

STRUCTURE, ISOTYPES, TARGETS, AND POST-TRANSLATIONAL MODIFICATIONS OF IMMUNOGLOBULINS AND THEIR ROLE IN INFECTION, INFLAMMATION AND AUTOIMMUNITY

EDITED BY: Sylvie Hermouet, Jean Harb and Bridget S. Wilson
PUBLISHED IN: *Frontiers in Immunology*





frontiers

Frontiers eBook Copyright Statement

The copyright in the text of individual articles in this eBook is the property of their respective authors or their respective institutions or funders. The copyright in graphics and images within each article may be subject to copyright of other parties. In both cases this is subject to a license granted to Frontiers.

The compilation of articles constituting this eBook is the property of Frontiers.

Each article within this eBook, and the eBook itself, are published under the most recent version of the Creative Commons CC-BY licence.

The version current at the date of publication of this eBook is CC-BY 4.0. If the CC-BY licence is updated, the licence granted by Frontiers is automatically updated to the new version.

When exercising any right under the CC-BY licence, Frontiers must be attributed as the original publisher of the article or eBook, as applicable.

Authors have the responsibility of ensuring that any graphics or other materials which are the property of others may be included in the CC-BY licence, but this should be checked before relying on the CC-BY licence to reproduce those materials. Any copyright notices relating to those materials must be complied with.

Copyright and source acknowledgement notices may not be removed and must be displayed in any copy, derivative work or partial copy which includes the elements in question.

All copyright, and all rights therein, are protected by national and international copyright laws. The above represents a summary only. For further information please read Frontiers' Conditions for Website Use and Copyright Statement, and the applicable CC-BY licence.

ISSN 1664-8714

ISBN 978-2-88966-046-9

DOI 10.3389/978-2-88966-046-9

About Frontiers

Frontiers is more than just an open-access publisher of scholarly articles: it is a pioneering approach to the world of academia, radically improving the way scholarly research is managed. The grand vision of Frontiers is a world where all people have an equal opportunity to seek, share and generate knowledge. Frontiers provides immediate and permanent online open access to all its publications, but this alone is not enough to realize our grand goals.

Frontiers Journal Series

The Frontiers Journal Series is a multi-tier and interdisciplinary set of open-access, online journals, promising a paradigm shift from the current review, selection and dissemination processes in academic publishing. All Frontiers journals are driven by researchers for researchers; therefore, they constitute a service to the scholarly community. At the same time, the Frontiers Journal Series operates on a revolutionary invention, the tiered publishing system, initially addressing specific communities of scholars, and gradually climbing up to broader public understanding, thus serving the interests of the lay society, too.

Dedication to Quality

Each Frontiers article is a landmark of the highest quality, thanks to genuinely collaborative interactions between authors and review editors, who include some of the world's best academicians. Research must be certified by peers before entering a stream of knowledge that may eventually reach the public - and shape society; therefore, Frontiers only applies the most rigorous and unbiased reviews.

Frontiers revolutionizes research publishing by freely delivering the most outstanding research, evaluated with no bias from both the academic and social point of view. By applying the most advanced information technologies, Frontiers is catapulting scholarly publishing into a new generation.

What are Frontiers Research Topics?

Frontiers Research Topics are very popular trademarks of the Frontiers Journals Series: they are collections of at least ten articles, all centered on a particular subject. With their unique mix of varied contributions from Original Research to Review Articles, Frontiers Research Topics unify the most influential researchers, the latest key findings and historical advances in a hot research area! Find out more on how to host your own Frontiers Research Topic or contribute to one as an author by contacting the Frontiers Editorial Office: researchtopics@frontiersin.org

STRUCTURE, ISOTYPES, TARGETS, AND POST-TRANSLATIONAL MODIFICATIONS OF IMMUNOGLOBULINS AND THEIR ROLE IN INFECTION, INFLAMMATION AND AUTOIMMUNITY

Topic Editors:

Sylvie Hermouet, INSERM U1232 Centre de Recherche en Cancérologie et Immunologie Nantes Angers (CRCINA), France

Jean Harb, INSERM U1064 Centre de Recherche en Transplantation et Immunologie, France

Bridget S. Wilson, University of New Mexico, United States

Citation: Hermouet, S., Harb, J., Wilson, B. S., eds. (2020). Structure, Isotypes, Targets, and Post-Translational Modifications of Immunoglobulins and Their Role in Infection, Inflammation and Autoimmunity. Lausanne: Frontiers Media SA.
doi: 10.3389/978-2-88966-046-9

Table of Contents

- 05 Editorial: Structure, Isotypes, Targets, and Post-translational Modifications of Immunoglobulins and Their Role in Infection, Inflammation and Autoimmunity**
Jean Harb, Bridget S. Wilson and Sylvie Hermouet
- 10 Peripheral IgE Repertoires of Healthy Donors Carry Moderate Mutation Loads and Do Not Overlap With Other Isotypes**
Marvyn T. Koning, Ignis J. M. Trollmann, Cornelis A. M. van Bergen, Diego Alvarez Saravia, Marcelo A. Navarrete, Szymon M. Kietbasa and Hendrik Veelken
- 18 Characterization of the C1q-Binding Ability and the IgG1-4 Subclass Profile of Preformed Anti-HLA Antibodies by Solid-Phase Assays**
Ana Navas, Juan Molina, María-Luisa Agüera, Ipek Guler, Aurora Jurado, Alberto Rodríguez-Benot, Corona Alonso and Rafael Solana
- 29 Low pH Exposure During Immunoglobulin G Purification Methods Results in Aggregates That Avidly Bind Fc γ Receptors: Implications for Measuring Fc Dependent Antibody Functions**
Ester Lopez, Nichollas E. Scott, Bruce D. Wines, P. Mark Hogarth, Adam K. Wheatley, Stephen J. Kent and Amy W. Chung
- 44 Development of a Potent and Protective Germline-Like Antibody Lineage Against Zika Virus in a Convalescent Human**
Fei Gao, Xiaohe Lin, Linling He, Ruoke Wang, Han Wang, Xuanling Shi, Fuchun Zhang, Chibiao Yin, Linqi Zhang, Jiang Zhu and Lei Yu
- 57 Anti-IL6 Autoantibodies in an Infant With CRP-Less Septic Shock**
Marketa Bloomfield, Zuzana Parackova, Tamara Cabelova, Iva Pospisilova, Pavel Kabicek, Hana Houstkova and Anna Sediva
- 63 Molecular Analysis of Goodpasture's Disease Following Hematopoietic Stem Cell Transplant in a Pediatric Patient, Recalls the Conformeropathy of Wild-Type Anti-GBM Disease**
Paul E. Gray, Hugh McCarthy, Owen M. Siggs, Moin A. Saleem, Tracy O' Brien, Katie Frith, John B. Ziegler, A. Richard Kitching, Agnes B. Fogo, Billy G. Hudson and Vadim Pedchenko
- 71 Diagnostic Profiling of the Human Public IgM Repertoire With Scalable Mimotope Libraries**
Anastas Pashov, Velizar Shivarov, Maya Hadzhieva, Victor Kostov, Dilyan Ferdinandov, Karen-Marie Heintz, Shina Pashova, Milena Todorova, Tchavdar Vassilev, Thomas Kieber-Emmons, Leonardo A. Meza-Zepeda and Eivind Hovig
- 85 An Inflammatory Story: Antibodies in Tuberculosis Comorbidities**
Milla R. McLean, Lenette L. Lu, Stephen J. Kent and Amy W. Chung
- 105 Minimal B Cell Extrinsic IgG Glycan Modifications of Pro- and Anti-Inflammatory IgG Preparations in vivo**
Anja Schaffert, Maja Hanić, Mislav Novokmet, Olga Zaytseva, Jasminka Krištić, Anja Lux, Lars Nitschke, Matthias Peipp, Marija Pezer, René Hennig, Erdmann Rapp, Gordan Lauc and Falk Nimmerjahn

- 121** *Predominant Role of Immunoglobulin G in the Pathogenesis of Splenomegaly in Murine Lupus*
Qian Zhang, Liping Xiang, Muhammad Haidar Zaman, Wenhui Dong, Guodan He and Guo-Min Deng
- 133** *The Proteolytic Cleavage of Therapeutic Monoclonal Antibody Hinge Region: More Than a Matter of Subclass*
Quentin Deveuue, Laurie Lajoie, Benjamin Barrault and Gilles Thibault
- 145** *A Comparison of Immunoglobulin Variable Region N-Linked Glycosylation in Healthy Donors, Autoimmune Disease and Lymphoma*
Esther M. Vletter, Marvyn T. Koning, Hans Ulrich Scherer, Hendrik Veelken and Rene E. M. Toes
- 157** *Analysis of the Targets and Glycosylation of Monoclonal IgAs From MGUS and Myeloma Patients*
Adrien Bosseboeuf, Célia Seillier, Nicolas Mennesson, Sophie Allain-Maillet, Maeva Fourny, Anne Tallet, Eric Piver, Philippe Lehours, Francis Mégraud, Laureline Berthelot, Jean Harb, Edith Bigot-Corbel and Sylvie Hermouet



Editorial: Structure, Isotypes, Targets, and Post-translational Modifications of Immunoglobulins and Their Role in Infection, Inflammation and Autoimmunity

Jean Harb^{1,2,3}, Bridget S. Wilson^{4,5} and Sylvie Hermouet^{2,6*}

¹ Centre de Recherche en Transplantation et Immunologie UMR1064, Inserm, Université de Nantes, Nantes, France,

² CRCINA, Inserm, Université de Nantes, Université d'Angers, Nantes, France, ³ Laboratoire de Biochimie, CHU de Nantes, Nantes, France, ⁴ University of New Mexico Comprehensive Cancer Center, Albuquerque, NM, United States, ⁵ Department of Pathology, University of New Mexico School of Medicine, Albuquerque, NM, United States, ⁶ Laboratoire d'Hématologie, CHU de Nantes, Nantes, France

Keywords: immunoglobulins, glycosylation, targets, inflammation, infection, autoimmunity

Editorial on the Research Topic

OPEN ACCESS

Edited by:

Deborah K. Dunn-Walters,
University of Surrey, United Kingdom

Reviewed by:

Roberta Pelanda,
University of Colorado School of
Medicine, United States

*Correspondence:

Sylvie Hermouet
sylvie.hermouet@univ-nantes.fr

Specialty section:

This article was submitted to
B Cell Biology,
a section of the journal
Frontiers in Immunology

Received: 29 May 2020

Accepted: 30 June 2020

Published: 07 August 2020

Citation:

Harb J, Wilson BS and Hermouet S
(2020) Editorial: Structure, Isotypes,
Targets, and Post-translational
Modifications of Immunoglobulins and
Their Role in Infection, Inflammation
and Autoimmunity.
Front. Immunol. 11:1761.
doi: 10.3389/fimmu.2020.01761

Structure, Isotypes, Targets, and Post-translational Modifications of Immunoglobulins and Their Role in Infection, Inflammation and Autoimmunity

Infection, autoimmunity, and cancer are accompanied by inflammation, which may alter the structure and function of immunoglobulins (Ig) and consequently, their pathogenicity (1–3). In addition, the isotype also influences the pathogenicity of Igs (4). During Dengue virus infection, the removal of core fucose residues selectively enhances the affinity of IgG for Fragment crystallizable (Fc)γRIIIa receptors, leading to increased antibody-dependent cell mediated cytotoxicity (ADCC) and decreased complement dependent cytotoxicity (CDC) (5). In patients infected by the human immunodeficiency virus (HIV), anti-gp120 antibodies are less galactosylated and sialylated in asymptomatic, long-term non-progressors, compared to symptomatic patients (6). The Fc domain of IgGs can trigger pro- or anti-inflammatory responses and there is abundant evidence that carbohydrates attached to the IgG Fc domain are essential for IgG function (7–9). The pro- or anti-inflammatory function of IgGs is mediated by different affinities for activating FcγRs (FcγRI, RIIa, RIIIa, and RIIb) and inhibiting FcγRIIb expressed by immune cells (10–12). A high level of sialylation of the IgG Fc fragment decreases ADCC potential through low affinity for activating receptors and conversely, bisecting N-acetylglucosamines on the Fc fragment are pro-inflammatory and enhance ADCC (13–16). In autoimmune diseases, such as rheumatoid arthritis, patients show low levels of IgG Fc sialylation, while increased IgG sialylation is associated with remission (17, 18). Thus, the glycosylation level of IgGs may explain their “protective” action. Similarly, Ig glycosylation plays an important role in IgA nephropathy, where IgA1s are deficient in galactose and not correctly cleared by anti-IgA1 antibodies (19).

The targets of Igs are also of increasing interest in human pathology, and important antigenic drivers are being discovered in monoclonal gammopathies of undetermined significance (MGUS) and myeloma, a blood cancer (20–26). The immunogenic glucolipid glucosylsphingosine (GlcSph)—also called lysoglucoylceramide (LGL1)—and infectious pathogens including Epstein-Barr virus (EBV) and hepatitis C virus (HCV), were recently shown to be the targets of monoclonal IgGs in MGUS and myeloma (20–26). Monoclonal IgGs bear very low levels of sialylated

glycans, which suggests a pro-inflammatory state and reinforces the notion that chronic antigenic stimulation and an abnormal immune response contribute to the pathogenesis of MGUS and myeloma (27). Importantly, therapies aiming at reducing the target of the monoclonal Ig can be proposed to patients. Recent reports described the beneficial effect for patients who presented a GlcSph (LGL-1)-reactive monoclonal Ig and who received treatments that reduced the level of immunogenic glucolipid; a clear reduction in monoclonal Ig was obtained for two patients (28). Similarly, antiviral treatment benefited both MGUS patients and myeloma patients with a monoclonal Ig that targeted HCV (29, 30).

This collection constituted of 13 original articles, 1 case report and 2 reviews from 112 authors, is divided into three sections. The first section presents recent knowledge on the variability in structure and isotype of Igs in clinical contexts. The second section is devoted to the targets and post-translational modifications of Igs in specific pathological contexts. The final section describes the consequences of Ig variability and targets in terms of pathogenicity and interest for the diagnosis, prognosis, monitoring, and treatment of patients.

STRUCTURE AND ISOTYPES OF IMMUNOGLOBULINS

The structure of Igs influences their function and also their fate (half-life, for instance) and subsequently, their efficacy. In this regard, the studies of Deveuue et al. highlight the importance of the hinge region of Igs, particularly for the development of new therapeutic monoclonal antibodies (TmAbs) (Deveuue et al.). They analyzed the proteolytic cleavage of the hinge region of IgG, which may occur by proteases of the microenvironment, including matrix metalloproteinase 12 (MMP12) or bacterial (*Streptococcus piogenes*) Ig-degrading enzymes (IdeS) and represents an escape mechanism to treatment by TmAbs. The authors compared the cleavage of 8 TmAbs of different isotypes and found the IgG2 TmAb more protease resistant than IgG1 and IgG4 TmAbs, and variable IdeS-sensitivity among IgG4 and IgG1 TmAbs. They propose that the variability in the cleavage sensitivity/resistance balance among IgG1 and IgG4 TmAbs results in part from characteristics of the Fab region (Deveuue et al.). They also show that a single cleavage of IgG1 TmAbs greatly decreases their affinity for FcγRIIIa and ability to induce FcγRIIIa-dependent functional responses from NK cells.

Allergy is dependent on the IgE isotype. Koning et al. studied IgE VDJ sequences from allergic patients, and compared them to the IgE repertoire from healthy, non-atopic individuals. They report that IgE repertoires were highly oligoclonal with preferential usage of certain IGHV genes. IgE sequences had no clonal relationship with the other isotypes, carried more somatic mutations than IgM but fewer than IgG and IgA. Thus, in healthy individuals, the mutational burden of IgE suggests an origin through direct class-switching from the IgM repertoire, and presumably low affinity for antigens.

The risk of transplant rejection is also affected by the isotype of antibodies developed by patients against human

leukocyte antigens (HLA). Navas et al. describe the results of the analysis of 1,285 anti-HLA antibodies identified in serum samples from 20 highly HLA-sensitized patients, and report that 36.8% of anti-HLA antibodies were C1q-binding. They found a strong association between C1q-binding ability and IgG1 strength, whereas weak or non-C1q-binding IgG2 and IgG4 subclasses were common. They conclude that the IgG1 subclass best correlates with the C1q-binding ability of anti-HLA antibodies.

TARGETS AND POST-TRANSLATIONAL MODIFICATIONS OF IMMUNO-GLOBULINS IN SPECIFIC PATHOLOGICAL CONTEXTS

Targets of Immunoglobulins

The antigenic targets of pathological Igs are relatively well-known in the context of allergy and auto-immune diseases. In the context of B-cell malignancies, the main objective is to eliminate the malignant clone and most studies aim to characterize tumoral cells and uncover the mechanisms of their resistance to treatments. Consequently, the antigenic targets of the Igs produced by malignant B-cell clones are rarely studied. Yet there is mounting evidence that chronic antigen stimulation as an important pathogenic mechanism in the development of B-cell malignancies. For instance, patients with somatically-mutated (antigen-driven) chronic lymphocytic leukemia (CLL) have a more favorable clinical course than other CLL patients (31, 32). Evidence in favor of chronic antigen stimulation has also been reported in MGUS and in myeloma (20–26). CLL-associated antigens appear to be mostly autoantigens, notably cytoskeleton components, or autoantigens found in apoptotic cells and bacteria (33–35). Cases of virus (HCV), HIV-driven CLL, MGUS or myeloma appear to be relatively rare (36). In MGUS and myeloma, the targets of monoclonal IgG reported include viruses (>25% cases, predominantly EBV and more rarely, herpes virus simplex (HSV) and HCV) and glucolipids, particularly GlcSph (LGL1) (~15% cases) or associated enzymes (22–26). Using a new assay based on the protein micro-array technology, Bosseboeuf et al. report that the purified monoclonal Ig from 42% of IgA MGUS and myeloma patients recognize EBV EBNA-1, HCV or LGL1. Altogether, a pathogenic model of antigen-driven disease may be valid for about half of CLL, MGUS, and myeloma cases. This model offers new therapeutic approaches: in addition to current therapeutic protocols aimed at eliminating the malignant clone, one can envision therapies designed to reduce or suppress the antigen responsible for disease initiation, i.e., the target of the patient's monoclonal Ig, whenever the target can be identified (28–30).

Unfortunately, the identification of the targets of pathogenic human IgG and IgA for diagnosis and therapeutic purposes is still not possible outside research laboratories. Similarly, the targets of IgMs from healthy individuals are rarely investigated and remain poorly known. To facilitate the study of human IgM antibodies, which are characterized by polyspecificity and autoreactivity, Pashov et al. propose a new peptide array consisting of 594

mimotopes that reflect the common IgM repertoire of 10,000 healthy donors.

Post-translational Modifications and Function of Immunoglobulins

To interpret the results of IgG functional studies, the conditions of preparation and purification of Igs are of great importance. Lopez et al. report that low pH exposure during IgG purification may result in aggregates that abnormally and avidly bind Fc γ receptors. These authors compared Protein G purification of IgG (at low pH) with an immunoaffinity method which elutes IgG at physiological pH, and investigated several factors known to impact Fc functionality and influence Fc γ R binding, including IgG subclass, N-glycosylation, aggregation, and conformational changes. They show that low pH elution of IgG enhances their recognition of Fc γ Rs, and increases IgG aggregation. Thus, differences in IgG purification methods may explain the poor reproducibility of studies of Fc-mediated antibody functions.

The important role played in immunity by the N-linked glycosylation of the Fc region of Igs is well-established but the function of N-linked glycosylation of the variable domains of Igs is less well-known. In their review, Vletter et al. report that N-linked glycans are present on autoantibodies, notably in rheumatoid arthritis, and in patients with B-cell follicular lymphoma (FL). N-linked glycosylation of the variable domain of Igs may confer a selective advantage, through interaction with lectins and/or microbiota. They analyzed the characteristics of autoantibodies and those of Igs from FL patients and healthy donors and found differences in variable domain glycan distribution, frequency and glycan composition, which led them to propose a classification of diseases according to the specific Ig variable domain glycosylation patterns observed in patients.

Sialylation may also modify therapeutic IgGs. Shaffert et al. analyzed changes in human intravenous IgG (IVIg) sialylation upon injection in mice deficient in B cells or lacking the sialyltransferase 1, which catalyzes the addition of α 2,6 linked sialic acid residues and conclude that the glycosylation of therapeutic IgGs is stable *in vivo* Schaffert et al.. Only a very small fraction of IgGs acquired sialic acid structures, mostly in the Fab portion, not in the Fc portion.

CONSEQUENCES IN TERMS OF DIAGNOSIS, PROGNOSIS, MONITORING OF PATIENTS, AND THERAPY

The detection of monoclonal or/and polyclonal Igs with identified targets is becoming of increasing importance in different clinical contexts, including severe infection, chronic inflammation, and certain blood cancers. It is also necessary to better understand the effects of therapeutic monoclonal antibodies used in the clinic, alone or associated with other treatments.

Infection

The interest of understanding the Ig response of patients in context of acute infection is illustrated by the report by

Bloomfield et al., who describe the case of an infant who presented with a normal C-reactive protein (CRP) level despite severe septic shock following *Staphylococcus aureus* infection, with clear biological evidence of systemic inflammation. Bloomfield et al. suspected a defect in the interleukin-6 (IL-6)/CRP axis, which was confirmed by the presence of neutralizing anti-IL-6 autoantibodies in the child's serum. These findings are of importance since clinical interference of IL-6 signaling, for instance with IL-6 receptor-targeting therapeutic antibodies such as tocilizumab or sarilumab, may alter IL-6-mediated innate immune responses and compromise host resistance to infections.

The complex role played by Igs in chronic infection is illustrated in the review by McLean et al. on the mechanisms of tuberculosis reactivation in individuals with comorbidities. They describe the Ig responses to *Mycobacterium tuberculosis* of patients with chronic conditions, such as co-infection with HIV, diabetes or kidney diseases, where inflammation may facilitate tuberculosis re-activation. McLean et al. propose that inflammatory IgG profiles may be important biomarkers for the detection of progressive tuberculosis. More studies are needed to distinguish inflammatory antibody profiles that are the consequences of co-morbidities from those that contribute to the reactivation of tuberculosis.

Regarding severe viral infections, neutralizing antibodies hold great promise both for antibody-based therapeutic intervention and for vaccine design. This is illustrated by the paper by Gao et al., who applied next-generation sequencing (NGS) to probe the development of ZK2B, a potent E DIII-specific antibody protective against Zika virus (ZIKV), isolated from a convalescent individual. The NGS-derived, germline-like ZK2B10 somatic variants neutralized ZIKV and protected mice from ZIKV challenge, without cross-reactivity with Dengue virus. Site-directed mutagenesis identified residues essential to the functional maturation of ZK2B10. The repertoire and lineage features unveiled in this study should help elucidate the developmental process and protective potential of anti-ZIKV antibodies.

Auto-Immunity

Gray et al. report on a rapidly progressive glomerulonephritis reproducing the auto-immune Goodpasture's disease (GP), caused by anti-glomerular basement membrane (GBM) antibodies developed after allogeneic haematopoietic stem cell transplantation (HSCT). In GP, autoantibodies bind neopeptides formed upon disruption of the structure of α 345 NC1 hexamer, a critical domain of α 345 collagen IV scaffolds. Upon hexamer disruption, α 3 and α 5 NC1 subunits become immunogens. Gray et al.'s is the first report of allo-incompatibility and antigenic specificity in anti-GBM disease after allogeneic HSCT. Both the patient and donor presented with the Goodpasture's susceptibility HLA-allele *DRB1*1501*, and the patient's anti-GBM antibodies recognized the E_A epitope of the α 3 NC1 monomer of collagen IV. Auto-antibody binding to native α 345 NC1 hexamer was minimal, and there were no polymorphic differences between the donor's and recipient's collagen IV genes. The authors conclude that their patient's was a case of classical GP disease, the anti-GBM antibodies emerging post transplantation

from the donor immune system. This hypothesis is supported by the finding that native a345 NC1 hexamer was not pathogenic in an animal model of GP disease, whereas immunization with dissociated hexamers induced glomerulonephritis (Gray et al.).

Another example is provided by systemic lupus erythematosus (SLE), where Zhang et al. investigated the role of IgG in spleen inflammation. They report that lupus IgGs are important pathological factors involved in the initiation of inflammation and further germinal center (GC) and plasma cell formation. Macrophages of the splenic marginal zone were dispensable for the GC response induced by lupus IgG, while red pulp macrophages were important for GC responses. Furthermore, lupus IgGs promoted inflammation and GC formation through the macrophage-mediated secretion of TNF- α . Interestingly, Syk

inhibitor treatment suppressed the changes in the histopathology of the spleen induced by lupus IgGs.

CONCLUSION

Accumulating new knowledge of the structure, targets, and glycosylation of pathogenic Igs should rapidly translate into improved diagnosis and treatments for patients suffering from acute or chronic infection, chronic inflammation, autoimmunity, or B-cell malignancies.

AUTHOR CONTRIBUTIONS

All authors listed have made a substantial, direct and intellectual contribution to the work, and approved it for publication.

REFERENCES

- Scallon BJ, Tam SH, McCarthy SG, Cai AN, Raju TS. Higher levels of sialylated Fc glycans in immunoglobulin G molecules can adversely impact functionality. *Mol. Immunol.* (2007) 44:1524–34. doi: 10.1016/j.molimm.2006.09.005
- Dalziel M, Crispin M, Scanlan CN, Zitzmann N, Dwek RA. Emerging principles for the therapeutic exploitation of glycosylation. *Science.* (2014) 343:1235681. doi: 10.1126/science.1235681
- Parekh RB, Dwek RA, Sutton BJ, Fernandes DL, Leung A, Stanworth D, et al. Association of rheumatoid arthritis and primary osteoarthritis with changes in the glycosylation pattern of total serum IgG. *Nature.* (1985) 316:452–7. doi: 10.1038/316452a0
- Nimmerjahn F, Ravetch JV. Divergent immunoglobulin γ subclass activity through selective Fc receptor binding. *Science.* (2005) 310:1510–2. doi: 10.1126/science.1118948
- Wang TT, Sewatanon J, Memoli MJ, Wrammert J, Bournazos S, Bhaumik SK, et al. IgG antibodies to dengue enhanced for Fc γ RIIIA binding determine disease severity. *Science.* (2017) 355:395–8. doi: 10.1126/science.aai8128
- Ackerman ME, Crispin M, Yu X, Baruah K, Boesch AW, Harvey DJ, et al. Natural variation in Fc glycosylation of HIV-specific antibodies impacts antiviral activity. *J. Clin. Invest.* (2013) 123:2183–92. doi: 10.1172/JCI65708
- Kaneko Y, Nimmerjahn F, Ravetch JV. Anti-inflammatory activity of immunoglobulin G resulting from Fc sialylation. *Science.* (2006) 313:670–3. doi: 10.1126/science.1129594
- Nimmerjahn F. Activating and inhibitory Fc γ Rs in autoimmune disorders. *Springer Semin. Immunopathol.* (2006) 28:305–19. doi: 10.1007/s00281-006-0052-1
- Anthony RM, Nimmerjahn F, Ashline DJ, Reinhold VN, Paulson JC, Ravetch JV. Recapitulation of IVIG anti-inflammatory activity with a recombinant IgG Fc. *Science.* (2008) 320:373–6. doi: 10.1126/science.1154315
- Anthony RM, Wermeling F, Karlsson MCI, Ravetch JV. Identification of a receptor required for the anti-inflammatory activity of IVIG. *Proc Natl Acad Sci USA.* (2008) 105:19571–8. doi: 10.1073/pnas.0810163105
- Schwab I, Mihai S, Seeling M, Kasperkiewicz M, Ludwig RJ, Nimmerjahn F. Broad requirement for terminal sialic acid residues and Fc γ RIIB for the preventive and therapeutic activity of intravenous immunoglobulins in vivo. *Eur J Immunol.* (2014) 44:1444–53. doi: 10.1002/eji.201344230
- Washburn N, Schwab I, Ortiz D, Bhatnagar N, Lansing JC, Medeiros A, et al. Controlled tetra-Fc sialylation of IVIG results in a drug candidate with consistent enhanced anti-inflammatory activity. *Proc Natl Acad Sci USA.* (2015) 112:E1297–306. doi: 10.1073/pnas.1512309112
- Umaña P, Jean-Mairet J, Moudry R, Amstutz H, Bailey JE. Engineered glycoforms of an antineuroblastoma IgG1 with optimized antibody-dependent cellular cytotoxic activity. *Nat. Biotechnol.* (1999) 17:176–80. doi: 10.1038/6179
- Gasdaska JR, Sherwood S, Regan JT, Dickey LF. An afucosylated anti-CD20 monoclonal antibody with greater antibody-dependent cellular cytotoxicity and B-cell depletion and lower complement-dependent cytotoxicity than rituximab. *Mol. Immunol.* (2012) 50:134–41. doi: 10.1016/j.molimm.2012.01.001
- Quast I, Keller CW, Maurer MA, Giddens JB, Tackenberg B, Wang L-X, et al. Sialylation of IgG Fc domain impairs complement-dependent cytotoxicity. *J Clin Invest.* (2015) 125:4160–70. doi: 10.1172/JCI82695
- Schwab I, Biburger M, Krönke G, Schett G, Nimmerjahn F. IVIg-mediated amelioration of ITP in mice is dependent on sialic acid and SIGNR1. *Eur J Immunol.* (2012) 42:826–30. doi: 10.1002/eji.201142260
- Parekh RB, Roitt IM, Isenberg DA, Dwek RA, Ansell BM, Rademacher TW. Galactosylation of IgG associated oligosaccharides: reduction in patients with adult and juvenile onset rheumatoid arthritis and relation to disease activity. *Lancet.* (1988) 1:966–9. doi: 10.1016/S0140-6736(88)91781-3
- van de Geijn FE, Wührer M, Selman MH, Willemsen SP, de Man YA, Deelder AM, et al. Immunoglobulin G galactosylation and sialylation are associated with pregnancy-induced improvement of rheumatoid arthritis and the postpartum flare: results from a large prospective cohort study. *Arthritis Res Ther.* (2009) 11:R193. doi: 10.1186/ar2892
- Novak J, Barratt J, Julian BA, Renfrow MB. Aberrant glycosylation of the IgA1 molecule in IgA nephropathy. *Semin Nephrol.* (2018) 38:461–76. doi: 10.1016/j.semnephrol.2018.05.016
- Hermouet S, Corre I, Gassin M, Bigot-Corbel E, Sutton CA, Casey JW. Hepatitis C virus, human herpesvirus-8 and the development of plasma cell leukemia. *New Engl J Med.* (2003) 348:178–9. doi: 10.1056/NEJM200301093480219
- Bigot-Corbel E, Gassin M, Corre I, Le Carrer D, Delaroche O, Hermouet S. Hepatitis C virus (HCV) infection, monoclonal immunoglobulin specific for HCV core protein, plasma-cell malignancy. *Blood.* (2008) 112:4357–8. doi: 10.1182/blood-2008-07-167569
- Nair S, Branagan AR, Liu J, Boddupalli CS, Mistry PK, Dhodapkar M V. Clonal immunoglobulin against lysolipids in the origin of myeloma. *New Engl J Med.* (2016) 374:555–61. doi: 10.1056/NEJMoa1508808
- Bosseboeuf A, Feron D, Tallet A, Rossi C, Charlier C, Garderet L, et al. Monoclonal IgG in MGUS and multiple myeloma target infectious pathogens. *J Clin Invest Insight Oct.* (2017) 5: 95367. doi: 10.1172/jci.insight.95367
- Nair S, Sng J, Sekhar Boddupalli C, Seckinger A, Chesi M, Fulciniti M, et al. Antigen-mediated regulation in monoclonal gammopathies and myeloma. *J Clin Invest Insight.* (2018) 3:e98259. doi: 10.1172/jci.insight.98259
- Preuss KD, Hollak CEM, Fadl N, van Oers M, Regitz E, Pfreundschuh M. Saposin C is a frequent target of paraproteins in Gaucher disease-associated MGUS/multiple myeloma. *Br J Haematol.* (2019) 184:384–91. doi: 10.1111/bjh.15659
- Bosseboeuf A, Mennesson N, Allain-Maillet S, Tallet A, Piver E, Moreau C, et al. Characteristics of MGUS and multiple myeloma according to the target

- of monoclonal immunoglobulins, glucosylsphingosine, or epstein-barr virus EBNA-1. *Cancers*. (2020) 12:E1254. doi: 10.3390/cancers12051254
27. Bosseboeuf A, Allain S, Mennesson N, Tallet A, Rossi C, Garderet L, et al. Pro-inflammatory state in MGUS and Myeloma is characterized by low sialylation of pathogen-specific and other monoclonal and polyclonal immunoglobulin G. *Front. Immunol.* (2017) 8:1347. doi: 10.3389/fimmu.2017.01347
 28. Nair S, Bar N, Xu ML, Dhodapkar M, Mistry PK. Glucosylsphingosine but not Saposin C, is the target antigen in Gaucher disease-associated gammopathy. *Mol Genet Metab.* (2020) 129:286–91. doi: 10.1016/j.ymgme.2020.01.009
 29. Panfilio S, D'Urso P, Annechini G, D'Elia GM, De Angelis F, Stefanizzi C, et al. Regression of a case of Multiple Myeloma with antiviral treatment in a patient with chronic HCV infection. *Leuk Res Rep.* (2013) 2:39–40. doi: 10.1016/j.lrr.2013.01.002
 30. Rodríguez García A, Linares M, Mennesson N, Sanchez-Vega B, Sanchez R, Alonso Fernandez R, et al. The role of Hepatitis C virus in the development of multiple myeloma: a case study. 60th Annual Meeting of the American Society of Hematology (ASH), San Diego, CA, USA, December 1–4, 2018. Abstract Nbr: 5592, Submission ID: 112842. *Blood.* (2018) 132:5592. doi: 10.1182/blood-2018-99-112842
 31. Damle RN, Wail T, Fais F, Ghiotto F, Valletto A, Allen SL, et al. Ig V gene mutation status and CD38 expression as novel prognostic indicators in chronic lymphocytic leukemia. *Blood.* (1999) 94:1840–7. doi: 10.1182/blood.V94.6.1840.418k06_1840_1847
 32. Hamblin TJ, Davis Z, Gardiner A, Oscier DG, Stevenson FK. Unmutated Ig VH genes are associated with a more aggressive form of chronic lymphocytic leukemia. *Blood.* (1999) 94:1848–54. doi: 10.1182/blood.V94.6.1848.418k05_1848_1854
 33. Chiorazzi N, Hatzi K, Albesiano E. B-cell chronic lymphocytic leukemia, a clonal disease of B lymphocytes with receptors that vary in specificity for (auto)antigens. *Ann N Y Acad Sci.* (2005) 1062:1–2. doi: 10.1196/annals.1358.002
 34. Citera R, Silverman GJ, Hatzi K, Seiler T, Didier S, Zhang L, et al. Chronic lymphocytic leukemia cells recognize conserved epitopes associated with apoptosis and oxidation. *Mol Med.* (2008) 14:665–74. doi: 10.2119/2008-00102.Citera
 35. Lanemo Myhrinder A, Hellqvist E, Sidorova E, Söderberg A, Baxendale H, Dahle C, et al. A new perspective: molecular motifs on oxidized LDL, apoptotic cells, and bacteria are targets for chronic lymphocytic leukemia antibodies. *Blood.* (2008) 111:3838–48. doi: 10.1182/blood-2007-11-125450
 36. Hwang K-K, Trama AM, Kozink DM, et al. IGHV1-69 B cell chronic lymphocytic leukemia antibodies cross-react with HIV-1 and hepatitis c virus antigens as well as intestinal commensal bacteria. *PLoS ONE.* (2014) 9:e90725. doi: 10.1371/journal.pone.0090725

Conflict of Interest: The authors declare that the research was conducted in the absence of any commercial or financial relationships that could be construed as a potential conflict of interest.

Copyright © 2020 Harb, Wilson and Hermouet. This is an open-access article distributed under the terms of the Creative Commons Attribution License (CC BY). The use, distribution or reproduction in other forums is permitted, provided the original author(s) and the copyright owner(s) are credited and that the original publication in this journal is cited, in accordance with accepted academic practice. No use, distribution or reproduction is permitted which does not comply with these terms.



Peripheral IgE Repertoires of Healthy Donors Carry Moderate Mutation Loads and Do Not Overlap With Other Isotypes

Marvyn T. Koning¹, Ignis J. M. Trollmann¹, Cornelis A. M. van Bergen¹, Diego Alvarez Saravia², Marcelo A. Navarrete^{2*}, Szymon M. Kielbasa³ and Hendrik Veelken¹

¹ Department of Hematology, Leiden University Medical Center, Leiden, Netherlands, ² School of Medicine, University of Magallanes, Punta Arenas, Chile, ³ Department of Biomedical Data Sciences, Leiden University Medical Center, Leiden, Netherlands

OPEN ACCESS

Edited by:

Bridget S. Wilson,
University of New Mexico,
United States

Reviewed by:

Mats Ohlin,
Lund University, Sweden
Hannah Gould,
King's College London,
United Kingdom

*Correspondence:

Marcelo A. Navarrete
marcelo.navarrete@umag.cl

Specialty section:

This article was submitted to
B Cell Biology,
a section of the journal
Frontiers in Immunology

Received: 04 February 2019

Accepted: 20 June 2019

Published: 03 July 2019

Citation:

Koning MT, Trollmann IJM, van Bergen CAM, Alvarez Saravia D, Navarrete MA, Kielbasa SM and Veelken H (2019) Peripheral IgE Repertoires of Healthy Donors Carry Moderate Mutation Loads and Do Not Overlap With Other Isotypes. *Front. Immunol.* 10:1543. doi: 10.3389/fimmu.2019.01543

IgE-mediated allergic disease represents an increasing health problem. Although numerous studies have investigated IgE sequences in allergic patients, little information is available on the healthy IgE repertoire. IgM, IgG, IgA, and IgE transcripts from peripheral blood B cells of five healthy, non-atopic individuals were amplified by unbiased, template-switching, isotype-specific PCR. Complete VDJ regions were sequenced to near-exhaustion on the PacBio platform. Sequences were analyzed for clonal relationships, degree of somatic hypermutation, IGHV gene usage, evidence of antigenic selection, and N-linked glycosylation motifs. IgE repertoires appeared to be highly oligoclonal with preferential usage of certain IGHV genes compared to the other isotypes. IgE sequences carried more somatic mutations than IgM, yet fewer than IgG and IgA. Many IgE sequences contained N-linked glycosylation motifs. IgE sequences had no clonal relationship with the other isotypes. The IgE repertoire in healthy individuals is derived from relatively few clonal expansions without apparent relations to immune reactions that give rise to IgG or IgA. The mutational burden of normal IgE suggests an origin through direct class-switching from the IgM repertoire with little evidence of antigenic drive, and hence presumably low affinity for specific antigens. These findings are compatible with a primary function of the healthy IgE repertoire to occupy Fcε receptors for competitive protection against mast cell degranulation induced by allergen-specific, high-affinity IgE. This background knowledge may help to elucidate pathogenic mechanisms in allergic disease and to design improved desensitization strategies.

Keywords: affinity maturation, allergy, B-cell receptor, class switching, IgE

INTRODUCTION

Type I hypersensitivity is an immune response triggered by allergen-specific IgE. Binding of allergen-bound IgE to Fcε receptors on mast cells leads to prompt degranulation, which provokes a range of clinical symptoms including atopic dermatitis, asthma, allergic rhinoconjunctivitis, urticarial, and anaphylaxis (1, 2). Despite the recognition that IgE-mediated diseases are becoming an ever increasing health burden, especially in urban societies (3), the mechanisms leading to

IgE-mediated disease, as well as the underlying principles causing clinical heterogeneity, remain incompletely understood (4, 5). An improved understanding of the development of IgE repertoires in healthy individuals may aid in the identification of these disease mechanisms and facilitates efficient design of anti-allergic strategies (6, 7).

Two distinct pathways to generate IgE have been identified in mouse models. In the direct pathway, functional B-cell receptor (BCR) genes undergo direct class-switch recombination (CSR) from IgM to IgE isotype and yield predominantly IgE with low affinity to antigen. In the indirect pathway, high-affinity IgE results from secondary CSR in B cells that express IgG or potentially IgA (8, 9). Along with increased affinity, IgE derived from IgG1 B cells also carry significantly more mutations than IgE in IgG1-deficient mice (10). The existence of multiple pathways has been further supported by flow cytometric analyses in humans showing subsets both dependent and independent of germinal centers (11).

Since low and high affinity IgE compete for occupation of the Fcε receptor, higher concentrations of low-affinity IgE than high-affinity IgE can theoretically provide protection against anaphylaxis (10). In non-allergic humans, very limited information on the extent and origin of the IgE repertoire is currently available and consists of only 60 near-full-length IgE sequences from two individuals (12). Although recently a number of studies have applied massive parallel sequencing to gain new insights in the IgE repertoire, none of them generated the full-length sequences essential for comprehensive analysis and/or used primer binding bias-free methodology (13–18).

This study aimed to provide in-depth characterization of the IgE repertoire in healthy, non-allergic individuals as an essential reference for comparative studies in allergic and desensitized individuals. We determined the peripheral blood IgE BCR repertoire of five non-allergic donors to near completion by unbiased, full-length massive parallel sequencing. IgE BCR repertoires were compared to IgM, IgG, and IgA repertoires to support the hypothesis that the direct pathway of IgE generation would be dominant in non-allergic human individuals.

MATERIALS AND METHODS

Material Collection and Storage

Cryopreserved aliquots of Ficoll-separated mononuclear cells (PBMC) from five healthy, asymptomatic stem cell donors were obtained from the biobank of the Leiden University Medical Center biobank in accordance with local guidelines. Absence of atopic constitution was confirmed by measurement of total IgM, IgG, IgA, and IgE immunoglobulin levels in time-matched serum samples.

Flow Cytometry Analysis for Expression of CD19 and IgE

IgE-expressing B cells were isolated from aliquots of 1×10^5 thawed PBMC by flow cytometry. To avoid artifacts from binding of IgE to Fcε receptor-expressing cells (19), cells were fixed in 200 μl 1% paraformaldehyde in phosphate-buffered saline (B. Braun, Melsungen, Germany) with 5% fetal bovine serum (Bodinco,

Alkmaar, The Netherlands) and 0.2% saponin (Sigma Aldrich, St. Louis, MO, USA) for 8 min at 4°C. After washing, fixed cells were permeabilized for 30 min at 4°C in 200 μl of the same buffer without paraformaldehyde. Cells were washed once more and stained with anti-CD19-FITC (BD Biosciences, Franklin Lakes, NJ, USA) and anti-IgE-APC (Miltenyi Biotec, Leiden, The Netherlands) for 30 min at 4°C in the dark, followed by another wash and resuspension. The abundance of CD19⁺ and IgE⁺ cells was determined by flow cytometry in live gated cells.

BCR Repertoire Sequencing

The ARTISAN PCR protocol for unbiased amplification of BCR repertoires (20) was adapted for IgE by designing a series of IgE constant region-specific reverse primers (ε.rt 5'-GGCATAGTGACCAGAGAGCG-3' for reverse transcription; ε.pcr1 5'-GGTCACCATCACCGGCTCCG-3' for initial PCR amplification; ε.pcr2 5'-GGCAGCCCAGAGTCACGG-3' for semi-nested PCR amplification; ε.bc 5'-[barcode]-CGGATGGGCTCTGTGTGG-3' for barcoding; barcodes: 5'-CCATCTCATATGTAGTACTCT-3', 5'-CGGATGGGCTCTGTGTGG-3', 5'-CGGATGGGCTCTGTGTGG-3', 5'-CGGATGGGCTCTGTGTGG-3' and 5'-CGGATGGGCTCTGTGTGG-3'). B cells were isolated from aliquots of thawed cells by removal of non-B cells with magnetic beads (B cell isolation kit II; Miltenyi Biotec, Leiden, The Netherlands) and routinely yielded a purity of >99% CD19⁺ B cells as assessed by flow cytometry. For each healthy donor, 2×10^6 B cells were divided into five aliquots.

Messenger RNA isolation and cDNA synthesis were performed separately for each aliquot with addition of the ε.rt primer to the ARTISAN cDNA synthesis mix (20). IgM, IgG, and IgA cDNA was amplified according to the original ARTISAN PCR protocol. Due to the low abundance of IgE⁺ B cells in healthy donor peripheral blood, amplification of functional IgE transcripts was extensively optimized with different primer combinations on serial dilutions (100–0.01%) of the IgE-expressing multiple myeloma cell line U266 (DSMZ, Braunschweig, Germany) in a background of healthy donor PBMCs. For IgE repertoires, cDNA was first amplified for 15 cycles with the ε.pcr1 primer. First-round IgE amplicons were purified by silica spin columns (Promega, Madison, WI, USA) and re-amplified for 15 cycles of semi-nested PCR using the ε.pcr2 primer. Libraries were barcoded at the 5' terminus to identify the donor and at the 3' terminus to identify individual aliquots. Pooled libraries were amplified as single molecules in rolling circles on a total of five SMRT cells on the RSII system (Pacific Biosciences, Menlo Park, CA, USA). IgE sequences were sequenced to high depth to achieve near-complete representation of all IgE⁺ B cells present in the sample.

Sequence and Statistical Analysis

Output sequence files were filtered with SMRT portal software for a minimum of eight sequencing passes. All sequences were annotated by IMGT HighV-QUEST (21). For statistical analyses, sequences with identical IGHV genes and amino acid CDR3 sequences within one aliquot were counted as a single sequence.

IGHV gene usage was compared between isotypes by Fisher's exact test and corrected for multiple testing by Bonferroni

TABLE 1 | Serum immunoglobulin concentrations in five healthy donors.

Subject	IgM (g/L)	IgG (g/L)	IgA (g/L)	IgE (kU/L)
1	1.56	8.67	2.17	12.4
2	1.19	9.68	1.93	76.8
3	0.38	8.02	1.32	41.8
4	0.53	9.20	1.78	23.7
5	0.67	6.45	0.61	14.9

correction. Cumulative differences in IGHV gene usage were calculated by determining the absolute differences in fractional IGHV usage between two isotypes for every IGHV gene and adding these to a cumulative difference with a theoretical maximum of 200. BCR mutational status and CDR3 length were compared between isotypes by unpaired *t*-test.

N-linked glycosylation motifs were identified as Asn-X-Ser/Thr motifs (where X may be any amino acid except proline) and their abundance, location, and the mutational status of the corresponding sequence were compared between isotypes using unpaired *t* and Fisher's exact tests.

Clonal B-cell expansions were defined as the presence of BCR sequences with identical V, D and J gene usage, identical CDR3 length and $\geq 95\%$ nucleotide overlap in CDR3 in either multiple aliquots or in more than one isotype of any individual donor. Intraclonal sequence variation was defined as the distance from the clonal consensus and determined for the largest 10 IgE clones, as well as the largest 5 IgM, IgG, and IgA clones.

Calculation of Sampling Depth

To assess how many cells from the sample were represented in the VDJ sequence libraries, we performed an *in silico* simulation to estimate the fraction of observed unique sequences sampled out of a large pool of sequences. A unique numerical identifier was assigned to each unique observed BCR sequence for each donor, and 5×10^5 copies of every identifier were pooled in the simulation. Consequently, random sequences were sampled from the pool up to the number of sequences obtained from massive parallel sequencing, and the number of unique identifiers was counted. This simulation was performed 100 times per donor, and the median number of unique samples identifiers per donor was calculated.

RESULTS

According to applicable stem cell donor regulations, all donors had no atopic constitution, denied any allergic symptoms, and had normal serum immunoglobulin and IgE concentrations (Table 1).

Sequence Acquisition

A median of 0.09% of peripheral blood B cells of healthy donors expressed IgE (Table 2), corresponding to a median of 2,000 cells per 2×10^6 B cells. A median of 3,254 total full-length, potentially functional VDJ IgE sequences were obtained per donor by ARTISAN PCR and deep PacBio sequencing, representing a median of 1.52 IgE sequences per IgE⁺ B cell

present in the sample. *In silico* simulations indicated that this amount of oversampling would theoretically return a median of 78% of unique sequences (Supplementary Data). In addition, medians of 2,088 IgM (range: 1,287–2,437), 1,221 IgG (range: 735–2,144), and 2,770 IgA (range: 1,351–3,012) unique, full-length and potentially functional VDJ sequences were obtained per donor.

Clonal B-Cell Expansions

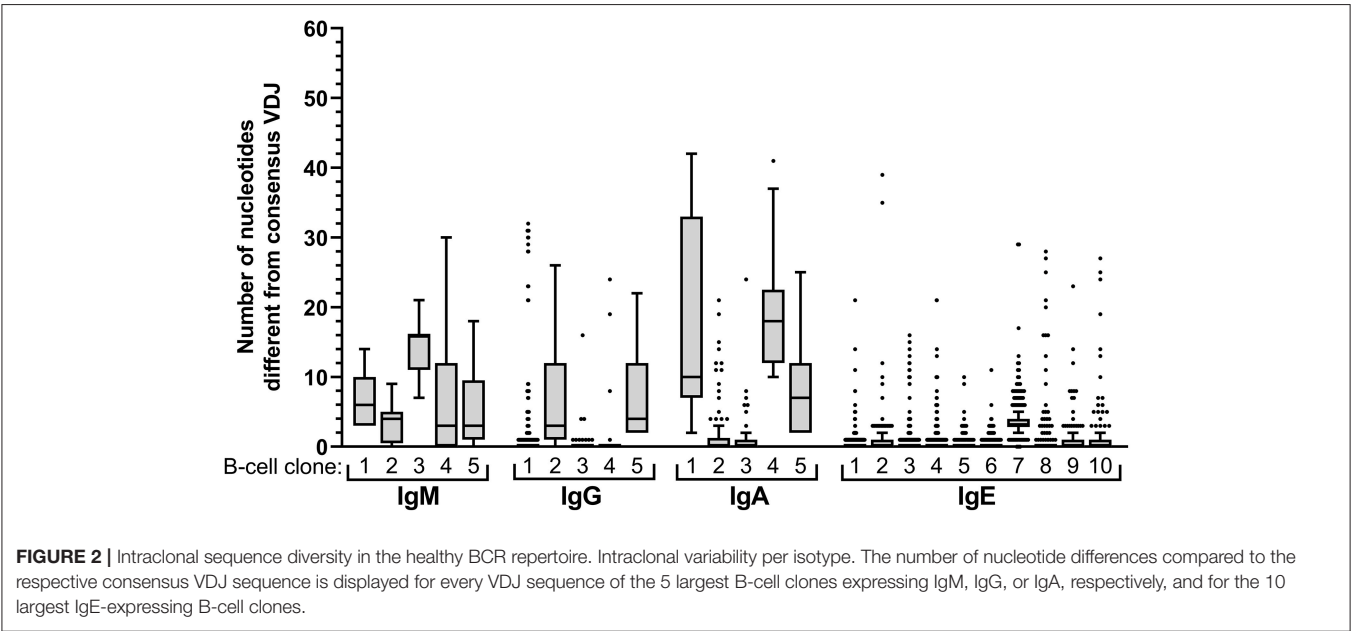
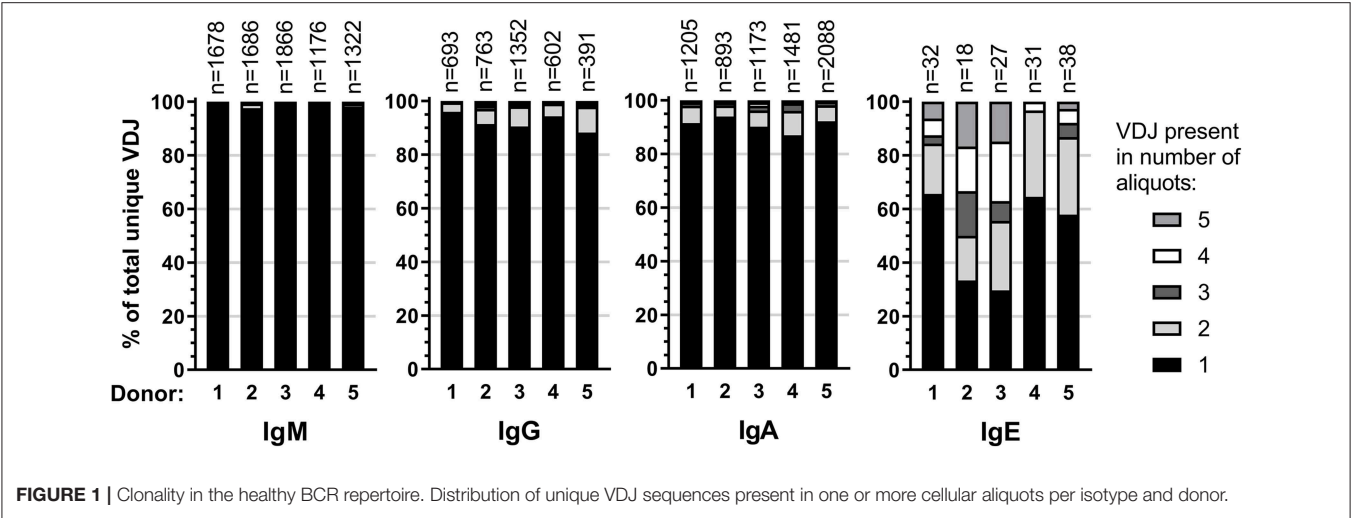
To identify and quantify clonal B cell expansions, we first assigned all individual VDJ sequences within an isotype of each donor to clonotypes according to stringent criteria developed rationally to minimize the calling of false-positive clonal relationships (Supplementary Data). This analysis identified a median of 39 (range: 23–46) putative unique IgE clonotypes per donor and indicated representation of each clonotype by an average of 85 closely related VDJ sequences. Additional manual inspection revealed that some of these putative clonotypes shared substantial numbers of individual mutations in their IGHV, strongly suggesting a common clonal origin despite less than 95% CDR3 identity and despite occasional variation in CDR3 length. Therefore, we combined putative clonotypes from an individual that shared at least 70% of their IGHV mutations regardless of CDR3 similarities into definitive clonotypes for all further analyses. We identified a total of 146 definitive IgE clonotypes (median per donor 31; range: 18–38). In a single instance, these criteria indicated the presence of a single clonotype in two donors. Since the libraries of these two donors were sequenced on the same SMRT cell, this phenomenon may originate from barcode contamination and does not permit to conclude the presence of canonical IgE clonotypes across individuals.

Expansion of an IgE-expressing B-cell clone was unequivocally demonstrated by the presence of 69 of the total of 146 IgE clonotypes (47%) in at least two B-cell aliquots (Figure 1), corresponding to a median of 12 (range: 11–19) clonal expansions of IgE-expressing B-cells per donor. In comparison, only 1.3 of IgM, 7.9 of IgG, and 9.1% of IgA VDJ clonotypes were found in multiple aliquots and therefore derived from clonally expanded B cells, corresponding to a median of 14 (range: 6–40; total 97), 46 (range: 28–128; total 301) and 115 (range: 54–192; total 625) clonal expansions per donor and isotype, respectively (Figure 1). IgE clonal expansions were fewer than IgG ($p = 0.034$) and IgA ($p = 0.0017$), but similar to IgM expansions ($p = 0.39$). Intraclonal sequence diversity was lower in IgE than in all other isotypes (IgM: $p = 0.0002$; IgG: $p = 0.0184$; IgA: $p = 0.0039$; Figure 2). Twelve VDJ clonotypes were present in both IgM and IgG BCR repertoires, 24 in IgM and IgA, and 45 in IgG and IgA. Seven clonotypes comprised IgM, IgG, and IgA isotypes. In marked contrast, no relationship was found between any IgE and non-IgE VDJ. Since this finding is in contrast with previous reports (22), we performed extensive *in silico* simulations that demonstrated frequent false-positive conclusions of clonal overlap when inappropriately relaxed criteria for clonal relationship are applied (Supplementary Data).

TABLE 2 | Quantification of IgE⁺ B cells and sequencing depth.

Donor	% CD19 ⁺	IgE ⁺ B cells		VDJ sequences		Median theoretical coverage (range)
	cells within live gate	% within CD19 ⁺ gate	per 2 × 10 ⁶ CD19 ⁺ cells	Total	per cell	
1	11.3	0.10	2,000	3,254	1.63	81% (79–82)
2	10.8	0.09	1,800	1,814	1.01	63% (62–66)
3	10.8	0.15	3,000	3,716	1.24	71% (69–73)
4	9.2	0.06	1,200	1,823	1.52	78% (76–81)
5	6.5	0.08	1,600	5,199	3.25	96% (95–97)
Median	10.8	0.09	2,000	3,254	1.52	78%

Coverage represents the amount of unique sequences sampled from the pool in an *in silico* simulation assuming no PCR amplification bias. Its range is based on the minimum and maximum values obtained from 100 simulations.



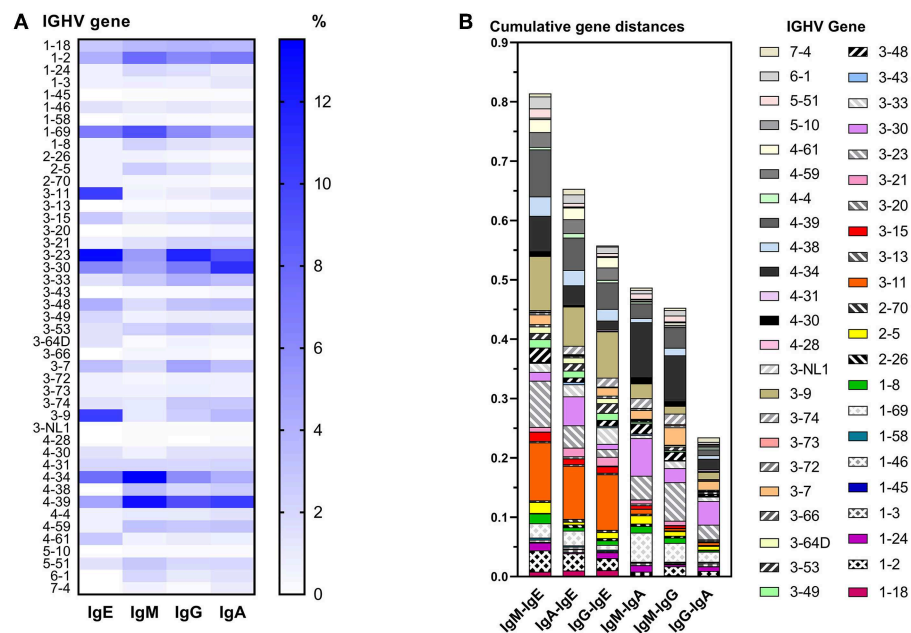


FIGURE 3 | Differential IGHV usage between isotypes. **(A)** Heat map indicating the relative frequency of all IGHV genes among unique VDJ sequences per isotype. For each isotype, the frequencies shown add up to 100%. **(B)** Pairwise comparison of cumulative IGHV gene distance between two isotypes. For each IGHV gene, the fractions of VDJ sequences containing that IGHV gene within an isotype were calculated, and the numerical difference of these fractions between two isotypes was determined per IGHV gene. For each pairwise comparison between isotypes, all differences of IGHV gene fractions were added to obtain their cumulative distance.

BCR Characteristics per Isotype

IgE VDJ utilized more frequently IGHV3-9 and IGHV3-11 ($p < 0.0001$), and less frequently IGHV4-39 than the remaining isotypes ($p = 0.0018$; **Figure 3A**). Concordantly, cumulative gene fraction distances between IgE and other isotypes were significantly larger than distances between IgM and IgG, IgM, and IgA, and IgG, and IgA (**Figure 3B**).

All isotypes had median CDR3 lengths of 15 amino acids (**Figure 4A**). Unique IgE VDJ carried fewer mutations (4.9%) than the other class-switched isotypes ($p < 0.001$) (**Figure 4B**).

Despite their moderate SHM burden, more IgE VDJ (23%) had acquired N-linked glycosylation motifs (NLGM) through SHM than IgG (16%; $p < 0.001$) and IgA (17%; $p < 0.001$). When considering all NLGM, i.e., both germline-encoded (from IGHV1-8, IGHV4-34, and IGHV5-10-1) and SHM-derived motifs, their prevalence of 27% in all IgE VDJ was significantly higher ($p < 0.0001$) than in IgM, IgG, and IgA (**Figure 4C**). This difference was largely attributable to preservation of germ-line-encoded NLGM in the IgE compartment (**Table 3**).

DISCUSSION

In conclusion, we provide the first comprehensive inventory of near-complete peripheral blood IgE repertoires from healthy individuals through tailored methodology that lacks primer binding bias, yields full-length VDJ sequences, and detects clonal expansions by standardized parallel analysis of several aliquots (20). The applicable regulations for volunteer stem cell

donors precluded the acquisition of additional epidemiological information such as dwelling and other living conditions that are associated with allergy. The observed frequency of 0.09% IgE-expressing cells among peripheral B cells is on the high end of the reported spectrum (23, 24). The consequences of a possible overestimation of the true prevalence of IgE⁺ B cells would predominantly imply that the sequencing of the IgE repertoires would have been even more exhaustive than indicated by our simulations. In this context, presence of clonally related IgE sequences in several cellular aliquots is a much more reliable indicator of clonal expansions than BCR sequence read counts in massive parallel sequencing experiments. Nevertheless, it is a striking observation that IgE sequences found in all 5 aliquots dominated the sequence libraries (not shown), suggesting that few IgE⁺ clones actually had expanded strongly.

The presence of SHM indicates that IgE⁺ B cells have passed through germinal center reactions. The intermediate SHM load of IgE between IgM and IgG/IgA could result from direct CSR of the majority of healthy donor PBMC from IgM to IgE (13). Alternatively, non-IgE B cells could have acquired higher SHM loads by repeated GC passages, whereas IgE⁺ B cells have only a limited presence in germinal centers, (25–27). The difference in IgE mutation rate compared to other isotypes was more striking than in another recent study of IgE in non-allergic subjects, yet not as low as in children with atopic dermatitis (15, 16). These findings call for further verification.

The striking lack of clonal relationships between IgE-expressing B cells and B cells expressing the other isotypes

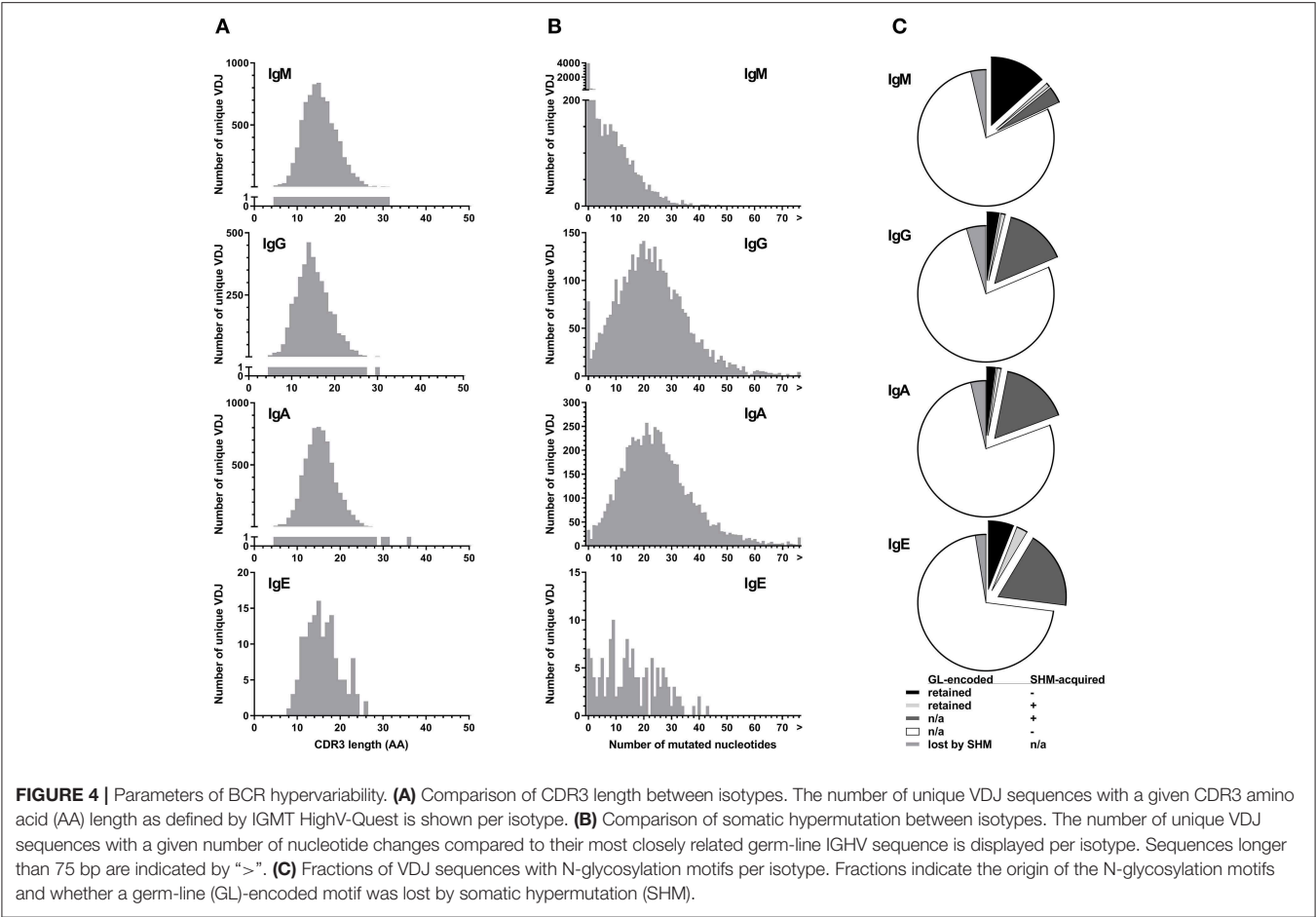


TABLE 3 | Preservation of germline-encoded N-linked glycosylation sites.

Isotype	Retention of germline N-linked glycosylation motifs		
	IGHV1-8	IGHV4-34	IGHV5-10-1
IgM	87%	89%	83%
IgG	51%	47%	43%
IgA	59%	44%	62%
IgE	94%	64%	N/A

No IGHV5-10-1-containing VDJ were found for IgE.

supports the important conclusion that IgE-expressing B cells emerge from qualitatively different immune responses. While the IgE repertoire has been sequenced to apparent exhaustion in our study, incomplete sampling of the other isotype compartments cannot completely exclude a low degree of clonal overlap. However, lack of clonal overlap is corroborated by a recent massive parallel sequencing study that also found virtually no clonal relationship between IgE and other isotypes in healthy donors (16). In contrast, marked overlap of allergen-specific IgE clones with IgG and IgA has been described in allergic individuals (14, 17, 28) and in immunized mice (13).

The distinct characteristics of the normal IgE repertoire, i.e., relatively low SHM burden, lack of intraclonal sequence variation, skewed usage of IGHV genes, marked oligoclonality, retention of germline-encoded NLGM, frequent acquisition of additional such motifs, and striking absence of clonal relatedness to IgM-expressing and non-IgE-class-switched B cells cumulatively indicates its origin from qualitatively different immune responses than IgG- and IgA-expressing B cells. Like allergic individuals (15, 17), healthy donors appear to have IgE repertoires composed of a small pool of highly expanded clones. However, in healthy donors, these likely represent rearrangements in a low affinity, non-antigen-specific, “static” state. As previously suggested, such low-affinity IgE could have a protective role against allergy by competition with high-affinity, type I hypersensitivity-inducing IgE for occupation of Fcε receptors (13, 29).

The novel hypothesis of a specific role of N-glycosylation in expansion and maintenance of IgE-expressing B cells in non-allergic individuals warrants further studies. Ubiquitous NLGM acquisition could have a disease-specific role in selection of IgE-expressing B-cells in similarity to follicular lymphoma (30), primary cutaneous follicle center lymphoma (31) and rheumatoid arthritis (32). On the other hand, glycosylation at NLGM positions could non-specifically

obstruct antigen recognition and effectively inhibit BCR affinity maturation (33).

Our findings also support direct class switch recombination from IgM to IgE as the origin of such low-affinity IgE antibodies as demonstrated in mouse studies (10, 13, 19).

Some, but not all (17, 18, 28), previous studies found preferential IGHV usage in allergic individuals, most notably of IGHV2, IGHV4, and IGHV5 family genes (15, 34–36). Our data do not indicate this particular IGHV bias in healthy individuals. Although theoretically attributable to study population differences, primer binding bias in multiplexed primer strategies creates an inherent risk of skewing repertoire analyses. Use of a forward primer binding to an artificial uniform sequence at the 5' cDNA termini effectively alleviates this risk (7, 20, 31, 37). Differential amplification efficiency of different IGHV genes may be another theoretical source of bias for observed IGHV usage. However, IgE sequences underwent only two additional thermocycles than the other isotypes, effectively limiting this particular risk. In addition, ARTISAN PCR employs long extension times to avoid such bias. In previous applications of this method, no preferential V allele amplification was actually observed (20).

In comparison to allergic individuals and derivatives of high-affinity murine clones, healthy donors appear to carry IgE sequences with fewer BCR mutations (12–15, 18, 28) and less restriction to few individual clonotypes (7, 12, 38, 39). Although IgE VDJ from allergic and parasite-exposed patients also lacked evidence of substantial antigenic selection (7, 15), these characteristics indicate that high-affinity (allergen-specific) IgE clones in allergic individuals are probably generated through indirect class switch recombination from IgG and IgA clonal expansions, preferentially utilizing a restricted repertoire of IGHV genes (13).

Overall, our results add various new aspects to the current knowledge on the IgE repertoire (7). Future projects investigating IgE repertoires in allergic disease should be generated by the same high-standard unbiased approach used here to allow for side-to-side comparison with healthy donors.

ETHICS STATEMENT

This study was carried out in accordance with the guidelines as outlined by the LUMC Biobank Committee with written informed consent from all subjects. All subjects gave written informed consent in accordance with the Declaration of Helsinki. The protocol was approved by the LUMC Medical Ethical Testing Committee.

AUTHOR CONTRIBUTIONS

CvB obtained samples. MK and IT obtained the data. MK analyzed the data. DA, MN, and SK provided bioinformatics support. MK and HV wrote the manuscript. All authors read and approved the manuscript.

FUNDING

MK was supported by a grant from the Professor Steenhuis Fund. MN and DA were supported by Fondecyt 11140542 and Fondecyt 1180882.

SUPPLEMENTARY MATERIAL

The Supplementary Material for this article can be found online at: <https://www.frontiersin.org/articles/10.3389/fimmu.2019.01543/full#supplementary-material>

REFERENCES

- Akdis CA. Allergy and hypersensitivity: mechanisms of allergic disease. *Curr Opin Immunol.* (2006) 18:718–26. doi: 10.1016/j.coi.2006.09.016
- Galli SJ, Tsai M, Piliponsky AM. The development of allergic inflammation. *Nature.* (2008) 454:445–54. doi: 10.1038/nature07204
- Ring J, Akdis C, Behrendt H, Lauener RP, Schappi G, Akdis M, et al. Davos declaration: allergy as a global problem. *Allergy.* (2012) 67:141–3. doi: 10.1111/j.1398-9995.2011.02770.x
- Akdis CA. Therapies for allergic inflammation: refining strategies to induce tolerance. *Nat Med.* (2012) 18:736–49. doi: 10.1038/nm.2754
- Lotvall J, Akdis CA, Bacharier LB, Björner L, Casale TB, Custovic A, et al. Asthma endotypes: a new approach to classification of disease entities within the asthma syndrome. *J Allergy Clin Immunol.* (2011) 127:355–60. doi: 10.1016/j.jaci.2010.11.037
- Akdis M, Akdis CA. Mechanisms of allergen-specific immunotherapy: multiple suppressor factors at work in immune tolerance to allergens. *J Allergy Clin Immunol.* (2014) 133:621–31. doi: 10.1016/j.jaci.2013.12.1088
- Gadermaier E, Levin M, Flicker S, Ohlin M. The human IgE repertoire. *Int Arch Allergy Immunol.* (2014) 163:77–91. doi: 10.1159/000355947
- Erazo A, Kutchukhidze N, Leung M, Christ AP, Urban JF Jr, Curotto de Lafaille MA, et al. Unique maturation program of the IgE response *in vivo*. *Immunity.* (2007) 26:191–203. doi: 10.1016/j.immuni.2006.12.006
- Mills FC, Thyphronitis G, Finkelman FD, Max EE. Ig mu-epsilon isotype switch in IL-4-treated human B lymphoblastoid cells. evidence for a sequential switch. *J Immunol.* (1992) 149:1075–85.
- Xiong H, Dolpady J, Wabl M, Curotto de Lafaille MA, Lafaille JJ. Sequential class switching is required for the generation of high affinity IgE antibodies. *J Exp Med.* (2012) 209:353–64. doi: 10.1084/jem.20111941
- Berkowska MA, Heeringa JJ, Hajdarbegovic E, van der Burg M, Thio HB, van Hagen PM, et al. Human IgE(+) B cells are derived from T cell-dependent and T cell-independent pathways. *J Allergy Clin Immunol.* (2014) 134:688–97 e6. doi: 10.1016/j.jaci.2014.03.036
- Dahlke I, Nott DJ, Ruhno J, Sewell WA, Collins AM. Antigen selection in the IgE response of allergic and nonallergic individuals. *J Allergy Clin Immunol.* (2006) 117:1477–83. doi: 10.1016/j.jaci.2005.12.1359
- He JS, Subramaniam S, Narang V, Srinivasan K, Saunders SP, Carbajo D, et al. IgG1 memory B cells keep the memory of IgE responses. *Nat Commun.* (2017) 8:641. doi: 10.1038/s41467-017-00723-0
- Hoh RA, Joshi SA, Liu Y, Wang C, Roskin KM, Lee JY, et al. Single B-cell deconvolution of peanut-specific antibody responses in allergic patients. *J Allergy Clin Immunol.* (2016) 137:157–67. doi: 10.1016/j.jaci.2015.05.029
- Kerzel S, Rogosch T, Struecker B, Maier RF, Kabesch M, Zemlin M. Unlike in children with allergic asthma, IgE transcripts from preschool children with atopic dermatitis display signs of superantigen-driven activation. *J Immunol.* (2016) 196:4885–92. doi: 10.4049/jimmunol.1402889

16. Kitaura K, Yamashita H, Ayabe H, Shini T, Matsutani T, Suzuki R. Different somatic hypermutation levels among antibody subclasses disclosed by a new next-generation sequencing-based antibody repertoire analysis. *Front Immunol.* (2017) 8:389. doi: 10.3389/fimmu.2017.00389
17. Levin M, King JJ, Glanville J, Jackson KJ, Looney TJ, Hoh RA, et al. Persistence and evolution of allergen-specific IgE repertoires during subcutaneous specific immunotherapy. *J Allergy Clin Immunol.* (2016) 137:1535–44. doi: 10.1016/j.jaci.2015.09.027
18. Levin M, Levander F, Palmason R, Greiff L, Ohlin M. Antibody-encoding repertoires of bone marrow and peripheral blood—a focus on IgE. *J Allergy Clin Immunol.* (2017) 139:1026–30. doi: 10.1016/j.jaci.2016.06.040
19. Wesemann DR, Magee JM, Boboila C, Calado DP, Gallagher MP, Portuguese AJ, et al. Immature B cells preferentially switch to IgE with increased direct Smu to Sepsilon recombination. *J Exp Med.* (2011) 208:2733–46. doi: 10.1084/jem.20111155
20. Koning MT, Kielbasa SM, Boersma V, Buermans HPJ, van der Zeeuw SAJ, van Bergen CAM, et al. ARTISAN PCR: rapid identification of full-length immunoglobulin rearrangements without primer binding bias. *Br J Haematol.* (2017) 178:983–6. doi: 10.1111/bjh.14180
21. Alamyar E, Duroux P, Lefranc MP, Giudicelli V. IMGT((R)) tools for the nucleotide analysis of immunoglobulin (IG) and T cell receptor (TR) V-(D)-J repertoires, polymorphisms, and IG mutations: IMGT/V-QUEST and IMGT/HighV-QUEST for NGS. *Methods Mol Biol.* (2012) 882:569–604. doi: 10.1007/978-1-61779-842-9_32
22. Looney TJ, Lee JY, Roskin KM, Hoh RA, King J, Glanville J, et al. Human B-cell isotype switching origins of IgE. *J Allergy Clin Immunol.* (2016) 137:579–86 e7. doi: 10.1016/j.jaci.2015.07.014
23. King CL, Nutman TB. IgE and IgG subclass regulation by IL-4 and IFN-gamma in human helminth infections. assessment by B cell precursor frequencies. *J Immunol.* (1993) 151:458–65.
24. King CL, Poindexter RW, Ragunathan J, Fleisher TA, Ottesen EA, Nutman TB. Frequency analysis of IgE-secreting B lymphocytes in persons with normal or elevated serum IgE levels. *J Immunol.* (1991) 146:1478–83.
25. He JS, Meyer-Hermann M, Xiangying D, Zuan LY, Jones LA, Ramakrishna L, et al. The distinctive germinal center phase of IgE+ B lymphocytes limits their contribution to the classical memory response. *J Exp Med.* (2013) 210:2755–71. doi: 10.1084/jem.20131539
26. Talay O, Yan D, Brightbill HD, Straney EE, Zhou M, Ladi E, et al. IgE(+) memory B cells and plasma cells generated through a germinal-center pathway. *Nat Immunol.* (2012) 13:396–404. doi: 10.1038/ni.2256
27. Yang Z, Sullivan BM, Allen CD. Fluorescent *in vivo* detection reveals that IgE(+) B cells are restrained by an intrinsic cell fate predisposition. *Immunity.* (2012) 36:857–72. doi: 10.1016/j.immuni.2012.02.009
28. Croote D, Darmanis S, Nadeau KC, Quake SR. High-affinity allergen-specific human antibodies cloned from single IgE B cell transcriptomes. *Science.* (2018) 362:1306–9. doi: 10.1126/science.aau2599
29. Nopp A, Johansson SG, Ankerst J, Bylin G, Cardell LO, Gronneberg R, et al. Basophil allergen threshold sensitivity: a useful approach to anti-IgE treatment efficacy evaluation. *Allergy.* (2006) 61:298–302. doi: 10.1111/j.1398-9995.2006.00987.x
30. Schneider D, Duhren-von Minden M, Alkhatib A, Setz C, van Bergen CA, Benkisser-Petersen M, et al. Lectins from opportunistic bacteria interact with acquired variable-region glycans of surface immunoglobulin in follicular lymphoma. *Blood.* (2015) 125:3287–96. doi: 10.1182/blood-2014-11-609404
31. Koning MT, Nteleah V, Veelken H, Navarrete MA. Template-switching anchored polymerase chain reaction reliably amplifies functional lambda light chain transcripts of malignant lymphoma. *Leuk Lymphoma.* (2014) 55:1212–4. doi: 10.3109/10428194.2013.828353
32. Vergoosen RD, Slot LM, Hafkenscheid L, Koning MT, van der Voort EIH, Grooff CA, et al. B-cell receptor sequencing of anti-citrullinated protein antibody (ACPA) IgG-expressing B cells indicates a selective advantage for the introduction of N-glycosylation sites during somatic hypermutation. *Ann Rheum Dis.* (2017) 77:956–8. doi: 10.1136/annrheumdis-2017-212052
33. Wright A, Tao MH, Kabat EA, Morrison SL. Antibody variable region glycosylation: position effects on antigen binding and carbohydrate structure. *EMBO J.* (1991) 10:2717–23. doi: 10.1002/j.1460-2075.1991.tb07819.x
34. Coker HA, Harries HE, Banfield GK, Carr VA, Durham SR, Chevetton E, et al. Biased use of VH5 IgE-positive B cells in the nasal mucosa in allergic rhinitis. *J Allergy Clin Immunol.* (2005) 116:445–52. doi: 10.1016/j.jaci.2005.04.032
35. Snow RE, Djukanovic R, Stevenson FK. Analysis of immunoglobulin E VH transcripts in a bronchial biopsy of an asthmatic patient confirms bias towards VH5, and indicates local clonal expansion, somatic mutation and isotype switch events. *Immunology.* (1999) 98:646–51. doi: 10.1046/j.1365-2567.1999.00910.x
36. van der Stoep N, van der Linden J, Logtenberg T. Molecular evolution of the human immunoglobulin E response: high incidence of shared mutations and clonal relatedness among epsilon VH5 transcripts from three unrelated patients with atopic dermatitis. *J Exp Med.* (1993) 177:99–107. doi: 10.1084/jem.177.1.99
37. Wang Y, Jackson KJ, Chen Z, Gaeta BA, Siba PM, Pomat W, et al. IgE sequences in individuals living in an area of endemic parasitism show little mutational evidence of antigen selection. *Scand J Immunol.* (2011) 73:496–504. doi: 10.1111/j.1365-3083.2011.02525.x
38. Edwards MR, Brouwer W, Choi CH, Ruhno J, Ward RL, Collins AM. Analysis of IgE antibodies from a patient with atopic dermatitis: biased V gene usage and evidence for polyreactive IgE heavy chain complementarity-determining region 3. *J Immunol.* (2002) 168:6305–13. doi: 10.4049/jimmunol.168.12.6305
39. Janezic A, Chapman CJ, Snow RE, Hourihane JO, Warner JO, Stevenson FK. Immunogenetic analysis of the heavy chain variable regions of IgE from patients allergic to peanuts. *J Allergy Clin Immunol.* (1998) 101:391–6. doi: 10.1016/S0091-6749(98)70253-2

Conflict of Interest Statement: The authors declare that the research was conducted in the absence of any commercial or financial relationships that could be construed as a potential conflict of interest.

Copyright © 2019 Koning, Trollmann, van Bergen, Alvarez Saravia, Navarrete, Kielbasa and Veelken. This is an open-access article distributed under the terms of the Creative Commons Attribution License (CC BY). The use, distribution or reproduction in other forums is permitted, provided the original author(s) and the copyright owner(s) are credited and that the original publication in this journal is cited, in accordance with accepted academic practice. No use, distribution or reproduction is permitted which does not comply with these terms.



Characterization of the C1q-Binding Ability and the IgG1-4 Subclass Profile of Preformed Anti-HLA Antibodies by Solid-Phase Assays

Ana Navas^{1,2}, Juan Molina^{1,2*}, María-Luisa Agüera^{1,3}, Ipek Guler¹, Aurora Jurado^{1,2}, Alberto Rodríguez-Benot^{1,3}, Corona Alonso^{1,2} and Rafael Solana^{1,2}

¹ Maimonides Biomedical Research Institute of Cordoba (IMIBIC), Reina Sofia University Hospital, University of Cordoba, Cordoba, Spain, ² Department of Immunology and Allergy, Reina Sofia University Hospital, Cordoba, Spain, ³ Department of Nephrology, Reina Sofia University Hospital, Cordoba, Spain

OPEN ACCESS

Edited by:

Jean Harb,
INSERM U1064 Centre de Recherche
en Transplantation et
Immunologie, France

Reviewed by:

Valérie Dubois,
Etablissement Français du Sang
Auvergne Rhône-Alpes, France
Jakob Nilsson,
University Hospital Zürich, Switzerland

*Correspondence:

Juan Molina
juan.e.molina.alcaide@gmail.com

Specialty section:

This article was submitted to
Alloimmunity and Transplantation,
a section of the journal
Frontiers in Immunology

Received: 20 April 2019

Accepted: 08 July 2019

Published: 02 August 2019

Citation:

Navas A, Molina J, Agüera M-L,
Guler I, Jurado A, Rodríguez-Benot A,
Alonso C and Solana R (2019)
Characterization of the C1q-Binding
Ability and the IgG1-4 Subclass Profile
of Preformed Anti-HLA Antibodies by
Solid-Phase Assays.
Front. Immunol. 10:1712.
doi: 10.3389/fimmu.2019.01712

Humoral alloimmunity, particularly that triggered by preformed antibodies against human leukocyte antigens (HLA), is associated with an increased prevalence of rejection and reduced transplant survival. The high sensitivity of solid phase assays, based on microbeads coated with single antigens (SAB), consolidated them as the gold-standard method to characterize anti-HLA antibodies, ensuring a successful allograft allocation. Mean fluorescence intensity (MFI) provided by SAB is regularly used to stratify the immunological risk, assuming it as a reliable estimation of the antibody-level, but it is often limited by artifacts. Beyond MFI, other properties, such as the complement-binding ability or the IgG1-4 subclass profile have been examined to more accurately define the clinical relevance of antibodies and clarify their functional properties. However, there are still unresolved issues. Neat serum-samples from 20 highly-sensitized patients were analyzed by SAB-panIgG, SAB-IgG1-4 subclass and SAB-C1q assays. All 1:16 diluted serum-samples were additionally analyzed by SAB-panIgG and SAB-IgG1-4 subclass assays. A total of 1,285 anti-HLA antibodies were identified as positive, 473 (36.8%) of which were C1q-binding. As expected, serum-dilution enhanced the correlation between the C1q-binding ability and the antibody-strength, measured as the MFI ($r_{\text{neat}} = 0.248$ vs. $r_{\text{diluted}} = 0.817$). SAB-subclass assay revealed at least one IgG1-4 subclass in 1,012 (78.8%) positive antibody-specificities. Among them, strong complement-binding subclasses, mainly IgG1, were particularly frequent (98.9%) and no differences were found between C1q- and non-C1q-binding antibodies regarding their presence (99.4 vs. 98.5%; $p = 0.193$). In contrast, weak or non-C1q-binding subclasses (IgG2/IgG4) were more commonly detected in C1q-binding antibodies (78.9 vs. 38.6%; $p < 0.001$). Interestingly, a strong association was found between the C1q-binding ability and the IgG1 strength ($r_{\text{IgG1dil}} = 0.796$). Though lower, the correlation between the IgG2 strength and the C1q-binding ability was also strong ($r_{\text{IgG2dil}} = 0.758$), being both subclasses closely related ($r_{\text{IgG1-IgG2}} = 0.817$).

We did not find any correlation with the C1q-binding ability considering the remaining subclasses. In conclusion, we demonstrate that a particular profile of IgG subclasses (IgG1/IgG3) itself does not determine at all the ability to bind complement of anti-HLA antibodies assessed by SAB-C1q assay. It is the IgG subclass strength, mainly of IgG1, which usually appears in combination with IgG2, that best correlates with it.

Keywords: anti-HLA antibodies, C1q-binding ability, humoral alloimmunity, IgG1-4 subclass profile, kidney transplantation, single antigen bead assay

INTRODUCTION

In the last few years, single antigen bead (SAB)-assay has revolutionized the allograft allocation algorithm of patients awaiting solid-organ transplantation through a non-invasive virtual cross-matching procedure (1), with the purpose of avoiding the allograft damage caused by antibodies directed against human leukocyte antigens (HLA) undetected by other less sensitive tests such as the complement-dependent cytotoxicity (2, 3). However, the high sensitivity of SAB-assay linked to the premise that the presence of any antibody supposes an unacceptable risk regardless of its properties, has limited the access to transplantation of sensitized patients, excessively prolonging their waiting time (4). Even though the standardization of solid-phase assays has maintained low rates of rejection (5, 6), the impact of anti-HLA antibodies only detected by these tests is still under discussion and indeed, a proportion of transplanted patients with circulating donor-specific anti-HLA antibodies (DSA) under a negative complement-dependent cytotoxicity result, have acceptable allograft outcomes (7–9).

Technical issues of SAB-assay seem to prevent the discrimination of clinically relevant from harmless anti-HLA antibodies (10). In the absence of additional information regarding functional properties and with the aim of improving the consolidated restrictive algorithm for allograft allocation, the immunological risk of anti-HLA antibodies has been stratified according to their mean fluorescence intensity (MFI) value (11–14), assuming that this is a reliable estimation of the antibody level. Although SAB-assay is not approved as a quantitative method and there is no consensus on the threshold which defines an antibody as harmful, many transplantation centers consider all those donor mismatches for which antibodies show MFI values above 5,000 as unacceptable (15–18).

Several studies have demonstrated a direct correlation between high-MFI levels of DSA and increased incidences of antibody-mediated rejection and premature allograft failure (19–21). However, some methodological aspects may lead to MFI measures far from the real level of alloantibodies (22), suggesting that this is not always an entirely precise method to assess their risk. The prozone effect is the most common phenomenon whereby high-titers of antibodies are detected as low-MFI antibodies (<5,000). This effect, particularly frequent

in highly-sensitized patients, masks potentially dangerous specificities. Similarly, forbidden antibodies considered as harmful due to their MFI value (>5,000) might not be highly concentrated (22).

Beyond the MFI value, the SAB-C1q assay has been proposed as a tool to discriminate the sub-set of antibodies capable of binding C1q and assess their pathogenic potential, considering that the complement cascade is the major pathway of antibody-mediated damage (23). Until now, some authors have reported strong correlations between the presence of pre- and post-transplantation C1q-binding DSA and the risk of allograft failure (24–27), despite the fact that it is not fully ascertained whether this increased risk is due to the high-level of DSA or to their own ability to bind C1q (21, 28). Certainly, there seems to be a direct relationship between the complement-binding ability of anti-HLA antibodies and their strength (22, 27, 29).

The main effector mechanisms through which alloantibodies can induce damage on transplanted allografts include the activation of cells to promote proliferation and inflammation, the development of Fc-receptor-mediated functions and mainly, the activation of the complement system (30, 31). Since the four subclasses of IgG exhibit different structural and functional properties (32), triggering different pathological mechanisms of allograft damage, they must produce different phenotypes of injury. Indeed, Lefaucheur et al. (33) reported that the presence of IgG3 as immunodominant DSA led to acute antibody-mediated rejection with increased microvascular injury and C4d deposition, whereas IgG4-immunodominant DSA led to subclinical antibody-mediated rejection with increased chronic lesions. Additionally, they showed that patients with IgG3-immunodominant DSA had a significantly lower allograft survival rate regarding the presence of other IgG subclasses. More recently, Hamdani et al. (34) in a small cohort of pediatric kidney-transplanted patients showed that IgG3-DSA were independently associated with graft dysfunction. These findings suggest the added value of the IgG subclass detection to predict allograft outcome.

Thus, under all these premises, the present study aimed to investigate the characteristics of circulating anti-HLA antibodies in a cohort of highly-sensitized patients awaiting single-kidney transplantation, including the MFI value (neat and 1:16 diluted-serum), the ability to bind C1q and the IgG1-4 subclass profile in order to improve our understanding of the relationship between the different properties of antibodies.

Abbreviations: DSA, donor-specific anti-HLA antibodies; HLA, human leukocyte antigens; MFI, mean fluorescence intensity; SAB, single antigen bead.

MATERIALS AND METHODS

Serum Samples of the Study Cohort

In this study, analyzed serum samples were obtained from 20 highly-sensitized patients (calculated panel reactive antibody $\geq 75\%$) awaiting single-kidney transplantation at Reina Sofia University Hospital (Cordoba, Spain). The study cohort included 11 (55%) males and 9 (45%) females and the mean age was 47.35 ± 11.5 . At the time of the analysis the mean calculated panel reactive antibody of all patients was 97.15 ± 4.69 by the Organ Procurement and Transplantation Network database. The recorded classical HLA sensitization events were previous transplant in 15 (75%) patients, two of whom had also been poly-transfused, pregnancy in 4 (20%) patients and multiple blood-transfusions in 1 (5%) patient. Among all, 9 (45%) had antibodies against Class I, 4 (20%) against Class II, and 7 (35%) against Class I + II molecules. Serum samples of each patient were tested to detect all circulating anti-HLA antibody-specificities using the standardized SAB-panIgG and a modified SAB-assay to detect their IgG1-4 subclass composition (SAB-subclass assay). The C1q-binding ability was assessed by the SAB-C1q assay. All the analyses were performed using a single batch of reagents. This study was conducted according to the Declaration of Helsinki and was approved by the Ethics Committee of the Reina Sofia University Hospital (ref. 2465). All participants in the study provided written informed consent.

Detection and Characterization of Anti-HLA Antibodies by the Standardized SAB-panIgG Assay: Neat and Diluted Sera

Neat-serum samples were tested to detect the presence of circulating anti-HLA-A, -B, -Cw, -DR, -DQ, and -DP antibodies. The standardized SAB-panIgG assay (LABScreen, One Lambda, Inc.) on a Luminex platform was used to determine anti-HLA antibody-specificities according to the manufacturer instructions. Luminex 100 IS version 2.3 was used as data acquisition software and Fusion 3.3 (One Lambda, Inc.) as analysis software.

Additionally, since Tambur et al. (22) and Zeevi et al. (29) reported that the majority of antibody-specificities reaches the highest MFI value at a 1:16 dilution, we analyzed the 1:16 dilution of all samples by the standardized SAB-panIgG assay to assess their true MFI value and avoid the prozone effect. The dilution of the samples was performed with phosphate buffer saline.

Mean fluorescence intensity (MFI) value $\geq 1,000$ was the threshold set for a reaction to be considered positive. MFI = 5,000 was the cut-off set to classify antibodies into weak (MFI < 5,000) and strong (MFI $\geq 5,000$) antibodies.

Detection and Characterization of Anti-HLA Antibodies by the Standardized SAB-panIgG Assay: Pre-treatment With Heat and EDTA

Serum samples were pre-treated to overcome the possible inhibitory effect caused by several confounding factors other

than the amount of IgG antibodies. For this purpose, neat-serum samples were pre-heated at 56°C for 30 min and then analyzed by the standardized SAB-panIgG assay according to the manufacturer instructions. In addition, neat-serum samples were tested by the standardized SAB-panIgG assay using EDTA pre-treatment as previously described (22, 35).

Characterization of the C1q-Binding Ability of Anti-HLA Antibodies by the Standardized SAB-C1q Assay

The C1q-binding ability of anti-HLA antibodies was assessed using SAB-C1q assay (One Lambda, Inc.) on neat-serum samples according to the manufacturer protocol. All neat-serum samples were heat pre-treated at 56°C for 30 min as is indicated in the protocol of the SAB-C1q assay in order to remove any endogenous C1q. MFI value ≥ 500 was the threshold set for a C1q-reaction to be considered positive.

Subclass Profile by IgG1-4 SAB-Subclass Assay

The SAB-subclass assay was performed as previously reported (36). The standardized SAB-panIgG assay was modified by replacing the phycoerythrin-conjugated goat anti-human pan-IgG by specific monoclonal antibodies against IgG1-4 subclasses (IgG1 clone HP6001, IgG2 clone 31-7-4, IgG3 clone HP6050, IgG4 clone HP6025; Southern Biotech). In brief, 20 μL of neat-serum was mixed with 2.5 μL of HLA-coated beads (LABScreen, One Lambda, Inc.) for 30 min in darkness at room temperature while being shaken. The beads were washed once for 5 min at 1,300 g with 150 μL of wash buffer (One Lambda, Inc.). After discarding the supernatant, 100 μL of each appropriately diluted phycoerythrin-labeled anti-IgG1-4 secondary antibody was added as reported by Lefaucheur et al. (33) and incubated for 30 min in darkness at room temperature while being shaken. After one wash, 80 μL of phosphate buffer saline was added to be acquired on the Luminex platform. All beads showing MFI values > 500 were considered positive. Additionally, we analyzed the 1:16 dilution of serum samples by the SAB-subclass assay.

Statistical Analysis

Mean and standard deviations were provided for the description of continuous variables, and total number and frequency for the description of non-continuous variables. χ^2 test was used to compare qualitative data, while Student's *T*-test was used to compare parametric quantitative data. Pearson's test was used as the correlation test. Correlation was classified according to the correlation coefficient (*r*) into weak ($r < 0.5$), moderate ($0.5 > r < 0.75$) and strong ($r > 0.75$) correlation. We considered the raw MFI value of anti-HLA antibodies in all detection assays to perform the statistical analyses. All studied sera were included in the analyses. Values of $p < 0.05$ were regarded as statistically significant.

RESULTS

Analysis of panIgG Anti-HLA Antibodies in Neat and 1:16 Diluted Sera

The standardized SAB-panIgG assay performed with neat-serum samples belonging to the 20 HLA-sensitized patients included in this study defined 1,236 (47.6%) panIgG antibody-specificities as positive (MFI $\geq 1,000$) of the 2,594 Luminex-beads analyzed. Among the 1,236 positive antibody-specificities, 727 (58.8%) exhibited strong-MFI values (MFI $\geq 5,000$), and 509 (41.2%) were characterized as weak-MFI antibodies (**Figure 1**).

Then, the SAB-panIgG assay was performed with the 1:16 diluted-serum samples. The dilution unmasked the presence of 49 antibody-specificities with strong-MFI values originally detected as negative (**Figure 1**). As a result, a total of 1,285 antibody-specificities (1,236 detected in neat-sera plus 49 revealed after the dilution) were now regarded as positive. Furthermore, as shown in **Figure 1**, 72 (14.1%) of 509 neat-sera weakly positive antibodies became strong-specificities. Similarly,

the serum dilution cleared the presence of 114 (15.7%) strong-specificities. Therefore, after the dilution, 235 (18.3%) antibody-specificities dramatically changed their status: 121 from negative or weak to strong-specificities and 114 from strong to negative. Details of the 1,285 antibody-specificities detected, 806 (62.7%) directed against Class I and 479 (37.3%) against Class II molecules, are shown in **Supplementary Table 1**.

Analysis of the C1q-Binding Ability: Effect of the 1:16 Dilution, EDTA, and Heat Pre-treatments

As others before us, we explored the relationship between the C1q-binding ability of antibodies and their strength, measured as the MFI value. Among the 1,285 positive antibodies pre-defined by SAB-panIgG, 473 (36.8%) were C1q-positive. Additionally, 13 antibody-specificities undetectable neither in neat nor in diluted-serum SAB-panIgG assay (**Figure 1**) were weakly C1q-positive (908.6 ± 253.4). No subclass was identified in any of these 13 specificities, therefore regarded as false positive C1q-reactions

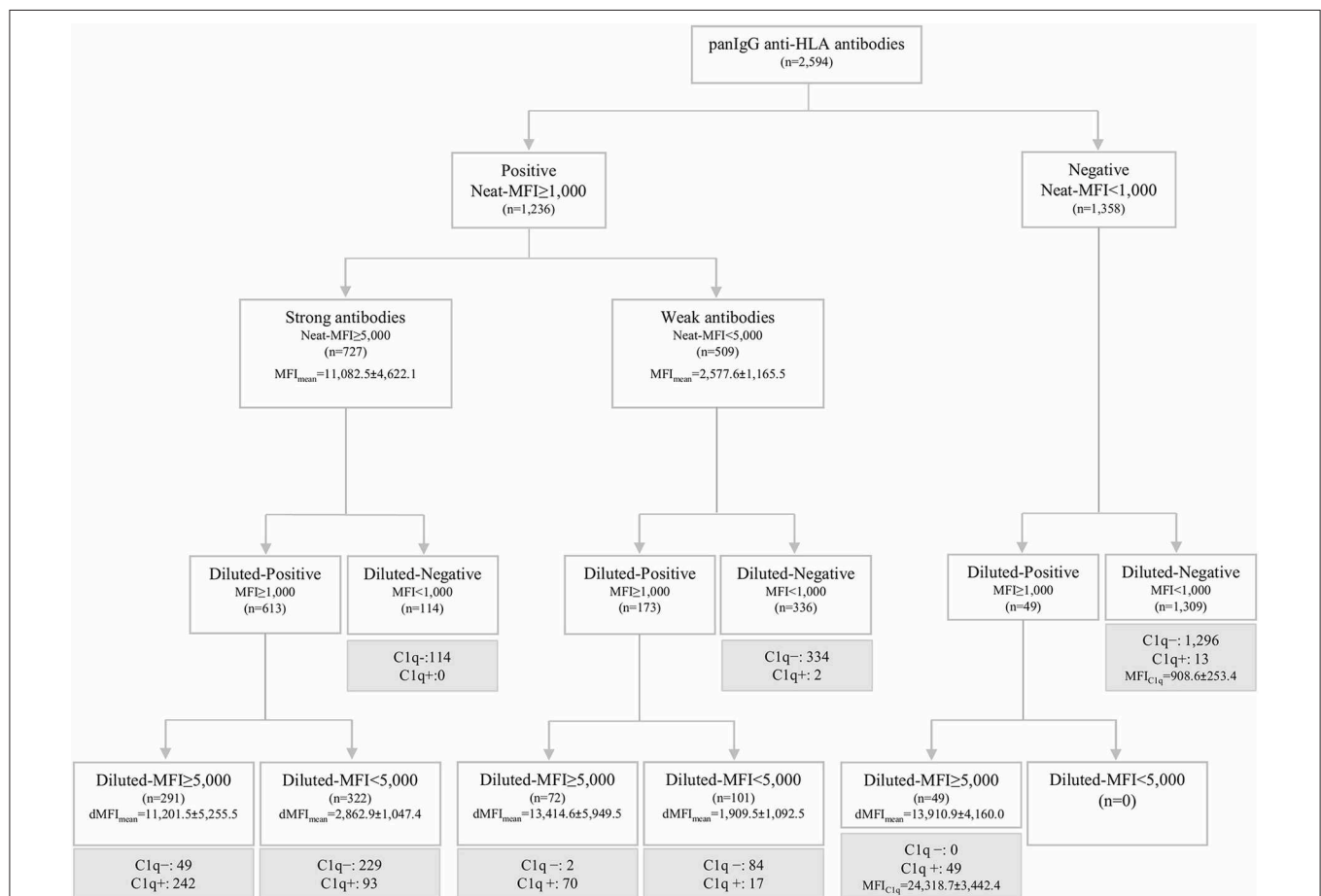


FIGURE 1 | Algorithm of classification of panIgG anti-HLA antibodies analyzed by the standardized single antigen bead (SAB)-panIgG assay in neat and 1:16 diluted-serum samples according to the different positivity and strength thresholds set. Diluted and neat-mean fluorescence intensity row values (MFI) of each group of antibodies are displayed. Within each re-classified group after the 1:16 serum dilution, anti-HLA antibodies were categorized into C1q+ or C1q- (in gray) according to the results obtained from SAB-C1q assay on neat-serum samples.

and not attributed to the presence of isolated IgM given the inactivating heat pre-treatment of the serum required to perform the SAB-C1q assay.

The mean MFI value in neat-serum SAB-panIgG assay of C1q-binding antibodies was significantly higher than that of non-C1q-binding antibodies ($9,204.6 \pm 6,302.3$ vs. $6,193.3 \pm 4,829.1$; $p < 0.001$). However, the correlation per bead between MFI values by SAB-panIgG and SAB-C1q assays was weak ($r_{\text{neat}} = 0.248$), as depicted in **Figure 2A**. Hence, 29.2% (138/473) of antibody-specificities capable of binding C1q exhibited weak neat-serum MFI values, whereas 53.9% (392/727) of strong antibodies were incapable of binding C1q.

As expected, after the dilution, the correlation between the C1q-binding ability and the strength of antibodies (**Figure 2B**) was enhanced ($r_{\text{dil}} = 0.817$). Among the 138 C1q-binding antibodies exhibiting low neat-serum MFI values in the standardized SAB-panIgG assay, 119 (86.2%) significantly increased their MFI value after the dilution ($1,777.1 \pm 1,583.8$ vs. $13,747.3 \pm 5,228.6$; $p < 0.001$). Likewise, the MFI value of the 392 non-C1q-binding strong antibodies significantly decreased ($10,149.1 \pm 4,082.3$ vs. $2,625.6 \pm 2,280.7$; $p < 0.001$).

Figure 2 also depicts the effect of heat (**Figure 2C**) and EDTA (**Figure 2D**) pre-treatments on the correlation between

the MFI value of panIgG anti-HLA antibodies and the ability to bind C1q. Both serum pre-treatments increased the correlation value with respect to that obtained with untreated neat-serum samples ($r_{\text{heat}} = 0.699$ and $r_{\text{EDTA}} = 0.656$, respectively) and seem to be particularly useful to prevent the prozone effect. The correlation per bead between MFI values obtained after heat and EDTA pre-treatments was noticeably high ($r = 0.952$; **Supplementary Figure 1**).

IgG1-4 Anti-HLA Antibodies

The modified SAB-subclass assay was performed to identify the IgG1-4 subclass distribution of the 1,285 antibody-specificities predefined by the standardized SAB-panIgG assay (**Table 1**). Our analyses revealed that 1,012 (78.8%) panIgG anti-HLA antibodies were comprised of at least one IgG1-4 subclass. Of these, IgG1 was by far the most frequent, being present in 95.3% of anti-HLA antibody-specificities, followed by IgG2 (54.7%), IgG3 (13.8%), and IgG4 (13.0%). No subclass was identified in 273 (21.2%) panIgG antibodies considered as positive, which predictably exhibited rather low panIgG MFI values ($2,774.7 \pm 2,457.1$).

Regarding the IgG subclass patterns, 419 (41.4%) panIgG positive antibody-specificities were comprised of isolated IgG1-4 subclasses, whereas the other 593 (58.6%) were comprised of

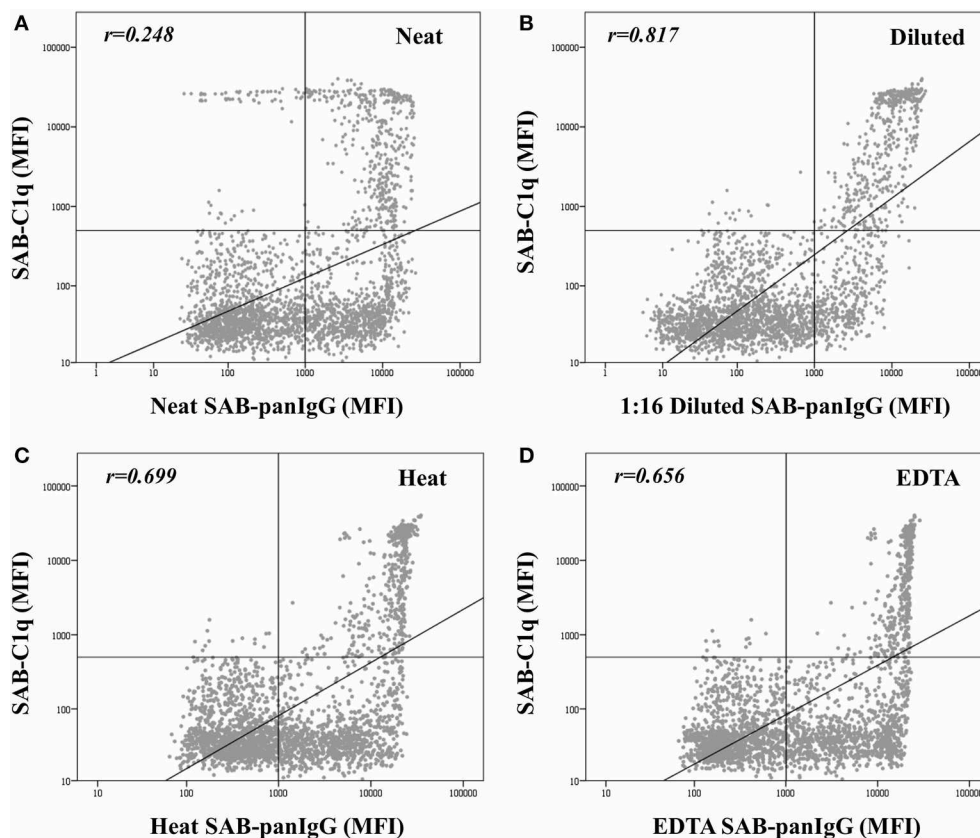


FIGURE 2 | Correlation between mean fluorescence intensity (MFI) row values of the 2,594 analyzed beads obtained by the standardized single antigen bead (SAB)-panIgG assay in neat-serum samples (**A**), 1:16 diluted-serum samples (**B**), heat pre-treated samples (**C**), and EDTA pre-treated samples (**D**) and MFI row values obtained by SAB-C1q assay. MFI values were graphed in a log-scatter plot. Correlation was assessed using Pearson's correlation.

TABLE 1 | IgG1-4 subclasses comprising panIgG anti-HLA antibodies analyzed according to SAB-subclass assay performed on neat-serum samples.

	Positive panIgG anti-HLA antibodies (<i>n</i> = 1,285)
None subclass detected, <i>n</i> (%)	273 (21.2)
Any subclass detected, <i>n</i> (%)^a	1,012 (78.8)
IgG1, <i>n</i> (%)	964 (95.3)
IgG2, <i>n</i> (%)	554 (54.7)
IgG3, <i>n</i> (%)	140 (13.8)
IgG4, <i>n</i> (%)	132 (13.0)
IgG1-4 patterns^a	
Isolated subclass, <i>n</i> (%)	419 (41.4)
Isolated IgG1, <i>n</i> (%)	373 (36.9)
Isolated IgG2, <i>n</i> (%)	5 (0.5)
Isolated IgG3, <i>n</i> (%)	36 (3.6)
Isolated IgG4, <i>n</i> (%)	5 (0.5)
Mixture of subclasses, <i>n</i> (%)	593 (58.6)
IgG1+IgG2, <i>n</i> (%)	376 (37.2)
IgG1+IgG3, <i>n</i> (%)	22 (2.2)
IgG1+IgG4, <i>n</i> (%)	21 (2.1)
IgG2+IgG3, <i>n</i> (%)	1 (0.1)
IgG2+IgG4, <i>n</i> (%)	1 (0.1)
IgG3+IgG4, <i>n</i> (%)	0 (0)
IgG1+IgG2+IgG3, <i>n</i> (%)	67 (6.6)
IgG1+IgG3+IgG4, <i>n</i> (%)	1 (0.1)
IgG2+IgG3+IgG4, <i>n</i> (%)	0 (0)
IgG1+IgG2+IgG4, <i>n</i> (%)	91 (9.0)
IgG1+IgG2+IgG3+IgG4, <i>n</i> (%)	13 (1.3)

^aPercentage of antibodies calculated considering only those with at least one detectable subclass.

a mixture of them. IgG1 + IgG2 was the most common pattern found, which comprised 37.2% of antibody-specificities, followed by isolated IgG1 (36.9%). Specificities comprised of a mixture of the four IgG subclasses (IgG1 + IgG2 + IgG3 + IgG4) or of isolated weak/non-C1q-binding subclasses (IgG2 and/or IgG4) were uncommon (1.3 and 1.1%, respectively). All subclass patterns are also shown in Table 1.

IgG Subclass Profile, Strength, and C1q-Reactivity of Anti-HLA Antibodies

Finally, we thoroughly studied the relationship between the pattern of IgG subclasses, the C1q-binding ability and the strength of panIgG anti-HLA antibodies. One of our main findings was that the presence of strong complement-binding subclasses (IgG1 and/or IgG3) was particularly high, comprising 1,001 (98.9%) of 1,012 positive panIgG anti-HLA antibody-specificities with at least one detectable subclass (Table 2). However, only 470 of them (46.9%) were capable of binding C1q, evincing that being potentially able to bind complement does not involve that an antibody-specificity was really detected as C1q-positive.

Notwithstanding the significant differences in the proportion of IgG1-4 subclasses according to the C1q-binding ability of

anti-HLA antibodies ($p < 0.001$), the presence of IgG1 and/or IgG3, the most relevant strong complement-binding subclasses, was noticeably high in both groups of antibodies. Indeed, no differences regarding the presence of IgG1 and/or IgG3 between the 473 C1q-binding and the 539 non-C1q-binding antibodies were found (99.4 vs. 98.5%; $p = 0.193$). Unexpectedly, whereas IgG2 and/or IgG4 were present in the 78.9% of C1q-binding antibodies, they were only present in the 38.6% of non-C1q-binding antibodies ($p < 0.001$). The presence of a mixture of IgG1-4 subclasses was more common in C1q-binding than in non-C1q-binding antibody-specificities (79.5 vs. 40.3%; $p < 0.001$). In addition, the 1:16 diluted-MFI value of antibodies comprised of a mixture of IgG1-4 subclasses was significantly higher than that of antibodies comprised of isolated subclasses ($8,394.5 \pm 6,520.4$ vs. $2,527.2 \pm 3,107.2$; $p < 0.001$). Finally, we found 3/473 (0.6%) positive antibody-specificities with the ability to bind C1q only comprised of isolated IgG2, which exhibited high MFI values in the diluted-sera analysis ($22,705.02 \pm 9,257.3$).

Beyond the profile of IgG subclasses, we explored the relationship between the IgG subclass strength, measured as the MFI value, and the C1q-binding ability. Regarding this, Figure 3 shows the correlation per bead between MFI row values of each IgG1-4 subclass in neat and 1:16 diluted serum-samples and MFI row values of panIgG anti-HLA antibodies in SAB-C1q assay. A strong correlation was found between IgG1 and the C1q-binding ability of antibodies after the dilution ($r_{\text{IgG1dil}} = 0.796$), revealing the close relationship between the presence of strong IgG1 comprising an antibody-specificity and its ability to bind C1q (Figure 3E). Conversely, this association was not found with regard to IgG3, probably due to its low prevalence (13.8%). Furthermore, Figure 3F shows that the correlation between the strength of IgG2 after the sample dilution and the C1q-binding ability of anti-HLA antibody-specificities was of $r_{\text{IgG2dil}} = 0.758$. This unexpectedly strong correlation could be explained by the fact that IgG2 was mainly found in combination with IgG1 (Table 2). Moreover, the correlation between the MFI value of IgG1 and the MFI value of IgG2 in 1:16 diluted-serum samples was strong ($r_{\text{IgG1-IgG2}} = 0.817$; Figure 4).

DISCUSSION

In this study, we aimed to elucidate the relationship between the properties of anti-HLA antibodies detected by the different solid-phase assays available and clarify those reactions which have not yet been outlined. Thus far, the data obtained from solid-phase to characterize the pathogenic potential of circulating anti-HLA antibodies has been considered too complex and has led to potential confusion about how to make clinical decisions (3). Furthermore, although the increased sensitivity of detection assays has improved transplantation success, waiting times of sensitized patients have also risen because of the expansion of the number of their unacceptable mismatches (37).

Among the isotypes of immunoglobulins, IgG is considered the main effector of humoral rejection through the activation of the complement pathway (38). Nevertheless, the four IgG

TABLE 2 | IgG subclass profile of C1q-binding and non-C1q-binding anti-HLA antibodies.

	C1q- (<i>n</i> = 539) ^a	C1q+ (<i>n</i> = 473) ^a	<i>p</i>
IgG1-4 subclass profile			<0.001
Isolated IgG subclasses, <i>n</i> (%)	322 (59.7)	97 (20.5)	<0.001
Isolated IgG1, <i>n</i> (%)	283 (52.5)	90 (19.0)	
Isolated IgG2, <i>n</i> (%)	2 (0.4)	3 (0.6)	
Isolated IgG3, <i>n</i> (%)	32 (5.9)	4 (0.8)	
Isolated IgG4, <i>n</i> (%)	5 (0.9)	0	
Mixture of IgG subclasses, <i>n</i> (%)	217 (40.3)	376 (79.5)	<0.001
IgG1+IgG2, <i>n</i> (%)	129 (23.9)	247 (52.2)	
IgG1+IgG3, <i>n</i> (%)	16 (3.0)	6 (1.3)	
IgG1+IgG4, <i>n</i> (%)	16 (3.0)	5 (1.1)	
IgG2+IgG3, <i>n</i> (%)	1 (0.2)	0	
IgG2+IgG4, <i>n</i> (%)	1 (0.2)	0	
IgG3+IgG4, <i>n</i> (%)	0	0	
IgG1+IgG2+IgG3, <i>n</i> (%)	31 (5.8)	36 (7.6)	
IgG1+IgG2+IgG4, <i>n</i> (%)	22 (4.1)	69 (14.6)	
IgG1+IgG3+IgG4, <i>n</i> (%)	1 (0.2)	0	
IgG2+IgG3+IgG4, <i>n</i> (%)	0	0	
IgG1+IgG2+IgG3+IgG4, <i>n</i> (%)	0	13 (2.7)	
Presence of IgG1 and/or IgG3, <i>n</i> (%)	531 (98.5)	470 (99.4)	0.193
Presence of IgG2 and/or IgG4, <i>n</i> (%)	208 (38.6)	373 (78.9)	<0.001

^aOnly those antibody-specificities with at least one detectable IgG1-4 subclass were considered. Therefore, 273 non-C1q-binding anti-HLA antibodies with undetectable IgG subclasses were excluded from the analysis.

subclasses exhibit different properties (31, 32, 39). Considering these issues, Chen et al. (40) introduced SAB-C1q as a modified assay to distinguish those hypothetically more dangerous complement-binding subclasses (IgG1/IgG3) from those which a priori suppose an acceptable short-term risk for transplantation (IgG2/IgG4). Several reports have been published to date predicting the risk of allograft failure according to the C1q-binding ability of anti-HLA antibodies before and after transplantation (24–27). However, some authors suggest that determining the complement-binding ability to predict the allograft loss in the clinical practice is unsuccessful (41, 42), and many others question whether the SAB-C1q assay really discriminates among IgG subclasses, given the close relationship observed between the real-strength of antibodies and their ability to bind C1q (21, 22, 28, 29).

Certainly, we found that the relationship between the neat-strength and the C1q-binding ability was weak ($r_{\text{neat}} = 0.248$). Indeed, 29.2% (138/473) of antibodies, usually considered as low-immunological risk because exhibiting MFI values lower than 5,000, were able to bind C1q. Moreover, 10.4% (49/473) were detected as negative. Conversely, 53.9% of antibodies with strong-MFI values ($>5,000$), which are habitually forbidden in the clinical practice, were not able to bind C1q. The dilution of the serum-samples allowed us to unmask the real-strength of a considerable proportion of antibodies. Hence, 121 antibodies changed their status from low-risk specificities with negative or weak-MFI values to high-risk specificities with strong-MFI values. Additionally, the 1:16 dilution cleared the presence of 114 specificities exhibiting neat-MFI values $\geq 5,000$. Therefore,

the dilution provided a better assessment of the strength of antibodies, which should be taken into consideration in those pre-transplant studies in which the MFI value is the unique criterion to ascertain the immunological risk and, although the correlation with the C1q-binding status was still not totally perfect ($r_{\text{dil}} = 0.817$), the data support the idea that the ability to bind C1q is tightly linked to the antibody real-strength. As depicted in **Figure 2**, the association between the C1q-binding ability of antibodies and their strength when pre-treating with heat and EDTA, even higher with respect to neat-serum ($r_{\text{heat}} = 0.699$ and $r_{\text{EDTA}} = 0.656$, respectively), was not as strong as with diluted-serum, which could be explained by a lower ability of heat and EDTA to effectively discriminate between different levels of antibodies, beyond the usefulness of both methods preventing the prozone effect.

Regardless of the strength, the IgG subclass composition should determine the potential complement-binding ability of antibodies. Considering the strong complement-binding subclasses (IgG1/IgG3), we identified that these were present in 98.9% of specificities detected, being only 470 of them (46.9%) capable of binding C1q. Indeed, 98.5% of non-C1q-binding antibodies with at least one detectable subclass had IgG1 and/or IgG3 in their profile. Our results were similar to those previously reported by Schaub et al. (28), who found that a negative C1q-reaction did not necessarily mean that the considered antibody was uniquely comprised of subclasses without the ability to activate the complement pathway. Unexpectedly, we found that IgG2 and/or IgG4 more frequently comprised C1q-binding than non-C1q-binding antibodies (78.9 vs. 38.6%; $p <$

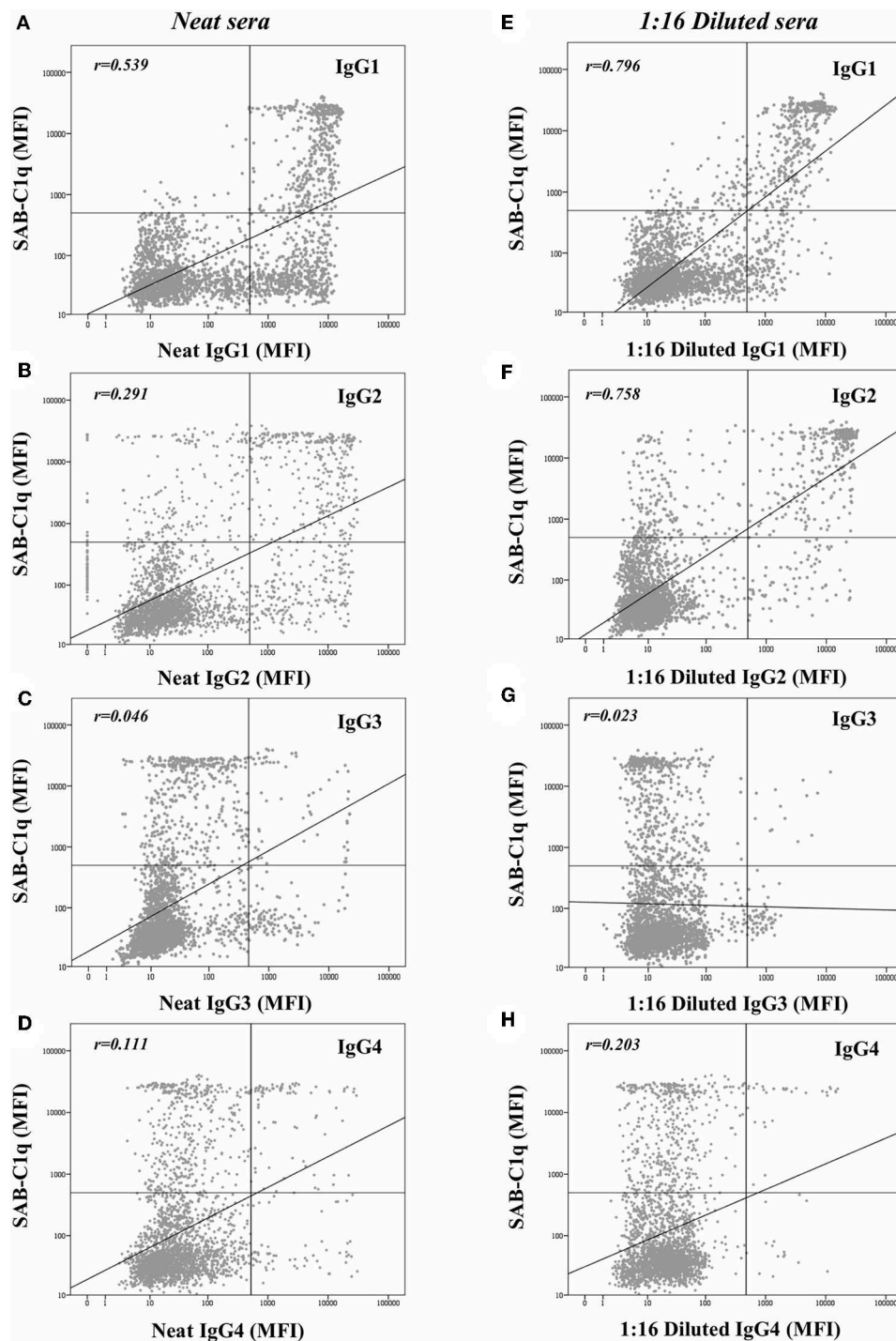
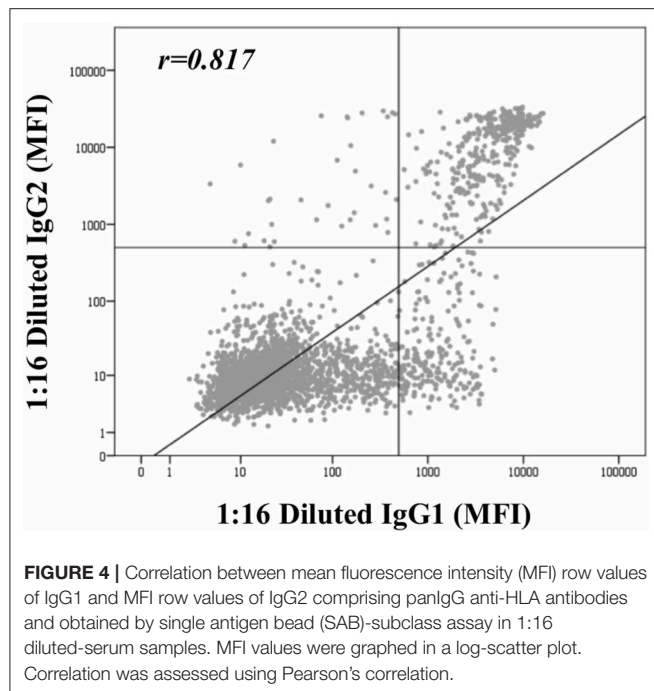


FIGURE 3 | Log-scatter plot for the correlation between the mean fluorescence intensity (MFI) row value of panIgG anti-HLA antibodies in single antigen bead (SAB)-C1q assay and the MFI row value of IgG1 (A), IgG2 (B), IgG3 (C), and IgG4 (D) in SAB-subclass assay of neat-serum samples and IgG1 (E), IgG2 (F), IgG3 (G), and IgG4 (H) in SAB-subclass assay of 1:16 diluted-serum samples. Correlation was assessed using Pearson's correlation.

0.001). Likewise, the presence of a mixture of IgG1-4 subclasses was more common in C1q-binding antibody-specificities (79.5 vs. 40.3%; $p < 0.001$). Antibodies comprised of a mixture of subclasses could be a sign of the more advanced immune

response, stimulated by a longer and more intense antigen exposure (39). As others before us (28, 33, 36, 43, 44), we found that the presence of isolated IgG2 and/or IgG4 subclasses was particularly low (1.1%). We also confirmed previous studies (33,



36) showing that positive panIgG antibodies without detectable IgG subclasses exhibited low MFI values, which might reflect the different sensitivity of the detection tests used.

Given that all these findings suggest that the complement-binding ability may not be merely explained by differences in the subclass composition, since both C1q-binding and non-C1q-binding antibodies were comprised of similar proportions of complement-binding subclasses (IgG1/IgG3), we decided to explore the strength of them (**Figure 3**). Our results demonstrate that the strength of IgG1, measured as the MFI value, exhibited the strongest correlation with the C1q-binding ability of panIgG antibodies, particularly after diluting the samples ($r_{\text{IgG1}} = 0.539$ and $r_{\text{IgG1dil}} = 0.796$). Despite the widely proven strong complement-binding ability of IgG3, its presence is unlikely to explain the complement-binding ability of a particular specificity due to its low prevalence (13.8%) and the low MFI value exhibited (**Figure 3C**). The evolution of IgG subclass switching follows the following sequence: IgG3 → IgG1 → IgG2 → IgG4 (39). We hypothesize that IgG3 is badly detectable because it is the first in order of class-switching and it has the shortest half-life in circulation (31).

It is widely described that triggering complement depends on the antigen density/epitopes and the concentration of antibodies (30). Wang et al. (45) elegantly revealed that the formation of C1q:IgG complexes predominantly assembles at a stoichiometry of 1:6. In the context of Luminex-beads, the C1q-binding must mainly depend on the density of antibodies bound to their target antigens on the bead surface, which in turn depends on their strength (amount, affinity, and avidity). Hence, high titers of strong C1q-binding subclasses, particularly IgG1, alone or combined with other IgG subclasses, mainly IgG2, may compose the hexamer formation to efficiently recruit the C1q

protein. These results are in line with those recently reported by Ponsirenas et al. (46), who, although without revealing the real-strength of IgG subclasses diluting serum-samples, found that C1q-binding was detected in high MFI antibodies comprised of IgG1 or multiple IgG subclasses. Only under certain conditions such as increased concentration of immunoglobulin, even IgG2 could effectively activate the complement (30). The C1q-positivity observed in the three beads comprised uniquely of IgG2 might be due to a considerable high strength of this subclass. However, these are extremely uncommon cases (0.6%). Beyond the antibody load, we found that the correlation of the IgG1 strength with the C1q-binding status was significantly different between HLA-loci ($p < 0.001$). In this regard, the best correlation was obtained for HLA-DQ antigen beads, as depicted in **Supplementary Figure 2**. These findings reinforce the premise that the C1q-binding ability of anti-HLA antibodies, defined by SAB-C1q assay, must also be affected by a different relative density of HLA antigens coating the bead surface.

The main limitation of our study was that we could not performed serial dilutions analyses to determine the titer of each antibody-specificity. The literature describes that the majority of antibody-specificities reaches the highest MFI value at a 1:16 dilution (22, 29), but some may be even more affected by the prozone effect. Furthermore, we did not study the correlation between the properties of antibodies and the allograft outcome. However, it was not our main purpose but to try to explain those until now incomprehensible reactions. Finally, although the cohort size was low and the number of antibodies analyzed was limited, the data obtained were enough to improve our knowledge about the relationship between the different properties of antibodies.

In conclusion, almost all antibodies are comprised by strongly complement-binding subclasses, mainly IgG1, regardless of their C1q-binding status. In contrast, the presence of IgG2/IgG4, weak and non-C1q-binding subclasses, respectively, is more commonly found in C1q-binding antibodies. The real strength of IgG1, alone or, more usually combined with IgG2, and not the IgG1-4 profile itself, comprising an antibody-specificity is which best correlates with its ability to bind C1q. C1q-binding antibodies exhibiting true low MFI value are not found, suggesting that this is an extremely uncommon event. Thus far, different antibody properties characterized by the available detection assays have been evaluated in an attempt to improve the immunological risk assessment under the presumption that they are unrelated. Herein, we demonstrate a close relationship between the circulating antibody strength, which could be better estimated by the measurement of the MFI value obtained after the serum dilution, the presence of a mixture of IgG subclasses, beyond the quasy omnipresent IgG1, and the C1q-binding ability.

DATA AVAILABILITY

All datasets generated for this study are included in the manuscript and/or the **Supplementary Files**.

ETHICS STATEMENT

This study was approved by the Ethics Committee of the Reina Sofia University Hospital (ref. 2465). All participants in the study provided written informed consent in accordance with the Declaration of Helsinki.

AUTHOR CONTRIBUTIONS

AN and RS designed the study. AN and JM conducted the laboratory experiments and wrote the draft. M-LA and AR-B provided and collected the clinical data. AN, JM,

and CA interpreted the results. AN, IG, and AJ performed the statistical analyses. AR-B, CA, and RS reviewed the final version and made significant conceptual contributions to the manuscript. All the authors provided intellectual content, contributed to the article writing, and approved the final version.

SUPPLEMENTARY MATERIAL

The Supplementary Material for this article can be found online at: <https://www.frontiersin.org/articles/10.3389/fimmu.2019.01712/full#supplementary-material>

REFERENCES

- Tait BD. Detection of HLA antibodies in organ transplant recipients—triumphs and challenges of the solid phase bead assay. *Front Immunol.* (2016) 7:570. doi: 10.3389/fimmu.2016.00570
- Haarberg KM, Tambur AR. Detection of donor-specific antibodies in kidney transplantation. *Br Med Bull.* (2014) 110:23–34. doi: 10.1093/bmb/ldu005
- Schinstock CA, Gandhi MJ, Stegall MD. Interpreting anti-HLA antibody testing data: a practical guide for physicians. *Transplantation.* (2016) 100:1619–28. doi: 10.1097/TP.0000000000001203
- Bostock IC, Alberu J, Arvizu A, Hernandez-Mendez EA, De-Santiago A, Gonzalez-Tableros N, et al. Probability of deceased donor kidney transplantation based on % PRA. *Transpl Immunol.* (2013) 28:154–8. doi: 10.1016/j.trim.2013.05.002
- Amico P, Honger G, Steiger J, Schaub S. Utility of the virtual crossmatch in solid organ transplantation. *Curr Opin Organ Transplant.* (2009) 14:656–61. doi: 10.1097/MOT.0b013e328331c169
- Amico P, Hirt-Minkowski P, Honger G, Gurke L, Mihatsch MJ, Steiger J, et al. Risk stratification by the virtual crossmatch: a prospective study in 233 renal transplantations. *Transpl Int.* (2011) 24:560–9. doi: 10.1111/j.1432-2277.2011.01235.x
- Susal C, Ovens J, Mahmoud K, Dohler B, Scherer S, Ruhenstroth A, et al. No association of kidney graft loss with human leukocyte antigen antibodies detected exclusively by sensitive luminex single-antigen testing: a collaborative transplant study report. *Transplantation.* (2011) 91:883–7. doi: 10.1097/TP.0b013e3182100f77
- Orandi BJ, Garonzik-Wang JM, Massie AB, Zachary AA, Montgomery JR, Van Arendonk KJ, et al. Quantifying the risk of incompatible kidney transplantation: a multicenter study. *Am J Transplant.* (2014) 14:1573–80. doi: 10.1111/ajt.12786
- Sicard A, Amrouche L, Suberbielle C, Carmagnat M, Candon S, Thervet E, et al. Outcome of kidney transplantations performed with preformed donor-specific antibodies of unknown etiology. *Am J Transplant.* (2014) 14:193–201. doi: 10.1111/ajt.12512
- Gebel HM, Bray RA. HLA antibody detection with solid phase assays: great expectations or expectations too great? *Am J Transplant.* (2014) 14:1964–75. doi: 10.1111/ajt.12807
- Caro-Oleas JL, Gonzalez-Escribano MF, Gonzalez-Roncero FM, Acevedo-Calado MJ, Cabello-Chaves V, Gentil-Govantes MA, et al. Clinical relevance of HLA donor-specific antibodies detected by single antigen assay in kidney transplantation. *Nephrol Dial Transplant.* (2012) 27:1231–8. doi: 10.1093/ndt/gfr429
- Kannabhiran D, Lee J, Schwartz JE, Friedlander R, Aull M, Muthukumar T, et al. Characteristics of circulating donor human leukocyte antigen-specific immunoglobulin G antibodies predictive of acute antibody-mediated rejection and kidney allograft failure. *Transplantation.* (2015) 99:1156–64. doi: 10.1097/TP.0000000000000511
- Salvade I, Aubert V, Venetz JP, Golshayan D, Saouli AC, Matter M, et al. Clinically-relevant threshold of preformed donor-specific anti-HLA antibodies in kidney transplantation. *Hum Immunol.* (2016) 77:483–9. doi: 10.1016/j.humimm.2016.04.010
- Viglietti D, Lefaucheur C, Glotz D. Evidence for an important role of both complement-binding and noncomplement-binding donor-specific antibodies in renal transplantation. *Curr Opin Organ Transplant.* (2016) 21:433–40. doi: 10.1097/MOT.0000000000000324
- Marfo K, Ajaimy M, Colovai A, Kayler L, Greenstein S, Lubetzky M, et al. Pretransplant immunologic risk assessment of kidney transplant recipients with donor-specific anti-human leukocyte antigen antibodies. *Transplantation.* (2014) 98:1082–8. doi: 10.1097/TP.0000000000000191
- Susal C, Roelen DL, Fischer G, Campos EF, Gerbase-DeLima M, Honger G, et al. Algorithms for the determination of unacceptable HLA antigen mismatches in kidney transplant recipients. *Tissue Antigens.* (2013) 82:83–92. doi: 10.1111/tan.12137
- Susal C, Seidl C, Schonemann C, Heinemann FM, Kauke T, Gombos P, et al. Determination of unacceptable HLA antigen mismatches in kidney transplant recipients: recommendations of the German Society for Immunogenetics. *Tissue Antigens.* (2015) 86:317–23. doi: 10.1111/tan.12682
- Zeher D, Bach C, Preiss A, Staudner C, Utpatel K, Evert M, et al. Analysis of luminex-based algorithms to define unacceptable HLA antibodies in CDC-crossmatch negative kidney transplant recipients. *Transplantation.* (2018) 102:969–77. doi: 10.1097/TP.0000000000002129
- Mizutani K, Terasaki P, Hamdani E, Esquenazi V, Rosen A, Miller J, et al. The importance of anti-HLA-specific antibody strength in monitoring kidney transplant patients. *Am J Transplant.* (2007) 7:1027–31. doi: 10.1111/j.1600-6143.2006.01721.x
- Lefaucheur C, Loupy A, Hill GS, Andrade J, Nochy D, Antoine C, et al. Preexisting donor-specific HLA antibodies predict outcome in kidney transplantation. *J Am Soc Nephrol.* (2010) 21:1398–406. doi: 10.1681/ASN.2009101065
- Yell M, Muth BL, Kaufman DB, Djamali A, Ellis TM. C1q binding activity of de novo donor-specific HLA antibodies in renal transplant recipients with and without antibody-mediated rejection. *Transplantation.* (2015) 99:1151–5. doi: 10.1097/TP.0000000000000699
- Tambur AR, Herrera ND, Haarberg KM, Cusick MF, Gordon RA, Leventhal JR, et al. Assessing antibody strength: comparison of MFI, C1q, and titer information. *Am J Transplant.* (2015) 15:2421–30. doi: 10.1111/ajt.13295
- Stegall MD, Chedid MF, Cornell LD. The role of complement in antibody-mediated rejection in kidney transplantation. *Nat Rev Nephrol.* (2012) 8:670–8. doi: 10.1038/nrneph.2012.212
- Loupy A, Lefaucheur C, Vernerey D, Prugger C, Duong van Huyen JP, Mooney N, et al. Complement-binding anti-HLA antibodies and kidney-allograft survival. *N Engl J Med.* (2013) 369:1215–26. doi: 10.1056/NEJMoa1302506
- Calp-Inal S, Ajaimy M, Melamed ML, Savchik C, Masiakos P, Colovai A, et al. The prevalence and clinical significance of C1q-binding donor-specific anti-HLA antibodies early and late after kidney transplantation. *Kidney Int.* (2016) 89:209–16. doi: 10.1038/ki.2015.275
- Malheiro J, Tafalo S, Dias L, Martins S, Fonseca I, Beirao I, et al. Determining donor-specific antibody C1q-binding ability improves the prediction of antibody-mediated rejection in human leukocyte antigen-incompatible kidney transplantation. *Transpl Int.* (2017) 30:347–59. doi: 10.1111/tri.12873

27. Molina J, Navas A, Agüera ML, Rodelo-Haad C, Alonso C, Rodríguez-Benot A, et al. Impact of preformed donor-specific anti-human leukocyte antigen antibody C1q-binding ability on kidney allograft outcome. *Front Immunol.* (2017) 8:1310. doi: 10.3389/fimmu.2017.01310
28. Schaub S, Honger G, Koller MT, Liwski R, Amico P. Determinants of C1q binding in the single antigen bead assay. *Transplantation.* (2014) 98:387–93. doi: 10.1097/TP.0000000000000203
29. Zeevi A, Lunz J, Feingold B, Shullo M, Bermudez C, Teuteberg J, et al. Persistent strong anti-HLA antibody at high titer is complement binding and associated with increased risk of antibody-mediated rejection in heart transplant recipients. *J Heart Lung Transplant.* (2013) 32:98–105. doi: 10.1016/j.healun.2012.09.021
30. Thomas KA, Valenzuela NM, Reed EF. The perfect storm: HLA antibodies, complement, fcγ receptors, and endothelium in transplant rejection. *Trends Mol Med.* (2015) 21:319–29. doi: 10.1016/j.molmed.2015.02.004
31. Hickey MJ, Valenzuela NM, Reed EF. Alloantibody generation and effector function following sensitization to human leukocyte antigen. *Front Immunol.* (2016) 7:30. doi: 10.3389/fimmu.2016.00030
32. Valenzuela NM, Hickey MJ, Reed EF. Antibody subclass repertoire and graft outcome following solid organ transplantation. *Front Immunol.* (2016) 7:433. doi: 10.3389/fimmu.2016.00433
33. Lefaucheur C, Viglietti D, Bentlejewski C, Duong van Huyen JP, Vernerey D, Aubert O, et al. IgG donor-specific anti-human HLA antibody subclasses and kidney allograft antibody-mediated injury. *J Am Soc Nephrol.* (2016) 27:293–304. doi: 10.1681/ASN.2014111120
34. Hamdani G, Goebel JW, Brailey P, Portwood EA, Hooper DK, Girnita AL. IGG3 anti-HLA donor-specific antibodies and graft function in pediatric kidney transplant recipients. *Pediatr Transplant.* (2018) 22:e13219. doi: 10.1111/ptr.13219
35. Schnaidt M, Weinstock C, Jurisic M, Schmid-Horch B, Ender A, Wernet D. HLA antibody specification using single-antigen beads—a technical solution for the prozone effect. *Transplantation.* (2011) 92:510–5. doi: 10.1097/TP.0b013e31822872dd
36. Honger G, Hopfer H, Arnold ML, Spriewald BM, Schaub S, Amico P. Pretransplant IgG subclasses of donor-specific human leukocyte antigen antibodies and development of antibody-mediated rejection. *Transplantation.* (2011) 92:41–7. doi: 10.1097/TP.0b013e31821cd0f0
37. Cecka JM. Calculated PRA (CPRA): the new measure of sensitization for transplant candidates. *Am J Transplant.* (2010) 10:26–9. doi: 10.1111/j.1600-6143.2009.02927.x
38. Khovanova N, Daga S, Shaikhina T, Krishnan N, Jones J, Zehnder D, et al. Subclass analysis of donor HLA-specific IgG in antibody-incompatible renal transplantation reveals a significant association of IgG4 with rejection and graft failure. *Transpl Int.* (2015) 28:1405–15. doi: 10.1111/tri.12648
39. Valenzuela NM, Schaub S. The biology of IgG subclasses and their clinical relevance to transplantation. *Transplantation.* (2018) 102:S7–13. doi: 10.1097/TP.0000000000001816
40. Chen G, Sequeira F, Tyan DB. Novel C1q assay reveals a clinically relevant subset of human leukocyte antigen antibodies independent of immunoglobulin G strength on single antigen beads. *Hum Immunol.* (2011) 72:849–58. doi: 10.1016/j.humimm.2011.07.001
41. Courant M, Visentin J, Linares G, Dubois V, Lepreux S, Guidicelli G, et al. The disappointing contribution of anti-human leukocyte antigen donor-specific antibodies characteristics for predicting allograft loss. *Nephrol Dial Transplant.* (2018) 33:1853–63. doi: 10.1093/ndt/gfy088
42. Crespo M, Torio A, Mas V, Redondo D, Perez-Saez MJ, Mir M, et al. Clinical relevance of pretransplant anti-HLA donor-specific antibodies: does C1q-fixation matter? *Transpl Immunol.* (2013) 29:28–33. doi: 10.1016/j.trim.2013.07.002
43. Lowe D, Higgins R, Zehnder D, Briggs DC. Significant IgG subclass heterogeneity in HLA-specific antibodies: implications for pathogenicity, prognosis, and the rejection response. *Hum Immunol.* (2013) 74:666–72. doi: 10.1016/j.humimm.2013.01.008
44. Arnold ML, Ntokou IS, Doxiadis II, Spriewald BM, Boletis JN, Iniotaki AG. Donor-specific HLA antibodies: evaluating the risk for graft loss in renal transplant recipients with isotype switch from complement fixing IgG1/IgG3 to noncomplement fixing IgG2/IgG4 anti-HLA alloantibodies. *Transpl Int.* (2014) 27:253–61. doi: 10.1111/tri.12206
45. Wang G, de Jong RN, van den Bremer ET, Beurskens FJ, Labrijn AF, Ugurlar D, et al. Molecular basis of assembly and activation of complement component C1 in complex with immunoglobulin G1 and antigen. *Mol Cell.* (2016) 63:135–45. doi: 10.1016/j.molcel.2016.05.016
46. Ponsirenas RVG, Cazarote HB, Araujo SA, Wanderley DC, Shimakura S, Valdameri JS, et al. Anti-HLA donor-specific IgG subclasses and C1q-binding evolution in posttransplant monitoring. *Transplant Direct.* (2018) 4:e385. doi: 10.1097/TXD.0000000000000823

Conflict of Interest Statement: The authors declare that the research was conducted in the absence of any commercial or financial relationships that could be construed as a potential conflict of interest.

Copyright © 2019 Navas, Molina, Agüera, Guler, Jurado, Rodríguez-Benot, Alonso and Solana. This is an open-access article distributed under the terms of the Creative Commons Attribution License (CC BY). The use, distribution or reproduction in other forums is permitted, provided the original author(s) and the copyright owner(s) are credited and that the original publication in this journal is cited, in accordance with accepted academic practice. No use, distribution or reproduction is permitted which does not comply with these terms.



Low pH Exposure During Immunoglobulin G Purification Methods Results in Aggregates That Avidly Bind Fcγ Receptors: Implications for Measuring Fc Dependent Antibody Functions

Ester Lopez¹, Nichollas E. Scott¹, Bruce D. Wines^{2,3,4}, P. Mark Hogarth^{2,3,4}, Adam K. Wheatley¹, Stephen J. Kent^{1,5,6} and Amy W. Chung^{1*}

OPEN ACCESS

Edited by:

Harry W. Schroeder,
University of Alabama at Birmingham,
United States

Reviewed by:

Masaki Hikida,
Akita University, Japan
Neil S. Greenspan,
Case Western Reserve University,
United States

*Correspondence:

Amy W. Chung
awchung@unimelb.edu.au

Specialty section:

This article was submitted to
B Cell Biology,
a section of the journal
Frontiers in Immunology

Received: 24 July 2019

Accepted: 26 September 2019

Published: 11 October 2019

Citation:

Lopez E, Scott NE, Wines BD, Hogarth PM, Wheatley AK, Kent SJ and Chung AW (2019) Low pH Exposure During Immunoglobulin G Purification Methods Results in Aggregates That Avidly Bind Fcγ Receptors: Implications for Measuring Fc Dependent Antibody Functions. *Front. Immunol.* 10:2415. doi: 10.3389/fimmu.2019.02415

¹ Department of Microbiology and Immunology, Peter Doherty Institute for Infection and Immunity, University of Melbourne, Parkville, VIC, Australia, ² Immune Therapies Group, Burnet Institute, Melbourne, VIC, Australia, ³ Department of Immunology and Pathology, Monash University, Melbourne, VIC, Australia, ⁴ Department of Clinical Pathology, The University of Melbourne, Melbourne, VIC, Australia, ⁵ Infectious Diseases Department, Melbourne Sexual Health Centre, Central Clinical School, Alfred Health, Monash University, Melbourne, VIC, Australia, ⁶ ARC Centre of Excellence in Convergent Bio-Nano Science and Technology, University of Melbourne, Parkville, VIC, Australia

Evaluating the biophysical and functional nature of IgG is key to defining correlates of protection in infectious disease, and autoimmunity research cohorts, as well as vaccine efficacy trials. These studies often require small quantities of IgG to be purified from plasma for downstream analysis with high throughput immunoaffinity formats which elute IgG at low-pH, such as Protein G and Protein A. Herein we sought to compare Protein G purification of IgG with an immunoaffinity method which elutes at physiological pH (Melon Gel). Critical factors impacting Fc functionality with the potential to significantly influence FcγR binding, such as IgG subclass distribution, N-glycosylation, aggregation, and IgG conformational changes were investigated and compared. We observed that transient exposure of IgG to the low-pH elution buffer, used during the Protein G purification process, artificially enhanced recognition of Fcγ Receptors (FcγRs) as demonstrated by Surface Plasmon Resonance (SPR), FcγR dimer ELISA, and a functional cell-based assay. Furthermore, low-pH exposed IgG caused conformational changes resulting in increased aggregation and hydrophobicity; factors likely to contribute to the observed enhanced interaction with FcγRs. These results highlight that methods employed to purify IgG can significantly alter FcγR-binding behavior and biological activity and suggest that the IgG purification approach selected may be a previously overlooked factor contributing to the poor reproducibility across current assays employed to evaluate Fc-mediated antibody effector functions.

Keywords: Fcγ receptors, IgG purification, protein G, melon gel, antibody, antibody dependent cellular phagocytosis (ADCP), Fc functions

INTRODUCTION

Antibodies are commonly purified prior to analysis, and high throughput easy to use immunoaffinity formats for small-scale purification of IgG have become increasingly popular. This is especially the case where purification of small quantities of IgG from plasma are required for various assays and downstream analysis. Purified IgG is often studied in large cohorts and vaccine trials, where the efficiency of antibody-induced effector functions are evaluated and compared.

Diverse approaches exist for the purification of IgG from plasma, other biological fluids, and culture medium. These include ammonium sulfate precipitation, ion exchange chromatography, and affinity purification on immobilized Protein A and Protein G. A relatively recent, novel approach however is the use of Melon Gel, a proprietary resin chemistry and optimized buffer system (Thermo Fisher Scientific, USA). In contrast with positive selection methods such as Protein G and Protein A, Melon Gel binds all non- γ -globulin and plasma proteins while allowing purified IgG to be collected in the flow-through fraction. This method presents several potential advantages, in particular the absence of harsh low pH elution conditions commonly used during IgG immunoaffinity purification procedures such as Protein G. In contrast, Protein G affinity matrices for purification of IgG consist of a bacterial protein which primarily binds IgG at the $\text{C}\gamma 2/\text{C}\gamma 3$ interface (1), as well as to a low-affinity site in the $\text{C}\gamma 1$ domain (2). Several studies have highlighted potentially undesirable consequences of exposing IgG to low pH, and it has been suggested that Protein A and Protein G immunoaffinity methods which elute in the range of pH 2–3 should be reconsidered (3–7). This concern has arisen from findings that exposure to low pH results in partial denaturation, dramatic alteration of antigen-binding behavior, and conformational changes leading to aggregation (6–9). This concern is further highlighted by high-resolution NMR demonstrating that the second constant domain ($\text{C}\gamma 2$) of IgG collapses entirely at pH 3.1 (8) while remaining intact at pH 3.5 and above. What effect these widely used purification approaches have on functional activity is however, poorly understood. A small number of studies on the antigen binding region of IgG have demonstrated that low-pH IgG purification approaches dramatically alter F(ab')_2 antigen recognition (5, 10, 11). Whether Fc dependent functions are also altered following IgG purification and low-pH elution, to our knowledge has not been investigated.

Several important functions of the immune system are associated with the Fc portion of IgG, such as binding to complement and Fc γ receptors (Fc γ Rs). Fc γ Rs play a central role in the immune system by connecting humoral and cell-based innate immunity, and the binding kinetics of IgG-Fc γ R interactions are key indicators of antibody functional performance. Crystal structures of the Fc fragment have proposed that Fc γ R bind asymmetrically to the top region of the $\text{C}\gamma 2$ domain, and the adjacent lower hinge of IgG (12, 13). The $\text{C}\gamma 2/\text{C}\gamma 3$ interface of the IgG Fc binds both Protein G and Protein A. Considering the aforementioned effects of low pH

immunoaffinity methods, particularly the stability of the $\text{C}\gamma 2$ domain critical in Fc γ Rs binding, it was hypothesized that exposure to low pH during Protein G purification might result in altered Fc γ R interactions, similar to the altered antigen recognition by the F(ab')_2 region observed in other studies (5, 10, 11). Herein we compare the traditional Protein G immunoaffinity method of purifying IgG from plasma, with a method which elutes at physiological pH (Melon Gel). For both methods Fc γ R interactions were examined, and well-recognized factors impacting Fc tail functionality with the potential to significantly influence IgG binding; such as IgG subclass distribution, N-glycosylation, and aggregation, were compared.

MATERIALS AND METHODS

Plasma Samples

Subsets of plasma samples used for this study were obtained from a previously published influenza vaccine cohort (14), consisting of 30 healthy HIV uninfected subjects, and 27 HIV positive subjects recently vaccinated against influenza. Ethics approval was provided by the Alfred Health and University of Melbourne Human Ethics Committees (IDs 432/14 and 1443420). All samples were collected at mean 28 days post vaccination with an intramuscular injection of trivalent influenza vaccine (Fluvax; bio-CSL, Australia) containing 15 μg of hemagglutinin (HA) from A/California/7/2009 (H1N1), A/South Australia/55/2014 (H3N2), and B/Phuket/3073/2013. A/South Australia/55/2014 is an A/Switzerland/9715293/2013 (H3N2)-like virus selected for inclusion in trivalent influenza vaccines for the Southern Hemisphere, with only a single K207R mutation (H3 numbering) differentiating these two antigenically similar strains. Thus A/Switzerland/9715293/2013 (H3N2) was used as a substitute HA antigen within this study.

IgG Purification

IgG was purified from plasma samples from healthy individuals, or from HIV positive individuals (14), via Protein G chromatography (Protein G HP Multitrap, GE Healthcare, Sweden) and Melon Gel chromatography (Melon Gel IgG Purification Kit, Thermo Fisher Scientific, USA). For Protein G sepharose purification, plasma was diluted 2-fold with binding buffer (20 mM sodium phosphate, pH 7.0) and incubated for 1 h. IgG was eluted with 0.1 M glycine-HCl (pH 2.7), into neutralizing buffer (1 M Tris-HCl, pH 9.0). IgG was purified from plasma samples by Melon Gel purification according to the manufacturer's protocol. Briefly, serum samples were diluted 1:10 and the diluted serum was added to a minispin column containing the Melon Gel resin. After 5 min incubation, the purified IgG was collected in the flow through following the manufacturer's instructions. Eluted IgG (Protein G) and flow through (Melon Gel) were concentrated, and buffer exchanged into PBS using a 30 kDa Amicon Ultra centrifugal filter (Millipore, USA). IgG concentrations were quantitated using the Human-IgG ELISA kit (Mabtech, Sweden).

Fcγ Receptor-Binding Kinetics of Protein G and Melon Gel Purified IgG

The kinetic constants of the interaction of Melon Gel and Protein G purified IgG and the low and high affinity variants of FcγRIIIa or FcγRIIa were determined by surface plasmon resonance BIACORE 3000; (GE Healthcare, Sweden). Biotinylated FcγRs >95% pure based on SDS-PAGE (SinoBiological Inc, China) were immobilized on a streptavidin sensor chip (GE Healthcare, Sweden) at a flow rate of 10 μl/min, with flow cell one left blank as a reference surface. Each FcγR was immobilized at the following ligand densities FcγRIIaH131: 270 RU, FcγRIIaR131: 917 RU, FcγRIIIa F158: 798 RU, and FcγRIIIaV158: 660 RU. To collect kinetic binding data, each analyte (purified IgG) in 10 mM HEPES, 150 mM NaCl, 0.005% P20, 0.1% Tween 20 pH 7.4, was injected over flow cells at concentrations of 333.3, 166.7, 83.3, 41.7, and 20.8 nM at a flow rate of 30 μl/min, and at a temperature of 25°C. For the FcγRIIIa ligands, the IgG was allowed to associate and dissociate for 120 and 360 s, respectively. The surfaces were regenerated with 2 × 5 μl injections of 10 mM Glycine HCl pH 2.25, for Protein G purified samples, and a single 5 μl injection of 10 mM Glycine HCl pH 3.0 for Melon Gel samples. For the FcγRIIa ligands, the complex was allowed to associate and dissociate for 120 and 360 s, respectively, and the surfaces were regenerated with 3 × 5 μl injections of 10 mM NaOH for Protein G, and a single 5 μl injection of 10 mM Glycine HCl pH 3.0 for Melon Gel samples. Data was double referenced and globally fitted to a 1:1 interaction model with Scrubber2 software (BioLogic Software, Australia).

Real-Time Interaction Analysis of the Binding of IgG to FcγRIIa Exposed to Varying pH

Melon Gel purified IgG (9.5 mg/ml) (pooled from plasma of healthy individuals) was exposed to 0.1 M glycine buffer (low pH 1.5, to high pH 9.5) for 1 min. The pH was then adjusted to pH 7.0 and the samples were buffer exchanged into PBS. Binding to the higher affinity variant of FcγRIIa-H131 was determined by surface plasmon resonance on a BIACORE 3000 (GE Healthcare, Sweden). ~200RU FcγRIIaH131 was immobilized on a streptavidin sensor chip (GE Healthcare, Sweden). IgG samples were diluted in 10 mM HEPES, 150 mM NaCl, 0.005% P20 pH 7.4 and run over flow cells at a concentration of 333.3 nM at a flow rate of 30 μl/min. For the native sample, a 1 in 100 dilution of a plasma pool was used. The IgG complexes were allowed to associate and dissociate for 120 and 300 s, respectively.

FcγR Dimer Receptor ELISA

An ELISA previously described (12, 15, 16) was used to characterize the FcγR potential functional capacity of IgG purified by Melon gel and Protein G from plasma. This assay employs dimeric recombinant soluble FcγR proteins (rsFcγR) to evaluate and model the cross-linking of antibody Fc with FcγRs as a measure of their potential to activate effector cells. Briefly, biotin tagged recombinant soluble homodimers of either FcγRIIIa or FcγRIIa were used to quantitate the FcγR-binding capacity of purified IgG from the subjects bound to influenza HA

H3N2 (A/Switzerland/9715293/2013, Sinobiological Inc, China), or of HIV exposed individuals to HIV-1_{BAL} gp120 (NIH-AIDS Reagent Repository, USA). The influenza or HIV antigens were prepared in PBS and adsorbed (50 ng/well) to 96 well plates (Nunc™ MaxiSorp™, Denmark) Wells were washed with PBS containing 0.05% Tween 20 and blocked with PBS containing 1 mM EDTA and 1% (w/v) BSA (Sigma-Aldrich, USA). Purified IgG samples were serially diluted from a starting concentration of 100–12.5 μg/ml, and then incubated for 1 h at 37°C. Plates were washed five times with PBS containing 0.05% Tween-20, and the Ab-bound plates were subsequently incubated with 0.1 μg/ml purified dimeric rsFcγRIIIa V158-biotin or 0.2 μg/ml purified dimeric rsFcγRIIa H131-biotin in PBS containing 1 mM EDTA, 0.05% Tween-20, and 1% (w/v) BSA for 1 h at 37°C. Following incubation plates were washed five times and High Sensitivity Streptavidin (Thermo Fisher Scientific, USA) 1/10,000 in diluent buffer was added for 1 h at 37°C. Plates were washed eight times and then developed with TMB Single Solution (Sigma-Aldrich, USA). The reaction was stopped by addition of 1 M HCl, and absorbance at 450 nm was determined. A standard curve was used to determine the geometric mean FcγR activating capacity of each IgG preparation, with standard curves generated with pooled human IgG: IVIg (Privigen®, CSL Behring, Australia), and HIV IgG (NIH-AIDS Reagent Repository, USA), respectively.

Antibody Dependent Cellular Phagocytosis Assay (ADCP)

The THP-1 ADCP phagocytosis assay was performed as previously described (17). Briefly, Influenza HA protein H3N2 A/Switzerland/9715293/2013 (Sinobiological Inc, China), was biotinylated using the EZ-Link Sulfo-NHS-LC-Biotin kit (Thermo Fisher Scientific, USA) following manufacturer's recommendations. Biotinylated HA antigen was then incubated overnight at 4°C with fluorescent 1 μM neutravidin beads (Molecular Probes Inc, USA), and subsequently washed twice to remove unbound antigen. Purified IgG (10 μg/ml) was added to each well, and the plate was incubated for 2 h at 37°C in order to allow antibodies to bind to the beads. Controls with no IgG antibody, and with unconjugated beads were also run to determine background phagocytosis of the beads. 1 × 10⁵ THP-1 cells (monocytic cell line, ATCC TIB-202) were then added to each well, and the plate was incubated overnight at 37°C. Following incubation, cells were fixed in 1% formaldehyde before being acquired on a LSR Fortessa (BD Biosciences, USA) Flow cytometer. Flow cytometry data was analyzed using FlowJo analysis software version 10.5.3. Phagocytic scores were calculated as the geometric mean fluorescent intensity (MFI) of the beads multiplied by the percentage bead uptake. As a control to rule out any possible contaminating differentiating factors in the purified IgG samples, each sample was also preincubated with unconjugated beads, and any non-specific background for each sample was subtracted. Both the percentage of THP-1 cells that ingested one or more beads (percent bead positive), and the "mean phago score," which was calculated by determining the percentage of cells that were bead-positive, and multiplying

by the mean fluorescence intensity (to provide a convenient quantitative measure of net phagocytosis), was determined for each duplicate sample. For ease of presentation, these scores were then divided by 10^5 .

Antibody Isotyping

Purified IgG or plasma samples were simultaneously quantified for IgG₁, IgG₂, IgG₃, IgG₄, IgA, and IgM using the Bio-Plex Pro™ Human Isotyping Panel, 6-plex kit (Bio-Rad, USA), according to the protocol provided by the manufacturer. Purified IgG and plasma samples were diluted 1/10,000 and 1/40,000, respectively. Plates were washed using a magnetic plate-washer (Bio-Plex Pro Wash station, Bio-rad, USA), read on a Bio-plex MAGPIX instrument, and analyzed on Bio-Plex Manager 6.1.1 (Bio-Rad, USA) software. The proportion of each IgG subclass was calculated as a total percentage of the sum of the concentration of all the four IgG subclasses.

Mass Spectrometry of IgG N-glycans SP3 Protein Clean Up and In-solution Digestion

Four Melon Gel and four matched Protein G IgG preparations (10 µg) were prepared for MS analysis using a modified SP3 sample preparation approach (18, 19). Briefly, samples were first denatured and reduced using 1% SDS, 10 mM DTT, 100 mM HEPES by boiling at 95°C, 1,000 rpm for 10 min. Samples were then cooled and alkylated with 40 mM 2-chloroacetamide (CAA) for 1 h at RT in the dark. The alkylation reactions were then quenched with 40 mM DTT for 10 min and then samples precipitated on to SeraMag Speed Beads (GE Healthcare, USA) with ethanol (final concentration 50% v/v). Samples were shaken for 10 min to allow complete precipitation onto beads, and then washed three times with 80% ethanol. The precipitated protein covered beads were then resuspended in 100 mM Ammonium Bicarbonate containing 1 µg of trypsin 1/10 (w/w) (Sigma-Aldrich, USA), and allowed to digest overnight at 37°C. Upon completion of the digests, samples were spun down at 14,000 g for 5 min to pellet the beads. The supernatant was then collected and desalted using homemade C18 stage tips (20) before being dried down and stored until analyzed by LC-MS. Prior to loading, samples were reconstituted in MS running buffer [2% acetonitrile (ACN), 0.1% trifluoroacetic acid (TFA)] to a concentration of 0.5 µg/µl of which 2 µg (4 µl) was loaded for analysis.

iBAQ Proteome and Glycoform Analysis by LC-MS

Purified peptides were resuspended in Buffer A and separated using a two-column chromatography set up comprising a PepMap100 C18 20 mm × 75 µm trap and a PepMap C18 500 mm × 75 µm analytical column (ThermoFisher Scientific). Samples were concentrated onto the trap column at 5 µl/min for 6 min and infused into either an Orbitrap Elite™ Mass Spectrometer (ThermoFisher Scientific) for iBAQ based analysis or an Orbitrap Fusion™ Lumos™ Tribrid™ (ThermoFisher Scientific) for glycopeptide analysis at 300 nl/min via the analytical column using a Dionex Ultimate 3000 UPLC (ThermoFisher Scientific). Sixty-five minutes gradients were run

altering the buffer composition from 1% buffer B to 28% B over 35 min, then from 28% B to 40% B over 10 min, then from 40% B to 100% B over 2 min, the composition was held at 100% B for 3 min, and then dropped to 3% B over 5 min and held at 3% B for another 10 min. The Orbitrap Elite™ Mass Spectrometer was operated in a data-dependent mode automatically switching between the acquisition of a single Orbitrap MS1 scan (120,000 resolution) followed by 20 data-dependent CID MS2 events (NCE 35) with 30 s dynamic exclusion enabled. The Orbitrap Fusion™ Lumos™ Mass Spectrometer was operated in a data-dependent mode automatically switching between the acquisition of a single FTMS MS1 scan (120,000 resolution) every 3 s and MS2 HCD fragmentation (NCE 30, a maximum injection time of 22 ms and AGC of 2×10^5) with 30 s dynamic exclusion enabled. If the HexNAc oxonium ion (m/z 204.087) and its associated ions m/z 186.075 and m/z 168.065 were detected within an HCD scan the putative glycopeptide precursor was subjected to addition characterization using ITMS CID (NCE 35) and FTMS EThCD (using charge dependent ETD reaction times, HCD NCE 25, a maximum injection time of 250 ms and AGC of 2×10^5).

Mass Spectrometry Data Analysis

For proteomic comparison of IgG preparations MS raw files were searched against the UNIPROT human proteome databases (UP000005640, downloaded July 2017) using MaxQuant [version 1.5.3.3 (21)]. Searches were performed using cysteine carbamidomethylation as a fixed modification, methionine oxidation and N-terminal acetylation as variable modifications with trypsin specificity and a maximum of two miss-cleavage events. The default MaxQuant instrument setting for Orbitrap FTMS (MS1 tolerance of ± 20 ppm for the first search and ± 4.5 ppm for the main search) and ITMS (MS1 tolerance of ± 0.6 Da) were used with the resulting data filtered to a False discovery rates (FDR) of 1% at the protein and peptide levels. To enable the assessment of relative protein amount within IgG preparations the IBAQ (22) setting was enabled. The resulting output file was then imported into R for generation for data visualization.

The identification of IgG glycoforms within IgG preparations were accomplished using Byonic [Protein Metrics, version 3.4 (23)]. Each MS raw file was searched with a MS1 tolerance of ± 10 ppm and a tolerance of ± 20 ppm was allowed for both HCD and EThCD MS2 scans. Searches were performed using cysteine carbamidomethylation as a fixed modification, methionine oxidation as a variable modification in addition to allowing N-linked glycosylation on asparagine. The default Byonic human N-linked no multiple fucose glycan database, which is composed of 182 mammalian N-glycans compiled from literature sources (7–10), was used. The proteases specificity was set to full trypsin specificity and a maximum of two miss-cleavage events allowed. Data searched against the UNIPROT human proteome databases (UP000005640, downloaded July 2017). Search was filtered to a 1% protein FDR as set in the Byonic parameters with the final results collated using R with an additional filtering step to remove glycopeptide assignments with Byonic score below 150 [as suggested by Lee et al. (24)] applied to remove low quality glycopeptide assignments and ensure a <1% FDR.

Only glycopeptides of the main IgG subclass IgG₁ were examined, as the other subclasses were confounded by the fact that in Caucasian populations the tryptic glycopeptide of IgG₃ generally has the same peptide sequence as IgG₂ (25), and IgG₄ counts were poor for many of the glycopeptides. Fc IgG1 glycosylation at site N180 was compared across all samples. To compare glycosylation, peptide spectrum matches (PSM) i.e., the count of each time the glycopeptides were identified was quantified. To permit comparison across the samples, all samples were normalized to total count (sum of each time the glycopeptide is identified across the samples). Glycosylation features were calculated from the data: fucosylation (% of glycans bearing a core fucose), bisection (% of glycans with a bisecting GlcNAc), and sialylation (% of antennae carrying a sialic acid).

Protein Aggregation Assay

A pool of Melon Gel purified IgG (9.5 mg/ml) was aggregated at 65°C for 30 min. At this point, the IgG was considered 100% aggregated (26). The aggregated IgG was then added in various proportions to unaggregated monomeric IgG to achieve percentages of aggregation, in order to create a standard curve as described by the manufacturer of 100, 80, 40, 20, 10.5, 2.5, and 0% aggregated IgG. Two microliters of ProteoStat® Fluorescent Dye (Enzo Life Sciences, USA) was added to each test sample containing 200 µg/ml of IgG in a 96-well black, clear flat-bottomed plate (Greiner Bio-One, Austria). This dye is widely used to detect protein aggregates (27) and is benchmarked with IgG by the manufacturer (28). The microplate containing test samples was incubated in the dark for 15 min at room temperature. Samples were excited at 530 nm and emission was read at 605 nm on a FLUOstar plate reader (BMG Labtech, Germany).

ANS Fluorescence

Melon Gel or Protein G purified IgG samples were prepared at 2 µM and incubated with 32 µM of 8-Anilino-1-naphthalenesulfonic acid (ANS) (Sigma-Aldrich, USA) in a clear bottom, black, non-binding 96 well plate (Greiner Bio One, Austria). For endpoint measurement samples were excited at 388 nm and Emission at 500 nm was recorded. The fluorescence emission spectra of ANS was also recorded between 400 and 600 nm on a CLARIOstar plate reader (BMG Labtech, Germany).

Statistical Analysis

Statistical analyses were performed using GraphPad Prism 8 (GraphPad Software, San Diego CA, USA). Data are summarized using descriptive measures such as median + IQR (interquartile range), mean ± SD, and percentage (%). Spearman's rank correlations were used to examine bivariate associations between variables. Wilcoxon matched pair signed rank tests were used to compare Melon Gel and Protein G data. The Friedman test with Dunn's multiple comparisons was used to compare data obtained from the IgG subclass analysis. In all cases *P*-values <0.05 were considered to indicate statistical significance. In figures, asterisks denote statistical significance (**p* ≤ 0.05; ***p* ≤ 0.01; ****p* ≤ 0.001; *****p* ≤ 0.0001; ns = not significant) with comparisons specified by connecting lines.

RESULTS

Low-pH Exposure in Protein G Purified Samples Induces Aggregation of IgG

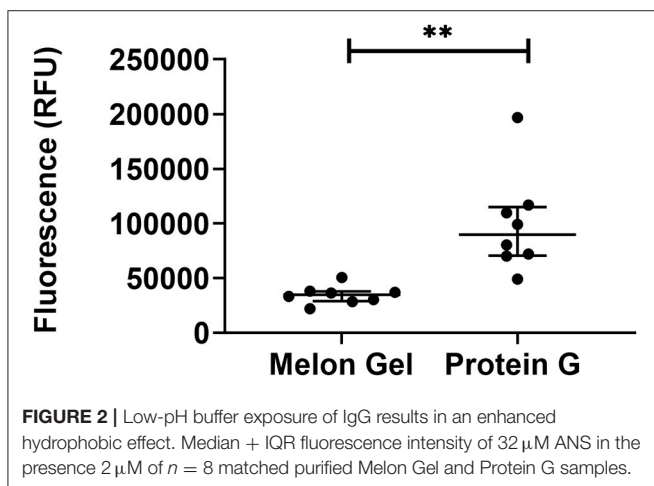
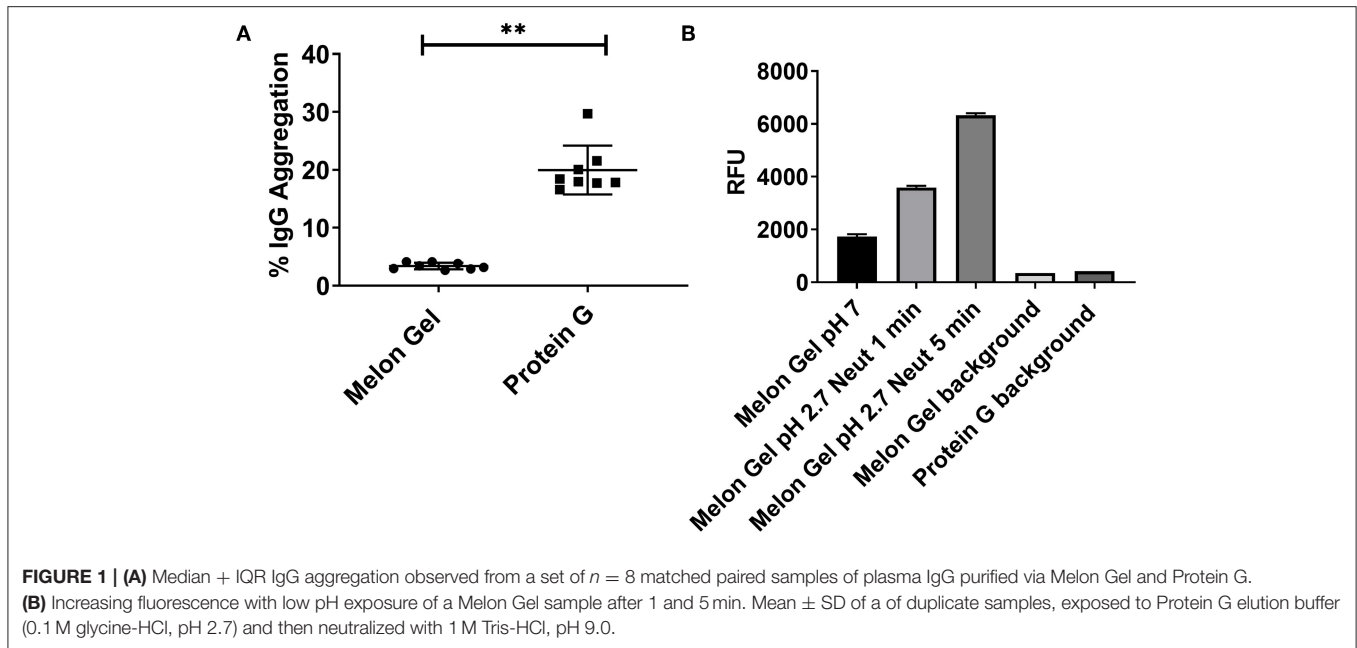
Potential differences in aggregation between Melon Gel and Protein G purified IgG were examined using a fluorescent dye, ProteoStat® (Enzo Life Sciences, USA). The fraction of aggregation in Melon Gel purified IgG from a subset of healthy serum samples (*n* = 8) was compared with that of equivalent IgG samples purified using Protein G. The Protein G purified samples were found to contain ~6-fold more aggregates than the Melon Gel purified IgG (Protein G median = 18.2 vs. Melon Gel median = 3.3, *p* = 0.0078; **Figure 1A**). In order to confirm the pH dependency of an aggregation affect, Melon Gel IgG was additionally exposed to the low pH elution buffer. When Melon Gel purified IgG was transiently exposed to the low-pH buffer conditions (pH 2.7) used in the elution of IgG in the Protein G purification process, the fluorescence of the ProteoStat® aggregate reporter dye almost doubled within a 1 min exposure and was increased 3-fold by 5 min (**Figure 1B**). The low pH elution step in the Protein G purification process is thus likely to strongly contribute to the higher aggregate content of IgG purified using Protein G.

Low pH Exposure Increases IgG Hydrophobicity as Evaluated by 8-anilnonaphthalene-1-sulfonate (ANS) Fluorescence

ANS is a fluorescent molecular probe which can change its fluorescent properties as it binds to hydrophobic regions of proteins, thereby making it a useful tool to study conformational changes. ANS was therefore used as a probe to evaluate whether low-pH buffer exposure during the Protein G purification process exposed new hydrophobic sites on IgG. Protein G samples incubated in the presence of ANS exhibited a significantly higher fluorescence in comparison to Melon Gel purified IgG samples (**Figure 2** *p* = 0.0078). Increased fluorescence intensity and a blue shift in the fluorescence maxima were also observed in the spectral scan recorded after excitation at 388 nm (**Figure 3A**), demonstrating the increased hydrophobicity of low-pH buffer-exposed IgG molecules. To confirm the low-pH dependency of this effect, a Melon Gel sample was also exposed to low pH for 1 and 5 min, and was also found to exhibit the same increased ANS fluorescence, consistent with an increased hydrophobicity upon exposure to low-pH (**Figure 3B**).

Aberrant Kinetics of Protein G Purified IgG With Immobilized FcγRIIIa and FcγRIIa

Protein G and Melon Gel purified IgG are widely used for the evaluation of antibody function, with many important functions mediated via Fc receptors. Whether the IgG purification method employed had any effect on the binding of purified IgG to Fc receptors was examined using surface plasmon resonance (SPR). The different Fc binding ectodomains of the allelic variants of FcγRIIIa and FcγRIIa were immobilized and reacted with either Protein G or Melon Gel purified IgG. Inspection of



representative sensograms (**Figure 4**) and the apparent binding constants derived from the analysis of $n = 15$ IgG samples (**Figure 5**), found stronger binding by the Protein G purified samples. Most striking was Protein G purified IgG binding profile to immobilized Fc γ RIIa, where the bound analyte dissociated more slowly and the apparent K_D^{app} obtained was about 20-fold lower than that of the Melon gel purified IgG ($p < 0.0001$). Notably, even the Melon Gel purified IgG showed biphasic binding profiles to immobilized Fc γ RIIa, that is characteristic of multivalent binding of aggregates but with a much smaller slow association and faster dissociation component than the Protein G-IgG. Nevertheless, even the low 3.3% level of aggregates in the Melon Gel purified IgG affected the binding sensograms and results in a higher apparent binding strength (Fc γ RIIa H131 $K_D^{app} = 0.14 \mu$ M and R131 $K_D^{app} = 0.24 \mu$ M) when fitted to

a 1:1 binding model, than the known micromolar binding of this receptor (13, 29). Fc γ RIIIa has higher affinity for IgG-Fc than Fc γ RIIa but also showed divergent binding sensograms for Protein G and Melon gel purified IgG, although this was less extreme than for Fc γ RIIa. The K_D^{app} of the Protein G IgG was over 2-fold lower ($p < 0.0001$), again consistent with the higher level of aggregates in this preparation contributing to stronger apparent binding to Fc γ RIIIa.

IgG Exposure to Low-pH Produces Aberrant Binding Kinetics With Immobilized Fc γ RIIa

The effect of the low pH elution buffer used in the Protein G purification process was evaluated by exposing IgG to the low-pH elution buffer, and the pH dependency of the binding to Fc γ RIIa was investigated. Here the binding profiles obtained after single injections of a pool of IgG purified via Melon gel transiently exposed to a range of low to high pH buffer were compared. Transient exposure of IgG at a pH of 1.5 or 2.5 strongly increased the binding of IgG to Fc γ RIIa, as evident by comparing the dissociation curve of the interaction to a pH of 3.5 and above (**Figure 6**). Pooled Melon gel IgG was also exposed to the binding buffer used in the Protein G purification procedure (20 mM sodium phosphate, pH 7.0), displaying a similar profile to that observed here at pH 7.5 (**Figure S1**).

IgG Aggregates in Protein G Preparations Show Increased Dimeric Fc γ R Binding

Dimeric rsFc γ R ectodomains have been used as a serological approach to evaluate the functional, Fc γ R-activating, capacity of IgG-immune complexes. The binding of dimeric rsFc γ R ectodomains in an ELISA requires avid binding to pairs of

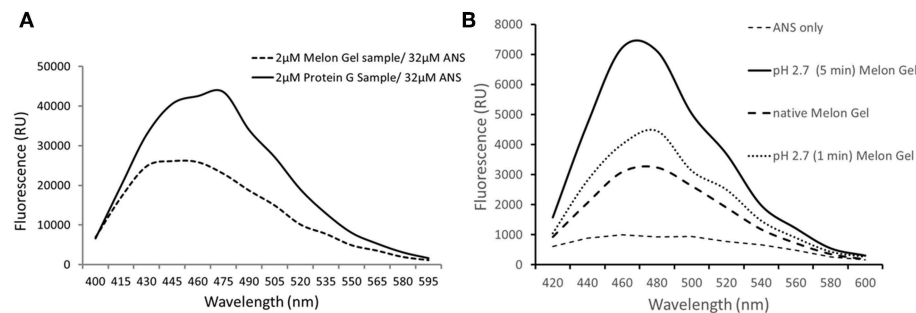


FIGURE 3 | (A) Emission spectra of 32 μ M ANS in the presence of 2 μ M of a Protein G sample and a Melon Gel sample. **(B)** Emission spectra of 32 μ M ANS in the presence of 2 μ M of a native and pH 2.7 buffer exposed (5 min or 1 min) Melon gel sample.

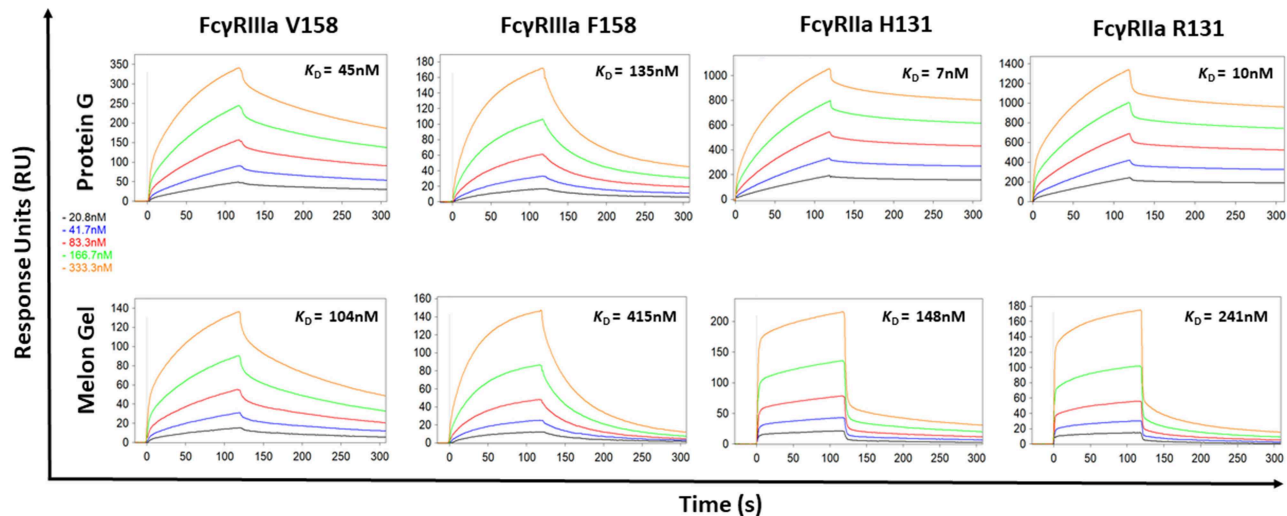


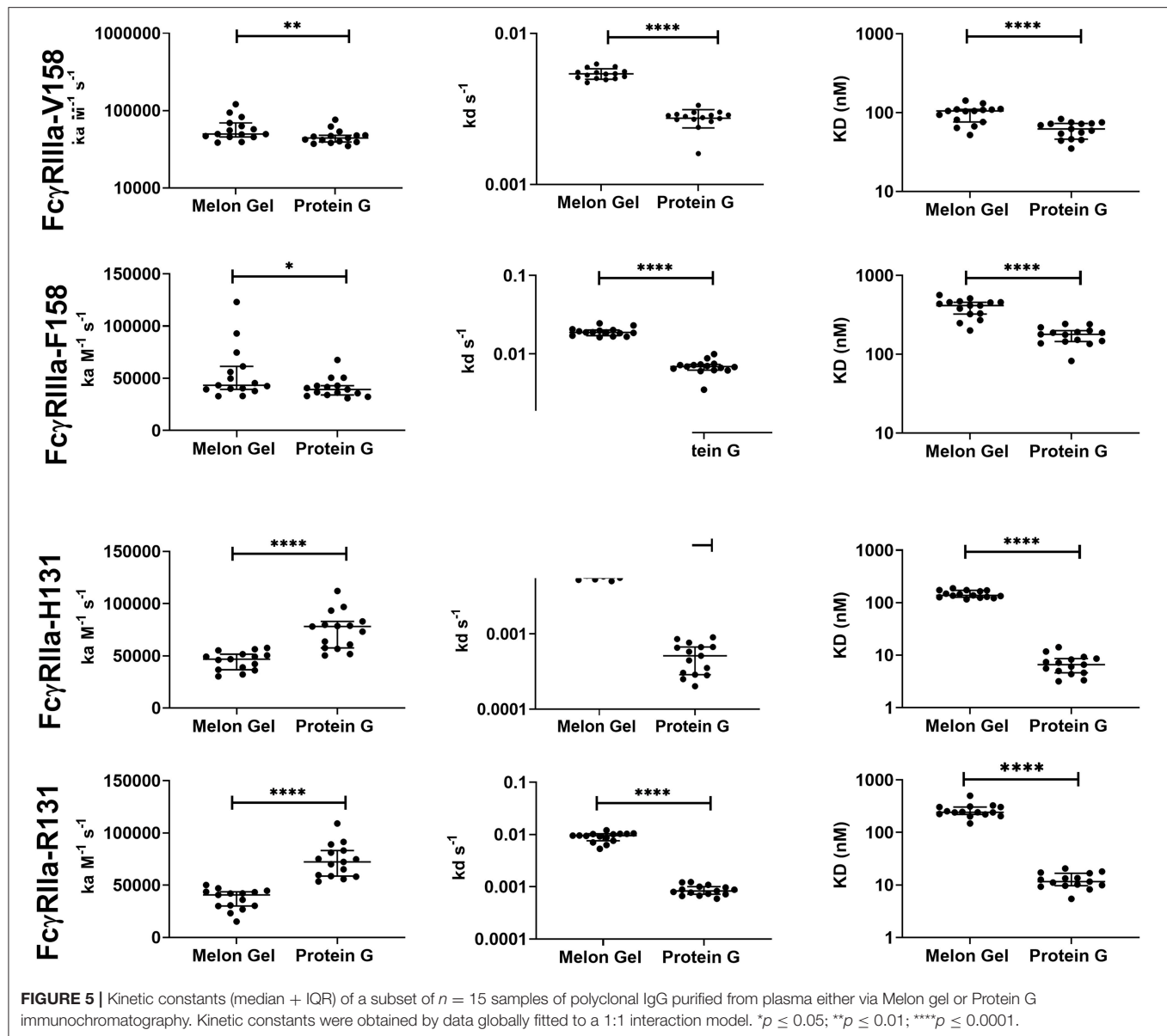
FIGURE 4 | Binding kinetics of the high and low affinity variants of Fc γ RIIIa and Fc γ RIIa to IgG purified via Melon Gel and Protein G. Real-time surface plasmon resonance sensorgrams and affinity constants determined from SPR analysis representative of an individual polyclonal IgG sample serially diluted 2-fold from 333.3 nM.

IgG-Fcs. Having found by SPR that aggregates in Protein G purified IgG bind avidly to Fc γ Rs, the dimeric rsFc γ R assay was employed to predict if these aggregates might also have Fc γ R activating capacity. Recombinant soluble biotin tagged homodimers of either Fc γ RIIIa or Fc γ RIIa high affinity variants were used to quantitate and compare the activating potential of IgG purified using the two distinct purification methods. IgG from 28 healthy individuals purified via Protein G and Melon Gel were incubated with Influenza H3 Switzerland hemagglutinin (HA) immobilized to ELSA plates and the capacity of these antigen immune complexes to bind dimeric rsFc γ Rs was measured. Increased binding to the Protein G IgG-immune complexes was observed for both dimeric rsFc γ RIIIa and dimeric rsFc γ RIIa ($p < 0.0001$, **Figures 7A,B**). Thus, HA-specific IgG in the Protein G preparations include some aggregated material which retains HA binding activity, and by virtue of aggregation, artefactually elevates binding avidity to Fc γ Rs. This observation was extended using a second separate cohort consisting of plasma samples from 25 HIV positive

individuals, from which polyclonal IgGs, were also purified using both methods and reacted with HIV gp120 antigen. Again dimeric rsFc γ RIIIa ($p < 0.0001$) and dimeric rsFc γ RIIa ($p = 0.0006$) rsFc γ R binding in the ELISA was higher for Protein G purified samples (**Figures 7C,D**). This increased binding for dimeric Fc γ RIIIa and Fc γ RIIa suggests that Protein G IgG purified samples have augmented capacity to activate Fc γ R effector cells.

Protein G Purified IgG Has Apparently Enhanced Effector Function

Next, we evaluated whether the aggregate-mediated increased avidity of Protein G purified IgG interactions with Fc γ Rs translates to enhanced Fc γ R function in a well-validated *in vitro* phagocytosis cell-based assay. THP-1 human monocytic cells which express Fc γ RI and Fc γ RIIa were incubated with influenza HA Switz conjugated fluorescent beads that were opsonized with IgG from Influenza vaccinated individuals purified using



either Melon Gel or Protein G. Phagocytosis of HA-beads by THP-1 cells (**Figure 8**) was significantly augmented when opsonized with Protein G purified IgG (**Figure 8A** % bead positive median = 35.7%; $p = 0.008$; **Figure 8B** Phagocytosis score $p = 0.008$; median = 2.45), compared to identical matched samples purified via Melon Gel (% bead positive median = 30.1%, Phagocytosis score median = 2.08). The MFI (representing the mean quantity of internalized antigen conjugated fluorescent beads per THP-1), was also observed to be significantly ($p = 0.0078$) higher in Protein G samples (Protein G median = 6,203 vs. Melon Gel median = 5,707, data not shown). Thus, antibody dependent cellular phagocytosis (ADCP) activity is artefactually increased upon purification using Protein G as are potentially other effector functions that depend on avid binding to FcγRs.

Effect of Purification Method on IgG Subclass Distribution and Fc N-glycan Composition

Since IgG interactions with FcγRs are influenced by IgG subclass and glycosylation (30, 31), it is possible some attributes of the augmented activity of the Protein G purified polyclonal IgG may be attributed to altering the subclass or glycan composition. First, the IgG subclass composition of Protein G and Melon gel preparations was examined. Although it is known that Protein G binds all human IgG subclasses, there is no published data as to whether either Protein G or Melon Gel purification alters the subclass composition of plasma IgG. Matched Melon gel and Protein G purified IgG from healthy donors, along with corresponding plasma samples were simultaneously quantified for IgG₁, IgG₂, IgG₃,

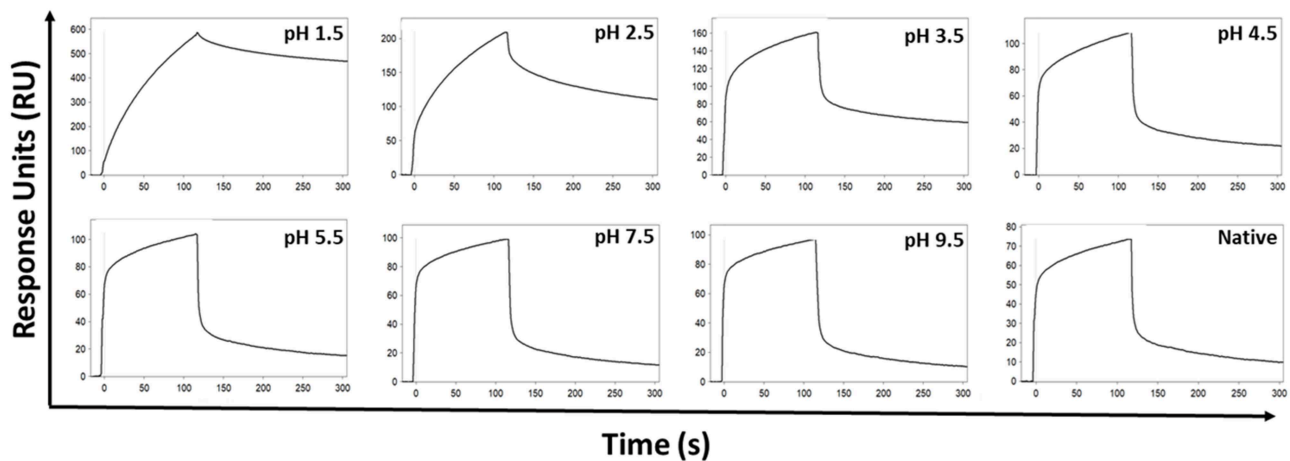


FIGURE 6 | SPR real-time interaction analysis of the binding of 333.3 nM IgG to FcγRIIa. IgG was exposed transiently over a range of low to high pH of 0.1 M glycine-HCl, and then neutralized with 1 M Tris-HCl, pH 9.0. Native IgG (1:100 dilution of plasma) was also run for comparison.

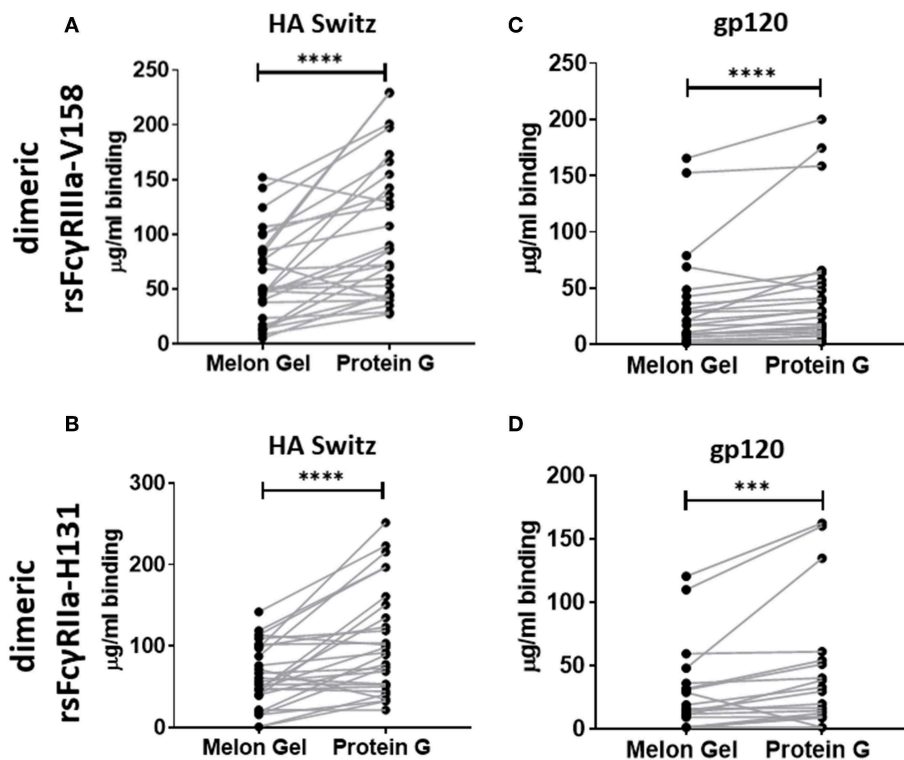


FIGURE 7 | Dimer ELISA binding Ab responses to HA from A/Switzerland/9715293/2013 (H3N2) (HA Switz) for FcγRIIIa V158 $n = 28$ (A) and FcγRIIIa H131 (B) and HIV gp120 protein (C,D) $n = 25$. IgG samples were serially diluted 4-fold from a starting concentration of 100 μg/ml. Melon Gel and Protein G responses were compared using the Wilcoxon matched-pair test. *** $p \leq 0.001$; **** $p \leq 0.0001$.

and IgG₄ via multiplex immunoassay, in order to determine which purification approach best reflected the IgG subclass distribution ratios observed in plasma (Figure 9). Compared to the subclass composition of plasma both the Melon Gel purified samples and Protein G purified IgG samples had lower levels of IgG₃ ($p < 0.0001$). A small deficit in the proportion

of IgG₄ in Melon gel preps contrasted with the Protein G preparations which had substantially decreased proportions of IgG₁, IgG₃, and IgG₄, while IgG₂ was overrepresented ($p < 0.0001$). The FcγRIIa-H131 allele is the only human FcγR that functionally binds human IgG₂. Thus, although Protein G preparations had increased proportions of IgG₂, the enhanced

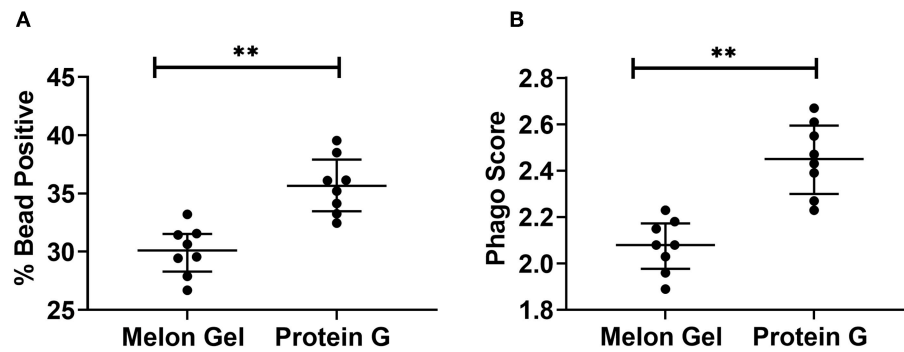


FIGURE 8 | (A) Median + IQR % bead positive THP-1 cells, and **(B)** phagocytic scores of purified Protein G or Melon Gel IgG from flu vaccinated individuals against hemagglutinin-coated beads. All samples were run in duplicate, and Melon Gel and Protein G responses were compared using the Wilcoxon matched-pair test.

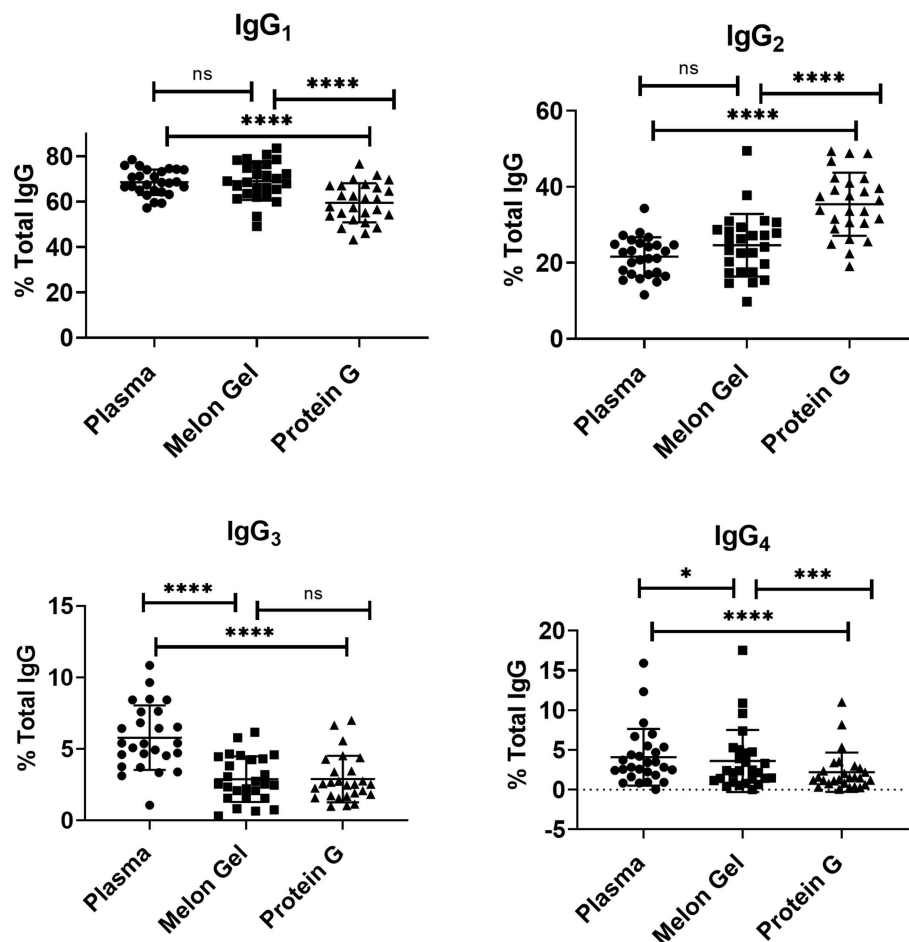


FIGURE 9 | Mean and SD of subclass percentage obtained for plasma and purified (Melon Gel and Protein G) IgG samples ($n = 26$) via Multiplex immunoassay. The Friedman test with Dunn's multiple comparisons was used to compare data from each group. * $p \leq 0.05$; *** $p \leq 0.001$; **** $p \leq 0.0001$.

binding of the low-IgG2 reactive FcγRIIa R131 allele with these preparations by SPR (Figures 4, 5) and dimeric receptor assay (Figure 7) indicates this enhanced activity is mediated, not by the higher IgG2 composition, but by the higher aggregate

composition in the Protein G preparations. However, these alterations in subclass composition, including increased IgG2, could have important effects in other functional evaluations. Nevertheless, both methods showed a significant correlation,

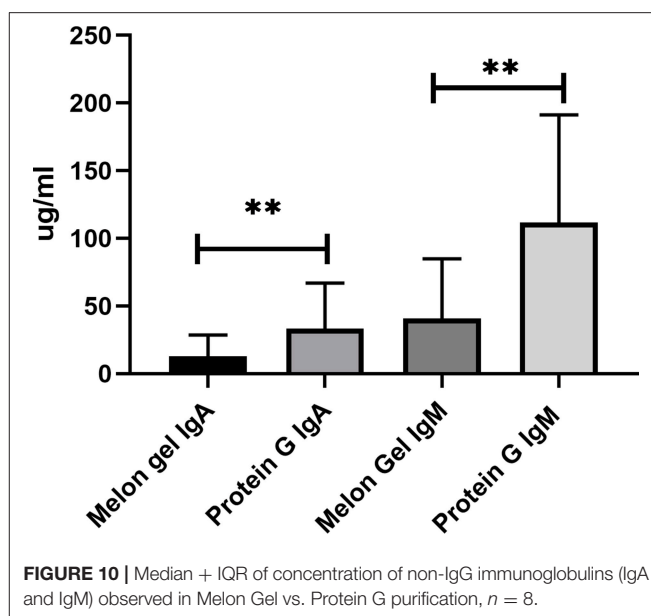
both to each other and to plasma with regard to IgG subclass distribution (Table S1).

Compared to antibody affinity purification with Protein A or Protein G, Melon Gel IgG Purification is reported to provide greater yields and higher purity by the manufacturer. Here, we also examined via multiplex immunoassay a subset of samples for the presence of contaminating immunoglobulins IgA and IgM by the two IgG purification approaches (Figure 10), with Protein G purified samples found to contain significantly more contaminating IgA ($p = 0.0078$) and IgM ($p = 0.0078$), equating to an almost 3-fold difference for both IgA (median = 12.9 vs. 33.3 $\mu\text{g/ml}$) and IgM (median = 41.0 vs. 111.9 $\mu\text{g/ml}$). Since the composition of asparagine (N) 297-linked glycans are well-known to modulate the binding affinity of IgG Fc to Fc γ receptors, an exploratory analysis using mass spectrometry was performed on four matched IgG samples purified via Melon Gel and Protein G. Fc IgG1 glycosylation at site Asn 297 (N180) was compared across all samples, however no differences were observed in this preliminary analysis (Figure S2).

DISCUSSION

Fc-functional antibodies are of growing interest in protection and control of diverse infectious diseases, such as HIV, Influenza, and Mycobacterium Tuberculosis (12, 30, 32, 33). Given that neutralizing antibody titers do not always correlate with protection, Fc-functional antibody assays are fundamental components of correlates of protection for the evaluation of these infectious disease research cohorts, as well as current and future vaccine efficacy trials (32–36). Quantitative functional antibody assays have however been reported to be difficult to standardize, and reliable assays that can be reproducibly used across different laboratories to measure Fc-dependent functions, such as antibody dependent cellular cytotoxicity (ADCC), have been described as limited (37–39). Consequently, there is a lack of consensus as to which Fc effector functions contribute to protection against a number of infectious diseases, such as HIV-1 (37, 39). Although a range of factors may be responsible for these for conflicting results, how the antibodies used in these functional assays have been purified, appears to be a technical factor which has been entirely overlooked. Given the wide array of diverse approaches that are available for researchers to purify IgG, it is reasonable to assume that the purification strategy employed, might also contribute to divergent results obtained across laboratories with respect to functional assays. Herein we compared two popular approaches for purifying IgG from human plasma and demonstrated that the method employed to purify IgG dramatically altered Fc γ R-binding behavior and Fc functional activity.

Typical purification processes which elute from affinity resins at low pH such as Protein A and Protein G, have been well-documented to promote formation of non-native IgG structures, particularly aggregates (40). Low-pH exposure of IgG has been found to be caused by Cy2 unfolding associated with protonation of specific acidic residues, with IgG aggregation primarily



determined by IgG subclass, and degree of Cy2 glycosylation (8). As demonstrated in the present study, such aggregates show enhanced avid binding to Fc receptors, thus significantly impacting antibody binding kinetics and apparent affinity. Low pH exposure in our study resulted in 6-fold higher median percentage of IgG aggregates in the Protein G samples compared to those purified via Melon Gel. Furthermore, even Melon Gel purified IgG with only 3% aggregation appeared to be influenced by these aggregates in the SPR sensograms, with increased apparent binding affinity and decreased dissociation. Similar results were also obtained by Dorion-Thibaudeau et al. where even small percentages (2%) of IgG aggregates were found to affect Fc receptor binding (41). A previous study which investigated the effect of IgG aggregates on Fc receptor binding, also found aggregates bind more strongly to Fc receptors, with a much slower off-rate, significantly impacting affinity determinations (42). This is the result of an increased avidity effect, rather than a true difference in IgG affinity. Significantly slower apparent off-rates (k_d) as observed via SPR were also a feature of Protein G purified samples in the present study. Indeed, in our study, the presence of aggregates in these low pH exposed Protein G samples was found to have a more profound effect on the low affinity Fc γ RIIa, where a 20-fold increase in apparent binding affinity was observed. The effect of aggregates for low affinity receptors, where the avidity effect would be more pronounced, has also been previously found to be much greater than that for high affinity receptors (43). The increased avidity of binding of Protein G purified IgG translated to apparently augmented effector function in our study, with Protein G purified IgG having an enhanced capacity to stimulate Fc γ Rs on THP-1 cells to trigger ADCP. Future studies exploring the effect of low pH purification methods upon other IgG Fc-mediated functions such as antibody mediated complement activation is warranted.

Together SPR and dimer ELISA analysis data revealed a profound impact on the binding kinetics of Protein G purified IgG binding FcγRIIIa and FcγRIIa. SPR which is widely used to examine the binding activities of different FcγRs (29), is sensitive enough to detect composition changes, such as the increased presence of dimers and aggregates in IgG samples. The increased avidity, and vast difference in the apparent binding kinetics of Protein G and Melon Gel purified IgG was further highlighted in our results by the need to modify the regeneration conditions necessary to dissociate the ligand-analyte interaction for all Protein G purified IgG samples described in the SPR methods. We also observed significantly enhanced binding to specific antigens (HIV gp120, and influenza HA) via a previously described dimer ELISA, demonstrating that aggregates also preserve their antigen binding activity.

By using ANS, a fluorescent molecular probe used to examine hydrophobicity of proteins, we confirmed that exposure of IgG to low-pH results in molecular modifications characterized by a significant increase in hydrophobicity as observed by a previous study (5). The authors of this study theorized that low-pH triggers the exposure of previously buried hydrophobic amino acids, thereby increasing the hydrophobicity of IgG. The fact that we were able to induce changes to Melon Gel IgG by transient exposure to the low pH elution buffer used in the Protein G purification process, suggests that it is most likely low pH and not any other aspect of the Protein G purification procedure that is responsible for these conformational changes. Where on the IgG molecule these hydrophobic changes occur, and how exactly they trigger IgG aggregation, or whether they alter Fc receptor binding remains to be determined. The authors of the previous study assumed that these conformational changes occur in the Fab region, as the objective of their study sought to investigate the phenomenon of low pH induced antigen polyreactivity (5). One study, published over 50 years ago, however demonstrated by infrared spectroscopy as well as by hydrogen-deuterium exchange measurements that at low pH, the original structure of the IgG Fc fragment is altered, whereas the conformational properties of the Fab fragments do not change significantly (44). A study 4 years later (45) also supported these findings suggesting the refractory nature of the Fab region. Our findings demonstrate that a significant increased apparent binding affinity is observed when IgG is exposed to a pH below 3.5. Whereas, from a pH of 3.5 upwards, binding was found to reflect a similar profile to native IgG. This observation is interestingly consistent with high-resolution NMR analysis demonstrating that the second constant domain (Cγ2) of IgG remains intact at pH 3.5 and is profoundly altered at pH 3.1 (8). It is therefore plausible that low pH induced conformational changes to the Cγ2 domain occur, in addition to the increased presence of IgG aggregates, however this remains to be determined. Investigating the relative contributions of low pH induced IgG aggregation in comparison to low pH induce protein hydrophobicity upon increased apparent FcγR binding and functions may provide further insights.

It is well-known that the binding affinity of an IgG for Fc receptors can be modulated by IgG subclass (46), and each of the IgG subclasses has a unique binding profile to each FcγR.

For the low affinity receptors FcγRIIa and FcγRIIIa examined in this study, binding affinity generally follows the hierarchy IgG₃ > IgG₁ >> IgG₂ = IgG₄, however, the allelic variant of FcγRIIa with a histidine at position 131 (H131) displays a higher affinity for IgG₂ and has the binding hierarchy, IgG₃ > IgG₁ ~ IgG₂ > IgG₄ (13). For both FcγRIIa and FcγRIIIa binding affinity is strongest for IgG₃, which did not differ significantly from the two purification methods. Furthermore, IgG₁, which follows IgG₃ in binding affinity, was significantly higher in the Melon Gel samples. It is therefore unlikely that absolute differences in IgG subclass ratios between the two purification methods contribute to the disparate binding profiles of IgG observed with the two purification methods. In particular the higher proportion of IgG₂ in Protein G purified IgG did not directly enhance FcγRIIa binding as this was enhanced to both the H131 allelic form and the low-IgG₂ binding R131 allelic form. It is relevant to note however, that IgG₂ has been found to exhibit greater aggregation under low-pH conditions than IgG₁ (8, 47). The greater proportion of IgG₂ observed in the Protein G/low pH purified samples may consequently promote aggregation that incorporates universally FcγR binding IgG₁ and IgG₃ subclasses in mixed aggregates.

Glycosylation of the Fc region of IgG is well-known to be critical for maintaining IgG structural integrity, and modulating Fc receptor binding (48). It has been reported that sialic acids may be lost when they are subjected to high temperature (>28°C) or extreme pH with prolonged exposure, possibly resulting in the formation of false glycans in the sample (49). Our analysis was limited to glycopeptides of the main IgG subclass IgG₁, as the other subclasses were confounded by the fact that in Caucasian populations the tryptic glycopeptide of IgG₃ generally has the same peptide sequence as IgG₂ (25), and IgG₄ counts were poor for many of the glycopeptides. Though our preliminary limited exploratory analysis of four samples examining Fc IgG₁ glycosylation analysis revealed no significant differences, this finding is not definitive, and whether diverse purification approaches impact Fc IgG glycosylation is a factor which warrants further investigation.

Much of the understanding surrounding IgG purification approaches, and IgG aggregation is known from biopharmaceutical antibody production (50) but may be less appreciated in the research community. Commercial monoclonal therapeutics are also often susceptible to aggregation during routine purification steps. For example, Nivolumab, an anti-programmed death (PD)1 IgG₄ antibody used as a cancer treatment was found to be significantly affected by low pH Fc induced aggregation during routine Protein A chromatography (9). This is especially important as aggregates, and polyreactive IgG can threaten safety and efficacy by eliciting undesirable immunogenic responses. As such, many mAb therapeutics have moved away from low pH elution chromatography approaches, and modifications in the manufacturing process have been introduced to either minimize or remove aggregates in the final product (50). A positive aspect of exposing IgG to low pH has however been the enhancement of the therapeutic potential of immunoglobulin

preparations such as IVIg in experimental systems (11). For example, low pH exposed, and not native treated intravenous immunoglobulin was found to improve the survival of mice with bacterial lipopolysaccharide-induced septic shock (5). The mechanisms behind this phenomenon have however been assumed to be attributed to structural modifications in the Fab region and the formation of aggregates, while the impact on Fc functionality has to our knowledge never been explored.

CONCLUSION

Herein we demonstrate that exposing IgG to low pH significantly affected Fc-binding behavior and Fc effector functions as a result of IgG aggregation. Taken together with previous studies of monoclonal and polyclonal IgG purified by low pH elution from Protein G and Protein A, these findings indicate that transient exposure of IgG to low pH (<3.5), leads to exposure of hydrophobic sites and significant aggregation, whilst preserving antigen and FcγR binding. This results in apparently enhanced functionality in the context of binding and cell activation assays that are sensitive to the avidity of interactions. Since the normal function of the low affinity FcγRs is the avid sensing of immune complexes and antibody opsonized targets, the unappreciated impact of aggregates on evaluating antibody effector functions is evident in the present study, though the potential impact on other major FcγR receptors remains to be determined. These observations contribute to the mounting evidence highlighting the potential undesirable consequences of purification processes which elute from affinity resins at low pH, such as Protein G and Protein A, and suggest that IgG cannot be assumed to be fully native following low-pH elution. Thus, the purification strategy chosen by researchers may profoundly influence the outcome and interpretation of experimental systems, and may consequently be a previously overlooked factor contributing to the current lack of reproducibility between assays employed to evaluate Fc-mediated effector functions. Researchers should actively consider antibody purification methods both upon design of experiments and in the interpretation of experimental data.

REFERENCES

1. Sauer-Eriksson AE, Kleywegt GJ, Uhlen M, Jones TA. Crystal structure of the C2 fragment of streptococcal protein G in complex with the Fc domain of human IgG. *Structure*. (1995) 3:265–78. doi: 10.1016/S0969-2126(01)00157-5
2. Lian LY, Barsukov IL, Derrick JP, Roberts GC. Mapping the interactions between streptococcal protein G and the Fab fragment of IgG in solution. *Nat Struct Biol*. (1994) 1:355–7. doi: 10.1038/nsb0694-355
3. Welfle K, Misselwitz R, Hausdorf G, Höhne W, Welfle H. Conformation, pH-induced conformational changes, and thermal unfolding of anti-p24 (HIV-1) monoclonal antibody CB4-1 and its Fab and Fc fragments. *Biochim Biophys Acta*. (1999) 1431:120–31. doi: 10.1016/S0167-4838(99)00046-1
4. Arakawa T, Philo JS, Tsumoto K, Yumioka R, Ejima D. Elution of antibodies from a Protein-A column by aqueous arginine solutions. *Protein Expr Purif*. (2004) 36:244–8. doi: 10.1016/j.pep.2004.04.009

DATA AVAILABILITY STATEMENT

The datasets generated for this study are available on request to the corresponding author.

ETHICS STATEMENT

The studies involving human participants were reviewed and approved by Alfred Health and University of Melbourne Human Ethics Committees (IDs 432/14 and 1443420). The patients/participants provided their written informed consent to participate in this study.

AUTHOR CONTRIBUTIONS

EL wrote the manuscript, conceived, designed and performed all experiments, with the exception of the mass spectrometry glycan analysis which was performed and analyzed by NS. Recombinant soluble Fc Receptors were provided by PH and BW. Plasma samples were provided by AW and SK. AC and SK contributed to the design of the research and together with BW interpreted the results. All authors reviewed and contributed to the final manuscript.

FUNDING

This work was supported by an Australian NHMRC project grant (APP1125164) and American Foundation for AIDS (amfAR) Mathilde Krim Fellowship (#109882).

ACKNOWLEDGMENTS

We thank the NIH AIDS Reagent repository for providing recombinant gp120 BaL and HIV IgG.

SUPPLEMENTARY MATERIAL

The Supplementary Material for this article can be found online at: <https://www.frontiersin.org/articles/10.3389/fimmu.2019.02415/full#supplementary-material>

5. Djoumerska-Alexieva IK, Dimitrov JD, Voynova EN, Lacroix-Desmazes S, Kaveri SV, Vassilev TL. Exposure of IgG to an acidic environment results in molecular modifications and in enhanced protective activity in sepsis. *FEBS J*. (2010) 277:3039–50. doi: 10.1111/j.1742-4658.2010.07714.x
6. Gagnon P, Nian R, Leong D, Hoi A. Transient conformational modification of immunoglobulin G during purification by protein A affinity chromatography. *J Chromatogr A*. (2015) 1395:136–42. doi: 10.1016/j.chroma.2015.03.080
7. Gagnon P, Nian R. Conformational plasticity of IgG during protein A affinity chromatography. *J Chromatogr A*. (2016) 1433:98–105. doi: 10.1016/j.chroma.2016.01.022
8. Latypov RF, Hogan S, Lau H, Gadgil H, Liu D. Elucidation of acid-induced unfolding and aggregation of human immunoglobulin IgG1 and IgG2 Fc. *J Biol Chem*. (2012) 287:1381–96. doi: 10.1074/jbc.M111.297697
9. Liu B, Guo H, Xu J, Qin T, Xu L, Zhang J, et al. Acid-induced aggregation propensity of nivolumab is dependent on the Fc. *Mabs*. (2016) 8:1107–1117. doi: 10.1080/19420862.2016.1197443

10. McMahon MJ, O'Kennedy R. Polyreactivity as an acquired artefact, rather than a physiologic property, of antibodies: evidence that monoreactive antibodies may gain the ability to bind to multiple antigens after exposure to low pH. *J Immunol Methods*. (2000) 241:1–10. doi: 10.1016/S0022-1759(00)00196-4
11. Djoumierska-Alexieva IK, Dimitrov JD, Nacheva J, Kaveri SV, Vassilev TL. Protein destabilizing agents induce polyreactivity and enhanced immunomodulatory activity in IVIg preparations. *Autoimmunity*. (2009) 42:365–7. doi: 10.1080/08916930902832181
12. Woof JM, Burton DR. Human antibody–Fc receptor interactions illuminated by crystal structures. *Nat Rev Immunol*. (2004) 4:89. doi: 10.1038/nri1266
13. Hogarth PM, Pietersz GA. Fc receptor-targeted therapies for the treatment of inflammation, cancer and beyond. *Nat Rev Drug Discov*. (2012) 11:311–31. doi: 10.1038/nrd2909
14. Kristensen AB, Lay WN, Ana-Sosa-Batiz F, Vandervan HA, Madhavi V, Laurie KL, et al. Antibody responses with Fc-mediated functions after vaccination of HIV-infected subjects with trivalent influenza vaccine. *J Virol*. (2016) 90:5724–34. doi: 10.1128/JVI.00285-16
15. Wines BD, Vandervan HA, Esparon SE, Kristensen AB, Kent SJ, Hogarth PM. Dimeric FcγR ectodomains as probes of the Fc receptor function of anti-influenza virus IgG. *J Immunol*. (2016) 197:1507–16. doi: 10.4049/jimmunol.1502551
16. Mclean MR, Madhavi V, Wines BD, Hogarth PM, Chung AW, Kent SJ. Dimeric Fcγ receptor enzyme-linked immunosorbent assay to study HIV-specific antibodies: a new look into breadth of Fcγ receptor antibodies induced by the RV144 vaccine trial. *J Immunol*. (2017) 199:816–26. doi: 10.4049/jimmunol.1602161
17. Ackerman ME, Moldt B, Wyatt RT, Dugast A-S, McAndrew E, Tsoukas S, et al. A robust, high-throughput assay to determine the phagocytic activity of clinical antibody samples. *J Immunol Methods*. (2011) 366:8–19. doi: 10.1016/j.jim.2010.12.016
18. Hughes CS, Foehr S, Garfield DA, Furlong EE, Steinmetz LM, Krijgsvelde J. Ultrasensitive proteome analysis using paramagnetic bead technology. *Mol Syst Biol*. (2014) 10:757. doi: 10.15252/msb.20145625
19. Hughes CS, Moggridge S, Müller T, Sorensen PH, Morin GB, Krijgsvelde J. Single-pot, solid-phase-enhanced sample preparation for proteomics experiments. *Nat Protoc*. (2019) 14:68. doi: 10.1038/s41596-018-0082-x
20. Rappsilber J, Mann M, Ishihama Y. Protocol for micro-purification, enrichment, pre-fractionation and storage of peptides for proteomics using StageTips. *Nat Protoc*. (2007) 2:1896. doi: 10.1038/nprot.2007.261
21. Cox J, Mann M. MaxQuant enables high peptide identification rates, individualized ppb-range mass accuracies and proteome-wide protein quantification. *Nat Biotechnol*. (2008) 26:1367. doi: 10.1038/nbt.1511
22. Schwanhäusser B, Busse D, Li N, Dittmar G, Schuchhardt J, Wolf J, et al. Global quantification of mammalian gene expression control. *Nature*. (2011) 473:337. doi: 10.1038/nature10098
23. Bern M, Kil YJ, Becker C. Byonic: advanced peptide and protein identification software. *Curr Protoc Bioinformatics*. (2012) Chapter 13:Unit13.20. doi: 10.1002/0471250953.bi1320s40
24. Lee LY, Moh ES, Parker BL, Bern M, Packer NH, Thaysen-Andersen M. Toward automated N-glycopeptide identification in glycoproteomics. *J Proteome Res*. (2016) 15:3904–15. doi: 10.1021/acs.jproteome.6b00438
25. Zauner G, Selman MH, Bondt A, Rombouts Y, Blank D, Deelder AM, et al. Glycoproteomic analysis of antibodies. *Mol Cell Proteomics*. (2013) 12:856–65. doi: 10.1074/mcp.R112.026005
26. Ostreiko K, Tumanova I, Sykulev YK. Production and characterization of heat-aggregated IgG complexes with pre-determined molecular masses: light-scattering study. *Immunol Lett*. (1987) 15:311–6. doi: 10.1016/0165-2478(87)90134-9
27. Oshinbolu S, Shah R, Finka G, Molloy M, Uden M, Bracewell DG. Evaluation of fluorescent dyes to measure protein aggregation within mammalian cell culture supernatants. *J Chem Technol Biotechnol*. (2018) 93:909–17. doi: 10.1002/jctb.5519
28. Shen D, Banks P. A Novel Protein Aggregation Assay for Biologics Formulation Studies and Production QA/QC. BioTek Instruments, Inc. Available online at: http://wolfson.huji.ac.il/purification/PDF/Protein_Refolding/BioTek_ProtoStatAggregMethod.pdf
29. Bruhns P, Iannascoli B, England P, Mancardi DA, Fernandez N, Jorieux S, et al. Specificity and affinity of human Fcγ receptors and their polymorphic variants for human IgG subclasses. *Blood*. (2009) 113:3716–25. doi: 10.1182/blood-2008-09-179754
30. Chung AW, Ghebremichael M, Robinson H, Brown E, Choi I, Lane S, et al. Polyfunctional Fc-effector profiles mediated by IgG subclass selection distinguish RV144 and VAX003 vaccines. *Sci Transl Med*. (2014) 6:228ra238. doi: 10.1126/scitranslmed.3007736
31. Damelang T, Rogerson SJ, Kent SJ, Chung AW. Role of IgG3 in infectious diseases. *Trends Immunol*. (2019) 40:197–211. doi: 10.1016/j.it.2019.01.005
32. Lu LL, Chung AW, Rosebrock TR, Ghebremichael M, Yu WH, Grace PS, et al. A functional role for antibodies in tuberculosis. *Cell*. (2016) 167:433–43. e414. doi: 10.1016/j.cell.2016.08.072
33. Vandervan HA, Jegaskanda S, Wines BD, Hogarth PM, Carmuglia S, Rockman S, et al. Antibody-dependent cellular cytotoxicity responses to seasonal influenza vaccination in older adults. *J Infect Dis*. (2017) 217:12–23. doi: 10.1093/infdis/jix554
34. Teo A, Feng G, Brown GV, Beeson JG, Rogerson SJ. Functional antibodies and protection against blood-stage malaria. *Trends Parasitol*. (2016) 32:887–98. doi: 10.1016/j.pt.2016.07.003
35. Chung AW, Alter G. Systems serology: profiling vaccine induced humoral immunity against HIV. *Retrovirology*. (2017) 14:57. doi: 10.1186/s12977-017-0380-3
36. Arnold KB, Chung AW. Prospects from systems serology research. *Immunology*. (2018) 153:279–89. doi: 10.1111/imm.12861
37. Huang Y, Ferrari G, Alter G, Forthal DN, Kappes JC, Lewis GK, et al. Diversity of antiviral IgG effector activities observed in HIV-infected and vaccinated subjects. *J Immunol*. (2016) 197:4603–12. doi: 10.4049/jimmunol.1601197
38. Wines BD, Billings H, Mclean MR, Kent SJ, Hogarth PM. Antibody functional assays as measures of Fc receptor-mediated immunity to HIV - new technologies and their impact on the HIV vaccine field. *Curr HIV Res*. (2017) 15:202–15. doi: 10.2174/1570162X15666170320112247
39. Lewis GK, Ackerman ME, Scarlatti G, Moog C, Robert-Guroff M, Kent S, et al. Knowns and unknowns of assaying antibody-dependent cell-mediated cytotoxicity against HIV-1. *Front Immunol*. (2019) 10:1025. doi: 10.3389/fimmu.2019.01025
40. Filipe V, Kükrer B, Hawe A, Jiskoot W. Transient molten globules and metastable aggregates induced by brief exposure of a monoclonal IgG to low pH. *J Pharm Sci*. (2012) 101:2327–39. doi: 10.1002/jps.23157
41. Dorion-Thibaudeau J, Raymond C, Lattová E, Perreault H, Durocher Y, and De Crescenzo G. Towards the development of a surface plasmon resonance assay to evaluate the glycosylation pattern of monoclonal antibodies using the extracellular domains of CD16a and CD64. *J Immunol Methods*. (2014) 408:24–34. doi: 10.1016/j.jim.2014.04.010
42. Geuijen KPM, Oppers-Tiemenis C, Egging DF, Simons PJ, Boon L, Schasfoort RBM, et al. Rapid screening of IgG quality attributes - effects on Fc receptor binding. *FEBS Open Bio*. (2017) 7:1557–74. doi: 10.1002/2211-5463.12283
43. Luo Y, Lu Z, Raso SW, Entrican C, Tangarone B. Dimers and multimers of monoclonal IgG1 exhibit higher *in vitro* binding affinities to Fcγ receptors. *MAbs*. (2009) 1:491–504. doi: 10.4161/mabs.1.5.9631
44. Abaturon L, Nezlin R, Vengerova T, Varshavsky JM. Conformational studies of immunoglobulin G and its subunits by the methods of hydrogen deuterium exchange and infrared spectroscopy. *Biochim Biophys Acta*. (1969) 194:386–96. doi: 10.1016/0005-2795(69)90099-3
45. Hill R. Quenching of tryptophan fluorescence in rabbit and bovine IgG. *Eur J Immunol*. (1973) 3:330–4. doi: 10.1002/eji.1830030603
46. Jefferis R, Pound J, Lund J, Goodall M. Effector mechanisms activated by human IgG subclass antibodies: clinical and molecular aspects. Review article. *Ann Biol Clin*. (1994) 52:57–65.
47. Franey H, Brych SR, Kolvenbach CG, Rajan RS. Increased aggregation propensity of IgG2 subclass over IgG1: role of conformational changes and covalent character in isolated aggregates. *Protein Sci*. (2010) 19:1601–15. doi: 10.1002/pro.434
48. Chung AW, Crispin M, Pritchard L, Robinson H, Gorny MK, Yu X, et al. Identification of antibody glycosylation structures that predict monoclonal antibody Fc-effector function. *AIDS*. (2014) 28:2523. doi: 10.1097/QAD.0000000000000444
49. Yang S, Zhang L, Thomas S, Hu Y, Li S, Cipollo J, et al. Modification of sialic acids on solid phase: accurate characterization of protein sialylation. *Anal Chem*. (2017) 89:6330–5. doi: 10.1021/acs.analchem.7b01048

50. Vázquez-Rey M, Lang DA. Aggregates in monoclonal antibody manufacturing processes. *Biotechnol Bioeng.* (2011) 108:1494–508. doi: 10.1002/bit.23155

Conflict of Interest: The authors declare that the research was conducted in the absence of any commercial or financial relationships that could be construed as a potential conflict of interest.

Copyright © 2019 Lopez, Scott, Wines, Hogarth, Wheatley, Kent and Chung. This is an open-access article distributed under the terms of the Creative Commons Attribution License (CC BY). The use, distribution or reproduction in other forums is permitted, provided the original author(s) and the copyright owner(s) are credited and that the original publication in this journal is cited, in accordance with accepted academic practice. No use, distribution or reproduction is permitted which does not comply with these terms.



Development of a Potent and Protective Germline-Like Antibody Lineage Against Zika Virus in a Convalescent Human

Fei Gao^{1†}, Xiaohu Lin^{2†}, Linling He², Ruoke Wang¹, Han Wang¹, Xuanling Shi¹, Fuchun Zhang³, Chibiao Yin³, Linqi Zhang^{1*}, Jiang Zhu^{2*} and Lei Yu^{3*}

¹ Department of Basic Medical Sciences, Comprehensive AIDS Research Center, Beijing Advanced Innovation Center for Structural Biology, School of Medicine, Tsinghua University, Beijing, China, ² Department of Integrative Structural and Computational Biology, Department of Immunology and Microbiology, The Scripps Research Institute, La Jolla, CA, United States, ³ Guangzhou Eighth People's Hospital, Guangzhou Medical University, Guangzhou, China

OPEN ACCESS

Edited by:

Sylvie Hermouet,
INSERM U1232 Centre de Recherche
en Cancérologie et Immunologie
Nantes Angers (CRCINA), France

Reviewed by:

Usha Nivarthi,
University of North Carolina at Chapel
Hill, United States
John Scribner Schieffelin,
Tulane University, United States

*Correspondence:

Linqi Zhang
zhanglinqi@mail.tsinghua.edu.cn
Jiang Zhu
jiang@scripps.edu
Lei Yu
leiyuforngs@126.com

[†]Co-first authors

Specialty section:

This article was submitted to
Viral Immunology,
a section of the journal
Frontiers in Immunology

Received: 14 June 2019

Accepted: 27 September 2019

Published: 24 October 2019

Citation:

Gao F, Lin X, He L, Wang R, Wang H,
Shi X, Zhang F, Yin C, Zhang L, Zhu J
and Yu L (2019) Development of a
Potent and Protective Germline-Like
Antibody Lineage Against Zika Virus in
a Convalescent Human.
Front. Immunol. 10:2424.
doi: 10.3389/fimmu.2019.02424

Zika virus (ZIKV) specific neutralizing antibodies hold great promise for antibody-based interventions and vaccine design against ZIKV infection. However, their development in infected patients remains unclear. Here, we applied next-generation sequencing (NGS) to probe the dynamic development of a potent and protective ZIKV E DIII-specific antibody ZK2B10 isolated from a ZIKV convalescent individual. The unbiased repertoire analysis showed dramatic changes in the usage of antibody variable region germline genes. However, lineage tracing of ZK2B10 revealed limited somatic hypermutation and transient expansion during the 12 months following the onset of symptoms. The NGS-derived, germline-like ZK2B10 somatic variants neutralized ZIKV potently and protected mice from lethal challenge of ZIKV without detectable cross-reactivity with Dengue virus (DENV). Site-directed mutagenesis identified two residues within the λ chain, N31 and S91, that are essential to the functional maturation of ZK2B10. The repertoire and lineage features unveiled here will help elucidate the developmental process and protective potential of E DIII-directed antibodies against ZIKV infection.

Keywords: Zika virus infection, Guillain-Barré syndrome, microcephaly, neutralizing antibody, antibody repertoire, next-generation sequencing

INTRODUCTION

Zika virus (ZIKV), a member of the *Flavivirus* genus of the *Flaviviridae* family, is an emerging mosquito-borne pathogen. ZIKV is closely related to other flaviviruses such as dengue (DENV 1, 2, 3, and 4), yellow fever (YFV), West Nile (WNV), Japanese encephalitis (JEV), and tick-borne encephalitis (TBEV) viruses (1). Since ZIKV was first identified in 1947 among rhesus macaques in the Zika forest of Uganda, its new variants have become increasingly prevalent and have adapted to the human population as recent outbreaks spread across the Americas, Caribbean, and Southeast Asia (2–5). At the peak of the 2016 outbreak, several incidents of imported ZIKV infection were identified in mainland China (6). In contrast to previous epidemics, the recent ZIKV outbreak has been associated with severe neurological complications such as Guillain-Barré syndrome in adults and microcephaly in fetuses and newborns (7–10). Currently, no ZIKV-specific therapeutics or vaccines are available. The high prevalence of the vectors and the continuing evolution of viral species have raised serious concerns about public health and ZIKV-related disease control (11).

The surface envelope glycoprotein (E) of flaviviruses mediates entry and presents a potential target for neutralizing antibodies. Large numbers of E-targeting monoclonal antibodies (mAbs) have been identified with potent neutralizing activity and epitope specificity (12–29). Previously, we isolated and characterized a panel of E-targeting mAbs from plasma and memory B cells from sequential blood samples of a DENV-naïve ZIKV-infected convalescent patient (Pt1) who acquired ZIKV infection in Venezuela during the 2016 outbreak and then returned to China (6, 24). Among these mAbs, ZK2B10 showed the highest neutralizing potency against ZIKV without any detectable reactivity with DENV 1 or 2 (24). ZK2B10 also demonstrated remarkable prophylactic and therapeutic activities against lethal challenge in the mouse models of ZIKV infection and microcephaly (30). Crystal structure and cryo-EM analysis revealed that ZK2B10 recognizes the lateral ridge of E DIII and blocks infection by inhibiting membrane fusion after cellular attachment (31). Since ZK2B10 may serve as a promising candidate for antibody-based interventions, the ontogeny of ZK2B10 could provide insight into the protective antibody response during ZIKV infection in humans and inform rational vaccine design. Furthermore, diverse vaccine candidates have demonstrated their ability to protect against ZIKV challenge in mice or nonhuman primates (NHPs) and have been evaluated in preclinical and clinical studies (16, 32, 33). It is therefore imperative to investigate the dynamics and characteristics of the antibody repertoire during ZIKV infection longitudinally, which will shed light on the molecular requirements necessary for the development of an effective ZIKV vaccine.

In this study, we applied long-read next-generation sequencing (NGS) and an unbiased repertoire capture method to longitudinally analyze the B cell repertoire of Pt1 from the early acute phase to the late convalescent phase (34). We obtained tens of millions of antibody sequences from a total of seven sequential time points including Day 4, Day 15, Month 2, Month 3, Month 6, Month 10 and Month 12 after the onset of symptoms. We first performed NGS analysis of the antibody repertoire with a focus on germline gene usage, CDR3 loop length, and degree of somatic hypermutation (SHM). Our data revealed that the antibody repertoire profile during ZIKV infection consisted of diverse germline gene usage combined with a steady distribution of CDR3 loops, in contrast to chronic HIV-1 infection, which often exhibits unusual repertoire profiles characteristic of high degree of SHM, skewed germline gene usage, and long HCDR3 loops (34, 35). The emergence of germline-like antibodies was observed at Day 15 after the onset of symptoms. We then traced the antibody lineage of ZK2B10 within the NGS-derived repertoire and investigated its maturation pathway. Our results show that ZK2B10 was generated with relatively low titers along with other germline-like antibodies at Day 15. Somatic variants of ZK2B10 were synthesized for functional characterization both *in vitro* and *in vivo*. Germline-like ZK2B10 heavy chain variants demonstrated strong neutralizing activity and protection against lethal ZIKV challenge in a mouse model. Of note, two substitutions occurred at positions N31 on LCDR1 and S91 on LCDR3 of λ -light chain were found to be critical for the functional maturation of ZK2B10. In summary, our repertoire

and lineage analyses elucidated the maturation pathway of a potentially neutralizing antibody, ZK2B10, and suggested that germline-like antibodies may play an important role in protective immunity against ZIKV infection.

MATERIALS AND METHODS

Donor and PBMCs Samples

The blood samples were donated by a 28-year-old Chinese ZIKV convalescent male patient (Pt1) who traveled from Venezuela to the southern metropolitan city Guangzhou, China, in February, 2016 (6). During his hospitalization and follow-up visits, a total of 7 sequential blood samples were collected at Day 4, Day 15, Month 2, Month 3, Month 6, Month 10, and Month 12 after the onset of symptoms. Samples were separated into plasma and peripheral blood mononuclear cells (PBMCs) by centrifugation through a Ficoll-Hypaque gradient (GE Healthcare). PBMCs were cryopreserved in freezing media and stored in liquid nitrogen until further analysis by antibody repertoire sequencing.

Sample Preparation Using 5'-RACE PCR

An improved version of the rapid amplification of cDNA 5'-ends (5'-RACE) polymerase chain reaction (PCR) protocol for sample preparation was reported in a recent study (34, 36). Here, total RNA was extracted from 1–5 million PBMCs into 30 ml of water with RNeasy Mini Kits (Qiagen, Valencia, CA). For unbiased repertoire analysis, 5'-RACE was performed with SMARTer RACE cDNA Amplification Kit (Clontech, Mountain View, CA). For ZK2B10 gene-specific lineage analysis, reverse transcription (RT) was performed with SuperScript III (Life Technologies) and oligo (dT). In both cases, the cDNA was purified and eluted in 20 μ l of elution buffer (NucleoSpin PCR Clean-up Kit, Clontech). The immunoglobulin PCRs were set up with Platinum Taq High-Fidelity DNA Polymerase (Life Technologies, Carlsbad, CA) in a total volume of 50 μ l, with 5 μ l of cDNA as template, 1 μ l of 5'-RACE primer or gene-specific forward primers, and 1 μ l of 10 μ M reverse primer. To facilitate deep sequencing on the Ion GeneStudio S5 system, the forward primers (both 5'-RACE and gene-specific) contained a P1 adaptor, while the reverse primer contained an A adaptor and an Ion Xpress™ barcode (Life Technologies) to differentiate the libraries from various time points. A total of 25 cycles of PCRs were performed and the PCR products (~600 bp for 5'-RACE PCR or ~500 bp for gene-specific PCR) were gel purified (Qiagen, Valencia, CA). A degenerate primer (SAGGTGCAGCTGGTGCAGTCTGG) was used as the forward gene-specific primer to cover potential variations at the 5'-end of ZK2B10 transcripts.

Next-Generation Sequencing (NGS) and Antibodyomics Analysis

Antibody NGS has been adapted to the Ion GeneStudio S5 system (35). Briefly, the antibody heavy and light (κ and λ) chain libraries were quantitated using Qubit® 2.0 Fluorometer with Qubit® dsDNA HS Assay Kits. Equal amounts of the heavy chain libraries from various time points were mixed and loaded onto an Ion 530 chip to increase the sequencing depth and to eliminate run-to-run variation. The κ and λ

chain libraries at each time point were mixed at a ratio of 1:1 prior to library pooling and chip loading. Template preparation and (Ion 530) chip loading was performed on the Ion Chef system using Ion 530 Ext Kits, followed by S5 sequencing with the default settings. Raw data was processed without 3'-end trimming in base calling to extend the read length. The human *Antibodyomics* pipeline version 1.0 (34, 36, 37) has been modified to improve data accuracy and computational efficiency (35). This new *Antibodyomics* pipeline was used to process and annotate Pt1 antibody NGS data for repertoire profiling and lineage tracing. The distributions of germline genes, germline divergence or degree of SHM, and CDR3 loop length derived from antibody NGS data as general repertoire profiles. The two-dimensional (2D) divergence/identity plots were constructed to visualize ZIKV-specific antibody lineages in the context of Pt1 antibody repertoire. A CDR3 identity of 95% was used as the cutoff for identifying sequences evolutionarily related to a reference antibody (shown as magenta dots on the 2D plots). The hierarchical clustering method was used to divide CDR3-defined somatic variants into groups based on an overall identity cutoff of 98% as previously described (34). In addition to the dominant sequences, a consensus or a manually selected sequence was used as the group representative for antibody synthesis and functional characterization. ZK2B10 were initially isolated from PBMCs of Pt1 as we previously reported (24).

Human Monoclonal Antibody (mAb) Clones Construction, Expression, and Purification

All of the synthetic variable region genes of antibody heavy chain (V_H) and light chain ($V_{K/L}$) were analyzed using the IMGT/V-Quest server (<http://www.imgt.org/IMGTindex/V-QUEST.php>). They were cloned into the backbone of antibody expression vectors containing the constant regions of human IgG1 as previously described (38). To produce full-length human mAbs, the recombinant clone was paired with the complementary chain of wild-type (WT) ZK2B10. The heavy and light chain expression plasmids were transiently co-transfected into HEK 293T cells for the production of full-length human IgGs, which were purified from the supernatant by affinity chromatography using protein A agarose (Thermo Scientific). The IgG concentration was determined using the BCA Protein Assay Kit (Thermo Scientific). We included previously reported MERS-CoV-specific mAb MERS-4 (38) for comparative analysis.

ZIKV E and ZIKV E DIII Protein and ELISA

The gene of either E protein or E DIII protein (residues 301–403) of ZIKV (GZ01, KU820898) without tag was cloned into pET28a vectors (Novagen) and expressed by IPTG-induction in BL21 (RIL) bacterial cells. The isolated inclusion bodies were solubilized and re-folded as reported (39). In the enzyme-linked immunosorbent assay (ELISA), the E proteins and E DIII proteins were captured separately onto ELISA plates overnight at 4°C. Each tested mAb was serially diluted and applied to the ZIKV E and E DIII protein-captured ELISA plates. Binding activities were detected using anti-human IgG labeled with HRP and TMB substrate.

Antibody Neutralization Assays

All ZIKV GZ01 (KU820898), ZIKV MR766 (AY632535), and DENV2 43 (AF204178) viruses were grown in C6/36 *Aedes Albopictus* cells and titrated on Vero cells before use. For neutralization assay, serial dilutions of mAbs were mixed with virus at 4°C for 1 h before being applied to Vero cells in the 6-well culture plates. After 1–2 h of infection, the antibody-virus mixture was aspirated and Vero cells were washed with PBS and overlaid with DMEM containing 2% heat-inactivated FBS and 1% SeaPlaque Agarose (Lonza, 50501). After 4–6 days, plaques were stained by 1% crystal violet and counted manually.

Antibody Prophylactic Potential Analysis in AG6 Mice

C57BL/6 mice deficient in interferon (IFN) α , β , and γ receptors (AG6 mice) were kindly provided by the Institute Pasteur of Shanghai, Chinese Academy of Sciences (IPS). The mice were bred and maintained in a pathogen-free animal facility. Groups of 4 sex-matched, 4- to 6-week-old AG6 mice were used for the animal studies. In prophylaxis assays, 300 μ g of each tested mAb or isotype control (MERS-4) was administered via the i.p. route. The following day, the animals were challenged with 10^4 PFUs of ZIKV (GZ01 strain) via i.p. injection. Survival was monitored for up to 14 days post challenge. At days 5 and 12 after challenge, whole blood was collected from each animal for ZIKV viral load measurement.

Quantitative Measurement of Viral Loads by TaqMan qPCR

Whole blood (10 μ L) was collected in an RNase free Eppendorf tube containing lysis buffer (QIAGEN) and stored at -80°C until use. Total RNA was extracted using RNeasy Mini Kits (74106, QIAGEN) and reverse-transcribed into cDNA using iScript cDNA Synthesis Kits (170-8890, Bio-Rad). Viral RNA copies were quantified through TaqMan qPCR amplification of ZIKV (GZ01) envelope gene. Measurements were expressed as \log_{10} viral RNA copies per millimeter calculated against a standard curve. Sequences for primers and probes were as follows: ZIKV-F CCGCTGCCCAACACAAG, ZIKV-R CCACTAACGTTCTTTTGCAGACAT, ZIKV-probe AGCCTA CCTTGACAAGCARTCAGACACTCAA (5'FAM, 3'TAMRA).

Multiple Sequence Alignment and Structural Analysis

Multiple sequence alignment (MSA) was calculated using BioEdit ClustalW. The crystal structure of ZIKV E DIII-ZK2B10 Fab complex has been determined and analyzed here to identify the 'hotspot' residues critical to ZK2B10 lineage development (31). For the intermolecular interactions shown in **Figure 5**, 4 Å was used as the maximal cut-off distance for hydrogen bonds. Illustrations of structural models were prepared using PyMOL Molecular Graphics System 1.5.0.4.

Statistical Methods

All data were analyzed using Prism6 software (GraphPad). The half-maximal effective concentrations (EC_{50}) were calculated using the dose-response stimulation model. The IC_{50} value for

each mAb was calculated using the dose-response inhibition model. For experiments involving AG6 mice, four animals were included in each assessment group to ensure equal representation and consistency of the data obtained. Statistical analysis was performed using Student's unpaired *t* test. Data were presented as mean \pm SEM. **p* < 0.05; ***p* < 0.01; and ****p* < 0.001.

Ethics Statement

The human study was approved by the Ethical Committee of the Guangzhou Eighth People's Hospital, Guangzhou Medical University. The research was conducted in strict accordance with the Chinese government rules and regulations for the protection of human subjects. The study subjects provided the written informed consents for research use of their blood samples. All procedures with animals were undertaken according to Experimental Animal Welfare and Ethics Committee of Tsinghua University. All experiments were performed under the guidelines of the Experimental Animal Welfare and Ethics Committee of Tsinghua University (16-ZLQ9).

RESULTS

Dynamic B Cell Repertoire Response Throughout ZIKV Infection

Next-generation sequencing (NGS) is a powerful tool for probing antibody response to natural infection and vaccination (40–42). Extensive studies of broadly neutralizing antibodies (bNAbs) and their lineage development using NGS have revealed the unexpected complexity and diversity of B cell repertoire in HIV-1-infected individuals during chronic infection (37, 43–45). Here, we performed a longitudinal NGS analysis of the antibody repertoire in Pt1 to delineate the dynamic B cell response to ZIKV infection following the procedure outlined in **Figure 1A**. We analyzed seven sequential time points from the acute phase (Day 4 and Day 15 after the onset of symptoms) to the convalescent phase (Month 2, 3, 6, 10, and 12 after the onset of symptoms). We combined 5'-RACE PCR and single reverse primers in template preparation to ensure the NGS in a long-read (600 bp) and unbiased manner as previously reported (**Figure S1**) (34, 36, 46–48). Deep sequencing yielded a total of 14.2 million heavy chains and 14.1 million light (κ and λ) chains in two separate NGS runs on the Ion S5 GeneStudio platform (**Table S1**). The *Antibodyomics* 2.0 pipeline was used to process, annotate, and analyze the NGS data, rendering 1.3 to 2.9 million reads per time point (**Table S1**) (35, 49). Of these sequences, 55.3 to 71.2% are high-quality, full-length antibody variable regions which were used for the in-depth analysis of B cell repertoire profiles (**Table S1**). Furthermore, we traced the lineage of ZK2B10 within the NGS-derived repertoire and synthesized representative somatic variants for functional characterization both *in vitro* and *in vivo* (**Figure 1A**).

Overall, Pt1 exhibited a diverse and dynamic distribution of germline gene usage (**Figure 1B**). A few germline genes are dominant in all seven time points such as IGHV1-69, IGKV3-20, and IGLV1-40 with an average of 15.21% or greater (**Figure 1B**, left). In contrast, some specific germline genes were observed with low frequency, such as IGHV1-8, the V_H

germline gene of ZK2B10, ranging from 0.98% to 4.80% in seven time points (**Figure 1B**, left). The V_L germline gene of ZK2B10, corresponding to IGLV1-47, ranged from 2.58 to 5.34% (**Figure 1B**, right). However, the low frequency of IGHV1-8 and IGLV1-47 was unexpected, suggesting that ZK2B10 did not represent a major B cell lineage in the repertoire spanning the acute and convalescent phases of ZIKV infection. In addition, there appeared to be no correlation between the potency of a ZIKV E-targeting mAb and its lineage expansion or prevalence, as indicated by the low frequency of the ZK2B10 germline gene family.

We then determined the degree of SHM, or germline divergence, at each time point from early acute phase to late convalescent phase. As shown in **Figure 1C**, there was a significant increase in the population of germline-like sequences at Day 15 for both heavy and light chains. As a result, the average SHM of heavy, κ and λ chain repertoires fell to 6.25, 5.92, and 5.91% at Day 15, respectively. Of note, the SHM decreased in most V gene families at Day 15, suggesting a repertoire-level response (**Figure S2**). As for the V_H germline gene of ZK2B10, IGHV1-8 showed only 6.45% SHM at Day 15 and varied between 7.23 and 13.60% at other time points (**Figure S2**, left). The V_L germline gene of ZK2B10, IGLV1-47, displayed 5.72% SHM at Day 15, and 6.70 to 9.04% at other time points studied (**Figure S2**, right). These results suggest a drastic shift in repertoire composition likely caused by a rapid plasmablast response during the acute phase of ZIKV infection. The emergence and development of ZK2B10 may serve as an example for this type of antibody response. These patterns are consistent with the fact that plasmablasts from ZIKV-infected, flavivirus-naïve individuals exhibited less somatic hypermutation or clonal expansion compared to those from ZIKV-infected, DENV-immune individuals, which may originate from common memory B cell clones (19, 50). Interestingly, similar patterns have also been reported for chronically infected HIV-1 patients in response to a rapidly evolving virus population (36).

Next, we determined the distribution of CDR3 loop length. Due to the diversity of the D gene, a rather dispersed distribution of HCDR3 loop length was observed as compared to a steady, canonical CDR3 loop length distribution obtained for κ and λ chains (**Figure 1D**). The HCDR3 loops were mainly distributed in the range of 9-aa to 15-aa (**Figure 1D**, left). As for the light chain, 9-aa KCDR3 loops accounted for 79.3 to 88.2% of the κ chain repertoire, while 9-aa to 11-aa LCDR3 loops accounted for 81.3 to 94.9% of the λ chain repertoire (**Figure 1D**, middle and right). Results from the case study of Pt1 have revealed unique features of human B cell repertoire during acute and transient ZIKV infection. Future studies with longitudinal samples from a larger cohort of infected donors would be needed to validate our findings.

ZK2B10 Lineage-Specific Antibody Response During ZIKV Infection

To probe the maturation pathway of ZK2B10, we traced the mAb lineage at each time point within the NGS-derived repertoire

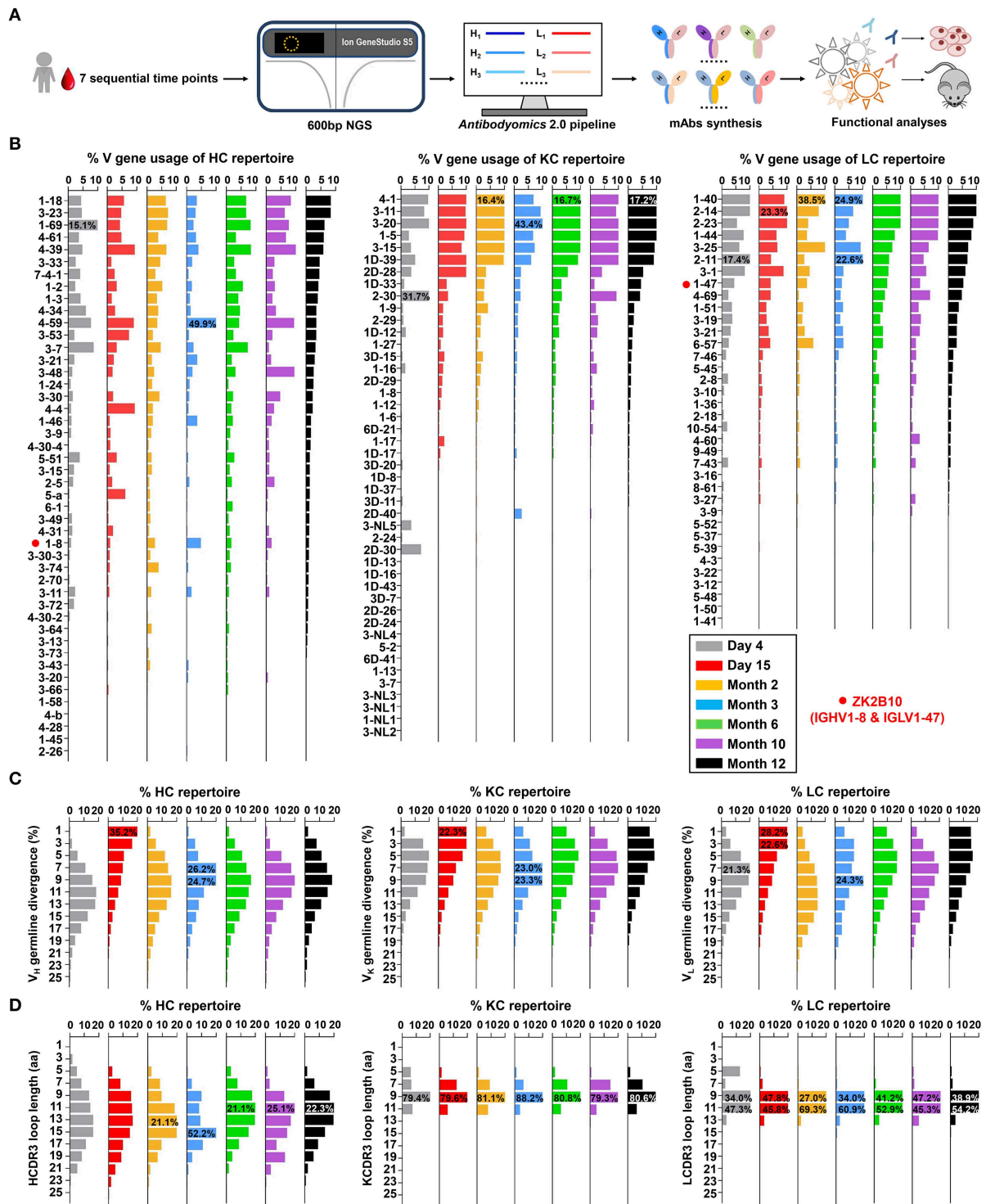


FIGURE 1 | Unbiased antibody repertoire profiles of donor Pt1 across ZIKV infection. **(A)** Schematic view of unbiased antibody repertoire analysis and ZK2B10 lineage tracing. PBMC samples from Pt1 were collected at 7 sequential time points after the onset of symptoms. 5'-RACE PCR was used to prepare antibody chain libraries for long-read (600 bp) next-generation sequencing (NGS) on the Ion GeneStudio S5 platform. The *Antibodyomics* 2.0 pipeline was used to process the NGS data for antibody repertoire profiling, while CDR3-based identification was used for ZK2B10 lineage tracing. Representative somatic variants were synthesized for functional characterization. **(B–D)** Distributions were plotted for **(B)** germline V gene usage, **(C)** germline divergence, and **(D)** CDR3 loop length for heavy chains (left panel), κ chains (middle panel), and λ chains (right panel). Color coding denotes the 7 sequential time points with Day 4 shown in gray, Day 15 in red, Month 2 in orange, Month 3 in sky blue, Month 6 in green, Month 10 in purple, and Month 12 in black. The germline V genes used by ZK2B10 (IGHV1-8 and IGLV1-47) are marked with red dots.

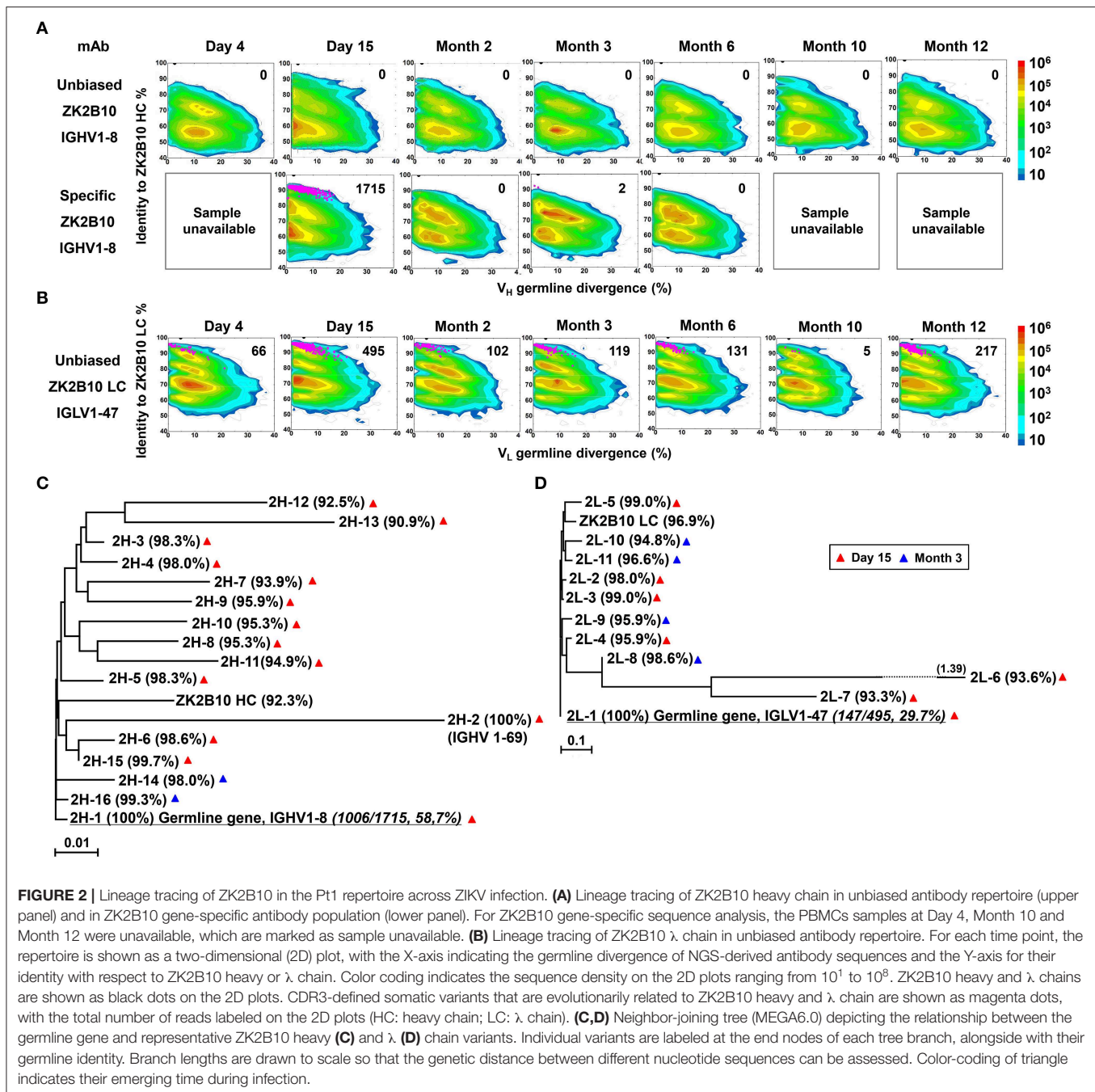


FIGURE 2 | Lineage tracing of ZK2B10 in the Pt1 repertoire across ZIKV infection. **(A)** Lineage tracing of ZK2B10 heavy chain in unbiased antibody repertoire (upper panel) and in ZK2B10 gene-specific antibody population (lower panel). For ZK2B10 gene-specific sequence analysis, the PBMCs samples at Day 4, Month 10 and Month 12 were unavailable, which are marked as sample unavailable. **(B)** Lineage tracing of ZK2B10 λ chain in unbiased antibody repertoire. For each time point, the repertoire is shown as a two-dimensional (2D) plot, with the X-axis indicating the germline divergence of NGS-derived antibody sequences and the Y-axis for their identity with respect to ZK2B10 heavy or λ chain. Color coding indicates the sequence density on the 2D plots ranging from 10^1 to 10^6 . ZK2B10 heavy and λ chains are shown as black dots on the 2D plots. CDR3-defined somatic variants that are evolutionarily related to ZK2B10 heavy and λ chain are shown as magenta dots, with the total number of reads labeled on the 2D plots (HC: heavy chain; LC: λ chain). **(C,D)** Neighbor-joining tree (MEGA6.0) depicting the relationship between the germline gene and representative ZK2B10 heavy **(C)** and λ **(D)** chain variants. Individual variants are labeled at the end nodes of each tree branch, alongside with their germline identity. Branch lengths are drawn to scale so that the genetic distance between different nucleotide sequences can be assessed. Color-coding of triangle indicates their emerging time during infection.

(Figures 2A,B). A CDR3 identity of 95% with respect to WT ZK2B10 heavy or λ chain was used as the cutoff for identifying sequences evolutionarily related to ZK2B10 (Figures 2A,B, shown as magenta dots on the 2D plots). As reported previously, WT ZK2B10 was derived from the memory B cells of Pt1 at Month 3 after the symptom onset (24). Unexpectedly, from the libraries of unbiasedly amplified germline gene families, we could not find any ZK2B10 heavy chain somatic variants in the repertoire at all seven time points, suggesting that the ZK2B10 lineage may have an extremely low frequency (Figure 2A, upper

panel). To gain more insight into the ZK2B10 lineage evolution, we performed an additional NGS experiment on four antibody libraries at Day 15, Months 2, 3, and 6, using a degenerate forward primer to target the ZK2B10 heavy chain and its putative germline gene, IGHV1-8 (Figure 2A, lower panel). Gene-specific NGS yielded 1715 ZK2B10-like heavy chains for Day 15 and only two for Month 3 (Figure 2A, lower panel). As for λ chain repertoire, ZK2B10 λ chain somatic variants were detectable at Day 4 but reached the peak at Day 15 with 495 identified variants, and persisted into Month 12 despite a noticeable decline

at Month 10 (**Figure 2B**). Of note, due to the lack of D gene segments, light chains do not possess unambiguous sequence signatures for CDR3-based lineage tracing. Nonetheless, our data suggests that ZK2B10 and its variants were induced rapidly and transiently at the end of acute phase during ZIKV infection. Interestingly, the majority of ZK2B10 somatic variants showed a germline divergence of <5.0% in both heavy and λ chain repertoires (**Figure 2A**, low panel and **Figure 2B**).

To further study the maturation pathway of ZK2B10, we selected representative somatic variants for antibody synthesis and functional characterization. A hierarchical clustering method was used for sequence selection, as previously described (34). In addition to the dominant sequences, a consensus selection was conducted based on the sequence characteristics to ensure broad coverage and representativeness (34). Of these, 16 representative heavy chains were selected with 14 from Day 15 and 2 from Month 3, and 11 representative λ chains with 7 from Day 15 and 4 from Month 3 (**Figures 2C,D**). These somatic variants were designated based on the order in which they were selected (e.g., 2H-1 is the 1st selected sequence of representative ZK2B10 heavy chain somatic variants). Surprisingly, 2H-1 and 2L-1 are 100% identical to their putative germline genes, corresponding to IGHV1-8 and IGLV1-47, with NGS read frequencies as high as 58.7% (1006/1715) and 29.7% (147/495), respectively (**Figures 2C,D**). Furthermore, all these ZK2B10 somatic variants showed a low degree of SHM: the average identity of representative heavy chains with respect to their putative germline gene, IGHV1-8, was 96.81%; as for λ chains, the average germline identity to IGLV1-47 was also as high as 96.79% (**Figures 2C,D**). Sequence alignment of variable regions of representative ZK2B10 somatic variants is shown in **Figure 3**. To summarize, the ZK2B10 antibody lineage represents a transient plasmablast response with a low degree of SHM at the end of acute phase of ZIKV infection.

Functional Characterization of ZK2B10 Somatic Variants

The representative ZK2B10 somatic variants were then synthesized and paired with their respective wild-type (WT) partner chains for full-length human IgG1 expression and functional characterization. Of the 16 synthesized ZK2B10 heavy chain somatic variants, 11 (2H-1, -2, -3, -4, -5, -6, -9, -10, -14, -15, and -16) could be expressed when paired with WT ZK2B10 λ chain (**Figure 4A**). We next measured their binding to E protein and E DIII of ZIKV by ELISA. Among the 11 mAbs, 8 (2H-1, -4, -5, -6, -9, -10, -15, and -16) demonstrated strong binding affinities for E and E DIII at a similar level to ZK2B10, with the half-maximal effective concentrations (EC_{50}) ranging from 3.4 to 11.2 ng/ml, while the remaining 3 mAbs (2H-2, -3, and -14) showed low affinities (**Figure 4A**). ZIKV E protein and E DIII were expressed in bacterial cells following the same procedure as previously described for the crystallographic analysis (31, 39). It must be noted that the affinity of a mAb may vary depending on the

expression system used to produce the antigen. Nonetheless, the affinity of WT ZK2B10 here ($EC_{50} = 3.3$ ng/ml) was comparable to that obtained using HEK293T-derived ZIKV E ($EC_{50} = 8.4$ ng/ml), confirming the antigen binding of ZK2B10 somatic variants (24). These mAbs were then employed in plaque reduction neutralization tests against two ZIKV strains, GZ01 (Asian) and MR766 (African), and DENV 2 (**Figure 4A**). Consistent with their binding affinities, the 8 strong binders (2H-1, -4, -5, -6, -9, -10, -15, and -16) neutralized GZ01 and MR766 potently (**Figure 4A**). The half-maximal inhibitory concentrations (IC_{50}) ranged from 14.1 to 82.4 ng/ml, which are comparable to WT ZK2B10 and other potent E-targeting mAbs isolated from ZIKV-infected, DENV-naïve human subjects (**Figure 4A**) (18, 20, 21, 24, 26). Not surprisingly, 2H-2 failed to show detectable potency ($IC_{50} > 500$ ng/ml) against both GZ01 and MR766, while 2H-3 exhibited only modest neutralizing activity ($IC_{50} = 289.4$ ng/ml to GZ01 and 334.1 ng/ml to MR766). Similarly, 2H-14 showed negligible or no neutralizing activity against the two ZIKV strains tested ($IC_{50} = 489.1$ ng/ml to GZ01 and $IC_{50} > 500$ ng/ml to MR766) (**Figure 4A**). All these mAbs showed no cross-neutralizing activity with DENV 2 (**Figure 4A**). Strikingly, with 100% identity to IGHV1-8, 2H-1 showed high affinity for full-length E and E DIII of ZIKV with EC_{50} values measured at 5.3 ng/ml and 3.4 ng/ml, respectively (**Figure 4A**). Consistently, 2H-1 also displayed potent neutralization against GZ01 and MR766, with IC_{50} values of 14.1 ng/ml and 19.4 ng/ml, respectively (b). Notably, 1006 out of 1715 (58.7%) ZK2B10-like heavy chains from Day 15 were identical to 2H-1, confirming that this germline-like mAb lineage emerged at the peak of plasmablast response. Based on the alignment with the IGHV1-8 germline sequence, the functional loss of 2H-2, -3, and -14 could potentially be explained by the mutation of D39 located toward the end of HCDR1 (**Figure 3A**). As for the 11 synthesized ZK2B10-like λ chains, 7 (2L-1, -2, -3, -6, -8, -9, and -11) were expressible when paired with WT ZK2B10 heavy chain. Of note, 5 of these 7 λ chain variants (2L-1, -3, -8, -9, and -11) failed to bind ZIKV E or E DIII and showed undetectable neutralization against ZIKV (**Figure 4B**). Among these λ chain variants, the sequence of 2L-1 is 100% identical to IGLV1-47 and represents a large portion of the Day 15 λ chains (147 out of 495, 29.7%) (**Figure 4B**). The reconstituted mAbs containing 2L-2 and 2L-6 demonstrated rather weak binding and neutralization compared to WT ZK2B10 (**Figure 4B**). These functional and repertoire observations, together with the sequence alignment, suggest that S31N on LCDR1 and A91S on LCDR3 could be critical for the maturation of ZK2B10 λ chain (**Figure 3B**).

Taken together, results from the functional characterization of ZK2B10 heavy chain somatic variants confirmed the hypothesis that this mAb lineage represents a transient yet effective naïve B cell response to ZIKV infection. The loss of function observed for most λ chain somatic variants, in which V_L was reverted to IGLV1-47, suggested that light chain maturation is crucial for the ZK2B10 lineage to acquire its potency and specificity, reminiscent of the HIV-1 bNAbs, VRC01 (36).

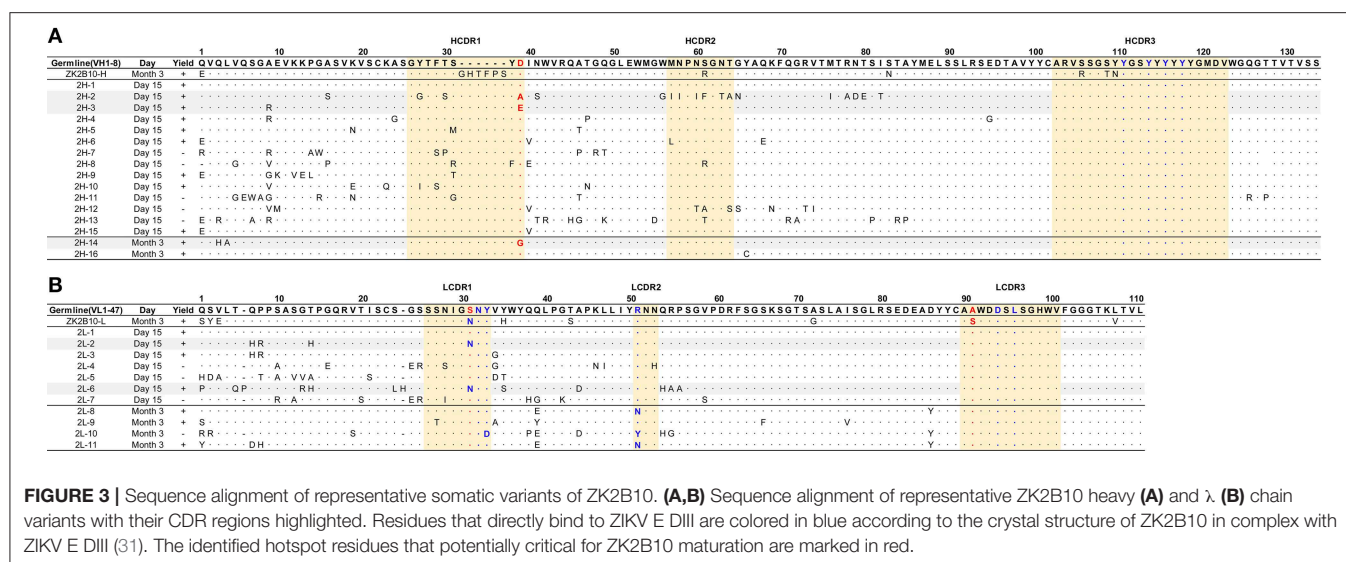


FIGURE 3 | Sequence alignment of representative somatic variants of ZK2B10. **(A,B)** Sequence alignment of representative ZK2B10 heavy **(A)** and λ **(B)** chain variants with their CDR regions highlighted. Residues that directly bind to ZIKV E DIII are colored in blue according to the crystal structure of ZK2B10 in complex with ZIKV E DIII (31). The identified hotspot residues that potentially critical for ZK2B10 maturation are marked in red.

Protective Potential of ZK2B10 Somatic Variants in a Mouse Model

Previously, we have demonstrated that ZK2B10 can protect mice from lethal ZIKV infection and microcephaly (24, 30). Conducting similar animal studies will not only confirm the accuracy of our repertoire analysis but also provide useful clues as to the functional diversity of the ZK2B10 lineage *in vivo*. To this end, we tested the *in vivo* protection of representative ZK2B10 somatic variants against ZIKV lethal infection in AG6 mice (C57BL/6 mice deficient in IFN α , β , and γ receptors) following the protocol outlined in **Figure 4C** (24, 30, 51, 52). Briefly, we administered 300 μ g of each ZK2B10-like mAb, ZK2B10 as positive control, or MERS-4 as negative control to groups of four AG6 mice, each 4–6 weeks in age, via the intraperitoneal (i.p.) route (Fig 4C) (38). On the following day, the animals were challenged with 10^4 plaque-forming units (PFUs) of ZIKV Asian strain GZ01 via the intraperitoneal (i.p.) route (**Figure 4C**). Animals were monitored for survival rate up to 14 days after ZIKV challenge, and for viral RNA level in the blood on days 5 and 12 post ZIKV challenge (**Figure 4C**). As expected, *in vivo* protection of mAbs was correlated with their *in vitro* neutralization, as previously reported (30). For example, the heavy chain variants with potent neutralizing activities *in vitro* (2H-1, -4, -6, -9, -10, -15, and -16) provided complete protection with a survival rate of 100% up to 14 days after ZIKV challenge (**Figure 4D**). The RNA load in these groups was suppressed in blood with distinguishable level from the MERS-4 group (**Figure 4F**). Conversely, 2H-2, -3, and -14 failed to offer any protection with a median survival time of 7.25 to 8 days after ZIKV challenge (**Figure 4D**). The viral RNA levels measured in mice treated by these variants were on average 3.72–4.45 log $_{10}$ greater than the ZK2B10 group at day 5 after ZIKV challenge (**Figure 4F**). In contrast, all λ chain variants demonstrated a consistent survival rate identical to that of the negative control MERS-4 and failed to suppress viral replication (**Figures 4E,G**). Therefore, *in vivo* evaluation of representative

ZK2B10 somatic variants confirmed the differential effect of heavy and λ -light chains on antibody function, consistent with the *in vitro* characterization by ELISA and neutralization assays.

Critical Residues for ZK2B10 Functional Maturation

To further investigate the maturation pathway of the ZK2B10 lineage, we performed reverse mutagenesis and structural analysis to identify “hotspot” residues. Initially, we aligned the amino acid sequences of representative ZK2B10 heavy and λ chain variants with their putative germline genes, IGHV1-8 and IGLV1-47, respectively (**Figure 3**). For heavy chain variants, 2H-2, 2H-3, and 2H-14 lost their potency to ZIKV both *in vitro* and *in vivo*. These 3 heavy chains possess a single substitution mutation at residue D39 with respect to their germline gene (**Figure 3A**). To assess whether this was the cause of the reduced potency, we conducted reverse mutagenesis on 2H-2 (A39D), 2H-3 (E39D), and 2H-14 (G39D) and characterized the function of these mutants by ELISA and neutralization assays. As shown in **Figure 5A**, 2H-3 (E39D), and 2H-14 (G39D) mutants regained their ZIKV E-binding and neutralizing activities, approaching the level of WT ZK2B10. Due to the use of a different V_H germline gene, IGHV1-69, the 2H-2 (A39D) mutant was ineffective (**Figure 5A**). This result suggested that the ZK2B10 lineage has a restricted V_H gene usage to achieve high affinity and potency against ZIKV. Based on the crystal structure of ZK2B10 in complex with ZIKV E DIII, four residues within the HCDR3 loop (Y111, Y114, Y116, and Y118) are directly involved in the contact interface (31). Although D39 is within the HCDR1 loop, it forms hydrogen bonds with Y115 and Y117 on the opposite side of the HCDR3 loop, thus stabilizing the HCDR3 conformation (**Figure 5C**). These results provide further evidence that the ZK2B10 lineage was indeed generated during the naïve B cell response to acute ZIKV infection, with critical residues encoded by the germline gene. For λ chain variants, two critical mutations were identified that potentially contribute

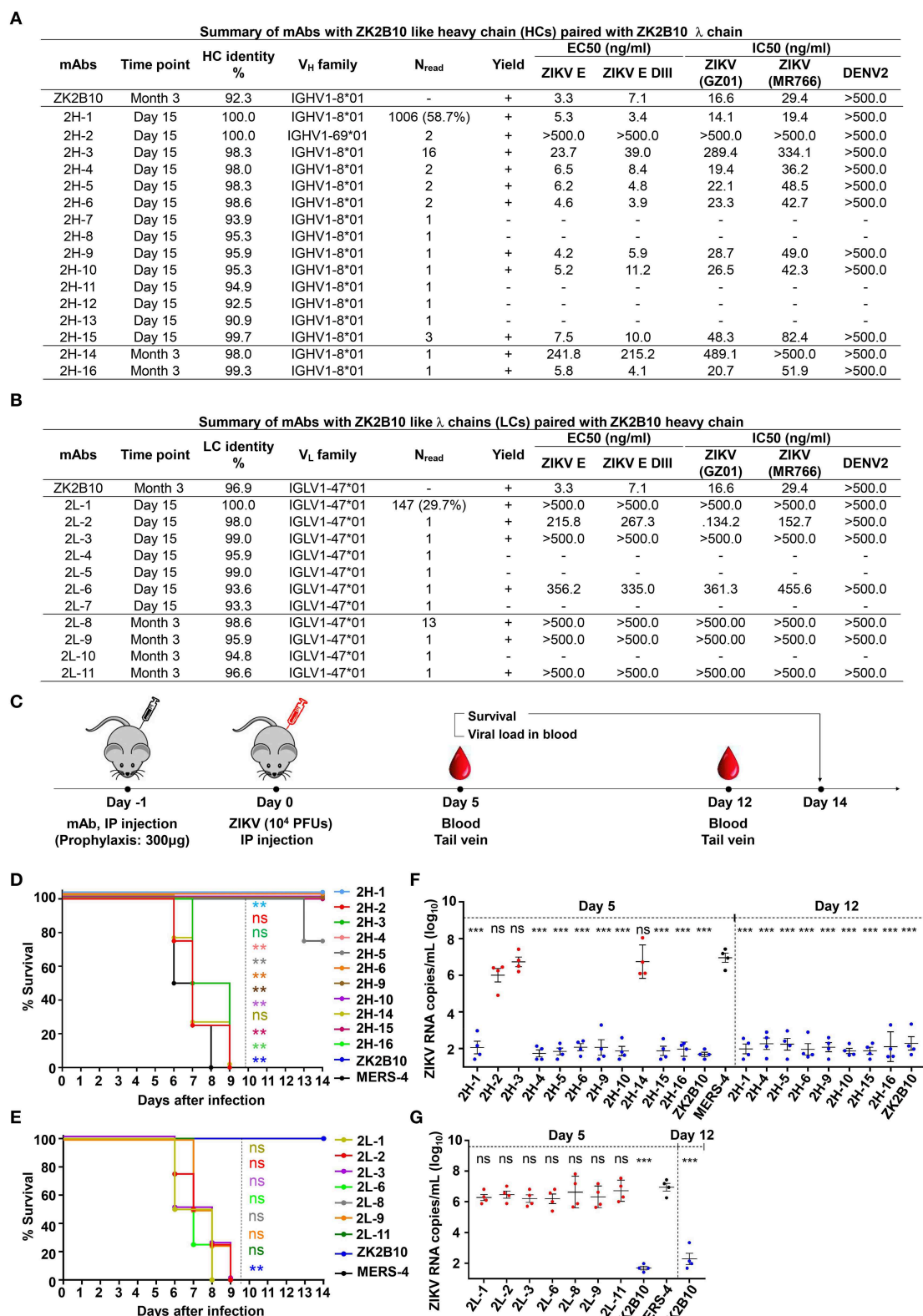


FIGURE 4 | Summary of somatic variants of the ZK2B10 antibody lineage. **(A,B)** ZK2B10 somatic variants are listed with the sampling time point, genetic characterization, sequencing read frequency (N_{read}), expression yield, and functional characterization. **(A)** 16 representative ZK2B10 heavy chain variants and **(B)** 11 (Continued)

FIGURE 4 | representative ZK2B10 λ chain variants identified from the Day 15 and Month 3 antibody repertoires. EC₅₀ represents the half-maximal effective concentrations for ELISA binding assays. IC₅₀ represents the half-maximal inhibitory concentrations for plaque neutralization assays. **(C–G)** Antibody protection against lethal ZIKV challenge in AG6 mice. Shown here: **(C)** timeline for mAb injection, ZIKV inoculation, and blood collection. The prophylactic potential of mAbs was assessed by monitoring survival rates for representative **(D)** heavy and **(E)** λ chain somatic variants of ZK2B10 up to 14 days post challenge, and ZIKV RNA copies in blood for **(F)** heavy and **(G)** λ chain somatic variants of ZK2B10 on 5 days and 12 days post challenge. Single measurement of ZIKV RNA copies in blood showed statistically significant difference among study groups, each containing four animals. All data are presented here as mean \pm SEM. * $p < 0.05$; ** $p < 0.01$; *** $p < 0.001$; ns, not significant.

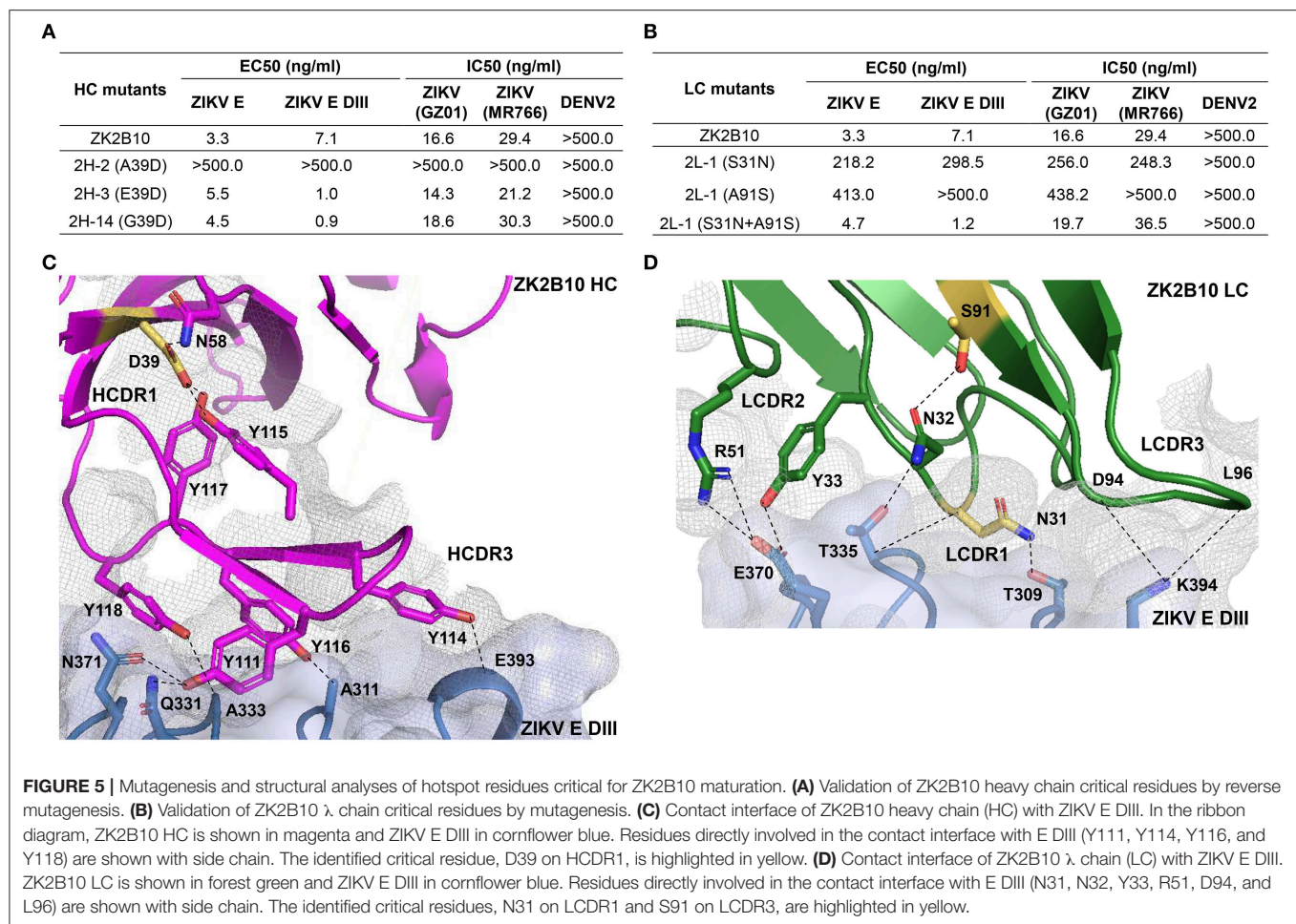
to the maturation of ZK2B10 lineage (**Figure 3B**). One such mutation, located on the LCDR1 loop, is N31, which is shared by two weakly functional variants, 2L-2 and 2L-6, as well as WT ZK2B10 λ chain (**Figure 3B**). The other mutation is at position 91 on LCDR3 loop, which is S91 in WT ZK2B10 λ chain but predominantly A91 in all weakly or non-functional λ chain variants (**Figure 3B**). Thus, N31 and S91 could potentially be the most critical mutations for ZK2B10 λ chain maturation. We first examined the effect of these two mutations individually by performing site-directed mutagenesis on 2L-1, which is 100% identical to germline gene IGLV1-47. Neither S31N nor A91S could render the germline antibody functional (**Figure 5B**). We then introduced a double mutation (S31N+A91S) into 2L-1, which, as expected, bound to ZIKV E and E DIII with high affinity and potently neutralized ZIKV at the same level of WT ZK2B10 (**Figure 5B**). As shown by the crystal structure, five residues within ZK2B10 λ chain (N31, N32, Y33, R51, D94, and L96) are directly involved in the contact interface (31). For the two NGS-identified hotspot residues, N31 directly interacts with T309 on ZIKV E DIII, while S91 forms a hydrogen bond with N32, which interacts with T335 on ZIKV E DIII (**Figure 5D**). In brief, our combined analysis of NGS data, antibody function, and complex structure confirms that residues N31 and S91 within the λ chain are essential to ZK2B10, thus representing a crucial event necessary for the functional maturation of this IGLV1-47-originated ZIKV E DIII-directed antibody lineage.

DISCUSSION

In this study, we delineated the B cell repertoire response of a ZIKV-infected individual (Pt1) during natural infection using an NGS-based approach. Future studies with sequential samples from more patients would be needed to validate and support our current findings. Our analysis showed an antibody repertoire profile with diverse germline usage, limited somatic hypermutation in variable genes, and steady CDR3 loop length. Tracing ZK2B10 in the NGS-derived antibody repertoire revealed the dynamics of an effective germline-encoded antibody lineage, which emerged prior to the convalescent phase of ZIKV infection. Germline-like somatic variants derived from the ZK2B10 lineage potently neutralized ZIKV and protected mice from lethal ZIKV challenge, while showing no cross-reactivity with DENV 2. We also demonstrated that two mutations, N31 and S91, within the germline-encoded λ -light chain are essential to the functional maturation of this IGHV1-8/IGLV1-47-encoded antibody lineage.

Two important aspects in this study are worth highlighting. One is the effective germline-encoded antibody response represented by the ZK2B10 lineage. We observed a significant increase in germline-like antibodies at Day 15 after the onset of symptoms. This drastic shift in repertoire composition was likely a result of rapid plasmablast response toward the end of the acute phase of ZIKV infection. Interestingly, this shift coincided with the emergence of the ZK2B10 lineage, which exemplifies the role of the germline-encoded antibody response during ZIKV infection. Similar patterns have been described in previous studies. For monoclonal antibodies, germline-like human mAbs m301 and m302 were reported that target ZIKV E DIII cryptic epitopes (C-C' loop) and neutralize ZIKV potently both *in vitro* and *in vivo* (22). Another human mAb, P1F12, originates from germline gene IGHV3-7 with an identity of 100% and neutralizes ZIKV potently as well (53). For the overall B cell response, plasmablast-derived antibodies from a ZIKV-infected, DENV-naïve donor showed low levels of SHM, supporting the mechanism of naïve B cell activation (19). Low levels of IgG SHM were also reported during acute DENV infection, which is consistent with an “innate-like” antiviral recognition mediated by B cells possessing antigen-specific naïve B cell receptors (54). Therefore, the induction of germline-encoded neutralizing antibodies is critical for effective protection against acute flavivirus infection. Diverse mechanisms of antibody lineage development have been found in chronic infections. During HIV-1 infection, rapidly emerged MPER-directed antibody lineages have been reported to achieve neutralizing breadth with low levels of SHM (55). In contrast, HIV-1 bNAbs VRC01 and PGT121, which target the CD4 binding site (CD4bs) and the V3 stem, respectively, require extensive mutation to achieve neutralizing breadth and potency (34, 36). In addition, long HCDR3 loops are required for bNAb PGT121 to penetrate the glycan shield of the envelope spike. In summary, our longitudinal analysis of Pt1 repertoire and ZK2B10 lineage development provides insight into the possible protective immunity against ZIKV infection. It must be noted that more ZIKV-infected donors need to be analyzed in future studies to confirm the B-cell repertoire dynamics in response to ZIKV infection observed for Pt1. However, longitudinal patient samples covering the entire course of infection are usually scarce due to the difficulties in early diagnosis and sample collection, posing a significant challenge for such studies.

The other important aspect of our study is its implication for rational design of a safe and effective ZIKV vaccine. As previously reported, ZK2B10 and other E DIII-specific mAbs, are ZIKV-specific, potently neutralizing, and can protect mice



from a lethal ZIKV challenge (18, 23, 24, 30). Structural studies revealed that ZK2B10 binds to the residues within the lateral ridge of DIII and blocks infection at a post-attachment step similar to other E DIII-specific potently neutralizing mAbs (31, 50). In addition, E DIII-specific antibodies are critical for controlling ZIKV as they correlate positively with high neutralization titers and their depletion results in reduced neutralizing activity in ZIKV-infected patient serum (24, 50). Our results indicate that only two mutations of the IGLV1-47 germline λ chain, N31 and S91, can sufficiently enable the IGHV1-8/IGLV1-47 germline antibodies to achieve potent ZIKV neutralization. Therefore, this barrier could be readily overcome by an antigen-activated B cell repertoire. The low degree of SHM observed for the ZK2B10 lineage suggests that elicitation of naïve protective B cell response against ZIKV may be achieved with a standard vaccination regimen. Furthermore, E DIII-based vaccine has been reported to avert lethal West Nile virus (WNV) infection without enhancing ZIKV or DENV infectivity (56). However, the low frequency and transient expansion of ZK2B10-like antibodies observed in the Pt1 repertoire suggest that overcoming the suboptimal immunogenicity of ZIKV E DIII, an elongated immunoglobulin-like domain, may prove to be a significant challenge for ZIKV vaccine development

(39, 57). While many E DIII-directed antibodies are potent neutralizers, antibodies targeting the quaternary epitopes have also been reported with exceptional neutralizing potency (13, 28, 58). Longitudinal analysis of such quaternary antibodies will provide valuable insight into the protective immunity against ZIKV infection and inform rational vaccine design, warranting further investigations.

DATA AVAILABILITY STATEMENT

The datasets analyzed in this manuscript are not publicly available. Requests to access the datasets should be directed to jiang@scripps.edu.

ETHICS STATEMENT

The studies involving human participants were reviewed and approved by Ethical Committee of the Guangzhou Eighth People's Hospital, Guangzhou Medical University. The patients/participants provided their written informed consent to participate in this study. The animal study was reviewed and approved by Experimental Animal Welfare and Ethics Committee of Tsinghua University.

AUTHOR CONTRIBUTIONS

Project design by FG, XL, LZ, JZ, and LY. Sample preparation by FG, XS, FZ, CY, and LZ. Library preparation and NGS by LH. Data processing and annotation by XL and JZ. Antibody lineage tracing by XL and JZ. Antibody sequence selection by FG, XL, and JZ. Antibody synthesis by FG, RW, and LZ. Antigen binding and neutralization assays by FG and LZ. ZIKV challenge and protection in mice by FG, HW, and LZ. Manuscript written by FG, LZ, JZ, and LY.

ACKNOWLEDGMENTS

We are grateful to the ZIKV convalescent patient for donating his blood samples from which mAbs were isolated and Drs. Jiang Wang, Wenxin Hong, and Lingzhai Zhao for providing the patient with treatment and care. We thank Drs. Cheng-Feng Qin and Gong Cheng for providing the Zika virus isolate GZ01 and MR766. We are also grateful for Institute

Pasteur of Shanghai, Chinese Academy of Sciences for kindly providing AG6 mice. This study was funded by the National Natural Science Foundation Award (81530065). The project was also supported by the National Science and Technology Major Projects (2017ZX10305501-003), the Special Program of Guangdong Provincial Department of Science and Technology (#2016A020248001), the Guangzhou Health Care and Cooperation Innovation Major grant (201704020229). The work related to the NGS analysis of Pt1 repertoire was funded in part by HIV Vaccine Research and Design (HIVRAD) program (P01 AI124337) (to JZ), and NIH Grants AI129698, AI140844, and AI123861 (to JZ).

SUPPLEMENTARY MATERIAL

The Supplementary Material for this article can be found online at: <https://www.frontiersin.org/articles/10.3389/fimmu.2019.02424/full#supplementary-material>

REFERENCES

- Miner JJ, Diamond MS. Zika virus pathogenesis and tissue tropism. *Cell Host Microbe*. (2017) 21:134. doi: 10.1016/j.chom.2017.01.004
- Dick GWA, Kitchen SE, Haddock AJ. Zika virus (I). isolations and serological specificity. *Trans R Soc Trop Med Hyg*. (1952) 46:509–20. doi: 10.1016/0035-9203(52)90042-4
- Petersen LR, Jamieson DJ, Powers AM, Honein MA. Zika virus. *N Engl J Med*. (2016) 374:1552–63. doi: 10.1056/NEJMra1602113
- Weaver SC, Costa F, Garcia-Blanco MA, Ko AI, Ribeiro GS, Saade G, et al. Zika virus: history, emergence, biology, and prospects for control. *Antiviral Res*. (2016) 130:69–80. doi: 10.1016/j.antiviral.2016.03.010
- Wikan N, Smith DR. Zika virus: history of a newly emerging arbovirus. *Lancet Infect Dis*. (2016) 16:e119–26. doi: 10.1016/S1473-3099(16)30010-X
- Zhang FC, Li XF, Deng YQ, Tong YG, Qin CF. Excretion of infectious Zika virus in urine. *Lancet Infect Dis*. (2016) 16:641–2. doi: 10.1016/S1473-3099(16)30070-6
- Brasil P, Jp P, Raja GC, Damasceno L, Wakimoto M, Ribeiro Nogueira RM, et al. Zika virus infection in pregnant women in Rio de Janeiro—preliminary report. *N Engl J Med*. (2016) 375:2321. doi: 10.1056/NEJMoa1602412
- França GVA, Schuler-Faccini L, Oliveira WK, Henriques CMP, Carmo EH, Pedi VD, et al. Congenital Zika virus syndrome in Brazil: a case series of the first 1501 livebirths with complete investigation. *Lancet*. (2016) 388:891–7. doi: 10.1016/S0140-6736(16)30902-3
- Rasmussen SA, Jamieson DJ, Honein MA, Petersen LR. Zika virus and birth defects—reviewing the evidence for causality. *N Engl J Med*. (2016) 374:1981–7. doi: 10.1056/NEJMSr1604338
- Oehler E, Watrin L, Larre P, Leparac-Goffart I, Lastère S, Valour F, et al. Zika virus infection complicated by Guillain-Barré syndrome – case report, French Polynesia, December 2013. *Eurosurveillance*. (2014) 19:20720. doi: 10.2807/1560-7917.ES2014.19.9.20720
- Lessler J, Chaisson LH, Kucirka LM, Bi Q, Grantz K, Salje H, et al. Assessing the global threat from Zika virus. *Science*. (2016) 353:aaf8160. doi: 10.1126/science.aaf8160
- Dowd KA, Pierson TC. Antibody-mediated neutralization of flaviviruses: a reductionist view. *Virology*. (2011) 411:306–15. doi: 10.1016/j.virol.2010.12.020
- Fernandez E, Dejnirattisai W, Cao B, Scheaffer SM, Supasa P, Wongwiwat W, et al. Human antibodies to the dengue virus E-dimer epitope have therapeutic activity against Zika virus infection. *Nat Immunol*. (2017) 18:1261. doi: 10.1038/ni.3849
- Heinz FX, Stiasny K. The antigenic structure of Zika virus and its relation to other flaviviruses: implications for infection and immunoprophylaxis. *Microbiol Mol Biol Rev*. (2017) 81:e00055–16. doi: 10.1128/MMBR.00055-16
- Magnani DM, Rogers TF, Beutler N, Ricciardi MJ, Bailey VK, Gonzalez-Nieto L, et al. Neutralizing human monoclonal antibodies prevent Zika virus infection in macaques. *Sci Transl Med*. (2017) 9:aan8184. doi: 10.1126/scitranslmed.aan8184
- Pierson TC, Graham BS. Zika virus: immunity and vaccine development. *Cell*. (2016) 167:625–31. doi: 10.1016/j.cell.2016.09.020
- Pierson TC, Diamond MS. Molecular mechanisms of antibody-mediated neutralisation of flavivirus infection. *Expert Rev Mol Med*. (2008) 10:e12. doi: 10.1017/S1462399408000665
- Robbiani DF, Bozzacco L, Keffe JR, Khouri R, Olsen PC, Gazumyan A, et al. Recurrent potent human neutralizing antibodies to Zika virus in Brazil and Mexico. *Cell*. (2017) 169:597–609. doi: 10.1016/j.cell.2017.04.024
- Rogers TF, Goodwin EC, Briney B, Sok D, Beutler N, Strubel A, et al. Zika virus activates de novo and cross-reactive memory B cell responses in dengue-experienced donors. *Sci Immunol*. (2017) 2:aan6809. doi: 10.1126/sciimmunol.aan6809
- Stettler K, Beltramello M, Espinosa DA, Graham V, Cassotta A, Bianchi S, et al. Specificity, cross-reactivity, and function of antibodies elicited by Zika virus infection. *Science*. (2016) 353:823–6. doi: 10.1126/science.aaf8505
- Wang Q, Yang H, Liu X, Dai L, Ma T, Qi J, et al. Molecular determinants of human neutralizing antibodies isolated from a patient infected with Zika virus. *Sci Transl Med*. (2016) 8:369ra179. doi: 10.1126/scitranslmed.aai8336
- Wu Y, Li S, Du L, Wang C, Peng Z, Hong B, et al. Neutralization of Zika virus by germline-like human monoclonal antibodies targeting cryptic epitopes on envelope domain III. *Emerg Microbes Infect*. (2017) 6:e89. doi: 10.1038/emi.2017.79
- Zhao H, Fernandez E, Dowd K, Speer S, Platt D, Gorman M, et al. Structural basis of Zika virus-specific antibody protection. *Cell*. (2016) 166:1016–27. doi: 10.1016/j.cell.2016.07.020
- Yu L, Wang R, Gao F, Li M, Liu J, Wang J, et al. Delineating antibody recognition against Zika virus during natural infection. *JCI Insight*. (2017) 2:93042. doi: 10.1172/jci.insight.93042
- Barba-Spaeth G, Dejnirattisai W, Rouvinski A, Vaney MC, Medits I, Sharma A, et al. Structural basis of potent Zika-dengue virus antibody cross-neutralization. *Nature*. (2016) 536:48. doi: 10.1038/nature18938
- Sappapapu G, Fernandez E, Kose N, Cao B, Fox JM, Bombardi RG, et al. Neutralizing human antibodies prevent Zika virus replication and fetal disease in mice. *Nature*. (2016) 540:443. doi: 10.1038/nature20564

27. Hasan SS, Miller A, Sapparapu G, Fernandez E, Klose T, Long F, et al. A human antibody against Zika virus crosslinks the E protein to prevent infection. *Nat Commun.* (2017) 8:14722. doi: 10.1038/ncomms14722
28. Rouvinski A, Guardado Calvo P, Barba Spaeth G, Duquerroy S, Vaney M-C, Kikutu CM, et al. Recognition determinants of broadly neutralizing human antibodies against dengue viruses. *Nature.* (2015) 520:109–13. doi: 10.1038/nature14130
29. Wanwisa D, Wiyada W, Sunpetchuda S, Xiaokang Z, Xinghong D, Alexander R, et al. A new class of highly potent, broadly neutralizing antibodies isolated from viremic patients infected with dengue virus. *Nat Immunol.* (2015) 16:170. doi: 10.1038/ni.3058
30. Li C, Gao F, Yu L, Wang R, Jiang Y, Shi X, et al. A single injection of human neutralizing antibody protects against Zika virus infection and microcephaly in developing mouse embryos. *Cell Rep.* (2018) 23:1424–34. doi: 10.1016/j.celrep.2018.04.005
31. Wang L, Wang R, Wang L, Ben H, Yu L, Gao F, et al. Structural basis for neutralization and protection by a Zika virus-specific human antibody. *Cell Rep.* (2019) 26:3360–8.e5. doi: 10.1016/j.celrep.2019.02.062
32. Abbink P, Stephenson KE, Barouch DH. Zika virus vaccines. *Nat Rev Microbiol.* (2018) 16:594–600. doi: 10.1038/s41579-018-0039-7
33. Abbasi J. Zika vaccine enters clinical trials. *JAMA.* (2016) 316:1249. doi: 10.1001/jama.2016.19328
34. He L, Sok D, Azadnia P, Hsueh J, Landais E, Simek M, et al. Toward a more accurate view of human B-cell repertoire by next-generation sequencing, unbiased repertoire capture and single-molecule barcoding. *Sci Rep.* (2014) 4:6778. doi: 10.1038/srep06778
35. He L, Lin X, De VN, Saye-Francisco KL, Mann CJ, Augst R, et al. Hidden lineage complexity of glycan-dependent HIV-1 broadly neutralizing antibodies uncovered by digital panning and native-like gp140 trimer. *Front Immunol.* (2017) 8:1025. doi: 10.3389/fimmu.2017.01025
36. Kong L, Ju B, Chen Y, He L, Ren L, Liu J, et al. Key gp120 glycans pose roadblocks to the rapid development of VRC01-class antibodies in an HIV-1-infected Chinese donor. *Immunity.* (2016) 44:939–50. doi: 10.1016/j.immuni.2016.03.006
37. Wu X, Zhou T, Zhu J, Zhang B, Georgiev I, Wang C, et al. Focused evolution of HIV-1 neutralizing antibodies revealed by structures and deep sequencing. *Science.* (2011) 333:1593–602. doi: 10.1126/science.1207532
38. Jiang L, Wang N, Zuo T, Shi X, Poon K-MV, Wu Y, et al. Potent neutralization of MERS-CoV by human neutralizing monoclonal antibodies to the viral spike glycoprotein. *Sci Transl Med.* (2014) 6:234ra59. doi: 10.1126/scitranslmed.3008140
39. Dai L, Song J, Lu X, Deng YQ, Musyoki AM, Cheng H, et al. Structures of the Zika virus envelope protein and its complex with a flavivirus broadly protective antibody. *Cell Host Microbe.* (2016) 19:696–704. doi: 10.1016/j.chom.2016.04.013
40. Koff WC, Burton DR, Johnson PR, Walker BD, King CR, Nabel GJ, et al. Accelerating next-generation vaccine development for global disease prevention. *Science.* (2013) 340:1232910. doi: 10.1126/science.1232910
41. Georgiou G, Ippolito GC, Beausang J, Busse CE, Wardemann H, Quake SR. The promise and challenge of high-throughput sequencing of the antibody repertoire. *Nat Biotechnol.* (2014) 32:158. doi: 10.1038/nbt.2782
42. Koff WC, Gust ID, Plotkin SA. Toward a human vaccines project. *Nat Immunol.* (2014) 15:589–92. doi: 10.1038/ni.2871
43. Wu X, Zhang Z, Schramm CA, Joyce MG, Kwon YD, Tongqing Z, et al. Maturation and diversity of the VRC01-antibody lineage over 15 years of chronic HIV-1 infection. *Cell.* (2015) 161:470–85. doi: 10.1016/j.cell.2015.03.004
44. Sok D, Pauthner M, Briney B, Lee JH, Saye-Francisco KL, Hsueh J, et al. A prominent site of antibody vulnerability on HIV envelope incorporates a motif associated with CCR5 binding and its camouflaging glycans. *Immunity.* (2016) 45:31–45. doi: 10.1016/j.immuni.2016.06.026
45. Zhu J, O'Dell S, Ofek G, Pancera M, Wu X, Zhang B, et al. Somatic populations of PGT135–137 HIV-1-neutralizing antibodies identified by 454 pyrosequencing and bioinformatics. *Front Microbiol.* (2012) 3:315. doi: 10.3389/fmicb.2012.00315
46. Dai K, He L, Khan SN, O'Dell S, McKee K, Tran K, et al. Rhesus macaque B-cell responses to an HIV-1 trimer vaccine revealed by unbiased longitudinal repertoire analysis. *mBio.* (2015) 6:e01375. doi: 10.1128/mBio.01375-15
47. Zhu J, Ofek G, Yang Y, Zhang B, Louder MK, Lu G, et al. Mining the antibodyome for HIV-1-neutralizing antibodies with next-generation sequencing and phylogenetic pairing of heavy/light chains. *Proc Natl Acad Sci USA.* (2013) 110:6470–5. doi: 10.1073/pnas.1219320110
48. Zhu J, Wu X, Zhang B, McKee K, O'Dell S, Soto C, et al. De novo identification of VRC01 class HIV-1-neutralizing antibodies by next-generation sequencing of B-cell transcripts. *Proc Natl Acad Sci USA.* (2013) 110:E4088–97. doi: 10.1073/pnas.1306262110
49. Tzarum N, Giang E, Kong L, He L, Prentoe J, Augestad E, et al. Genetic and structural insights into broad neutralization of hepatitis C virus by human VH1–69 antibodies. *Sci Adv.* (2019) 5:eav1882. doi: 10.1126/sciadv.aav1882
50. Pierson TC, Diamond MS. The emergence of Zika virus and its new clinical syndromes. *Nature.* (2018) 560:573–81. doi: 10.1038/s41586-018-0446-y
51. Orozco S, Schmid MA, Parameswaran P, Lachica R, Henn MR, Beatty R, et al. Characterization of a model of lethal dengue virus 2 infection in C57BL/6 mice deficient in the alpha/beta interferon receptor. *J Gen Virol.* (2012) 93:2152–7. doi: 10.1099/vir.0.045088-0
52. Liu J, Liu Y, Nie K, Du S, Qiu J, Pang X, et al. Flavivirus NS1 protein in infected host sera enhances viral acquisition by mosquitoes. *Nat Microbiol.* (2016) 1:16087. doi: 10.1038/nmicrobiol.2016.87
53. Magnani DM, Cgt S, Rosen BC, Ricciardi MJ, Pedreño-Lopez N, Gutman MJ, et al. A human inferred germline antibody binds to an immunodominant epitope and neutralizes Zika virus. *PLoS Negl Trop Dis.* (2017) 11:e0005655. doi: 10.1371/journal.pntd.0005655
54. Godoy-Lozano E, Téllez-Sosa J, Sánchez-González G, Sámano-Sánchez H, Aguilar-Salgado A, Salinas-Rodríguez A, et al. Lower IgG somatic hypermutation rates during acute dengue virus infection is compatible with a germinal center-independent B cell response. *Genome Med.* (2016) 8:23. doi: 10.1186/s13073-016-0276-1
55. Krebs SJ, Kwon YD, Schramm CA, Law WH, Donofrio G, Zhou KH, et al. Longitudinal analysis reveals early development of three MPER-directed neutralizing antibody lineages from an HIV-1-infected individual. *Immunity.* (2019) 50:677–91.e13. doi: 10.1016/j.immuni.2019.02.008
56. Lai H, Paul AM, Sun H, He J, Yang M, Bai F, et al. A plant-produced vaccine protects mice against lethal West Nile virus infection without enhancing Zika or dengue virus infectivity. *Vaccine.* (2018) 36:1846–52. doi: 10.1016/j.vaccine.2018.02.073
57. Sirohi D, Chen Z, Sun L, Klose T, Pierson TC, Rossmann MG, et al. The 3.8 Å resolution cryo-EM structure of Zika virus. *Science.* (2016) 352:467. doi: 10.1126/science.aaf5316
58. Abbink P, Larocca RA, Dejnirattisai W, Peterson R, Nkolola JP, Borducchi EN, et al. Therapeutic and protective efficacy of a dengue antibody against Zika infection in rhesus monkeys. *Nat Med.* (2018) 24:721–3. doi: 10.1038/s41591-018-0056-0

Conflict of Interest: The authors declare that the research was conducted in the absence of any commercial or financial relationships that could be construed as a potential conflict of interest.

Copyright © 2019 Gao, Lin, He, Wang, Wang, Shi, Zhang, Yin, Zhang, Zhu and Yu. This is an open-access article distributed under the terms of the Creative Commons Attribution License (CC BY). The use, distribution or reproduction in other forums is permitted, provided the original author(s) and the copyright owner(s) are credited and that the original publication in this journal is cited, in accordance with accepted academic practice. No use, distribution or reproduction is permitted which does not comply with these terms.



Anti-IL6 Autoantibodies in an Infant With CRP-Less Septic Shock

Marketa Bloomfield^{1,2*}, Zuzana Parackova^{1†}, Tamara Cabelova², Iva Pospisilova^{2,3}, Pavel Kabicek², Hana Houstkova² and Anna Sediva¹

¹ Department of Immunology, 2nd Faculty of Medicine, Charles University and Motol University Hospital, Prague, Czechia,

² Department of Pediatrics, 1st Faculty of Medicine, Thomayer's Hospital and Charles University, Prague, Czechia,

³ Department of Clinical Chemistry, 1st Faculty of Medicine, Thomayer's Hospital and Charles University, Prague, Czechia

OPEN ACCESS

Edited by:

Sylvie Hermouet,
INSERM U1232 Centre de Recherche
en Cancérologie et Immunologie
Nantes Angers (CRCINA), France

Reviewed by:

Toshio Tanaka,
Osaka University Hospital, Japan
Lawrence Albert Potempa,
Roosevelt University, United States

*Correspondence:

Marketa Bloomfield
marketa.bloomfield@fmotol.cz

[†]These authors have contributed
equally to this work

Specialty section:

This article was submitted to
Autoimmune and Autoinflammatory
Disorders,
a section of the journal
Frontiers in Immunology

Received: 16 August 2019

Accepted: 23 October 2019

Published: 08 November 2019

Citation:

Bloomfield M, Parackova Z,
Cabelova T, Pospisilova I, Kabicek P,
Houstkova H and Sediva A (2019)
Anti-IL6 Autoantibodies in an Infant
With CRP-Less Septic Shock.
Front. Immunol. 10:2629.
doi: 10.3389/fimmu.2019.02629

Background: Interleukin-6 (IL-6) is a pleiotropic cytokine with a multitude of pro-inflammatory effects. Serum C-reactive protein (CRP) is an acute phase protein induced mainly by IL-6 in response to inflammatory conditions, particularly infection. The biological functions of CRP include opsonisation, induction of phagocytosis, complement activation, or chemotaxis enhancement. Factors interfering with IL-6-mediated recruitment of innate immune responses, such as the presence of anti-IL6 antibodies, may therefore compromise the host resistance to microbial pathogens. This has major implications for the use of IL-6-targeting biologics, such as tocilizumab or sarilumab in rheumatologic, immune dysregulation diseases, and cancer.

Case presentation: 20-month-old Czech female developed severe septic shock with clinical and laboratory signs of systemic inflammation but no increase of CRP or IL-6. The offending pathogen was most likely *Staphylococcus aureus*, detected in a throat swab; the response to antibiotic treatment was prompt. A defect in the integrity of IL-6/CRP axis was suspected and verified by the detection of neutralizing IL-6 antibodies in the serum of the child.

Conclusion: We report a first case of systemic bacterial infection in a patient with anti-IL6 autoantibodies. Disturbed IL-6 signaling, whether iatrogenic by targeted IL-6 blockade or endogenous due to the presence of autoantibodies against IL-6, represents a risk factor for increased infectious susceptibility. Patients with severe bacterial infection without elevation of CRP should be examined for the presence of anti-IL6 autoantibodies.

Keywords: interleukin 6, C-reactive protein, anti-IL6 autoantibodies, tocilizumab, siltuximab, sarilumab

BACKGROUND

Interleukin 6 (IL-6), originally described as B-cell stimulatory factor in 1985, is now known as a pleiotropic cytokine with multitude of key biological functions, including inflammatory and immune responses, hematopoiesis, and oncogenesis. It is transiently produced by immune cells, such as monocytes and macrophages, but also by other cell lineages upon various stimuli, e.g. infection or tissue injury (1). IL-6 binds to its receptor, which exists in two forms; a membrane-bound protein or a soluble form. In short, upon IL-6 binding the downstream signaling molecules Janus kinases (JAKs) recruit either signal transducer and activator of transcription 3 (STAT3) or mitogen-activated protein kinases (MAPKs) via receptor-associated molecule gp130. This initiates the transcription of IL-6-inducible genes (2) and results, inter alia, in the production of proteins such as C-reactive protein (CRP), fibrinogen and serum amyloid A.

CRP is an acute phase reactant produced by hepatocyte-derived IL-6-dependent biosynthesis in inflammatory conditions, particularly in response to infection. Its biologic functions are promotion of innate immune processes, including opsonisation, complement activation, induction of release of pro-inflammatory cytokines or promotion of phagocytosis and chemotaxis (3). CRP serum levels begin to rise by 6 hours and peak within 2–3 days from induction (4).

Procalcitonin (PCT) is produced in health in thyroid cells and immediately converted to the hormone calcitonin. On the other hand, the inflammatory PCT is released mainly by adipocytes and white blood cells, triggered by various microbial peptides or inflammatory mediators such as IL-6 or tumor necrosis factor- α (TNF α). PCT is utilized as a diagnostically accurate tool for bacterial infection and a useful discriminator of sepsis. Its levels increase more rapidly than CRP, between 2 and 6 hours and peak within 6–24 hours during infection (5).

Sepsis is defined as systemic inflammatory response to infection (6) or, more recently, as life-threatening organ dysfunction caused by a dysregulated host response to infection (7). Septic shock is clinically identified as sepsis with cardiovascular dysfunction (6). During sepsis, an array of cytokines and chemokines is produced, such as interleukin 1 β (IL-1 β), IL-6, TNF- α , or soluble CD14 (5). Currently, IL-6, CRP and PCT are the most commonly used biomarkers of sepsis, which severity and outcome prediction capacity is of high clinical research interest.

Given the role of IL-6 in immune responses, an enhanced infectious susceptibility is a rational concern in any therapeutic strategy targeting IL-6 signaling, e.g. IL-6 receptor (IL6R) (tocilizumab, sarilumab) or IL-6 (siltuximab), increasingly utilized in treatment of rheumatoid arthritis (RA), juvenile idiopathic arthritis (JIA), or Castleman's disease (8).

To date, three patients only were reported to suffer severe bacterial infections while having detectable neutralizing antibodies to IL-6 and impaired acute phase response (9, 10). The hereby-presented case describes the fourth such patient, who is also the first to present with severe systemic inflammatory response.

CASE PRESENTATION

Clinical Vignette

A Czech female was born in 36th gestational week to a mother with history of intravenous methylamphetamine abuse during

pregnancy. She suffered severe perinatal asphyxia and multiple ileal perforations requiring a stoma, which was closed at 4 months. At the age of 5 months, she suffered another ileal perforation, during which an increase of CRP (86,7 mg/L) and leucocytosis ($19,7 \times 10^9/L$) were noted. The subsequent infectious susceptibility was inconspicuous; she thrived relatively well, received hexavalent combined vaccine (diphtheria, tetanus, pertussis, poliomyelitis, *Haemophilus influenzae type B*, and hepatitis B) and developed within the neurologic limitations of her perinatal insult. At the age of 20 months, she suffered a short paroxysm of generalized seizures in a second day of fevers of 38, 0–38, 5°C. Upon admission, she presented with dehydration, circulatory instability with hypotension, tachycardia, tachypnea, and anuria. Her laboratory workup showed mild leukopenia $5.8 \times 10^9/L$ (ref. range 6.0–17.5), thrombocytopenia $64 \times 10^9/L$ (ref. range 150–450), severe electrolyte imbalance, increased renal parameters (creatinin 132 $\mu\text{mol/L}$, ref. range 8–45; urea 25 mmol/L, ref. range 3.2–9.0), signs of rhabdomyolysis (increased aspartate aminotransferase, serum creatine kinase, myoglobin) and elevated D-dimers, activated partial thromboplastin time but unincreased fibrinogen 2.82 g/L (ref. range 1.45–3.48). An extreme elevation of PCT 378.0 $\mu\text{g/L}$ (electrochemiluminescence, ref. range 0.0–0.5) but, curiously, no increase of CRP 2.9 mg/L (immunoturbidimetry, ref. range 0.0–5.0) or IL-6 16.2 ng/L (electrochemiluminescence, ref. range 0.0–20.0) were noted. *Staphylococcus aureus* was cultured from throat swabs, other microbiologic investigations were negative, including blood cultures. She was diagnosed with septic shock, required massive intravenous volume expansion and received 10 days of antibiotic treatment (third generation cephalosporin and gentamicin) that controlled the infection and the laboratory parameters normalized. During the following 6 months, she experienced no other infections.

The patient's basic immune profiling suggested no gross abnormality (Table 1). However, intrigued by the peculiar dynamics of the inflammatory markers during sepsis, especially the lack of IL-6 and CRP response along the high PCT elevation (Figure 1A), we prompted investigation of the integrity of IL-6 signaling axis, which we tested in the following steps.

The Ability to Synthesize IL-6 by Patient's CD14⁺ Monocytes Is Normal

In order to establish a normal cellular ability to produce IL-6, patient's whole blood was stimulated with lipopolysaccharide (LPS) in presence of Brefeldin A. Flow cytometric trace of IL-6 (Figure 1B), IL-1 β and TNF α (Supplementary Figure 1) in CD14⁺ monocytes was analyzed. We observed an increased unstimulated production of IL-6 and IL-1 β in the time of sepsis, which further increased after LPS stimulation, demonstrating an unskewed ability to synthesize these cytokines. The production of TNF α was similar to healthy controls.

The Ability to Release IL-6 Into Extracellular Space by Patient's Cells Is Normal

Having established a normal intracellular IL-6 synthesis, we sought to determine the patient's cells ability to release the

Abbreviations: Abs, antibodies; AD HIES, autosomal dominant HyperIgE syndrome; Anti-IL6 abs, antibodies against interleukin 6; Anti-IL6 autoAbs, autoantibodies against interleukin 6; CM, complete medium; CRP, C reactive protein; DOCK8, dedicator of cytokinesis 8; FBS, fetal bovine serum; IFN- γ , interferon gamma; IL12, IL-17A, IL-17F, IL-22, IL-23, interleukin of corresponding enumeration; IL-6, interleukin 6; IL6R, interleukin 6 receptor; IRAK-4, interleukin 1 receptor-associated kinase 4; JAKs, Janus kinases; JIA, juvenile idiopathic arthritis; LPS, lipopolysaccharide; MAPKs, mitogen-activated protein kinases; MyD88, myeloid differentiation primary response 88; NEMO, nuclear factor-kappa B essential modulator; PBMC, peripheral blood mononuclear cells; PBS, phosphate-buffered saline; PCT, procalcitonin; pSTAT3, phosphorylated signal transducer and activator of transcription 3; RA, rheumatoid arthritis; ref.range, reference range; STAT3, signal transducer and activator of transcription 3; TNF α , tumor necrosis factor- α .

TABLE 1 | Patient's basic immune profile.

Patient's immune profile	Value	Age-matched reference values
Leukocytes (cells/ μ L)	10,100	6,000–17,000
Lymphocytes (cells/ μ L)	7,180	2,900–12,400
Neutrophils (cells/ μ L)	1,550	1,300–8,200
Monocytes (cells/ μ L)	1,010	150–1,280
Eosinophils (cells/ μ L)	610	0–1,200
CD3 ⁺ (% ^a , cells/ μ L)	76 \uparrow / 5,457 \uparrow	56–75/1,400–3,700
CD3 ⁺ CD4 ⁺ (% ^a , cells/ μ L)	42/3,016 \uparrow	28–47/700–2,200
CD3 ⁺ CD8 ⁺ (% ^a , cells/ μ L)	27/1,939 \uparrow	16–30/490–1,300
Naïve CD4 ⁺ (% ^b)	36	36–97
(CD3 ⁺ CD4 ⁺ CD45RA ⁺ CD27 ⁺)		
Naïve CD8 ⁺ (% ^c)	19	19–95
(CD3 ⁺ CD8 ⁺ CD45RA ⁺ CD27 ⁺)		
CD19 ⁺ (% ^a , cells/ μ L)	18/1,292	14–33/390–1,400
Naïve CD19 ⁺ (% ^d)	91	49–100
(CD19 ⁺ CD27 ⁺ IgD ⁺)		
Switched memory CD19 ⁺ (% ^d)	3 \downarrow	5–25.6
(CD19 ⁺ CD27 ⁺ IgD ⁺)		
CD16 ⁺ /CD56 ⁺ (% ^a , cells/ μ L)	4.4 /316	4–17/130–720
Immunoglobulins		
IgG (g/L)	4.76 \downarrow	5.53–10.20
IgG1 (g/L)	2.4 \downarrow	2.90–8.50
IgG2 (g/L)	1.33	0.45–2.60
IgG3 (g/L)	0.42	0.15–1.13
IgG4 (g/L)	0.61	0.01–0.79
IgA (g/L)	0.31 \downarrow	0.33–0.91
IgM (g/L)	0.47	0.47–1.55
IgE (IU/mL)	60.6 \uparrow	0.0–30.0
IgD (IU/mL)	<5.65	0.0–100.0
a-tetanus, a-diphtheria, a-hemophilus postvaccination IgG	Normal	NA
Autoantibodies (ANA, ENA, a-dsDNA, RF, ANCA, a-TPO, a-TG, a-TSHR, a-EM, a-TTG, a-GD)	Neg	NA
Complement activation (%):		Reference ranges
Classic pathway	94	69–129
Alternative pathway	53.4	30–113
MBL pathway	0.4 \downarrow	>10
Burst test PMA and <i>E.coli</i> , NBT test	Normal	NA

^a% of total peripheral lymphocytes.^b% of CD4⁺.^c% of CD8⁺.^d% of CD19⁺.

NA, not applicable; SCIG, subcutaneous immunoglobulins; Neg, negative; ANA, antinuclear antibodies; ENA, extractable nuclear antigen antibodies; a-dsDNA, anti-double stranded DNA antibodies; RF, rheumatoid factor IgG, IgA and IgM; ANCA, anti-neutrophil cytoplasm antibodies; a-TPO, anti-thyroperoxidase antibodies; a-TG, anti-thyroglobulin antibodies; a-TSHR, TSH receptor antibodies; a-EM, anti-endomysium IgG and IgA antibodies; a-TTG, anti-tissue transglutaminase antibodies IgG and IgA; a-GD, anti-deamidated gliadin IgA and IgG; MBL, mannan binding lectine; PMA, Phorbolmyristate acetate; NBT, nitroblue tetrazolium. \uparrow , \downarrow , value above, below reference range, respectively.

cytokine extracellularly. Patient's peripheral blood mononuclear cells (PBMCs) were stimulated with LPS overnight. The supernatants were harvested and the IL-6 was determined using a commercial IL-6 Elisa assay. We found the PBMCs of the patient to be capable of substantial IL-6 extracellular release, even if slightly decreased compared to a healthy control (**Figure 1C**).

The Patient's Serum Has IL-6 Neutralizing Property

Because of the patient's uncompromised ability to produce CRP at the age of 5 months, we hypothesized that an induction of anti-IL6 antibodies (abs) may underlie the acquired IL-6/CRP irresponsiveness. The healthy donors' PBMCs were stimulated according to the protocol above or left unstimulated in complete media (CM) supplemented either with patient's serum obtained from 2 different time points (in time of sepsis and 1 month later) or with fetal bovine serum (FBS). We noted a profound decrease of the cytokine in the presence of patient's serum. This indicated that the patient's serum contained a component interfering with the IL-6 detection (**Figure 1D**).

The Patient's Serum Contains Anti-IL6 Autoantibodies

The anti-IL6 abs were detected in the patient's and healthy donors' sera using a commercial Elisa kit (MyBiosource, details available in List of Methods). While the control samples were negative for anti-IL6 abs, the patient's serum was found positive in time of sepsis as well as 1 month after the infection (**Figure 1E**).

The Patient's Serum Decreases the Intracellular IL-6-Mediated Signal Transduction

Finally, we investigated whether the IL-6 abs found in the patient's serum cause a corresponding depression of IL-6 signal transduction downstream of IL-6 receptor (IL6R). To do this, we cultivated recombinant IL-6 in phosphate-buffered saline (PBS) supplemented with patient's serum obtained from 3 different time-points (in sepsis, 1 and 3 months later) or with FBS. Then, control full blood ($n = 2$) was stimulated with IL-6 in the respective media and STAT3 phosphorylation (pSTAT3) was analyzed in peripheral T cells and monocytes. We observed a significantly lower pSTAT3 signal from samples containing patient's serum from all 3 time-points (**Figure 1F**). The results suggest that the IL-6 abs have a neutralizing effect and indicate the persistence of the IL-6 abs even beyond acute phase of the infection.

DISCUSSION AND CONCLUSIONS

We present a child with septic shock, which most likely developed on the grounds of serum anti-IL6 autoAbs. Based on the lack of detectable IL-6, CRP and fibrinogen response during a clinically manifested systemic inflammation, together with the disturbed IL-6/STAT3-mediated signaling observed in cells exposed to patient's serum, we suggest that these abs have neutralizing property and contributed to the severity of the infection. Meanwhile, the undisturbed functionality of other proinflammatory cytokines, such as IL-1 β or TNF α probably explains the patient's retained ability to develop other features of inflammatory response, such as fever or increased PCT. PCT, a strong IL-6 independent biomarker of bacterial infection, rises sooner than CRP. Yet, due to its biologic half-life its increase should later overlap with CRP elevation. Therefore, the

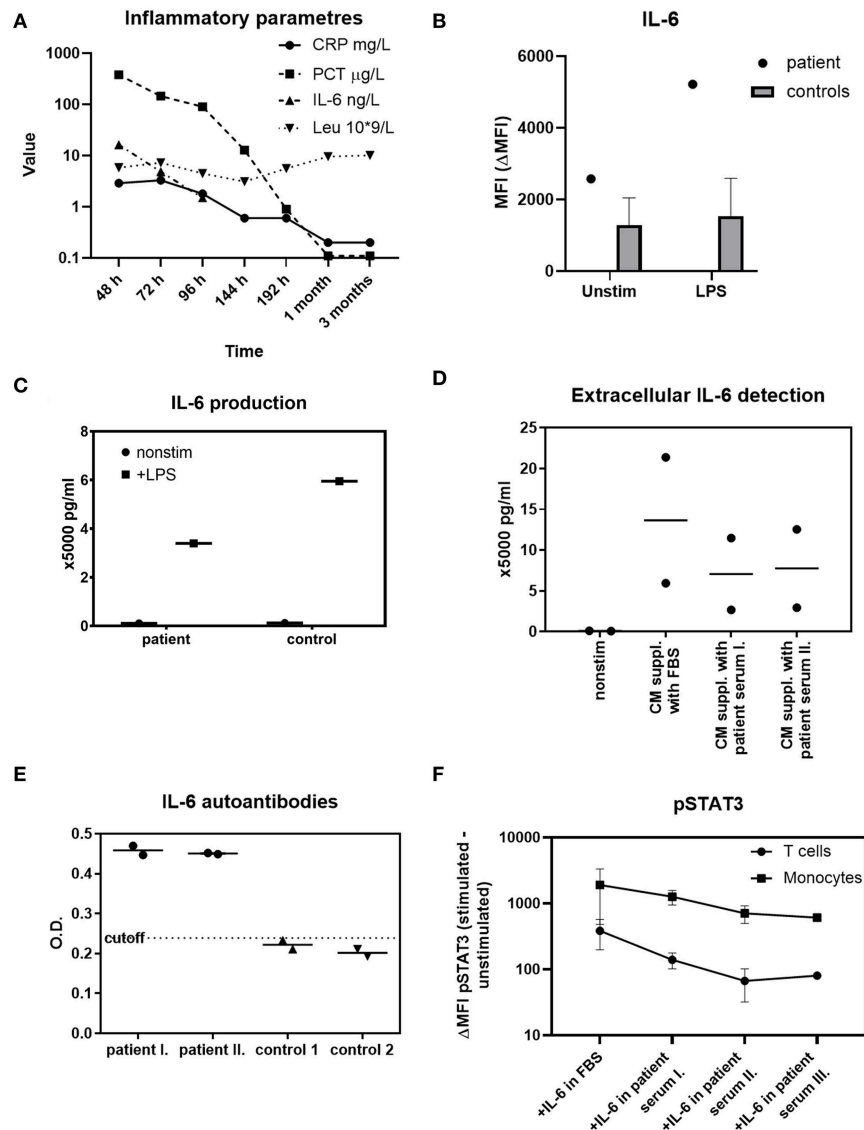


FIGURE 1 | Investigations of IL-6 functions in the patient. **(A)** The dynamics of IL-6, CRP, PCT, and absolute leukocytes count in various time-points during sepsis, 1 and 3 months afterwards (h-hours from onset of fever, m-month/s). An extreme elevation of PCT is not accompanied with IL-6 or CRP increases over the normal reference value. Reference ranges: CRP 0.0–5.0 mg/L; PCT 0.0–0.5 μ g/L; IL-6 0.0–20.0 ng/L; Leu $6.0\text{--}17.5 \times 10^9$ /L. **(B)** Intracellular IL-6 production in patient's monocytes at the time of sepsis compared to 59 healthy controls' monocytes after 1 μ g/ml LPS determined with flow cytometry. Unstimulated state is expressed as MFI (mean fluorescence intensity). The effect of LPS stimulation is expressed as Δ MFI (stimulated minus unstimulated MFI). The synthesis of IL-6 by patient's monocytes is unskewed. **(C)** Detection of extracellular IL-6 from patient's PBMCs after 1 μ g/ml LPS stimulation determined by ELISA. The release of IL-6 into extracellular space by patient's cells is normal. **(D)** Suppression of extracellular IL-6 by patient's serum analyzed by ELISA. Healthy age-matched controls' PBMCs ($n = 2$) were stimulated with LPS, cultivated in complete media (CM) supplemented either with fetal bovine serum (FBS) or 10% patient serum in time of sepsis (I) and 1 month later (II). The amount of IL-6 detected in the presence of patient's serum is decreased in both time-points. **(E)** Anti-IL-6 autoantibodies detection in patient serum obtained in time of sepsis (I), 1 month later (II), and in 2 healthy age-matched controls with ELISA. The patient's serum, but not the control serum, contains anti-IL-6 autoantibodies. OD, optical density. **(F)** STAT3 phosphorylation (pSTAT3) in control ($n = 2$) T cells and monocytes after 10 ng/ml recombinant IL-6 stimulation. The peripheral blood was stimulated with IL-6 diluted in PBS containing 20% patient serum obtained in sepsis (I), 1 month later (II), 3 months later (III), or in fetal bovine serum (FBS). The patient's serum decreases the pSTAT3 signal in all three time-points. Data are expressed as Δ MFI (stimulated minus unstimulated MFI). MFI, mean fluorescence intensity.

PCT/IL-6/CRP discrepancy during the acute phase of infection in our patient supports the hypothesis of isolated defect in IL-6-mediated CRP induction.

To our knowledge, this is the first patient with anti-IL6 autoAbs reported to suffer a severe systemic infection. Previously,

Puel et al. reported a Haitian boy with recurrent *Staphylococcus aureus* subcutaneous abscesses and cellulitis (9) and Nanki et al. referred two adult Japanese patients presenting with *Staphylococcal aureus* cellulitis and *Streptococcus intermedius* and *Escherichia coli* empyema (10) (**Supplementary Table 1**).

Eventhough very likely, a causative link between the anti-IL6 abs and the infectious susceptibility may not be unequivocally established in our patient. With no human IL-6 deficiency reported to date, the corresponding phenotype and the exact underlying molecular mechanisms of such defects are yet to be elucidated. Nevertheless, some clues may be derived from patients with genetic loss of proteins involved in IL-6/gp130/STAT3 signaling pathway. Two patients were recently reported to harbor homozygous IL6R mutations resulting in a phenotype of recurrent infections, absence of CRP increase during acute phase of clinically apparent infections, elevated IgE and eczema (11). A single case of bilallelic gp130 mutation has been described to present as early onset severe bacterial infections including *Staphylococcus aureus*, eczema, impaired acute phase response and increased IgE (12). Similar features are associated with hypomorphic STAT3 mutations, which constitute the autosomal dominant HyperIgE syndrome (AD HIES) [reviewed in (13)]. Additionally, an IL-6 knockout murine model was shown to develop normally, but the inflammatory acute-phase response after tissue damage or infection was severely compromised (14).

The apparently impeded resistance to *Staphylococcus aureus* in subjects with IL-6 signaling disruption is intriguing. Various primary immunodeficiencies (PIDs) predispose to abnormal, but not selective staphylococcal susceptibility, such as X-linked chronic granulomatous disease, NEMO deficiency syndrome, IRAK-4 deficiency, MyD88 deficiency, or DOCK8 deficiency. Mechanistically, the most relevant to our case is the STAT3 loss-of-function AD HIES, classically hallmarked by recurrent staphylococcal skin and lung infections, and the IL6R deficiency with both reported cases suffering with staphylococcal infections (11). Such similarity strongly suggests that the functional integrity of IL-6/STAT3 pathway is particularly important in antistaphylococcal immunity, however, the exact mechanism is not yet clear. It may involve the lack of CRP-mediated protection or other aspects, such as disturbed Th17 functions or diminished circulating T follicular helper cell induction, which was observed in AD HIES and IL6R deficiency.

Interestingly, several PIDs have recently been coupled with their phenocopies that arise from the presence of anti-cytokine abs. For example, an increased susceptibility to weakly virulent mycobacteria due to IFN- γ autoAbs resembles a rare PID called Mendelian susceptibility to mycobacterial diseases due to monogenic defects in IL-12/IFN- γ circuit. Similarly, abs against Th17-related cytokines IL-17A, IL-17F, IL-22, IL-23 underlie increased susceptibility to fungal infections resembling chronic mucocutaneous candidiasis due to various genetic etiologies [reviewed in (15)].

Naturally occurring anti-IL6 autoAbs were found in 0.1% healthy population but these are likely low concentration and lack the neutralizing property due to their low affinity (16). As with the majority of human autoantibodies, the reason why our patient developed blocking anti-IL6 autoAbs is unknown. A genetic predisposition might play a role. However, having been able to develop a normal acute phase response,

including a CRP increase, at the age of 5 months, a single gene inborn error is unlikely. Of note, the two adult subjects reported previously to produce blocking IL-6 abs were not affected with increased infectious susceptibility until 56 and 67 years of age (10). These aspects suggest that “multiple hits” may be required in the disease pathophysiology. Also, our patient’s severe perinatal history may underlie an immune dysbalance, owing to early abnormal exposure to pathogens or self-antigens, which may result in autoAbs induction. Nevertheless, no other clinically relevant abs were detected in the patient’s blood.

Finally, two IL6R and one IL-6 blocking agents are currently approved and widely used in diseases such as RA, JIA and Castleman’s disease (8). While some studies identified a higher incidence of severe infections in RA patients receiving anti-IL6R blockade compared to anti-TNF α biologics (17, 18), others did not (19). However, the suppression of CRP in RA patients receiving monoclonal anti-IL6R abs has been well-recognized, in fact CRP has been suggested as an outcome predictor and treatment monitoring tool (20). In the same context, CRP has also been reported to be a poor predictor of severe infectious complications (21). Several ongoing clinical trials investigate the efficacy and tolerability of IL-6 targeting in various other immune dysregulation or oncologic diseases and novel compounds interfering with IL-6 signaling are being rapidly developed (8). Therefore, given the severity of presentation in our patient, we suggest that extra care in exercised in patients receiving IL-6 blocking agents, especially when administered together with other immune suppressant drugs.

Of note, an excess of soluble IL-6R, which would bind the IL-6 and interfere with its detection was not excluded in our patient. This is a limitation of our study, however the documented presence of anti-IL6 autoAbs amply explains the observed phenomena.

To conclude, disturbed IL-6/STAT3/CRP axis due to endogenous production of anti-IL6 autoAbs was a likely cause of severe septic shock in our patient who failed to mount an efficient acute phase response. We suggest that patients with severe bacterial infection without elevation of CRP should be examined for the presence of anti-IL6 antibodies.

DATA AVAILABILITY STATEMENT

All data generated or analyzed during this study are included in the article/**Supplementary Material** and are also available from the corresponding author on reasonable request.

ETHICS STATEMENT

Ethical review and approval was not required for the study on human participants in accordance with the local legislation and institutional requirements. Written informed consent to participate in this study and for publication was provided by the participants’ legal guardian/next of kin.

AUTHOR CONTRIBUTIONS

MB treated the patient, established the hypothesis and wrote the manuscript. ZP designed and performed the experiments and co-wrote the manuscript. TC treated the patient and revised the manuscript. IP performed the routine tests and revised the manuscript. PK and HH supervised the patient treatment, manuscript preparation and revisions. AS supervised the experiments, manuscript preparation and revisions. All authors have contributed in a substantive and intellectual manner.

FUNDING

This work was supported by grant AZV NV18-05-00162 from Ministry of Health of the Czech Republic, GAUK 954218 and 460218, both issued by the Charles University in Prague, Czech Republic.

REFERENCES

- Akira S, Taga T, Kishimoto T. Interleukin-6 in biology and medicine. *Adv Immunol.* (1993) 53:1–78. doi: 10.1016/S0065-2776(08)60532-5
- Wolf J, Rose-John S, Garbers C. Interleukin-6 and its receptors: a highly regulated and dynamic system. *Cytokine.* (2014) 70:11–20. doi: 10.1016/j.cyt.2014.05.024
- Sproston NR, Ashworth JJ. Role of C-reactive protein at sites of inflammation and infection. *Front Immunol.* (2018) 9:754. doi: 10.3389/fimmu.2018.00754
- Pepys MB, Hirschfield GM. C-reactive protein: a critical update. *J Clin Invest.* (2003) 111:1805–12. doi: 10.1172/JCI18921
- Vijayan AL, Vanimaya, Ravindran S, Saikant R, Lakshmi S, Kartik R, G M. Procalcitonin: a promising diagnostic marker for sepsis and antibiotic therapy. *J Intensive Care.* (2017) 5:51. doi: 10.1186/s40560-017-0246-8
- Goldstein B, Giroir B, Randolph A. International pediatric sepsis consensus conference: definitions for sepsis and organ dysfunction in pediatrics. *Pediatr Crit Care Med.* (2005) 6:2–8. doi: 10.1097/01.PCC.0000149131.72248.E6
- Singer M, Deutschman CS, Seymour C, Shankar-Hari M, Annane D, Bauer M, et al. The third international consensus definitions for sepsis and septic shock (sepsis-3). *JAMA.* (2016) 315:801–10. doi: 10.1001/jama.2016.0287
- Kang S, Tanaka T, Narazaki M, Kishimoto T. Targeting interleukin-6 signaling in clinic. *Immunity.* (2019) 50:1007–23. doi: 10.1016/j.immuni.2019.03.026
- Puel A, Picard C, Lorrot M, Pons C, Chrabieh M, Lorenzo L, et al. Recurrent Staphylococcal cellulitis and subcutaneous abscesses in a child with autoantibodies against IL-6. *J Immunol.* (2008) 180:647–54. doi: 10.4049/jimmunol.180.1.647
- Nanki T, Onoue I, Nagasaka K, Takayasu A, Ebisawa M, Hosoya T, et al. Suppression of elevations in serum C reactive protein levels by anti-IL-6 autoantibodies in two patients with severe bacterial infections. *Ann Rheum Dis.* (2013) 72:1100–2. doi: 10.1136/annrheumdis-2012-02768
- Spencer S, Köstel Bal S, Egner W, Lango Allen H, Raza SI, Ma CA, et al. Loss of the interleukin-6 receptor causes immunodeficiency, atopy, and abnormal inflammatory responses. *J Exp Med.* (2019) 216:1986–98. doi: 10.1084/jem.20190344
- Schwerd T, Twigg SRF, Aschenbrenner D, Manrique S, Miller KA, Taylor IB, et al. A biallelic mutation in IL6ST encoding the GP130 co-receptor causes immunodeficiency and craniosynostosis. *J Exp Med.* (2017) 214:2547–62. doi: 10.1084/jem.20161810
- Freeman AF, Holland SM. The hyper-IgE syndromes. *Immunol Allergy Clin North Am.* (2008) 28:277–91. doi: 10.1016/j.iac.2008.01.005

ACKNOWLEDGMENTS

We would like to thank the family of our patient for their willingness to participate in our study.

SUPPLEMENTARY MATERIAL

The Supplementary Material for this article can be found online at: <https://www.frontiersin.org/articles/10.3389/fimmu.2019.02629/full#supplementary-material>

Supplementary Figure 1 | Cytokine production by patient's monocytes in time of sepsis: IL-1 β and TNF α production determined by flow cytometry compared to 65 and 30 healthy controls, respectively. Unstimulated state is expressed as MFI (mean fluorescence intensity). LPS stimulation is expressed as Δ MFI (stimulated—unstimulated MFI).

Supplementary Table 1 | An overview of reported cases of patients with anti-IL-6 autoantibodies and severe bacterial infections.

- Kopf M, Baumann H, Freer G, Freudenberg M, Lamers M, Kishimoto T, et al. Impaired immune and acute-phase responses in interleukin-6-deficient mice. *Nature.* (1994) 368:339–42. doi: 10.1038/368339a0
- Barcenas-Morales G, Cortes-Acevedo, P, Doffinger R. Anticytokine autoantibodies leading to infection early recognition, diagnosis and treatment options. *Curr Opin Infect Dis.* (2019) 32:330–6. doi: 10.1097/QCO.0000000000000561
- Galle P, Svenson M, Bendtzen K, Hansen MB. High levels of neutralizing IL-6 autoantibodies in 0.1% of apparently healthy blood donors. *Eur J Immunol.* (2004) 34:3267–75. doi: 10.1002/eji.200425268
- Rutherford AI, Subesinghe S, Hyrich KL, Galloway JB. Serious infection across biologic-treated patients with rheumatoid arthritis: results from the British Society for Rheumatology Biologics Register for Rheumatoid Arthritis. *Ann Rheum Dis.* (2018) 77:905–10. doi: 10.1136/annrheumdis-2017-212825
- Pawar A, Desai RJ, Solomon DH, Santiago Ortiz AJ, Gale S, Bao M, et al. Risk of serious infections in tocilizumab versus other biologic drugs in patients with rheumatoid arthritis: a multidatabase cohort study. *Ann Rheum Dis.* (2019) 78:456–64. doi: 10.1136/annrheumdis-2018-214367
- Nishimoto N, Ito K, Takagi N. Safety and efficacy profiles of tocilizumab monotherapy in Japanese patients with rheumatoid arthritis: meta-analysis of six initial trials and five long-term extensions. *Mod Rheumatol.* (2010) 20:222–32. doi: 10.1007/s10165-010-0279-5
- Kojima T, Yabe Y, Kaneko A, Hirano Y, Ishikawa H, Hayashi M, Miyake H, Takagi H, Kato T, Terabe K, et al. Monitoring C-reactive protein levels to predict favourable clinical outcomes from tocilizumab treatment in patients with rheumatoid arthritis. *Mod Rheumatol.* (2013) 23:977–85. doi: 10.3109/s10165-012-0782-y
- Bari SF, Khan A, Lawson T. C reactive protein may not be reliable as a marker of severe bacterial infection in patients receiving tocilizumab. *Case Reports.* (2013) 2013:bcr2013010423. doi: 10.1136/bcr-2013-010423

Conflict of Interest: The authors declare that the research was conducted in the absence of any commercial or financial relationships that could be construed as a potential conflict of interest.

Copyright © 2019 Bloomfield, Parackova, Cabelova, Pospisilova, Kabicek, Houstkova and Sediva. This is an open-access article distributed under the terms of the Creative Commons Attribution License (CC BY). The use, distribution or reproduction in other forums is permitted, provided the original author(s) and the copyright owner(s) are credited and that the original publication in this journal is cited, in accordance with accepted academic practice. No use, distribution or reproduction is permitted which does not comply with these terms.



Molecular Analysis of Goodpasture's Disease Following Hematopoietic Stem Cell Transplant in a Pediatric Patient, Recalls the Conformeropathy of Wild-Type Anti-GBM Disease

Paul E. Gray^{1,2*}, Hugh McCarthy³, Owen M. Siggs⁴, Moin A. Saleem⁵, Tracy O' Brien^{2,6}, Katie Frith¹, John B. Ziegler^{1,2}, A. Richard Kitching⁷, Agnes B. Fogo^{8,9,10}, Billy G. Hudson^{9,10,11} and Vadim Pedchenko¹⁰

¹ Department of Immunology and Infectious Diseases, Sydney Children's Hospital, Sydney, NSW, Australia, ² Faculty of Medicine, School of Women's and Children's Health, University of New South Wales, Sydney, NSW, Australia, ³ Department of Nephrology, Sydney Children's Hospital, Sydney, NSW, Australia, ⁴ Immunology Division, Garvan Institute of Medical Research, Darlinghurst, NSW, Australia, ⁵ Faculty of Health Sciences, Bristol Medical School, University of Bristol, Bristol, United Kingdom, ⁶ Kid's Cancer Centre, Sydney Children's Hospital, Sydney, NSW, Australia, ⁷ Faculty of Medicine, Nursing & Health Sciences, Centre for Inflammatory Diseases, Monash University, Clayton, VIC, Australia, ⁸ Department of Pediatrics, Vanderbilt University School of Medicine, Nashville, TN, United States, ⁹ Department of Pathology, Microbiology and Immunology, Vanderbilt University School of Medicine, Nashville, TN, United States, ¹⁰ Division of Nephrology, Department of Medicine, Vanderbilt University Medical Center, Nashville, TN, United States, ¹¹ Department of Biochemistry, Vanderbilt University School of Medicine, Nashville, TN, United States

OPEN ACCESS

Edited by:

Sylvie Hermouet,
INSERM U1232 Centre de Recherche
en Cancérologie et Immunologie
Nantes Angers (CRCINA), France

Reviewed by:

Dorin-Bogdan Borza,
Meharry Medical College,
United States
Mårten Segeelmark,
Linköping University, Sweden

*Correspondence:

Paul E. Gray
paul.gray1@health.nsw.gov.au

Specialty section:

This article was submitted to
Alloimmunity and Transplantation,
a section of the journal
Frontiers in Immunology

Received: 24 July 2019

Accepted: 28 October 2019

Published: 14 November 2019

Citation:

Gray PE, McCarthy H, Siggs OM,
Saleem MA, O' Brien T, Frith K,
Ziegler JB, Kitching AR, Fogo AB,
Hudson BG and Pedchenko V (2019)
Molecular Analysis of Goodpasture's
Disease Following Hematopoietic
Stem Cell Transplant in a Pediatric
Patient, Recalls the Conformeropathy
of Wild-Type Anti-GBM Disease.
Front. Immunol. 10:2659.
doi: 10.3389/fimmu.2019.02659

Background: Goodpasture's disease (GP) is mediated by autoantibodies that bind the glomerular and alveolar basement membrane, causing rapidly progressive glomerulonephritis with or without pulmonary hemorrhage. The autoantibodies bind neopeptides formed upon disruption of the quaternary structure of $\alpha345$ NC1 hexamer, a critical structural domain of $\alpha345$ collagen IV scaffolds. Hexamer disruption leads to a conformational changes that transitions $\alpha3$ and $\alpha5$ NC1 subunits into immunogens, however, the trigger remains unknown. This contrasts with another anti-GBM disease, Alports' post-transplant nephritis (APTn), where the pathogenic alloantibody binds directly to native NC1 hexamer. The current report includes the first study of antigenic specificity and allo-incompatibility in anti-GBM disease occurring after allogeneic haematopoietic stem cell transplant (HSCT).

Results: The anti-GBM antibodies were found to be directed predominantly against the E_A epitope of the $\alpha3$ NC1 monomer of collagen IV and developed rapidly in patient serum reaching peak level within 5 weeks. Autoantibody binding to native $\alpha345$ NC1 hexamer was minimal; however, binding was greatly increased upon dissociation of the native hexamer. There were no polymorphic genetic differences between donor and recipient collagen IV genes which would be predicted to cause a significant NC1 conformational change or to provide a target for antibody binding. Both patient and donor possessed the Goodpasture's susceptibility HLA-allele *DRB1*1501*.

Conclusions: The current report includes the first in-depth study of allo-incompatibility and antigenic specificity in anti-GBM disease occurring after allogeneic haematopoietic

stem cell transplant (HSCT). No polymorphic genetic differences were identified between donor and recipient collagen IV genes which would be predicted to provide a target for antibody binding. Furthermore, autoantibody binding to native $\alpha345\text{NC1}$ hexamer was minimal, increasing greatly upon dissociation of the native hexamer, resembling wild-type GP diseases and marking this as the first example of a post-HSCT conformeropathy.

Keywords: Goodpastures, glomerular basement membrane, conformeropathy, GvHD, anti-GBM, alloimmunity, autoimmunity

INTRODUCTION

Goodpasture's (GP) disease is mediated by autoantibodies, commonly known as anti-GBM antibodies, that target $\alpha345$ scaffold of collagen IV of the kidney glomerular (GBM) and lung alveolar basement membrane causing rapidly progressive glomerulonephritis and pulmonary hemorrhage. In GP disease, the autoantibodies bind neoepitopes formed on $\alpha3$ and $\alpha5$ NC1 subunits upon disruption of the quaternary structure of native $\alpha345\text{NC1}$ hexamer, a critical structural domain of $\alpha345$ collagen IV scaffolds (1, 2). Hexamer disruption is concomitant with conformational changes that transitions subunits into immunogens. The pathogenesis of the ensuing anti-GBM nephritis contrasts with that of Alport's post-transplant nephritis (APTn). In APTn, $\alpha345$ collagen IV scaffold is seen as foreign within the transplanted kidney, owing to its absence in the GBM of the recipient Alport patient. Of particular importance, while both auto- and alloantibodies target the same $\alpha345\text{NC1}$ hexamer, they bind different epitopes (1). In GP disease, epitopes are formed after dissociation of hexamer subunits, whereas in APTn alloantibody epitopes are located on the surface of the $\alpha345\text{NC1}$ hexamer (3, 4). The trigger for conformational changes that transition subunits into immunogens in GP disease remains unknown. We describe the first case of anti-GBM disease occurring post haematopoietic stem cell transplant where the pathogenesis including antibody specificity and the local determinants of antibody binding have been extensively studied.

We previously reported the first patient with X-linked lymphoproliferative (XLP) disease-associated cerebral vasculitis to successfully undergo a hematopoietic stem cell transplant (HSCT) (5). However, at day +169 post-transplant the patient developed anti-GBM disease, a complication rarely reported post-HSCT. This case presented a unique opportunity to investigate whether the anti-GBM nephritis phenocopied alloimmune response, as in APTn, or autoimmune response, as in GP disease. In addition, serum from this patient was available prior to and during the onset of anti-GBM disease, providing a window into both the emergence, evolution, antibody specificity, and the temporal relationship between antibody production and the development of renal failure.

MATERIALS AND METHODS

Patient serum was collected prior to the onset of anti-GBM disease and through the time when plasma exchange and immunosuppressive drug treatment were initiated. Serum collected at the disease onset at dilutions of 1:50 to 1:250 was

applied to frozen sections of normal human kidney, and binding of circulating anti-GBM antibody to the normal GBM was detected using fluorescein labeled anti-IgG secondary antibody. For immunoadsorption, patient serum was preincubated with NHS-activated magnetic beads coated with 100 $\mu\text{g}/\text{mg}$ of recombinant $\alpha3\text{NC1}$ domain of collagen IV. In a separate experiment, immunofluorescent staining was also performed after treatment of normal kidney sections with 6 M urea in 0.1 M glycine-HCl, pH 2.2 for 10 min prior to addition of GP serum.

Antigens and Anti-GBM ELISA

Recombinant human $\alpha1\text{NC1}$ through $\alpha6\text{NC1}$ domains of collagen IV in monomer form and $\alpha3/\alpha1$ chimeras were purified from culture medium of stably transfected human embryonic kidney (HEK) 293 cells using anti-FLAG agarose as previously described (6). $\alpha3/\alpha1\text{NC1}$ chimeras corresponding to the E_A and E_B epitopes of the $\alpha3\text{NC1}$ domain were constructed by PCR mutagenesis as previously described (7). The native NC1 hexamers of collagen IV were isolated from bovine or human GBM after collagenase digestion and size-exclusion FPLC chromatography. Binding of antibody to recombinant NC1 domains or chimeras was performed using indirect enzyme-linked immunosorbent assay, with alkaline phosphatase-conjugated goat anti-human IgG or IgM (Sigma, 1:2,000) secondary antibody as described (1).

Sequencing and Analysis

Next generation gene sequencing was performed by the Bristol genetics laboratory using the *HaloPlex* Target Enrichment System kit including all coding regions for a range of basement membrane associated genes. Analysis was focused specifically on the COL4A3, COL4A4, and COL4A5 genes to identify non-reference sequence variations (hg19) between donor and recipient, which were assessed using the Grantham score of physicochemical change.

Statistical Analysis

The results for all quantitative experiments are reported as mean \pm SD of three independent experiments. To determine differences between groups, we used analysis of variance with multiple groups comparison by Holm-Sidak method (SigmaStat) with $P < 0.05$ considered to indicate statistical significance.

RESULTS

A 12-year-old boy underwent unrelated cord blood transplant (UCBT) for X-linked lymphoproliferative (XLP) disease caused by a mutation c.96G>C in the *SH2D1A* gene. The patient's

primary disease has been reported elsewhere regarding novel features of XLP, with presentation including cerebral vasculitis, aplastic anemia, acute respiratory distress syndrome, and arthropathy (5). Features of the transplant potentially pertinent to the current investigations include that an initial 6/6 HLA matched UCBT failed to engraft and he underwent a second transplant with a 5/6 matched UCBT, which engrafted with 100% donor chimerism. His main side effects during the acute phase of the transplant were BK virus-associated hemorrhagic cystitis with bladder perforation and a possible NK cell immune reconstitution syndrome, including bilateral pulmonary infiltrates. At 169 days post-transplant when he had been engrafted and well for some time, he presented with fever, hematuria and acute renal failure, and was identified as having anti-GBM antibodies on indirect immunofluorescence of serum and characteristic crescentic glomerulonephritis injury with direct linear GBM immunofluorescence staining for IgG on renal biopsy. He was treated with plasmapheresis for 1 month with initial 2nd daily exchanges, high dose corticosteroids and cyclophosphamide before having B-cell depletion with rituximab. He went into remission, becoming anti-GBM antibody negative, with residual moderate chronic kidney disease. He is currently well with a glomerular filtration rate of 43 ml/min/1.73 m², with no proteinuria or hematuria.

The biopsy showed characteristic features of crescentic glomerulonephritis, with >90% of the 32 glomeruli sampled (8 globally sclerosed) displaying cellular or fibrocellular crescents, with segmental fibrinoid necrosis and with extensive acute tubular injury and focal, 10–20% interstitial fibrosis and tubular atrophy (**Figure 1A**). When applied to frozen sections of normal human kidney, the patient's serum at 1:50 dilution demonstrated strong linear anti-GBM staining, which was greatly enhanced by acidic urea treatment (**Figures 1B,C**). The specificity of the staining and the nature of deposited antibody were established by immunoadsorption of serum on α 3NC1-coated magnetic beads, which nearly abolished staining in parallel with removal of α 3NC1 antibody (**Figures 1E,F**). The findings are diagnostic of severe anti-GBM antibody-mediated glomerulonephritis.

Serum collected at initial presentation showed that a majority of antibody targeting the α 3NC1 monomer of collagen IV with weaker reactivity against α 1 and α 5NC1 monomers, indicating that α 3NC1 is the primary autoantigen (**Figure 2A**). This was further supported by measuring the affinity of circulating antibodies toward human α 1, α 3, and α 5NC1 domains (**Figure 2B**). Patient serum was pre-incubated with increasing concentrations of the NC1 monomers and binding to immobilized α 1, α 3, and α 5NC1, respectively was measured by inhibition ELISA. The strongest inhibition by the α 3NC1 monomers indicates that the anti- α 3 antibodies have highest affinity, followed by the anti- α 5, and low affinity anti- α 1 antibody. Furthermore, adsorption of patient serum on α 3NC1-coated magnetic beads not only removes α 3 specific antibodies, but significantly reduces immunoreactivity to α 1 and α 5NC1 (**Figure 2C**), indicating at least partial cross-reactivity of the major α 3-specific antibody with the α 1 and α 5NC1 domains.

Circulating antibodies from the HSCT patient targeted predominantly the E_A epitope of α 3NC1 monomer with lower

reactivity toward E_B epitope (**Figure 2D**) suggesting a key role of the E_A region in the initiation of anti-GBM disease in this case. This is consistent with previously reported E_A-specific antibody titers as a primary predictor of renal outcome in Goodpasture's disease (8) and proven pathogenicity of E_A- α 3 chimeric protein in rat model of glomerulonephritis (9). Since targeting of the additional non-GP epitopes could not be excluded in this type of assay, we performed the competition ELISA for antibody binding to the α 3NC1 domain. For this experiment, GP antibodies were purified by affinity chromatography on α 3NC1 domain coupled to agarose beads and labeled with biotin. Patient serum antibodies efficiently competed with binding of biotinylated GP antibody to coated α 3NC1 in a dose-dependent manner and was undistinguishable from the control mix of GP sera (**Figure 2E**), showing that current patient's circulating antibody targets the same epitopes as in patients with classical GP disease.

Finally, although there was minimal antibody reactivity with native α 345NC1 hexamers from bovine or human GBM, binding of antibody was significantly increased upon hexamer dissociation by a protein denaturant (**Figure 2F**). This closely resembled the enhanced immunofluorescent staining of human kidney sections after acidic urea (**Figure 1C**). Therefore, in terms of epitope specificity and binding to dissociated NC1 hexamers, the anti-GBM antibodies in the current post-HSCT case clearly phenocopy classical Goodpasture autoantibodies, but not APTN alloantibodies.

ELISA analysis revealed the rapid development of antibodies to the α 3NC1 monomer of collagen IV in patient serum over a period of 5 weeks (**Figure 2G**). Surprisingly, we did not detect IgM reactivity to any of collagen IV NC1 domains either prior or at the onset of the anti-GBM disease (**Figure 2H**). By quantitative analysis using purified GP antibodies as standard, we found that concentration of α 3-specific IgG reached peak concentration about 400 μ g/ml or 4% of total IgG, which is considerably higher than ~1% median value for GP patients.

Given that there is a strong association between susceptibility to Goodpasture's disease and HLA DRB1*15:01 (10–12), we also assessed the HLA alleles and found that both the recipient and the donor of the cord blood, which engrafted 100%, carried a single Goodpasture's associated HLA DRB1*15:01 allele.

We then questioned whether the pathogenesis of anti-GBM disease in this HSCT patient involved alloreactivity between the incoming donor immune system and genetic variation in the recipient's α 345 collagen IV scaffold. An absence of genetic alterations within the part of the COL4A3 gene encoding the NC1 domain in Goodpasture's patients has been reported previously, suggesting that NC1 mutations are not a major factor in the etiology of classical Goodpasture's disease (13). However, we hypothesized that genetic variations may occur in HSCT patient that alters the fine specificity of T and B cell tolerance to α 3NC1 or the structure of the of the recipient's α 345 NC1 hexamer. Such an alteration could promote appearance of the abnormally folded NC1 hexamer or an unassembled full length α 3 chain recognized as foreign to the incoming donor immune system and thereby inducing antibody production.

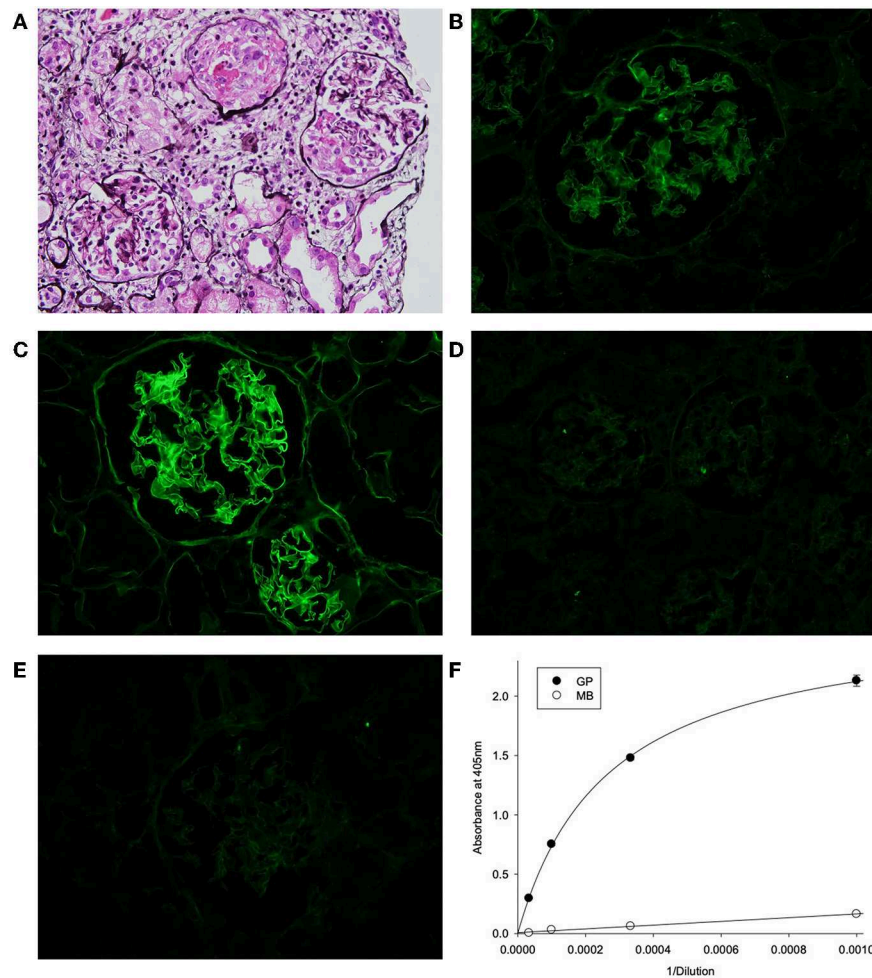


FIGURE 1 | (A) Kidney lesions in post-HSCT patient showing characteristic features of crescentic glomerulonephritis, with >90% of the 32 glomeruli sampled displaying cellular or fibrocellular crescents, with segmental fibrinoid necrosis and with extensive acute tubular injury and focal, 10–20% interstitial fibrosis and tubular atrophy (Jones' silver stain). **(B–E)** Binding of patient serum antibodies to frozen sections from normal human kidney (immunofluorescent staining). **(B)** Distinct linear staining of GBM observed on intact kidney section, which is strongly increased after pre-treatment with acidic urea **(C)**. **(D)** There is no staining with normal human serum (1:50). **(E)** GBM staining was abolished by adsorption of patient serum on α 3NC1-coated magnetic beads **(E)**, which removed 95% of α 3-antibody as demonstrated by testing of original (GP) and absorbed (MB) serum using indirect ELISA of on α 3NC1-coated plate **(F)**.

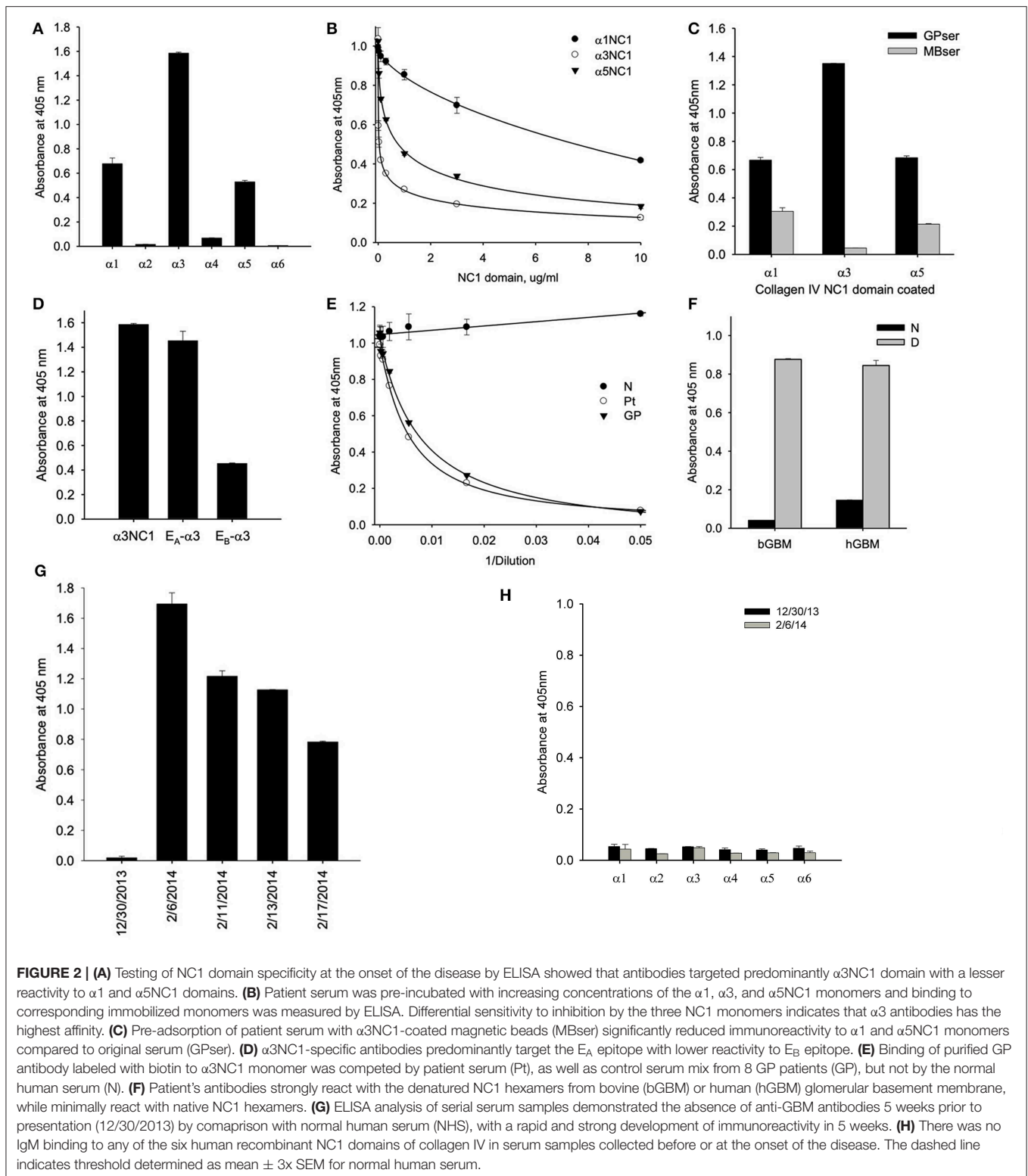
We detected two missense variants in each of *COL4A3* and *COL4A4*, and none in *COL4A5* genes in the recipient, but not in the donor, which are listed in **Table 1**. Mutation mapping shows that all four variants fall within the triple-helical region of *COL4A4/COL4A3* chains distant to the target E_A - α 3 and E_B - α 3 epitopes of the NC1 domain (**Figure 3**) and would not be predicted to directly influence the quaternary structure of the native α 345NC1 hexamer. No variants were detected which differed between donor and recipient, in the α 3, α 4 or α 5NC1 domains.

DISCUSSION

Autoimmune disease occurring post-HSCT, i.e., antibodies from the graft against “self,” is not uncommon, and is more common with transplants are performed for certain monogenic

indications (14). Wiskott Aldrich syndrome, a disease which predisposes to autoimmunity, is associated with a high rate of post-transplant autoimmunity, a predilection which is associated with reduced donor cell chimerism (15). HSCT for another entity, chronic granulomatous disease, may also predispose to a high risk of autoimmune cytopenias, neuropathy and thyroid disease (16), and in this case the tendency appears to occur despite excellent donor cell engraftment. There is no particular predilection reported of post-transplant autoimmunity in patients transplanted for XLP1.

The post-HSCT antibody-mediated disease where there is the greatest knowledge of antigenic target is autoimmune haemolytic anemia. Preformed recipient allo-antibodies against donor derived red cells resemble red cell alloantibodies important for transfusion reactions, and are therefore well-understood (17). However, there is little information of antigenic targets



and in particular epitope specificities involved in less common post-HSCT allo- or autoimmune entities, with the exception of data on the cell surface targets of antibodies relevant to chronic graft vs. host disease (GVHD) (18).

The current patient is the first described case of anti-GBM disease post-cord blood transplant. Two cases of anti-GBM nephritis were reported originating as a graft-vs.-host (GVH) phenomenon post hematopoietic stem cell transplant (HSCT).

TABLE 1 | Missense variants in genes encoding collagen IV chains.

Variant	Gene	gnomAD MAF	SNP ref.	Amino acid change	Grantham score
g.2,228163453,C,A	COL4A3	4.7%	rs57611801	Asp1269Glu	45
g.2,228121101,G,T	COL4A3	16.7%	rs55703767	Asp326Tyr	160
g.2,227946893,C,G	COL4A4	2.8%	rs1800516	Gly545Ala	60
g.2,227915832,G,A	COL4A4	52%	rs1800517	Pro1004Leu	98

The gnomAD (r2.0.2) allele frequency (AF) reflects that these are common variants, however the Grantham scores (range 5–215) reveal that in particular rs55703767 (radical change), might be expected to impose a significant effect on the physicochemical properties of the α 3 chain of collagen IV. MAF, minor allele frequency.



FIGURE 3 | Patient-restricted coding variants within type IV collagen proteins. Domain architecture and relative locations of missense variants within COL4A3 (Uniprot: Q01955) and COL4A4 (Uniprot: P53420) proteins that differed between the patient and the cord-blood donor. No patient-restricted variants were observed in COL4A5. The black bars represent anti-GBM disease-associated E_A- α 3 and E_B- α 3 epitopes.

A 42-year-old female patient received a bone marrow transplant (BMT) and developed systemic vasculitis with a combination of anti-neutrophil cytoplasmic (ANCA) and anti-GBM antibodies (19). In another study, a series of biopsies in patients suffering renal disease post-HSCT identified a single case of an elderly BMT patient with anti-GBM disease (20). Neither of these cases was analyzed with regard to antigen specificity of anti-GBM antibody.

Given the rarity of anti-GBM nephritis post-HSCT, we determined whether the specificity and binding properties of the anti-GBM antibodies of the HSCT patient resembled those of APTN or GP disease. This disease involved a donor immune system and genetically mismatched kidney, similar to the case with APTN, and therefore we had anticipated that the antibodies would behave analogous to that of APTN alloantibodies by binding to the native α 345NC1 hexamer, and specifically to the α 3 or α 5NC1 subunits. Surprisingly, the HSCT antibodies did not bind the native α 345NC1 hexamer but bound to the dissociated α 3 and α 5NC1 subunits via the E_A and E_B neoepitopes. Thus, the anti-GBM antibodies of the HSCT patient phenocopied GP autoantibodies. Furthermore, no genetic variants were found in the recipient collagen IV genes which might have led to a structural perturbation in the immunogen, eliciting antibody production.

We conclude that this is a case of classical Goodpasture’s disease, as shown by the specificity of the antibodies phenocopying that of antibodies bound to native kidney and elicited by the native immune system of GP patients. These antibodies emerged post transplantation from a donor immune system. But what caused this patient to suffer this novel complication? The properties of his circulating antibodies, which were non-reactive to the native α 345NC1 hexamer, but fully reactive to dissociated α 3NC1 subunit, strongly suggest

that the inciting immunogen was the dissociated subunit harboring the E_A and E_B neoepitopes. This supposition is supported by the finding that native α 345NC1 hexamer is not pathogenic in an animal model of GP disease, whereas immunization with hexamer dissociated by acid treatment induced glomerulonephritis (21, 22). Yet, in the unique case of APTN, the native hexamer elicited alloantibody production, revealing it to be the immunogen in the kidney allograft (3, 4). While it is not possible to pinpoint the inciting factor that triggered hexamer dissociation into immunogenic subunits in the HSCT case, several possibilities exist. For example, after transplant he suffered an episode of bilateral pulmonary infiltrates, which could cause structural damage to the α 345NC1 hexamer in the alveolar basement membrane (23), transitioning subunits into immunogens. Such a structural damage in lungs could also occur due to a bacterial or one of his viral infections (BK, HHV-7) or by the immunosuppression therapy. Indeed, lung injury has been associated with GP disease etiology, wherein cigarette smoking and inhalation of hydrocarbons are risk factors in numerous patients (24, 25).

The process of immune reconstitution may be relevant for GP disease etiology in HCT patients. The current paradigm suggests that the loss of tolerance in autoimmune disease is often a failure of multiple checkpoints that ultimately unmask autoreactive T and B cells (26). There have been reports of anti-GBM disease occurring with recovery following alemtuzumab treatment (27). Further, patients with HIV/AIDS, who have severe immune dysregulation, develop frequent autoantibodies, including anti-GBM, although anti-GBM disease is very rare (28). Both recipient and donor were homozygous for the HLA allele associated with Goodpasture’s disease, *HLA DRB1*15:01* (DR15) (11, 12). Homozygosity at the DR locus meant that there was no expression of dominantly protective DR allomorphs

such as DR1 or DR7 (10), setting the scene for the loss of tolerance to α 3NC1 under unfavorable conditions. In the context of DR15, central tolerance to α 3NC1 is poor, as CD4⁺ Foxp3[−] conventional T cells even from healthy people bearing DR15 react with the immunodominant T cell epitope α 3_{135–145}, and can be differentiated into effector Th1 cells, Th17 cells and T follicular helper (Tfh) cells (12). Antigen-specific Tfh cells are critical in generating antibody responses to most antigens, likely including the Goodpasture antigen. As the Tfh subset is deficient in *SH2D1A* deficiency (29), in our patient aberrant or exuberant reconstitution resulting in the development of autoreactive Tfh cells may have played a role in loss of tolerance to α 3NC1 and the generation of anti-GBM antibodies.

The availability of serum prior to and during early stages of anti-GBM disease in this HSCT patient provided a unique opportunity to assess the time frame for development of GP disease. The case demonstrated the rapidity, in a matter of weeks, with which a patient can go from being antibody negative to accumulating high titers of pathogenic antibody with development of rapidly progressive glomerulonephritis. Importantly, our findings reiterate the ultimate importance for early diagnosis and timely treatment (30) with potential recovery of kidney function despite very high level of circulating α 3 and α 5NC1 antibodies. Furthermore, our patient shows that the antibody phenocopies the autoimmune GP disease, rather than the antibody specificity seen in Alport patients with anti-GBM developing after kidney transplant.

DATA AVAILABILITY STATEMENT

All datasets generated for this study are included in the article/supplementary material.

REFERENCES

- Pedchenko V, Bondar O, Fogo AB, Vanacore R, Voziyan P, Kitching AR, et al. Molecular architecture of the Goodpasture autoantigen in anti-GBM nephritis. *N Engl J Med.* (2010) 363:343–54. doi: 10.1056/NEJMoa0910500
- Cui Z, Zhao MH, Jia XY, Wang M, Hu SY, Wang SX, et al. Antibodies to alpha5 chain of collagen IV are pathogenic in Goodpasture's disease. *J Autoimmun.* (2016) 70:1–11. doi: 10.1016/j.jaut.2016.04.001
- Wang XP, Fogo AB, Colon S, Giannico G, Abul-Ezz SR, Miner JH, et al. Distinct epitopes for anti-glomerular basement membrane alport alloantibodies and goodpasture autoantibodies within the noncollagenous domain of alpha3(IV) collagen: a janus-faced antigen. *J Am Soc Nephrol.* (2005) 16:3563–71. doi: 10.1681/ASN.2005060670
- Kang JS, Kashtan CE, Turner AN, Heidet L, Hudson BG, Borza DB. The alloantigenic sites of alpha3alpha4alpha5(IV) collagen: pathogenic X-linked alport alloantibodies target two accessible conformational epitopes in the alpha5NC1 domain. *J Biol Chem.* (2007) 282:10670–7. doi: 10.1074/jbc.M611892200
- Gray PE, O'Brien TA, Wagle M, Tangye SG, Palendira U, Roscioli T, et al. Cerebral vasculitis in X-linked lymphoproliferative disease cured by matched unrelated cord blood transplant. *J Clin Immunol.* (2015) 35:604–9. doi: 10.1007/s10875-015-0194-9
- Sado Y, Boutaud A, Kagawa M, Naito I, Ninomiya Y, Hudson BG. Induction of anti-GBM nephritis in rats by recombinant alpha 3(IV)NC1 and alpha 4(IV)NC1 of type IV collagen. *Kidney Int.* (1998) 53:664–71. doi: 10.1046/j.1523-1755.1998.00795.x
- Netzer KO, Leinonen A, Boutaud A, Borza DB, Todd P, Gunwar S, et al. The goodpasture autoantigen. Mapping the major conformational epitope(s) of alpha3(IV) collagen to residues 17-31 and 127-141 of the NC1 domain. *J Biol Chem.* (1999) 274:11267–74. doi: 10.1074/jbc.274.16.11267
- Hellmark T, Burkhardt H, Wieslander J. Goodpasture disease. Characterization of a single conformational epitope as the target of pathogenic autoantibodies. *J Biol Chem.* (1999) 274:25862–8. doi: 10.1074/jbc.274.36.25862
- Chen L, Hellmark T, Wieslander J, Bolton WK. Immunodominant epitopes of alpha3(IV)NC1 induce autoimmune glomerulonephritis in rats. *Kidney Int.* (2003) 64:2108–20. doi: 10.1046/j.1523-1755.2003.00332.x
- Phelps RG, Rees AJ. The HLA complex in Goodpasture's disease: a model for analyzing susceptibility to autoimmunity. *Kidney Int.* (1999) 56:1638–53. doi: 10.1046/j.1523-1755.1999.00720.x
- Ooi JD, Chang J, O'Sullivan KM, Pedchenko V, Hudson BG, Vandenbark AA, et al. The HLA-DRB1*15:01-restricted Goodpasture's T cell epitope induces GN. *J Am Soc Nephrol.* (2013) 24:419–31. doi: 10.1681/ASN.2012070705
- Ooi JD, Petersen J, Tan YH, Huynh M, Willett ZJ, Ramarathnam SH, et al. Dominant protection from HLA-linked autoimmunity by antigen-specific regulatory T cells. *Nature.* (2017) 545:243–7. doi: 10.1038/nature22329
- Persson U, Hertz JM, Carlsson M, Hellmark T, Juncker I, Wieslander J, et al. Patients with Goodpasture's disease have two normal COL4A3 alleles encoding the NC1 domain of the type IV collagen alpha 3 chain. *Nephrol Dial Transpl.* (2004) 19:2030–5. doi: 10.1093/ndt/gfh355

ETHICS STATEMENT

This study has been approved by the Human Research Ethics Committee of the South Eastern Sydney Local Health Network—Northern Sector HREC Ref 11/107, and written informed consent obtained from the parents of the participant for the publication of this case.

AUTHOR CONTRIBUTIONS

PG, KF, and TO'B managed the patient. TO'B contributed regarding post-transplant autoimmunity. KF regarding immune reconstitution. PG and JZ envisaged the project. PG liaised with VP who performed the serological and staining work with BH and AF. PG and HM worked with MS who performed genetics in Bristol and OS helped with data interpretation, while AK advised regarding HLA testing and interpretation. PG and VP worked together to bring the manuscript together with the help of other investigators.

FUNDING

This work was supported by the grant R01 DK18381 from the National Institutes of Health to BH.

ACKNOWLEDGMENTS

We thank Ms. Ellen Donnert for expert technical assistance with tissue immunofluorescence staining.

14. Hou HA, Tang JL, Hsu SC, Yu CL, Chen YC, Yao M. Acquisition and cure of autoimmune disease following allogeneic hematopoietic stem cell transplantation. *J Formos Med Assoc.* (2007) 106:779–83. doi: 10.1016/S0929-6646(08)60040-6
15. Moratto D, Giliani S, Bonfim C, Mazzolari E, Fischer A, Ochs HD, et al. Long-term outcome and lineage-specific chimerism in 194 patients with Wiskott-Aldrich syndrome treated by hematopoietic cell transplantation in the period 1980–2009: an international collaborative study. *Blood.* (2011) 118:1675–84. doi: 10.1182/blood-2010-11-319376
16. Yanir AD, Hanson IC, Shearer WT, Noroski LM, Forbes LR, Seeborg FO, et al. High incidence of autoimmune disease after hematopoietic stem cell transplantation for Chronic Granulomatous Disease. *Biol Blood Marrow Transplant.* (2018) 24:1643–50. doi: 10.1016/j.bbmt.2018.03.029
17. Holbro A, Passweg JR. Management of hemolytic anemia following allogeneic stem cell transplantation. *Hematol Am Soc Hematol Educ Program.* (2015) 2015:378–84. doi: 10.1182/asheducation-2015.1.378
18. Wang KS, Kim HT, Nikiforow S, Heubeck AT, Ho VT, Koreth J, et al. Antibodies targeting surface membrane antigens in patients with chronic graft-versus-host disease. *Blood.* (2017) 130:2889–99. doi: 10.1182/blood-2017-08-801001
19. Shetty HB, Howat AJ, Anderton JG. ANCA +ve/anti-GBM +ve vasculitis following bone marrow transplantation. *Nephrol Dial Transpl.* (2002) 17:2280–1. doi: 10.1093/ndt/17.12.2280
20. Brinkerhoff BT, Houghton DC, Troxell ML. Renal pathology in hematopoietic cell transplant recipients: a contemporary biopsy, nephrectomy, and autopsy series. *Mod Pathol.* (2016) 29:637–52. doi: 10.1038/modpathol.2016.61
21. Bolton WK, May WJ, Sturgill BC. Proliferative autoimmune glomerulonephritis in rats: a model for autoimmune glomerulonephritis in humans. *Kidney international* (1993) 44:294–306. doi: 10.1038/ki.1993.244
22. Kalluri R, Gattone VH III, Noelken ME, Hudson BG. The alpha 3 chain of type IV collagen induces autoimmune Goodpasture syndrome. *Proc Natl Acad Sci USA.* (1994) 91:6201–5. doi: 10.1073/pnas.91.13.6201
23. Gunwar S, Bejarano PA, Kalluri R, Langeveld JP, Wisdom BJ Jr, Noelken ME, et al. Alveolar basement membrane: molecular properties of the noncollagenous domain (hexamer) of collagen IV and its reactivity with Goodpasture autoantibodies. *Am J Respir Cell Mol Biol.* (1991) 5:107–12. doi: 10.1165/ajrcmb.5.2.107
24. Donaghy M, Rees AJ. Cigarette smoking and lung haemorrhage in glomerulonephritis caused by autoantibodies to glomerular basement membrane. *Lancet.* (1983) 2:1390–3. doi: 10.1016/S0140-6736(83)90923-6
25. Bombassei GJ, Kaplan AA. The association between hydrocarbon exposure and anti-glomerular basement membrane antibody-mediated disease (Goodpasture's syndrome). *Am J Indus Med.* (1992) 21:141–53. doi: 10.1002/ajim.4700210204
26. Goodnow CC. Multistep pathogenesis of autoimmune disease. *Cell.* (2007) 130:25–35. doi: 10.1016/j.cell.2007.06.033
27. Meyer D, Coles A, Oyuela P, Purvis A, Margolin DH. Case report of anti-glomerular basement membrane disease following alemtuzumab treatment of relapsing-remitting multiple sclerosis. *Mult Scler Relat Disord.* (2013) 2:60–3. doi: 10.1016/j.msard.2012.07.002
28. Singh P, Barry M, Tzamaloukas A. Goodpasture's disease complicating human immunodeficiency virus infection. *Clin Nephrology.* (2011) 76:74–7. doi: 10.5414/cn106607
29. Deenick EK, Chan A, Ma CS, Gatto D, Schwartzberg PL, Brink R, et al. Follicular helper T cell differentiation requires continuous antigen presentation that is independent of unique B cell signaling. *Immunity.* (2010) 33:241–53. doi: 10.1016/j.immuni.2010.07.015
30. Hirayama K, Yamagata K, Kobayashi M, Koyama A. Anti-glomerular basement membrane antibody disease in Japan: part of the nationwide rapidly progressive glomerulonephritis survey in Japan. *Clin Exp Nephrol.* (2008) 12:339–47. doi: 10.1007/s10157-008-0051-8

Conflict of Interest: The authors declare that the research was conducted in the absence of any commercial or financial relationships that could be construed as a potential conflict of interest.

Copyright © 2019 Gray, McCarthy, Siggs, Saleem, O'Brien, Frith, Ziegler, Kitching, Fogo, Hudson and Pedchenko. This is an open-access article distributed under the terms of the Creative Commons Attribution License (CC BY). The use, distribution or reproduction in other forums is permitted, provided the original author(s) and the copyright owner(s) are credited and that the original publication in this journal is cited, in accordance with accepted academic practice. No use, distribution or reproduction is permitted which does not comply with these terms.



Diagnostic Profiling of the Human Public IgM Repertoire With Scalable Mimotope Libraries

Anastas Pashov^{1*}, Velizar Shivarov^{2,3}, Maya Hadzhieva¹, Victor Kostov^{1,4}, Dilyan Ferdinandov⁴, Karen-Marie Heintz⁵, Shina Pashova^{1,6}, Milena Todorova¹, Tchavdar Vassilev⁷, Thomas Kieber-Emmons⁸, Leonardo A. Meza-Zepeda⁵ and Eivind Hovig^{5,9}

¹ Laboratory of Experimental Immunotherapy, Department of Immunology, Stephan Angeloff Institute of Microbiology, Bulgarian Academy of Sciences, Sofia, Bulgaria, ² Laboratory of Clinical Immunology, Department of Clinical Hematology, Sofamed University Hospital, Sofia, Bulgaria, ³ Faculty of Biology, Sofia University "St. Kliment Ohridski," Sofia, Bulgaria, ⁴ Neurosurgery Clinic, St. Ivan Rilsky Hospital, Sofia MU, Sofia, Bulgaria, ⁵ Department of Tumor Biology, Institute for Cancer Research, Oslo University Hospital, Oslo, Norway, ⁶ Department of Molecular Immunology, Institute of Biology and Immunology of Reproduction, Bulgarian Academy of Sciences, Sofia, Bulgaria, ⁷ Institute of Biology and Biomedicine, N.I. Lobachevsky University, Nizhny Novgorod, Russia, ⁸ Winthrop P. Rockefeller Cancer Research Center, UAMS, Little Rock, AR, United States, ⁹ Centre for Bioinformatics, Department of Informatics, University of Oslo, Oslo, Norway

OPEN ACCESS

Edited by:

Bridget S. Wilson,
University of New Mexico,
United States

Reviewed by:

Michael Zemlin,
Saarland University Hospital, Germany
Paolo Casali,
University of Texas Health Science
Center San Antonio, United States

*Correspondence:

Anastas Pashov
a_pashov@microbio.bas.bg

Specialty section:

This article was submitted to
B Cell Biology,
a section of the journal
Frontiers in Immunology

Received: 23 July 2019

Accepted: 14 November 2019

Published: 03 December 2019

Citation:

Pashov A, Shivarov V, Hadzhieva M, Kostov V, Ferdinandov D, Heintz K-M, Pashova S, Todorova M, Vassilev T, Kieber-Emmons T, Meza-Zepeda LA and Hovig E (2019) Diagnostic Profiling of the Human Public IgM Repertoire With Scalable Mimotope Libraries. *Front. Immunol.* 10:2796. doi: 10.3389/fimmu.2019.02796

Specific antibody reactivities are routinely used as biomarkers, but the antibody repertoire reactivity (igome) profiles are still neglected. Here, we propose rationally designed peptide arrays as efficient probes for these system level biomarkers. Most IgM antibodies are characterized by few somatic mutations, polyspecificity, and physiological autoreactivity with housekeeping function. Previously, probing this repertoire with a set of immunodominant self-proteins provided a coarse analysis of the respective repertoire profiles. In contrast, here, we describe the generation of a peptide mimotope library that reflects the common IgM repertoire of 10,000 healthy donors. In addition, an appropriately sized subset of this quasi-complete mimotope library was further designed as a potential diagnostic tool. A 7-mer random peptide phage display library was panned on pooled human IgM. Next-generation sequencing of the selected phage yielded 224,087 sequences, which clustered in 790 sequence clusters. A set of 594 mimotopes, representative of the most significant sequence clusters, was shown to probe symmetrically the space of IgM reactivities in patients' sera. This set of mimotopes can be easily scaled including a greater proportion of the mimotope library. The trade-off between the array size and the resolution can be explored while preserving the symmetric sampling of the mimotope sequence and reactivity spaces. BLAST search of the non-redundant protein database with the mimotopes sequences yielded significantly more immunoglobulin J region hits than random peptides, indicating a considerable idiotypic connectivity of the targeted igome. The proof of principle predictors for random diagnoses was represented by profiles of mimotopes. The number of potential reactivity profiles that can be extracted from this library is estimated at more than 10^{70} . Thus, a quasi-complete IgM mimotope library and a scalable representative subset thereof are found to address very efficiently the dynamic diversity of the human public IgM repertoire, providing informationally dense and structurally interpretable IgM reactivity profiles.

Keywords: diagnostic, phage display, antibody repertoire, mimotope, systems immunology

INTRODUCTION

The repertoire of human IgM contains a considerable proportion of moderately autoreactive antibodies, characterized by low intrinsic affinity/low specificity (1). They function as a first line of defense and as scavengers of senescent cells and debris (2–6) and even in tumor surveillance (7). It is becoming increasingly clear that the human antibody repertoire has an organization similar to that of its murine counterpart (8–12). About one fourth of the murine splenic B lymphocytes that respond to lipopolysaccharide have B-cell receptors that are moderately autoreactive. Practically unaffected by somatic mutations and follicular evolution, the physiological self-reactivities largely overlap with the germline-encoded polyspecific antibodies (13–15). Eighty percent of murine serum IgM falls in this category and is referred to as natural antibodies (nAbs) (16, 17). Apart from the polyspecific splenic B cells, the source of nAbs in mice seems to be mostly a population of B1-related IgM⁺ plasma cells residing in a unique IL-5-dependent bone marrow niche (18).

IgM antibodies appear early in the course of an infection. However, they fall relatively fast, even after restimulation, providing a dynamic signal. By interacting with structures of the self and carrying housekeeping tasks, this part of the antibody repertoire is coupled to changes in the internal environment. Consequently, IgM antibodies have gained interest as biomarkers of physiological or pathological processes (19–23). Yet they remain underused in immunodiagnosics, although their interactions with sets of antigens have been studied in a range of platforms (19, 22–25). The reasons IgM antibodies are rarely considered are probably their low specificity and transitory expression due to which particular specificities are used mostly to detect recent infection.

The study of the IgM repertoire (igome) might be expected to give information about interactions that occur mostly in the blood and the tissues with fenestrated vessels, because, unlike IgG, IgM cannot easily cross the normal vascular wall. Yet IgM tissue deposits are a common finding in diverse inflammatory conditions (26–28) and especially in the disorganized vasculature of the tumors, where they are a key element of the innate immune surveillance mechanism (7, 29, 30). Changes in the IgM repertoire further reflect B-cell function affected by antigenic, danger, and inflammatory signals, but also by anatomical changes leading to vascular permeability or disruption. Thus, IgM repertoire monitoring has the potential to provide clinically relevant information about most of the pathologies involving inflammation and vascular remodeling, as well as all types of cancer.

Our goal was to demonstrate that an essential part of the human polyspecific IgM repertoire involved in homeostasis could be probed by a set of mimotopes, which could be rationally scaled to sizes appropriate for the diagnostic tasks. Essentially, our approach does not specifically target disease specific antibody reactivities but rather the natural antibody repertoire as a universal biosensor of changes of the internal environment. The existing approaches for immunosignature (31, 32) or immunomic (33) analysis of the immunoglobulin repertoires focus mostly on IgG and have used arrays of either

10² proteins or 10⁴–10⁵ random peptides. The IgM repertoire has been previously probed by protein arrays (34), containing a physiologically determined representative set of autoantigens, which is a structurally coarse approach. We set out to explore the feasibility of a method that, similar to the self-protein “homunculus” arrays (15, 23), targets a small set of rationally selected probes but also preserves the structural interpretability of peptides in a format applicable for routine diagnostics.

MATERIALS AND METHODS

Deep Panning

Human IgM was isolated from a sample of IgM enriched IVIg, IgM-Konzentrat (Biotest AG, Dreieich, Germany, generously provided by Prof. Srinivas Kaveri), whereas human monoclonal IgM paraprotein was isolated from an IgM myeloma patient's serum selected from the biobank at the Center of Excellence for Translational Research in Hematology at the National Hematology Hospital, Sofia (with the kind cooperation of Dr. Lidiya Gurcheva). In both cases, IgM was purified using affinity chromatography with polyclonal anti-μ antibody coupled to agarose (A9935, SIGMA-ALDRICH, USA). A 7-mer random peptide library (E8100S, Ph.D.-7, New England Biolabs, USA) was panned overnight at 4°C on pooled human IgM adsorbed on polystyrene plates at a concentration of 0.1 mg/ml, washed, eluted with glycine buffer at pH 2.7, and immediately brought to pH 7. The eluate was transferred to a plate coated with monoclonal IgM and incubated according to the same protocol, but this time, the phage solution was collected after adsorption and amplified once, following the procedure described by Matochko et al. (35). Briefly, the phage DNA was extracted, and the peptide-coding fragment amplified by PCR. The amplicons were subjected to deep sequencing using the NextSeq platform (Illumina, USA), performed at the Sequencing Core Facility of Oslo University Hospital.

Patients' Sera

Sera were obtained from randomly selected patients with glioblastoma multiforme (GBM), brain metastases of breast (MB) or lung (ML) cancers, and non-tumor-bearing patients (C) (herniated disc surgery, trauma, etc.) of the Neurosurgery Clinic of St. Ivan Rilski University Hospital, Sofia. The samples were acquired according to the rules of the ethics committee of the Medical University in Sofia, after its approval and obtaining informed consent. The sera were aliquoted and stored at –20°C. Before staining, the sera were thawed; incubated for 30 min at 37°C for dissolution of IgM complexes; diluted 1:100 with phosphate-buffered saline (PBS), pH 7.4, and 0.05% Tween 20 with 0.1% bovine serum albumin (BSA); further incubated for 30 min at 37°C; and filtered through 0.22-μm filters before use. The serum IgM reactivity was analyzed on different sets of peptides defined in microarray format.

Peptide Microarray

The customized microarray chips were produced by PEPperPRINT™ (Heidelberg, Germany) by synthesis *in situ* as 7-mer peptides attached to the surface through their

C-terminus and a common spacer GGGs. The layout was in a format of a single field of up to 5,500 or five fields of up to 600 peptides in randomly positioned duplicates. The chips were blocked for 60 min using PBS, pH 7.4, and 0.05% Tween 20 with 1% BSA on a rocker; washed 3×1 min with PBS, pH 7.4, and 0.05% Tween 20; and incubated with sera in dilutions equivalent to 0.01 mg/ml IgM ($\sim 1:100$ serum dilution) on a rocker overnight at 4°C. After 3×1 -min washing, the chips were incubated with secondary antibodies at room temperature (RT), washed, rinsed with distilled water, and dried by spinning in a vertical position in empty 50-ml test tubes at $100 \times g$ for 2 min.

Microarray Data Analysis

The microarray images were acquired using a GenePix 4000 Microarray Scanner (Molecular Devices, USA). The densitometry was done using the GenePix® Pro v6.0 software. All further analysis was performed using publicly available packages of the R statistical environment for Windows (v3.4.1) (Bioconductor; Biostrings, limma, pepStat, sva, e1071, Rtsne, clvalid, entropy, RankProd, multcomp, etc.) as well as in-house developed R scripts (<https://github.com/ansts/IgMimPap1> and <https://github.com/ansts/IgMimPap2>). For algorithm details, see **Supplementary Methods**.

BLAST Search for Homologous Peptides

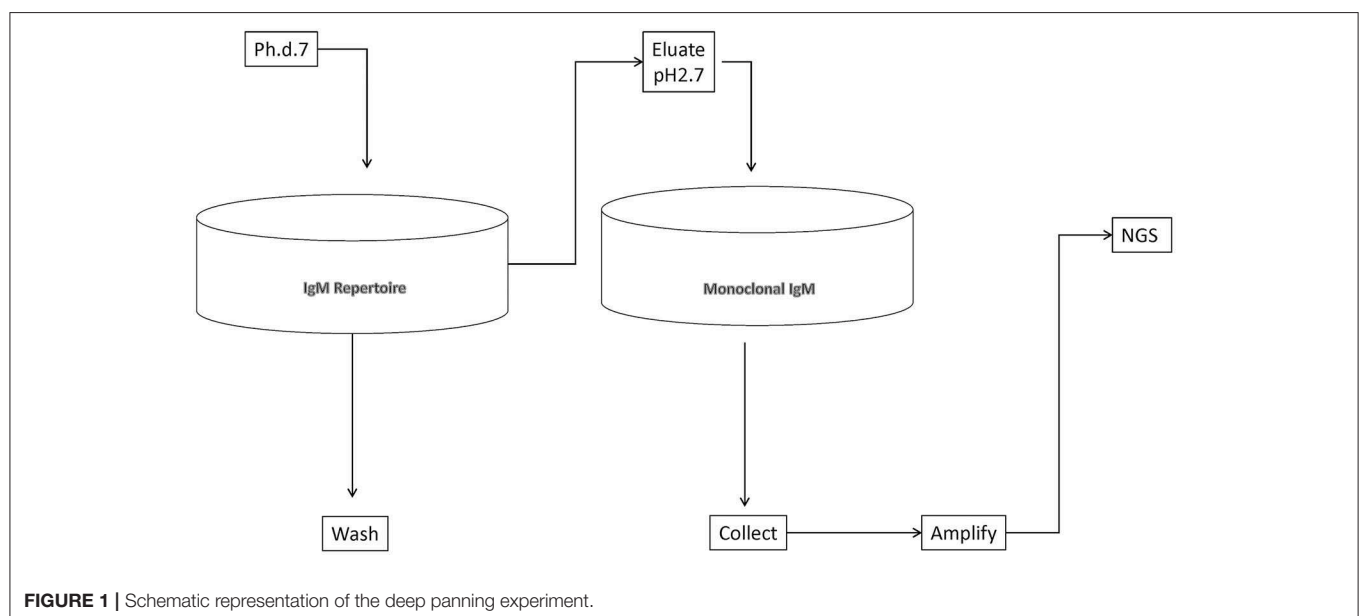
Sections of protein sequences homologous to the studied peptides were identified using the blastp function and the non-redundant human protein database of NCBI (36–38). The parameters were automatically adjusted for short sequences, and the results further restricted to those with a minimum of six positive positions and a minimum of six identity position with no gaps. The alignments are provided as **Supplemental Files**. This search was performed for three of the libraries: SYM, RND, and NGR. The NGR sequences introduced as negative control in the library SYM were removed so it represented only 519 sequences. For all libraries, the hits of each peptide were classified

into (1) immunoglobulin if at least one of the hits was in the heavy or light chain of the immunoglobulin genes, (2) non-immunoglobulin (hit in any other human protein sequence), and (3) no hit. The number of hits in immunoglobulin J region sequences greatly exceeded the length of those in other parts of the immunoglobulin sequences, and also J regions are naturally overrepresented in the database. Therefore, we considered with some approximation that the majority of the immunoglobulin hits were in J regions and if occasionally not, then in variable regions. The proportion of hits in immunoglobulin sequences were compared using the chi-square test.

RESULTS

Selection of 7-Mer Mimotopes

We set out to define as complete as possible a library of mimotopes of the normal human broadly expressed IgM repertoire. To this end, we chose to pan a commercially available 7-mer random peptide phage display library (Ph.D.-7, New England Biolabs) of diversity 10^9 . Thus, the size of the mimotopes would be in the range of the shortest linear B-cell epitopes in the IEDB database (<http://www.iedb.org/>). At the same time, an almost complete diversity of sequences of that length could be interrogated. As a repertoire template, we used an experimental preparation of human immunoglobulins for intravenous use enriched in IgM. It represents a pool of the repertoire of $\sim 10,000$ healthy donors. Total IgM was isolated from it by affinity purification. The phage eluted from the IgM repertoire was adsorbed on a monoclonal IgM to filter out phage binding to the constant regions, thereby focusing only on the mimotopes (**Figure 1**). The peptide inserts were amplified and deep sequenced using the approach described by Matochko et al. (35). Two separate experiments starting with 20% of the original phage library were performed (experiments A and B), whereas in a third one (C), the starting point was a preamplified 20% sample



of the original library. The yield was 688,860 (experiment A), 518,533 (experiment B), and 131,475 (experiment C) unique reads. Based on the distribution of the reads by copy number in the selections from the native and preamplified library, two thresholds were determined, that is, 2 and 11 copies, and the reads within these limits (exclusively) were considered further (see **Supplementary Methods**). The lower limit ensured the acceptable sequencing error level, and the upper was used to avoid overgrowing phage clones.

Sequence Properties of the Mimotope Clusters

The overall amino acids residues frequencies (AAF) in the mimotopes selected from the phage library showed a skewing in favor of G, W, A, R, T, H, M, P, and Q and against C, F, N, Y, I, L, and S (**Figure 2A**), when compared with the average overall amino acid frequencies of the Ph.D.-7 library. When studied by position, the distribution of AAF visualized by the respective sequence logos showed a highly skewed distribution for the N-terminus (**Figure 2B**). The actual frequencies by position are shown in **Figure 2C**. The residues of W, D, and E appear in similar frequencies, but owing to the much lower abundance of W in the phage library, in **Figure 2A**, it comes up as selected and D and E as slightly disfavored. The N-terminal frequency skewing and the preference for A, P, and T proved to be properties of the library. This became evident after comparing the AAF by position of a non-selected but amplified library [based on the data from Matochko et al. (35) **Figure 2D**]. The evidence of selection by IgM stood out in the distribution by position only after using the position weight matrix (PWM) of the non-selected amplified library as background frequencies to describe the actual enrichment in our mimotope library (**Figure 2E**). It showed a slight divergence from the background distribution of the frequencies in the middle of the sequence. Overrepresentation of proline in positions 2–7 appears to be a property of the amplified library, whereas the IgM binding selected for negatively charged residues, as well as glycine and tryptophan.

To gain insight into the mimotope sequence space, the set of 224,087 selected mimotope sequences was subjected to clustering using the GibbsCluster-2.0 method (39). This algorithm was applied originally for inferring the specificity of multiple peptide ligands tested on multiple major histocompatibility complex (MHC) receptors. The number of clusters was optimized by scanning the range of 100 to 2,500 clusters and using the Kullback–Leibler divergence (KLD) criterion. This is an information theory-based measure of similarity between two distributions. Here, it was used to compare the sequence alignments by cluster to the background model of random sequences (39). The cluster number scan indicated optimal clustering in 790 clusters (**Figure 3**). The range of cluster numbers was chosen on the basis of biological relevance (100) and computational complexity (2,500), and the choice proved suitable as much as there was a single global maximum of the criterion in this range. Position-weighted matrices were calculated next from each cluster (**Supplement File 2**).

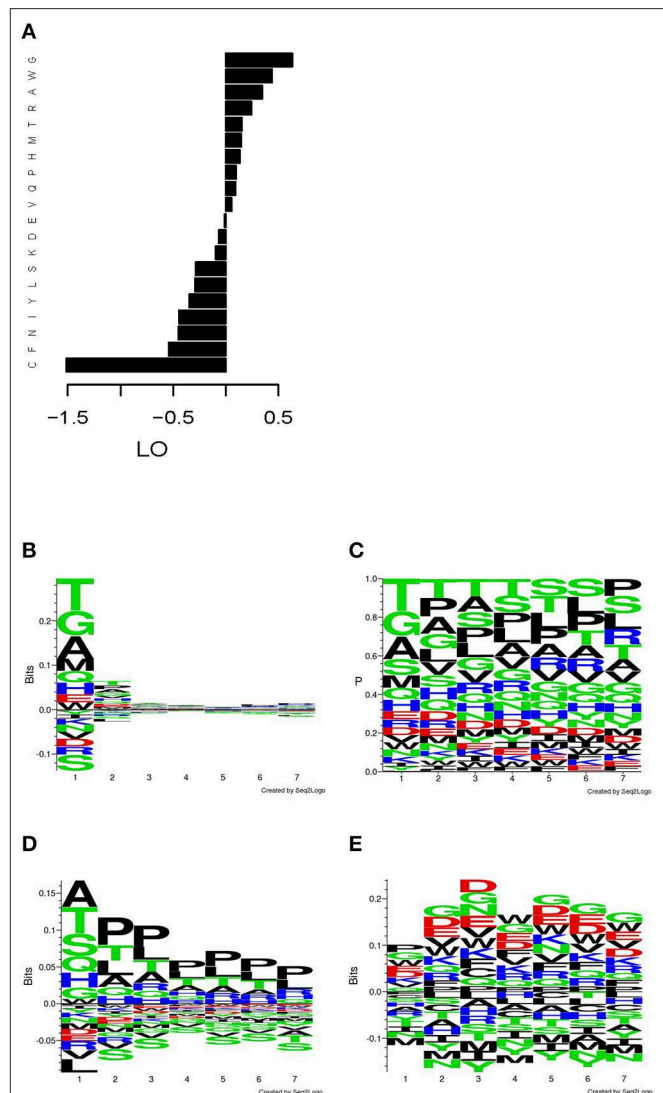
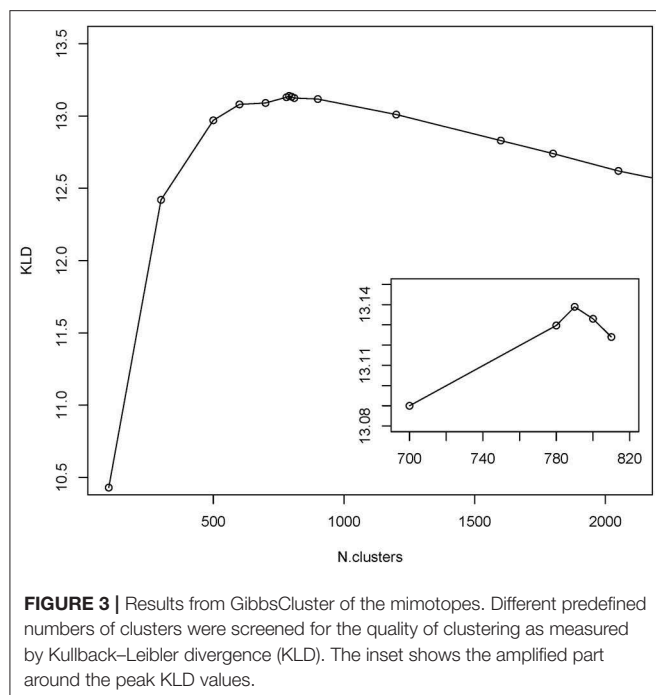


FIGURE 2 | Distribution of the amino acid residues in the mimotope library. **(A)** Log odds (LO) relative to background frequencies. **(B)** Sequence logo of the LO by position relative to the overall background frequencies. **(C)** Sequence logo of the frequencies by position. **(D)** Sequence logo of the LO by position in an amplified Ph.D.-7 phage library without ligand selection relative to the overall background frequencies (based on W. L. Matochko, R. Derda. "Error analysis of deep sequencing of phage libraries: peptides censored in sequencing". *Comput Math Methods Med*, 2013, 491612. 2013., <http://www.chem.ualberta.ca/~derda/parasitepaper/rawfiles/PhD7-GAC-30FuR.txt>). **(E)** Sequence logo of the LO by position relative to the frequencies by position in the amplified, unselected library shown in **(D)**. The skewing of the distribution in the free N-terminus appears to be property of the library, whereas the selection by the IgM repertoire leads to slight skewing in the middle of the sequence toward negatively charged residues, glycine and tryptophan.

Generation of a Mimotope Library for Practical Probing of the IgM Igome

The mimotope library of more than 200,000 sequences is a rich source of potential mimotope candidates for vaccine or diagnostics. Yet the size of a probe containing an array of 10^5 peptides is impractical for routine diagnostic use. A way



to scale down the mimotope probe array would be to include a representative sequence of each of the naturally existing 790 clusters. Only the sequence with the top score from each cluster was kept as a mimotope prototype for the cluster. These are expected to sample evenly (symmetrically) the mimotope sequence space, as ensured by the GibbsCluster algorithm.

The mimotope sequence diversity in each cluster was significant. Thus, cutting down so much the list of representative sequences would seem counterintuitive with respect to our goals. Nevertheless, this approach was chosen because such a symmetric sequence set was hypothesized to address a much wider range of IgM clones than the mere number of mimotopes chosen because of the well-documented polyspecificity of the majority of the antibodies probed.

The sequence clusters were found to vary with respect to the probability of random occurrence of such a group of sequences, which was used to rank them by significance (Supplementary Methods). As the optimal format of the microarrays used included five fields of 600 peptides, the top 519 clusters cluster representative sequences were considered further. Finally, 75 sequences from the negative control library NGR (see below) were added to a total of 594 peptides. This library was labeled SYM for symmetric.

The relevance of this mimotope library to the complete repertoire of broadly expressed IgM reactivities and the scope of their diversity could be established by comparing several different peptide libraries with different properties.

An alternative sequence library was constructed *in silico* to check the representativeness of the selected mimotope set and the relevance of the clustering found. To this end, 2.3×10^6 random 7-mer sequences were scored and ranked according to

TABLE 1 | Libraries of 7-mer peptides studied.

Library	Description	Number of peptides
SYM	A library that samples symmetrically the mimotope sequence space. Contains the sequence with the highest score for the respective position weight matrix from each significant cluster (significant clusters are those for which the number of sequences with more than median PWM score is greater than the expected number of occurrences of such score in random peptides— $p < 0.0001$ by binomial test).	594
C5_1	A group of 5 of the 288 clusters with best binomial $p < 1e-16$: clusters #2, 6, 9, 10, and 11. This library is an example of a lower diversity set.	600
C5_2	A group of 5 of the 288 clusters with best binomial $p < 1e-16$: clusters #115, 61, 55, 53, and 258. This library is an example of lower diversity set.	1,193
C5P	150 random* sequences with log odds scores greater than the median score of the respective cluster for each of 5 clusters (clusters #2, 6, 9, 10, and 11). This library tests the capacity of the sequence profiles to capture the antigenic properties of the mimotopes.	750
NG1	The lowest scoring sequence (using KLD) from each significant cluster. These sequences are least certain to belong to any of the 790 clusters.	594
NG2	Among the set of the lowest scoring sequences (NG1) using GibbsCluster's own "Corrected" score—those with score < 5 (39). Another version of the previous library.	82
NGR	The max scores for each of a set of 2×10^6 random* 7-mer sequences after testing against each cluster PWM are ranked, and the sequences with the lowest ranks are retained representing sequences least related to the mimotope library.	753
RND	800 random peptides.	800
Total		5,366

The number of sequences per library was constrained by the size of the microarray chip used for their testing. PWM, position weight matrix.

**The random sets are constructed with underlying frequencies in phage display library Ph.D.-7.*

their similarity to each of the 790 clusters of mimotopes defined above. The random sequences that were the least related to any of the clusters in the selected library were used as a negative control (library NGR—see Supplementary Methods).

Other libraries of peptides generated for further comparison were as follows: (1) uncertainly clustered sequences as reflected in their KLD scores as shown by the GibbsCluster algorithm (NG1 and NG2); (2) two groups of five high scoring clusters as lower diversity libraries (C5_1 and C5_2); (3) random 7-mer sequences predicted to belong to some of the five highest scoring clusters based on PWM profile scores (C5P); and (4) random 7-mer sequences (RND) (see Table 1 for description of all libraries).

Comparison Between Libraries

IgM reactivity in sera from patients with GBM ($n = 3$), MB ($n = 3$), and non-tumor-bearing neurosurgery patients (C, $n = 4$) was analyzed using the sets of peptides described in Table 1. The peptide libraries were synthesized in an oriented

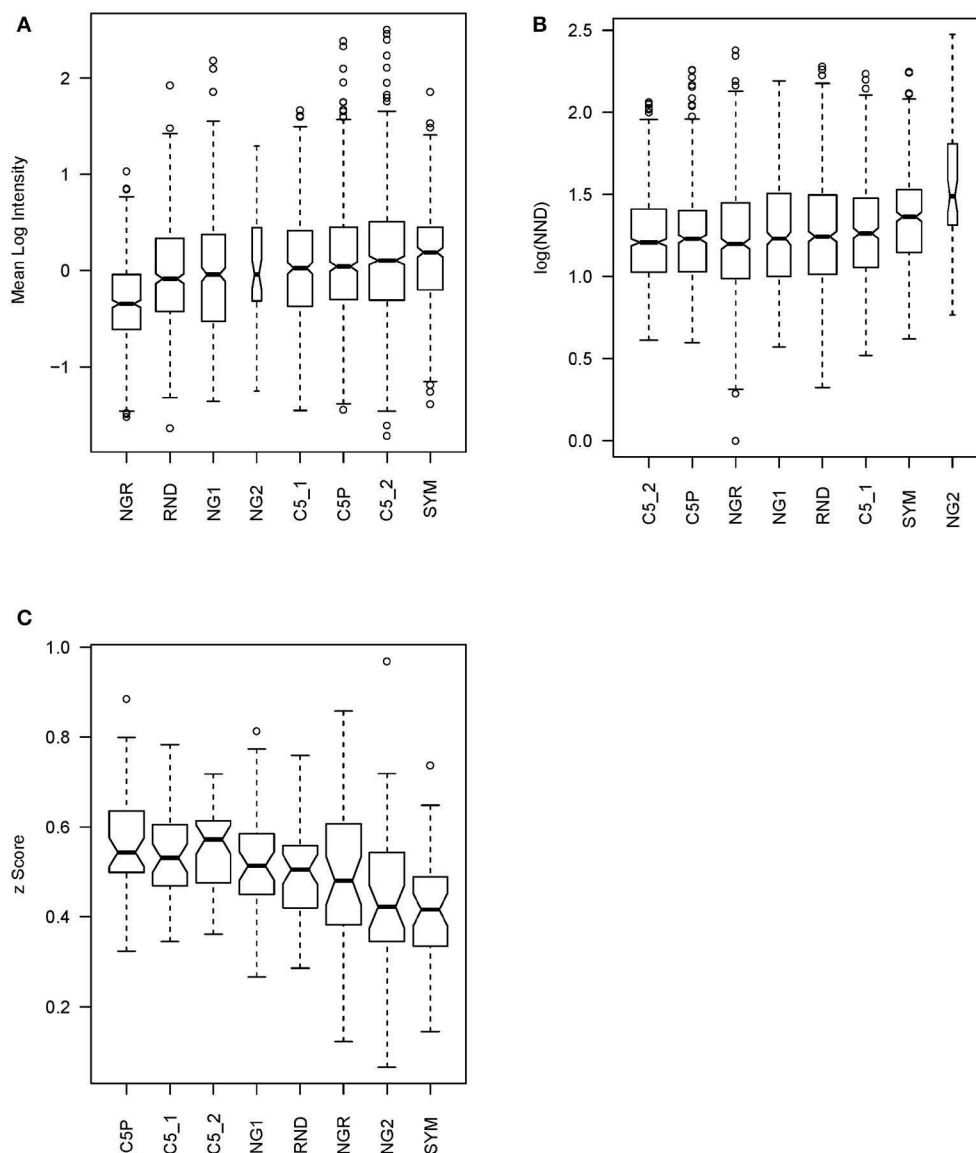


FIGURE 4 | Statistics testing the libraries' capacity to probe the mimotope reactivity space. **(A)** Mean reactivity of each peptide across patients grouped by library. The optimized library SYM has the highest reactivity. For library content, see **Table 1**. **(B)** Mean nearest neighbor distance of the peptide profiles across 10 patients in each library. **(C)** Mean correlation of patient profiles across the peptides in each library compared after z transformation. This test has a similar meaning as the previous but is performed on the transposed matrix. The optimized library SYM provides the least correlated patient reactivity profiles, which indicates a high potential to reflect the natural diversity of the human population but increases the requirements for the size of the teaching sets to extract models of good generalization. The optimized library SYM appears to sample the mimotope reactivity space evenly. The width of the bars is proportional to the size of the sample.

(C-terminus attached) planar microarray format. In the first round of experiments, the eight different libraries defined were compared based on the IgM reactivity in the sera from 10 patients (**Supplementary Figures 4, 5**). The data on the mean serum IgM reactivity of the peptides with the different sera, grouped by library, were used to compare the libraries for their overall reactivity using linear models (**Figure 4A**). The proposed optimized small library (SYM) had significantly higher ($p < 0.001$) average reactivity than NG1, RND, or NGR. Interestingly, the library NGR, which was *in silico* purged of

sequences scoring high with the 790 profiles of mimotope clusters defined, had indeed the lowest reactivity. It was significantly lower than that of both the weakly clustering peptides (NG1) and the random sequences (RND) (**Supplementary Table 1**). This is considered an indication that the mimotope library of the order of 10^5 sequences is a quasi-complete igeome image. Also, this fact is in support of the hypothesis that the 790 cluster profiles summarize in sufficient detail the salient sequence features that define the mimotopes of the public human IgM repertoire.

TABLE 2 | Rank product test of three criteria for optimal mimotope library.

Library	Rank products	p value
C5_1	4.380	0.650
C5P	5.518	0.853
NG1	5.313	0.823
NG2	2.154	0.099
NGR	5.241	0.812
C5_2	4.579	0.692
SYM	1.260	0.007
RND	4.820	0.739

Next, the capacity of the different libraries to sample symmetrically the space of 7-mer IgM mimotope reactivities in the IgM repertoire was tested. The mean nearest neighbor distance (MNND) was used for that purpose as a statistic indicating clustering of the data. Peptides that have similar reactivity profiles with different sera (thus carrying redundant information) would map to points in the reactivity space that lie close to each other. This clustering in some regions of the space would lead to a lower MNND. The library SYM ranked second only to NG2 (**Figure 4B**) by this parameter and had a significantly higher MNND than all the other libraries (**Supplementary Table 2**).

The correlations between the patient profiles of reactivity were also used as a measure of the capacity of the libraries to extract information from the IgM repertoire. We tested all pairwise correlations between the patient profiles with the peptides from a given library. After z transformation of the correlation coefficients to allow for comparison by linear models, the means of those z values for each library were used to compare the libraries (**Figure 4C**). Again, the SYM library exhibited the lowest mean correlation—significantly lower than the correlation between the reactivities with the other libraries except for NGR and NG2 (**Supplementary Table 3**).

Finally, all three criteria were summarized using a rank product test, which proved that reactivity with SYM stands out from all the other tested libraries as the best among them for probing the IgM repertoire (**Table 2**).

Visualization of the Mimotope Sequence Space

T-distributed stochastic neighbor embedding (t-sne) was used to visualize the structure of the mimotope sequence space as represented by the general mimotope library produced by deep panning. To represent the sequences as vectors of real numbers, each amino acid residue was represented by five scores based on the z_1 – z_5 scales published by Sandberg et al. (40) (see **Supplementary Methods** for details). Thus, each 7-mer sequence was parameterized as a 35-dimensional vector. These vectors were then represented in two dimensions by t-sne transformation. The map of the mimotope library, thus generated, resembled that of an equal number of random 7-mer

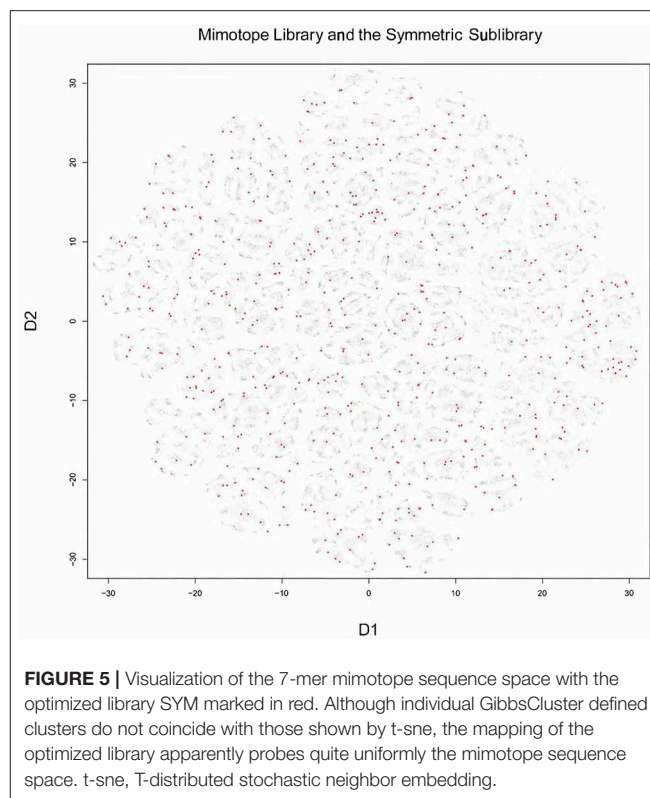


FIGURE 5 | Visualization of the 7-mer mimotope sequence space with the optimized library SYM marked in red. Although individual GibbsCluster defined clusters do not coincide with those shown by t-sne, the mapping of the optimized library apparently probes quite uniformly the mimotope sequence space. t-sne, T-distributed stochastic neighbor embedding.

sequences constructed using the residue background frequencies of the phage display library (**Supplementary Figure 7**). Next, the representation of some of the clusters of mimotopes described above was mapped in this new mapping. Although the five most significant among 790 sequence clusters (the C5_1 library, **Supplementary Figure 7**) mapped to rather scattered clusters in the t-sne representation, the mapping of the optimized library (SYM) still covered symmetrically the mimotope sequence space (**Figure 5**). Both the clustering and the mapping do not give unique solutions and fail to capture the full information in the general mimotope data set. Yet the symmetry of the optimized library SYM, designed rationally on the basis of the clustering, is nevertheless reflected in the t-sne mapping.

SYM Overrepresents Mimotopes of Idiotype

An important aspect of the usage of mimotopes as igeome probes is their interpretability. Using large mimotope libraries provides an opportunity to generalize the type of structures targeted by the antibody repertoire studied. The numerous tests may allow for signal to emerge despite the noise due to poor representativeness of conformational epitopes, polyspecificity, mimotope/epitope sequence length disparity, etc.

To explore the capacity of the library SYM to reveal general properties of the antigens targeted by the natural IgM repertoire, we used NCBI blastp program to find SYM homologous short sequences in the non-redundant (nr) database of human proteins

(36, 37). The parameters of the search were automatically adjusted to short sequences. Owing to the extremely short length of the query sequences, the expectation values were high. The proteins containing sequences homologous to SYM mimotopes were very often immunoglobulin junction region. This is not surprising as the diversity of the immunoglobulin J regions included in the human nr database is on the same scale as the overall diversity of the proteome. We were somewhat surprised, though, to see a highly significant preference to immunoglobulin J regions in the alignments of the SYM library as compared with the RND and especially with the NGR library as well as in the RND compared with NGR (**Figure 6**). The NGR sequences attached to SYM as controls were excluded for this search, yielding only 519 mimotopes. Despite the small number of sequences, the profile derived for GBM (see below) had even higher number of homologies in J regions.

Diagnostic Potential of a Rationally Designed Restricted Mimotope Library

To test the diagnostic potential of the SYM library, we chose to look for reactivity profiles able to separate sera from patients with different brain tumors. Although somewhat questionable, our expectation to find IgM repertoire correlates of brain tumor diseases was justified by (1) reports by Merbl et al. (23) that both IgG and IgM natural autoreactive antibody profiling with self-antigens can discriminate between murine tumors and from O'Donnell et al. (41) that 3×10^5 random peptide-based profiling of antibody repertoires can discriminate GBM from other tumors; (2) reports indicating the role of natural IgM antibodies in the immune surveillance against tumors (7, 30–39, 41–43); and (3) reports of diagnostic or therapeutic natural IgM binding-defined tumor antigens (44–46). Furthermore, cancer is a suitable test for the natural IgM igome's diagnostic utility because of the localized inflammation and shedding of tumor-specific and tumor-associated antigens. Therefore, this type of pathology serves better to test a “biosensor” property of the functional repertoire. It would surely be easier to show SYM profile changes studying diseases affecting the repertoire itself, which cause large-scale distortion like hyper-IgM syndrome, myeloma, and reconstitution after ablative therapy, but this was deemed insufficient.

For this assay, we used sera from a set of 34 patients with brain tumors. The main goal was a “proof of principle” test demonstrating the capacity of the assay to provide mimotope reactivity profiles suitable for building predictors for randomly selected pathology. The distribution of patients by diagnosis (GBM, ML, MB, and C) is shown in **Table 3**. The microarray data were cleaned and normalized locally and globally, and the group sizes were balanced, which warranted the use of the ComBat function (47) for the batch effect compensation. The reactivity data, thus obtained, represented 28 patients' serum IgM binding to 586 peptides. No reactivity was found specifically expressed in any of the diagnostic groups. Each patient's serum, though, reacted significantly with most of the mimotopes as compared with the pool of the rest of the patients. The reactivities with individual sera were between 339 and 390 (mean, 368) out of

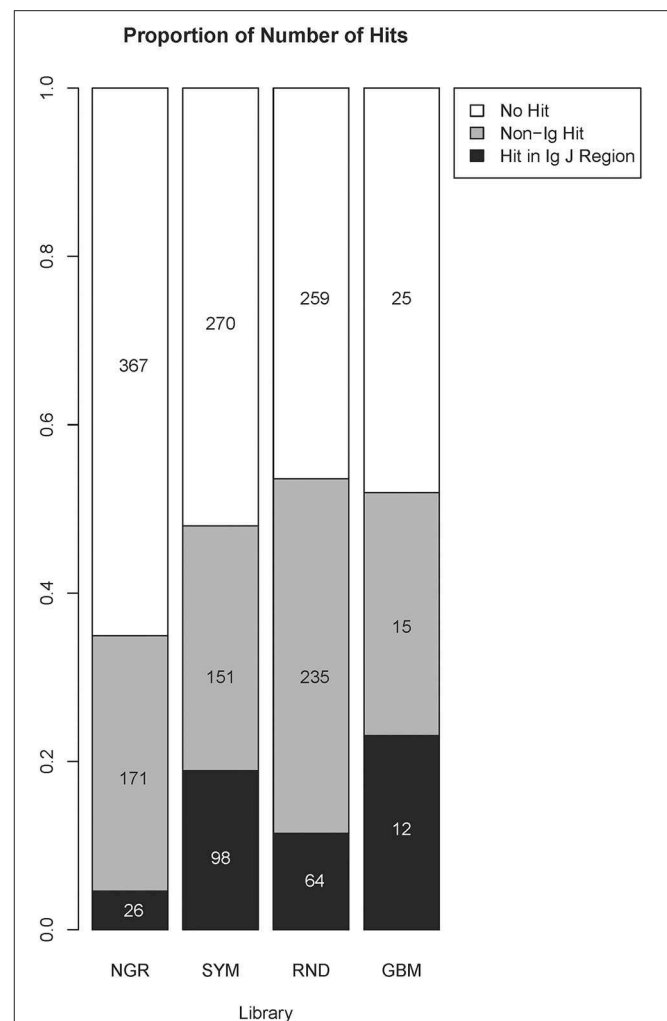


FIGURE 6 | Comparison between the number of homologous sequences found by BLAST search of the non-redundant human protein database classified as immunoglobulin J regions or non-immunoglobulin hits. The numbers and the size of the shaded bars correspond to the number of peptides having this type of homolog in the targeted database, and the proportion these peptides represent the volume of the library. A peptide was considered to be homologous to an immunoglobulin J region if the search returned at least one hit in a variable J region. The parameters were automatically adjusted for short sequences, and the results further restricted to those with a minimum of six positive positions and a minimum of six identity position. The alignment length was set equal to the number of positive positions, and no gaps were allowed. The proportions were compared using the chi-square test followed by pairwise multicomparison with false discovery rate correction (overall, $p = 2 \times 10^{-16}$; SYM/Ig vs. RND/Ig, $p = 1.2 \times 10^{-6}$; SYM/non-Ig vs. RND/non-Ig, $p = 3.6 \times 10^{-9}$; NGR/Ig vs. RND/Ig, $p = 2 \times 10^{-8}$; GBM/Ig vs. RND/Ig, $p = 0.045$). GBM, glioblastoma multiforme.

586. Altogether, 582/586 reactivities were significant in at least one patient.

A two-dimensional projection of the cases on the 582 positive reactivities by multidimensional scaling (MDS) showed no separation (data not shown). This is expected because the peptide library is not targeted to any particular pathology. It represents

TABLE 3 | Patients tested using the optimized library.

Diagnosis	Abbr.	Batches			Total
		G	P	R	
Non-tumor bearing (control)	C	1	3	4	8
Glioblastoma multiforme	GBM	2	4	9 (5)*	15 (11)*
Lung cancer (brain metastasis)	ML	2	4	3	9
Breast cancer (brain metastasis)	MB	0	0	2 (0)*	2 (0)*
Total					34

*To balance the group sizes between batches, only 5/9 GBM samples from batch “R” were used, and the breast cancer cases were omitted before batch compensation using the ComBat function. All cases in batch “R” were used in the validation step; those omitted from the training step served as a testing set.

rather a universal tool for IgM repertoire probing and mapping to a highly multidimensional feature space. The information in the reactivity profiles when all features are used is so rich that it makes practically each patient unique and a generalization impossible. In addition, the “curse of dimensionality” makes differentiating in 582 dimensional space hard. Therefore, a feature selection step would be necessary to construct a predictor for any diagnostic task.

A combination of filtering and wrapping feature selection techniques was applied next. The filtering method used was a selection of individual features with highly significant expression in at least one patient. The wrapping techniques were recursive feature elimination followed by a forward selection algorithm. The feature to remove (respectively to add) at each step was selected so as to improve maximally the separation of the patient data clusters of interest when mapped on the remaining features. This iteration was repeated until no further improvement of the separation is possible (see **Supplementary Methods** section for details). This algorithm produced SYM subsets of 60 up to 220 features depending on variations of the clustering criterion (recursive feature elimination derived sets [RFEDSs]). Using this approach, we tested the capacity of the respective RFEDSs to separate dichotomously GBM from the rest of the cases. For the consecutive steps, the cases omitted before the batch compensation were used as a testing set. A support vector machine (SVM) model based on GBM-RFEDSs separated well the patient groups in the training set. Still, it suffered from overfitting when tested in a leave-one-out validation (data not shown) performed within the limits of the overall training set. To achieve generalization, next, we explored the variation of the GBM-RFEDSs using patient data sets that differed by 2/28 cases (using the leave-one-out scheme—**Supplementary Methods**). It was surprising to find that so similar patient groups produced different GBM-RFEDSs that contained between 15 and 194/582 reactivities (median = 54) with only one feature common for all GBM-RFEDSs generated. The reason for this could be the variability between individuals and the capacity of the mimotope library to reflect it. Another reason could be the hypothesized highly convoluted nature of the profiles—each IgM clone should be represented by a number of reactivities, and each peptide

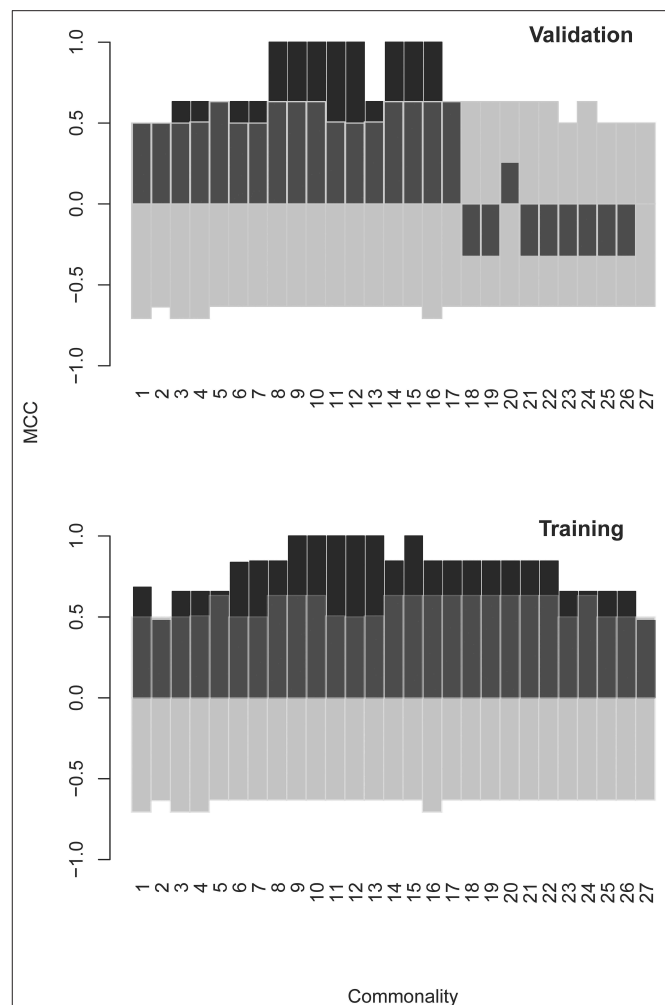


FIGURE 7 | Matthews correlation coefficient (MCC) as a measure of the quality of SVM models using different optimized feature sets. The models were constructed using GBM specific feature sets derived by a combination of filtering and backward and forward feature selection steps. Finally, consensus feature sets were formed from at least n “leave one out” groups of patients: $n = 1$ means all features from all groups were pooled, and $n = 27$ means the set contains only the three features found in all 27 groups (there was only one feature found in all 28 groups). The testing set consists of the cases in batch “R” that were omitted from the batch compensated pooled patient group. The model predicts correctly the classification of these cases. As the values in batch “R” were not subject to batch compensation, the validation also serves as a control against artifacts introduced by the ComBat function. The transparent bars indicate the 5% and the 95% confidence limits of MCC calculated on the basis of 1,000 scrambled matrices. SVM, support vector machine; GBM, glioblastoma multiforme.

possibly reacts with more than one clone. Nevertheless, a good prediction both of the training and of the testing sets using SVM was possible when combining features that recur widely in the GBM-RFEDSs. The best performing feature set represented a pool of 43 features each found in at least 15 of the 28 GBM-RFEDSs (**Figure 7**, see **Supplementary Methods** for further details).

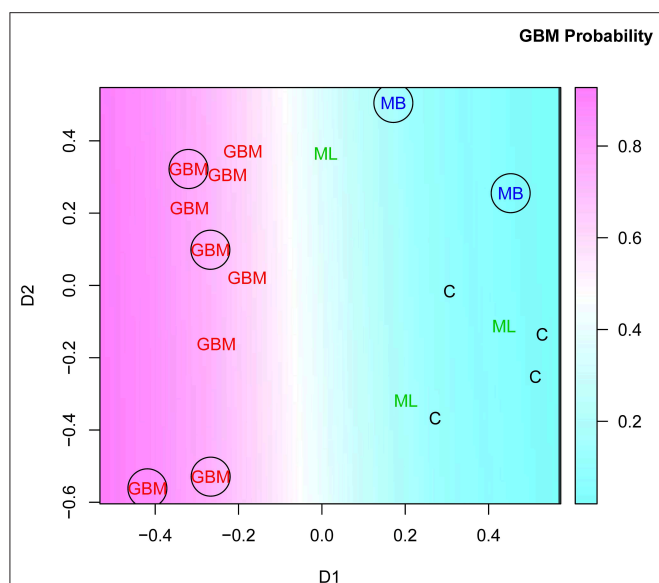


FIGURE 8 | Multidimensional scaling plot of cases in batch “R” based on the set of GBM-related features found in at least 15/28 of the “leave on out” patient groups. See **Figure 7** and **Supplementary Methods** for details. The encircled points correspond to the testing set. GBM, glioblastoma multiforme.

Interestingly, this two-stage feature selection strategy (bootstrapping RFEDS variability and pooling recurring features) helped improve the generalization considerably. Testing of the model of 43 dimensional data with just a few cases is impractical. Therefore, the dimensionality of the IgM reactivity data was reduced from 43 to 2 using MDS. The SVM model, constructed on the basis of the two surrogate features obtained by MDS, successfully classified the GBM and non-GBM cases not only of the training but also of the testing set of sera (**Figure 8**).

Thus, we were able to show that a rationally designed small library of 586 IgM mimotopes contains potentially a huge number of mimotope profiles that can differentiate randomly selected diagnoses after appropriate feature selection.

DISCUSSION

High-throughput omics screening methods have extracted profiles from different dynamic diversities (proteome, genome, glycome, secretome, etc.) and used them as biomarkers. The use of the antibody repertoire as a source of biomarkers has also been defined and approached in multiple ways. First came the technically minimalistic, but conceptually loaded, semiquantitative immunoblotting, developed 20 years ago (48–53). The further development produced methods that have been referred to as functional immunomics (33) in terms of protein reactivities or as immunosignaturing (31) in terms of random peptide libraries or described as a deep panning technique (54) in terms of complete set of mimotopes (igome) selected from random phage display libraries. Here, we describe the design of the first mimotope library for the analysis of the human

IgM repertoire of reactivities recurrent in most individuals also referred to as public repertoire (12, 55, 56). The focusing on broad reactivities is a consequence of panning on IgM pooled from at least 10,000 donors, which dilutes the unique specificities.

The deep panning approach relies on next-generation sequencing (NGS) and thus requires balancing between sequence fidelity and diversity. Even with diversity affected by discarding sequences of one and two copies on the one hand, and overgrowth of phage clones on the other, our strategy still manages to find a general representation of the mimotope sequence space by identifying clusters of mimotopes. This relatively small set of sequence classes is hypothesized to be related to the modular organization of the repertoire defined previously (57). Alternatively, it can also be an artifact of the sequence clustering algorithm depending on the size and diversity of the sequence set. In the latter case, the clustering may not reflect a biological phenomenon but still provides a tool for the classification of the sequences.

The central role of prolines in the nAb mimotopes has been observed previously (58). Tchernychev et al. also used a phage display library. Now, it is clear that the high proline content of nAb mimotopes that they found is related to the bias of the particular phage display library. This property of the library may facilitate the discovery of mimotopes because prolines are associated with turns and flanking structures and proline abundance also reduces the entropic component of the binding. In our experiments, the selection by the IgM repertoire led to an enrichment of tryptophan and negatively charged residues in the middle of the sequences. This suggests that the broad IgM reactivity has a preference for loop-like mimotopes (facilitated by the presence of prolines) with negative charges. The abundance of tryptophan is also interesting in terms of its propensity (together with proline) to mimic carbohydrate structures (59).

The mimotope library of diversity 10^5 derived by deep panning reflects the recurrent IgM specificities found in the human population. A library of random peptides with sequences selected to be least related to the observed 790 cluster profiles reacted very weakly with IgM from patients' sera. This fact suggests that not only does the library of a little over 200,000 mimotopes represents the IgM mimotope space but also that the 790 cluster profile matrices are collectively a promising model of it. The good coverage of the IgM reactivity space by this mimotope library most probably is facilitated by the polyspecific binding of IgM and the small, flexible peptides.

Although the large mimotope library can be used as is in peptide arrays when applicable, its size is not very practical for routine diagnostics. The classification in 790 clusters was used to produce a smaller and more applicable library, SYM, for clinical use. It contains basically representative sequences from the most significant clusters. SYM represents more efficiently the mimotopes' main reactivity patterns found in the phage selection experiment when compared with seven other libraries chosen to represent key alternative concepts. The precision of that representation can be adjusted by expanding the small library if necessary. Including more mimotopes from the set of 224,087 can be done in a similar fashion, sampling further the existing sequence clusters. Another improvement may be to

include a couple of related sequences to each of the mimotopes, for example, those immediately adjacent in the same cluster, for a statistically robust signal.

An interesting though not unexpected property of the public IgM igome found is its idiotypic connectivity. Overlap with immunoglobulin variable domain J regions proved the prominent feature of the human protein sequence fragments homologous to the peptides in SYM library. The actual epitopes of IgM should be mostly conformational. Nevertheless, both linear idiotypic epitopes (idiotopes) and fragments of them are probably represented in the CDR3 loops so as to produce statistically detectable signal in the BLAST results. It has long been known that linear epitope models yield clear structural idiotypic representation in CDR3 loops (60). Interestingly, the overall number of hits in the human proteome for the SYM library was smaller than that for the random library RND, which may reflect the overall tolerance of the igome for self to the background of higher idiotypic connectivity. The considerable self-referential (immunoglobulin-immunoglobulin) component of the igome means that the signal that can be read off it as a biosensor should be viewed in terms of global connectivity perturbations at least as much as in terms of local antibody–autoantigen interactions. Indeed, this idiotypic component is preserved and even somewhat enhanced in the specific profile found for GBM.

SYM could be used as a tool for the study of the IgM repertoire, as a source of mimotopes for design of immunotherapeutics (61–64), but mostly it may be applied as a multipurpose diagnostic tool. As a diagnostic tool, SYM has some key properties that distinguish it from other omics sets. When used to probe sera from patients with different brain tumors, no single reactivity correlated strongly with a whole diagnostic group. Still, quantitative profiles of subsets of reactivities collectively could separate the diagnoses by decision boundaries, which can be non-linear. Thus, appropriate feature selection algorithms are essential for the design of predictors based on the natural, polyspecific igome. With the use of the proposed algorithms, the typical feature sets tuned for dichotomous separation of diagnoses contained between 28 and 111 sequences (median = 66). Keeping only features recurring in at least half of the sets generated in the bootstrapped feature selection algorithm helped remedy the overfitting of the models and achieve the necessary generalization.

The optimal feature set for GBM diagnosis we find has 43 mimotopes. If the library provides in the order of 500 significant reactivities and the profiles are typically of around 50 features, the theoretical capacity of this approach is $>10^{70}$ different subsets. This is an estimate of only the qualitative outcome—presence or absence of reactivity. Thus, the information provided by a typical IgM binding assay with the library is probably enough to describe any physiological or pathological state of clinical relevance reflected in the IgM repertoire. Of course, this is just an estimate of the resolution of the method. The number of naturally occurring profiles and their correlation with clinically relevant states will determine the actual capacity. Another important consideration is the significant probability to find profiles correlating to any state by chance. Therefore,

extensive testing of the models to prove their ability to generalize is indispensable.

The novelty of our approach is based on the combination of several previously existing concepts.

First, early studies have argued that the physiologically autoreactive nAbs comprise a consistent, organized immunological compartment (50, 53, 65–68). The consistency of the nAb self-reactivity among individuals was considered evidence for the existence of preferred self-antigens. Such “public reactivities” are most probably related to the germline repertoire of antibodies generated by evolutionarily encoded paratope features and negative/positive selection (34, 69, 70). They were hypothesized to represent the repertoire compartment characterized also by idiotypic interactions (71). These antibodies were targeted using protein microarrays, the utility of which has been previously demonstrated (23, 33, 34, 57). Recently, the existence of structurally distinct public V-regions has been analyzed using repertoire sequencing (12), noting again that they are often found in nAbs. If the repertoire should be read as a source consistent patterns that can be mapped to a wide variety of physiological and pathological states, the public natural IgM autoreactivity seems to be a suitable but underappreciated compartment.

Second, germline variable regions are characterized by polyspecificity or cross-reactivity with protein and non-protein antigens (14). It seems that going for epitopes could be a way to approach the repertoire convolution. Yet the actual epitopes will be mostly conformational and hard to study. In similar tasks, mimotopes are often used (72–75). On the other hand, M. H. Van Regenmortel argues that mimotopes are of little use to structural prediction of a B-cell epitope (74). Apparently, this is less of a problem when the whole repertoire is used to address classes of epitopes whereby a statistically significant signal can be detected.

Third, peptide arrays have been used for some time now as probes of the antibody repertoire (54, 76–79). This includes the use of random peptide arrays for extracting repertoire immunosignatures (32) or deep panning of phage display libraries to analyze antibody response (54). Here, we combined these two approaches. An antibody can often cross-react with a linear sequence that is part of the nominal conformational epitope (74). The 7 aa residue long peptides can be viewed as a simplified set of long “syllables” in the epitope “vocabulary” that can cross-react with the respective antibodies. They represent also a set of small complete epitopes. For instance, in the Immunoepitope Database (<http://www.iedb.org>) collection of 4×10^4 linear B-cell epitopes close to 5,000 entries are <8 residues long. Thus, the peptide length of seven residues makes possible the interrogation of the repertoire with a library of 10^9 *k*-mers, which is at the same time complete and highly diverse.

The phage display-generated library provides a rich source of mimotopes that can be screened for different theranostic tools focused on particular targets. On an omics scale, the smaller optimized mimotope library proposed here probes the repertoire of broadly expressed IgM reactivities efficiently, mapping its dynamic diversity to a space of potentially over 10^{70} distinct profiles. The major tasks ahead are (1) exploring the concept of reproducibility for the sequences of IgM mimotopes by

further deep panning experiments and (2) designing studies aimed at efficiently extracting specific diagnostic profiles and building appropriate predictors, for example, for predicting immunotherapy responders or side effects and predicting the risk of malignancy in chronic inflammation as well as other conditions involving immune activity.

DATA AVAILABILITY STATEMENT

The datasets generated for this study can be found in the GITHUB (<https://github.com/ansts/IgMimoPap1> and <https://github.com/ansts/IgMimoPap2>).

ETHICS STATEMENT

The studies involving human participants were reviewed and approved by Ethics Committee at the Medical University Sofia. The patients/participants provided their written informed consent to participate in this study.

AUTHOR CONTRIBUTIONS

AP conceptualized the project, analyzed the results performing all the *in silico* work, supervised experiments except for the sequencing as well as the overall project execution, and prepared the manuscript. MH ran the phage display experiments. VK and MT ran the microarray experiments up to data processing and cataloged and maintained the seroteque. VS participated in the conceptualizing of the paper and the overall design of

the experiments, supervised the phage display experiments, and together with K-MH and LM-Z carried out the DNA isolation, PCR, and sequencing. EH supervised the sequencing task and participated in conceptualizing the project and the preparation of the manuscript. SP and MT performed the data processing of microarray scans. TV and TK-E participated in conceptualizing the project, analysis of the results, and the preparation of the manuscript. DF was responsible for the patient selection, informed consent, ethics committee protocol preparation, blood collection, and serum preparation.

FUNDING

This work was performed with the support of EEA/Norway Grant BG09/D03-103 and the Bulgarian Fund for Scientific Research Grant D01-11/2016. This manuscript has been released as a Pre-Print at (80).

ACKNOWLEDGMENTS

The authors wish to thank Prof. Radha Nagarajan, Prof. Ivanka Tsakovska, and Prof. Soren Hairabedian for critically reading the manuscript.

SUPPLEMENTARY MATERIAL

The Supplementary Material for this article can be found online at: <https://www.frontiersin.org/articles/10.3389/fimmu.2019.02796/full#supplementary-material>

REFERENCES

- Baumgarth N, Herman OC, Jager GC, Brown LE, Herzenberg LA, Chen J. B-1 and B-2 cell-derived immunoglobulin M antibodies are non-redundant components of the protective response to influenza virus infection. *J Exp Med.* (2000) 192:271–80. doi: 10.1084/jem.192.2.271
- Ochsenbein AF, Fehr T, Lutz C, Suter M, Brombacher F, Hengartner H, et al. Control of early viral and bacterial distribution and disease by natural antibodies. *Science.* (1999) 286:2156–9. doi: 10.1126/science.286.5447.2156
- Vollmers HP, Brandlein S. Tumors: too sweet to remember? *Mol Cancer.* (2007) 6:78. doi: 10.1186/1476-4598-6-78
- Matter MS, Ochsenbein AF. Natural antibodies target virus-antibody complexes to organized lymphoid tissue. *Autoimmun Rev.* (2008) 7:480–6. doi: 10.1016/j.autrev.2008.03.018
- Avrameas S, Guilbert B, Dighiero G. Natural antibodies against tubulin, actin myoglobin, thyroglobulin, fetuin, albumin and transferrin are present in normal human sera, and monoclonal immunoglobulins from multiple myeloma and Waldenstrom's macroglobulinemia may express similar antibody specificities. *Ann Immunol.* (1981) 132C:231–6. doi: 10.1016/0769-2625(81)90031-3
- Panda S, Zhang J, Tan NS, Ho B, Ding JL. Natural IgG antibodies provide innate protection against ficolin-opsonized bacteria. *EMBO J.* (2013) 32:2905–19. doi: 10.1038/emboj.2013.199
- Vollmers HP, Brandlein S. Natural antibodies and cancer. *N Biotechnol.* (2009) 25:294–8. doi: 10.1016/j.nbt.2009.03.016
- Prieto JMB, Felipe MJB. Development, phenotype, and function of non-conventional B cells. *Comp Immunol Microb Infect Dis.* (2017) 54:38–44. doi: 10.1016/j.cimid.2017.08.002
- Lobo PI. Role of natural autoantibodies and natural IgM anti-leucocyte autoantibodies in health and disease. *Front Immunol.* (2016) 7:198. doi: 10.3389/fimmu.2016.00198
- Rothstein TL, Griffin DO, Holodick NE, Quach TD, Kaku H. Human B-1 cells take the stage. *Ann NY Acad Sci.* (2013) 1285:97–114. doi: 10.1111/nyas.12137
- Weller S, Braun MC, Tan BK, Rosenwald A, Cordier C, Conley ME, et al. Human blood IgM “memory” B cells are circulating splenic marginal zone B cells harboring a pre-diversified immunoglobulin repertoire. *Blood.* (2004) 104:3647–54. doi: 10.1182/blood-2004-01-0346
- Greiff V, Weber CR, Palme J, Bodenhofer U, Miho E, Menzel U, et al. Learning the high-dimensional immunogenomic features that predict public and private antibody repertoires. *J Immunol.* (2017) 199:2985–97. doi: 10.4049/jimmunol.1700594
- Van Regenmortel MH. Specificity, polyspecificity, and heterospecificity of antibody-antigen recognition. *J Mol Recognit.* (2014) 27:627–39. doi: 10.1002/jmr.2394
- Willis JR, Briney BS, DeLuca SL, Crowe JE Jr, Meiler J. Human germline antibody gene segments encode polyspecific antibodies. *PLoS Comput Biol.* (2013) 9:e1003045. doi: 10.1371/journal.pcbi.1003045
- Cohen IR, Young DB. Autoimmunity, microbial immunity and the immunological homunculus. *Immunol Today.* (1991) 12:105–10. doi: 10.1016/0167-5699(91)90093-9
- Avrameas S, Guilbert B, Mahana W, Matsiota P, Ternynck T. Recognition of self and non-self constituents by polyspecific autoreceptors. *Int Rev Immunol.* (1988) 3:1–15. doi: 10.3109/08830188809051179
- Avrameas S. Natural autoantibodies: from ‘horror autotoxicus’ to ‘gnothi seauton’. *Immunol Today.* (1991) 12:154–9. doi: 10.1016/S0167-5699(05)80045-3

18. Reynolds AE, Kuraoka M, Kelsø G. Natural IgM is produced by CD5- plasma cells that occupy a distinct survival niche in bone marrow. *J Immunol.* (2015) 194:231–42. doi: 10.4049/jimmunol.1401203
19. Silverman GJ, Srikrishnan R, Germar K, Goodyear CS, Andrews KA, Ginzler EM, et al. Genetic imprinting of autoantibody repertoires in systemic lupus erythematosus patients. *Clin Exp Immunol.* (2008) 153:102–16. doi: 10.1111/j.1365-2249.2008.03680.x
20. B-Sharron Z, Dror YK, Gittit D, Asaf M, Yifat M, Francisco JQ, et al. Individual and meta-immune networks. *Phys Biol.* (2013) 10:025003. doi: 10.1088/1478-3975/10/2/025003
21. Mao J, Ladd J, Gad E, Rastetter L, Johnson MM, Marzbani E, et al. Mining the pre-diagnostic antibody repertoire of TgMMTV-neu mice to identify autoantibodies useful for the early detection of human breast cancer. *J Transl Med.* (2014) 12:121. doi: 10.1186/1479-5876-12-121
22. Butvilovskaya VI, Poplateva SB, Chechetkin VR, Zubtsova ZI, Tsybulskaya MV, Samokhina LO, et al. Multiplex determination of serological signatures in the sera of colorectal cancer patients using hydrogel biochips. *Cancer Med.* (2016) 5:1361–72. doi: 10.1002/cam4.692
23. Merbl Y, Itzhak R, Vider-Shalit T, Louzoun Y, Quintana FJ, Vadai E, et al. A systems immunology approach to the host-tumor interaction: large-scale patterns of natural autoantibodies distinguish healthy and tumor-bearing mice. *PLoS ONE.* (2009) 4:e6053. doi: 10.1371/journal.pone.0006053
24. Stafford P, Wrapp D, Johnston SA. General assessment of humoral activity in healthy humans. *Mol Cell Proteomics.* (2016) 15:1610–21. doi: 10.1074/mcp.M115.054601
25. Campbell CT, Gulley JL, Oyeleran O, Hodge JW, Schlom J, Gildersleeve JC. Serum antibodies to blood group A predict survival on PROSTVAC-VF. *Clin Cancer Res.* (2013) 19:1290–9. doi: 10.1158/1078-0432.CCR-12-2478
26. Kulthanan K, Pinkaew S, Suthipinittharm P. Diagnostic value of IgM deposition at the dermo-epidermal junction. *Int J Dermatol.* (1998) 37:201–5. doi: 10.1046/j.1365-4362.1998.00288.x
27. Borrelli M, Maglio M, Agnese M, Paparo F, Gentile S, Colicchio B, et al. High density of intraepithelial $\gamma\delta$ lymphocytes and deposits of immunoglobulin (IgM) anti-tissue transglutaminase antibodies in the jejunum of coeliac patients with IgA deficiency. *Clin Exp Immunol.* (2010) 160:199–206. doi: 10.1111/j.1365-2249.2009.04077.x
28. Chan RK, Ding G, Verna N, Ibrahim S, Oakes S, Austen WG Jr, et al. IgM binding to injured tissue precedes complement activation during skeletal muscle ischemia-reperfusion. *J Surg Res.* (2004) 122:29–35. doi: 10.1016/j.jss.2004.07.005
29. Hensel F, Hermann R, Schubert C, Abe N, Schmidt K, Franke A, et al. Characterization of glycosylphosphatidylinositol-linked molecule CD55/decay-accelerating factor as the receptor for antibody SC-1-induced apoptosis. *Cancer Res.* (1999) 59:5299–306.
30. Vollmers HP, Brandlein S. The “early birds”: natural IgM antibodies and immune surveillance. *Histol Histopathol.* (2005) 20:927–37. doi: 10.14670/HH-20.927
31. Hughes AK, Cichacz Z, Scheck A, Coons SW, Johnston SA, Stafford P. Immunosignaturing can detect products from molecular markers in brain cancer. *PLoS ONE.* (2012) 7:e40201. doi: 10.1371/journal.pone.0040201
32. Stafford P, Halperin R, Legutki JB, Magee DM, Galgiani J, Johnston SA. Physical characterization of the “immunosignaturing effect”. *Mol Cell Proteomics.* (2012) 11:M111.011593. doi: 10.1074/mcp.M111.011593
33. Quintana FJ, Hagedorn PH, Elizur G, Merbl Y, Domany E, Cohen IR. Functional immunomics: microarray analysis of IgG autoantibody repertoires predicts the future response of mice to induced diabetes. *Proc Natl Acad Sci USA.* (2004) 101 (Suppl. 2):14615–21. doi: 10.1073/pnas.0404848101
34. Merbl Y, Zucker-Toledano M, Quintana FJ, Cohen IR. Newborn humans manifest autoantibodies to defined self molecules detected by antigen microarray informatics. *J Clin Invest.* (2007) 117:712–8. doi: 10.1172/JCI29943
35. Matokho WL, Chu K, Jin B, Lee SW, Whitesides GM, Derda R. Deep sequencing analysis of phage libraries using Illumina platform. *Methods.* (2012) 58:47–55. doi: 10.1016/j.jymeth.2012.07.006
36. Coordinators NR. Database resources of the national center for biotechnology information. *Nucleic Acids Res.* (2016) 44:D7–19. doi: 10.1093/nar/gkv1290
37. Protein. Bethesda MD: National Library of Medicine (US), National Center for Biotechnology Information [1988–2019]. Available online at: <https://www.ncbi.nlm.nih.gov/nucleotide/>
38. Altschul SF, Madden TL, Schaffer AA, Zhang J, Zhang Z, Miller W, et al. Gapped BLAST and PSI-BLAST: a new generation of protein database search programs. *Nucleic Acids Res.* (1997) 25:3389–402. doi: 10.1093/nar/25.17.3389
39. Andreatta M, Lund O, Nielsen M. Simultaneous alignment and clustering of peptide data using a Gibbs sampling approach. *Bioinformatics.* (2013) 29:8–14. doi: 10.1093/bioinformatics/bts621
40. Sandberg M, Eriksson L, Jonsson J, Sjostrom M, Wold S. New chemical descriptors relevant for the design of biologically active peptides. A multivariate characterization of 87 amino acids. *J Med Chem.* (1998) 41:2481–91.
41. O'Donnell B, Maurer A, Papandreou-Suppappola A, Stafford P. Time-frequency analysis of peptide microarray data: application to brain cancer immunosignatures. *Cancer Informat.* (2015) 14:219–33. doi: 10.4137/CIN.S17285
42. Brandlein S, Pohle T, Ruoff N, Wozniak E, Muller-Hermelink HK, Vollmers HP. Natural IgM antibodies and immunosurveillance mechanisms against epithelial cancer cells in humans. *Cancer Res.* (2003) 63:7995–8005.
43. Devarapu SK, Mamidi S, Plöger F, Dill O, Blixt O, Kirschfink M, et al. Cytotoxic activity against human neuroblastoma and melanoma cells mediated by IgM antibodies derived from peripheral blood of healthy donors. *Int J Cancer.* (2016) 138:2963–73. doi: 10.1002/ijc.30025
44. Rosenes Z, Mulhern TD, Hatters DM, Ilag LL, Power BE, Hosking C, et al. The anti-cancer IgM monoclonal antibody PAT-SM6 binds with high avidity to the unfolded protein response regulator GRP78. *PLoS ONE.* (2012) 7:e44927. doi: 10.1371/journal.pone.0044927
45. Rodriguez-Zhurbenko N, Rabade-Chediak M, Martinez D, Grinan T, Hernandez AM. Anti-NeuGcGM3 reactivity: a possible role of natural antibodies and B-1 cells in tumor immunosurveillance. *B-1 Cell Dev Function.* (2015) 1362:224–38. doi: 10.1111/nyas.12827
46. Diaz-Zaragoza M, Hernandez-Avila R, Viedma-Rodriguez R, Arenas-Aranda D, Ostoa-Saloma P. Natural and adaptive IgM antibodies in the recognition of tumor-associated antigens of breast cancer (Review). *Oncol Rep.* (2015) 34:1106–14. doi: 10.3892/or.2015.4095
47. Nygaard V, Rodland EA, Hovig E. Methods that remove batch effects while retaining group differences may lead to exaggerated confidence in downstream analyses. *Biostatistics.* (2016) 17:29–39. doi: 10.1093/biostatistics/kxv027
48. Haury M, Grandien A, Sundblad A, Coutinho A, Nobrega A. Global analysis of antibody repertoires. I. An immunoblot method for the quantitative screening of a large number of reactivities. *Scand J Immunol.* (1994) 39:79–87. doi: 10.1111/j.1365-3083.1994.tb03343.x
49. Stahl D, Yeshurun M, Gorin NC, Sibrowski W, Kaveri SV, Kazatchkine MD. Reconstitution of self-reactive antibody repertoires of autologous plasma IgM in patients with non-hodgkin's lymphoma following myeloablative therapy. *Clin Immunol.* (2001) 98:31–8. doi: 10.1006/clim.2000.4949
50. Mouthon L, Haury M, Lacroix-Desmazes S, Barreau C, Coutinho A, Kazatchkine MD. Analysis of the normal human IgG antibody repertoire. Evidence that IgG autoantibodies of healthy adults recognize a limited and conserved set of protein antigens in homologous tissues. *J Immunol.* (1995) 154:5769–78.
51. Lacroix-Desmazes S, Mouthon L, Coutinho A, Kazatchkine MD. Analysis of the natural human IgG antibody repertoire: life-long stability of reactivities towards self antigens contrasts with age-dependent diversification of reactivities against bacterial antigens. *Eur J Immunol.* (1995) 25:2598–604. doi: 10.1002/eji.1830250929
52. Nobrega A, Haury M, Grandien A, Malanchere E, Sundblad A, Coutinho A. Global analysis of antibody repertoires. II. Evidence for specificity, self-selection and the immunological “homunculus” of antibodies in normal serum. *Eur J Immunol.* (1993) 23:2851–9. doi: 10.1002/eji.1830231119
53. Mouthon L, Nobrega A, Nicolas N, Kaveri SV, Barreau C, Coutinho A, et al. Invariance and restriction toward a limited set of self-antigens characterize neonatal IgM antibody repertoires and prevail in autoreactive repertoires of healthy adults. *Proc Natl Acad Sci USA.* (1995) 92:3839–43. doi: 10.1073/pnas.92.9.3839
54. Ryvkin A, Ashkenazy H, Smelyanski L, Kaplan G, Penn O, Weiss-Ottolenghi Y, et al. Deep panning: steps towards probing the IgOme. *PLoS ONE.* (2012) 7:e41469. doi: 10.1371/journal.pone.0041469
55. Truck J, Ramasamy MN, Galson JD, Rance R, Parkhill J, Lunter G, et al. Identification of antigen-specific B cell receptor

- sequences using public repertoire analysis. *J Immunol.* (2015) 194:252–61. doi: 10.4049/jimmunol.1401405
56. Gu H, Tarlinton D, Muller W, Rajewsky K, Forster I. Most peripheral B cells in mice are ligand selected. *J Exp Med.* (1991) 173:1357–71. doi: 10.1084/jem.173.6.1357
 57. Madi A, Hecht I, Bransburg-Zabary S, Merbl Y, Pick A, Zucker-Toledano M, et al. Organization of the autoantibody repertoire in healthy newborns and adults revealed by system level informatics of antigen microarray data. *Proc Natl Acad Sci USA.* (2009) 106:14484–9. doi: 10.1073/pnas.0901528106
 58. Tchernychev B, Cabilly S, Wilchek M. The epitopes for natural polyreactive antibodies are rich in proline. *Proc Natl Acad Sci USA.* (1997) 94:6335–9. doi: 10.1073/pnas.94.12.6335
 59. Luo P, Agadjanyan M, Qiu J, Westerink MA, Steplewski Z, Kieber-Emmons T. Antigenic and immunological mimicry of peptide mimotopes of Lewis carbohydrate antigens. *Mol Immunol.* (1998) 35:865–79. doi: 10.1016/S0161-5890(98)00067-4
 60. Garcia KC, Desiderio SV, Ronco PM, Verroust PJ, Amzel LM. Recognition of angiotensin II: antibodies at different levels of an idiotypic network are superimposable. *Science.* (1992) 257:528–31. doi: 10.1126/science.1636087
 61. Scott JK. Discovering peptide ligands using epitope libraries. [Review]. *Trends Biochem Sci.* (1992) 17:241–5. doi: 10.1016/0968-0004(92)90401-T
 62. Westerink MA, Giardina PC, Apicella MA, Kieber-Emmons T. Peptide mimicry of the meningococcal group C capsular polysaccharide. *Proc Natl Acad Sci USA.* (1995) 92:4021–5. doi: 10.1073/pnas.92.9.4021
 63. Kieber-Emmons T. Peptide mimotopes of carbohydrate antigens. *Immunol Res.* (1998) 17:95–108. doi: 10.1007/BF02786435
 64. Pashov A, Canziani G, Monzavi-Karbassi B, Kaveri SV, Macleod S, Saha R, et al. Antigenic properties of peptide mimotopes of HIV-1-associated carbohydrate antigens. *J Biol Chem.* (2005) 280:28959–65. doi: 10.1074/jbc.M502964200
 65. Cohen IR. The cognitive paradigm and the immunological homunculus. *Immunol Today.* (1992) 13:490–4. doi: 10.1016/0167-5699(92)90024-2
 66. Cohen IR. Autoantibody repertoires, natural biomarkers, and system controllers. *Trends Immunol.* (2013) 34:620–5. doi: 10.1016/j.it.2013.05.003
 67. Lacroix-Desmazes S, Mouthon L, Pashov A, Barreau C, Kaveri SV, Kazatchkine MD. Analysis of antibody reactivities toward self antigens of IgM of patients with Waldenström's macroglobulinemia. *Int Immunol.* (1997) 9:1175–83. doi: 10.1093/intimm/9.8.1175
 68. Mouthon L, Lacroix-Desmazes S, Nobrega A, Barreau C, Coutinho A, Kazatchkine MD. The self-reactive antibody repertoire of normal human serum IgM is acquired in early childhood and remains stable throughout life. *Scand J Immunol.* (1996) 44:243–51. doi: 10.1046/j.1365-3083.1996.d01-306.x
 69. Hardy RR, Hayakawa K. Positive and negative selection of natural autoreactive B cells. *Adv Exp Med Biol.* (2012) 750:227–38. doi: 10.1007/978-1-4614-3461-0_17
 70. Noviski M, Tan C, Huizar J, Vykunta V, Mueller JL, Zikherman J. Optimal development of mature B cells requires recognition of endogenous antigens. *J Immunol.* (2019) 203:418–28. doi: 10.4049/jimmunol.1900175
 71. Varela F, Coutinho A. Second generation immune networks. *Immunol Today.* (1991) 12:159–66. doi: 10.1016/0167-5699(91)90081-4
 72. Putterman C, Deocharan B, Diamond B. Molecular analysis of the autoantibody response in peptide-induced autoimmunity. *J Immunol.* (2000) 164:2542–9. doi: 10.4049/jimmunol.164.5.2542
 73. Pashov A, Monzavi-Karbassi B, Kieber-Emmons T. Immune surveillance and immunotherapy: lessons from carbohydrate mimotopes. *Vaccine.* (2009) 27:3405–15. doi: 10.1016/j.vaccine.2009.01.074
 74. Van Regenmortel MH. What is a B-cell epitope? *Methods Mol Biol.* (2009) 524:3–20. doi: 10.1007/978-1-59745-450-6_1
 75. Huang J, He B, Zhou P. Mimotope-based prediction of B-cell epitopes. *Methods Mol Biol.* (2014) 1184:237–43. doi: 10.1007/978-1-4939-1115-8_13
 76. Weber LK, Palermo A, Kugler J, Armant O, Isse A, Rentschler S, et al. Single amino acid fingerprinting of the human antibody repertoire with high density peptide arrays. *J Immunol Methods.* (2017) 443:45–54. doi: 10.1016/j.jim.2017.01.012
 77. Weiss-Ottolenghi Y, Gershoni JM. Profiling the IgOme: meeting the challenge. *FEBS Lett.* (2014) 588:318–25. doi: 10.1016/j.febslet.2013.11.005
 78. Navalkar KA, Johnston SA, Stafford P. Peptide based diagnostics: are random-sequence peptides more useful than tiling proteome sequences? *J Immunol Methods.* (2014) 417:10–21. doi: 10.1016/j.jim.2014.12.002
 79. Legutki JB, Zhao ZG, Greving M, Woodbury N, Johnston SA, Stafford P. Scalable high-density peptide arrays for comprehensive health monitoring. *Nat Commun.* (2014) 5:4785. doi: 10.1038/ncomms5785
 80. Pashov AD, Shivarov V, Hadzhieva M, Kostov V, Ferdinandov D, Heinz M-K, et al. A rationally designed mimotope library for profiling of the human IgM repertoire. *bioRxiv.* (2018). doi: 10.1101/308973

Conflict of Interest: The authors declare that the research was conducted in the absence of any commercial or financial relationships that could be construed as a potential conflict of interest.

Copyright © 2019 Pashov, Shivarov, Hadzhieva, Kostov, Ferdinandov, Heintz, Pashova, Todorova, Vassilev, Kieber-Emmons, Meza-Zepeda and Hovig. This is an open-access article distributed under the terms of the Creative Commons Attribution License (CC BY). The use, distribution or reproduction in other forums is permitted, provided the original author(s) and the copyright owner(s) are credited and that the original publication in this journal is cited, in accordance with accepted academic practice. No use, distribution or reproduction is permitted which does not comply with these terms.



An Inflammatory Story: Antibodies in Tuberculosis Comorbidities

Milla R. McLean¹, Lenette L. Lu², Stephen J. Kent^{1,3,4} and Amy W. Chung^{1*}

¹ Department of Microbiology and Immunology, Peter Doherty Institute for Infection and Immunity, University of Melbourne, Melbourne, VIC, Australia, ² Division of Infectious Disease and Geographic Medicine, Department of Internal Medicine, University of Texas Southwestern Medical Center, Dallas, TX, United States, ³ Infectious Diseases Department, Melbourne Sexual Health Centre, Alfred Health, Central Clinical School, Monash University, Brisbane, VIC, Australia, ⁴ ARC Centre of Excellence in Convergent Bio-Nano Science and Technology, University of Melbourne, Melbourne, SA, Australia

OPEN ACCESS

Edited by:

Sylvie Hermouet,
INSERM U1232 Centre de Recherche
en Cancérologie et Immunologie
Nantes Angers (CRCINA), France

Reviewed by:

Martin Bachmann,
University of Bern, Switzerland
Martin Gengenbacher,
Center for Discovery and Innovation,
Hackensack Meridian Health,
United States

*Correspondence:

Amy W. Chung
awchung@unimelb.edu.au

Specialty section:

This article was submitted to
B Cell Biology,
a section of the journal
Frontiers in Immunology

Received: 26 August 2019

Accepted: 19 November 2019

Published: 09 December 2019

Citation:

McLean MR, Lu LL, Kent SJ and
Chung AW (2019) An Inflammatory
Story: Antibodies in
Tuberculosis Comorbidities.
Front. Immunol. 10:2846.
doi: 10.3389/fimmu.2019.02846

Mycobacterium tuberculosis (*Mtb*) resides in a quarter of the world's population and is the causative agent for tuberculosis (TB), the most common infectious reason of death in humans today. Although cellular immunity has been firmly established in the control of *Mtb*, there is growing evidence that antibodies may also modulate the infection. More specifically, certain antibody features are associated with inflammation and are divergent in different states of human infection and disease. Importantly, TB impacts not just the healthy but also those with chronic conditions. While HIV represents the quintessential comorbid condition for TB, recent epidemiological evidence shows that additional chronic conditions such as diabetes and kidney disease are rising. In fact, the prevalence of diabetes as a comorbid TB condition is now higher than that of HIV. These chronic diseases are themselves independently associated with pro-inflammatory immune states that encompass antibody profiles. This review discusses isotypes, subclasses, post-translational modifications and Fc-mediated functions of antibodies in TB infection and in the comorbid chronic conditions of HIV, diabetes, and kidney diseases. We propose that inflammatory antibody profiles, which are a marker of active TB, may be an important biomarker for detection of TB disease progression within comorbid individuals. We highlight the need for future studies to determine which inflammatory antibody profiles are the consequences of comorbidities and which may potentially contribute to TB reactivation.

Keywords: antibody, glycosylation, tuberculosis, HIV, diabetes, kidney disease, co-infection, inflammation

INTRODUCTION

Mycobacterium tuberculosis (*Mtb*) is a leading cause of mortality and morbidity across the globe with an estimated 10 million new infections annually and a quarter of the world's population infected (1). The spectrum of tuberculosis (TB) in humans is most widely characterized by two clinical states: active TB and latent TB. Individuals with active TB exhibit symptoms such as hemoptysis, fever and weight loss with detectable bacteria, while individuals with latent TB are not overtly clinically ill, have no detectable *Mtb*, and therefore no transmission risk (see **Table 1**). An important reason for the significant burden of TB today, is our poor understanding of the human immune response to *Mtb* infection. More specifically, why 5–10% of infected individuals progress to active disease while others remain latent is not known (4). In many low to middle

income countries where TB is endemic, there exists a double burden of such communicable diseases with the rapid rise in chronic and non-communicable diseases (5). The HIV-1 and TB co-infection syndemic is highly alarming (6) with TB being the leading cause of death in people living with HIV-1 (7). An estimated 49% of HIV-1 infected individuals are unaware of their co-infection and post-mortems on HIV-1 infected adults showed 64% had evidence of disseminated *Mtb* (7, 8).

Studies in the context of comorbid conditions in humans as well as animal models have helped identify some of the mechanisms underlying this transition from latent infection to active disease (9). Specifically, the HIV epidemic has highlighted T cell function as an important component of immune protection. Besides HIV, there remains many other significant conditions in which the risk of *Mtb* acquisition and or progression from latent infection to active disease is increased (10–12).

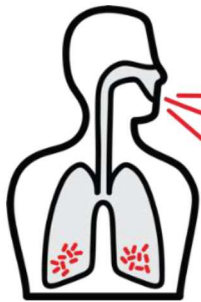
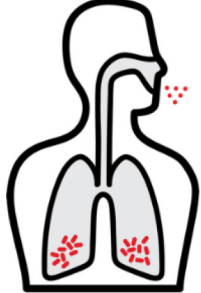
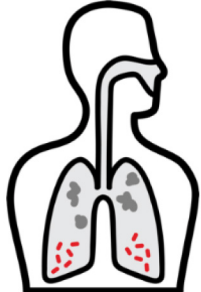

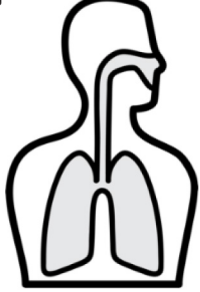
Diabetes as an epidemiological risk factor for TB is well-reported (13). Spanning back to 1947, a review of diabetes and *Mtb* co-infection reported that 50% of diabetics succumbed to pulmonary TB (10). In recent years the epidemic has grown, with the number of individuals with Diabetes-TB overtaking those with HIV-TB (14); which can be attributed in part, to the positive impacts that antiretroviral therapy is having on reducing TB-HIV co-infection (15). Moreover, a recent multi-country cohort study found that patients with Diabetes-TB had more severe TB disease compared to individuals without diabetes (16). Thus, diabetes presents an independent risk factor for acquisition of *Mtb* infection and also progression of disease.

Chronic Kidney Disease (CKD) associated with and also independent of diabetes, represents an additional risk factor for TB. Patients with late-stage CKD, called end stage renal disease (ESRD) requiring dialysis have a ~50-fold higher risk of latent TB reactivation (11). Additionally, TB contributes to mortality in individuals with CKD, and with a global rise in total CKD [18.4% increase since 2005 (17)], it is expected that cases of CKD/TB comorbidity will increase in prevalence (18, 19). The immunological causes of TB reactivation, however, are not well-understood in patients with these chronic diseases and thus we have a significant gap in our understanding of the immune response to *Mtb* infection.

While the importance of T cells in TB control is firmly established, the fact that other comorbid conditions and healthy individuals with intact T cell responses (as far as we know) can progress from latent infection to active TB, suggests that there are additional immune mediated mechanisms of protection. Moreover, T cell based diagnostics fail to distinguish between latent and active TB and these tests cannot reliably detect TB in HIV-1 infected individuals (20, 21). Finally, the BCG vaccine inducing potent T cell responses is sub optimally protective (22, 23). Thus, a broader understanding of the immune response to TB is needed.

In recent years, there has been more focus on investigating the role of antibodies and innate cells in TB infection and disease (24, 25). This interest in humoral immunity in *Mtb* is evidenced

TABLE 1 | Clinical spectrum of TB (2, 3).

Active TB	 <ul style="list-style-type: none"> • Severe symptoms • High transmission • Smear and culture <i>Mtb</i> positive • Highest bacillary burden <p>Diagnostically</p> <ul style="list-style-type: none"> ✓ TST positive ✓ IGRA positive (if immunocompetent) ✓ Chest X-Ray positive
Subclinical TB	 <ul style="list-style-type: none"> • Mild symptoms or asymptomatic • Intermittent transmission • Smear or culture <i>Mtb</i> positive • Moderate bacillary burden <p>Diagnostically</p> <ul style="list-style-type: none"> ✓ TST positive ✓ IGRA positive (if immunocompetent) ✓ Chest X-Ray positive
Incipient TB	 <ul style="list-style-type: none"> • Asymptomatic • Low transmission • Culture negative • Moderate bacillary burden <p>Diagnostically</p> <ul style="list-style-type: none"> ✓ TST positive ✓ IGRA positive (if immunocompetent) ✓ Chest X-Ray showing upper-lobe opacities
Latent TB	 <ul style="list-style-type: none"> • Asymptomatic • Low transmission • Smear negative and culture negative • Low bacillary burden <p>Diagnostically</p> <ul style="list-style-type: none"> ✓ TST positive ✓ IGRA positive (if immunocompetent) ✓ Chest X-Ray negative
“Resisters”	 <ul style="list-style-type: none"> • Asymptomatic • No transmission • Smear and culture negative • Low bacillary burden <p>Diagnostically</p> <ul style="list-style-type: none"> ✓ TST Negative ✓ IGRA Negative (if immunocompetent) ✓ Chest x-Ray Negative

TST, Tuberculin Skin Test; IGRA, interferon- γ -release assay.

by a mounting number of studies that have identified specific antibody targets, and structural or functional differences that are observed during different TB disease states (26–30). For example, while *Mtb*-specific IgG titers alone have been insufficient in distinguishing between latent and active TB, refinement of these correlates using additional isotypes, subclasses, and other Fc modifications are underway (see **Figure 1**) (31–35). Moreover, incorporating data including multiple instead of single *Mtb* antigens as well as Fab affinity and avidity to *Mtb* targets may improve sensitivity and specificity (36–40). Thus, assessing more specific antibody features may improve our understanding of humoral immune correlates of infection and disease.

This review examines the antibody profiles (isotypes, subclasses, functions, and post translational modifications) in TB and diseases in which TB has high rates of reactivation, focusing primarily on HIV-1, type 2 diabetes mellitus (T2DM), and CKD (see **Figure 2**). We draw together what is known about antibodies and their role in inflammation in infectious and non-communicable diseases, a novel take on examining humoral immunity in co-infection. Further, we discuss antibody characteristics described in the limited studies of *Mtb* comorbidity cohorts. Understanding antibody characteristics in *Mtb* infection, conditions where TB reactivates and their comorbidities will assist in drawing links between immune states in each disease and potential common mechanisms of TB reactivation (25). We speculate whether these antibody characteristics may ultimately find utility as biomarkers in assessing a patient's real-time risk of TB reactivation to personalize treatment plans and follow-up.

ANTIBODY STRUCTURE

The antibody glycoprotein exists within the immunoglobulin (Ig) superfamily. The Y-shaped heterodimeric protein consists of two light chains (C_L) and two heavy chains (C_H). Its tertiary structure can be functionally divided into the Fab region proximally and the Fc region distally, between which lies a flexible hinge region (41). Antibodies can be viewed as a “bridge” between innate and adaptive immunity since they have the capacity to bind targets via the Fab region and activate innate immune effector cells via Fc-receptors (42, 43). The functional capacity of an antibody is determined by a range of characteristics; including the antibody isotype and subclass, but also the many complex modifications that ensue post-translationally.

Antibody Isotypes and Subclasses

Within the range of human antibodies, there exists 5 isotypes; IgM, IgD, IgG, IgE, and IgA. IgG predominates in human serum and can be subclassed into IgG1, IgG2, IgG3, and IgG4 in order of most to least abundance, while IgA predominates in mucosal sites and can be subclassed into IgA1 and IgA2 (44, 45). IgG, IgA, and IgE isotypes can be further classified into allotypes which exist as genetic polymorphisms within the C_L and C_H (46, 47).

Antibody isotypes and subclasses differentially interact with Fc receptors (FcR) thus determining the range of effectors cells activated and their immune response. Antibody isotype and subclass class switch recombination is modulated by B cell factors

and toll-like receptor stimuli [e.g., Activation-induced deaminase and CPG (48)] and is often influenced by T cell help (e.g., CD40L) and specific cytokines secreted by a range of classical T helper cells and non-classical T cells such as NK T and gamma-delta T cells (49–51). In general, extracellular bacterial infections skew subclass responses toward IgG1 and IgG2, which are elicited in response to the high polysaccharide and protein composition of these bacteria. These antibodies have the ability to neutralize bacterial toxins, opsonize capsular polysaccharides for phagocytosis, as well as activate the complement membrane-attack complex for bacterial lysis (52–56). Viral infections and intracellular bacteria primarily elicit IgG1 and IgG3 subclasses. Antiviral IgG1 and IgG3 antibodies are commonly divided into neutralizing antibodies which bind free virus preventing cell entry and non-neutralizing antibodies, though there is a growing awareness of neutralizing antibodies with the capacity to activate non-neutralizing functions (57, 58).

Antibody Glycosylation

Post-translational modifications of antibodies have substantial downstream effects on their engagement of cells and cellular diversity, antibody localization, protein half-life, and stability (59, 60). The most comprehensively studied in relation to antibodies is N-glycosylation, where research mainly focuses upon how glycosylation of antibodies can improve monoclonal antibody therapeutics (61, 62).

Glycosylation is the covalent addition of sugar moieties to portions of an antibody in the endoplasmic reticulum and golgi. The glycan molecules which can be added include galactose, sialic acid, fucose, and bisecting N-acetylglucosamine (GlcNAc) (60). There is a key N-glycosylation site on all IgG Fc regions at an Asn-297 residue of IgG CH_2 heavy chains. In addition, approximately 10–20% of serum antibody Fab regions contain N-linked glycans, while O-linked glycans are also present in the hinge region of IgG3 and IgA1 (63, 64).

Glycosylation of IgG holds the two heavy chains in an open confirmation, allowing binding to Fc γ -receptors (65). Fully deglycosylated IgG have reduced capacity to engage most Fc Receptors (66–68). Agalactosylated antibodies (G0) are upregulated in inflammatory diseases that are commonly associated with enhanced presence of pro-inflammatory cytokines in serum. These agalactosylated G0 antibodies have the capacity to activate alternative and mannose-binding lectin complement pathways (69). Bisecting GlcNAc on IgG1 has been associated with increased Fc γ RIIIa binding (70) while the presence of core fucose residues reduces Fc γ RIIIa binding and subsequent ADCC (71). On the other hand, sialylated antibodies enhance anti-inflammatory activities via engagement with DC-Sign and inhibitory Fc γ RIIb binding (64, 72). Recent studies suggest that antibody glycosylation can also affect antigen binding affinity and affinity maturation (73, 74).

Antibody Fc Functions

Antibody Fc functions link the adaptive and innate immunity. Fc-functional antibodies can simultaneously bind a target via the Fab region and an innate immune FcR effector cell via the Fc region. Cross-linking of these antibodies on the surface

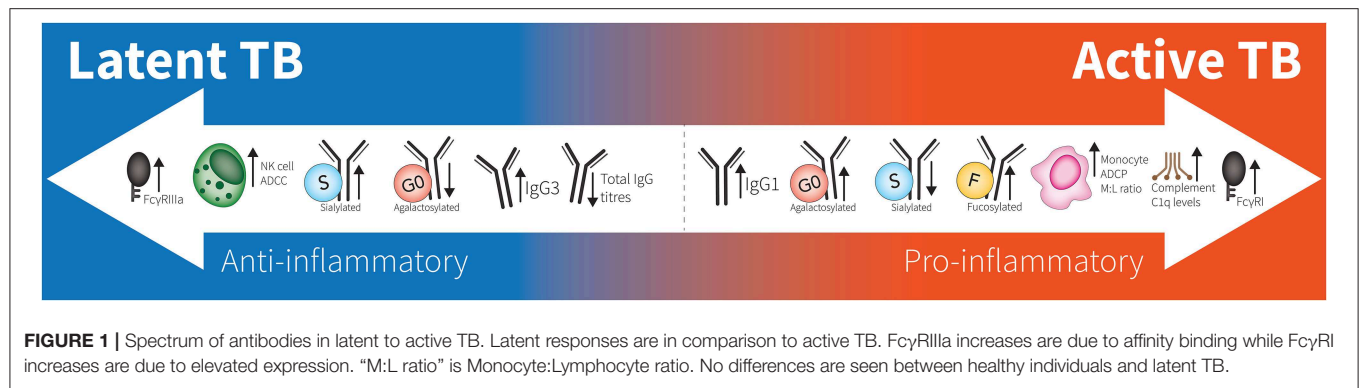


FIGURE 1 | Spectrum of antibodies in latent to active TB. Latent responses are in comparison to active TB. FcγRIIIa increases are due to affinity binding while FcγRI increases are due to elevated expression. “M:L ratio” is Monocyte:Lymphocyte ratio. No differences are seen between healthy individuals and latent TB.

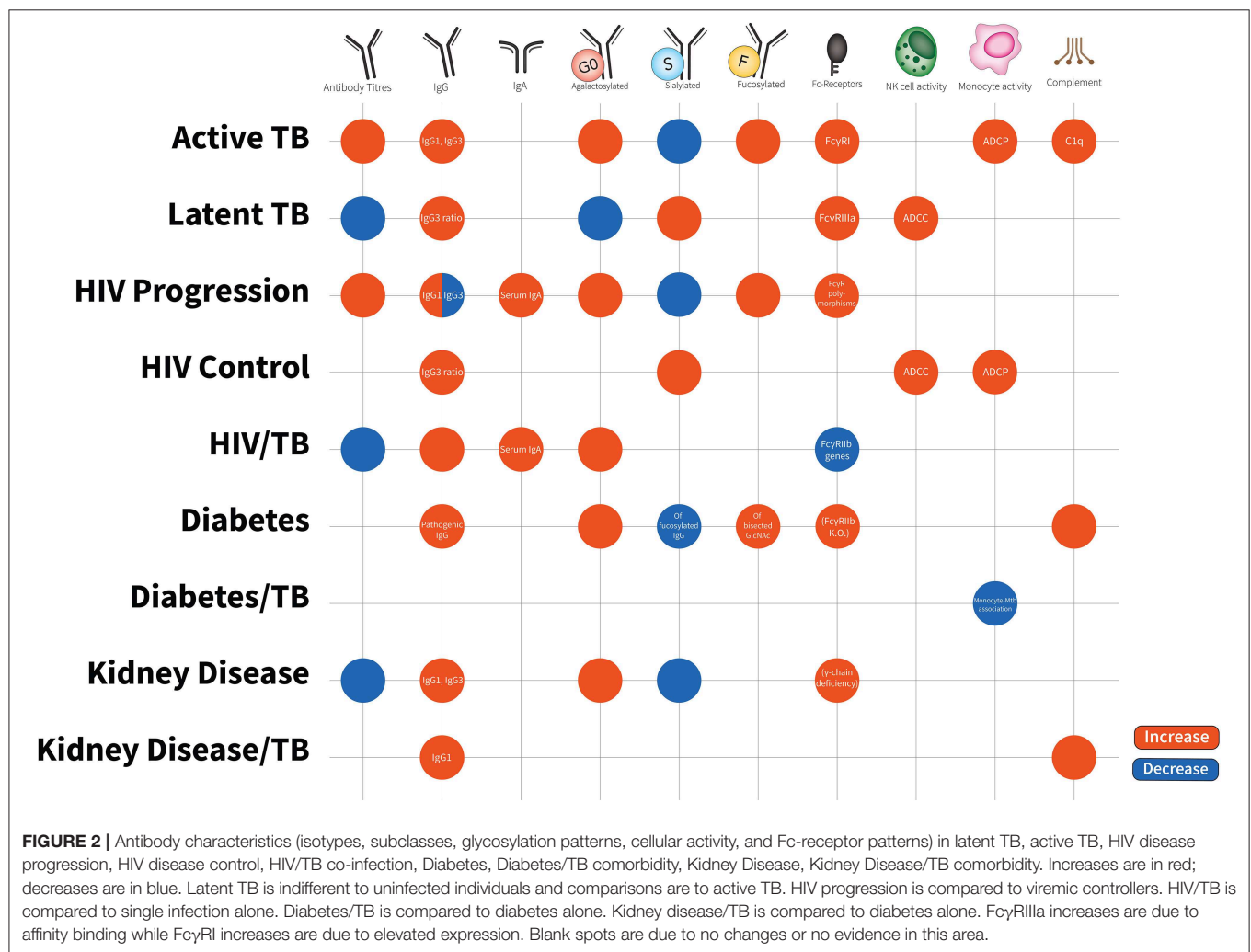


FIGURE 2 | Antibody characteristics (isotypes, subclasses, glycosylation patterns, cellular activity, and Fc-receptor patterns) in latent TB, active TB, HIV disease progression, HIV disease control, HIV/TB co-infection, Diabetes, Diabetes/TB comorbidity, Kidney Disease, Kidney Disease/TB comorbidity. Increases are in red; decreases are in blue. Latent TB is indifferent to uninfected individuals and comparisons are to active TB. HIV progression is compared to viremic controllers. HIV/TB is compared to single infection alone. Diabetes/TB is compared to diabetes alone. Kidney disease/TB is compared to diabetes alone. FcγRIIIa increases are due to affinity binding while FcγRI increases are due to elevated expression. Blank spots are due to no changes or no evidence in this area.

of effector cells leads to a downstream activating signaling cascade, inducing a range of effector functions including targeted cell killing, otherwise known as antibody-dependent-cellular-cytotoxicity (ADCC), antibody-dependent-phagocytosis (ADP), cytokine, chemokine and/or enzyme release (75, 76). The FcR syntax for IgA is FcαR, IgE is FcεR, and IgG is FcγR, of which there exists different isoforms (42). Different effector

cells can express a different combination of activating FcγR (e.g., FcγRI/IIa/IIc/IIIa/IIIb) and/or inhibitory FcγR (FcγRIIb) receptors on their surface. Further, IgG subclasses differentiate in their binding affinity to different FcγRs with IgG3 and IgG1 being subclasses with the highest affinity (77, 78). The affinity, diversity, and polymorphisms of FcγR and IgG subclasses is reviewed elsewhere (79).

TUBERCULOSIS (TB)

Mtb infection in humans produces a spectrum of clinical and subclinical disease. This continuum can be loosely grouped into active TB, subclinical TB, incipient TB, latent TB, and “Resisters.” Individuals with active TB have detectable bacillary burden by culture or PCR and commonly have a positive interferon- γ (IFN- γ) releasing assay (IGRA) or tuberculin skin test (TST) with cough, weight loss, and fever. Subclinical TB is defined as asymptomatic disease but with a loss of bacterial containment which can be observed with inflammation as detected radiographically by positron emission tomography (PET). At the other end of the spectrum, latent TB is identified as persistent asymptomatic infection, TST or IGRA positive with no transmission capacity (2). Unlike subclinical TB, individuals with latent infection do not demonstrate areas of PET avidity consistent with active disease. Finally, a subset of TST and IGRA negative individuals have been identified called “Resisters” who appear to have non canonical immune responses to *Mtb* antigens in the context of high levels of exposure (80). Clinical and diagnostic details of these TB disease groups have been recently reviewed by Furin et al. (3) and are summarized in **Table 1**.

Pro-Inflammatory Indicators in *Mycobacterium tuberculosis* Infection

While delineating mechanisms of protection is important in understanding TB pathogenesis, enhancement of disease is a physiologically important component of the host response. The full spectrum of clinical presentations from latency to disseminated extra-pulmonary TB initiates varying and complex host-pathogen interactions (81, 82). The role of IFN- γ releasing CD4+ T cells is complex and somewhat paradoxical. IFN- γ knock-out mice succumb to early *Mtb* infection compared to wildtype (83, 84). In humans, IFN- γ releasing T_H1 CD4+ cells are widely recognized as the predominate cell-type that responds to *Mtb* infection with their numbers increasing post-infection and at granuloma sites, where bacteria are surrounded by innate and adaptive immune cells (85, 86). Mutations in IFN signaling are associated with non-tuberculous mycobacterial infections (87), and the use of inhibitors of TNF- α , another important inflammatory cytokine, as disease modifying antirheumatic drugs in patients with autoimmune diseases is associated with increased risk of TB (88, 89). The induction of IFN- γ releasing cells has also been a primary aim of many TB vaccine efforts with vaccine correlate studies focusing on eliciting high T cell release of type 1 cytokines including IFN- γ , TNF- α , and IL-2 (90–93). Moreover, a recent study into BCG vaccine-induced IFN- γ releasing T cells reported that these cells protect if expanded in response to vaccination (94). Thus, multiple lines of evidence in animal models and humans across *Mtb* and BCG demonstrate the protective potential of IFN- γ and TNF- α .

However, more recent evidence brings to light that IFN- γ , and also TNF- α , in TB is not solely protective and the landscape is in fact more complex. A growing number of studies correlate IFN- γ releasing T_H1 cells (22, 23, 93, 95, 96) and TNF (97) post-infection with enhanced disease burden and reduced survival. Indeed, with PD-1 inhibitor blockade in pre-clinical models

and in humans, *Mtb* specific CD4+ T cells producing IFN- γ increase in the blood, correlating with progression of TB disease (98, 99). Finally, an immune correlates study looking at BCG vaccination in infants, showed that the induction of type-1 cytokines released from peripheral blood CD4+ T cells co-expressing IFN- γ , TNF- α , and IL-2 did not correlate with TB protection (100). This lack of correlation is also seen in tissue specific *Mtb*-reactive CD4+ T cell responses in mice (22). Extending from children to adults, double positive TNF- α +/IFN- γ + CD4+ T cells and single positive TNF- α + CD4+ T cells were substantially elevated in active compared to latent TB (101, 102). One possible explanation for this complexity is that the timing of *Mtb*-specific CD4+ T cell responses may be critical to their role in TB protection or burden as in whether the cell population and subsequent inflammation expands before or after *Mtb* infection (25, 103). Thus, pre-existing T cell responses induced by vaccination and or exposure may protect against disease, but expansion of T cells in the context of disease progression may not be helpful. In fact, phagocytosis alone stimulates substantial IL-12 release which alongside IFN- γ drives a switch to the inflammatory T_H1 phenotype (104). As such, pro-inflammatory cytokine profiles, including IFN- γ , IL-1, IL-2, IL-13, and TNF- α , mark the state of active TB in patients (105, 106). Moreover, excess proinflammatory signaling can result in tissue remodeling and destruction (107, 108), and high levels of TNF- α can be detrimental, in some circumstances contributing to cachexia and weight loss (97, 101, 102, 109–111). However, orthogonal pro-inflammatory cytokines can be potentially protective in individuals with latent infection or those who have been highly exposed to *Mtb* (30, 112). One study looking at healthcare workers in frequent contact with TB patients, found no differences in IFN- γ release from PBMCs in response to purified protein derivative compared to culture-positive TB patients (113). In the study by Lu et al. latent TB individuals had greater IFN- γ release from *Mtb*-specific CD4+ T cells than “resisters” who reported almost no IFN- γ response despite the “resister” population having *Mtb*-specific IgM and IgG (30). The magnitude of the IFN- γ response in the resister population may be a function of lower antigen load, as “resisters” are thought to have no replicative bacteria. How antibodies may inform on these inflammatory states remains to be fully elucidated.

Antibody Isotypes and Subclasses in *Mycobacterium tuberculosis* Infection

In the broadest of strokes, antibody titers increase as *Mtb* burden increases, presumably due to increased antigen availability (26, 37, 114, 115). More specifically, some but not all studies show that active pulmonary TB elicits an *Mtb*-specific IgG isotype response with the elevation of both *Mtb*-specific and total IgG1 and IgG3 subclasses in serum (37, 116–118). *In vitro*, IgG1 mediates TNF- α release from human monocytes but does not increase the anti-inflammatory cytokine IL-10 (109, 110). IgG1 and IgG3 subclasses are also the main antibodies capable of activating complement (119). Consistent with these associations, complement C1q levels are higher in active TB compared to

latent TB, and complement cascade molecules are upregulated 18 months before progression from *Mtb* infection to TB disease (120–122). Moreover, some monoclonal *Mtb* IgG1 can enhance bacterial replication *in vitro*, demonstrating the potential to exacerbate disease (27). Finally, polyclonal serum from *Mtb* infected rabbits can enhance BCG infection in mice (123). Thus, specific subclasses such as IgG1 and IgG3 in the context of monoclonality or polyclonality may participate in the induction of pro-inflammatory downstream consequences as seen in active TB disease and potentially favor the bacteria.

However, not all IgG is pathogenic. Passive transfer into mice of purified polyclonal IgG from some healthcare workers highly exposed to *Mtb* with detectable *Mtb* specific IgG can decrease *Mtb* burden in the lung (28). Similarly, serum from mice immunized by a variety of antigens thought to be cross reactive to *Mtb* capsular macromolecules can delay *Mtb* outgrowth from a variety of organs and increase survival time in mice (124, 125). This protective impact, along with decreased associated pulmonary pathology, can even be seen with intact intravenous immunoglobulin (IVIG) preparations of pooled polyclonal IgG from multiple healthy humans used to clinically treat autoimmune diseases (126, 127). Notably, the protective effect appears to be abrogated with enzymatic removal of glycan residues (127). Therefore, *Mtb* reactive IgG with intact glycosylation in these complex polyclonal responses may participate in controlling bacterial burden. Further studies capturing the antigen specificities and glycan signatures of these antibodies will illuminate the mechanistic basis of these findings.

Beyond IgG, IgA has been a focus of interest due to the importance of this isotype in mucosal immunity within the pulmonary compartment, the main route of TB infection, acquisition and subsequent transmission. While analysis of bronchoalveolar lavage (BAL) (128, 129) from individuals diagnosed with pulmonary TB demonstrates the presence of *Mtb*-specific IgA in addition to IgG, not all IgA is protective. In mice, transfer of B cells induced by an *Mtb* subunit mucosal vaccine that produces detectable antigen-specific IgA in the lung is not protective compared to the T cell counterparts (130). This may be in part due to the lack of the Fc α -receptor/CD89 human homolog in mice as one of the many challenges in translating between species (131). Indeed, the protective effect of intranasal delivery of one monoclonal *Mtb* IgA is dependent on the presence of CD89 expressed transgenically (132). Yet, mice deficient in IgA have increased susceptibility to *Mycobacterium bovis* in the context of subunit vaccination (133), suggesting that non Fc α R mediated qualities could also be involved. In fact, intratracheal delivery of a different monoclonal *Mtb* IgA into mice has shown some protection with decreased bacterial burden and pulmonary pathology in absence of CD89 (134). Consistent with these findings, a recent *in vitro* study observed that monoclonal IgA were able to inhibit *Mtb* growth, while IgG antibodies to the same targets promoted infection (27). Intriguingly, this isotype mediated control of *Mtb* appears to be modulated via Fc α R/Fc γ R independent mechanisms, as these results were observed when using epithelial cell lines that lack these FcR receptors. The authors hypothesize that the IgG *Mtb* uptake and infection may instead have been mediated by FcRn binding, though

no mechanistic studies were conducted to confirm this. While monoclonal antibodies differ compared to polyclonal humoral immune responses in infection due to both antigen specificity and antibody glycosylation, these monoclonal studies suggest that IgA may mediate control of bacterial burden through both Fc α R dependent and independent mechanisms.

Glycosylation Patterns in *Mycobacterium tuberculosis*

Going beyond subclass and isotypes, post translational modifications of antibodies such as glycosylation are linked to inflammation. Antibody glycosylation patterns can be applied to TB in order to distinguish latent from active TB. In the area of autoimmunity, glycosylation of IgG has been extensively studied as a biomarker of disease severity. Agalactosylated IgG is considered pro-inflammatory and is a prominent biomarker in rheumatoid arthritis where increases in agalactosylated IgG with fucose is associated with increased disease severity (135). In inflammatory bowel disease where substantial granulomatous T cell pathology occurs, agalactosylation of IgG increases with greater T cell-mediated tissue damage and elevated C-Reactive Protein (136). On the other hand, the addition of sialic acid on IgG appears to transform it from a pro-inflammatory to anti-inflammatory entity (137).

In two independent and geographically distinct human cohorts, the active TB antibody glycome of total IgG exhibits agalactosylation and less sialic acid, but more fucose compared to latent TB IgG (26). While the lack of galactose is associated with inflammation in general, more specifically, agalactosylated IgG has been hypothesized to activate the mannose binding lectin complement pathway (69). This would be consistent with blood transcriptional profiling demonstrating elevated complement levels in individuals with active TB (138). The presence of sialic acid is associated with an anti-inflammatory state in rheumatological diseases (135), and this would be consistent with less inflammation in the context of latent compared to active TB (26). Antibodies with less fucose are better at engaging Fc γ RIIIa on NK cells to mediate ADCC in the monoclonal antibody literature (71, 139). Lu et al. did find higher binding of polyclonal IgG to Fc γ RIIIa along with enhanced TB-specific ADCC in latent compared to active TB (26). Intriguingly, an independent study of multiple human cohorts of latent and active TB demonstrated an NK cell signature associated with latent infection. This study also observed that PBMCs from latent TB individuals had increased capacity to mediated ADCC responses compared to uninfected controls, although this same analysis was not conducted using PBMCs from active TB individuals (140). Further studies will be important in orthogonally validating the link between specific IgG glycan patterns and Fc effector functions in human TB infection.

In contrast to IgG, the glycosylation of pentameric IgM is far more complex (141, 142) and therefore less well-characterized and understood. In a mouse model consistent with active TB, IgM glycosylation in BCG naïve mice after *Mtb* infection had a 5-fold increase in fucosylated IgM as well as less sialylation (143). Overall, mice receiving BCG had less fucosylation (143).

What this means for downstream effector functions is less clear. Moreover, the respective similarities and differences between mice and human glycosylation regulation are less well-described. Thus, IgM glycosylation within and even beyond TB is an area that would benefit from significant further studies.

Antibody Function in *Mycobacterium tuberculosis*

With differential glycosylation, isotypes, and subclasses, antibody Fc-domain engagement of Fc receptors on immune cells help modulate pro- and anti- inflammatory signals, the balance of which, in TB, can contribute to outcome (79). Despite lower *Mtb*-specific IgG titers in latent compared to active TB, there is higher affinity for the activating FcγRIIIa and no difference in the activating FcγRIIa or inhibitory FcγRIIb (26). Studies in mice deficient of the inhibitory FcγRIIb have greater control of *Mtb* bacterial burden, whereas complete knock-out of the Fcγ-chain region, which is essential for activating FcγR signaling, resulted in more severe disease in pulmonary pathology (144). Additionally, there are higher levels of FcγRI receptor gene expression in individuals with active TB compared to latent TB (145), and these levels decrease over the course of therapy (146). FcγRI is an activating receptor, which is upregulated by cytokines such as IFN-γ and GM-CSF and binds with high affinity to IgG1, IgG3, and IgG4 in comparison to the low affinity FcγRIIIa or IIa (79). As such, high FcγRI levels in active TB may either be a marker of or contribute to the inflammation. These lines of evidence at an Fc receptor level suggest that while too much immune complex activity identified in active TB may contribute to inflammation and pathology, some antibody mediated cellular effector functions may be important for bacterial control.

At a cellular level, immune cells expressing Fc-receptors have been implicated in both the enhancement of bacterial uptake, as well as the control of bacterial fate, in the context of antibodies. Early studies by Fong et al. (147) and Armstrong and Hart (148) coated *Mtb* with serum from BCG immunized rabbits. Though there was enhancement of uptake *in vitro* demonstrated by Armstrong and Hart, there were no significant difference in intracellular *Mtb* growth in rabbit (147) or murine (148) peritoneal macrophages. In humans, THP-1 monocytes demonstrated enhancement of BCG opsonophagocytosis using human serum after vaccination, inducing a humoral response that included IgG reactive to arabinomannan, a component of mycobacterial cell wall (149). This enhanced microbial uptake can be extended to primary human neutrophils, monocytes, and macrophages and attributed for the most part to IgG by depletion assays (150). Importantly, unlike Fong et al. and Armstrong and Hart, when both Chen et al. and De Valliere et al. examined the resulting *in vitro* bacterial burden, there was decreased growth rate of BCG when opsonized with post-compared to pre- vaccination serum in both neutrophils and monocytes/macrophages. Demonstrating that despite increased initial uptake of BCG, the fate of these bacteria surrounded by antigen-specific antibodies inside a cell was death. Whether differences in mycobacterial species (*Mtb* vs. BCG) with

partially overlapping antigenic repertoires and/or host species FcR repertoires (rabbit vs. human vs. mouse) explains these differential findings, remains to be clarified. However, the more recent studies using human serum with human cells may provide a path toward overcoming species differences in modeling *Mtb in vitro*, particularly in the context of antibodies.

In studies with human cells and *Mtb*, macrophages, NK cells, and alveolar epithelial cells have been demonstrated to both potentially inhibit and also enhance bacterial growth in the context of antibodies. Opsonization of *Mtb* with polyclonal IgG purified from individuals with latent and active TB appeared to lead to similar bacterial uptake in primary human monocyte derived macrophages (26). However, upon the addition of purified polyclonal IgG after *Mtb* infection, intracellular bacterial burden is decreased in the context of antibodies from latent compared to active TB individuals (26). Whether or not this is due to cis- or trans- ADCC mediated by bystander macrophages in place of canonical NK cells remains unclear, but could provide a scenario in which this cellular effector mechanism (which is noted to be increased with *Mtb* antigen coated beads and NK cells in the context of latent compared to active TB IgG) could be directly linked (26). Finally, using arabinomannan reactive monoclonal antibodies to opsonize *Mtb*, Zimmerman et al. demonstrated that IgG1 on THP1 monocytes had no significant difference on bacterial counts compared to isotype control whereas the IgA1 isotype did (27). Indeed, when this experimental setup was expanded to the A549 human alveolar epithelial cell line expressing FcRn but not FcγRI, FcγRIII, FcγRII, or FcαR there was an enhancement of CFU noted upon infection with *Mtb* opsonized with monoclonal IgG isotype and inhibition with the IgA isotype. These studies demonstrate that bacterial fate is determined by both the antibody itself as well as the host cell.

A plethora of FcR expressing cells and associated downstream cellular processes can be recruited by *Mtb* reactive antibodies. Specifically, the classical antibody elicited effector functions of NK cell activation and subsequent production of granzysin to mediated ADCC has been observed (26, 140, 151). Moreover, Lu et al. demonstrated that phagolysosomal fusion, inflammasome activation, and IL-1β production could be elicited more with polyclonal IgG purified from individuals with latent compared to active TB. This is consistent with monoclonal antibodies enhancing BCG lysosomal co-localization (152). However, additional macrophage-mediated cellular processes in the context of *Mtb* include the production of additional cytokines, antimicrobial peptides, and even autophagy. These specific processes in mice and humans can contribute to protection as well as pathology (153, 154). Thus, even if these cellular functions are linked to antibodies, the implications for overall disease and outcome are not straight forward. These nuances may in fact help explain how enhanced survival (155) and or protection against dissemination (156) can be mediated by some monoclonal antibodies without impact on bacterial burden itself, highlighting further the immunomodulation and inflammatory balance that may be critical for TB control.

CONDITIONS ASSOCIATED WITH TB REACTIVATION: HIV-1 INFECTION

Inflammation in HIV-1

In acute HIV-1 infection the viral load rapidly increases alongside a burst of cytokines such as IFN- α and overstimulated pro-apoptotic CD4+ T cells; the immunological hallmark of HIV-1 infection (157). There is mounting evidence that chronic HIV-1 disease progression is characterized by systemic immune activation and oxidative stress, which can occur even while viremia is controlled with antiretrovirals (158–160). This systemic inflammation is thought to be caused by a number of factors; namely gut permeability, activated monocytes and cytokine derangement (160–163). High levels of viremia are accompanied by high levels of IFN- γ , TNF- α , IFN- α , and other inflammatory markers (164–166). The elevation of inflammatory serum markers is also correlated with onset of AIDS, cardiovascular disease, and lymphoma (165, 167–169).

Antibody Isotypes and Subclasses in HIV-1

Recent studies showing the importance of non-neutralizing antibodies in HIV-1 control and in protection have expanded the framework of antibodies beyond direct neutralization (170). These antibodies have been relatively well-characterized in HIV-1, with momentum gaining after the RV144 HIV-1 vaccine immune correlates analysis showed non-neutralizing V1V2 HIV-1 Envelope (Env) IgG was associated with protection (171–174). Antibody responses in the first months of HIV-1 infection are governed by non-neutralizing antibodies directed against Env (175). While initially thought to be ineffective, these early antibodies display some viral inhibition, while higher ADCC activity of vaccine-induced IgG has been associated with reduced peak viral load in macaque SHIV trials (176–178). The isotypes that predominate during this time are IgM followed by class-switching to IgG and IgA (179, 180). Anti-Env IgM titers decline after 1 month of infection while anti-env IgG levels remain raised and neutralizing IgG titers emerge months to years later in infection (181, 182). The role of IgA in HIV is controversial. Vaccine-specific serum IgA was correlated with reduce vaccine efficacy in the RV144 trial, as did an elevated IgA:IgG ratio (171, 183). Further, serum IgA has been associated with HIV disease progression (184, 185). However, mucosal IgA may be functionally distinct compared to serum IgA, and there are promising results from non-human primate SHIV infection studies, where mucosal administration of IgA appears to be protective (186).

During acute infection, IgG3 is elicited first in the IgG subclass response but eventually is surpassed by higher IgG1 titers against Env (187). Multiple studies have associated HIV-specific IgG3 with viral control and enhanced Fc-functions (172, 178, 188, 189). IgG1 and IgG2 against internal HIV-1 p24 protein have also associated with viral control though the mechanisms are still not understood (190, 191). As with active TB, IgG1, and IgG3 subclass predominates in HIV-1, however the connection between these specific IgG subclasses and inflammation in the context of HIV-1 is yet to be investigated. Studies have identified a greater breadth of IgG neutralizing antibodies in HIV controllers

who had high inflammatory markers such as TNF- α (192). Given the observation that neutralization breadth is a product of persistent viral replication (182), the high inflammatory markers in this study may point to a lack of viral control. In the context of HIV-1, some inflammation may be somewhat beneficial with cytokines and stimulated T cells encouraging the rate of somatic hypermutation in B cells to produce cross-reactive antibodies. However, in the context of a co-infected patient with latent TB, one could hypothesize that this HIV-associated inflammation involving inflammatory cytokines and T cell activation may tip the inflammatory balance too far, encouraging *Mtb* replication and development of active TB.

Glycosylation of Antibodies in HIV-1

Glycosylation of antibodies in HIV-1 infection differ between bulk IgG and HIV-specific IgG (193). Chronic progressive HIV infection exhibits highly agalactosylated IgG compared to controls, which as previously discussed, is typical of inflammation. In studies of HIV-1 glycosylation, this highly agalactosylated IgG has been shown to engage the complement cascade (193–195). The subclass that exhibits most agalactosylation in HIV-1 infection was IgG1 followed by IgG2 and IgG4 (194). The ability to categorize IgG1 as protective or destructive may rely on its galactosylation status and subsequent impact on downstream inflammatory outcomes such as tissue destruction and innate cell activation via Fc γ Rs. The role of sialylation and fucosylation in HIV-1 is not as clear. A recent study observed decreased sialylation and increased fucosylation of IgG in HIV-infected individuals (195). This increase in fucosylation was associated with reduced ADCC activity, meaning beneficial innate responses were decreased thereby reducing anti-inflammatory activities. Further, a significant association was observed between anti-inflammatory sialylated IgG, higher CD4+ counts and lower T cell activation (195). One caveat of this study is that they assessed the total IgG glycome and not HIV-specific IgG, meaning that we cannot comment on how specific IgG glycosylation impacts the ability of the antibody to fight HIV. While the global IgG glycome is an antibody inflammatory biomarker reflecting activated immune cells and therefore influencing an individual's susceptibility to disease, the glycosylation patterns of those specific antibodies which neutralize or function with ADCC/ADP to fight disease is also an important measure of the targeted immune response.

Antibody Function in HIV-1

Multiple studies have demonstrated the importance of antibody Fc function in HIV-1 control and vaccine-mediated protection (196–200). ADCC responses to Env have been associated with improved clinical outcomes and places mutation pressure on HIV-1 virus (196, 199, 201–203). While historically HIV studies have focused upon NK cell mediated ADCC, recent research has demonstrated the importance of other Fc functions mediated by neutrophils, macrophages, monocytes, and complement activation (204, 205), such that polyfunctional antibody responses may be beneficial (172, 206, 207). Through the strong engagement of these particular Fc receptors in HIV infection, cells are activated resulting in downstream release

of inflammatory cytokines and cytotoxic granules. A study looking at cytokines before pre- and post-ART (anti-retroviral therapy) in individuals with HIV-infection alone, found that TNF- α and IL-6 (pro-inflammatory) and IL-10, IL-4, and TGF- β (anti-inflammatory) were higher before ART while IFN- γ levels were lower before ART (208). In a different study of ART-naïve individuals co-infected with HIV/TB, *Mtb* culture-positive status correlated with high TNF- α , IL-2, IL-12, and also IFN- γ (209). It may be possible, that those with HIV-infection and substantial TB reactivation risk exhibit an over-inflammatory state involving more pro-inflammatory cytokines such as IFN- γ , but the involvement of antibodies in this inflammation is yet to be studied.

HIV-1 and *Mycobacterium tuberculosis* Co-infection

Infection with HIV-1 is a major risk factor for progression from latent to active TB, with the risk of reactivation 20-fold higher than the general population (158). The risk of developing active TB infection doubles in the first year of HIV-1 infection (210). The lack of T cells in HIV infection is one reason for the increased risk of TB acquisition and progression to active disease. However, even with effective ART such that viral loads are suppressed, CD4+ counts are >500 cells/ μ L and opportunistic infection risk is normalized, the risk of TB acquisition or reactivation is still increased (211). One study in South Africa, found that despite the widespread roll-out of ART, HIV prevalence among TB patients remained at 49% (212). Bucşan et al. recently found in a SIV/TB co-infection model that depleting CD4+ T cells in macaques was not sufficient to induce latent TB reactivation (213). The group propose SIV-associated reactivation may involve inflammatory imbalance. This could be due, in part, to inflammatory antibodies in HIV infection. Regardless, there may be other immune mechanisms than CD4+ T cell reduction that contribute to HIV-associated TB reactivation.

HIV-1 perturbs the *Mtb* immune response by impacting granuloma formation, *Mtb*-specific T cell response and macrophage activity (138). In an SIV-*Mtb* co-infection model, latent TB reactivated within 47 weeks of uncontrolled SIV infection (214). Immune Reconstitution Inflammatory Syndrome (IRIS), is a syndrome marked by innate cell cytotoxicity and cytokine dysregulation typically following the commencement of ART in HIV-1 infection. In IRIS, as the function of immune cells is reinstated, excessive inflammation and inflammatory driven organ-damage ensues. TB associated reactivation with IRIS can occur within 8 weeks of ART being commenced, particularly in the setting of advanced HIV-1 infection, indicating the role that this inflammatory state may play in TB reactivation (215–217). Further, *Mtb* and HIV co-infection increases the incidence of IRIS by 2-fold and HIV-infected patients with IRIS are at risk of acquiring TB (218, 219). The “unmasking” of other dormant pathogens, has also been observed in this hyperinflammatory state (220). The role of antibodies in the reactivation of dormant pathogens such as *Mtb* in the context of inflammation must be further explored.

Antibodies in TB/HIV-1 Co-infection

While IgG is formed against *Mtb* antigens in patients co-infected with *Mtb* and HIV-1, some studies observe substantially lower titers of *Mtb*-specific IgG and other isotypes (221, 222). Yu et al. (222) show correlations between IgG2 and IgG3 as well as IgG1 and IgG3 levels in HIV/TB co-infection (222). The group consider HIV-associated hypergammaglobulinemia as a cause of the IgG correlations and comment that the TB serology they assessed is more complicated in HIV negative individuals than in HIV/TB co-infected patients. It is pertinent to consider the impacts of losing T-cell help on isotype and subclass switching in the context of this HIV co-infection.

In contrast to these findings, other groups have found an increase in *Mtb*-specific antibody titers and reactivity in HIV/TB co-infection which they attribute to a high *Mtb* bacillary burden in HIV infected individuals (223). Yu et al. also highlight in their discussion, the counterintuitive nature of TB antibody and IFN- γ research, in that some show them to be protective, but others find that high antibody and IFN levels correlate with bacterial burden. The authors warn against speculating whether specific immune mechanisms can be concluded from their own study. One could hypothesize that some level of bacterial load is necessary for the instigation of an immune response but if that replication is overbearing, infection cannot be controlled.

Studies into the breadth of the antibody response in HIV/TB co-infection are limited. One recent study proposes the measurement of serum LAM as a biomarker for active TB (224) and Yu et al. (222) assessed *Mtb* polysaccharide responses and found elevated arabinomannan-specific IgG2 had the highest titers in all TB-infected groups. The fact that different subclasses predominate based on the antigen type is unsurprising as IgG2 is predominately generated against polysaccharide antigens. This does highlight the complexity of *Mtb* being both bacterial (generating typically a Th2 response) and an intracellular pathogen (needing Th1 responses too) and informs us as to why the ability to delineate protective vs. pathogenic immune responses to *Mtb* are so difficult to characterize.

Mtb-specific antibody titers decrease with HIV/TB co-infection as does the binding avidity of these antibodies to *Mtb* targets such as Ag85A (38). This group attribute the reduced avidity to dampened B cell responses, possibly caused by reduced T cell help that occurs with HIV infection, and the reduction in avidity means the *Mtb*-specific antibody responses are not as effective. It is important to investigate whether these ineffective antibody responses may contribute to a lack of *Mtb* control in HIV/TB co-infection. One genomics study found the deletion of Fc γ RIIIb genes was higher in patients co-infected with HIV and TB compared to HIV-1 alone (225). Fc γ RIIIb is a low-affinity activating receptor only expressed on neutrophils and basophils (79). The effects of this gene deletion on downstream receptor-expression and antibody function in co-infection merits further investigation. Regarding glycosylation in co-infection, a study of HIV-1 infected individuals with *Mycobacterium avium* infection showed that co-infected individuals have higher levels of agalactosylated IgG as well as elevated serum IgA levels (226). Whether agalactosylation is also increased in

HIV-1 co-infection with *Mtb* is yet to be studied. If future studies find that agalactosylated IgG are increased in HIV/TB co-infection, we would consider whether these inflammatory antibodies are involved in TB reactivation by enhancing a state of over-inflammation.

CONDITIONS ASSOCIATED WITH TB REACTIVATION: DIABETES MELLITUS

Diabetes Mellitus and Inflammation

Type II diabetes mellitus (T2DM) is typically caused by nutritional, lifestyle, and genetic factors causing obesity-induced insulin resistance and eventual depletion of insulin-secreting cells altogether. T2DM is characterized by a proinflammatory milieu with CD8+ T cell and T_H1 activity promoting insulin resistance and glucose intolerance (227–229). High-fat diets contribute to inflammation in diabetes and obesity in that they supply high levels of fatty acids which stimulate immune receptors such as toll-like receptors on innate cells and non-immune cells in adipose tissue. This cell activation encourages secretion of pro-inflammatory cytokines and skews the activation state of immune cells such as macrophages and B cells to one of inflammation. This pro-inflammatory milieu includes high neutrophil activation, macrophage adipose and pancreatic infiltration, increased pro-inflammatory cytokines such as IL-1 β , IL-8, and TNF as well as decreased anti-inflammatory cytokines such as IL-10 (230–233). IL-10 typically inhibits activity of T_H1 cells, macrophages and NK cells as well as regulating class-switching of B cells to IgM and IgG plasmablasts (234, 235).

Macrophage and CD4+ T cell activation in T2DM pathogenesis is well-described (236, 237). Studies show upregulation of T_H1 cells in T2DM adipose tissue with pro-inflammatory signatures (238). Not dissimilar to active TB, increases in TNF- α secretion by T_H1 and T_H17 CD4+ T cells are attributed to T2DM pathogenesis (239). One recurring cell-type in diseases where TB reactivation is high, are macrophages and monocytes. The immune environment of high TNF increases monocyte infiltration and IL-1, IL-6, and IL-12 are associated with macrophage and monocyte activation (240). With these two cell types being the primary targets of *Mtb* infection, it could be proposed that the induction of this macrophage-driven inflammation in some diseases increases TB reactivation risk, providing an environment within which *Mtb* can replicate. The complexity of the macrophage-TB response has been detailed by Guirado et al. in the following review (241).

Antibodies Isotypes in Diabetes Mellitus

The involvement of antibodies in T2DM pathogenesis is not well-understood. One study in patients with T2DM found a smaller percentage of antigen-specific antibody secreting plasmablasts, but when stimulated with LPS, T2DM B cells produced greater IgM and IgG titers (233). There were no differences in IgA titers to healthy controls. Further, the B cell phenotype in T2DM is similar to that found in obese individuals, yet those with T2DM failed to elicit protective B cell responses to an influenza vaccine while obese individuals did elicit protective responses (233). This may indicate that in the proinflammatory

environment, T2DM patients have readily activated B cells producing antibody isotypes IgG and IgM, however that these antibodies may be undirected or enhance disease, counteracting any protective neutralization effects seen otherwise. IgG has also been implicated in its association and specificity to long chain saturated fatty acids found in the serum of T2DM patients (242).

High fat diets are associated with systemic immune activation and the secretion of “pathogenic” IgG which promotes insulin resistance (243). This study transferred IgG from mice that received a high fat diet into recipient mice with a normal diet and found that post-transfer, recipient mice had elevated TNF- α and “pathogenic” IgG which promoted glucose intolerance and insulin resistance via Fc engagement (243). The authors discuss phenotypic changes to macrophages and B cells in adipose tissue that results in inflammatory cytokine release and “pathogenic” IgG.

Further, an IgG autoantibody was associated with T2DM prevalence and earlier disease onset in a Southwest American Indian cohort (244). It is thought that IgG antibodies form immune complexes in visceral adipose tissue and engage Fc γ R on B cells and macrophages, inducing inflammatory cytokines (243, 245). Pathological autoantibodies exist in other autoimmune diseases such as systemic lupus erythematosus where autoantibody subclasses in the order IgG1>IgG3>IgG2 are substantially elevated (246, 247). There are case reports of TB infection in autoimmune affected individuals, however this review does not discuss these cases as immunological data lacks in these cohorts (248). Looking at the role of IgG subclasses in T2DM, total IgG2 has been associated with insulin-resistance in mouse skeletal muscle through activation of epithelial Fc γ RIIb, an inhibitory Fc-receptor, and the impairment of insulin epithelial translocation (243, 249, 250). For endothelial cells, since Fc γ RIIb is engaged in insulin translocation it is necessary to maintain insulin sensitivity as shown by the attenuation of Fc γ RIIb resulting in impaired insulin translocation in skeletal muscle of obese mice (250). With elevated levels of IgG2 binding to Fc γ RIIb, insulin translocation is impaired. While this FcR-binding mechanism may not directly increase inflammation, it may be a by-product of an overactive immune system which encourages the over-production of “pathogenic” IgG.

Antibody Glycosylation and Function in Diabetes Mellitus

The first large study on antibody N-glycans in T2DM patients found that T2DM IgG derived glycans had substantially increased agalactosylation and decreased sialylation of all fucosylated structures (251). The authors refer to their findings as “reflective of an overall pro-inflammatory state” (251). The implications of these findings are that T2DM IgG engage more readily with the complement cascade, bind with higher affinity to Fc γ R and impact insulin resistance. Further, this study found increased fucosylation of IgG structures with bisecting GlcNAc, and decreased fucosylation of IgG glycans without bisecting GlcNAc in T2DM. The glycosylation of antigen-specific antibodies in T2DM is not well-understood and would merit from further investigation as to elucidate whether they mechanistically cause

inflammation. In mice, reduced N-glycan IgG sialylation was associated with insulin resistance and glucose intolerance as associated with a T2DM phenotype (250). When IgG from T2DM humans was transferred into B-cell deficient mice, insulin resistance developed. Interestingly, this obesity-related insulin resistance and glucose intolerance could be reversed by normalizing the sialylation patterns of IgG. Further, C-reactive protein (CRP), a marker of inflammation in T2DM, caused insulin resistance in this same study. They also determined that CRP acted on the inhibitory receptor FcγRIIb present on epithelial cells, stopping translocation of insulin through the epithelial membrane (250). Mice that were FcγRIIb-knockout, were protected from insulin resistance.

In the chronic hyperglycemic state of diabetes, there is another type of glycosylation which can occur. This process is called non-enzymatic glycosylation of plasma proteins which occurs when plasma is saturated with glucose due to hyperglycemia and attaches spontaneously to plasma proteins. Unlike N-linked glycans, non-enzymatic glycosylation has been well-documented in diabetes and other diseases for many years (252). Non-enzymatic glycosylation of IgG has been implicated in diabetes pathogenesis affecting renal clearance of IgG with subsequent effects on renal function. Further, glycosylated IgG has been suggested as a comparable biomarker to the well-known glycosylated hemoglobin (HbA1c) (253, 254).

Antibodies in Diabetes Mellitus and Tuberculosis Comorbidity

Diabetes with associated *Mtb* infection is a substantial global health issue. There are now more individuals comorbid with TB/Diabetes than those with TB/HIV-1 (14). Diabetics with associated pulmonary TB infection have higher levels of type-1 pro-inflammatory cytokines such as IFN-γ and TNF-α as well as a reduction in anti-inflammatory cytokine IL-22 (255). The elevation of IFN-γ and TNF-α and reduction in anti-inflammatory cytokines mean that inflammatory pathways in innate cells and T cells are discharged which contributes to immunopathology and poor *Mtb* control in diabetic individuals (255). Further, T2DM co-infected with TB have a pro-atherogenic, dyslipidaemic plasma profile exacerbating metabolic disease which is postulated to contribute to TB reactivation (256). There are a number of studies that characterize the DM/TB co-infection T cell and innate cell phenotypes but none include a characterization of antibody responses in DM/TB co-infection (257–259). A study by Gomez et al. (260) demonstrated that monocytes cultured with serum from diabetics do not associate via classical or alternative complement pathways with *Mtb* *in vitro*, and they attribute this to reduced FcγR and complement receptor defects (260, 261). Defective FcγR would impact IgG isotype binding and functionality. The group do not report antibody nor complement protein titers in these individuals which would have addressed the question of whether reduced antibody titer in diabetics is a potential cause for the lack of *Mtb* association. Given the increasing burden of DM/TB co-infection, urgent attention needs to be given to potential immune biomarkers of reactivation, such as antibodies.

CONDITIONS ASSOCIATED WITH TB REACTIVATION: CHRONIC KIDNEY DISEASE

Chronic Kidney Disease and Inflammation

Chronic Kidney Disease (CKD) and its further progressed End-Stage Renal Disease (ESRD) are associated with substantial immune perturbation and inflammation (262). Despite the varied etiology of CKD, the end point of inflammation encompassing renal impairment, metabolic waste accumulation and treatment with dialysis is universal to CKD patients. The impact of hemodialysis includes chronic activation of the alternative complement pathway, antigenic stimulation and disruption of mucocutaneous barriers (263). CKD is a systemic disease not only affecting the kidneys, with “uremia” affecting other organs including the lungs. Pro-inflammatory cytokines such as TNF-α, IFN-γ, and IL-6 are elevated while IL-10 levels are suppressed (262, 264). Further, T_H1 responses are elevated in ESRD and Kato et al. discuss this immune dysfunction in ESRD in more detail (264). Impaired immune function in CKD leads to higher rates of infection while the exaggerated inflammatory immune response in the condition contributes to different immune-related events such as atherosclerotic cardiovascular disease (262). This is thought to occur in HIV-1 and T2DM also. It may be possible that the dysregulated immunity with excessive IFN-γ, TNF-α, and T_H1 responses, promotes macrophage activation and contributes to an environment which may favor *Mtb* replication.

Antibody Isotypes and Subclasses in Chronic Kidney Disease

A number of studies have documented reduced titers of antigen-specific IgG, IgA, and IgM in patients with chronic renal insufficiency. Most in-depth serum antibody analyses involve antigen-specific responses to vaccination or infection in CKD cohorts. The antibody response to Hepatitis B vaccine is muted in CKD individuals, with low seroconversion and rapid reduction in titers post-vaccination (265). Further, in Hemophilus influenza A-vaccinated CKD patients, there are reduced absolute B cell numbers and less functional bactericidal antigen-specific IgG and IgM (266). In a recent study, aiming to elucidate the role of the T-cell inhibitory receptor CTLA-4 in pathogenesis of glomerulonephritis, a major cause of CKD, levels of IgM inversely correlated with lower CTLA-4, as did IgG and IgA to a lesser extent, with the proposition that this may reflect inappropriate IgM function in ESRD (267). Further, many causes of CKD are auto-immune based and involve the generation of autoantibodies against kidney tissue. These auto-antibodies tend to be of the subclasses IgG1 and IgG3 and are reviewed at a greater depth by Tecklenborg et al. (268).

Glycosylation and Function of Antibodies in Chronic Kidney Disease

There is very little data on glycosylation of antibodies in CKD. The most recent study found a predominance of pro-inflammatory agalactosylated IgG Fc-glycosylation in patients with CKD and in those with agalactosylated IgG but no CKD,

they were at higher risk of developing CKD (269). Further, IgG Fc N-linked glycans in kidney disease patients are more likely to lack a core-fucose, a phenotype associated with substantially increased Fc γ RIIIa binding affinity and ADCC. Individuals with sialylated, core-fucosylated with bisecting GlcNAc IgG had greater CKD risk. This group also found that levels of anti-inflammatory IgG Fc-glycan sialylation were decreased in patients with CKD (269). One group also discovered a γ -chain deficiency in mice, thereby preventing the function of activating Fc γ Rs, resulting in kidney disease protection (270). These findings amongst those on glycosylation in CKD, are consistent with the idea that CKD progression is linked to pro-inflammatory mechanisms, some of which are enacted by antibodies. Anti-neutrophil cytoplasmic autoantibody vasculitis is one cause of CKD and Fc N-glycan patterns of IgG1 in this disease has also been described as pro-inflammatory, with high agalactosylation and low sialylation patterns (271).

Antibodies and Immunity in Chronic Kidney Disease and Tuberculosis Comorbidity

Despite notably high rates of co-infection between TB and CKD, the diagnosis of latent TB is difficult in this population. This is due to lowered sensitivity of the IGRA assay in detecting *Mtb* in ESRD groups which has been attributed to defective T cell function (272). $\gamma\delta$ T cells in this co-infected population showed lowered expression of lung-homing receptors while MAIT cells were depleted in the periphery, with particular reductions in cells also associated with lung-trafficking (273, 274). This indicates a potential role for unconventional T cells in controlling pulmonary TB infection. However, very little research has looked into characterizing antibody profiles in patients comorbid with kidney disease and TB. This is to the exception of IgA-nephropathy, a leading cause of primary kidney disease which is due to deposition of IgA in renal tubules leading to glomerulonephritic disease and eventually CKD. In a cohort of IgA-nephropathic patients co-infected with TB, levels of anti-Ag85A antibody were higher in co-infected patients indicating an ability to generate *Mtb*-specific antibody (275). It is thought that elevated *Mtb*-specific IgA levels contribute to IgA nephropathy co-infection, glomerulonephritis and ensuing CKD (276). The pathogenesis of this involves alternative complement activation, lectin activation and deposition of IgA-complexes in the kidney (275, 276). Deposits of IgA1 are found at higher levels of co-infected individuals as well as patients presenting with renal TB (275). Further, high levels of TGF- β 1 are correlated with defective IgA1 generation and TGF- β 1 increases in both TB and IgA nephropathy (276). These papers together propose that *Mtb* infection increases the levels of IgA in serum which aggregate to form pathogenic complexes leading to nephritic disease. This then exacerbates kidney disease and the cycle of inflammation, which may worsen TB disease. More than that, it may be possible that these serum IgA1 antibodies act more readily on inflammation in the kidney hence the association with higher TB renal disease in this population.

Studies assessing *Mtb* proteins and kidney injury found the *Mtb* antigen, ESAT-6, contributed to renal injury in mice injected with a high dose of ESAT-6 by upregulating the expression of pro-inflammatory microRNA-155 via the MyD88 innate cell

pathway (275, 277, 278). While the dose of ESAT-6 used in these studies may not reflect those found in physiological disease, this evidence may show a cyclical worsening of disease in CKD/TB coinfection exacerbated by kidney inflammation caused by TB and CKD independently.

TB mortality is also very high amongst ESRD patients after kidney transplant. A recent retrospective analysis discovered that kidney transplant recipients receiving the immunotherapy Belatacept, a fusion protein of anti-CTLA-4 and the Fc-portion of IgG1 (CTLA4-Ig), had a significantly higher incidence of TB reactivation and infection (279). The incidence of TB in the group receiving Belatacept was higher at 17.6% compared to other immunosuppressive drugs where the incidence was <2.5% indicating that the immunosuppressive actions of these drugs may not have been the root cause for TB reactivation in these groups (279). This is interesting given the previous studies discussed above provide some evidence to support the proinflammatory actions of IgG1 may worsen TB disease prognosis. Belatacept or CTLA4-Ig, was developed to not only stimulate T cells through inhibiting CTLA-4, but to induce ADCC and complement-dependent cytotoxicity via the IgG1 Fc region (280). The findings of TB reactivation in this anti-CTLA4 immunotherapy group echo the recent case reports of TB reactivation with PD-1 inhibitors (96, 98, 99, 281). Exaggerated T_H1 responses due to PD-1 inhibitors have been proposed as the mechanism by which TB reactivates in these patients (99).

CONCLUSIONS

Mtb infection and its frequent association with HIV, T2DM, and CKD are growing global health burdens. With a quarter of the world latently infected with *Mtb* and the rise of non-communicable diseases such as T2DM and CKD in both developed and developing countries, we must pay attention to this double burden of disease. There is a notable lack of research on the mechanisms of TB reactivation in different immune environments. The paradoxical evidence around T cell responses and type 1 cytokines suggests that high IFN- γ , TNF- α , and IL-2 CD4⁺ T cells induced in response to vaccination or before the establishment of TB disease is beneficial to TB control, but when these responses are too late or they expand after *Mtb* has established, they are detrimental. A better understanding of TB reactivation would allow the rational design of preventative measures to reduce associated mortality and burden on individuals and their healthcare systems. In this review, we describe antibody characteristics of isotypes and subclasses, glycosylation patterns and function across TB, HIV-1, T2DM, and CKD (see summary in **Supplementary Table 1**). There is a large volume of evidence from both arms of the immune system that point to the role of a pro-inflammatory milieu in assisting TB reactivation. HIV-1, T2DM, and CKD are highly inflammatory chronic diseases, and this is reflected by their antibody profiles, especially IgG subclasses and post-translational modifications. However, clearly this review also highlights the many gaps in our knowledge. To genuinely understand the causes of TB reactivation, we must look at the interface at which antibodies, T cells and innate cells all interact to create an

inflammatory response. Much can be learnt from the actions and patterns of antibodies from these diseases. Furthermore, antibodies are a real-time measure of immunocompetency and assessing serum antibodies is comparatively more reliable, cost-effective and high-throughput in comparison to cell-based assays. Understanding antibody characteristics is essential to decode these patterns in disease, and we are gaining in momentum and understanding.

AUTHOR CONTRIBUTIONS

MM and AC contributed to conception of the review. MM compiled literature, wrote and edited drafts, and created figures. MM, LL, AC, and SK contributed to the manuscript editing and revisions and approved the submitted version.

REFERENCES

- World Health Organization. *Global Tuberculosis Report 2018*. Geneva: World Health Organization (2018).
- Achkar JM, Jenny-Avital ER. Incipient and subclinical tuberculosis: defining early disease states in the context of host immune response. *J Infect Dis.* (2011) 204(Suppl 4):S1179–86. doi: 10.1093/infdis/jir451
- Furin J, Cox H, Pai M. Tuberculosis. *Lancet.* (2019) 393:1642–56. doi: 10.1016/S0140-6736(19)30308-3
- Rao M, Ippolito G, Mfinanga S, Ntouni F, Yeboah-Manu D, Vilaplana C, et al. Latent TB Infection (LTBI) - *Mycobacterium tuberculosis* pathogenesis and the dynamics of the granuloma battleground. *Int J Infect Dis.* (2019) 80S:S58–S61. doi: 10.1016/j.ijid.2019.02.035
- Magee MJ, Salindri AD, Gujral UP, Auld SC, Bao J, Haw JS, et al. Convergence of non-communicable diseases and tuberculosis: a two-way street? *Int J Tuberc Lung Dis.* (2018) 22:1258–68. doi: 10.5588/ijtld.18.0045
- Montales MT, Chaudhury A, Beebe A, Patil S, Patil N. HIV-associated TB syndemic: a growing clinical challenge worldwide. *Front Public Health.* (2015) 3:281. doi: 10.3389/fpubh.2015.00281
- World Health Organisation. *TB Causes 1 in 3 HIV Deaths*. World Health Organisation (2018). Available online at: <https://www.who.int/hiv/mediacentre/news/hiv-tb-patient-centred-care/en/>
- Gupta RK, Lucas SB, Fielding KL, Lawn SD. Prevalence of tuberculosis in post-mortem studies of HIV-infected adults and children in resource-limited settings: a systematic review and meta-analysis. *AIDS.* (2015) 29:1987–2002. doi: 10.1097/QAD.0000000000000802
- Abel L, Fellay J, Haas DW, Schurr E, Srikrishna G, Urbanowski M, et al. Genetics of human susceptibility to active and latent tuberculosis: present knowledge and future perspectives. *Lancet Infect Dis.* (2018) 18:e64–e75. doi: 10.1016/S1473-3099(17)30623-0
- Gauld WR, Lyall A. Tuberculosis as a complication of diabetes mellitus. *Br Med J.* (1947) 1:677–9. doi: 10.1136/bmj.1.4506.677
- Hussein MM, Mooij JM, Roujoleh H. Tuberculosis and chronic renal disease. *Semin Dial.* (2003) 16:38–44. doi: 10.1046/j.1525-139X.2003.03010.x
- Marais BJ, Lonnroth K, Lawn SD, Migliori GB, Mwaba P, Glaziou P, et al. Tuberculosis comorbidity with communicable and non-communicable diseases: integrating health services and control efforts. *Lancet Infect Dis.* (2013) 13:436–48. doi: 10.1016/S1473-3099(13)70015-X
- Cadena J, Rathinavelu S, Lopez-Alvarenga JC, Restrepo BI. The re-emerging association between tuberculosis and diabetes: lessons from past centuries. *Tuberculosis.* (2019) 116S:S89–S97. doi: 10.1016/j.tube.2019.04.015
- Restrepo BI. Diabetes and tuberculosis. *Microbiol Spectr.* (2016) 4:1–21. doi: 10.1128/microbiolspec.TNMI7-0023-2016
- Tomita A, Smith CM, Lessells RJ, Pym A, Grant AD, De Oliveira T, et al. Space-time clustering of recently-diagnosed tuberculosis and impact of ART scale-up: evidence from an HIV hyper-endemic rural South African population. *Sci Rep.* (2019) 9:1072. doi: 10.1038/s41598-019-46455-7

FUNDING

This work was supported by an Australian NHMRC project grant APP1163790.

ACKNOWLEDGMENTS

We would like to acknowledge Jennifer Juno for the valuable discussions about this review topic.

SUPPLEMENTARY MATERIAL

The Supplementary Material for this article can be found online at: <https://www.frontiersin.org/articles/10.3389/fimmu.2019.02846/full#supplementary-material>

- Ugarte-Gil C, Alisjahbana B, Ronacher K, Riza AL, Koesoemadinata RC, Malherbe ST, et al. Diabetes mellitus among pulmonary tuberculosis patients from four TB-endemic countries: the TANDEM study. *Clin Infect Dis.* (2019) ciz284. doi: 10.1093/cid/ciz284. [Epub ahead of print].
- Neuen BL, Chadban SJ, Demaio AR, Johnson DW, Perkovic V. Chronic kidney disease and the global NCDs agenda. *BMJ Glob Health.* (2017) 2:e000380. doi: 10.1136/bmjgh-2017-000380
- Lozano R, Naghavi M, Foreman K, Lim S, Shibuya K, Aboyans V, et al. Global and regional mortality from 235 causes of death for 20 age groups in 1990 and 2010: a systematic analysis for the Global Burden of Disease Study 2010. *Lancet.* (2012) 380:2095–128. doi: 10.1016/S0140-6736(12)61728-0
- Romanowski K, Clark EG, Levin A, Cook VJ, Johnston JC. Tuberculosis and chronic kidney disease: an emerging global syndemic. *Kidney Int.* (2016) 90:34–40. doi: 10.1016/j.kint.2016.01.034
- Mandalakas AM, Hesselning AC, Chegou NN, Kirchner HL, Zhu X, Marais BJ, et al. High level of discordant IGRA results in HIV-infected adults and children. *Int J Tuberc Lung Dis.* (2008) 12:417–23. Available online at: <https://www.ingentaconnect.com.ezp.lib.unimelb.edu.au/content/iautld/ijtld/2008/00000012/00000004/art00013>
- Lange C, Pai M, Drobniewski F, Migliori GB. Interferon-gamma release assays for the diagnosis of active tuberculosis: sensible or silly? *Eur Respir J.* (2009) 33:1250–3. doi: 10.1183/09031936.00019709
- Mittrucker HW, Steinhoff U, Kohler A, Krause M, Lazar D, Mex P, et al. Poor correlation between BCG vaccination-induced T cell responses and protection against tuberculosis. *Proc Natl Acad Sci USA.* (2007) 104:12434–9. doi: 10.1073/pnas.0703510104
- Sharpe S, White A, Sarfas C, Sibley L, Gleeson F, McIntyre A, et al. Alternative BCG delivery strategies improve protection against *Mycobacterium tuberculosis* in non-human primates: protection associated with mycobacterial antigen-specific CD4 effector memory T-cell populations. *Tuberculosis.* (2016) 101:174–90. doi: 10.1016/j.tube.2016.09.004
- Casadevall A. To be or not be a (functional) antibody against TB. *Cell.* (2016) 167:306–7. doi: 10.1016/j.cell.2016.09.041
- Zeng G, Zhang G, Chen X. Th1 cytokines, true functional signatures for protective immunity against TB? *Cell Mol Immunol.* (2018) 15:206. doi: 10.1038/cmi.2017.113
- Lu LL, Chung AW, Rosebrock TR, Ghebremichael M, Yu WH, Grace PS, et al. A functional role for antibodies in tuberculosis. *Cell.* (2016) 167:433–43.e414. doi: 10.1016/j.cell.2016.08.072
- Zimmermann N, Thormann V, Hu B, Kohler AB, Imai-Matsushima A, Loch C, et al. Human isotype-dependent inhibitory antibody responses against *Mycobacterium tuberculosis*. *EMBO Mol Med.* (2016) 8:1325–39. doi: 10.15252/emmm.201606330
- Li H, Wang XX, Wang B, Fu L, Liu G, Lu Y, et al. Latently and uninfected healthcare workers exposed to TB make protective antibodies against *Mycobacterium tuberculosis*. *Proc Natl Acad Sci USA.* (2017) 114:5023–8. doi: 10.1073/pnas.1611776114

29. Abebe F, Belay M, Legesse M, KLMCF, Ottenhoff THM. IgA and IgG against *Mycobacterium tuberculosis* Rv2031 discriminate between pulmonary tuberculosis patients, *Mycobacterium tuberculosis*-infected and non-infected individuals. *PLoS ONE*. (2018) 13:e0190989. doi: 10.1371/journal.pone.0190989
30. Lu LL, Smith MT, Yu KQ, Luedemann C, Suscovich TJ, Grace PS, et al. IFN- γ -independent immune markers of *Mycobacterium tuberculosis* exposure. *Nat Med*. (2019) 25:977–87. doi: 10.1038/s41591-019-0441-3
31. Davidow A, Kanauija GV, Shi L, Kaviar J, Guo X, Sung N, et al. Antibody profiles characteristic of *Mycobacterium tuberculosis* infection state. *Infect Immun*. (2005) 73:6846–51. doi: 10.1128/IAI.73.10.6846-6851.2005
32. Osada-Oka M, Tateishi Y, Hirayama Y, Ozeki Y, Niki M, Kitada S, et al. Antigen 85A and mycobacterial DNA-binding protein 1 are targets of immunoglobulin G in individuals with past tuberculosis. *Microbiol Immunol*. (2013) 57:30–7. doi: 10.1111/j.1348-0421.2012.12005.x
33. Baumann R, Kaempfer S, Chegou NN, Oehlmann W, Loxton AG, Kaufmann SH, et al. Serologic diagnosis of tuberculosis by combining Ig classes against selected mycobacterial targets. *J Infect*. (2014) 69:581–9. doi: 10.1016/j.jinf.2014.05.014
34. Senoputra MA, Shiratori B, Hasibuan FM, Koesoemadinata RC, Apriani L, Ashino Y, et al. Diagnostic value of antibody responses to multiple antigens from *Mycobacterium tuberculosis* in active and latent tuberculosis. *Diagn Microbiol Infect Dis*. (2015) 83:278–85. doi: 10.1016/j.diagmicrobio.2015.07.021
35. Awoniyi DO, Baumann R, Chegou NN, Kriel B, Jacobs R, Kidd M, et al. Detection of a combination of serum IgG and IgA antibodies against selected mycobacterial targets provides promising diagnostic signatures for active TB. *Oncotarget*. (2017) 8:37525–37. doi: 10.18632/oncotarget.16401
36. Broger T, Basu Roy R, Filomena A, Greef CH, Rimmele S, Havumaki J, et al. Diagnostic performance of tuberculosis-specific IgG antibody profiles in patients with presumptive tuberculosis from two continents. *Clin Infect Dis*. (2017) 64:947–55. doi: 10.1093/cid/cix023
37. De Araujo LS, Da Silva NBM, Leung JAM, Mello FCQ, Saad MHF. IgG subclasses' response to a set of mycobacterial antigens in different stages of *Mycobacterium tuberculosis* infection. *Tuberculosis*. (2018) 108:70–6. doi: 10.1016/j.tube.2017.10.010
38. Kimuda SG, Biraro IA, Bagaya BS, Raynes JG, Cose S. Characterising antibody avidity in individuals of varied *Mycobacterium tuberculosis* infection status using surface plasmon resonance. *PLoS ONE*. (2018) 13:e0205102. doi: 10.1371/journal.pone.0205102
39. Chiliza TE, Pillay M, Naidoo K, Pillay B. Immunoscreening of the M. tuberculosis F15/LAM4/KZN secretome library against TB patients' sera identifies unique active- and latent-TB specific biomarkers. *Tuberculosis*. (2019) 115:161–70. doi: 10.1016/j.tube.2019.03.005
40. Maekura R, Kitada S, Osada-Oka M, Tateishi Y, Ozeki Y, Fujicawa T, et al. Serum antibody profiles in individuals with latent *Mycobacterium tuberculosis* infection. *Microbiol Immunol*. (2019) 63:130–8. doi: 10.1111/1348-0421.12674
41. Burton DR, Woof JM. Human antibody effector function. *Adv Immunol*. (1992) 51:1–84. doi: 10.1016/S0065-2776(08)60486-1
42. Hogarth PM. Fc receptors are major mediators of antibody based inflammation in autoimmunity. *Curr Opin Immunol*. (2002) 14:798–802. doi: 10.1016/S0952-7915(02)00409-0
43. Panda S, Ding JL. Natural antibodies bridge innate and adaptive immunity. *J Immunol*. (2015) 194:13–20. doi: 10.4049/jimmunol.1400844
44. Delacroix DL, Dive C, Rambaud J, Vaerman J. IgA subclasses in various secretions and in serum. *Immunology*. (1982) 47:383.
45. Vidarsson G, Dekkers G, Rispens T. IgG subclasses and allotypes: from structure to effector functions. *Front Immunol*. (2014) 5:520. doi: 10.3389/fimmu.2014.00520
46. Woof JM, Kerr MA. IgA function—variations on a theme. *Immunology*. (2004) 113:175. doi: 10.1111/j.1365-2567.2004.01958.x
47. Damelang T, Rogerson SJ, Kent SJ, Chung AW. Role of IgG3 in infectious diseases. *Trends Immunol*. (2019) 40:197–211. doi: 10.1016/j.it.2019.01.005
48. Pone EJ, Zan H, Zhang J, Al-Qahtani A, Xu Z, Casali P. Toll-like receptors and B-cell receptors synergize to induce immunoglobulin class-switch DNA recombination: relevance to microbial antibody responses. *Crit Rev Immunol*. (2010) 30:1–29. doi: 10.1615/CritRevImmunol.v30.i1.10
49. Horner AA, Jabara H, Ramesh N, Geha RS. gamma/delta T lymphocytes express CD40 ligand and induce isotype switching in B lymphocytes. *J Exp Med*. (1995) 181:1239–44. doi: 10.1084/jem.181.3.1239
50. Stavnezer J. Immunoglobulin class switching. *Curr Opin Immunol*. (1996) 8:199–205. doi: 10.1016/S0952-7915(96)80058-6
51. Bai L, Deng S, Reboulet R, Mathew R, Teyton L, Savage PB, et al. Natural killer T (NKT)-B-cell interactions promote prolonged antibody responses and long-term memory to pneumococcal capsular polysaccharides. *Proc Natl Acad Sci USA*. (2013) 110:16097–102. doi: 10.1073/pnas.1303218110
52. Tarr PI, Hosea SW, Brown EJ, Schneerson R, Sutton A, Frank MM. The requirement of specific anticapsular IgG for killing of *Haemophilus influenzae* by the alternative pathway of complement activation. *J Immunol*. (1982) 128:1772–5.
53. Frank MM, Joiner K, Hammer C. The function of antibody and complement in the lysis of bacteria. *Rev Infect Dis*. (1987) 9(Suppl 5):S537–45. doi: 10.1093/clinids/9.Supplement_5.S537
54. Shackelford PG, Granoff DM, Nelson SJ, Scott MG, Smith DS, Nahm MH. Subclass distribution of human antibodies to *Haemophilus influenzae* type b capsular polysaccharide. *J Immunol*. (1987) 138:587–92.
55. Ferrante A, Beard LJ, Feldman RG. IgG subclass distribution of antibodies to bacterial and viral antigens. *Pediatr Infect Dis J*. (1990) 9:S16–24. doi: 10.1097/00006454-199008001-00004
56. Schechter MC, Satola SW, Stephens DS. Host defenses to extracellular bacteria. In: Rich RR, Fleisher TA, Shearer WT, Schroeder HW, Frew AJ Jr, Weyand CM, editors. *Clinical Immunology: Principles and Practice*. Amsterdam: Elsevier (2018). p. 391–402.e391.
57. Hessel AJ, Hangartner L, Hunter M, Havenith CE, Beurskens FJ, Bakker JM, et al. Fc receptor but not complement binding is important in antibody protection against HIV. *Nature*. (2007) 449:101–4. doi: 10.1038/nature06106
58. Parsons MS, Chung AW, Kent SJ. Importance of Fc-mediated functions of anti-HIV-1 broadly neutralizing antibodies. *Retrovirology*. (2018) 15:58. doi: 10.1186/s12977-018-0438-x
59. Garber E, Demarest SJ. A broad range of Fab stabilities within a host of therapeutic IgGs. *Biochem Biophys Res Commun*. (2007) 355:751–7. doi: 10.1016/j.bbrc.2007.02.042
60. Houde D, Peng Y, Berkowitz SA, Engen JR. Post-translational modifications differentially affect IgG1 conformation and receptor binding. *Mol Cell Proteomics*. (2010) 9:1716–28. doi: 10.1074/mcp.M900540-MCP200
61. Walsh G, Jefferis R. Post-translational modifications in the context of therapeutic proteins. *Nat Biotechnol*. (2006) 24:1241–52. doi: 10.1038/nbt1252
62. Chung AW, Crispin M, Pritchard L, Robinson H, Gorny MK, Yu X, et al. Identification of antibody glycosylation structures that predict monoclonal antibody Fc-effector function. *AIDS*. (2014) 28:2523–30. doi: 10.1097/QAD.0000000000000444
63. Van De Bovenkamp FS, Hafkenscheid L, Rispens T, Rombouts Y. The emerging importance of IgG fab glycosylation in immunity. *J Immunol*. (2016) 196:1435–41. doi: 10.4049/jimmunol.1502136
64. Baum LG, Cobb BA. The direct and indirect effects of glycans on immune function. *Glycobiology*. (2017) 27:619–24. doi: 10.1093/glycob/cwx036
65. Gornik O, Lauc G. Glycosylation of serum proteins in inflammatory diseases. *Dis Markers*. (2008) 25:267–78. doi: 10.1155/2008/493289
66. Boesch AW, Brown EP, Cheng HD, Ofori MO, Normandin E, Nigrovic PA, et al. Highly parallel characterization of IgG Fc binding interactions. *Mabs*. (2014) 6:915–27. doi: 10.4161/mabs.28808
67. Dashivets T, Thomann M, Rueger P, Knaupp A, Buchner J, Schlothauer T. Multi-angle effector function analysis of human monoclonal IgG glycovariants. *PLoS ONE*. (2015) 10:e0143520. doi: 10.1371/journal.pone.0143520
68. Geuijen KPM, Oppers-Tiemenissen C, Egging DF, Simons PJ, Boon L, Schasfoort RBM, et al. Rapid screening of IgG quality attributes - effects on Fc receptor binding. *FEBS Open Bio*. (2017) 7:1557–74. doi: 10.1002/2211-5463.12283
69. Malhotra R, Wormald MR, Rudd PM, Fischer PB, Dwek RA, Sim RB. Glycosylation changes of IgG associated with rheumatoid arthritis can

- activate complement via the mannose-binding protein. *Nat Med.* (1995) 1:237–43. doi: 10.1038/nm0395-237
70. Umana P, Jean-Mairet J, Moudry R, Amstutz H, Bailey JE. Engineered glycoforms of an antineuroblastoma IgG1 with optimized antibody-dependent cellular cytotoxic activity. *Nat Biotechnol.* (1999) 17:176–80. doi: 10.1038/6179
 71. Shields RL, Lai J, Keck R, O'Connell LY, Hong K, Meng YG, et al. Lack of fucose on human IgG1 N-linked oligosaccharide improves binding to human FcγRIII and antibody-dependent cellular toxicity. *J Biol Chem.* (2002) 277:26733–40. doi: 10.1074/jbc.M202069200
 72. Anthony RM, Ravetch JV. A novel role for the IgG Fc glycan: the anti-inflammatory activity of sialylated IgG Fcs. *J Clin Immunol.* (2010) 30(Suppl 1):S9–14. doi: 10.1007/s10875-010-9405-6
 73. Lofano G, Gorman MJ, Yousif AS, Yu WH, Fox JM, Dugast AS, et al. Antigen-specific antibody Fc glycosylation enhances humoral immunity via the recruitment of complement. *Sci Immunol.* (2018) 3:eaat7796. doi: 10.1126/sciimmunol.aat7796
 74. Van De Bovenkamp FS, Derksen NIL, Ooijsvaar-De Heer P, Van Schie KA, Kruithof S, Berkowska MA, et al. Adaptive antibody diversification through N-linked glycosylation of the immunoglobulin variable region. *PNAS.* (2018) 115:1901–6. doi: 10.1073/pnas.1711720115
 75. Takasugi J, Koide Y, Takasugi M. Reconstitution of natural cell-mediated cytotoxicity with specific antibodies. *Eur J Immunol.* (1977) 7:887–92. doi: 10.1002/eji.1830071213
 76. Clement MV, Haddad P, Soulie A, Legros-Maida S, Guillet J, Cesar E, et al. Involvement of granzyme B and perforin gene expression in the lytic potential of human natural killer cells. *Res Immunol.* (1990) 141:477–89. doi: 10.1016/0923-2494(90)90017-S
 77. Bruhns P, Iannascoli B, England P, Mancardi DA, Fernandez N, Jorieux S, et al. Specificity and affinity of human FcγRIII receptors and their polymorphic variants for human IgG subclasses. *Blood.* (2009) 113:3716–25. doi: 10.1182/blood-2008-09-179754
 78. Anania JC, Chenoweth AM, Wines BD, Hogarth PM. The human FcγRIII (CD32) family of leukocyte FcR in health and disease. *Front Immunol.* (2019) 10:464. doi: 10.3389/fimmu.2019.00464
 79. Hogarth PM, Pietersz GA. Fc receptor-targeted therapies for the treatment of inflammation, cancer and beyond. *Nat Rev Drug Discov.* (2012) 11:311–31. doi: 10.1038/nrd2909
 80. Simmons JD, Stein CM, Seshadri C, Campo M, Alter G, Fortune S, et al. Immunological mechanisms of human resistance to persistent *Mycobacterium tuberculosis* infection. *Nat Rev Immunol.* (2018) 18:575–89. doi: 10.1038/s41577-018-0025-3
 81. Ilgazli A, Boyaci H, Basyigit I, Yildiz F. Extrapulmonary tuberculosis: clinical and epidemiologic spectrum of 636 cases. *Arch Med Res.* (2004) 35:435–41. doi: 10.1016/j.arcmed.2004.05.008
 82. Modlin RL, Bloom BR. TB or not TB: that is no longer the question. *Sci Transl Med.* (2013) 5:213sr216. doi: 10.1126/scitranslmed.3007402
 83. Cooper AM, Dalton DK, Stewart TA, Griffin JP, Russell DG, Orme IM. Disseminated tuberculosis in interferon gamma gene-disrupted mice. *J Exp Med.* (1993) 178:2243–7. doi: 10.1084/jem.178.6.2243
 84. Flynn JL, Chan J, Triebold KJ, Dalton DK, Stewart TA, Bloom BR. An essential role for interferon gamma in resistance to *Mycobacterium tuberculosis* infection. *J Exp Med.* (1993) 178:2249–54. doi: 10.1084/jem.178.6.2249
 85. Randhawa PS. Lymphocyte subsets in granulomas of human tuberculosis: an *in situ* immunofluorescence study using monoclonal antibodies. *Pathology.* (1990) 22:153–5. doi: 10.1019/00313029009063555
 86. Feng CG, Bean AG, Hooi H, Briscoe H, Britton WJ. Increase in gamma interferon-secreting CD8(+), as well as CD4(+), T cells in lungs following aerosol infection with *Mycobacterium tuberculosis*. *Infect Immun.* (1999) 67:3242–7.
 87. Ottenhoff TH, Kumararatne D, Casanova JL. Novel human immunodeficiencies reveal the essential role of type-I cytokines in immunity to intracellular bacteria. *Immunol Today.* (1998) 19:491–4. doi: 10.1016/S0167-5699(98)01321-8
 88. Navarra SV, Tang B, Lu L, Lin HY, Mok CC, Asavatanabodee P, et al. Risk of tuberculosis with anti-tumor necrosis factor-α therapy: substantially higher number of patients at risk in Asia. *Int J Rheum Dis.* (2014) 17:291–8. doi: 10.1111/1756-185X.12188
 89. Xie X, Li F, Chen JW, Wang J. Risk of tuberculosis infection in anti-TNF-α biological therapy: from bench to bedside. *J Microbiol Immunol Infect.* (2014) 47:268–74. doi: 10.1016/j.jmii.2013.03.005
 90. Hanekom WA, Dockrell HM, Ottenhoff TH, Doherty TM, Fletcher H, McShane H, et al. Immunological outcomes of new tuberculosis vaccine trials: WHO panel recommendations. *PLoS Med.* (2008) 5:e145. doi: 10.1371/journal.pmed.0050145
 91. Hawkrige T, Scriba TJ, Gelderbloem S, Smit E, Tameris M, Moyo S, et al. Safety and immunogenicity of a new tuberculosis vaccine, MVA85A, in healthy adults in South Africa. *J Infect Dis.* (2008) 198:544–52. doi: 10.1086/590185
 92. Kaufmann SH. Fact and fiction in tuberculosis vaccine research: 10 years later. *Lancet Infect Dis.* (2011) 11:633–40. doi: 10.1016/S1473-3099(11)70146-3
 93. Tameris MD, Hatherill M, Landry BS, Scriba TJ, Snowden MA, Lockhart S, et al. Safety and efficacy of MVA85A, a new tuberculosis vaccine, in infants previously vaccinated with BCG: a randomised, placebo-controlled phase 2b trial. *Lancet.* (2013) 381:1021–8. doi: 10.1016/S0140-6736(13)60177-4
 94. Du G, Chen CY, Shen Y, Qiu L, Huang D, Wang R, et al. TCR repertoire, clonal dominance, and pulmonary trafficking of mycobacterium-specific CD4+ T effector cells in immunity against tuberculosis. *J Immunol.* (2010) 185:3940–7. doi: 10.4049/jimmunol.1001222
 95. Leal IS, Smedegard B, Andersen P, Appelberg R. Failure to induce enhanced protection against tuberculosis by increasing T-cell-dependent interferon-γ generation. *Immunology.* (2001) 104:157–61. doi: 10.1046/j.1365-2567.2001.01305.x
 96. Sakai S, Kauffman KD, Sallin MA, Sharpe AH, Young HA, Ganusov VV, et al. CD4 T cell-derived IFN-γ plays a minimal role in control of pulmonary *Mycobacterium tuberculosis* infection and must be actively repressed by PD-1 to prevent lethal disease. *PLoS Pathog.* (2016) 12:e1005667. doi: 10.1371/journal.ppat.1005667
 97. Bekker LG, Maartens G, Steyn L, Kaplan G. Selective increase in plasma tumor necrosis factor-α and concomitant clinical deterioration after initiating therapy in patients with severe tuberculosis. *J Infect Dis.* (1998) 178:580–4. doi: 10.1086/517479
 98. Picchi H, Mateus C, Chouaid C, Besse B, Marabelle A, Michot JM, et al. Infectious complications associated with the use of immune checkpoint inhibitors in oncology: reactivation of tuberculosis after anti PD-1 treatment. *Clin Microbiol Infect.* (2018) 24:216–8. doi: 10.1016/j.cmi.2017.12.003
 99. Barber DL, Sakai S, Kudchadkar RR, Fling SP, Day TA, Vergara JA, et al. Tuberculosis following PD-1 blockade for cancer immunotherapy. *Sci Transl Med.* 11:eaat2702. doi: 10.1126/scitranslmed.aat2702
 100. Kagina BM, Abel B, Scriba TJ, Hughes EJ, Keyser A, Soares A, et al. Specific T cell frequency and cytokine expression profile do not correlate with protection against tuberculosis after bacillus Calmette-Guérin vaccination of newborns. *Am J Respir Crit Care Med.* (2010) 182:1073–9. doi: 10.1164/rccm.201003-0334OC
 101. Harari A, Rozot V, Bellutti Enders F, Perreau M, Stalder JM, Nicod LP, et al. Dominant TNF-α+ *Mycobacterium tuberculosis*-specific CD4+ T cell responses discriminate between latent infection and active disease. *Nat Med.* (2011) 17:372–6. doi: 10.1038/nm.2299
 102. Tebruegge M, Ritz N, Donath S, Dutta B, Forbes B, Clifford V, et al. Mycobacteria-specific mono- and polyfunctional CD4+ T cell profiles in children with latent and active tuberculosis: a prospective proof-of-concept study. *Front Immunol.* (2019) 10:431. doi: 10.3389/fimmu.2019.00431
 103. Fletcher HA, Snowden MA, Landry B, Rida W, Satti I, Harris SA, et al. T-cell activation is an immune correlate of risk in BCG vaccinated infants. *Nat Commun.* (2016) 7:11290. doi: 10.1038/ncomms11290
 104. Ladel CH, Szalay G, Riedel D, Kaufmann SH. Interleukin-12 secretion by *Mycobacterium tuberculosis*-infected macrophages. *Infect Immun.* (1997) 65:1936–8.
 105. Tebruegge M, Dutta B, Donath S, Ritz N, Forbes B, Camacho-Badilla K, et al. Mycobacteria-specific cytokine responses detect tuberculosis infection and distinguish latent from active tuberculosis. *Am J Respir Crit Care Med.* (2015) 192:485–99. doi: 10.1164/rccm.201501-0059OC

106. Clifford V, Tebruegge M, Zufferey C, Germano S, Forbes B, Cosentino L, et al. Cytokine biomarkers for the diagnosis of tuberculosis infection and disease in adults in a low prevalence setting. *Tuberculosis*. (2019) 114:91–102. doi: 10.1016/j.tube.2018.08.011
107. Kim DH, Cheon JH. Pathogenesis of inflammatory bowel disease and recent advances in biologic therapies. *Immune Netw.* (2017) 17:25–40. doi: 10.4110/in.2017.17.1.25
108. Michels Da Silva D, Langer H, Graf T. Inflammatory and molecular pathways in heart failure-ischemia, HFpEF and transthyretin cardiac amyloidosis. *Int J Mol Sci.* (2019) 20:E2322. doi: 10.3390/ijms20092322
109. Hussain R, Shiratsuchi H, Ellner JJ, Wallis RS. PPD-specific IgG1 antibody subclass upregulate tumour necrosis factor expression in PPD-stimulated monocytes: possible link with disease pathogenesis in tuberculosis. *Clin Exp Immunol.* (2000) 119:449–55. doi: 10.1046/j.1365-2249.2000.01139.x
110. Hussain R, Shiratsuchi H, Phillips M, Ellner J, Wallis RS. Opsonizing antibodies (IgG1) up-regulate monocyte proinflammatory cytokines tumour necrosis factor- α (TNF- α) and IL-6 but not anti-inflammatory cytokine IL-10 in mycobacterial antigen-stimulated monocytes-implications for pathogenesis. *Clin Exp Immunol.* (2001) 123:210–8. doi: 10.1046/j.1365-2249.2001.01439.x
111. Cantini F, Niccoli L, Goletti D. Tuberculosis risk in patients treated with non-anti-tumor necrosis factor- α (TNF- α) targeted biologics and recently licensed TNF- α inhibitors: data from clinical trials and national registries. *J Rheumatol Suppl.* (2014) 91:56–64. doi: 10.3899/jrheum.140103
112. Essone PN, Leboueny M, Maloupazoa Siawaya AC, Alame-Emane AK, Aboumegone Biyogo OC, Dapnet Tadatsin PH, et al. *M. tuberculosis* infection and antigen specific cytokine response in healthcare workers frequently exposed to tuberculosis. *Sci Rep.* (2019) 9:8201. doi: 10.1038/s41598-019-50847-0
113. Menon J, Hoepfner VH, Judd A, Power CA, Bretscher PA. A hypothesis for the existence of two types of tuberculosis, reflecting two distinct types of immune failure to control the pathogen, based upon prevalence of mycobacterium-specific IgG subclasses. *Scand J Immunol.* (2018) 87:e12665. doi: 10.1111/sji.12665
114. Lenzini L, Rottoli P, Rottoli L. The spectrum of human tuberculosis. *Clin Exp Immunol.* (1977) 27:230–7.
115. Achkar JM, Jenny-Avital E, Yu X, Burger S, Leibert E, Bilder PW, et al. Antibodies against immunodominant antigens of *Mycobacterium tuberculosis* in subjects with suspected tuberculosis in the United States compared by HIV status. *Clin Vaccine Immunol.* (2010) 17:384–92. doi: 10.1128/CVI.00503-09
116. Hussain R, Dawood G, Abrar N, Toossi Z, Minai A, Dojki M, et al. Selective increases in antibody isotypes and immunoglobulin G subclass responses to secreted antigens in tuberculosis patients and healthy household contacts of the patients. *Clin Diagn Lab Immunol.* (1995) 2:726–32.
117. Sousa AO, Henry S, Maroja FM, Lee FK, Brum L, Singh M, et al. IgG subclass distribution of antibody responses to protein and polysaccharide mycobacterial antigens in leprosy and tuberculosis patients. *Clin Exp Immunol.* (1998) 111:48–55. doi: 10.1046/j.1365-2249.1998.00452.x
118. Mattos AM, Chaves AS, Franken KL, Figueiredo BB, Ferreira AP, Ottenhoff TH, et al. Detection of IgG1 antibodies against *Mycobacterium tuberculosis* DosR and Rpf antigens in tuberculosis patients before and after chemotherapy. *Tuberculosis*. (2016) 96:65–70. doi: 10.1016/j.tube.2015.11.001
119. Michaelsen TE, Garred P, Aase A. Human IgG subclass pattern of inducing complement-mediated cytotoxicity depends on antigen concentration and to a lesser extent on epitope patchiness, antibody affinity and complement concentration. *Eur J Immunol.* (1991) 21:11–6. doi: 10.1002/eji.1830210103
120. Cai Y, Yang Q, Tang Y, Zhang M, Liu H, Zhang G, et al. Increased complement C1q level marks active disease in human tuberculosis. *PLoS ONE.* (2014) 9:92340. doi: 10.1371/journal.pone.0092340
121. Scriba TJ, Penn-Nicholson A, Shankar S, Hraha T, Thompson EG, Sterling D, et al. Sequential inflammatory processes define human progression from *M. tuberculosis* infection to tuberculosis disease. *PLoS Pathog.* (2017) 13:e1006687. doi: 10.1371/journal.ppat.1006687
122. Lubbers R, Sutherland JS, Goletti D, De Paus RA, Van Moersel CHM, Veltkamp M, et al. Complement component C1q as serum biomarker to detect active tuberculosis. *Front Immunol.* (2018) 9:2427. doi: 10.3389/fimmu.2018.02427
123. Forget A, Benoit JC, Turcotte R, Gusew-Chartrand N. Enhancement activity of anti-mycobacterial sera in experimental *Mycobacterium bovis* (BCG) infection in mice. *Infect Immun.* (1976) 13:1301–6.
124. Hamasur B, Haile M, Pawlowski A, Schroder U, Williams A, Hatch G, et al. *Mycobacterium tuberculosis* arabinomannan-protein conjugates protect against tuberculosis. *Vaccine.* (2003) 21:4081–93. doi: 10.1016/S0264-410X(03)00274-3
125. Glatman-Freedman A, Casadevall A, Dai Z, Jacobs WR Jr, Li A, Morris SL, et al. Antigenic evidence of prevalence and diversity of *Mycobacterium tuberculosis* arabinomannan. *J Clin Microbiol.* (2004) 42:3225–31. doi: 10.1128/JCM.42.7.3225-3231.2004
126. Roy E, Stavropoulos E, Brennan J, Coade S, Grigorieva E, Walker B, et al. Therapeutic efficacy of high-dose intravenous immunoglobulin in *Mycobacterium tuberculosis* infection in mice. *Infect Immun.* (2005) 73:6101–9. doi: 10.1128/IAI.73.9.6101-6109.2005
127. Olivares N, Marquina B, Mata-Espinoza D, Zatarain-Barron ZL, Pinzon CE, Estrada I, et al. The protective effect of immunoglobulin in murine tuberculosis is dependent on IgG glycosylation. *Pathog Dis.* (2013) 69:176–83. doi: 10.1111/2049-632X.12069
128. Raja A, Baughman RP, Daniel TM. The detection by immunoassay of antibody to mycobacterial antigens and mycobacterial antigens in bronchoalveolar lavage fluid from patients with tuberculosis and control subjects. *Chest.* (1988) 94:133–7. doi: 10.1378/chest.94.1.133
129. Demkow U, Bialas-Chromiec B, Filewska M, Sobiecka M, Kus J, Szturmowicz M, et al. Humoral immune response against mycobacterial antigens in bronchoalveolar fluid from tuberculosis patients. *J Physiol Pharmacol.* (2005) 56(Suppl 4):79–84. Available online at: <https://europepmc.org/abstract/med/16204779>
130. Khera AK, Afkhami S, Lai R, Jeyanathan M, Zganiacz A, Mandur T, et al. Role of B cells in mucosal vaccine-induced protective CD8+ T cell immunity against pulmonary tuberculosis. *J Immunol.* (2015) 195:2900–7. doi: 10.4049/jimmunol.1500981
131. Reljic R. In search of the elusive mouse macrophage Fc- α receptor. *Immunol Lett.* (2006) 107:80–1. doi: 10.1016/j.imlet.2006.04.014
132. Balu S, Reljic R, Lewis MJ, Pleass RJ, McIntosh R, Van Kooten C, et al. A novel human IgA monoclonal antibody protects against tuberculosis. *J Immunol.* (2011) 186:3113–9. doi: 10.4049/jimmunol.1003189
133. Rodriguez A, Tjarnlund A, Ivanji J, Singh M, Garcia I, Williams A, et al. Role of IgA in the defense against respiratory infections IgA deficient mice exhibited increased susceptibility to intranasal infection with *Mycobacterium bovis* BCG. *Vaccine.* (2005) 23:2565–72. doi: 10.1016/j.vaccine.2004.11.032
134. Lopez Y, Yero D, Falero-Diaz G, Olivares N, Sarmiento ME, Sifontes S, et al. Induction of a protective response with an IgA monoclonal antibody against *Mycobacterium tuberculosis* 16kDa protein in a model of progressive pulmonary infection. *Int J Med Microbiol.* (2009) 299:447–52. doi: 10.1016/j.ijmm.2008.10.007
135. Seeling M, Bruckner C, Nimmerjahn F. Differential antibody glycosylation in autoimmunity: sweet biomarker or modulator of disease activity? *Nat Rev Rheumatol.* (2017) 13:621–30. doi: 10.1038/nrrheum.2017.146
136. Dube R, Rook GA, Steele J, Brealey R, Dwek R, Rademacher T, et al. Agalactosyl IgG in inflammatory bowel disease: correlation with C-reactive protein. *Gut.* (1990) 31:431–4. doi: 10.1136/gut.31.4.431
137. Pagan JD, Kitaoka M, Anthony RM. Engineered sialylation of pathogenic antibodies *in vivo* attenuates autoimmune disease. *Cell.* (2018) 172:564–77.e513. doi: 10.1016/j.cell.2017.11.041
138. Esmail H, Riou C, Bruyn ED, Lai RP, Harley YXR, Meintjes G, et al. The immune response to *Mycobacterium tuberculosis* in HIV-1-coinfected persons. *Annu Rev Immunol.* (2018) 36:603–38. doi: 10.1146/annurev-immunol-042617-053420
139. Masuda K, Kubota T, Kaneko E, Iida S, Wakitani M, Kobayashi-Natsume Y, et al. Enhanced binding affinity for Fc γ 3b1a of fucose-negative antibody is sufficient to induce maximal antibody-dependent cellular cytotoxicity. *Mol Immunol.* (2007) 44:3122–31. doi: 10.1016/j.molimm.2007.02.005
140. Roy Chowdhury R, Vallania F, Yang Q, Lopez Angel CJ, Darboe F, Penn-Nicholson A, et al. A multi-cohort study of the immune factors

- associated with *M. tuberculosis* infection outcomes. *Nature*. (2018) 560:644–8. doi: 10.1038/s41586-018-0439-x
141. Arnold JN, Wormald MR, Suter DM, Radcliffe CM, Harvey DJ, Dwek RA, et al. Human serum IgM glycosylation: identification of glycoforms that can bind to mannan-binding lectin. *J Biol Chem*. (2005) 280:29080–7. doi: 10.1074/jbc.M504528200
 142. Moh ES, Lin CH, Thaysen-Andersen M, Packer NH. Site-specific N-glycosylation of recombinant pentameric and hexameric human IgM. *J Am Soc Mass Spectrom*. (2016) 27:1143–55. doi: 10.1007/s13361-016-1378-0
 143. Kumagai T, Palacios A, Casadevall A, Garcia MJ, Toro C, Tiemeyer M, et al. Serum IgM glycosylation associated with tuberculosis infection in mice. *mSphere*. (2019) 4:e00684-18. doi: 10.1128/mSphere.00684-18
 144. Maglione PJ, Xu J, Casadevall A, Chan J. Fc gamma receptors regulate immune activation and susceptibility during *Mycobacterium tuberculosis* infection. *J Immunol*. (2008) 180:3329–38. doi: 10.4049/jimmunol.180.5.3329
 145. Sutherland JS, Loxton AG, Haks MC, Kassa D, Ambrose L, Lee JS, et al. Differential gene expression of activating Fc gamma receptor classifies active tuberculosis regardless of human immunodeficiency virus status or ethnicity. *Clin Microbiol Infect*. (2014) 20:O230–8. doi: 10.1111/1469-0691.12383
 146. Cliff JM, Lee JS, Constantinou N, Cho JE, Clark TG, Ronacher K, et al. Distinct phases of blood gene expression pattern through tuberculosis treatment reflect modulation of the humoral immune response. *J Infect Dis*. (2013) 207:18–29. doi: 10.1093/infdis/jis499
 147. Fong J, Chin D, Akiyama HJ, Elberg SS. Studies on tubercle bacillus-monocyte relationship. III Conditions affecting the action of serum and cells; modification of bacilli in an immune system. *J Exp Med*. (1959) 109:523–43. doi: 10.1084/jem.109.6.523
 148. Armstrong JA, Hart PD. Phagosome-lysosome interactions in cultured macrophages infected with virulent tubercle bacilli. Reversal of the usual nonfusion pattern and observations on bacterial survival. *J Exp Med*. (1975) 142:1–16. doi: 10.1084/jem.142.1.1
 149. Chen T, Blanc C, Eder AZ, Prados-Rosales R, Souza AC, Kim RS, et al. Association of human antibodies to Arabinomannan with enhanced mycobacterial opsonophagocytosis and intracellular growth reduction. *J Infect Dis*. (2016) 214:300–10. doi: 10.1093/infdis/jiw141
 150. De Valliere S, Abate G, Blazevic A, Heuertz RM, Hoft DF. Enhancement of innate and cell-mediated immunity by antimycobacterial antibodies. *Infect Immun*. (2005) 73:6711–20. doi: 10.1128/IAI.73.10.6711-6720.2005
 151. Bruns H, Meinken C, Schauenberg P, Harter G, Kern P, Modlin RL, et al. Anti-TNF immunotherapy reduces CD8+ T cell-mediated antimicrobial activity against *Mycobacterium tuberculosis* in humans. *J Clin Invest*. (2009) 119:1167–77. doi: 10.1172/JCI38482
 152. Joller N, Weber SS, Muller AJ, Sporri R, Selchow P, Sander P, et al. Antibodies protect against intracellular bacteria by Fc receptor-mediated lysosomal targeting. *Proc Natl Acad Sci USA*. (2010) 107:20441–6. doi: 10.1073/pnas.1013827107
 153. Mishra BB, Rathinam VA, Martens GW, Martinot AJ, Kornfeld H, Fitzgerald KA, et al. Nitric oxide controls the immunopathology of tuberculosis by inhibiting NLRP3 inflammasome-dependent processing of IL-1beta. *Nat Immunol*. (2013) 14:52–60. doi: 10.1038/ni.2474
 154. Kimmey JM, Stallings CL. Bacterial pathogens versus autophagy: implications for therapeutic interventions. *Trends Mol Med*. (2016) 22:1060–76. doi: 10.1016/j.molmed.2016.10.008
 155. Teitelbaum R, Glatman-Freedman A, Chen B, Robbins JB, Unanue E, Casadevall A, et al. A mAb recognizing a surface antigen of *Mycobacterium tuberculosis* enhances host survival. *Proc Natl Acad Sci USA*. (1998) 95:15688–93. doi: 10.1073/pnas.95.26.15688
 156. Pethe K, Alonso S, Biet F, Delogu G, Brennan MJ, Locht C, et al. The heparin-binding haemagglutinin of *M. tuberculosis* is required for extrapulmonary dissemination. *Nature*. (2001) 412:190–4. doi: 10.1038/35084083
 157. Cohen MS, Shaw GM, McMichael AJ, Haynes BF. Acute HIV-1 infection. *N Engl J Med*. (2011) 364:1943–54. doi: 10.1056/NEJMra1011874
 158. Pawlowski A, Jansson M, Skold M, Rottenberg ME, Kallenius G. Tuberculosis and HIV co-infection. *PLoS Pathog*. (2012) 8:e1002464. doi: 10.1371/journal.ppat.1002464
 159. Musisi E, Matovu DK, Bukonya A, Kaswabuli S, Zawedde J, Andama A, et al. Effect of anti-retroviral therapy on oxidative stress in hospitalized HIV-infected adults with and without TB. *Afr Health Sci*. (2018) 18:512–22. doi: 10.4314/ahs.v18i3.7
 160. Kroeze S, Wit FW, Rossouw TM, Steel HC, Kityo CM, Siwale M, et al. Plasma biomarkers of HIV-related systemic inflammation and immune activation in sub-Saharan Africa before and during suppressive antiretroviral therapy. *J Infect Dis*. (2019) 220:1029–33. doi: 10.1093/infdis/jiz252
 161. Spadaro F, Cecchetti S, Fantuzzi L. Macrophages and phospholipases at the intersection between inflammation and the pathogenesis of HIV-1 infection. *Int J Mol Sci*. (2017) 18:E1390. doi: 10.3390/ijms18071390
 162. Neff CP, Krueger O, Xiong K, Arif S, Nusbacher N, Schneider JM, et al. Fecal microbiota composition drives immune activation in HIV-infected individuals. *EBioMedicine*. (2018) 30:192–202. doi: 10.1016/j.ebiom.2018.03.024
 163. Siedner MJ, Zanni M, Tracy RP, Kwon DS, Tsai AC, Kakuhire B, et al. Increased systemic inflammation and gut permeability among women with treated HIV infection in rural Uganda. *J Infect Dis*. (2018) 218:922–6. doi: 10.1093/infdis/jiy244
 164. McGinty T, Mirmonsef P, Mallon PW, Landay AL. Does systemic inflammation and immune activation contribute to fracture risk in HIV? *Curr Opin HIV AIDS*. (2016) 11:253–60. doi: 10.1097/COH.0000000000000275
 165. Dirajlal-Fargo S, Sattar A, Kulkarni M, Funderburg N, Mccomsey GA. Soluble TWEAK may predict carotid atherosclerosis in treated HIV infection. *HIV Clin Trials*. (2017) 18:156–63. doi: 10.1080/15284336.2017.1366001
 166. Matuzkova A, Pshenichnaya N, Suladze A, Tverdokhlebova T, Dosyagaeva L, Zhuravlev A. Markers of systemic inflammation in HIV-infected patients with different HIV RNA level. *Int J Infect Dis*. (2019) 79:85. doi: 10.1016/j.ijid.2018.11.214
 167. Musselwhite LW, Sheikh V, Norton TD, Rupert A, Porter BO, Penzak SR, et al. Markers of endothelial dysfunction, coagulation and tissue fibrosis independently predict venous thromboembolism in HIV. *AIDS*. (2011) 25:787–95. doi: 10.1097/QAD.0b013e3283453fcb
 168. Sandler NG, Wand H, Roque A, Law M, Nason MC, Nixon DE, et al. Plasma levels of soluble CD14 independently predict mortality in HIV infection. *J Infect Dis*. (2011) 203:780–90. doi: 10.1093/infdis/jiq118
 169. Flepisi BT, Bouic P, Sissolak G, Rosenkranz B. Biomarkers of HIV-associated cancer. *Biomark Cancer*. (2014) 6:11–20. doi: 10.4137/BIC.S15056
 170. Kim JH, Excler JL, Michael NL. Lessons from the RV144 Thai phase III HIV-1 vaccine trial and the search for correlates of protection. *Annu Rev Med*. (2015) 66:423–37. doi: 10.1146/annurev-med-052912-123749
 171. Haynes BF, Gilbert PB, Mcelrath MJ, Zolla-Pazner S, Tomaras GD, Alam SM, et al. Immune-correlates analysis of an HIV-1 vaccine efficacy trial. *N Engl J Med*. (2012) 366:1275–86. doi: 10.1056/NEJMoa1113425
 172. Chung AW, Ghebremichael M, Robinson H, Brown E, Choi I, Lane S, et al. Polyfunctional Fc-effector profiles mediated by IgG subclass selection distinguish RV144 and VAX003 vaccines. *Sci Transl Med*. (2014) 6:228ra238. doi: 10.1126/scitranslmed.3007736
 173. Yates NL, Liao HX, Fong Y, Decamp A, Vandergrift NA, Williams WT, et al. Vaccine-induced Env V1-V2 IgG3 correlates with lower HIV-1 infection risk and declines soon after vaccination. *Sci Transl Med*. (2014) 6:228ra239. doi: 10.1126/scitranslmed.3007730
 174. Chung AW, Kumar MP, Arnold KB, Yu WH, Schoen MK, Dunphy LJ, et al. Dissecting polyclonal vaccine-induced humoral immunity against HIV using systems serology. *Cell*. (2015) 163:988–98. doi: 10.1016/j.cell.2015.10.027
 175. Forthal D, Hope TJ, Alter G. New paradigms for functional HIV-specific nonneutralizing antibodies. *Curr Opin HIV AIDS*. (2013) 8:393–401. doi: 10.1097/COH.0b013e328363d486
 176. Gomez-Roman VR, Patterson LJ, Venzon D, Liewehr D, Aldrich K, Florese R, et al. Vaccine-elicited antibodies mediate antibody-dependent cellular cytotoxicity correlated with significantly reduced acute viremia in rhesus macaques challenged with SIVmac251. *J Immunol*. (2005) 174:2185–9. doi: 10.4049/jimmunol.174.4.2185
 177. Forthal DN, Landucci G, Chohan B, Richardson BA, McClelland RS, Jaoko W, et al. Antibody-dependent cell-mediated virus inhibition antibody activity does not correlate with risk of HIV-1 superinfection. *J Acquir Immune Defic Syndr*. (2013) 63:31–3. doi: 10.1097/QAI.0b013e3282874d41

178. Sadanand S, Das J, Chung AW, Schoen MK, Lane S, Suscovich TJ, et al. Temporal variation in HIV-specific IgG subclass antibodies during acute infection differentiates spontaneous controllers from chronic progressors. *AIDS*. (2018) 32:443–50. doi: 10.1097/QAD.0000000000001716
179. Cooper DA, Imrie AA, Penny R. Antibody response to human immunodeficiency virus after primary infection. *J Infect Dis*. (1987) 155:1113–8. doi: 10.1093/infdis/155.6.1113
180. Tomaras GD, Yates NL, Liu P, Qin L, Fouda GG, Chavez LL, et al. Initial B-cell responses to transmitted human immunodeficiency virus type 1: virion-binding immunoglobulin M (IgM) and IgG antibodies followed by plasma anti-gp41 antibodies with ineffective control of initial viremia. *J Virol*. (2008) 82:12449–63. doi: 10.1128/JVI.01708-08
181. Richman DD, Wrin T, Little SJ, Petropoulos CJ. Rapid evolution of the neutralizing antibody response to HIV type 1 infection. *Proc Natl Acad Sci USA*. (2003) 100:4144–9. doi: 10.1073/pnas.0630530100
182. Mikell I, Sather DN, Kalams SA, Altfeld M, Alter G, Stamatatos L. Characteristics of the earliest cross-neutralizing antibody response to HIV-1. *PLoS Pathog*. (2011) 7:e1001251. doi: 10.1371/journal.ppat.1001251
183. Tomaras GD, Ferrari G, Shen X, Alam SM, Liao HX, Pollara J, et al. Vaccine-induced plasma IgA specific for the C1 region of the HIV-1 envelope blocks binding and effector function of IgG. *Proc Natl Acad Sci USA*. (2013) 110:9019–24. doi: 10.1073/pnas.1301456110
184. Fling JA, Fischer JR Jr, Boswell RN, Reid MJ. The relationship of serum IgA concentration to human immunodeficiency virus (HIV) infection: a cross-sectional study of HIV-seropositive individuals detected by screening in the United States Air Force. *J Allergy Clin Immunol*. (1988) 82:965–70. doi: 10.1016/0091-6749(88)90132-7
185. Coates RA, Farewell VT, Raboud J, Read SE, Klein M, Macfadden DK, et al. Using serial observations to identify predictors of progression to AIDS in the Toronto Sexual Contact Study. *J Clin Epidemiol*. (1992) 45:245–53. doi: 10.1016/0895-4356(92)90084-Z
186. Lopez E, Shattock RJ, Kent SJ, Chung AW. The multifaceted nature of immunoglobulin A and its complex role in HIV. *AIDS Res Hum Retroviruses*. (2018) 34:727–38. doi: 10.1089/aid.2018.0099
187. Yates NL, Lucas JT, Nolen TL, Vandergrift NA, Soderberg KA, Seaton KE, et al. Multiple HIV-1-specific IgG3 responses decline during acute HIV-1: implications for detection of incident HIV infection. *AIDS*. (2011) 25:2089–97. doi: 10.1097/QAD.0b013e32834b348e
188. Dugast AS, Stamatatos L, Tonelli A, Suscovich TJ, Licht AF, Mikell I, et al. Independent evolution of Fc- and Fab-mediated HIV-1-specific antiviral antibody activity following acute infection. *Eur J Immunol*. (2014) 44:2925–37. doi: 10.1002/eji.201344305
189. Mclean MR, Madhavi V, Wines BD, Hogarth PM, Chung AW, Kent SJ. Dimeric fcgamma receptor enzyme-linked immunosorbent assay to study HIV-specific antibodies: a new look into breadth of fcgamma receptor antibodies induced by the RV144 vaccine trial. *J Immunol*. (2017) 199:816–26. doi: 10.4049/jimmunol.1602161
190. Tjiam MC, Sariputra L, Armitage JD, Taylor JP, Kelleher AD, Tan DB, et al. Control of early HIV-1 infection associates with plasmacytoid dendritic cell-reactive opsonophagocytic IgG antibodies to HIV-1 p24. *AIDS*. (2016) 30:2757–65. doi: 10.1097/QAD.0000000000001242
191. Chung AW, Mabuka JM, Ndlovu B, Licht A, Robinson H, Ramlakhan Y, et al. Viral control in chronic HIV-1 subtype C infection is associated with enrichment of p24 IgG1 with Fc effector activity. *AIDS*. (2018) 32:1207–17. doi: 10.1097/QAD.0000000000001812
192. Dugast AS, Arnold K, Lofano G, Moore S, Hoffner M, Simek M, et al. Virus-driven inflammation is associated with the development of bNAbs in spontaneous controllers of HIV. *Clin Infect Dis*. (2017) 64:1098–104. doi: 10.1093/cid/cix057
193. Ackerman ME, Crispin M, Yu X, Baruah K, Boesch AW, Harvey DJ, et al. Natural variation in Fc glycosylation of HIV-specific antibodies impacts antiviral activity. *J Clin Invest*. (2013) 123:2183–92. doi: 10.1172/JCI65708
194. Moore JS, Wu X, Kulhavy R, Tomana M, Novak J, Moldoveanu Z, et al. Increased levels of galactose-deficient IgG in sera of HIV-1-infected individuals. *AIDS*. (2005) 19:381–9. doi: 10.1097/01.aids.0000161767.21405.68
195. Vadrevu SK, Trbojevic-Akmagic I, Kossenkova AV, Colomb F, Giron LB, Anzurez A, et al. Frontline science: plasma and immunoglobulin G galactosylation associate with HIV persistence during antiretroviral therapy. *J Leukoc Biol*. (2018) 104:461–71. doi: 10.1002/JLB.3HI1217-500R
196. Baum LL, Cassutt KJ, Knigge K, Khattri R, Margolick J, Rinaldo C, et al. HIV-1 gp120-specific antibody-dependent cell-mediated cytotoxicity correlates with rate of disease progression. *J Immunol*. (1996) 157:2168–73.
197. Forthal DN, Landucci G, Haubrich R, Keenan B, Kuppermann BD, Tilles JG, et al. Antibody-dependent cellular cytotoxicity independently predicts survival in severely immunocompromised human immunodeficiency virus-infected patients. *J Infect Dis*. (1999) 180:1338–41. doi: 10.1086/314988
198. Chung AW, Rollman E, Center RJ, Kent SJ, Stratov I. Rapid degranulation of NK cells following activation by HIV-specific antibodies. *J Immunol*. (2009) 182:1202–10. doi: 10.4049/jimmunol.182.2.1202
199. Chung AW, Navis M, Isitman G, Wren L, Silvers J, Amin J, et al. Activation of NK cells by ADCC antibodies and HIV disease progression. *J Acquir Immune Defic Syndr*. (2011) 58:127–31. doi: 10.1097/QAI.0b013e31822c62b9
200. Lee WS, Kent SJ. Anti-HIV-1 antibody-dependent cellular cytotoxicity: is there more to antibodies than neutralization? *Curr Opin HIV AIDS*. (2018) 13:160–6. doi: 10.1097/COH.0000000000000439
201. Chung AW, Isitman G, Navis M, Kramski M, Center RJ, Kent SJ, et al. Immune escape from HIV-specific antibody-dependent cellular cytotoxicity (ADCC) pressure. *Proc Natl Acad Sci USA*. (2011) 108:7505–10. doi: 10.1073/pnas.1016048108
202. Johansson SE, Rollman E, Chung AW, Center RJ, Hejdeman B, Stratov I, et al. NK cell function and antibodies mediating ADCC in HIV-1-infected viremic and controller patients. *Viral Immunol*. (2011) 24:359–68. doi: 10.1089/vim.2011.0025
203. Wren LH, Chung AW, Isitman G, Kelleher AD, Parsons MS, Amin J, et al. Specific antibody-dependent cellular cytotoxicity responses associated with slow progression of HIV infection. *Immunology*. (2013) 138:116–23. doi: 10.1111/imm.12016
204. Sips M, Krykbaeva M, Diefenbach TJ, Ghebremichael M, Bowman BA, Dugast AS, et al. Fc receptor-mediated phagocytosis in tissues as a potent mechanism for preventive and therapeutic HIV vaccine strategies. *Mucosal Immunol*. (2016) 9:1584–95. doi: 10.1038/mi.2016.12
205. Worley MJ, Fei K, Lopez-Denman AJ, Kelleher AD, Kent SJ, Chung AW. Neutrophils mediate HIV-specific antibody-dependent phagocytosis and ADCC. *J Immunol Methods*. (2018) 457:41–52. doi: 10.1016/j.jim.2018.03.007
206. Ackerman ME, Mikhailova A, Brown EP, Dowell KG, Walker BD, Bailey-Kellogg C, et al. Polyfunctional HIV-specific antibody responses are associated with spontaneous HIV control. *PLoS Pathog*. (2016) 12:e1005315. doi: 10.1371/journal.ppat.1005315
207. Richardson SI, Chung AW, Natarajan H, Mabvakure B, Mkhize NN, Garrett N, et al. HIV-specific Fc effector function early in infection predicts the development of broadly neutralizing antibodies. *PLoS Pathog*. (2018) 14:e1006987. doi: 10.1371/journal.ppat.1006987
208. Osuji FN, Onyenekwe CC, Ahaneku JE, Ukibe NR. The effects of highly active antiretroviral therapy on the serum levels of pro-inflammatory and anti-inflammatory cytokines in HIV infected subjects. *J Biomed Sci*. (2018) 25:88. doi: 10.1186/s12929-018-0490-9
209. Kisuya J, Chemtai A, Raballah E, Okumu W, Keter A, Ouma C. The role of *Mycobacterium tuberculosis* antigen specific cytokines in determination of acid fast bacilli culture status in pulmonary tuberculosis patients co-infected with human immunodeficiency virus. *Pan Afr Med J*. (2018) 31:166. doi: 10.11604/pamj.2018.31.166.17294
210. Sonnenberg P, Glynn JR, Fielding K, Murray J, Godfrey-Faussett P, Shearer S. How soon after infection with HIV does the risk of tuberculosis start to increase? A retrospective cohort study in South African gold miners. *J Infect Dis*. (2005) 191:150–8. doi: 10.1086/426827
211. Gupta RK, Lawn SD, Bekker LG, Caldwell J, Kaplan R, Wood R. Impact of human immunodeficiency virus and CD4 count on tuberculosis diagnosis: analysis of city-wide data from Cape Town, South Africa. *Int J Tuberc Lung Dis*. (2013) 17:1014–22. doi: 10.5588/ijtld.13.0032
212. Kaplan R, Hermans S, Caldwell J, Jennings K, Bekker LG, Wood R. HIV and TB co-infection in the ART era: CD4 count distributions and TB case fatality in Cape Town. *BMC Infect Dis*. (2018) 18:356. doi: 10.1186/s12879-018-3256-9

213. Bucsan AN, Chatterjee A, Singh DK, Foreman TW, Lee TH, Threeton B, et al. Mechanisms of reactivation of latent tuberculosis infection due to SIV coinfection. *J Clin Invest.* (2019) 129:125810. doi: 10.1172/JCI125810
214. Diedrich CR, Mattila JT, Klein E, Janssen C, Phuah J, Sturgeon TJ, et al. Reactivation of latent tuberculosis in cynomolgus macaques infected with SIV is associated with early peripheral T cell depletion and not virus load. *PLoS ONE.* (2010) 5:e9611. doi: 10.1371/journal.pone.0009611
215. Crump JA, Tyrer MJ, Lloyd-Owen SJ, Han LY, Lipman MC, Johnson MA. Military tuberculosis with paradoxical expansion of intracranial tuberculomas complicating human immunodeficiency virus infection in a patient receiving highly active antiretroviral therapy. *Clin Infect Dis.* (1998) 26:1008–9. doi: 10.1086/517636
216. Pornprasert S, Leechanachai P, Klinbuayem V, Leenasirimakul P, Promping C, Inta P, et al. Unmasking tuberculosis-associated immune reconstitution inflammatory syndrome in HIV-1 infection after antiretroviral therapy. *Asian Pac J Allergy Immunol.* (2010) 28:206–9. Available online at: <https://www.apjai-journal.org/wp-content/uploads/2017/12/16UnmaskingtuberculosisassociatedVol28No2-3June-September2010P206-209.pdf>
217. Tan HY, Yong YK, Andrade BB, Shankar EM, Ponnampalavanar S, Omar SF, et al. Plasma interleukin-18 levels are a biomarker of innate immune responses that predict and characterize tuberculosis-associated immune reconstitution inflammatory syndrome. *AIDS.* (2015) 29:421–31. doi: 10.1097/QAD.0000000000000557
218. Meintjes G, Lawn SD, Scano F, Maartens G, French MA, Worodria W, et al. Tuberculosis-associated immune reconstitution inflammatory syndrome: case definitions for use in resource-limited settings. *Lancet Infect Dis.* (2008) 8:516–23. doi: 10.1016/S1473-3099(08)70184-1
219. Walker NF, Stek C, Wasserman S, Wilkinson RJ, Meintjes G. The tuberculosis-associated immune reconstitution inflammatory syndrome: recent advances in clinical and pathogenesis research. *Curr Opin HIV AIDS.* (2018) 13:512–21. doi: 10.1097/COH.0000000000000502
220. Murdoch DM, Venter WD, Van Rie A, Feldman C. Immune reconstitution inflammatory syndrome (IRIS): review of common infectious manifestations and treatment options. *AIDS Res Ther.* (2007) 4:9. doi: 10.1186/1742-6405-4-9
221. Sartain MJ, Slayden RA, Singh KK, Laal S, Belisle JT. Disease state differentiation and identification of tuberculosis biomarkers via native antigen array profiling. *Mol Cell Proteomics.* (2006) 5:2102–13. doi: 10.1074/mcp.M600089-MCP200
222. Yu X, Prados-Rosales R, Jenny-Avital ER, Sosa K, Casadevall A, Achkar JM. Comparative evaluation of profiles of antibodies to mycobacterial capsular polysaccharides in tuberculosis patients and controls stratified by HIV status. *Clin Vaccine Immunol.* (2012) 19:198–208. doi: 10.1128/CVI.05550-11
223. Samanich K, Belisle JT, Laal S. Homogeneity of antibody responses in tuberculosis patients. *Infect Immun.* (2001) 69:4600–9. doi: 10.1128/IAI.69.7.4600-4609.2001
224. Correia-Neves M, Froberg G, Korshun L, Viegas S, Vaz P, Ramanlal N, et al. Biomarkers for tuberculosis: the case for lipoarabinomannan. *ERJ Open Res.* (2019) 5:00115–2018. doi: 10.1183/23120541.00115-2018
225. Machado LR, Bowdrey J, Ngaimisi E, Habtewold A, Minzi O, Makonnen E, et al. Copy number variation of Fc gamma receptor genes in HIV-infected and HIV-tuberculosis co-infected individuals in sub-Saharan Africa. *PLoS ONE.* (2013) 8:e78165. doi: 10.1371/journal.pone.0078165
226. Hernandez-Munoz HE, Stanford JL. IgA and IgG antibodies to distinct serotypes of *Mycobacterium avium* in HIV seropositivity and AIDS. *J Med Microbiol.* (1996) 44:165–9. doi: 10.1099/00222615-44-3-165
227. Shoelson SE, Herrero L, Naaz A. Obesity, inflammation, and insulin resistance. *Gastroenterology.* (2007) 132:2169–80. doi: 10.1053/j.gastro.2007.03.059
228. Winer S, Chan Y, Paltser G, Truong D, Tsui H, Bahrami J, et al. Normalization of obesity-associated insulin resistance through immunotherapy. *Nat Med.* (2009) 15:921–9. doi: 10.1038/nm.2001
229. Goldfine AB, Fonseca V, Shoelson SE. Therapeutic approaches to target inflammation in type 2 diabetes. *Clin Chem.* (2011) 57:162–7. doi: 10.1373/clinchem.2010.148833
230. Jagannathan M, McDonnell M, Liang Y, Hasturk H, Hetzel J, Rubin D, et al. Toll-like receptors regulate B cell cytokine production in patients with diabetes. *Diabetologia.* (2010) 53:1461–71. doi: 10.1007/s00125-010-1730-z
231. Esser N, Legrand-Poels S, Piette J, Scheen AJ, Paquot N. Inflammation as a link between obesity, metabolic syndrome and type 2 diabetes. *Diabetes Res Clin Pract.* (2014) 105:141–50. doi: 10.1016/j.diabres.2014.04.006
232. Sefil F, Ulutas KT, Dokuyucu R, Sumbul AT, Yengil E, Yagiz AE, et al. Investigation of neutrophil lymphocyte ratio and blood glucose regulation in patients with type 2 diabetes mellitus. *J Int Med Res.* (2014) 42:581–8. doi: 10.1177/0300060513516944
233. Zhai X, Qian G, Wang Y, Chen X, Lu J, Zhang Y, et al. Elevated B cell activation is associated with type 2 diabetes development in obese subjects. *Cell Physiol Biochem.* (2016) 38:1257–66. doi: 10.1159/000443073
234. Couper KN, Blount DG, Riley EM. IL-10: the master regulator of immunity to infection. *J Immunol.* (2008) 180:5771–7. doi: 10.4049/jimmunol.180.9.5771
235. Heine G, Drozdenko G, Grun JR, Chang HD, Radbruch A, Worm M. Autocrine IL-10 promotes human B-cell differentiation into IgM- or IgG-secreting plasmablasts. *Eur J Immunol.* (2014) 44:1615–21. doi: 10.1002/eji.201343822
236. Touch S, Clement K, Andre S. T cell populations and functions are altered in human obesity and type 2 diabetes. *Curr Diab Rep.* (2017) 17:81. doi: 10.1007/s11892-017-0900-5
237. Xia C, Rao X, Zhong J. Role of T lymphocytes in type 2 diabetes and diabetes-associated inflammation. *J Diabetes Res.* (2017) 2017:6494795. doi: 10.1155/2017/6494795
238. McLaughlin T, Liu LF, Lamendola C, Shen L, Morton J, Rivas H, et al. T-cell profile in adipose tissue is associated with insulin resistance and systemic inflammation in humans. *Arterioscler Thromb Vasc Biol.* (2014) 34:2637–43. doi: 10.1161/ATVBAHA.114.304636
239. Ip B, Cifone NA, Belkina AC, Defuria J, Jagannathan-Bogdan M, Zhu M, et al. Th17 cytokines differentiate obesity from obesity-associated type 2 diabetes and promote TNFalpha production. *Obesity.* (2016) 24:102–12. doi: 10.1002/oby.21243
240. Arango Duque G, Descoteaux A. Macrophage cytokines: involvement in immunity and infectious diseases. *Front Immunol.* (2014) 5:491. doi: 10.3389/fimmu.2014.00491
241. Guirado E, Schlesinger LS, Kaplan G. Macrophages in tuberculosis: friend or foe. *Semin Immunopathol.* (2013) 35:563–83. doi: 10.1007/s00281-013-0388-2
242. Nicholas DA, Salto LM, Boston AM, Kim NS, Larios M, Beeson WL, et al. Identification of anti-long chain saturated fatty acid igg antibodies in serum of patients with type 2 diabetes. *Mediators Inflamm.* (2015) 2015:196297. doi: 10.1155/2015/196297
243. Winer DA, Winer S, Shen L, Wadia PP, Yantha J, Paltser G, et al. B cells promote insulin resistance through modulation of T cells and production of pathogenic IgG antibodies. *Nat Med.* (2011) 17:610–7. doi: 10.1038/nm.2353
244. Chang DC, Piaggi P, Hanson RL, Knowler WC, Bogardus C, Krakoff J. Autoantibodies against PFDN2 are associated with an increased risk of type 2 diabetes: a case-control study. *Diabetes Metab Res Rev.* (2017) 33:e2922. doi: 10.1002/dmrr.2922
245. Mallat Z. The B-side story in insulin resistance. *Nat Med.* (2011) 17:539–40. doi: 10.1038/nm0511-539
246. Kay RA, Wood KJ, Bernstein RM, Holt PJ, Pumphrey RS. An IgG subclass imbalance in connective tissue disease. *Ann Rheum Dis.* (1988) 47:536–41. doi: 10.1136/ard.47.7.536
247. Zhang H, Li P, Wu D, Xu D, Hou Y, Wang Q, et al. Serum IgG subclasses in autoimmune diseases. *Medicine.* (2015) 94:e387. doi: 10.1097/MD.0000000000000387
248. Bhattacharya PK, Jamil M, Roy A, Talukdar KK. SLE and tuberculosis: a case series and review of literature. *J Clin Diagn Res.* (2017) 11:OR01–3. doi: 10.7860/JCDR/2017/22749.9398
249. Fiorentino TV, Succurro E, Arturi F, Giancotti A, Peronace C, Quirino A, et al. Serum IgG2 levels are specifically associated with whole-body insulin-mediated glucose disposal in non-diabetic offspring of type 2 diabetic individuals: a cross-sectional study. *Sci Rep.* (2018) 8:13616. doi: 10.1038/s41598-018-32108-8
250. Tanigaki K, Sacharidou A, Peng J, Chambliss KL, Yuhanna IS, Ghosh D, et al. Hyposialylated IgG activates endothelial IgG receptor FcgammaRIIB to

- promote obesity-induced insulin resistance. *J Clin Invest.* (2018) 128:309–22. doi: 10.1172/JCI89333
251. Lemmers RFH, Vilaj M, Urda D, Agakov F, Simurina M, Klaric L, et al. IgG glycan patterns are associated with type 2 diabetes in independent European populations. *Biochim Biophys Acta Gen Subj.* (2017) 1861:2240–9. doi: 10.1016/j.bbagen.2017.06.020
 252. Ahmad S, Khan MS, Akhter F, Khan MS, Khan A, Ashraf JM, et al. Glycosylation of biological macromolecules: a critical approach to halt the menace of glycation. *Glycobiology.* (2014) 24:979–90. doi: 10.1093/glycob/cwu057
 253. Kalia K, Sharma S, Mistry K. Non-enzymatic glycosylation of immunoglobulins in diabetic nephropathy. *Clin Chim Acta.* (2004) 347:169–76. doi: 10.1016/j.cccn.2004.04.016
 254. Mistry K, Kalia K. Non enzymatic glycosylation of IgG and their urinary excretion in patients with diabetic nephropathy. *Indian J Clin Biochem.* (2009) 24:159–65. doi: 10.1007/s12291-009-0029-7
 255. Kumar NP, Sridhar R, Banurekha VV, Jawahar MS, Fay MP, Nutman TB, et al. Type 2 diabetes mellitus coincident with pulmonary tuberculosis is associated with heightened systemic type 1, type 17, and other proinflammatory cytokines. *Ann Am Thorac Soc.* (2013) 10:441–9. doi: 10.1513/AnnalsATS.201305-112OC
 256. Vrieling F, Ronacher K, Kleynhans L, Van Den Akker E, Walz G, Ottenhoff THM, et al. Patients with concurrent tuberculosis and diabetes have a pro-atherogenic plasma lipid profile. *EBioMedicine.* (2018) 32:192–200. doi: 10.1016/j.ebiom.2018.05.011
 257. Kumar Nathella P, Babu S. Influence of diabetes mellitus on immunity to human tuberculosis. *Immunology.* (2017) 152:13–24. doi: 10.1111/imm.12762
 258. Prada-Medina CA, Fukutani KF, Pavan Kumar N, Gil-Santana L, Babu S, Lichtenstein F, et al. Systems immunology of diabetes-tuberculosis comorbidity reveals signatures of disease complications. *Sci Rep.* (2017) 7:1999. doi: 10.1038/s41598-017-01767-4
 259. Rao S, Rahim M, Iqbal K, Haroon F, Hasan Z. Impact of diabetes on mechanisms of immunity against *Mycobacterium tuberculosis*. *J Pak Med Assoc.* (2019) 69:94–8. Available online at: https://jpma.org.pk/article-details/9007?article_id=9007
 260. Gomez DI, Twahirwa M, Schlesinger LS, Restrepo BI. Reduced *Mycobacterium tuberculosis* association with monocytes from diabetes patients that have poor glucose control. *Tuberculosis.* (2013) 93:192–7. doi: 10.1016/j.tube.2012.10.003
 261. Restrepo BI, Twahirwa M, Rahbar MH, Schlesinger LS. Phagocytosis via complement or Fc-gamma receptors is compromised in monocytes from type 2 diabetes patients with chronic hyperglycemia. *PLoS ONE.* (2014) 9:e92977. doi: 10.1371/journal.pone.0092977
 262. Syed-Ahmed M, Narayanan M. Immune dysfunction and risk of infection in chronic kidney disease. *Adv Chronic Kidney Dis.* (2019) 26:8–15. doi: 10.1053/j.ackd.2019.01.004
 263. Goldblum SE, Reed WP. Host defenses and immunologic alterations associated with chronic hemodialysis. *Ann Intern Med.* (1980) 93:597–613. doi: 10.7326/0003-4819-93-4-597
 264. Kato S, Chmielewski M, Honda H, Pecoits-Filho R, Matsuo S, Yuzawa Y, et al. Aspects of immune dysfunction in end-stage renal disease. *Clin J Am Soc Nephrol.* (2008) 3:1526–33. doi: 10.2215/CJN.00950208
 265. Bel'eed K, Wright M, Eadington D, Farr M, Sellars L. Vaccination against hepatitis B infection in patients with end stage renal disease. *Postgrad Med J.* (2002) 78:538–40. doi: 10.1136/pmj.78.923.538
 266. Gaultier GN, McCreedy W, Ulanova M. Natural immunity against *Haemophilus influenzae* type a and B-cell subpopulations in adult patients with severe chronic kidney disease. *Vaccine.* (2019) 37:3677–84. doi: 10.1016/j.vaccine.2019.05.036
 267. Grywalska E, Smarz-Widelska I, Mertowski S, Gosik K, Mielnik M, Podgajna M, et al. CTLA-4 expression inversely correlates with kidney function and serum immunoglobulin concentration in patients with primary glomerulonephritides. *Arch Immunol Ther Exp.* (2019) 67:335–49. doi: 10.1007/s00005-019-00548-3
 268. Tecklenborg J, Clayton D, Siebert S, Coley SM. The role of the immune system in kidney disease. *Clin Exp Immunol.* (2018) 192:142–50. doi: 10.1111/cei.13119
 269. Barrios C, Zierer J, Gudelj I, Stambuk J, Ugrina I, Rodriguez E, et al. Glycosylation profile of IgG in moderate kidney dysfunction. *J Am Soc Nephrol.* (2016) 27:933–41. doi: 10.1681/ASN.2015010109
 270. Lopez-Parra V, Mallavia B, Lopez-Franco O, Ortiz-Munoz G, Oguiza A, Recio C, et al. Fc-gamma receptor deficiency attenuates diabetic nephropathy. *J Am Soc Nephrol.* (2012) 23:1518–27. doi: 10.1681/ASN.2011080822
 271. Lardinois OM, Deterding LJ, Hess JJ, Poulton CJ, Henderson CD, Jennette JC, et al. Immunoglobulins G from patients with ANCA-associated vasculitis are atypically glycosylated in both the Fc and Fab regions and the relation to disease activity. *PLoS ONE.* (2019) 14:e0213215. doi: 10.1371/journal.pone.0213215
 272. Juno JA, Waruk JLM, Mesa C, Lopez C, Bueti J, Ball TB, et al. Maintenance of *Mycobacterium tuberculosis*-specific T cell responses in End Stage Renal Disease (ESRD) and implications for diagnostic efficacy. *Clin Immunol.* (2016) 168:55–63. doi: 10.1016/j.clim.2016.05.004
 273. Juno JA, Waruk JLM, Harris A, Mesa C, Lopez C, Bueti J, et al. gammadelta T-cell function is inhibited in end-stage renal disease and impacted by latent tuberculosis infection. *Kidney Int.* (2017) 92:1003–14. doi: 10.1016/j.kint.2017.03.036
 274. Juno JA, Waruk JLM, Wragg KM, Mesa C, Lopez C, Bueti J, et al. Mucosal-associated invariant T cells are depleted and exhibit altered chemokine receptor expression and elevated granulocyte macrophage-colony stimulating factor production during end-stage renal disease. *Front Immunol.* (2018) 9:1076. doi: 10.3389/fimmu.2018.01076
 275. Zhao N, Sun JY, Xu HP, Sun FY. Early diagnosis of tuberculosis-associated IgA nephropathy with ESAT-6. *Tohoku J Exp Med.* (2017) 241:271–9. doi: 10.1620/tjem.241.271
 276. Wang Y, Tao Y. Tuberculosis-associated IgA nephropathy. *J Int Med Res.* (2018) 46:2549–57. doi: 10.1177/0300060518774127
 277. Gao YT, Sun L, Feng JM. Roles of *mycobacterium tuberculosis* ESAT-6 in the development of renal injury. *Int J Clin Exp Med.* (2015) 8:21964–74.
 278. Zhou ZQ, Wang ZK, Zhang L, Ren YQ, Ma ZW, Zhao N, et al. Role of ESAT-6 in renal injury by regulating microRNA-155 expression via TLR4/MyD88 signaling pathway in mice with *Mycobacterium tuberculosis* infection. *Biosci Rep.* (2017) 37:BSR20170021. doi: 10.1042/BSR20170021
 279. Viana LA, Cristelli MP, Santos DW, Tavares MG, Dantas MTC, Felipe CR, et al. Influence of epidemiology, immunosuppressive regimens, clinical presentation, and treatment on kidney transplant outcomes of patients diagnosed with tuberculosis: a retrospective cohort analysis. *Am J Transplant.* (2019) 19:1421–31. doi: 10.1111/ajt.15220
 280. Gupta G, Womer KL. Profile of belatacept and its potential role in prevention of graft rejection following renal transplantation. *Drug Des Devel Ther.* (2010) 4:375–82. doi: 10.2147/DDDT.S10432
 281. Lee JJ, Chan A, Tang T. Tuberculosis reactivation in a patient receiving anti-programmed death-1 (PD-1) inhibitor for relapsed Hodgkin's lymphoma. *Acta Oncol.* (2016) 55:519–20. doi: 10.3109/0284186X.2015.1125017

Conflict of Interest: The authors declare that the research was conducted in the absence of any commercial or financial relationships that could be construed as a potential conflict of interest.

Copyright © 2019 McLean, Lu, Kent and Chung. This is an open-access article distributed under the terms of the Creative Commons Attribution License (CC BY). The use, distribution or reproduction in other forums is permitted, provided the original author(s) and the copyright owner(s) are credited and that the original publication in this journal is cited, in accordance with accepted academic practice. No use, distribution or reproduction is permitted which does not comply with these terms.



Minimal B Cell Extrinsic IgG Glycan Modifications of Pro- and Anti-Inflammatory IgG Preparations *in vivo*

Anja Schaffert¹, Maja Hanić², Mislav Novokmet², Olga Zaytseva², Jasminka Krištić², Anja Lux¹, Lars Nitschke¹, Matthias Peipp³, Marija Pezer², René Hennig^{4,5}, Erdmann Rapp^{4,5}, Gordan Lauc^{2,6*} and Falk Nimmerjahn^{1*}

¹ Department of Biology, Institute of Genetics, University of Erlangen-Nuremberg, Erlangen, Germany, ² Glycoscience Research Laboratory, Genos Ltd., Zagreb, Croatia, ³ Department of Medicine II, Christian-Albrechts University Kiel and University Medical Center Schleswig-Holstein, Kiel, Germany, ⁴ glyXera GmbH, Magdeburg, Germany, ⁵ Max Planck Institute for Dynamics of Complex Technical Systems, Magdeburg, Germany, ⁶ Faculty of Pharmacy and Biochemistry, University of Zagreb, Zagreb, Croatia

OPEN ACCESS

Edited by:

Jean Harb,
INSERM U1064 Centre de Recherche
en Transplantation et
Immunologie, France

Reviewed by:

Gillian Dekkers,
Sanquin Diagnostic
Services, Netherlands
Isaak Quast,
Monash University, Australia

*Correspondence:

Gordan Lauc
glauc@genos.hr
Falk Nimmerjahn
falk.nimmerjahn@fau.de

Specialty section:

This article was submitted to
B Cell Biology,
a section of the journal
Frontiers in Immunology

Received: 26 July 2019

Accepted: 10 December 2019

Published: 09 January 2020

Citation:

Schaffert A, Hanić M, Novokmet M,
Zaytseva O, Krištić J, Lux A,
Nitschke L, Peipp M, Pezer M,
Hennig R, Rapp E, Lauc G and
Nimmerjahn F (2020) Minimal B Cell
Extrinsic IgG Glycan Modifications of
Pro- and Anti-Inflammatory IgG
Preparations *in vivo*.
Front. Immunol. 10:3024.
doi: 10.3389/fimmu.2019.03024

Select residues in the biantennary sugar moiety attached to the fragment crystallizable of immunoglobulin G (IgG) antibodies can modulate IgG effector functions. Thus, afucosylated IgG glycovariants have enhanced cytotoxic activity, whereas IgG glycovariants rich in terminal sialic acid residues can trigger anti-inflammatory effects. More recent evidence suggests that terminal α 2,6 linked sialic acids can be attached to antibodies post IgG secretion. These findings raise concerns for the use of therapeutic antibodies as they may change their glycosylation status in the patient and hence affect their activity. To investigate to what extent B cell extrinsic sialylation processes modify therapeutic IgG preparations *in vivo*, we analyzed changes in human intravenous IgG (IVIg) sialylation upon injection in mice deficient in B cells or in mice lacking the sialyltransferase 1, which catalyzes the addition of α 2,6 linked sialic acid residues. By performing a time course of IgG glycan analysis with HILIC-UPLC-FLR (plus MS) and xCGE-LIF our study suggests that therapeutic IgG glycosylation is stable upon injection *in vivo*. Only a very small fraction of IgG molecules acquired sialic acid structures predominantly in the Fab- but not the Fc-portion upon injection *in vivo*, suggesting that therapeutic antibody glycosylation will remain stable upon injection *in vivo*.

Keywords: glycosylation, sialylation, IVIg, IgG, B cells, antibody

INTRODUCTION

Immunoglobulin G (IgG) antibodies are glycoproteins with pro- and anti-inflammatory effector functions. Thus, binding of IgG to Fc γ receptors (Fc γ Rs) can trigger effector functions such as the release of pro-inflammatory mediators, phagocytosis of opsonized pathogens, or antibody dependent cellular cytotoxicity (ADCC) (1, 2). Apart from host defense, IgG autoantibodies play a major role in tissue destruction and inflammation during autoimmune diseases including the primary Sjögren's syndrome, Systemic Lupus Erythematosus or Rheumatoid Arthritis (3). Moreover, pooled IgG preparations from thousands of donors, called IVIg (intravenous immunoglobulin G), are used as an anti-inflammatory treatment in the therapy of several autoimmune diseases, and during chronic inflammation (4).

The sugar moiety attached to each of two conserved asparagine 297 residues in the constant domain 2 (CH2) of the IgG fragment crystallizable (Fc) is essential for both, the pro- and anti-inflammatory activities of IgG (5) and keeps the IgG molecule in its typical horseshoe shape critical for FcγR binding (6–8). Apart from IgG Fc-glycosylation, about 10–15% of serum IgG contains an N-linked sugar moiety in the IgG fragment antigen binding (Fab) domain, which is generated *de novo* during the process of IgG hypermutation (9, 10). More recent evidence suggests that IgG Fab glycosylation helps to regulate IgG specificity (11). With respect to IVIg, especially terminal sialic acid residues were shown to be responsible for its anti-inflammatory activity. Thus, while desialylated IVIg lost its capacity to suppress a wide variety of autoimmune diseases in mice (12, 13), IVIg preparations enriched for terminal sialic acid residues showed an enhanced anti-inflammatory activity (5, 14). Of note, enriching cytotoxic antibodies for terminal sialic acid residues decreased their activity *in vivo* and *in vitro* in some but not all studies (15). Consistent with this reduced activity a reduction in affinity of highly sialylated IgGs for select activating FcγRs was noted (5). Due to the potent immune modulating functions of select IgG glycoforms, new therapeutic approaches try to alter IgG activity by modulating its glycosylation *ex vivo* (5, 16), or by changing the glycosylation status in the patient by enzymatic approaches (17–19).

Due to the potent immunomodulatory activity of the IgG sugar moiety, a precise monitoring of therapeutic IgG glycosylation has become standard before using new recombinant antibody preparations or consecutive batches of already approved antibodies in patients. This in-depth characterization relies on the fact that once an IgG antibody is injected into the patient, the sugar structures remain stable and are not subject to *in vivo* processing. However, recent studies suggest that terminal α2,6-linked sialic acids may be attached independently of the B cell secretory pathway (20, 21). According to these results, B cell independent IgG sialylation is achieved in the liver by secreted ST6Gal1 produced by cells lining the liver central veins. As a sugar donor, CMP-sialic acid at least partially derived from degranulating platelets may be used. More recently, it was suggested that in addition to antibodies the surface of cells may also become sialylated through this process (22). With respect to therapeutic antibody preparations, these findings raise the severe concern, that this process may alter the activity of therapeutic antibodies in the patient. Thus, cytotoxic antibodies may become less active due to decreased binding to activating FcγRs, while intravenous IgG preparation may become more active and may in the worst-case lead to an unwanted strong immune suppression. Moreover, the genetic heterogeneity of the human population and age dependent alterations of immune responses may further complicate to predict how stable therapeutic antibodies are in individual patients and with respect to glycosylation.

To address this issue and identify to what extent therapeutic IgG preparations are subject to B cell independent sialylation, we made use of two mouse strains lacking either B cells or ST6Gal1, which is the responsible enzyme for adding terminal sialic acid residues to the IgG sugar moiety (23–25). Both mouse strains

were injected with human IVIg preparations having either a normal or strongly reduced level of sialylated IgG glycoforms. IgG N-glycan analysis by HILIC-UPLC-FLR (plus MS-detection) and xCGE-LIF of mouse serum for several consecutive days after IVIg administration revealed that IVIg glycosylation is very stable upon injection *in vivo*. Only a very small fraction, predominantly of disialylated IgG N-glycans attached to the Fab- rather than the IgG Fc-portion appeared to increase over time. In summary, our results suggest that B cell extrinsic IgG sialylation may not modulate therapeutic IgG activity post injection *in vivo*.

MATERIALS AND METHODS

Mice

C57BL/6 mice were bought from Janvier, μMT^{-/-} mice were obtained from The Jackson Laboratory. Rag2/γc/FcεRγ/FcγR2b^{-/-} were generated by breeding Rag2/γc/FcεRγ/FcγR2b^{-/-} mice (26) with FcγR2b^{-/-} mice. ST6Gal1^{-/-} mice were kindly provided by Prof. Dr. rer. nat. Lars Nitschke (FAU Erlangen, Germany). Rag2/γc/FcεRγ/FcγR2b^{-/-}, μMT^{-/-}, and ST6Gal1^{-/-} mice were kept in the animal facilities of Friedrich-Alexander-University Erlangen-Nuremberg under specific pathogen-free conditions in individually ventilated cages, in accordance with the guidelines of the NIH and the legal requirements of Germany and the USA. All animal experiments conducted in the animal facility of the FAU were approved by government of Lower Franconia.

Reagents

Human IVIg was purchased from Biotest AG (Intratect, 100 mg/ml). α2-3,6,8 neuraminidase was purchased from New England BioLabs (P0720L, 50,000 U/ml) and used at a concentration of 0,04 U/μg IVIg. Rituximab (MabThera®, Roche) was kindly provided by Prof. Dr. rer. nat. Matthias Peipp (Christian-Albrechts-University Kiel, Germany). TA99-mIgG2c was purchased from BioXcell (USA).

Fluorescence-Activated Cell Sorting Analysis

Murine blood was obtained from the retroorbital plexus and erythrocytes were lysed. To reduce unspecific binding to Fc receptors, cells were incubated on ice for at least 10 min with Fc-block (clone 2.4G2, 10 μg/ml). Cells were washed and incubated on ice for at least 15 min with combinations of the following antibodies: APC-Fire750-conjugated CD45 (clone 30-F11), BV510-conjugated CD11b (clone M1/70), and PE-conjugated NKp46 (clone 29A1.4), PE-conjugated Ly6G (clone 1A8), PE-conjugated TCRβ (clone H57-597), and PE-Cy7-conjugated CD19 (clone 6D5) (all purchased from Biolegend). FITC-conjugated SNA was purchased from Vector Laboratories. Analysis was restricted to viable cells, which were identified by exclusion of cells positive for the nucleic acid binding dye 4'6-diamino-2-phenylindol (DAPI). Experiments were acquired on a FACS Canto II (BD) and analyzed using FACS Diva software (BD).

ELISA

Sera of 8–9 week old C57BL/6, μ MT and ST6Gal1^{-/-} mice were collected and stored at -20°C until further use. For quantification of total serum IgM and IgG the Mouse IgM ELISA Quantification Kit and the Mouse IgG ELISA Quantification Kit (Bethyl) were used according to the manufacturer's instructions: ELISA plates were coated with 100 ng/well goat anti-mouse IgM or IgG in Carbonate/Bicarbonate for 1 h at room temperature. After washing unspecific binding was blocked with PBS/1% BSA for 1 h at room temperature. Sera were diluted 1:2,500 (IgM) or 1:10,000 (IgG) in PBS/1% BSA and incubated for 1 h at room temperature and, after adequate washing, bound IgM and IgG antibodies were detected by 1:20,000 diluted (in PBS/1% BSA) anti-IgM-HRP or anti-IgG-HRP antibody in PBS/1% BSA (incubated for 1 h at room temperature). For detection, TMB Solution was added and the reaction was stopped with 6% orthophosphoric acid. OD was measured with VersaMax tunable microplate reader (Molecular Devices) at 450 and 650 nm. For detection of remaining human IVIg or neuraminidase treated IVIg in the sera of ST6Gal1^{-/-} mice the Human IgG ELISA Quantification Kit (Bethyl) was used according to the above-described protocol. ELISA plates were coated with 100 ng/well goat anti-human IgG. Sera were diluted 1:50,000.

In vivo Experiments

10 mg IVIg (Intratect, Biotest, Germany), 10 mg neuraminidase treated IVIg (NeuIVIg) or 1 mg of the murine antibody TA99-mIgG2c (BioXcell, USA), which is directed against the glycoprotein 75 (gp75), was injected into eight- to nine-week old μ MT or ST6Gal1^{-/-} mice. Two, four and six days after injection sera were collected and analyzed by HILIC-UPLC-FLR (hydrophilic interaction ultra performance liquid chromatography with fluorescence detection; IVIg and NeuIVIg treated serum samples) or xCGE-LIF (multiplexed capillary gel electrophoresis with laser-induced fluorescence detection; IVIg, NeuIVIg and TA99 treated serum samples) to analyze IgG specific glycan structures.

Rituximab-IgG-Induced B Cell Depletion in PBMC Humanized

Rag2/ γ c/Fc ϵ R γ /Fc γ R2b^{-/-}

PBMCs were isolated by density centrifugation from individual buffy coats. Isolated PBMCs were frozen and stored in liquid nitrogen until further use. Adult Rag2/ γ c/Fc ϵ R γ /Fc γ R2b^{-/-} mice were irradiated with 6 Gy and injected intraperitoneally with 1×10^7 human peripheral blood mononuclear cells (PBMCs) 6 h after irradiation as described previously (27). Eighteen hours after PBMC transfer, an equal amount of 0.5 μ g anti-CD20 rituximab IgG1 (MabThera[®]) in the serum of rituximab injected mice was given intraperitoneally and 24 h later B cell counts in the peritoneum were analyzed by flow cytometry.

Glycan Analysis

IgG Isolation

The IgG was isolated using protein G monolithic plates (BIA Separations, Ajdovščina, Slovenia) as described previously (28).

Briefly, 100–400 μ l of serum was diluted in ratio 1:7 with $1 \times$ PBS, pH 7.4 and filtered through 0.45 μ m GHP filter plate (Pall Corporation, Ann Arbor, MI, USA). After filtration, serum samples were applied to the protein G plate and instantly washed with $1 \times$ PBS, pH 7.4, to remove unbound proteins. IgGs were eluted with 1 ml of 0.1 M formic acid (Merck, Darmstadt, Germany) and neutralized with 1 M ammonium bicarbonate (Merck, Darmstadt, Germany).

Sample Preparation for HILIC-UPLC-FLR Analysis of Glycans

Methanol Desalting

Volumes of eluates corresponding to 100 μ g of IgG were dried in a vacuum concentrator. Samples were then desalted by methanol precipitation. For methanol desalting 1 mL of cold (-20°C) methanol (MeOH) was added to each sample and resuspended. The plate containing samples was then closed with adhesive seal and centrifuged at 2,200 g for 15 min. After centrifugation, 970 μ L of MeOH was discarded and 1 ml of cold MeOH was added again to each sample and resuspended. After that, the plate was again centrifuged at 2,200 g for 15 min. After a second centrifugation, the 970 μ L of MeOH again was discarded and the remaining sample was then dried by vacuum centrifugation.

Glycan Release

The dried, desalted samples were dissolved in 30 μ L 1.33% SDS (w/v) (Invitrogen, Carlsbad, CA, USA) and denatured by incubation at 65°C for 10 min. After incubation, samples were left to cool down to room temperature for 30 min. Subsequently, 10 μ L of 4% Igepal-CA630 (Sigma-Aldrich, St. Louis, MO, USA) was added to the samples and incubated on a shaker for 15 min. After shaking, 1.2 U of PNGase F (Promega, Madison, WI, USA) in 10 μ L $5 \times$ PBS were added and incubated overnight at 37°C for N-glycan release.

Glycan Labeling

The released N-glycans were labeled with 2-aminobenzamide (2-AB). The labeling mixture was freshly prepared by dissolving 2-AB (Sigma-Aldrich, St. Louis, MO, USA) in DMSO (Sigma-Aldrich, St. Louis, MO, USA) and glacial acetic acid (Merck, Darmstadt, Germany) mixture (70:30, v/v) and by adding 2-picoline borane (Sigma-Aldrich, St. Louis, MO, USA) to a final concentration of 19.2 mg/mL for 2-AB and 44.8 mg/mL for 2-picoline borane. A volume of 25 μ L of labeling mixture was added to each N-glycan sample in the 96-well plate and the plate was sealed using adhesive tape. Samples were mixed by a 10 min shaking step, followed by 2 h incubation at 65°C. After incubation, samples were left to cool down to room temperature for 30 min.

HILIC-SPE

The samples (in a volume of 75 μ L) were mixed with 700 μ L of cold 100% ACN (Sigma-Aldrich, St. Louis, MO, USA). Free label and reducing agent were removed from the samples using HILIC-SPE on a 0.2 μ m GHP filter plate (Pall Corporation, Ann Arbor, MI, USA). Solvent was removed by application of vacuum using a vacuum manifold (Millipore Corporation, Billerica, MA, USA).

All wells were prewashed using 200 μ L of 70% ethanol (Carlo Erba Reagents, Val de Reuil, France), followed by 200 μ L water and equilibrated with 200 μ L of cold 96% ACN. The samples were loaded onto GHP filter plate and incubated for 2 min before the vacuum application. The wells were subsequently washed 5 \times using 200 μ L of cold 96% ACN. The last washing step was followed by centrifugation at $165 \times g$ for 5 min. Glycans were eluted two times with 90 μ L of ultrapure water after 15 min of shaking at room temperature followed by centrifugation at $165 \times g$ for 5 min. The combined eluates were stored at -20°C until usage.

HILIC-UPLC-FLR Analysis of IgG Glycans

Fluorescently labeled N-glycans were separated by HILIC on a Waters Acquity UPLC instrument (Milford, MA, USA) consisting of a quaternary solvent manager, sample manager and a fluorescence (FLR) detector set with excitation and emission wavelengths of 250 and 428 nm, respectively. The instrument was under the control of Empower 3 software, build 3471 (Waters, Milford, MA, USA). The UPLC-FLR system was equipped with a hydrophilic interaction liquid chromatography (HILIC) column, a Waters BEH Glycan chromatography column (100 \times 2.1 mm i.d., 1.7 μ m BEH particles). The separation used a gradient of 75% solvent B (100% ACN; solvent A: 100 mM ammonium formate pH 4.4) to 62% solvent B over 27 min, with a flow of 0.4 ml/min. Solvent B was maintained at 62% for an additional 5 min. The column was then washed for 2 min with 100% of solvent A. Initial conditions were restored in 1 min and held for an additional 5 min to ensure column re-equilibration. Samples were maintained at 10°C before injection, and the separation temperature was 60°C . The system was calibrated using an external standard of hydrolyzed and 2-AB labeled glucose oligomers from which the retention times for the individual glycans were converted to glucose units (GU). The chromatographic glycan peaks resulting from the HILIC-UPLC-FLR analysis were integrated using an automatic processing method with a traditional integration algorithm after which each chromatogram was manually corrected to maintain the same intervals of integration for all samples. The amount of glycans in each peak was expressed as % of total integrated area. Peak annotation of human and murine IgG was performed according to Pućić et al. (28) and Kristic et al. (29).

HILIC-UPLC-FLR-MS/MS

2AB labeled N-glycans were separated and measured on an Acquity UPLC H-class instrument coupled to Compact Q-TOF mass spectrometer via Ion Booster ion source. Both instruments were operated under HyStar software version 3.2 (Bruker Daltonics). N-glycans were separated on a Waters BEH Glycan chromatography column, 100 \times 2.1 mm, 1.7 μ m BEH particles, using 100 mM ammonium formate, pH 4.4, as solvent A and acetonitrile as solvent B. Solvent A was prepared by diluting 2 M stock solution of ammonium formate, pH 4.4 with ultrapure water. For separation linear gradient of 25–38% of solvent A at the flow rate of 0.4 mL/min in a 32 min analytical run was used. Sample was maintained at 10°C before injection, while the separation temperature was 60°C . Fluorescent detector was

set with excitation and emission wavelengths of 250 and 428 nm, respectively. Data processing was performed using an automatic processing method with a traditional integration algorithm after which each chromatogram was manually corrected to maintain the same intervals of integration for all the samples. Relative abundance of each obtained peak was expressed as percentage of total integrated area. Mass spectrometer was operated in a positive ion mode with capillary voltage set to 2,250 V and nebulizing gas at pressure of 5.5 Bar. Drying gas (nitrogen) was applied to source at a flow rate of 4 L/min and temperature of 300°C , while vaporizer temperature was set to 300°C and flow rate of 5 L/min. Nitrogen was used as a source gas, while argon was used as collision gas. Ion energy was set to 4 eV, transfer time was 100 μ s. Spectra were recorded in m/z range of 50–3,000 at a 0.5 Hz frequency. N-glycan structures were assigned based on retention time, measured mass and fragmentation spectra using GlycoMod (30) (<http://web.expasy.org/glycomod/>) and GlycoWorkbench (31).

Sample Preparation for xCGE-LIF Analysis of Glycans

Preparation of Fc and Fab Fractions of Antibodies

IgG-Fc beads (6 μ L; CaptureSelect™ IgG-Fc (ms) Affinity Matrix, Thermo Scientific, USA) were dispensed into each well of Orochem filter plate (Orochem Technologies Inc., USA) in order to capture antibodies through their Fc region and washed three times with 200 μ L 1 \times PBS (pH 7.4) on a vacuum manifold. Eluates obtained after isolation on Protein G plate were added to each well of the Orochem filter plate in a volume ranging from 200 to 400 μ L (~ 90 μ g of antibody) and incubated for 1 h at room temperature. Samples were washed four times with 200 μ L 1 \times PBS (pH 7.4) to remove unbound antibodies. The recombinant streptococcal IdeS enzyme (FabRICATOR, Genovis, Lund, Sweden; 1 U per 1 μ g of protein) was combined with 35 μ L 1 \times PBS (pH 6.6) and added to each sample. Samples were incubated in a humid chamber at 37°C for 18 h. Fab fractions were collected by centrifugation for 2 min at $50 \times g$ in a PCR plate (Thermo Fischer Scientific, MA, USA). Remaining Fc fractions were washed three times with 200 μ L 1 \times PBS (pH 7.4) and additional three times with 200 μ L ultrapure water. For elution of Fc fragments, 100 μ L of 0.1 M formic acid (pH 2.5) was added to each well of Orochem filter plate and neutralized with 17 μ L 1 M ammonium bicarbonate. Fc fragments were collected in a clean PCR plate and neutralized with 17 μ L 1 M ammonium bicarbonate.

Methanol Desalting

Volumes of IgG eluates corresponding from 3 to 10 μ g of IgG were dried in a vacuum concentrator and desalted following previously described protocol for methanol precipitation.

N-Glycan Release

The dried, desalted samples were dissolved in 3 μ L of 1.66 \times PBS with 4 μ L 0.5% SDS (w/v) (Invitrogen, Carlsbad, CA, USA) and denatured by incubation at 65°C for 10 min. After incubation, 2 μ L of 4% Igepal-CA630 (Sigma-Aldrich, St. Louis, MO, USA) was added to the samples and incubated on a shaker

for 15 min. After shaking, 1.2 U of PNGase F (Promega, Madison, WI, USA) in 1 μ L 5 \times PBS was added and incubated for 3 h at 37°C for N-glycan release. Samples were dried in a vacuum concentrator afterward.

Glycan Labeling and HILIC-SPE

Dried samples were labeled with 8-aminopyrene-1,3,6-trisulfonic acid (APTS, Sigma-Aldrich, St. Louis, MO, USA) and cleaned by HILIC-SPE on BioGel P10 (Bio-Rad, Hercules, CA, USA) in 96-well format as described previously (32).

Multiplexed Capillary Gel Electrophoresis With Laser-Induced Fluorescence (xCGE-LIF)

First xCGE-LIF measurement was carried out without internal normalization standard to visually assess signal intensities in the samples. Reaction mixture consisted of 3 μ L of N-glycan post-cleanup eluate, 1 μ L GeneScan 500 LIZ Size Standard (Applied Biosystems, Foster City, CA, USA; 1:50 dilution in Hi-Di Formamide) and 6 μ L Hi-Di Formamide (Applied Biosystems, Foster City, CA, USA) pipetted into MicroAmp Optical 96-well Reaction Plate (Applied Biosystems, Foster City, CA, USA), sealed with a 96-well plate septa (Applied Biosystems, Foster City, CA, USA) and briefly centrifuged to avoid air bubbles at the bottom of the wells. Second measurement was also carried out in total volume of 10 μ L and contained 3 μ L of N-glycan post-cleanup eluate (depending on the signal intensity in the first xCGE-LIF run), 1 μ L GeneScan 500 LIZ Size Standard (1:50 dilution in Hi-Di Formamide), 1 μ L of NormMix (glyXera, Magdeburg, Germany) in Hi-Di Formamide. The xCGE-LIF measurement was performed in a 3130 Genetic Analyzer (Applied Biosystems, Foster City, CA, USA), equipped with a 50 cm 4-capillary array filled with POP-7 polymer (Applied Biosystems, Foster City, CA, USA). Electrokinetic sample injection was performed at 7.5–15 kV for 5 or 10 s depending on the signal intensity; samples were analyzed with a running voltage of 15 kV and run time of 3,400 s. Raw data files were converted to.xml file format using DataFileConverter (Applied Biosystems, Foster City, CA, USA) and analyzed using the glycan analysis tool glyXtoolTM (glyXera, Magdeburg, Germany). GlyXtoolTM software was used for structural identification by patented migration time normalization to an internal standard and N-glycan database driven peak annotation, for data comparison and for integration of normalized peak heights (33, 34).

Statistical Analysis

The statistical significance of the data was determined as indicated in the figure legends. In brief, the Kruskal-Wallis test, followed by Dunn's multiple comparison test, or repeated measures two-way ANOVA with Bonferroni post-test were used to determine statistical differences between more than two groups. To indicate different levels of significance, a p 0.05 was assigned one asterisk, a value smaller than 0.05 but larger than 0.001 was assigned two asterisks and a value smaller than 0.001 was assigned three asterisks.

RESULTS

Model System to Study B Cell Independent Sialylation of Therapeutic IgG

To determine to what extent therapeutic IgG preparations are subject to B cell independent sialylation, we made use of two mouse strains, namely ST6Gal1 deficient (ST6Gal1^{-/-}) and μ MT mice. While ST6Gal1^{-/-} mice lack the sialyltransferase 1, catalyzing the addition of α 2,6 linked sialic acid residues (23, 35), μ MT mice have a disruption of the gene encoding the μ -chain constant region resulting in an arrest of B cell development at the pre-B-cell stage (36). As shown in **Figure 1**, we started with a characterization of the two *in vivo* model systems with respect to B cell development and the presence of α 2,6-linked sialic acid residues. As expected, μ MT mice had no B cells in the blood, while the amount of B cells of ST6Gal1^{-/-} mice was comparable to C57BL/6 mice (**Figure 1A**). Consistent with the absence of B cells in μ MT mice, no IgM and IgG antibodies were detectable in the serum (**Figure 1B**). In contrast, ST6Gal1^{-/-} mice showed normal levels of B cells, strongly reduced levels of serum IgM and a trend toward higher levels of serum IgG as described before (**Figure 1B**) (35, 37). Staining with SNA (sambucus nigra agglutinin)—a plant lectin specifically detecting α 2,6 linked sialic acids—demonstrated that ST6Gal1^{-/-} mice were negative for SNA on B and T cells, whereas μ MT mice showed a T cell SNA staining pattern comparable to C57BL/6 mice (**Figure 1C**). Finally, the serum IgG glycosylation pattern of C57BL/6, μ MT and ST6Gal1^{-/-} mice was analyzed by HILIC-UPLC-FLR confirming the absence of α 2,6 linked sialic acid species on serum IgG of ST6Gal1^{-/-} mice (**Figure 1D**). In addition, we analyzed the sugar structures present in IVIg and neuraminidase digested IVIg preparations (NeuIVIg), which were used for studying B cell independent sialylation *in vivo* (**Figure 1D**). As expected, no sialic acid containing sugar moieties were detectable in neuraminidase digested IVIg, allowing a detection of extrinsic *de novo* sialylation *in vivo* with the greatest possible sensitivity.

Analysis of B Cell Extrinsic IVIg Sialylation *in vivo*

To address if therapeutic IgG preparations are subject to B cell extrinsic *de novo* sialylation *in vivo*, we injected 10 mg IVIg in B cell deficient μ MT mice and analyzed alterations in IVIg glycosylation in the serum of these animals by hydrophilic interaction ultra-performance liquid chromatography with fluorescence detection (HILIC-UPLC-FLR). In addition, the identity of each peak, where sialylation was expected (GP15–26), was confirmed by mass spectrometry (fragmentation spectra see **Figure S1**). As mouse IgG glycans terminate with N-glycolylneuraminic acid (Neu5Gc), while human IgGs carry terminal N-acetylneuraminic acids (Neu5Ac), the injection of human IgG into mice allows an unequivocal detection of B cell independent sialylation (29, 38–40). An overview of all detected murine and human glycan structures is shown in **Figure S2**. When we compared the HILIC-UPLC-FLR profiles of IVIg before and 6 days after injection in μ MT mice we found that the IVIg glycosylation profiles overlapped almost completely (**Figure 2A**). However, some small additional glycan

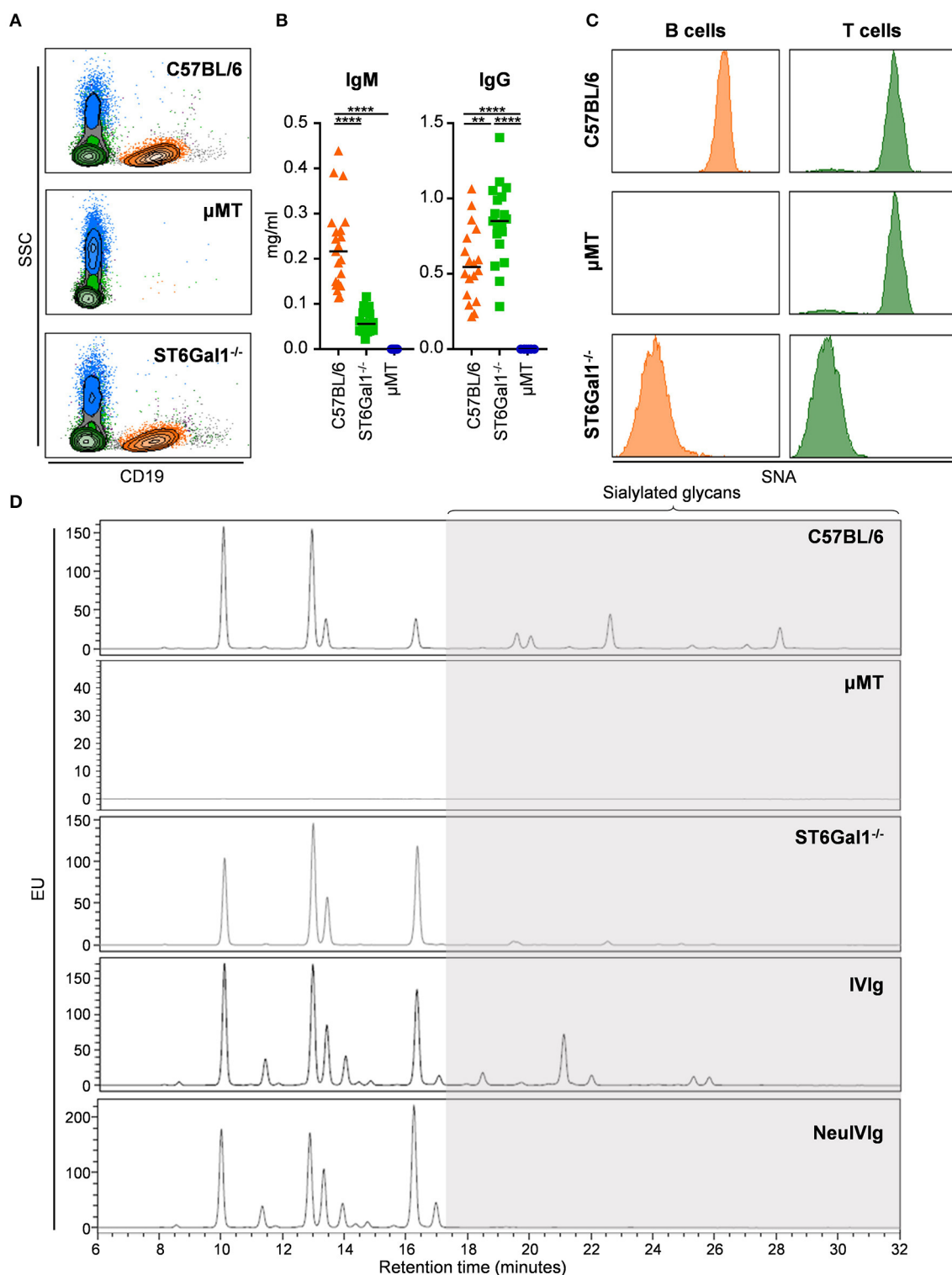


FIGURE 1 | Characterization of the experimental system to study extrinsic IgG sialylation. **(A–C)** C57BL/6, μ MT, and ST6Gal1^{-/-} mice were analyzed for the presence of B cells in the blood by FACS analysis **(A)**, serum IgM and IgG by ELISA **(B)** as well as for the presence of α 2,6-linked sialic acid residues on the surface of B and T cells by staining with sambucus nigra agglutinin (SNA). **(D)** Shown are representative glycoanalysis of serum IgG from the indicated mouse strains and of IVIg or neuraminidase treated IVIg (NeuVIg) by HILIC-UPLC-FLR. Statistical significance was evaluated with a one-way ANOVA test and a Bonferroni correction.

** $p = 0.01$, **** $p = 0.0001$. Horizontal lines in **(B)** represent mean values ($n = 10$ – 20). SSC, side scatter; EU, emission units.

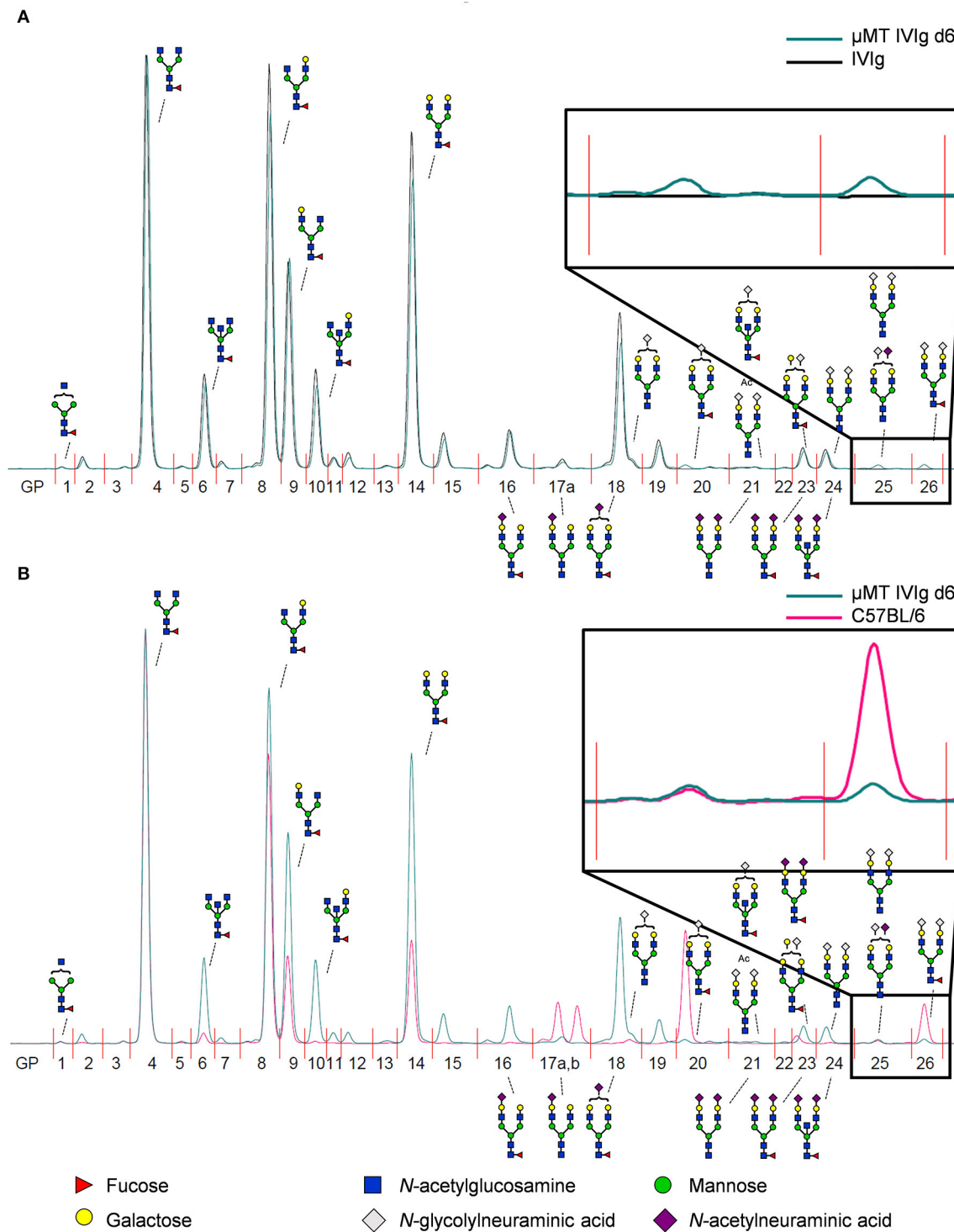


FIGURE 2 | Detection of *de novo* sialylated IgG glycoforms *in vivo*. **(A)** Shown is an overlay of a representative HILIC-UPLC-FLR analysis of IVIg before and 6 days after injection into μ MT mice (μ MT IVIg d6). **(B)** Depicted is an overlay of a HILIC-UPLC-FLR analysis of mouse serum IgG and IVIg 6 days post injection into μ MT mice. Enlarged insets highlight additional glycan peaks (GP) that were not present in the original IVIg preparation. Schematic drawings of the most prominent sugar structures (mouse structures on top, human structures on the bottom) are assigned to the respective peaks. Legend at the bottom of the figure explains the symbols used for individual sugar structures. See also **Figure S2** for additional peak information.

peaks (GP20, GP25, GP26) were detected that were not present in the original IVIg preparation (enlarged inset in **Figure 2A**). Interestingly all of those novel glycan peaks overlapped with sialic acid containing sugar structures (GP20 containing one sialic acid residue, GP25 and GP26 containing two sialic acid residues with (GP26) or without (GP25) fucose) selectively present in serum IgG from C57BL/6 mice (**Figure 2B**), suggesting that a very small level of extrinsic sialylation of IVIg can occur in mice.

We next analyzed the kinetics of B cell independent IgG sialylation by studying changes in IVIg sialylation 2, 4, and 6 days after injection into μ MT mice (**Figure 3** and **Figure S3**). As some studies suggest, that the level of IgG sialylation may affect antibody half-life and FcRn binding (41, 42), we first assessed if both, sialylated and non-sialylated IVIg preparations had a comparable half-life. As shown in **Figure S3A**, however, we noted no effect in the half-life of sialylated and asialylated IVIg (5), ensuring that both IVIg preparations had a comparable chance to become resialylated *in vivo*. Indeed, the presence of both disialylated sugar structures (GP25 and 26) slowly increased over time (**Figure 3A**). To increase the amount of acceptor sites for extrinsic IgG sialylation we also injected IVIg pretreated with neuraminidase (NeuIVIg). As shown in **Figure 3B**, however, this only mildly increased the level of extrinsic IgG sialylation on afucosylated sugar moieties, despite the availability of large amounts of IgG-G2 glycosylation variants. In total, only 1% of IgG glycovariants present in NeuIVIg acquired a disialylated sugar moiety 6 days after injection into μ MT mice. To further validate these results, we repeated this experiment in ST6Gal1^{-/-} mice, which are not able to add α 2,6-linked sialic acid residues and therefore served as a negative control. As shown in **Figures 3C,D** and **Figure S3**, the sialylation of IVIg or neuraminidase digested IVIg did not change over time in these animals, suggesting that the increase in GP25 and GP26 were indeed due to *de novo* IgG sialylation by ST6Gal1. In contrast, the small increase in monosialylated fucosylated IgG glycostructures (GP20) was also evident in ST6Gal1 deficient mice (**Figures S3B,C**). Moreover, afucosylated monosialylated glycan forms (GP18, A2G2Z1) of IVIg or NeuIVIg (**Figure 4B**) did not increase over time (**Figure S3**). Importantly however, the monosialylated glycoforms in GP18 comprise almost completely of human FA2G2S1 and it is therefore difficult to quantify murine monosialylated glycostructure by HILIC-UPLC-FLR. This prompted us to perform further studies.

Detection of B Cell Extrinsic IgG Sialylation by xCGE-LIF

To ensure that the inability to detect changes in *de novo* generated monosialylated IgG glycoforms was not due to technical reasons, we decided to use multiplexed capillary gel electrophoresis with laser-induced fluorescence detection (xCGE-LIF) to confirm our results. The advantage of xCGE-LIF is that very small amounts of IgG preparations can be analyzed with high sensitivity allowing better resolution for sialylated species. The characteristic glycan profiles of murine and human IgG preparations by xCGE-LIF as well as the structure and peak assignment are depicted in **Figure S4**. Based on the fact that neuraminidase digested IVIg allowed the most clear-cut identification of *de novo* IgG sialylation *in vivo*, we focused on NeuIVIg-injected μ MT and

ST6Gal1^{-/-} mice (**Figures 4, 5**). As shown for HILIC-UPLC-FLR analysis, additional glycan peaks became detectable on NeuIVIg 6 days after injection in B cell deficient μ MT mice, which overlapped with IgG sugar structures selectively present on mouse but not human IgG (**Figure 4B**). Fully consistent with HILIC-UPLC-FLR, the glycan peaks that appeared *de novo* and were increasing over time were mono- (P11 and P13) and disialylated sugar structures (P2 and P4) with (P4 and P13) or without (P2 and P11) core-fucose (**Figures 4, 5**). Injection of NeuIVIg into ST6Gal1^{-/-} mice did not lead to any detectable changes in IVIg sialylation *in vivo* (**Figures 5B,C**). Moreover, agalactosylated (G0), mono-galactosylated (G1), and digalactosylated (G2) IgG glycoforms were not changed over time (**Figure S5**). Thus, xCGE-LIF analysis allowed a better detection of mono- and disialylated IgG sugar structures.

To exclude that the observed minimal level of extrinsic IgG sialylation is due to the use of human IgG in mice, we performed a similar experiment where we injected 1 mg of the murine TA99-IgG2c antibody—directed against the glycoprotein 75—into B cell deficient μ MT mice and analyzed alterations in IgG glycosylation in the serum of these animals 10 min as well as 2, 4, and 6 days after injection by xCGE-LIF. As shown in **Figure S6** murine IgG acquired sialic acid residues to a similar extend as human IgG. Again, especially disialylated sugar structures (P2 and P4) were increasing over time. The sugar structure FA2G2Z1 (P13) might co-migrate with the large peak present in initial TA99-mIgG2c antibody (around 250 MTU²) and therefore could not be clearly distinguished. In summary, the data obtained with HILIC-UPLC-FLR and xCGE-LIF analysis suggest that a very small amount of IgG molecules—both human and murine—containing two galactose residues can become modified with one or two sialic acid residues *in vivo* in the absence of B cells.

To further characterize extrinsic IgG sialylation, we also discriminated *de novo* generated IgG glycoforms between Fab and Fc. For this purpose, the isolated serum IgG preparations from NeuIVIg injected μ MT mice (4 days after NeuIVIg injection) were separated into Fab and Fc portions before glycoanalysis by xCGE-LIF. Individual analysis of the separated IgG fragments revealed that extrinsic IgG sialylation occurred almost exclusively on N-glycosylation sites of the Fab (**Figure 6A**) but not of the Fc (**Figure 6B**) fragment. Again, minimal amounts of especially disialylated IgG sugar structures were appearing. In the two mouse serum samples $1.57 \pm 0.3\%$ of all IgG glycoforms on the Fab fragment corresponded to disialylated sugar structures, while only $0.89 \pm 0.15\%$ were monosialylated. In contrast, no additional murine sialic acids could be detected on the Fc fragment (**Figure 6B**). Therefore, predominantly the N-linked sugar moieties of the easily accessible Fab fragment in the IVIg preparations seems to be the target for *de novo* sialylation.

Impact of Extrinsic Sialylation on IgG Effector Function

To evaluate the impact of extrinsic sialylation on cytotoxic IgG effector functions, we injected μ MT and ST6Gal1^{-/-} mice with the CD20 specific antibody rituximab, which is broadly used in patients with autoimmune diseases and cancer. As rituximab selectively recognizes human but not mouse CD20, the injection into ST6Gal1 deficient mice with Rituximab does

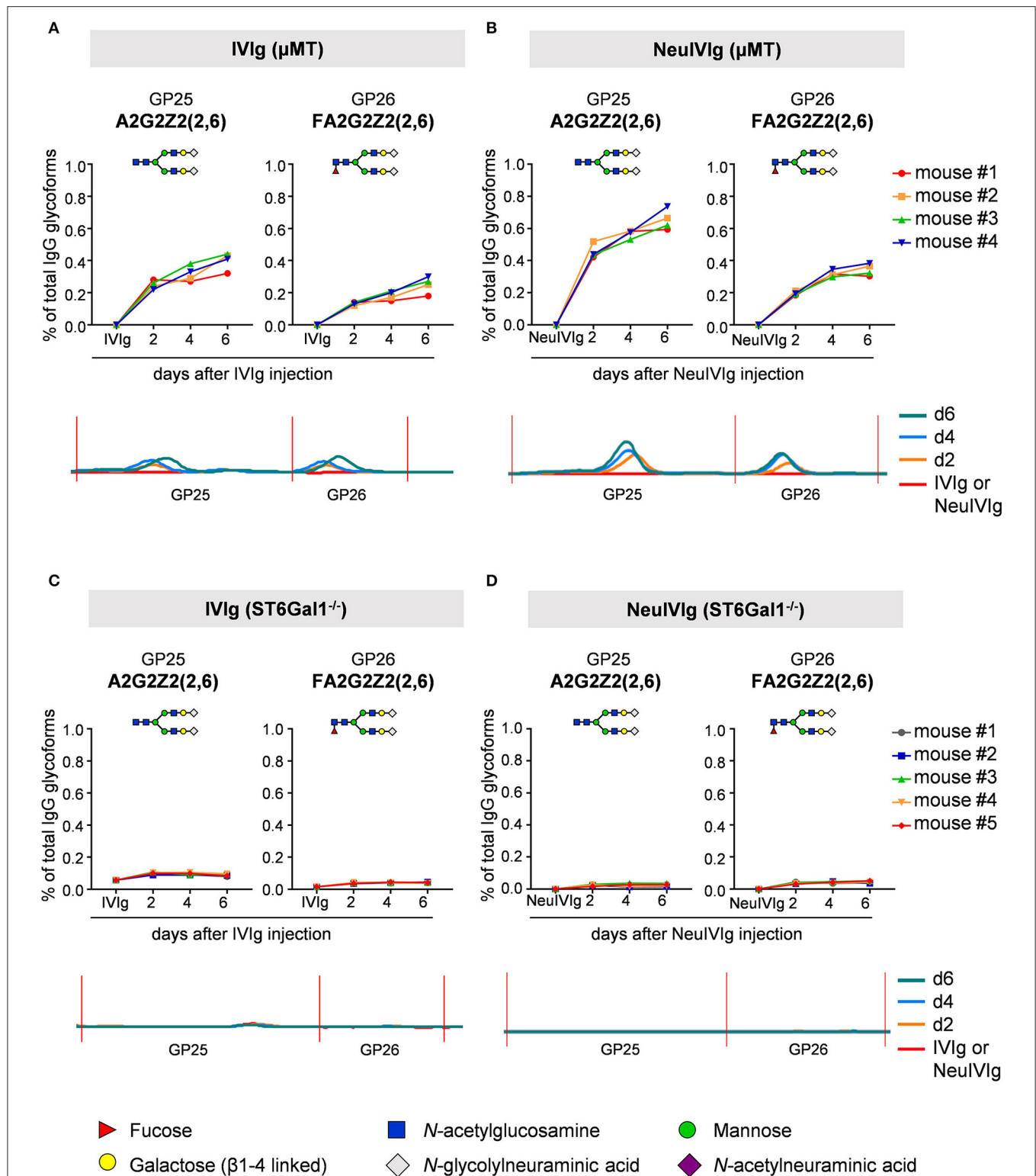


FIGURE 3 | Kinetics of extrinsic IgG sialylation in μ MT and ST6Gal1 deficient mice. Shown are the relative changes (% of total IgG glycoforms in the preparation) in glycopeaks (GP) 25 and 26 in IVIg (**A,C**) or neuraminidase treated IVIg (**B,D**) before (IVIg or NeuIVIg) and 2, 4, and 6 days after injection into μ MT (**A,B**) or ST6Gal1 deficient mice (**C,D**) by HILIC-UPLC-FLR analysis. Changes in the respective glycopeak in individual mice are shown at the top of each figure ($n = 4-5$). The bottom of each Figure shows a representative HILIC-UPLC-FLR trace of GP25 and 26. In each subfigure a schematic drawing of the sugar structure for GP25 and 26 is depicted. The Figure legend at the bottom explains the symbols used for the schematic representation of the sugar moieties.

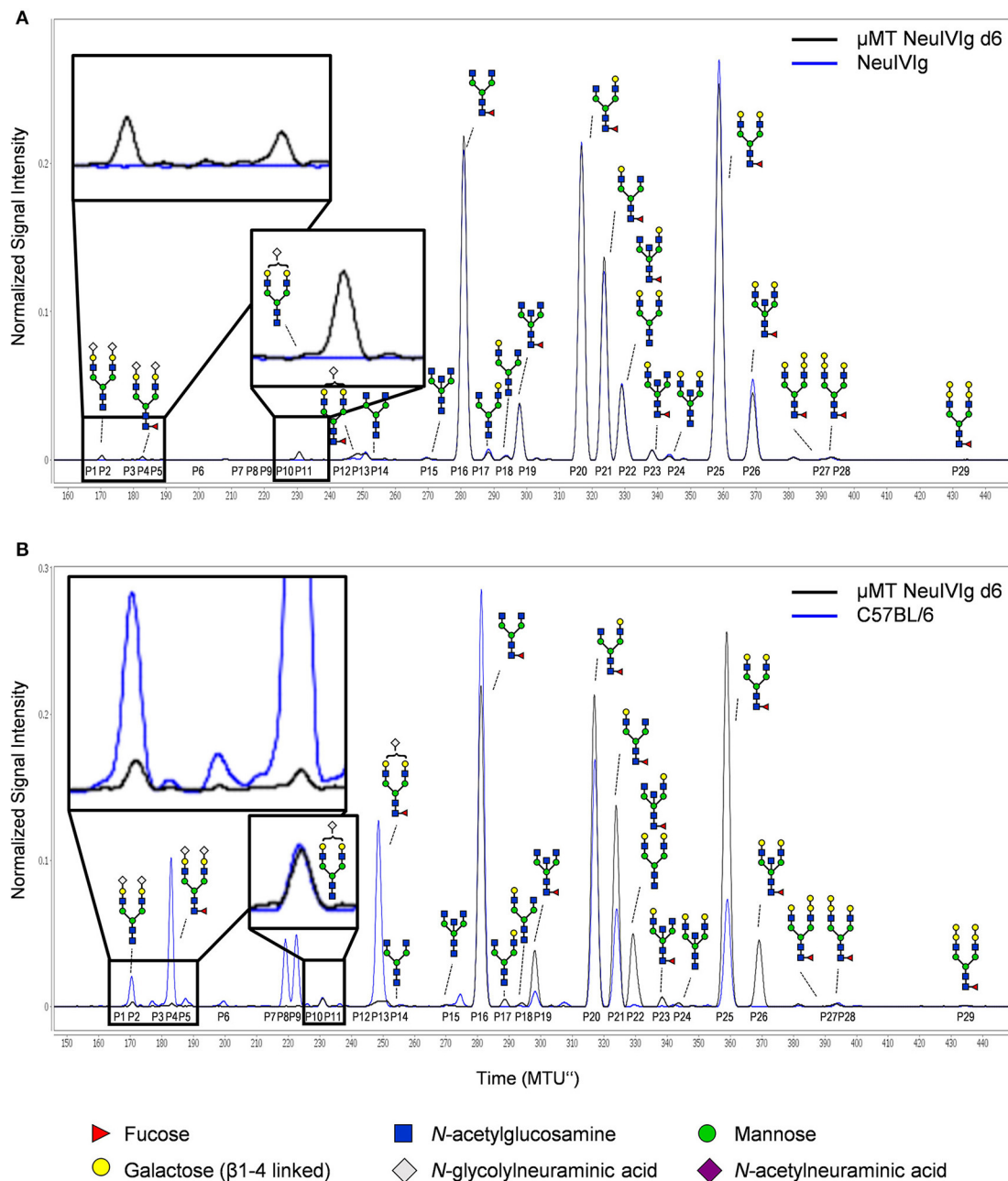


FIGURE 4 | Detection of *de novo* sialylation of human IgG *in vivo* by xCGE-LIF. **(A)** Depicted are representative overlays of xCGE-LIF IgG glycoanalysis of neuraminidase treated IVlg (NeuIVlg) before and 6 days after injection into μ MT mice (μ MT NeuIVlg d6). **(B)** Shown are representative overlays of xCGE-LIF glycoanalysis of serum IgG from C57BL/6 mice or from μ MT mice 6 days post injection with neuraminidase treated IVlg. Schematic drawings of the sugar moieties are depicted for the major peaks. Enlarged insets emphasize peaks detected selectively on NeuIVlg 6 days post injection into μ MT mice. The Figure legend at the bottom of the Figure depicts the symbols used for individual sugar residues. See also **Figure S2** for additional peak information. MTU'', normalized migration time units.

not affect B cell numbers. Four days after injection, serum from μ MT and ST6Gal1 knockout mice was collected, the level of human IgG determined and extrinsic IgG sialylation assessed by xCGE-LIF. As shown in **Figure 7A**, very low amounts of exclusively disialylated IgG structures were found in rituximab injected μ MT mice. To assess the functional activity of human CD20 antibodies present in the serum

of μ MT and ST6Gal1 deficient mice, a serum equivalent containing 0.5 μ g rituximab was injected into immunodeficient Rag2/ γ c/Fc ϵ R γ /Fc γ R2b $^{-/-}$ mice, which were irradiated and reconstituted with human peripheral blood mononuclear cells 18 h before (**Figure 7B**). As shown in **Figures 7C,D**, rituximab treatment via serum transfer of rituximab-injected μ MT and ST6Gal1 $^{-/-}$ mice led to a significant depletion of B cells in

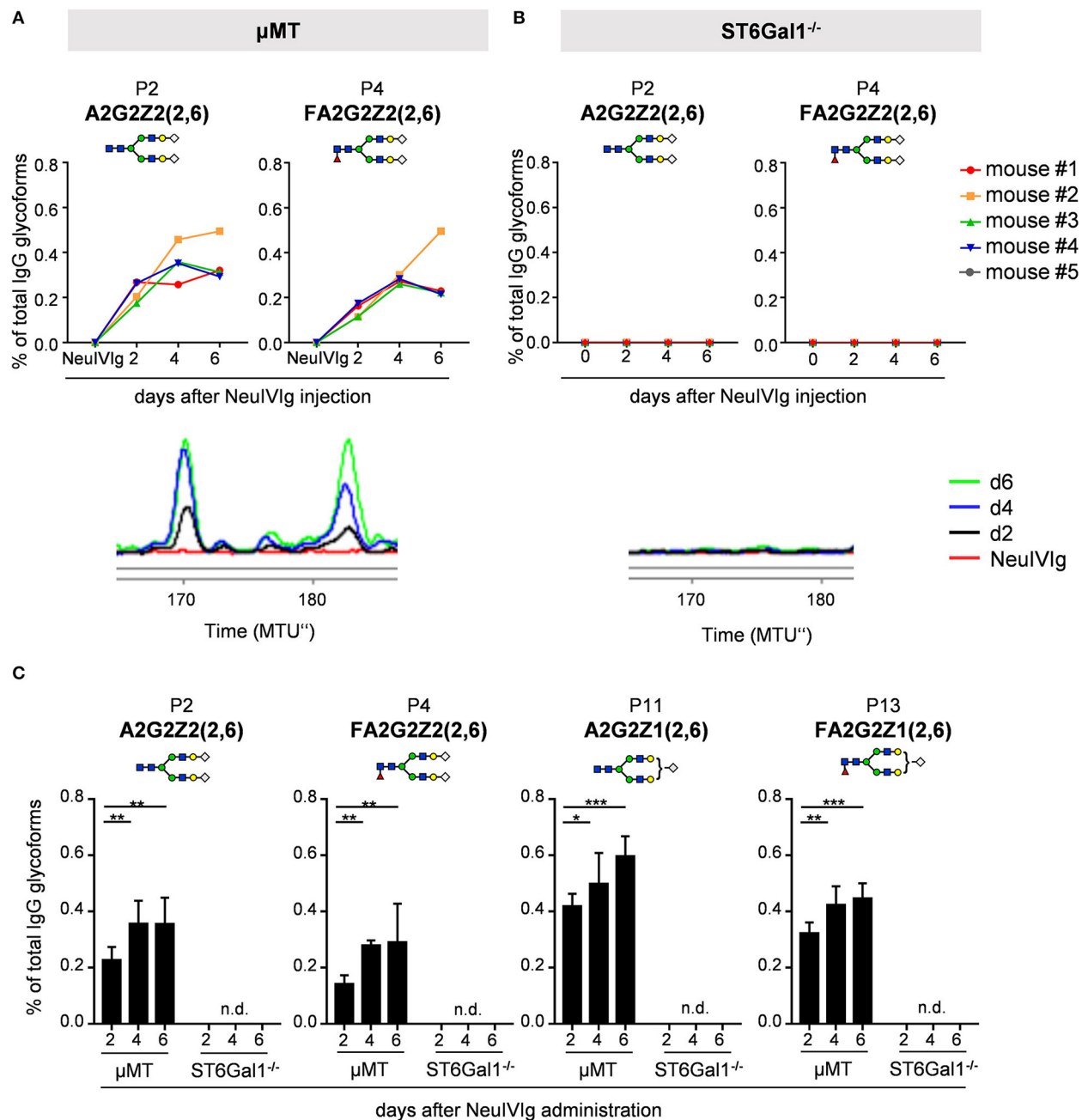
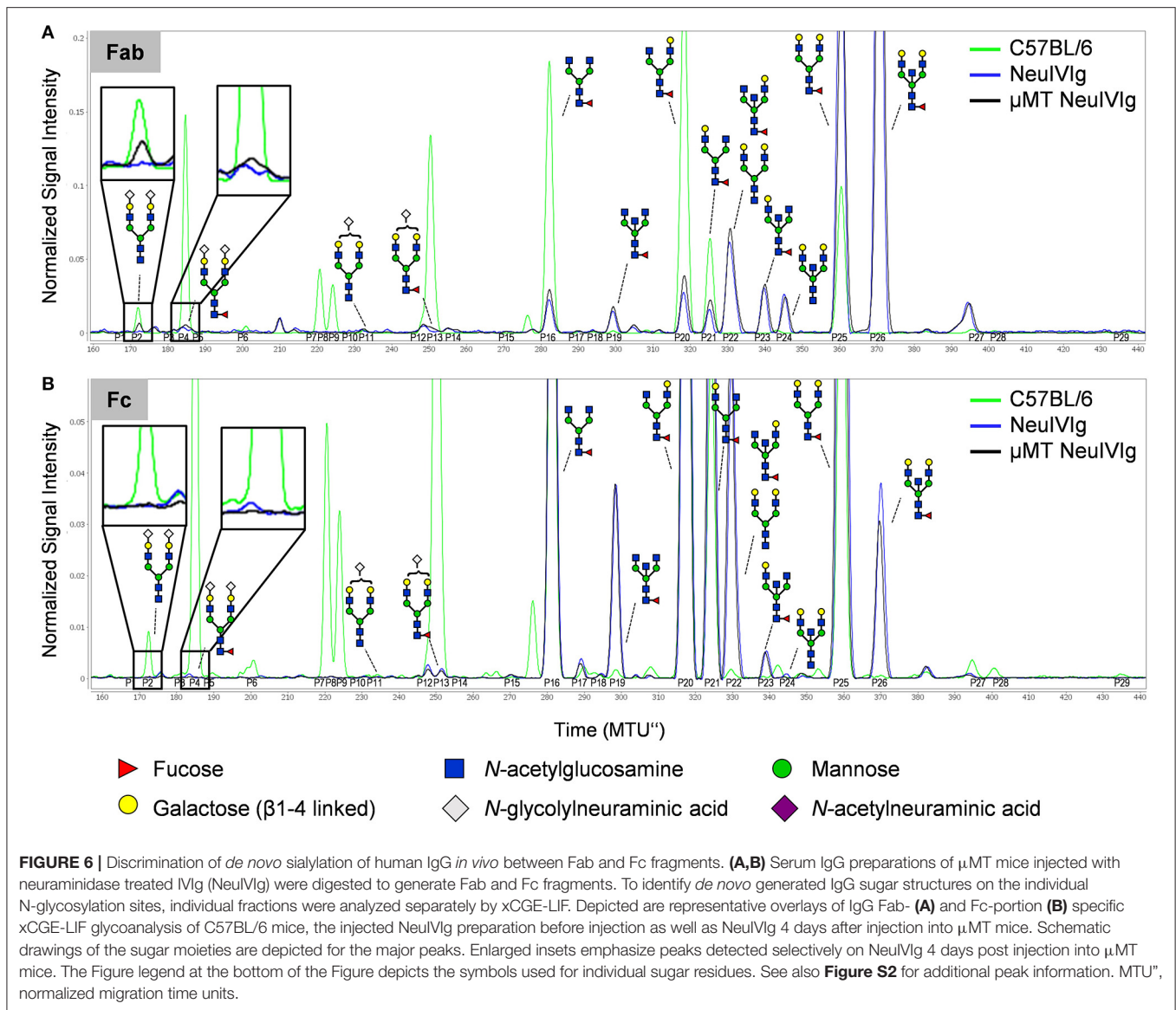


FIGURE 5 | Kinetics of appearance of *de novo* sialylated IgG glycoforms as detected with xCGE-LIF. **(A,B)** Shown are the relative changes (% of total IgG glycoforms in the preparation) in glycopeaks (P) 2 and 4 in neuraminidase treated IVlg (NeuIVlg) before and 2, 4, and 6 days after injection into μ MT **(A)** or ST6Gal1 deficient mice **(B)** by xCGE-LIF analysis for individual mice. In the bottom of each Figure a representative xCGE-LIF trace of glycopeaks P2 and 4 is depicted. **(C)** Quantification of all sialylated glycan peaks P2, P4, P11, and P13 2, 4, and 6 days after injection of NeuIVlg into μ MT or ST6Gal1^{-/-} mice, respectively. Bars represent mean \pm SD. * p = 0.05, ** p = 0.01, *** p = 0.001 by repeated measures two-way ANOVA. n = 4–5. In each Figure, a schematic drawing of the sugar structure for the respective glycopeak is depicted. MTU^o, normalized migration time units; n.d., not detectable.

the peritoneal cavity, while B cell counts in PBS-serum treated mice were not affected. In line with the low efficiency of the extrinsic sialylation pathway, when we compared B cell depletion between rituximab-containing ST6Gal1^{-/-} and μ MT serum, no significant differences in cytotoxic antibody activity were detected.

DISCUSSION

An important step in the process of introducing a new therapeutic IgG antibody or a new batch of an already approved antibody into the clinic is an in-depth characterization of the IgG glycovariants present in the antibody preparation. It is



well-known that many factors, such as the cell line in which a therapeutic antibody is produced (43) or the specific culture conditions (44), can alter IgG glycosylation. The importance of detecting alterations in IgG glycosylation have been emphasized by the fact that relatively minor changes in the composition of the biantennary complex sugar structure attached to both of the IgG Fc-domains can dramatically alter IgG activity. Thus, IgG antibodies lacking fucose, sialic acid, and galactose have been described to have an enhanced pro-inflammatory activity, while antibody glycoforms rich in terminal sialic acid residues have an active anti-inflammatory and immunomodulatory activity (5, 14, 45, 46). Until recently, it was believed that IgG glycosylation is established exclusively within the cells in which the antibody is produced and remains rather stable upon injection *in vivo*. However, more recent evidence suggests that IgG glycosylation may be actively altered *in vivo* (20, 21, 47). Thus, IgG antibodies

were described to become sialylated post secretion from plasma cells. As enhanced IgG sialylation was shown to impact IgG activity, this would represent a major concern for the use of therapeutic antibodies in patients, prompting us to analyze to what extent this extrinsic IgG sialylation pathway affects passively transferred antibodies. Technically this represents a major challenge as *in vivo* several factors may lead to an altered abundance in IgG glycoforms over time. For example, a more rapid clearance of select IgG isotypes or glycoforms may lead to an increase in other IgG glycoforms with a longer IgG half-life (41, 48). In a similar manner, using mouse strains with a cell subset specific deletion of ST6Gal1, the enzyme that catalyzes the addition of α 2,6-linked terminal sialic acid residues on IgG antibodies, may overestimate the level of B cell extrinsic sialylation if the deletion in the target cell population is incomplete and if B cell subsets that have escaped ST6Gal1

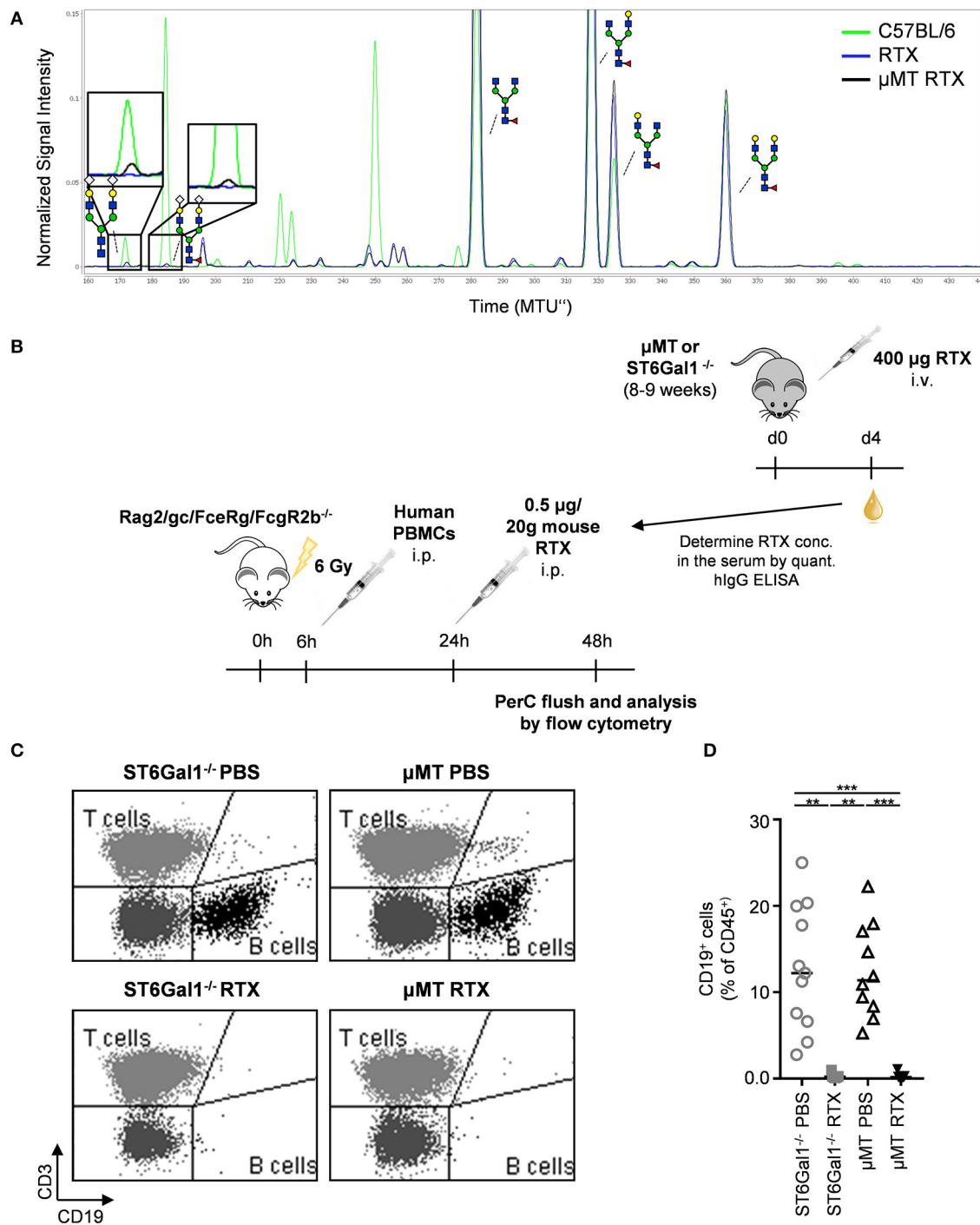


FIGURE 7 | Impact of IgG *de novo* sialylation on cytotoxic antibody activity. Shown is a representative overlay of xCGE-LIF IgG glycoanalysis of rituximab (RTX) treated μMT mice **(A)**, a schematic overview of the experimental setup **(B)**, and its respective results **(C,D)**. **(A)** μMT mice were injected with 400 μg RTX (μMT RTX) and 4 days later serum IgG was analyzed by xCGE-LIF to identify *de novo* generated IgG glycoforms. Schematic drawings of the sugar moieties are depicted for the major peaks. Enlarged insets emphasize peaks detected selectively on RTX 4 days post injection into μMT mice. **(B)** Immunodeficient Rag2/gc/FceRg/FcγR2b^{-/-} mice were irradiated (6 Gy) and reconstituted with human PBMC in the peritoneal cavity. Eighteen hours later mice ($n = 5-6$) received equal amounts of rituximab (0.5 μg/20 g mouse) derived from μMT or ST6Gal1^{-/-} mice, which had been injected with rituximab 4 days before. Twenty-four hours after RTX injection, cells of the peritoneal cavity were analyzed by flow cytometry. Shown are representative FACS plots **(C)** and the quantification **(D)** of human B cell counts in the peritoneal cavity 1 day after rituximab or PBS injection. Statistical significance was evaluated with a Kruskal-Wallis test followed by Dunns *post-hoc* test. ** $p = 0.01$, *** $p = 0.001$. Horizontal lines represent median values.

deletion have a competitive advantage over those with a deletion of the enzyme.

To study this in a most informative setting we decided to analyze changes in human IgG sialylation in mice lacking mature B cells and serum antibodies. To get the most complete picture we used human intravenous immunoglobulin preparations (IVIg), as IVIg contains all human IgG subclasses present in serum. In this experimental scenario, human IgG molecules represent the only antibody isotype in the serum and hence should be fully accessible for *de novo* sialylation. Moreover, mouse terminal sialic acid residues (Neu5Gc) can be distinguished from human sialic acid residues (Neu5Ac) by analytical techniques allowing an unequivocal identification of newly added mouse derived sialic acid residues to the transferred human antibodies *in vivo* (38). By using two independent analytical techniques to assess extrinsic *de novo* IgG sialylation *in vivo*, our results suggest that the addition of sialic acid residues is a very rare, but nonetheless detectable event. Interestingly the acceptor sugar moieties accessible for the *de novo* mono- or disialylation seemed to contain two terminal galactose residues (G2 glycoform), while in principle also monogalactosylated (G1) glycoforms could have served as acceptor structures for *de novo* sialylation and are normally present in mice *in vivo*. Moreover, both core fucosylated G2 and non-fucosylated G2 sugar moieties were able to acquire terminal Neu5Gc. Of note, increasing the amount of potential acceptor sugar structures by pre-treating human IgG with neuraminidase only marginally increased the level of IgG sialylation, further strengthening the notion, that extrinsic IgG sialylation is a rather inefficient process. However, it has to be considered that also the monosialylated structures as potential acceptor structures were removed. More importantly, when IgG preparations such as IVIg were used, in which IgG molecules present additionally containing N-linked sugar moieties in the Fab portion as potential acceptor sites for extrinsic sialylation, an almost exclusive sialylation occurred in these more easily accessible sugar domains (although not at a higher efficacy). As Fab arm glycosylation may modify antibody specificity, it will be interesting to study if extrinsic Fab arm glycosylation affects target antigen binding (49). If no Fab associated sugar moieties were present, however, minor changes in Fc-linked sugar moieties could be detected for mouse and human monoclonal antibodies. As the extent of B cell extrinsic IgG sialylation was similar for mouse and human IgG, we would exclude that human IgG molecules become sialylated less efficiently in mice due to some species barrier effects. Furthermore, as the amount of *de novo* sialylated IgG never exceeded two percent of the total IgG present *in vivo*, one would not expect functional consequences for IgG activity. Indeed, the human CD20 specific antibody

Rituximab did not show an altered activity when passaged through B cell deficient mice.

In summary, our study demonstrates that the process of B cell extrinsic *de novo* sialylation of IgG antibodies *in vivo* is only affecting a minor subset in the pool of IgG glycovariants present in IVIg and cytotoxic IgG preparations and hence may not trigger altered pro- or anti-inflammatory IgG activities.

DATA AVAILABILITY STATEMENT

The datasets generated for this study are available on request to the corresponding author.

ETHICS STATEMENT

The animal study was reviewed and approved by the government of Lower Franconia.

AUTHOR CONTRIBUTIONS

AS designed, performed, and analyzed the experiments. MH, MN, OZ, and JK analyzed the samples. RH and ER developed the method and software for xCGE-LIF analysis. AS and FN wrote the paper. AL, LN, and MPei provided material. MH, OZ, JK, AL, MPez, GL, MPei, and LN discussed the data. All authors read, reworked, and approved the manuscript.

FUNDING

This work was funded by the Research Training Group GRK1660, CRC1181-TPA07, FOR2953, and NI711/12 of the German Research Foundation (DFG) to FN. The glycan analysis was supported by the European Structural and Investment Funds IRI (Grant #KK.01.2.1.01.0003) and Croatian Center of Research Excellence in Personalized Healthcare (Grant #KK.01.1.1.01.0010).

ACKNOWLEDGMENTS

We thank Dr. Jamey Marth, UC Santa Barbara, for the ST6Gal1 KO mice.

SUPPLEMENTARY MATERIAL

The Supplementary Material for this article can be found online at: <https://www.frontiersin.org/articles/10.3389/fimmu.2019.03024/full#supplementary-material>

REFERENCES

1. Ravetch JV, Clynes RA. Divergent roles for Fc receptors and complement *in vivo*. *Annu Rev Immunol*. (1998) 16:421–32. doi: 10.1146/annurev.immunol.16.1.421
2. Nimmerjahn F, Ravetch JV. Antibody-mediated modulation of immune responses. *Immunol Rev*. (2010) 236:265–75. doi: 10.1111/j.1600-065X.2010.00910.x
3. Nimmerjahn F, Ravetch JV. Fcγ receptors as regulators of immune responses. *Nat Rev Immunol*. (2008) 8:34–47. doi: 10.1038/nri2206

4. Nimmerjahn F, Ravetch JV. The antiinflammatory activity of IgG: the intravenous IgG paradox. *J Exp Med.* (2007) 204:11–5. doi: 10.1084/jem.20061788
5. Kaneko Y, Nimmerjahn F, Ravetch JV. Anti-inflammatory activity of immunoglobulin G resulting from Fc sialylation. *Science.* (2006) 313:670–3. doi: 10.1126/science.1129594
6. Tao MH, Morrison SL. Studies of aglycosylated chimeric mouse-human IgG. Role of carbohydrate in the structure and effector functions mediated by the human IgG constant region. *J Immunol.* (1989) 143:2595–601.
7. Walker MR, Lund J, Thompson KM, Jefferis R. Aglycosylation of human IgG1 and IgG3 monoclonal antibodies can eliminate recognition by human cells expressing Fc gamma RI and/or Fc gamma RII receptors. *Biochem J.* (1989) 259:347–53. doi: 10.1042/bj2590347
8. Lund J, Tanaka T, Takahashi N, Sarmay G, Arata Y, Jefferis R. A protein structural change in aglycosylated IgG3 correlates with loss of huFc gamma R1 and huFc gamma R111 binding and/or activation. *Mol Immunol.* (1990) 27:1145–53. doi: 10.1016/0161-5890(90)90103-7
9. Dunn-Walters D, Boursier L, Spencer J. Effect of somatic hypermutation on potential N-glycosylation sites in human immunoglobulin heavy chain variable regions. *Mol Immunol.* (2000) 37:107–13. doi: 10.1016/S0161-5890(00)00038-9
10. Anumula KR. Quantitative glycan profiling of normal human plasma derived immunoglobulin and its fragments Fab and Fc. *J Immunol Methods.* (2012) 382:167–76. doi: 10.1016/j.jim.2012.05.022
11. Van De Bovenkamp FS, Derksen NIL, Ooijselaar-De Heer P, Van Schie KA, Kruihof S, Berkowska MA, et al. Adaptive antibody diversification through N-linked glycosylation of the immunoglobulin variable region. *Proc Natl Acad Sci USA.* (2018) 115:1901–6. doi: 10.1073/pnas.1711720115
12. Schwab I, Biburger M, Kronke G, Schett G, Nimmerjahn F. IVIg-mediated amelioration of ITP in mice is dependent on sialic acid and SIGNR1. *Eur J Immunol.* (2012) 42:826–30. doi: 10.1002/eji.201142260
13. Schwab I, Mihai S, Seeling M, Kasperkiewicz M, Ludwig RJ, Nimmerjahn F. Broad requirement for terminal sialic acid residues and Fc gamma RIIB for the preventive and therapeutic activity of intravenous immunoglobulins *in vivo*. *Eur J Immunol.* (2014) 44:1444–53. doi: 10.1002/eji.201344230
14. Schwab I, Nimmerjahn F. Intravenous immunoglobulin therapy: how does IgG modulate the immune system? *Nat Rev Immunol.* (2013) 13:176–89. doi: 10.1038/nri3401
15. Guhr T, Bloem J, Derksen NI, Wuhler M, Koenderman AH, Aalberse RC, et al. Enrichment of sialylated IgG by lectin fractionation does not enhance the efficacy of immunoglobulin G in a murine model of immune thrombocytopenia. *PLoS ONE.* (2011) 6:e21246. doi: 10.1371/journal.pone.0021246
16. Anthony RM, Nimmerjahn F, Ashline DJ, Reinhold VN, Paulson JC, Ravetch JV. Recapitulation of IVIG anti-inflammatory activity with a recombinant IgG Fc. *Science.* (2008) 320:373–6. doi: 10.1126/science.1154315
17. Nandakumar KS, Collin M, Olsen A, Nimmerjahn F, Blom AM, Ravetch JV, et al. Endoglycosidase treatment abrogates IgG arthritogenicity: importance of IgG glycosylation in arthritis. *Eur J Immunol.* (2007) 37:2973–82. doi: 10.1002/eji.200737581
18. Albert H, Collin M, Dudziak D, Ravetch JV, Nimmerjahn F. *In vivo* enzymatic modulation of IgG glycosylation inhibits autoimmune disease in an IgG subclass-dependent manner. *Proc Natl Acad Sci USA.* (2008) 105:15005–9. doi: 10.1073/pnas.0808248105
19. Collin M, Shannon O, Björck L. IgG glycan hydrolysis by a bacterial enzyme as a therapy against autoimmune conditions. *Proc Natl Acad Sci USA.* (2008) 105:4265–70. doi: 10.1073/pnas.0711271105
20. Jones MB, Oswald DM, Joshi S, Whiteheart SW, Orlando R, Cobb BA. B-cell-independent sialylation of IgG. *Proc Natl Acad Sci USA.* (2016) 113:7207–12. doi: 10.1073/pnas.1523968113
21. Dougher CWL, Buffone AJr, Nemeth MJ, Nasirikenari M, Irons EE, Bogner PN, et al. The blood-borne sialyltransferase ST6Gal-1 is a negative systemic regulator of granulopoiesis. *J Leukoc Biol.* (2017) 102:507–16. doi: 10.1189/jlb.3A1216-538RR
22. Manhardt CT, Punch PR, Dougher CWL, Lau JTY. Extrinsic sialylation is dynamically regulated by systemic triggers *in vivo*. *J Biol Chem.* (2017) 292:13514–20. doi: 10.1074/jbc.C117.795138
23. Kitagawa H, Paulson JC. Differential expression of five sialyltransferase genes in human tissues. *J Biol Chem.* (1994) 269:17872–8.
24. Harduin-Lepers A, Recchi MA, Delannoy P. 1994, the year of sialyltransferases. *Glycobiology.* (1995) 5:741–58. doi: 10.1093/glycob/5.8.741
25. Lo NW, Lau JT. Transcription of the beta-galactoside alpha 2,6-sialyltransferase gene in B lymphocytes is directed by a separate and distinct promoter. *Glycobiology.* (1996) 6:271–9. doi: 10.1093/glycob/6.3.271
26. Lux A, Seeling M, Baerenwaldt A, Lehmann B, Schwab I, Repp R, et al. A humanized mouse identifies the bone marrow as a niche with low therapeutic IgG activity. *Cell Rep.* (2014) 7:236–48. doi: 10.1016/j.celrep.2014.02.041
27. Kao D, Danzer H, Collin M, Gross A, Eichler J, Stambuk J, et al. A monosaccharide residue is sufficient to maintain mouse and human IgG subclass activity and directs IgG effector functions to cellular Fc receptors. *Cell Rep.* (2015) 13:2376–85. doi: 10.1016/j.celrep.2015.11.027
28. Pucic M, Knezevic A, Vidic J, Adamczyk B, Novokmet M, Polasek O, et al. High throughput isolation and glycosylation analysis of IgG-variability and heritability of the IgG glycome in three isolated human populations. *Mol Cell Proteom.* (2011) 10:M111.010090. doi: 10.1074/mcp.M111.010090
29. Kristic J, Zaytseva OO, Ram R, Nguyen Q, Novokmet M, Vuckovic F, et al. Profiling and genetic control of the murine immunoglobulin G glycome. *Nat Chem Biol.* (2018) 14:516–24. doi: 10.1038/s41589-018-0034-3
30. Cooper CA, Gasteiger E, Packer NH. GlycoMod—a software tool for determining glycosylation compositions from mass spectrometric data. *Proteomics.* (2001) 1:340–9. doi: 10.1002/1615-9861(200102)1:2<340::AID-PROT340>3.0.CO;2-B
31. Ceroni A, Maass K, Geyer H, Geyer R, Dell A, Haslam SM. GlycoWorkbench: a tool for the computer-assisted annotation of mass spectra of glycans. *J Proteome Res.* (2008) 7:1650–9. doi: 10.1021/pr7008252
32. Huffman JE, Pucic-Bakovic M, Klaric L, Hennig R, Selman MH, Vuckovic F, et al. Comparative performance of four methods for high-throughput glycosylation analysis of immunoglobulin G in genetic and epidemiological research. *Mol Cell Proteom.* (2014) 13:1598–610. doi: 10.1074/mcp.M113.037465
33. Hennig R, Reichl U, Rapp E. A software tool for automated high-throughput processing of CGE-LIF based glycoanalysis data, generated by a multiplexing capillary DNA sequencer. *Glycoconjugate J.* (2011) 28:331. doi: 10.1007/s10719-011-9334-5
34. Hennig R, Rapp E, Kottler R, Cajic S, Borowiak M, Reichl U. N-glycosylation fingerprinting of viral glycoproteins by xCGE-LIF. *Methods Mol Biol.* (2015) 1331:123–43. doi: 10.1007/978-1-4939-2874-3_8
35. Hennes T, Chui D, Paulson JC, Marth JD. Immune regulation by the ST6Gal sialyltransferase. *Proc Natl Acad Sci USA.* (1998) 95:4504–9. doi: 10.1073/pnas.95.8.4504
36. Kitamura D, Roes J, Kühn R, Rajewsky K. A B cell-deficient mouse by targeted disruption of the membrane exon of the immunoglobulin μ chain gene. *Nature.* (1991) 350:423–6. doi: 10.1038/350423a0
37. Jellusova J, Nitschke L. Regulation of B cell functions by the sialic acid-binding receptors siglec-G and CD22. *Front Immunol.* (2011) 2:96. doi: 10.3389/fimmu.2011.00096
38. Raju TS, Briggs JB, Borge SM, Jones AJ. Species-specific variation in glycosylation of IgG: evidence for the species-specific sialylation and branch-specific galactosylation and importance for engineering recombinant glycoprotein therapeutics. *Glycobiology.* (2000) 10:477–86. doi: 10.1093/glycob/10.5.477
39. Blomme B, Van Steenkiste C, Grassi P, Haslam SM, Dell A, Callewaert N, et al. Alterations of serum protein N-glycosylation in two mouse models of chronic liver disease are hepatocyte and not B cell driven. *Am J Physiol Gastrointest Liver Physiol.* (2011) 300:G833–42. doi: 10.1152/ajpgi.0022.8.2010
40. Maresch D, Altmann F. Isotype-specific glycosylation analysis of mouse IgG by LC-MS. *Proteomics.* (2016) 16:1321–30. doi: 10.1002/pmic.201500367
41. Bas M, Terrier A, Jacque E, Dehenne A, Pochet-Beghin V, Beghin C, et al. Fc sialylation prolongs serum half-life of therapeutic antibodies. *J Immunol.* (2019) 202:1582–94. doi: 10.4049/jimmunol.1800896

42. Wada R, Matsui M, Kawasaki N. Influence of N-glycosylation on effector functions and thermal stability of glycoengineered IgG1 monoclonal antibody with homogeneous glycoforms. *MAbs*. (2019) 11:350–72. doi: 10.1080/19420862.2018.1551044
43. Goh JB, Ng SK. Impact of host cell line choice on glycan profile. *Crit Rev Biotechnol*. (2018) 38:851–67. doi: 10.1080/07388551.2017.1416577
44. Ehret J, Zimmermann M, Eichhorn T, Zimmer A. Impact of cell culture media additives on IgG glycosylation produced in Chinese hamster ovary cells. *Biotechnol Bioeng*. (2019) 116:816–30. doi: 10.1002/bit.26904
45. Shinkawa T, Nakamura K, Yamane N, Shoji-Hosaka E, Kanda Y, Sakurada M, et al. The absence of fucose but not the presence of galactose or bisecting N-acetylglucosamine of human IgG1 complex-type oligosaccharides shows the critical role of enhancing antibody-dependent cellular cytotoxicity. *J Biol Chem*. (2003) 278:3466–73. doi: 10.1074/jbc.M210665200
46. Nimmerjahn F, Ravetch JV. Divergent immunoglobulin g subclass activity through selective Fc receptor binding. *Science*. (2005) 310:1510–2. doi: 10.1126/science.1118948
47. Lee-Sundlov MM, Ashline DJ, Hanneman AJ, Grozovsky R, Reinhold VN, Hoffmeister KM, et al. Circulating blood and platelets supply glycosyltransferases that enable extrinsic extracellular glycosylation. *Glycobiology*. (2017) 27:188–98. doi: 10.1093/glycob/cww108
48. Mankarious S, Lee M, Fischer S, Pyun KH, Ochs HD, Oxelius VA, et al. The half-lives of IgG subclasses and specific antibodies in patients with primary immunodeficiency who are receiving intravenously administered immunoglobulin. *J Lab Clin Med*. (1988) 112:634–40.
49. Seeling M, Bruckner C, Nimmerjahn F. Differential antibody glycosylation in autoimmunity: sweet biomarker or modulator of disease activity? *Nat Rev Rheumatol*. (2017) 13:621–30. doi: 10.1038/nrrheum.2017.146

Conflict of Interest: GL is the founder and CEO of Genos—a private research organization that specializes in high-throughput glycomic analysis and has several patents in the field. MH, MN, OZ, JK, and MPez are employees of Genos. ER is founder, CEO and CSO of glyXera GmbH and RE is an employee of glyXera GmbH. glyXera provides high-throughput glycomic analysis and holds several patents for xCGE-LIF based glycoanalysis.

The remaining authors declare that the research was conducted in the absence of any commercial or financial relationships that could be construed as a potential conflict of interest.

Copyright © 2020 Schaffert, Hanić, Novokmet, Zaytseva, Krištić, Lux, Nitschke, Peipp, Pezer, Hennig, Rapp, Lauc and Nimmerjahn. This is an open-access article distributed under the terms of the Creative Commons Attribution License (CC BY). The use, distribution or reproduction in other forums is permitted, provided the original author(s) and the copyright owner(s) are credited and that the original publication in this journal is cited, in accordance with accepted academic practice. No use, distribution or reproduction is permitted which does not comply with these terms.



Predominant Role of Immunoglobulin G in the Pathogenesis of Splenomegaly in Murine Lupus

Qian Zhang^{1*}, Liping Xiang^{1,2}, Muhammad Haidar Zaman¹, Wenhui Dong¹, Guodan He¹ and Guo-Min Deng^{3*}

¹ Key Laboratory of Antibody Techniques, National Health Commission, Nanjing Medical University, Nanjing, China,

² Department of Clinical Laboratory, Nanjing Jiangning Hospital, The Affiliated Jiangning Hospital of Nanjing Medical University, Nanjing, China, ³ Department of Rheumatology, Union Hospital Affiliated to Tongji Medical College, Huazhong

University of Science and Technology, Wuhan, China

OPEN ACCESS

Edited by:

Bridget S. Wilson,
University of New Mexico,
United States

Reviewed by:

Trine N. Jorgensen,
Case Western Reserve University,
United States
Andras Perl,
Upstate Medical University,
United States

*Correspondence:

Qian Zhang
zhangqian01@njmu.edu.cn
Guo-Min Deng
gmdeng@hust.edu.cn

Specialty section:

This article was submitted to
Autoimmune and Autoinflammatory
Disorders,
a section of the journal
Frontiers in Immunology

Received: 03 September 2019

Accepted: 10 December 2019

Published: 24 January 2020

Citation:

Zhang Q, Xiang L, Zaman MH,
Dong W, He G and Deng G-M (2020)
Predominant Role of Immunoglobulin
G in the Pathogenesis of
Splenomegaly in Murine Lupus.
Front. Immunol. 10:3020.
doi: 10.3389/fimmu.2019.03020

Systemic lupus erythematosus (SLE) is characterized by high levels of autoantibodies and multiorgan tissue damage. The pathogenesis of splenomegaly in SLE remains unknown. In this study, the role of immunoglobulin G (IgG) generation and deposition in the inflammation of the spleen and associated dysfunction in SLE was investigated. In the lupus mice, we observed the development of spontaneous splenomegaly, and we found that lupus serum IgG is an important pathological factor involved in the initiation of inflammation and further germinal center (GC) and plasma cell formation. We discovered that macrophages of the splenic marginal zone are dispensable for the GC response induced by lupus IgG, but red pulp macrophages are important for GC responses. Furthermore, we found that pathogenic lupus IgG promotes inflammation and GC formation through the macrophage-mediated secretion of TNF- α . Syk inhibitor treatment suppressed the changes in the histopathology of the spleen induced by lupus IgG. This study will contribute to the understanding of the pathogenesis of splenomegaly in lupus and promote the development of an effective therapeutic strategy for SLE.

Keywords: immunoglobulin G, systemic lupus erythematosus, spleen, inflammation, macrophages, germinal center

INTRODUCTION

Systemic lupus erythematosus (SLE) is a chronic autoimmune disease characterized by high levels of autoantibodies and multiorgan damage. The unknown interaction of genetics factors, environmental elements, and hormone levels results in abnormal immune cell activation and the release of cytokines, leading to damage multiple organs, such as the kidney, skin, lungs, brain, and joints (1, 2). The immunologic disturbances in SLE involve autoantibodies and the formation and deposition of immune complexes. SLE patients and murine lupus models exhibit increased autoantibody and nuclear self-antigens levels in the circulation, which causes tissue damage, immune complex deposition, complement activation, and cytokine secretion (3, 4). It has been reported that circulating immune complexes can activate plasmacytoid dendritic cells to induce type I IFN responses, which stimulate the differentiation of monocyte-derived dendritic cells and promote B cell activation and humoral autoimmunity (5). Both innate and adaptive immune systems are involved in the immune response in SLE pathogenesis.

The spleen is an important peripheral lymphoid organ for antibacterial and antifungal immunity. As the site of immunocyte proliferation and differentiation, the spleen combines the innate and adaptive immune responses in an exclusively organized manner. The red pulp macrophage and marginal zone macrophage (MZM) populations in the spleen enable the efficient removal of aging erythrocytes and blood-borne pathogens, respectively (6, 7). MZMs located in the marginal zone barrier, express the type I scavenger receptor MARCO and type C lectin SIGN-R1, which recognizes pathogens (8). White pulp containing T, B, and follicular dendritic cells are involved in adaptive immunity (9, 10). After antigen-specific differentiation in the splenic follicles, plasma cells produce and migrate into the red pulp. Autoantibodies are produced by B cells recruited to the germinal center (GC). The GC is an important site of B cell differentiation into long-lived memory and plasma cells. Traditionally, high-affinity autoantibodies are associated with the GC response, but recent studies have indicated that B cell activation and differentiation also occurs in the extrafollicular pathway in SLE. In SLE, autoantibodies are secreted by plasma cells in the spleen through both extrafollicular and GC pathways (11).

Splenomegaly is infrequently observed in SLE patients and lupus mice, although it has been reported as a manifestation of active SLE (12, 13). Splenomegaly may be caused by increased splenic function, congestion, or infiltration (14–16). Although the spleen is not considered a common target organ in SLE, but the function of the spleen in producing antibodies cannot be neglected. Thus, it is important to understand the pathogenesis and features of splenomegaly and inflammation of spleen in lupus.

T cells, B cells, and macrophages are known to contribute in the pathogenesis of SLE. Autoantibodies are involved in the pathogenesis of autoimmune diseases (17). Previous studies showed that lupus patient serum induces tissue damage (18–20). Serum IgG from lupus patients activates inflammatory cells, such as monocytes/macrophages, dendritic cells and neutrophils, which produce cytokines and subsequently induce tissue damage (21–23). Fcγ receptors (FcγRs) are receptors for IgG, and the balance between activating and inhibitory FcγRs determines the threshold of immune cells activation (24). B cells express only the inhibitory receptor FcγRIIb. It has been reported that FcγRIIb-deficient mice display an increased frequency of autoreactive B cells and lupus-like manifestations (25, 26). Although monocyte/macrophage abnormalities play a pivotal role in the pathogenesis of SLE, the role of macrophages in spleen inflammation and splenomegaly is still unknown. Spleen tyrosine kinase (Syk) is a member of the Src family of non-receptor tyrosine kinases that associate with surface receptors, including the B cells receptor (BCR) and Fcγ receptors, and is involved in the signal transduction pathways of PI3K/Akt, Ras/ERK, PLCc/NFAT, and IKK/NF-κB (27, 28). Treatment with the Syk inhibitor R788 completely abrogates skin inflammation induced by serum from lupus patients and suppresses established skin injury in lupus-prone mice (29), but whether inhibiting Syk suppresses spleen inflammation remains unknown.

In the present study, we investigated the histopathological features and pathogenesis of splenomegaly in lupus mice. We found that in lupus mice, IgG is an important pathological factor in red pulp inflammation and GC responses; pathogenic lupus IgG promoted GC formation through the macrophage-mediated secretion of TNF-α. Inhibiting Syk suppressed inflammation of the spleen induced by lupus IgG. This study broadens the understanding of the pathogenesis of splenomegaly in lupus mice.

MATERIALS AND METHODS

Mice and Reagents

C57BL/6 (B6) mice were obtained from the Animal Center of Nanjing Medical University. B6.MRL-Fas^{lpr}/J (B6.MRL/lpr; 000482) mice were purchased from the Model Animal Research Center of Nanjing University. MRL/MpJ (MRL; 000486), MRL/MpJ-Fas^{lpr}/J (MRL/lpr; 000485), FcγRIIb^{-/-} (002848), FcγRIII^{-/-} (003171), and TNF-α^{-/-} (005540) mice were purchased from Jackson Laboratories (USA). Pathogen-free environments were provided at the Animal Core Facility of Nanjing Medical University. All animal experiments were approved by the Nanjing Medical University Institutional Animal Care and Use Committee (IACUC-1710012). All experiments used in this study were approved by the Institutional Ethics Committee of Nanjing Medical University.

SLE patient and healthy human sera were provided by the First Affiliated Hospital of Nanjing Medical University and the Third Affiliated Hospital of Nanjing Medical University. From the provided serum, SLE patients with ≥4 of the 11 revised criteria of the American College of Rheumatology (ACR) for the classification of SLE were selected. All patients had SLE disease-activity index scores ranging from 0 to 20. Serum from healthy individuals was used as a control. Informed consent was received from all patients under the Nanjing Medical University Review Board-approved protocol. Mice sera were collected from B6.MRL/lpr and C57BL/6 mice.

Lupus IgG was extracted from the SLE patient serum using Protein G Agarose beads (Millipore, USA) following the manufacturer's protocol, as described previously. The Syk inhibitor R406 (sc-364595A) was purchased from Santa Cruz Biotechnology (Dallas, USA). Clodronate liposomes (CLs) were purchased from FormuMax (California, USA).

Histopathology, Histochemistry, Immunohistochemistry (IHC), and Microscopy

For histological examinations, spleens were fixed in 4% paraformaldehyde. After fixation, the samples were dehydrated in ethanol, embedded in paraffin, cut into 5-μm sections, and stained with hematoxylin and eosin (HE). The spleen inflammation severity was scored from 0 to 4: grade 0 = normal, grade 1 = mild inflammation in the red pulp, grades 2–3 = different quantities of infiltrating inflammatory cells in the red pulp and under the capsule, and grade 4 = increased numbers of infiltrating inflammatory cells in the red pulp and a large number

of megakaryocytes (megakaryocyte hyperplasia). For the IHC assay, the tissue slides were incubated with primary anti-mouse IgG (ab190475, Abcam), anti-MARCO (sc-65353, Santa Cruz), anti-CD138 (10593-1-AP, Proteintech), anti-F4/80 (ab6640, Abcam), and anti-human IgG (ab109489, Abcam) antibodies followed by incubation with biotinylated secondary antibodies and avidin–biotin–peroxidase complex treatment. Then, 3,3'-diaminobenzidine was used for development, and all slides were counterstained with Mayer's hematoxylin. Biotin-conjugated PNA (Vector Laboratories B-1075) was used to identify the GC, which was captured with a Zeiss LSM700 microscope (Carl Zeiss, USA).

Histochemistry of reticular fibers in paraffin sections (8 μ m) was assessed by the silver impregnation method previously described by Gordon and Sweets (30). Frozen sections were air-dried and fixed with ice-cold acetone and then detected by acid phosphatase using the previously described Gomori acid phosphatase method (31).

Injection Protocol and Macrophage Depletion

For ink injection, B6 mice and B6.MRL/lpr mice (30 weeks) were injected with Indian ink (0.1 ml/10 g) containing 50–100 nm carbon particles. India ink diluted 1:10 in PBS was injected intravenously after anesthesia with 10% chloral hydrate (Sigma, Aldrich). The spleens were collected 30 min after injection, and formalin-fixed paraffin sections (5 μ m) were assessed using light microscopy and HE staining.

Intrasplenic injections were administered to C57BL/6 mice to induce IgG deposition and inflammation in the spleen after mice anesthetized intraperitoneally with 10% chloral hydrate (Sigma, Aldrich). Following disinfection, an \sim 1 cm incision (without opening the peritoneal cavity) was made at the left loin, and then lupus serum was injected into the spleen *in situ*. Mice received the same volume of PBS or healthy human serum as the control. C57BL/6 mice used in this study were female with 6–8 weeks of age, unless otherwise indicated.

Macrophages were depleted with 1 mg (40 mg/kg) CLs administered to C57BL/6 mice by intraperitoneal injection 48 h before lupus IgG (200 μ g) injection. To selectively deplete the MZMs, 162 μ g (6.5 mg/kg) of CLs was injected intraperitoneally. The same volume of empty liposome-phosphate-buffered saline (control liposomes) was injected as a control.

Flow Cytometry

The spleen was isolated and mashed into RPMI 1640 medium containing 2% FBS. After erythrocytes were lysed, a single cell suspension of splenocytes was prepared and then stained with the cell surface markers. For GC B cell staining, cells were stained with anti-B220-PE (RA3-6B2, Biolegend), anti-Fas-APC (15A7, eBioscience), and anti-GL-7-FITC (GL-7, Biolegend). For marginal zone B (MZB) cell staining, cells were stained with anti-B220-FITC (RA3-6B2, BD), anti-CD21-APC (7G6, BD), and anti-CD23-PE (B3B4, BD). For IgG-secreting plasma cells, after surface staining of anti-CD138-APC (IB17-R0268, Miltenyi), cells were fixed, permeabilized, and stained for anti-IgG-FITC (Poly4060, BD). For MZM staining, cells were stained with

anti-F4/80-PE (BM8, Biolegend), anti-CD11b-Alexa Fluor 488 (M1/70, Biolegend), anti-SIGNR1-APC (22D1, eBioscience), and anti-MHC II (I-Ab)-eFluor 450 (AF6-120.1, eBioscience). All samples were detected on a flow cytometer (Beckman Coulter, USA) and analyzed with Cytexpert 2.0 software.

Isolation and Culture of Bone Marrow-Derived Macrophages

To obtain bone marrow-derived macrophages (BMMs), C57BL/6, Fc γ RII $^{-/-}$, and Fc γ RIII $^{-/-}$ mice were sacrificed by cervical dislocation, and the bone marrow cells were flushed from the femoral shafts using serum-free DMEM. After the adherent cells were removed at 3 h, the non-adherent cells in suspension were cultured with 30 ng/ml M-CSF (PeproTech) for 6 days, and the medium was changed every 3 days. After incubation, the adherent BMMs were obtained. The adherent BMMs were then cultured in fresh complete culture medium for stimulation with 50, 100, 200, and 300 μ g/ml lupus IgG that extracted from the SLE patient serum.

Western Blotting

Isolated BMMs were lysed in RIPA buffer. The cell lysates were subjected to SDS-PAGE and transferred to polyvinylidene difluoride (PVDF) membranes (Millipore). The primary antibodies p-Syk (CST, 2717), Syk (CST, 2712), p-NF- κ B p65 (CST, 3033), and NF- κ B p65 (CST, 4764) were diluted with 1/1,000. The evaluation of immunoreactivity was performed with the ECL analysis system.

ELISA Assay

TNF- α and MCP-1 levels were measured using ELISA kits (R&D Systems, USA). The blood serum and cell supernatant were diluted and studied using a standard curve. All of the samples were measured in triplicate. The procedure was performed according to the manufacturer's instructions.

Anti-dsDNA antibody levels in the serum were determined by ELISA, as described previously (32). Briefly, 96-well microtiter plates (Costar) were pretreated with calf thymus dsDNA (Sigma-Aldrich) for 2 h at 37°C and then placed overnight at 4°C. After being washed with PBS containing 0.05% Tween-20 (PBST), the plates were blocked with 1% BSA for 1 h. After the plates were incubated with a 1:100 dilution of mouse serum, the levels of anti-dsDNA antibodies were detected with horseradish peroxidase (HRP)-conjugated goat anti-mouse IgG, anti-mouse IgG1, anti-mouse IgG2a, anti-mouse IgG2b, anti-mouse IgG2c, anti-mouse IgG3, anti-mouse IgM, anti-mouse IgA, and anti-mouse IgE (all from Southern Biotech). Tetramethylbenzidine (TMB) substrate was used for the development, and absorbance at 450 nm was measured on a Thermo Multiskan Spectrum 1500.

Statistical Analysis

All data are shown as the mean \pm SEM. Statistical analyses were performed using GraphPad PRISM with Student's *t*-test. The differences were considered significant at **P* < 0.05, ***P* < 0.01, and ****P* < 0.001. All experiments were repeated at least three times with four to five mice in each group.

RESULTS

Lupus Mice Spontaneously Develop Splenomegaly

To understand the changes in the spleen during SLE, we observed lupus mice that spontaneously develop lupus-like clinical manifestations. We found that splenomegaly spontaneously develops in B6.MRL/lpr and MRL/lpr mice. The length and weight of the lupus mice spleens were much greater than those of the normal mice (**Figure 1A**). Histopathology showed increased numbers of accumulated cells in the white pulp in the spleens of lupus mice (**Figure 1B**).

To investigate the architectural changes in the spleen in lupus mice, we used silver impregnation to assess the reticular fibers. We found increased reticular fiber density in the white pulp. Acid phosphatase staining revealed increased numbers of phagocytes in the splenic red pulp of the lupus mice (**Figure 1C**). We used ink injection to evaluate the physiological function of the spleen and found that carbon particles were disseminated into the red pulp of lupus mice, while particles were retained exclusively in the marginal zone of normal mice (**Figure 1D**). These data suggest that the antigen capture ability is weakened in the spleens of lupus mice. Since MZMs act as a barrier to the entry of circulating pathogens into the follicles of the spleen, we investigated the distribution of MZMs in the spleens of lupus MRL/lpr mice. We found that the numbers of MARCO+ cells were significantly reduced in the spleens of lupus MRL/lpr mice (**Figure 1E**). MZBs, which are an innate non-recirculating B cell population responsible for antigen transport from the marginal zone into the follicles and can be induced to differentiate rapidly into plasma cells, are located close to MZMs. We found that the MZB cell population was largely expanded in the marginal zone of the spleen at 12 weeks in MRL/lpr mice but decreased at 30 weeks in MRL/lpr mice (**Figure 1F**). These data suggest that there are structural defects in the spleen in lupus mice.

IgG Production and Deposition Are Involved in the Pathogenesis of Splenomegaly in Lupus Mice

Since autoantibody-IgG is a major contributor to the development of tissue inflammation in SLE, we detected IgG deposition in the spleens of lupus MRL/lpr mice of different ages and found that IgG was deposited in the red pulp of the spleen in MRL/lpr mice of different ages. We also investigated plasma cells by detecting CD138 in the spleen and found that plasma cells were present in the red pulp in the spleens of mice of various ages (**Figure 2A**).

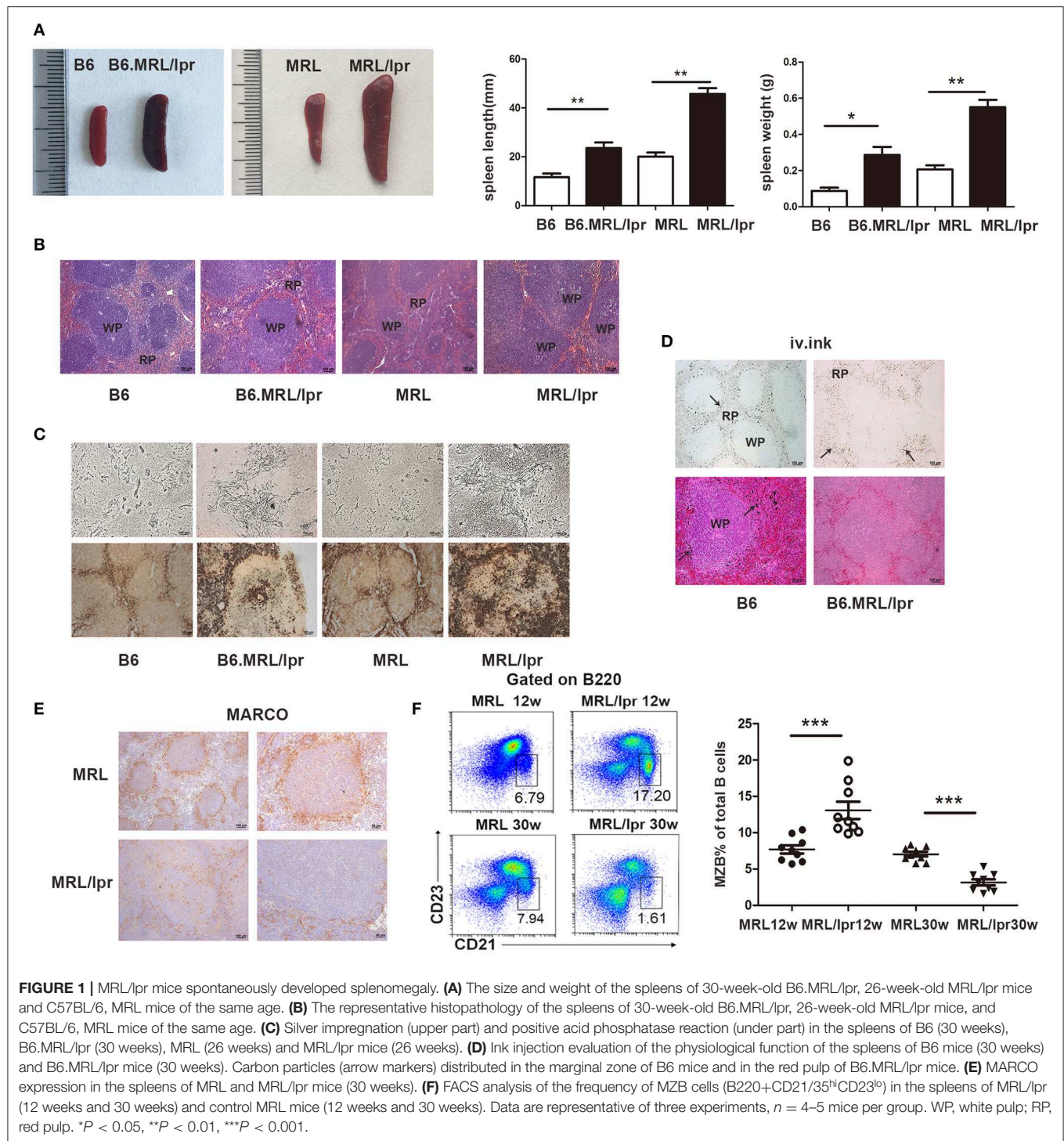
To determine whether the levels of autoantibodies in the peripheral blood reflect the levels of IgG deposition in the spleen of lupus mice, we detected immunoglobulin isotypes and anti-dsDNA antibodies. We found that the level of anti-dsDNA IgG in the blood increased as the age of MRL/lpr mice increased; IgG1, IgG2a, IgG2b, and IgG3 of anti-dsDNA

were predominant in the blood of MRL/lpr mice (**Figure 2B**). Autoantibodies are generated by plasma cells; we found that the number of IgG-secreting plasma cells in the spleen increased from 6 to 30 weeks in MRL/lpr mice (**Figure 2C**). These results suggest that antibody-secreting cells produce pathogenic IgG autoantibodies that deposit in the spleen and secrete into the periphery.

Lupus IgG-induced Splenic Red Pulp Inflammation and GC Responses

In this study, we found a large amount of IgG secretion and deposition in extrafollicular foci in the spleens of the lupus mice (**Figure 2**). To confirm that deposited IgG further induces immune responses in the spleen, we established a model with IgG deposition in the mouse spleen by intrasplenic injection of serum from SLE patients and healthy individuals. The results showed that serum from SLE patients induced red pulp inflammation, while PBS and serum from healthy humans did not (**Figure 3A**). We further used serum from lupus mice and normal mice to repeat this experiment. We also found that serum from lupus mice induced inflammation in the spleen, but serum from normal mice and young lupus mice did not (**Figure 3A**). To determine whether the severity of inflammation induced by lupus serum in the spleen is related to the volume injected, we used various volumes of lupus serum. We found that the severity of inflammation in the spleen is related to the volume of injected lupus serum (**Figure 3B**). We also investigated the kinetics of inflammation induced by lupus serum in the spleen and found that inflammation developed at 6h and peaked at 3 days after intrasplenic injection (**Figure 3B**). We used IHC staining to determine the cell types in the inflamed spleens. We found that spleen inflammation was characterized by the infiltration of F4/80 macrophages in the red pulp (**Figure 3C**). IgG deposition was observed in the spleens of C57BL/6 mice receiving intrasplenic injections of lupus serum (**Figure 3C**). We did not observe any inflammation and IgG deposition following intravenous and intraperitoneal injection of the same volume of lupus patient serum (**Figure S1**).

To confirm the role of IgG in inflammation induced by lupus serum, we used IgG-depleted lupus serum. We found that at 3 days after injection, the severity of inflammation was significantly decreased in the red pulp of mice injected with IgG-depleted SLE serum compared to mice injected with whole SLE serum (**Figure 3D**). Lupus IgG from SLE serum significantly induced spleen inflammation compared to IgG from healthy human serum (**Figure S2**). This finding suggests that IgG plays an important role in the development of inflammation induced by lupus serum in the spleen. MZB cells located in the marginal zone of the spleen differentiate directly into plasma cells in extrafollicular responses. GCs are important sites of autoreactive B cell activation in autoimmune diseases. Antibodies are secreted by plasma cells in the spleen through extrafollicular and GC pathways (11). We investigated whether lupus serum IgG induces extrafollicular responses, GC responses, and plasma cell formation using flow cytometry.



The results showed that the numbers of GC and IgG-secreting plasma cells increased at 8 days after injection of SLE patient serum, whereas GC and plasma cell numbers decreased in mice injected with IgG-depleted SLE serum (Figure 3E). We found an approximately five-fold reduction in GCs and plasma cells in the spleens of mice injected with IgG-depleted SLE serum compared to mice injected with whole SLE serum.

MZB cell numbers decreased at 8 days after injection of SLE patient serum. There were no significant changes in MZB cell numbers between mice injected with SLE patient serum and mice injected with IgG-depleted SLE patient serum. The injection of healthy human serum did not induce obvious changes in GCs and plasma cell numbers (Figure S3). These data suggest that IgG is an important factor in the development

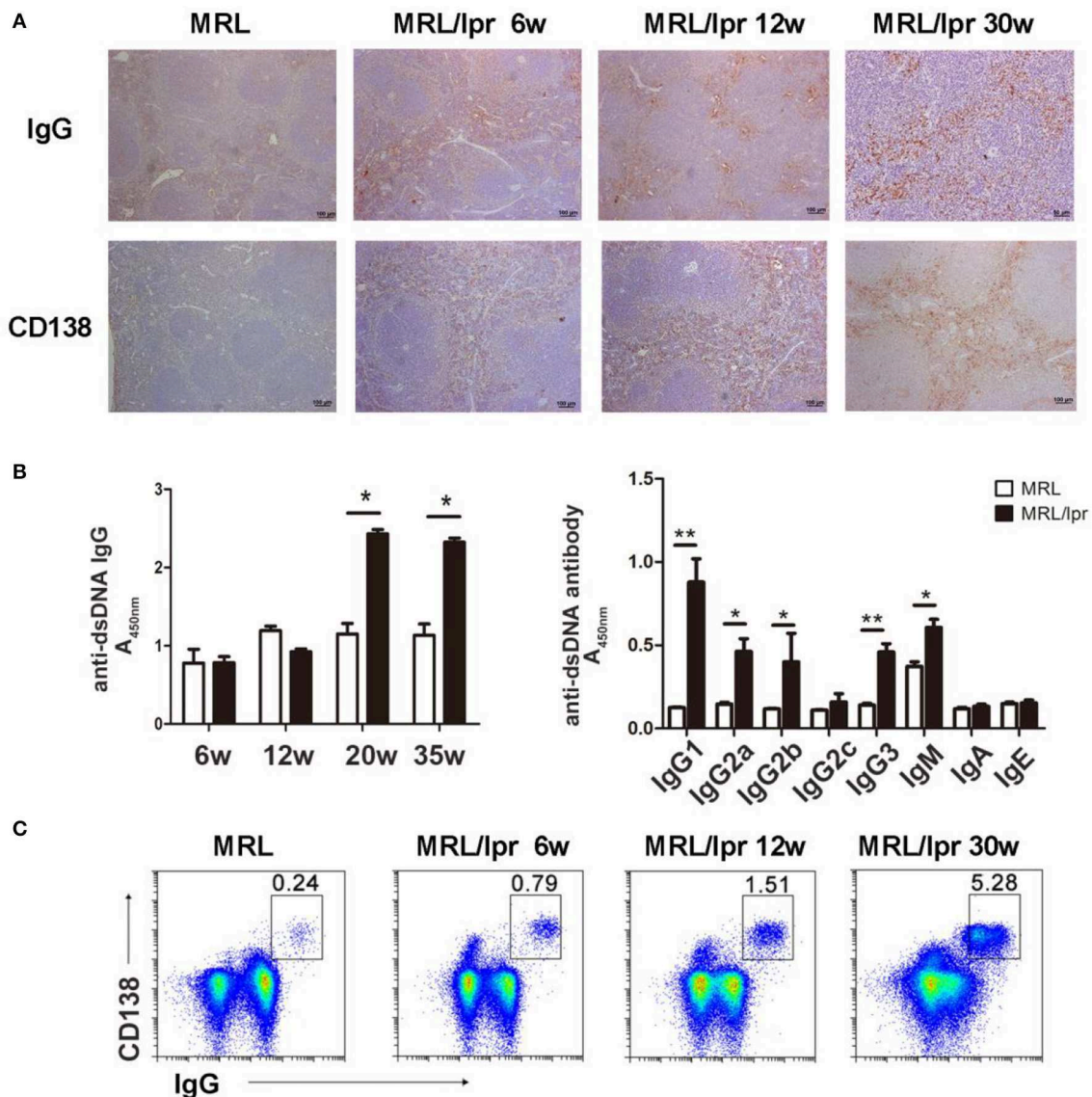


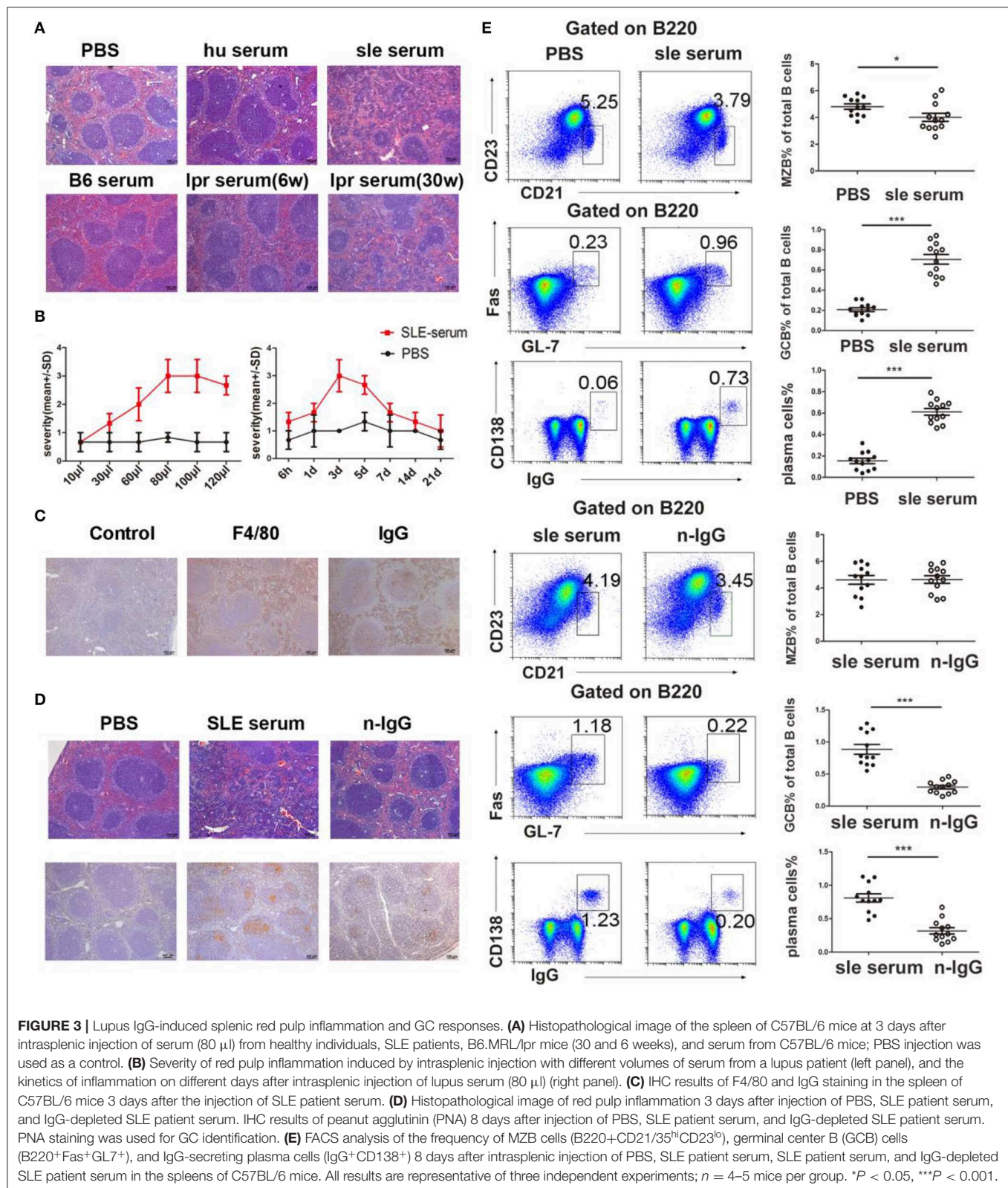
FIGURE 2 | IgG production and deposition in the spleens of lupus mice. **(A)** IHC showing that IgG and CD138 are distributed in the splenic red pulp in 6-, 12-, and 30-week-old MRL/lpr mice. **(B)** Serum levels of the anti-dsDNA antibody in MRL/lpr mice (left panel) at different ages (6, 12, 20, and 35 weeks). Levels of anti-dsDNA antibody immunoglobulin isotypes in 35-week-old MRL/lpr mice (right panel). * $P < 0.05$, ** $P < 0.01$. **(C)** Flow cytometry analysis of IgG-secreting plasma cells (IgG+CD138+) in 6-, 12-, and 30-week-old MRL/lpr mice. The results are representative of three independent experiments, $n = 4-5$ mice per group.

of lupus serum-induced red pulp inflammation and the GC response.

Macrophages Are Required for the Development of Spleen Inflammation and GC Responses Induced by Lupus IgG

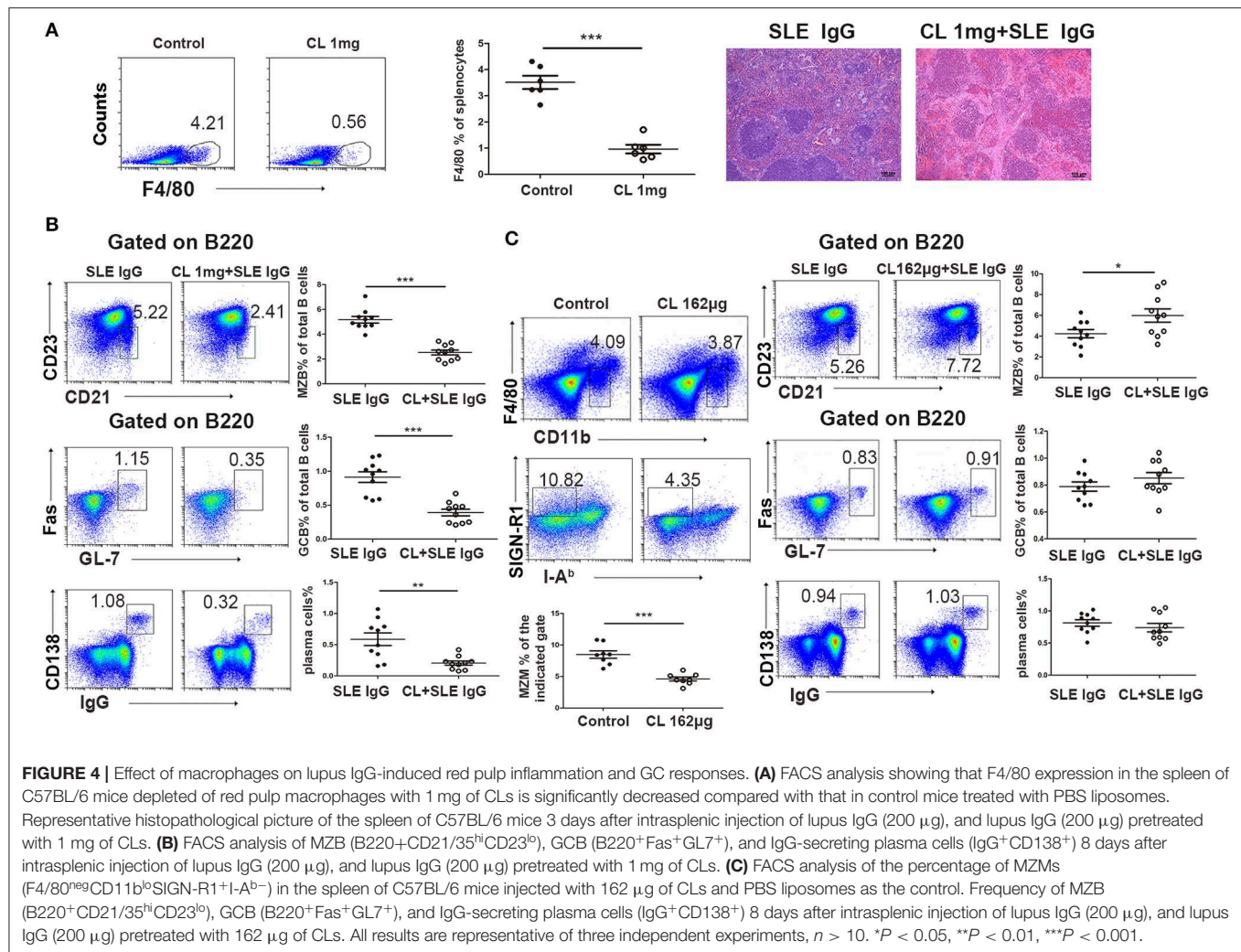
It has been reported that macrophages play a critical role in tissue damage in SLE (18). It is unclear whether macrophages are involved in spleen inflammation and the GC response induced by lupus IgG.

To determine the role of macrophages in lupus IgG-induced spleen inflammation and the GC response, we depleted macrophages in experimental mice by using various doses of CLs (33). We treated mice with high (40 mg/kg) and low doses (6.5 mg/kg) of CLs, which depleted red pulp macrophages, and MZMs, respectively. We found that the inflammation induced by lupus IgG was alleviated in red pulp macrophage-depleted mice compared to mice without depletion of red pulp macrophages (**Figure 4A**). This finding suggests that red pulp macrophages are crucial for the initial inflammation induced by lupus IgG. Since MZMs expressing MARCO are



deficient in the spleens of lupus MRL/lpr mice (**Figure 1E**), we further determined whether lupus IgG affects GC and plasma cells in red pulp macrophages and the MZM deficiency.

The results showed that depletion of red pulp macrophages (pretreated with 40 mg/kg CLs) decreased MZB, GCB, and plasma cell populations in the spleens of mice injected with



lupus IgG (**Figure 4B**). MZM deficiency (pretreatment with 6.5 mg/kg CLs) increased the number of MZB cells, which may respond to lupus IgG, but did not affect GCB and plasma cell populations (**Figure 4C**; **Figure S4**). These data suggest that lupus IgG can promote the formation of GCs and plasma cells without MZMs. Red pulp macrophages are indispensable for the development of spleen inflammation and the formation of GCB and plasma cells.

The Role of Syk, FcγR, and TNF-α in Inflammation and the GC Response Induced by Lupus IgG

Syk plays an important role in lupus IgG-induced signal transduction. We examined the lupus IgG-induced Syk-NF-κB signaling pathway in BMMs and found that lupus IgG induced Syk and NF-κB p65 phosphorylation in a dose-dependent manner (**Figure 5A**; **Figure S5**). To further confirm the effect of lupus IgG on the activation of Syk and NF-κB, we used a Syk inhibitor. We found that the Syk inhibitor treatment suppressed p-Syk and NF-κB p-p65 activation induced by lupus IgG (**Figure 5B**).

The FcγRs, which are IgG receptors, include activating receptors FcγRI and FcγRIII and the inhibitory receptor FcγRII. We used FcγRII- and FcγRIII-deficient BMMs to determine the role of these receptors in the lupus IgG-induced Syk-NF-κB signaling pathway. The results showed that deficiency of the activating receptor FcγRIII decreased Syk and NF-κB p65 activation induced by lupus IgG, while deficiency of the inhibitory receptor FcγRII increased Syk and NF-κB p65 activation induced by lupus IgG (**Figure 5B**).

To investigate the cytokine release by macrophages stimulated with lupus IgG, we detected TNF-α and MCP-1 levels in the supernatant of BMMs stimulated with lupus IgG. We found that lupus IgG increased the levels of TNF-α and MCP-1, whereas Syk inhibitor treatment significantly inhibited TNF-α and decreased MCP-1 expression, but the difference in MCP-1 expression was not significant (**Figure 5C**).

To further understand whether Syk regulates spleen inflammation induced by lupus IgG, we compared changes in the histopathology of spleens from mice treated with or without a Syk inhibitor. The results showed that the Syk inhibitor treatment obviously decreased the red pulp inflammation induced by lupus IgG (**Figure 5D**). Since lupus IgG increased the

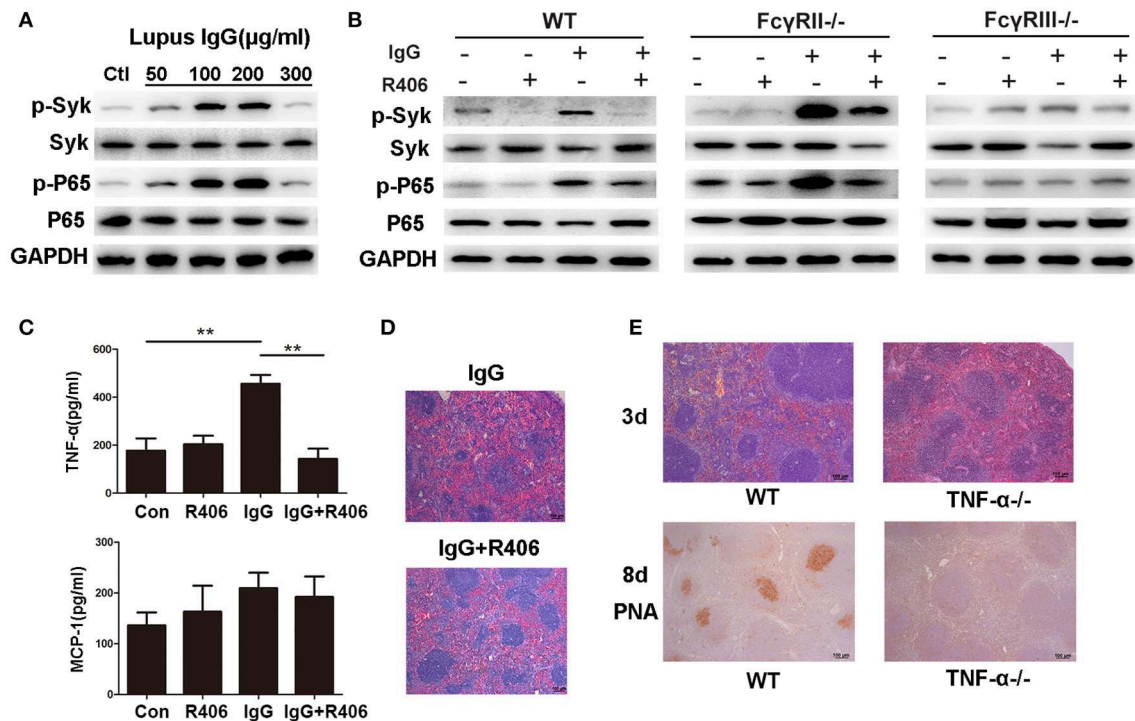


FIGURE 5 | Lupus IgG promoted inflammation and GC formation through TNF- α secretion by macrophages. **(A)** Western blot detected phosphorylated Syk (p-Syk) and total Syk, phosphorylated NF- κ B p65 (p-p65), and p65 in BMMs stimulated with various doses of lupus IgG for 20 min. The results are from three independent experiments. **(B)** Western blot detected p-Syk, Syk, p-p65, and p65 in BMMs stimulated with 100 μ g/ml lupus IgG in the presence or absence of R406 (2 μ M) for 30 min. BMMs were isolated from WT, Fc γ RII $^{-/-}$, and Fc γ RIII $^{-/-}$ mice. The results are from three independent experiments. **(C)** ELISA results of TNF- α and MCP-1 in the supernatant of WT-derived BMMs stimulated with 100 μ g/ml lupus IgG for 18 h in the presence or absence of R406 (2 μ M). ** P < 0.01, the result is representative of three independent experiments. **(D)** Histopathological image of the spleen in C57BL/6 mice treated with or without the Syk inhibitor R406 (10 mg/kg) after 3 days of intrasplenic injection of lupus IgG (200 μ g) from an SLE patient. The results are representative of three independent experiments, n = 5 mice per group. **(E)** Histopathological image of the spleen 3 days after intrasplenic injection of lupus IgG (200 μ g) in WT (C57BL/6) and TNF- α $^{-/-}$ mice. PNA was expressed 8 days after intrasplenic injection of lupus IgG in WT and TNF- α $^{-/-}$ mice. The result is representative of three independent experiments, n = 5 mice per group.

level of TNF- α in the supernatant of BMMs, we speculated that lupus IgG could promote GC formation through the secretion of TNF- α by macrophages. To confirm this speculation, we used TNF- α -deficient mice. The histopathology demonstrated that red pulp inflammation induced by lupus IgG was significantly decreased in TNF- α -deficient mice compared to wild-type (WT) mice. The IHC staining showed that GC formation induced by lupus IgG was also significantly reduced in TNF- α -deficient mice compared to WT mice (Figure 5E). In TNF- α -deficient mice, we found that lupus IgG decreased the initial red pulp inflammation and further inhibited GC formation.

DISCUSSION

Splenomegaly has been reported in lupus mice and patients, but there is little information available about the mechanism of splenomegaly in SLE patients. Although the pathogenesis of SLE remains unclear, evidence suggests that SLE may be caused by immunological abnormalities, including immunotolerance deficiency, abnormal interactions of T and B cells, immune cell hyperactivity, and defective clearance of autoantigens (34). The spleen is the largest

peripheral lymphoid organ and has a specialized structural organization for immunocyte proliferation and differentiation, and interaction with the circulation. Sustained autoantigen and immune complex deposition in the spleen may enhance the abnormalities and promote the progression of SLE. Our study demonstrates that lupus mice spontaneously develop splenomegaly, and the architectural injury of the spleen in lupus mice may be due to the production and deposition of large amounts of pathogenic IgG, which is an important pathological factor in spleen inflammation and immunological abnormalities.

SLE is a disease mainly driven by autoantibodies (35). We found large amounts of IgG and quantities of plasma cells in the spleens of MRL/lpr mice; the accumulation of anti-dsDNA IgG in the peripheral blood is related to age. The dsDNA antibody is an important parameter for both diagnosis and treatment in SLE (36, 37). It has been reported that autoantibodies in SLE are mainly produced by B cells through affinity maturation and somatic hypermutation in GCs and also extrafollicular responses (11, 38). Plasma cells can arise through B cell activation and direct differentiation in the extrafollicular site or in the T-dependent GC response. Antigens can activate B cells in a

T-independent or T-dependent manner. There are no definite markers that discriminate plasma cells by their pathway of differentiation. We and others have shown that IgG isolated from SLE patient serum can induce organ damage (18, 20, 39). Therefore, we established animal models of IgG deposition in the spleen by intrasplenic injection of lupus serum. Based on this model, we investigated whether lupus IgG induced inflammation and further GC and plasma cell formation. The results showed that the intrasplenic injection of lupus serum-induced red pulp inflammation at 3 days and further increased GC and plasma cells differentiation at 8 days. However, compared to mice injected with lupus serum containing IgG, mice injected with IgG-depleted lupus serum displayed decreased GC and plasma cell formation. Therefore, lupus IgG in SLE serum is the important pathological factor inducing red pulp inflammation, and dysfunctional adaptive immune responses in the spleen in lupus.

It has been shown that MZMs surrounding the splenic follicles can clear autoantigens or blood-borne antigens. The absence of MZMs results in the retention of apoptotic cell debris within the marginal zone and increased loading of antigens on MZB cells, stimulating the autoimmune response (3). MZMs have been reported to interact with MZB cells in the spleens of BXD2 lupus mice with the membrane lymphotoxin- $\alpha 1\beta 2$ and lymphotoxin β receptor. The abnormal follicular shuttling of MZB cells causes the loss of MZMs and thus downregulates the clearance of autoantigens (40). Our data demonstrate that depletion of MZMs increased the number of MZB cells, but did not affect the presentation of antigens and induction of the GC response, which is consistent with a report by Aichele (41). MZB cells can differentiate directly into plasma cells in extrafollicular responses and can also deliver antigens to the follicles, enhancing T-dependent responses (42). We found that lupus serum IgG decreased MZB cell numbers, but it is not clear if lupus IgG affects extrafollicular responses or the delivery of antigens to the follicles. MZMs and red pulp macrophages are known to interact with apoptotic cells entering the spleen from the circulation. There are many studies on the defects in the MZM-mediated regulation of inflammation and tolerance in autoimmune diseases, but not many on red pulp macrophages. Red pulp macrophages are known to increase the phagocytosis of apoptotic cells in the absence of MZMs (33), but information on how red pulp macrophages regulate inflammation and adaptive immunity in autoimmune diseases is lacking. Macrophages in the red pulp of the spleen express receptors for IgG or IgG-opsonized erythrocytes (43). In our study, red pulp macrophages were found to influence inflammation and GC responses induced by lupus IgG. The removal of F4/80 splenic macrophages can inhibit the development of autoantibodies and lupus pathology in mice (33). Therefore, this finding suggests that macrophages play a role in the pathogenesis of SLE.

IgG deposition in tissue can activate complement or engage in the activation of the Fc γ R to mediate antibody-dependent cell cytotoxicity (ADCC) and initiate inflammation (44). In this

study, we found that the effect of lupus IgG was mediated by its binding to the Fc γ R on macrophages. Lupus IgG activated Syk and NF- κ B signaling, leading to the release of TNF- α . In the *in vivo* experiment, we found that red pulp macrophages play an important role in initial inflammation and GC and plasma cell formation. Lupus IgG promotes inflammation through macrophage-mediated secretion of TNF- α and further promotes GC formation. TNF- α is important for the development of skin and liver injuries induced by lupus serum (18, 20). However, whether macrophages interact with T cells induced by lupus IgG requires further investigation. Syk plays a central role in Fc γ R-mediated macrophage activation. In the current study, we inhibited Syk downstream of Fc γ R, which decreased the inflammation induced by lupus IgG, and decreased NF- κ B signaling and TNF- α secretion induced by lupus IgG in macrophages. Numerous studies have described Syk abnormalities in BCR-mediated signaling in B cells and Syk inhibition in the progression of glomerulonephritis in SLE (45), but there is little information regarding the role of Fc γ R-mediated signaling in the progression of spleen inflammation and immune responses. Syk is an important therapeutic target for the spleen inflammation. Fc γ R-mediated signaling transduction is dependent on immune-receptor tyrosine-based activation motifs (ITAM), which are located in its cytoplasmic tail. Syk binds these phosphorylated ITAM motifs and activates downstream signaling. We confirmed that inhibiting Syk suppressed spleen inflammation and macrophage activation in the *in vitro* experiment and spleen inflammation model. Furthermore, we observed that inhibitor of Syk also treated splenomegaly in our previous study (29).

In conclusion, our study demonstrates that IgG plays an important role in the pathogenesis of splenomegaly in lupus mice. IgG production and deposition in the spleen is an important pathological factor in spleen inflammation and immunological abnormalities. Red pulp macrophages, instead of marginal zone macrophages, are indispensable for inflammation and GC responses in splenomegaly. Lupus IgG promotes the GC response through TNF- α production by macrophages. Syk is a therapeutic target for the suppression of inflammation in splenomegaly in SLE. These findings will contribute to future research for the development of therapeutic strategies for splenomegaly in SLE.

DATA AVAILABILITY STATEMENT

All datasets generated for this study are included in the article/**Supplementary Material**.

ETHICS STATEMENT

This study was carried out in accordance with the recommendations of the Institutional Animal Care and Use Committee (IACUC) guidelines of Nanjing Medical

University. The protocol was approved by the Institutional Ethics Committee of Nanjing Medical University.

AUTHOR CONTRIBUTIONS

QZ and G-MD designed the research and wrote the manuscript with the contribution from MZ. QZ, LX, and WD performed the experiments. QZ and GH analyzed the data for this manuscript.

FUNDING

This research was supported by the National Natural Science Foundation of China (QZ, 31700793), the Key Project of Science and Technology Development of Nanjing Medical University (QZ, 2016NJMUZD007), the Research Initiating Fund of Nanjing

Medical University (G-MD, KY101RC071203), and the National Natural Science Foundation of China (G-MD, 81472111).

ACKNOWLEDGMENTS

We thank Prof. Xiaoming Wang for his comments and the analysis of flow cytometry, and Dr. Binbin Pan for providing the lupus serum from the Third Affiliated Hospital of Nanjing Medical University.

SUPPLEMENTARY MATERIAL

The Supplementary Material for this article can be found online at: <https://www.frontiersin.org/articles/10.3389/fimmu.2019.03020/full#supplementary-material>

REFERENCES

- Collison J. Systemic lupus erythematosus: new pathway blocks disease in lupus-prone mice. *Nat Rev Rheumatol.* (2017) 13:131. doi: 10.1038/nrrheum.2017.2
- Buyon JP. *Systemic Lupus Erythematosus. Primer on the Rheumatic Diseases.* New York, NY: Springer (2008). p. 303–38. doi: 10.1007/978-0-387-68566-3_15
- Li H, Wu Q, Li J, Yang P, Zhu Z, Luo B, et al. Cutting edge: defective follicular exclusion of apoptotic antigens due to marginal zone macrophage defects in autoimmune BXD2 mice. *J Immunol.* (2013) 190:4465–9. doi: 10.4049/jimmunol.1300041
- McGaha TL, Karlsson MC. Apoptotic cell responses in the splenic marginal zone: a paradigm for immunologic reactions to apoptotic antigens with implications for autoimmunity. *Immunol Rev.* (2016) 269:26–43. doi: 10.1111/immr.12382
- Huang X, Dorta-Estremera S, Yao Y, Shen N, Cao W. Predominant role of plasmacytoid dendritic cells in stimulating systemic autoimmunity. *Front Immunol.* (2015) 6:526. doi: 10.3389/fimmu.2015.00526
- Lewis SM, Williams A. Structure and function of the immune system in the spleen. *Sci Immunol.* (2019) 4:eau6085. doi: 10.1126/sciimmunol.aau6085
- Borges da Silva H, Fonseca R, Pereira RM, Cassado Ados A, Alvarez JM, D'Imperio Lima MR. Splenic macrophage subsets and their function during blood-borne infections. *Front Immunol.* (2015) 6:480. doi: 10.3389/fimmu.2015.00480
- Mebius RE, Kraal G. Structure and function of the spleen. *Nat Rev Immunol.* (2005) 5:606–16. doi: 10.1038/nri1669
- Alsufyani F, Mattoo H, Zhou D, Cariappa A, Van Buren D, Hock H, et al. The Mst1 kinase is required for follicular B cell homing and B-1 B cell development. *Front Immunol.* (2018) 9:2393. doi: 10.3389/fimmu.2018.02393
- Moran I, Avery DT, Payne K, Lenthall H, Davies EG, Burns S, et al. B cell-intrinsic requirement for STK4 in humoral immunity in mice and humans. *J Allergy Clin Immunol.* (2019) 143:2302–5. doi: 10.1016/j.jaci.2019.02.010
- Malkiel S, Barlev AN, Atisha-Fregoso Y, Suurmond J, Diamond B. Plasma cell differentiation pathways in systemic lupus erythematosus. *Front Immunol.* (2018) 9:427. doi: 10.3389/fimmu.2018.00427
- Colmegna I, deBoisblanc BP, Gimenez CR, Espinoza LR. Slow development of massive splenomegaly, portal and pulmonary hypertension in systematic lupus erythematosus: can nodular regenerative hyperplasia of the liver explain all these findings? *Lupus.* (2005) 14:976–8. doi: 10.1191/0961203305lu2237xx
- Zuckerman E, Rosner I, Yeshurun D. Massive splenomegaly: a manifestation of active systemic lupus erythematosus. *Clin Exp Rheumatol.* (1993) 11:698–9.
- Yang QB, He YL, Peng CM, Qing YF, He Q, Zhou JG. Systemic lupus erythematosus complicated by noncirrhotic portal hypertension: a case report and review of literature. *World J Clin Cases.* (2018) 6:688–93. doi: 10.12998/wjcc.v6.i13.688
- Tsai F, Homan PJ. Bim suppresses the development of SLE by limiting myeloid inflammatory responses. *J Exp Med.* (2017) 214:3753–73. doi: 10.1084/jem.20170479
- Palmieri C, Tettamanti C, Scarpelli MP, Tse R. The forensic spleen: morphological, radiological, and toxicological investigations. *Foren Sci Int.* (2019) 214:3753–73. doi: 10.1016/j.forsci.2019.01.042
- Almaani S, Rovin BH. B-cell therapy in lupus nephritis: an overview. *Nephrol Dial Transplant.* (2019) 34:22–9. doi: 10.1093/ndt/gfy267
- Deng GM, Liu L, Kytteris VC, Tsokos GC. Lupus serum IgG induces skin inflammation through the TNFR1 signaling pathway. *J Immunol.* (2010) 184:7154–61. doi: 10.4049/jimmunol.0902514
- Li X, Guo X, Liu H, Gao G, Xu G, Fei X, et al. Skin inflammation induced by lupus serum was inhibited in IL-1R deficient mice. *Clin Immunol.* (2017) 180:63–8. doi: 10.1016/j.clim.2017.03.015
- Fang X, Zaman MH, Guo X, Ding H, Xie C, Zhang X, et al. Role of hepatic deposited immunoglobulin G in the pathogenesis of liver damage in systemic lupus erythematosus. *Front Immunol.* (2018) 9:1457. doi: 10.3389/fimmu.2018.01457
- Yu X, Lazarus AH. Targeting FcγR3s to treat antibody-dependent autoimmunity. *Autoimmun Rev.* (2016) 15:510–2. doi: 10.1016/j.autrev.2016.02.006
- Clatworthy MR, Aronin CE, Mathews RJ, Morgan NY, Smith KG, Germain RN. Immune complexes stimulate CCR7-dependent dendritic cell migration to lymph nodes. *Nat Med.* (2014) 20:1458–63. doi: 10.1038/nm.3709
- Joo H, Coquery C, Xue Y, Gayet I, Dillon SR, Punaro M, et al. Serum from patients with SLE instructs monocytes to promote IgG and IgA plasmablast differentiation. *J Exp Med.* (2012) 209:1335–48. doi: 10.1084/jem.20111644
- Nimmerjahn F, Ravetch JV. FcγR3s as regulators of immune responses. *Nat Rev Immunol.* (2008) 8:34–47. doi: 10.1038/nri2206
- Su K, Yang H, Li X, Li X, Gibson AW, Cafardi JM, et al. Expression profile of FcγR3s on leukocytes and its dysregulation in systemic lupus erythematosus. *J Immunol.* (2007) 178:3272–80. doi: 10.4049/jimmunol.178.5.3272
- Ondee T, Surawut S, Taratummarat S, Hirankarn N, Palaga T, Pisitkun P, et al. FcγR3 receptor IIB deficient mice: a lupus model with increased endotoxin tolerance-related sepsis susceptibility. *Shock.* (2017) 47:743–52. doi: 10.1097/SHK.0000000000000796
- Braegelmann C, Holzel M, Ludbrook V, Dickson M, Turan N, Ferring-Schmitt S, et al. Spleen tyrosine kinase (SYK) is a potential target for the treatment of cutaneous lupus erythematosus patients. *Exp Dermatol.* (2016) 25:375–9. doi: 10.1111/exd.12986
- Deng GM, Tsokos GC. The role of SYK in cutaneous lupus erythematosus. *Exp Dermatol.* (2016) 25:674–5. doi: 10.1111/exd.13018
- Deng GM, Liu L, Bahjat FR, Pine PR, Tsokos GC. Suppression of skin and kidney disease by inhibition of spleen tyrosine kinase in lupus-prone mice. *Arthritis Rheum.* (2010) 62:2086–92. doi: 10.1002/art.27452

30. Sun X, Liu E, Wang T, Zhang Q, Yang P, Ahmed N, et al. The novel histological evidence of the blood-spleen barrier in duck (*Anas platyrhynchos*). *Histol Histopathol.* (2019) 34:33–45. doi: 10.14670/HH-18-019
31. Zhang Q, Chen B, Yang P, Zhang L, Liu Y, Ullah S, et al. Identification and structural composition of the blood-spleen barrier in chickens. *Vet J.* (2015) 204:110–6. doi: 10.1016/j.tvjl.2015.01.013
32. Zhang W, Wu J, Qiao B, Xu W, Xiong S. Amelioration of lupus nephritis by serum amyloid P component gene therapy with distinct mechanisms varied from different stage of the disease. *PLoS ONE.* (2011) 6:e22659. doi: 10.1371/journal.pone.0022659
33. McGaha TL, Chen Y, Ravishanker B, van Rooijen N, Karlsson MC. Marginal zone macrophages suppress innate and adaptive immunity to apoptotic cells in the spleen. *Blood.* (2011) 117:5403–12. doi: 10.1182/blood-2010-11-320028
34. Zhang J, Jacobi AM, Wang T, Berlin R, Volpe BT, Diamond B. Polyreactive autoantibodies in systemic lupus erythematosus have pathogenic potential. *J Autoimmun.* (2009) 33:270–4. doi: 10.1016/j.jaut.2009.03.011
35. Iwata S, Tanaka Y. B-cell subsets, signaling and their roles in secretion of autoantibodies. *Lupus.* (2016) 25:850–6. doi: 10.1177/0961203316643172
36. Wen Z, Xu L, Chen X, Xu W, Yin Z, Gao X, et al. Autoantibody induction by DNA-containing immune complexes requires HMGB1 with the TLR2/microRNA-155 pathway. *J Immunol.* (2013) 190:5411–22. doi: 10.4049/jimmunol.1203301
37. Deshmukh US, Bagavant H, Fu SM. Role of anti-DNA antibodies in the pathogenesis of lupus nephritis. *Autoimmun Rev.* (2006) 5:414–8. doi: 10.1016/j.autrev.2005.10.010
38. William J, Euler C, Christensen S, Shlomchik MJ. Evolution of autoantibody responses via somatic hypermutation outside of germinal centers. *Science.* (2002) 297:2066–70. doi: 10.1126/science.1073924
39. Rosetti F, Tsuboi N, Chen K, Nishi H, Hernandez T, Sethi S, et al. Human lupus serum induces neutrophil-mediated organ damage in mice that is enabled by Mac-1 deficiency. *J Immunol.* (2012) 189:3714–23. doi: 10.4049/jimmunol.1201594
40. Li H, Fu YX, Wu Q, Zhou Y, Crossman DK, Yang P, et al. Interferon-induced mechanosensing defects impede apoptotic cell clearance in lupus. *J Clin Invest.* (2015) 125:2877–90. doi: 10.1172/JCI81059
41. Aichele P, Zinke J, Grode L, Schwendener RA, Kaufmann SH, Seiler P. Macrophages of the splenic marginal zone are essential for trapping of blood-borne particulate antigen but dispensable for induction of specific T cell responses. *J Immunol.* (2003) 171:1148–55. doi: 10.4049/jimmunol.171.3.1148
42. Cinamon G, Zachariah MA, Lam OM, Foss FW Jr, Cyster JG. Follicular shuttling of marginal zone B cells facilitates antigen transport. *Nat Immunol.* (2008) 9:54. doi: 10.1038/ni1542
43. Nagelkerke SQ, Bruggeman CW, den Haan JMM, Mul EPJ, van den Berg TK, van Bruggen R, et al. Red pulp macrophages in the human spleen are a distinct cell population with a unique expression of Fc-gamma receptors. *Blood Adv.* (2018) 2:941–53. doi: 10.1182/bloodadvances.2017015008
44. Nimmerjahn F, Gordan S, Lux A. Fc-gammaR dependent mechanisms of cytotoxic, agonistic, and neutralizing antibody activities. *Trends Immunol.* (2015) 36:325–36. doi: 10.1016/j.it.2015.04.005
45. Tanaka Y, Kubo S, Iwata S, Yoshikawa M, Nakayama S. B cell phenotypes, signaling and their roles in secretion of antibodies in systemic lupus erythematosus. *Clin Immunol.* (2018) 186:21–5. doi: 10.1016/j.clim.2017.07.010

Conflict of Interest: The authors declare that the research was conducted in the absence of any commercial or financial relationships that could be construed as a potential conflict of interest.

Copyright © 2020 Zhang, Xiang, Zaman, Dong, He and Deng. This is an open-access article distributed under the terms of the Creative Commons Attribution License (CC BY). The use, distribution or reproduction in other forums is permitted, provided the original author(s) and the copyright owner(s) are credited and that the original publication in this journal is cited, in accordance with accepted academic practice. No use, distribution or reproduction is permitted which does not comply with these terms.



The Proteolytic Cleavage of Therapeutic Monoclonal Antibody Hinge Region: More Than a Matter of Subclass

Quentin Deveuve¹, Laurie Lajoie^{1*}, Benjamin Barrault¹ and Gilles Thibault^{1,2*}

¹ EA7501 Groupe Innovation et Ciblage Cellulaire, Equipe Fc Récepteurs, Anticorps et MicroEnvironnement, Université de Tours, Tours, France, ² Laboratoire d'Immunologie, CHRU de Tours, Tours, France

OPEN ACCESS

Edited by:

Jean Harb,

INSERM U1064 Centre de Recherche
en Transplantation et
Immunologie, France

Reviewed by:

Laureline Berthelot,

Institut National de la Santé et de la
Recherche Médicale
(INSERM), France

Falk Nimmerjahn,

University of Erlangen-Nuremberg,
Germany

*Correspondence:

Laurie Lajoie

laurie.lajoie@univ-tours.fr

Gilles Thibault

gilles.thibault@univ-tours.fr

Specialty section:

This article was submitted to
B Cell Biology,
a section of the journal
Frontiers in Immunology

Received: 26 July 2019

Accepted: 21 January 2020

Published: 11 February 2020

Citation:

Deveuve Q, Lajoie L, Barrault B and
Thibault G (2020) The Proteolytic
Cleavage of Therapeutic Monoclonal
Antibody Hinge Region: More Than a
Matter of Subclass.
Front. Immunol. 11:168.
doi: 10.3389/fimmu.2020.00168

The hinge region of immunoglobulin G (IgG) is involved in C1q and FcγRIIIA-expressing natural killer (NK) cell recruitment. Both heavy chains (HCs) of the hinge region can be cleaved sequentially by several proteases of the tumor/inflammatory/infectious microenvironment, including matrix metalloproteinase 12 (MMP12), or immunoglobulin-degrading enzyme from *Streptococcus pyogenes* (IdeS), impairing Fc-mediated functions. The cleavage of therapeutic monoclonal antibodies (TmAbs), which are based on a human IgG1, IgG2 or IgG4 structure, has been poorly investigated, although it may represent an escape mechanism to these treatments. Therefore, we used non-reducing SDS-PAGE to compare the cleavage kinetics of five IgG1 TmAbs (trastuzumab, rituximab, cetuximab, infliximab, ipilimumab), one IgG2 TmAb (panitumumab), and two IgG4 TmAbs (nivolumab and pembrolizumab) by MMP12 and IdeS, which were found to cleave the first and second HCs with different kinetics. Panitumumab was more protease-resistant than IgG1 and IgG4 TmAbs. The latter were usually more protease-sensitive, whereas IgG1 TmAbs were usually cleaved with intermediate kinetics. However, we observed intra-subclass variability among IgG4 and IgG1 TmAbs. Nivolumab and pembrolizumab were cleaved similarly by MMP12, whereas pembrolizumab was more IdeS-resistant. Ipilimumab was more IdeS-sensitive and MMP12-resistant than the other IgG1 TmAbs, regardless of G1m allotype. In addition the Fc fragment of IgG1 TmAbs were highly resistant to cleavage by MMP12, whereas their cleavage kinetic by IdeS was very similar to that observed with the intact forms (excluding ipilimumab). Importantly, the cleavage kinetic of ipilimumab Fc fragment by IdeS was superimposable to that of trastuzumab, cetuximab and infliximab Fc fragment, showing that the variability observed for intact ipilimumab is unrelated to its Fc portion. We propose that the variability in the cleavage sensitivity/resistance balance among TmAbs of IgG1 and IgG4 subclasses results partially, from TmAb characteristics related to and/or located in the Fab region. Finally, with ELISA and flow cytometry, we observed that a single cleavage of IgG1 TmAbs greatly decreased their affinity for FcγRIIIA and C1q and their ability to induce FcγRIIIA-dependent functional responses of NK cells. Overall, our results indicate that the cleavage of the hinge region should be considered with TmAbs treatment and in the development of new molecules.

Keywords: therapeutic monoclonal antibodies, hinge region, proteolytic cleavage, MMP12, ideS, immunoglobulin G subclass, C1q, FcγRIIIA

INTRODUCTION

Therapeutic monoclonal antibodies (TmAbs), which are extensively used for treatment in cancer or chronic inflammatory diseases, are based on a human IgG1, IgG2, or IgG4 structure. The choice among the three subclasses during the design and development of an mAb is mainly directed by its expected mechanism of action. The IgG1 format efficiently binds C1q and FcγRs and triggers complement-dependent cytotoxicity or antibody-dependent cell-mediated cytotoxicity (ADCC) (1, 2). Therefore, this subclass is used to develop cytolytic mAbs. Conversely, the IgG2 or IgG4 format, which weakly binds C1q and FcγR, is usually favored when developing neutralizing/antagonist TmAbs. The binding sites of C1q and FcγR on human IgG are relatively close and are partially located in the lower hinge region (defined by the sequence ²³³PAPELLGGP²⁴¹ in IgG1) (1–3).

Previous studies have shown that in addition to the papain and pepsin sensitivity of the hinge region (4, 5), the lower hinge region of IgG1 is cleaved by tumor-, inflammatory-, and/or infectious-associated proteases such as matrix metalloproteinases (MMPs) or immunoglobulin-degrading enzyme from *Streptococcus pyogenes* (IdeS) (6–11). A first cleavage of one heavy chain (HC) generates single-cleaved IgG (sc-IgG), which retains its whole structure via CH3-CH3 and glycan weak interactions (9). Nevertheless, the cleavage sites are located within or proximal to the binding sites for C1q and FcγR, thus reducing their binding and ultimately Fc-mediated functional responses (1, 2, 6). The cleavage of the second HC is usually slower and generates F(ab')₂, which obviously loses the Fc-dependent interactions. The cleavage of trastuzumab or pertuzumab (anti-HER2, used in breast cancer therapy) impairs ADCC and has been associated with a weakened therapeutic effect in a mouse xenograft tumor model (12, 13). Furthermore, high levels of cleaved IgG were detected in serum from individuals with inflammatory bowel diseases, who did not respond to anti-TNFα TmAbs (10). Therefore, the proteolytic cleavage could be an immune evasion mechanism in IgG1 TmAbs treatment.

By contrast, IgG2s are almost completely MMP-resistant and only partially cleaved by IdeS. This resistance has been linked to the sequence of their lower hinge region. Indeed, replacing the ²³⁴PELLGG²⁴⁰ (EU numbering) of an IgG1 mAb hinge region with the ²³¹PPVA-G²³⁶ sequence of an IgG2 resulted in complete resistance to the cleavage by MMPs (14). Finally, the cleavage of IgG4 has been poorly documented, although Ryan et al. suggested that IgG1 and IgG4 mAbs were similarly cleaved by MMP3 and IdeS (6). Besides the amino acid composition of the lower hinge region related to the subclasses, the numerous available TmAbs feature other structural and/or conformational variations. Some are natural, such as the four IgG1 allotypes resulting from the combination of genetic markers (Gms) (K214/R214 and D356-L358/E356-M358 defining the G1m17/G1m3 and G1m1/G1m-1 allotypes, respectively) or Fc glycosylation. Other variations are related to bioengineering such as the type of humanization (chimeric, humanized, or full human) or the S228P mutation introduced to stabilize the core hinge region of IgG4 (15). The

effect of this subclass-independent structural heterogeneity of engineered TmAbs on protease sensitivity is unknown.

In this context, we aimed to compare the cleavage of a panel of eight widely used TmAbs (three chimeric, two humanized, and three full-human) regrouping five IgG1s that include the four allotypes, one IgG2 TmAb, and two IgG4 TmAbs. We chose IdeS as a model protease (12–14, 16) and MMP12, secreted by macrophages in the tumor microenvironment or in chronic inflammatory diseases, as a more relevant pathophysiological protease. We used SDS-PAGE to kinetically analyze the proteolytic fragments for each TmAbs. Moreover, we analyzed the effect of the cleavage on the binding of C1q and membrane FcγRIIIA as well as its functional consequences by ELISA or multicolor flow cytometry.

MATERIALS AND METHODS

Monoclonal Antibodies

TmAbs obtained from the CHRU de Tours included five IgG1 molecules: cetuximab (anti-EGFR), infliximab (anti-TNFα), ipilimumab (anti-CTLA4), rituximab (anti-CD20), trastuzumab (anti-HER2), one IgG2 (panitumumab [anti-EGFR]), and two IgG4 molecules (nivolumab and pembrolizumab [both anti-PD1]). MAb including unconjugated anti-CD16 (clone 3G8) and FITC-conjugated anti-CD16 (clone 3G8) and PE-conjugated anti-IFNγ (clone 45.15) were from Beckman Coulter and PE-Cy5-conjugated CD107a (clone H4A3) was from BD Biosciences. Horseradish peroxidase-conjugated anti-C1q was from Abcam. Allotypes of rituximab were produced by Evitria (Schlieren, Switzerland) were constructed following the same strategy as described by Ternant et al. (17).

Enzymes and Proteolytic Cleavage

Recombinant IdeS and IgdE were from Genovis. The human recombinant MMP12 catalytic domain was from Sinobiological Inc. The proteolytic cleavage of 50 μg TmAbs (1 mg/mL) involved 0.05 U IdeS/μg TmAbs or 10 μg/mL MMP12 in phosphate buffered saline (PBS, pH 7.4) and tris buffered saline (pH 7.5), respectively. MMP12 activity required the addition of 10 mM CaCl₂. At the indicated times, a sample of the reaction was stopped by 10 mM iodoacetamide (Sigma Aldrich) for IdeS or 1 mM EDTA for MMP12. To generate single-cleaved TmAbs (sc-TmAbs) for binding and functional experiments, TmAbs were incubated at 3 mg/mL with 0.1 U IdeS/μg TmAbs in PBS for 6 min. All reactions were performed at 37°C.

In order to produce Fc fragments, 50 μg TmAbs were incubated with 1 U IgdE/μg TmAbs either in PBS (pH 7.4) or TBS (pH 7.5) at 37°C for 48 h.

SDS-PAGE

Proteolytic fragments were analyzed by SDS-PAGE in NuPAGE MES SDS running buffer (ThermoScientific) on 6% (or 10% for the cleavage of the Fc domain) homemade gels under non-reducing conditions. Samples were heated at 95°C for 10 min in Laemmli buffer before electrophoresis. SeeBlue Plus2 Pre-stained Protein Standard (Invitrogen) was used as a weight molecular marker. Proteins were stained with Coomassie Blue and images

were acquired on a Fusion Fx (Vilber Lourmat). Relative percentages of each fragment were obtained by densitometry using ImageJ (1.50i) software.

Binding Property of TmAbs to FcγRIIIA

CD16-transduced NK92 cells (2×10^4) were incubated with FITC-conjugated anti-CD16 3G8 (dilution 1:100) and increasing concentrations of TmAbs or sc-TmAbs (30 min at 4°C) and were analyzed by flow cytometry as described (18).

Functional Responses of CD16-Transduced NK92 Cells

IgG2 mouse mAb, mouse anti-CD16 mAb, or (sc-)TmAbs (5 µg/mL) was used to sensitize Nunc Maxisorp 96-well culture plates (ThermoScientific) overnight at 4°C. Then, 100 µL CD16-transduced NK92 cells (2×10^4) were plated on non-sensitized or sensitized plates and incubated at 37°C in 5% CO₂ humidified air for 4 h with anti-CD107a mAb (dilution 1:20) and 0.1 µg/mL BD GolgiPlug containing Brefeldin A (BD Biosciences). Cells were fixed and permeabilized by using the BD Cytofix/cytoperm Plus kit (BD Biosciences) and stained with anti-IFNγ mAbs (dilution 1:10) for 30 min at 4°C. Data were acquired with a Gallios flow cytometer (Beckman Coulter) and were analyzed by using Kaluza v1.3.

C1q ELISA

Nunc Maxisorp 96-well culture plates were coated with saturating concentrations of (sc-)TmAbs (10 µg/mL) in 0.05 mol/L bicarbonate buffer (pH 9.5) overnight at 4°C. Wells were washed three times with PBS containing 0.05% Tween-20, then blocked with PBS-0.05% Tween-1% BSA for 1 h at 37°C. After three washes, 0.01–30 µg/mL C1q was added. After incubation for 2 h at 37°C, wells were washed three times with PBS-0.05% Tween-20 and incubated with horseradish peroxidase-conjugated anti-C1q (dilution 1:200) for 1 h at 37°C. 3,3',5,5'-Tetramethylbenzidine (Thermo Scientific) was used as a substrate. Absorbance was measured at 405 nm on a Mithras LB940 (Berthold Technologies).

RESULTS

Comparison of MMP12- and IdeS-Mediated Cleavage of TmAbs

To kinetically compare the proteolytic cleavage of TmAbs, we first incubated five IgG1 TmAbs (trastuzumab, rituximab, cetuximab, infliximab, and ipilimumab), one IgG2 TmAb (panitumumab), and two IgG4 TmAbs (nivolumab and pembrolizumab) with MMP12 for various times. The generated fragments were analyzed by non-reducing SDS-PAGE. An example of the cleavage (rituximab) is shown in **Figure 1A**. The ≈148 kDa band (intact rituximab) started to decrease after 5–15 min and almost completely disappeared after 6 h. After 15 min, two bands corresponding to the cleavage of one HC were detected: one ≈125 kDa (sc-TmAbs) and one ≈30–35 kDa [hemi-Fc (Fc(m)) released in denaturing conditions]. The sc-TmAb band increased up to 4–6 h and disappeared at 24 h, while the Fc(m) band increased over time. A fourth band of

≈98 kDa (F(ab')₂), corresponding to the cleavage of the second HC, was observed after 30 min. It increased with time and was the major band detected after 24 h. Finally, two additional slight bands of ≈50–55 kDa were observed after 4 h when IgG1 TmAbs were tested. The bands corresponding to the intact TmAbs, sc-TmAbs and F(ab')₂ were quantified (**Figure 1B**).

The IgG2 mAb panitumumab was highly resistant to cleavage by MMP12: the intact form represented >90% after 24 h (**Figure 1B** left). By contrast, intact forms of the two IgG4 TmAbs pembrolizumab and nivolumab decreased rapidly and disappeared after 6 h. Sc-TmAbs increased rapidly (up to ≈40% at 1–2 h), then decreased and became undetectable after 24 h (**Figure 1B** middle). The proportion of F(ab')₂ increased constantly to represent >80 and >90% after 6 and 24 h, respectively (**Figure 1B**, right). Finally, among IgG1 TmAbs, trastuzumab, rituximab, cetuximab, and infliximab showed an intermediate cleavage kinetics: about 20% of the intact form still observed after 6 h of incubation, with the maximum of sc-TmAbs (up to ≈40%) observed at 4–6 h, followed by almost complete disappearance. The proportion of F(ab')₂ increased constantly to represent ≈30 and >80% after 6 and 24 h, respectively (**Figure 1B**, middle and right). Unexpectedly, the cleavage of ipilimumab, the fifth IgG1 TmAb, was markedly slower and close to that of panitumumab: the intact form was still ≈70% after 24 h and the sc-TmAb and F(ab')₂ forms did not exceed 20%, whatever the time.

We then studied cleavage by IdeS. As shown in **Figure 1C** for rituximab and **Figure 1D** for all TmAbs, the cleavage by IdeS was actually faster than that by MMP12 (**Figure 1D**, left). IdeS cleaved the first HC very rapidly: almost all intact forms were converted in sc-TmAbs (**Figure 1D**, middle) when F(ab')₂ became detectable (**Figure 1D**, right). However, the latter form did not exceed 75% after 24 h, whatever the TmAb. Finally, we did not detect any additional bands as observed in MMP12 experiments.

The proteolytic profile of the eight TmAbs with IdeS according to their subclass differed from that observed with MMP12. First, the cleavage of the first HC (leading to sc-TmAb) was similar whatever the TmAb studied, except for the panitumumab: maximal sc-panitumumab proportion was observed after ≈2 h vs. 30 min for the other TmAbs (**Figure 1D**, middle). Therefore, the differences between the TmAbs mainly affected the cleavage of the second HC, as observed by the simultaneous decrease of sc-TmAbs and increase of F(ab')₂ forms (**Figure 1D**, middle and right). The panitumumab second HC was highly resistant to this cleavage by IdeS [≈30% of F(ab')₂ at 24 h]. Secondly, the two IgG4 TmAbs did not behave similarly. The cleavage of the second HC of pembrolizumab was slower than that of nivolumab: F(ab')₂ increased from ≈20 to 45% between 1 and 24 h and from ≈25 to 75% between 1 and 24 h. Finally, the cleavage of the second HC of trastuzumab, rituximab, cetuximab and infliximab was similar [≈40–50% of sc-TmAbs and F(ab')₂ at 24 h] and intermediate between that of IdeS-resistant panitumumab and IdeS-sensitive nivolumab. The profile of ipilimumab was once again different from that of the other IgG1-TmAbs and was close to that of nivolumab. Indeed, after 30 min, sc-ipilimumab decreased,

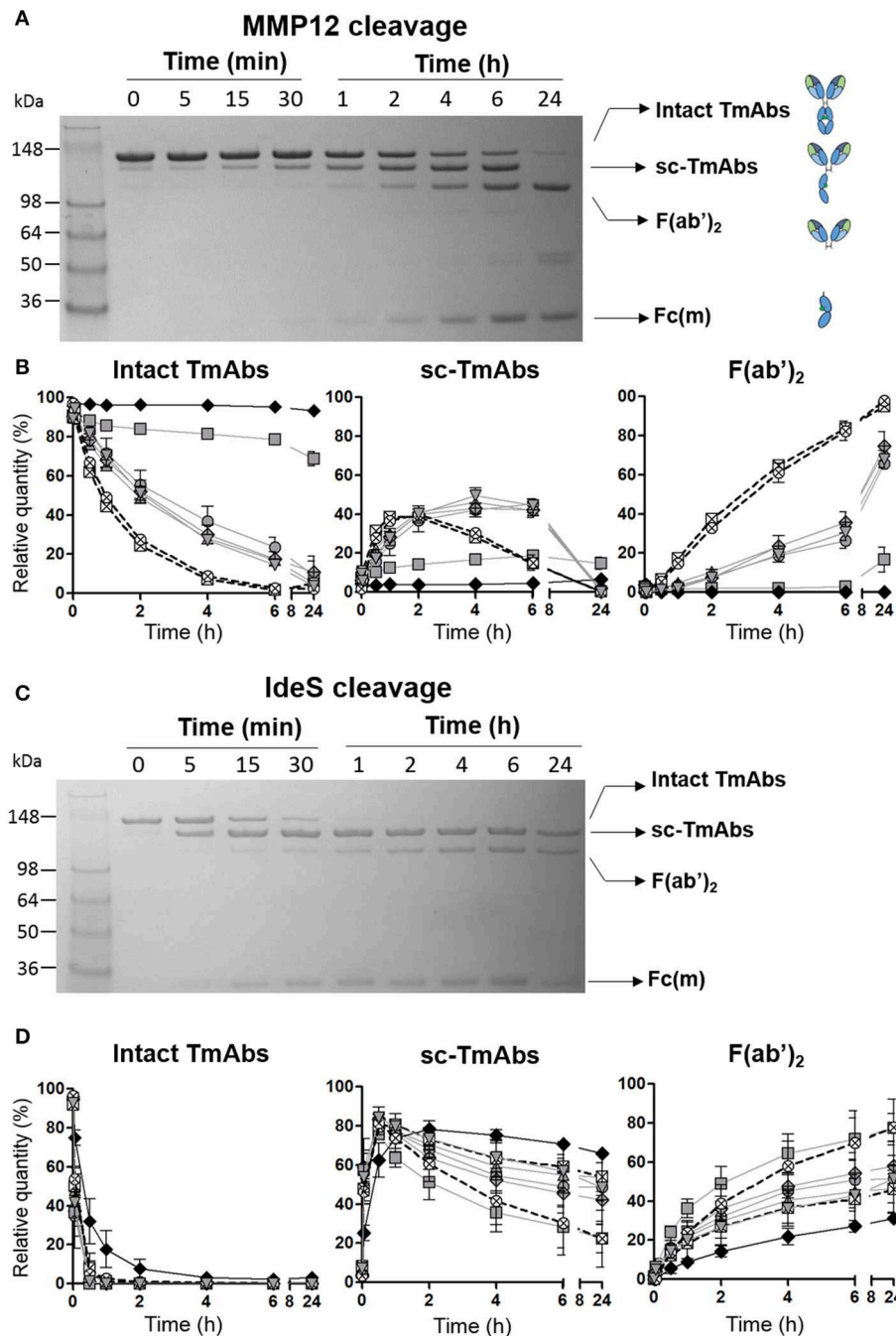


FIGURE 1 | Cleavage of TmAbs by MMP12 or IdeS. Non-reducing SDS-PAGE for rituximab without or with MMP12 (A) or IdeS (C) incubation (representative example). (B,D) show the relative quantity of cleavage product: intact TmAbs (left), single-cleaved forms (middle), and F(ab')₂ (right) at different times after incubation with MMP12 (B) or IdeS (D). The eight TmAbs (IgG1 in gray line, IgG2 black line, and IgG4 dotted line) are indicated: trastuzumab (circle), cetuximab (triangle), infliximab (crossed diamond), ipilimumab (square), rituximab (inverted triangle), panitumumab (diamond), nivolumab (crossed circle), and pembrolizumab (crossed square). Each band was quantified by densitometry with ImageJ. Data are mean (SD) ($n = 3$).

leaving only $\approx 20\%$ of this form and $\approx 80\%$ of F(ab')₂ after 24 h (Figure 1D).

The five IgG1 TmAbs included the four possible G1m allotypes, that is, G1m3;1 (cetuximab), G1m3;1 (ipilimumab),

G1m17;1 (infliximab and trastuzumab), and G1m17;1 (rituximab). We wondered whether the G1m allotype could be related to the variability of IgG1 TmAbs cleavage. We compared the cleavage kinetics by MMP12 (Figure 2A) and IdeS

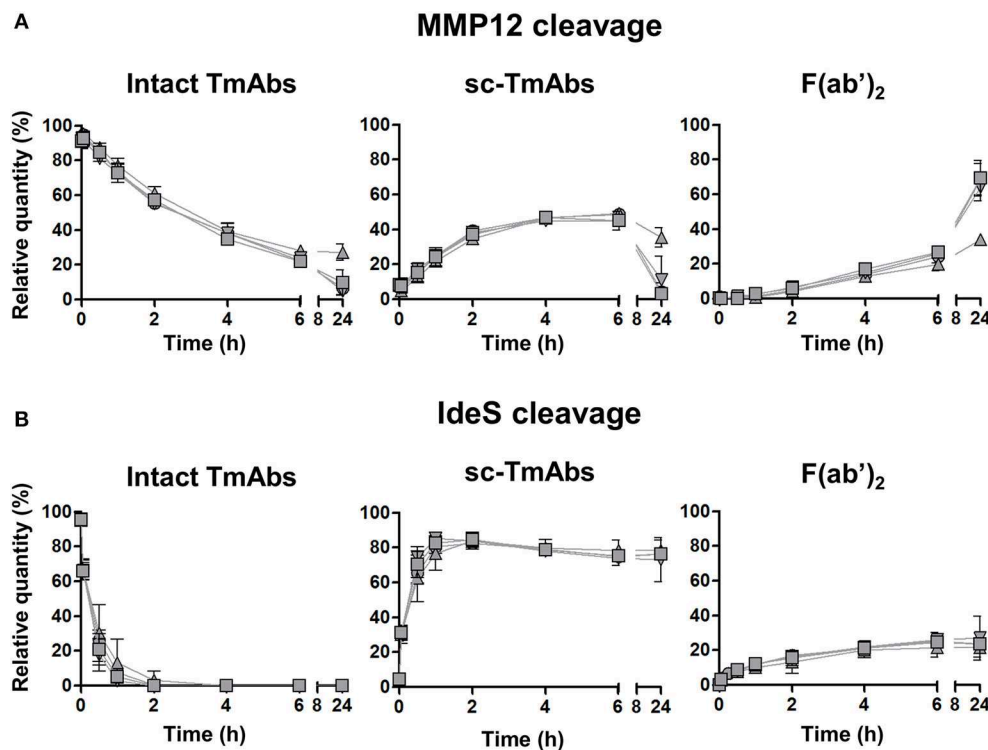


FIGURE 2 | Cleavage of rituximab allotypes by MMP12 or IdeS. The relative quantity of intact TmAbs (left panel), single-cleaved forms (middle panel) and F(ab')₂ (right panel) of the four allotypes based on the rituximab format G1m3;-1 (inverted triangle), G1m3;1 (square), G1m17;-1 (circle) or G1m17;1 (triangle) after incubation with MMP12 (A) or IdeS (B), as described in Figure 1. Data are mean (SD) ($n = 3$).

(Figure 2B) of the four allotypes constructed on the rituximab structure. Their general profiles were very similar to those of IgG1 TmAbs excluding ipilimumab. The cleavage kinetics of the four allotypes by IdeS was superimposable, as was that with MMP12 until 6 h. After 24 h, we detected 27% of the G1m17;1 intact form vs. only 5–10% of the other mAbs (Figure 2A, left panel). Accordingly, the amount of both sc-mAbs and F(ab')₂ of G1m17;1 was reduced (Figure 2A, middle and right). The results show the limited influence of the G1m allotype on the MMP12- and IdeS-mediated cleavage of mAbs.

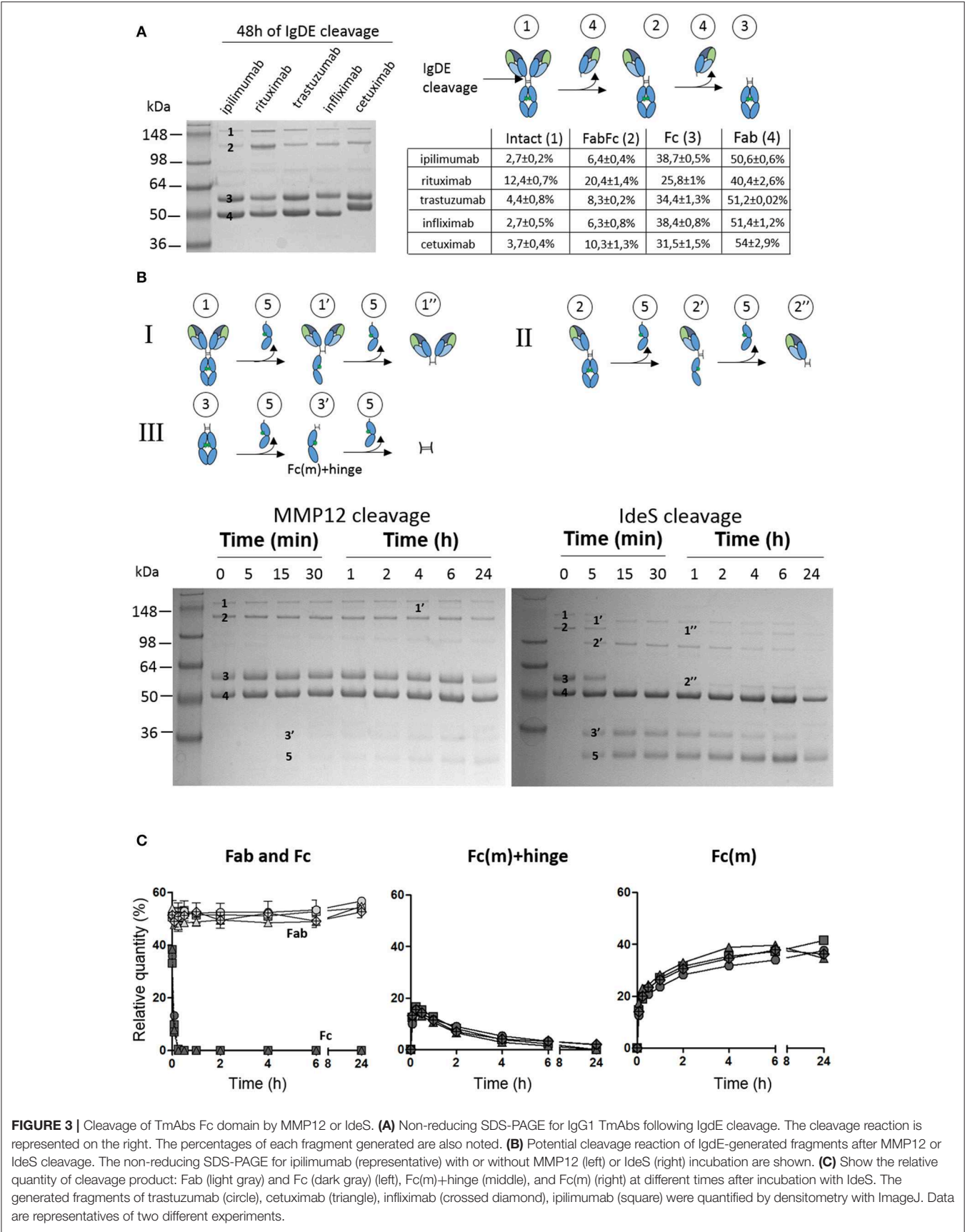
Overall, the ranking of MMP12- and IdeS-mediated TmAbs cleavage (IgG4 TmAbs > IgG1 TmAbs > ipilimumab > IgG2 TmAb and nivolumab=ipilimumab > IgG1 TmAbs ≥ pembrolizumab > IgG2 TmAb, respectively) clearly differed, which shows that the proteolytic profile of a TmAb on incubation with a given protease may differ from that of other TmAbs of the same subclass.

MMP12 and IdeS-Mediated Cleavage of IgG1 TmAbs Fc Fragment

We then wondered whether the variability of IgG1 TmAbs cleavage could be related to their Fc portion. To this end, IgG1 TmAbs were firstly incubated for 48 h with Igde, which cleaves the upper hinge region (19), followed by MMP12 and IdeS cleavage. The fragments obtained after Igde cleavage were analyzed as described in Figures 1, 2. We observed four bands

for each TmAbs: one ≈148 kDa (intact TmAbs), one ≈120 kDa corresponding to the cleavage of the first HC upper hinge region by Igde (FabFc), one ≈55 kDa corresponding to the cleavage of the second HC upper hinge region (Fc) and finally one ≈50 kDa corresponding to the Fab (Figure 3A left). It is of note that cetuximab Fab domains are glycosylated explaining the slightly higher MW of its Fab compared to other IgG1 TmAbs. The intensity of the Fab and Fc bands was substantially higher than that of intact TmAbs or FabFc bands, whatever the TmAbs, showing that Igde cleaved the upper hinge region efficiently in our conditions. The percentage of intact/FabFc TmAbs were very low (ranging from 8 to 14%) after cleavage of ipilimumab, trastuzumab, infliximab and cetuximab, while it reached ≈30% after cleavage of rituximab. Given this discrepancy, which may be related to the A221V mutation located very close to the upper hinge region of rituximab (20), this TmAb was not included in the following experiments.

The sequential cleavage by IdeS and MMP12 of the lower hinge region of intact and FabFc TmAbs results in the production of Fc(m) associated with several fragments >50 kDa (Figure 3B, reaction I and II). Moreover, cleavage of the first HC of a Fc fragment results in the simultaneous production of Fc(m) and Fc(m)+hinge (band ≈35 kDa), whereas cleavage of the second HC results in the disappearance of the latter and production of Fc(m) (Figure 3B, reaction III). Given that Fc(m) may result from cleavage of intact TmAbs, FabFc or Fc fragment, its



monitoring is obviously insufficient to evaluate the cleavage of the Fc. However, the first and second cleavage of the Fc portion may be accurately monitored by evaluating the intensity over time of the Fc and Fc(m)+hinge bands, respectively.

Using this approach, we unexpectedly found that the intensity of the Fc band was almost unchanged over time after MMP12 incubation. Accordingly, almost no Fc(m)+hinge was observed even after 24 h of incubation, whatever the TmAb (the example of ipilimumab is shown in **Figure 3B**, left). This result demonstrates the inability of MMP12 to cleave the Fc fragment of the four tested IgG1 TmAbs. By contrast, the Fc decreased very rapidly and disappeared after 15 min on incubation with IdeS. This was associated with a simultaneous rapid increase of Fc(m)+hinge and Fc(m) (reflecting the cleavage of the first HC). It was followed after 30 min by the progressive decrease (and disappearance at 24 h) of the Fc(m)+hinge and increase of the Fc(m) (reflecting the cleavage of the second HC). We then compared the cleavage kinetics of the four IgG1 TmAbs (**Figure 3C**). The amount of Fab was unchanged over 24 h showing that the IgD remaining in the medium did not further cleave the Fab-containing fragments (**Figure 3C**, left panel). Interestingly, the cleavage kinetic of the Fc by IdeS was very similar to that observed with intact IgG1 TmAbs excluding ipilimumab (shown in **Figure 1D**): the cleavage of the first HC was almost completed after ≈ 15 min [all Fc were converted in Fc(m)+hinge and Fc(m)], while the cleavage of the second HC was slower, increasing progressively from ≈ 30 min up to 24 h (reflected by the simultaneous decrease from ≈ 20 to 0% of Fc(m)+hinge and increase from ≈ 20 to 35–40% of Fc(m) (**Figure 3C** middle and right panel). Finally, and importantly, the cleavage kinetics of the four IgG1 TmAbs tested, including ipilimumab, were superimposable.

Overall, these results show that ipilimumab Fc fragment and that of trastuzumab, cetuximab, and infliximab were cleaved similarly by IdeS, whereas MMP12 was inefficient in our conditions.

Effect of a Single Cleavage of TmAbs on Binding to Membrane Fc γ RIIIA and Fc γ RIIIA-Dependent Functional Responses of NK Cells

We then compared the effect of single cleavage on binding of the TmAbs to the Fc γ RIIIA expressed on NK cells. We measured the inhibition of the FITC-conjugated anti-CD16 mAb (3G8) binding to Fc γ RIIIA/CD16⁺ NK92 cells by the intact TmAbs and sc-TmAbs. Intact IgG2 and IgG4 TmAbs poorly competed with binding of the 3G8 (**Figure 4A**, left), which shows their extremely weak binding to membrane Fc γ RIIIA. Accordingly, we did not detect an effect of the cleavage on Fc γ RIIIA binding, because the curves obtained with sc-TmAbs and their respective intact forms were similar. The inhibition curves revealed that the five intact IgG1 TmAbs bound efficiently to Fc γ RIIIA (**Figure 4A**, right). The curves were similar, starting at 0.03 mg/mL and reached maximal inhibition ($\approx 80\%$) at 3 mg/mL. The binding of the single-cleaved IgG1 TmAbs was substantially reduced because the inhibition was detected at 0.3 mg/mL and reached

an upper limit (at 3 mg/mL) of 35–60% depending on the TmAbs (**Figure 4A**, right).

We then compared the ability of sc-TmAbs to trigger NK functional responses upon Fc γ RIIIA engagement. Given the lack of a cell expressing all antigens (at similar level) recognized by the eight TmAbs, we could not compare the functional responses in a target cell-based assay (such as ADCC). Therefore, we used a target cell-independent assay with Fc γ RIIIA-expressing NK92 cells incubated in plates sensitized overnight with a saturating concentration of intact or sc-TmAbs and analyzed by flow cytometry (**Figure 4B**, row 1). In accordance with their low affinity for Fc γ RIIIA, degranulation and IFN γ production were low after incubation with intact or single-cleaved forms of IgG2 and IgG4 TmAbs (**Figure 4B**, row 2 and 3). By contrast, incubation with intact IgG1 TmAbs resulted in substantial responses. The percentages of responding cells were decreased (4–5-fold lower) after incubation with the corresponding single-cleaved forms (**Figure 4B**, row 4 and 5).

Effect of a Single Cleavage of TmAbs on C1q Binding

We then compared the effect of single cleavage of the eight TmAbs on the binding of C1q. We used an ELISA method with increasing concentrations of C1q added to plates sensitized with intact or single-cleaved TmAbs. The binding of C1q to intact or single-cleaved forms of IgG2 and IgG4 TmAbs was, as expected, extremely weak, detected at C1q > 2 mg/mL (**Figure 5**, left). Conversely, we detected C1q binding to the intact IgG1 TmAbs at C1q ≥ 0.2 mg/mL and peaking at ≈ 10 mg/mL (**Figure 5**, right). The binding of C1q to rituximab was slightly higher of its binding to the other IgG1 TmAbs. The binding of C1q to the single-cleaved IgG1 TmAbs was similar and was decreased by about 10-fold as compared with the binding to their intact counterpart. In this case, the binding was detected at C1q ≥ 3 mg/mL without reaching a maximum even at C1q ≥ 20 mg/mL.

DISCUSSION

To the best of our knowledge, this study is the first to compare kinetically the cleavage of the lower hinge region of a panel of TmAbs. Our results clearly demonstrate that TmAbs with the IgG1 and IgG4 format are both MMP12- and IdeS-sensitive, whereas a TmAb with an IgG2 format was more resistant. Comparing ipilimumab to the other IgG1 TmAbs or pembrolizumab to nivolumab showed that their cleavage kinetics on incubation with a given protease differed substantially and different ranking with IdeS and MMP12 incubation. Moreover, our results indicate that the specific cleavage kinetics of ipilimumab were unrelated to its allotype and did not extend to its Fc portion. We have also shown that the affinity for C1q and Fc γ RIIIA of all IgG1 TmAbs decreased greatly after a single cleavage, reaching the level observed with IgG2 or IgG4 TmAbs. Accordingly, IgG1 sc-TmAbs lost their Fc γ RIIIA-dependent functional responses. Our results show that the cleavage kinetics by proteases present in pathological microenvironments should be considered in the design and development of TmAbs.

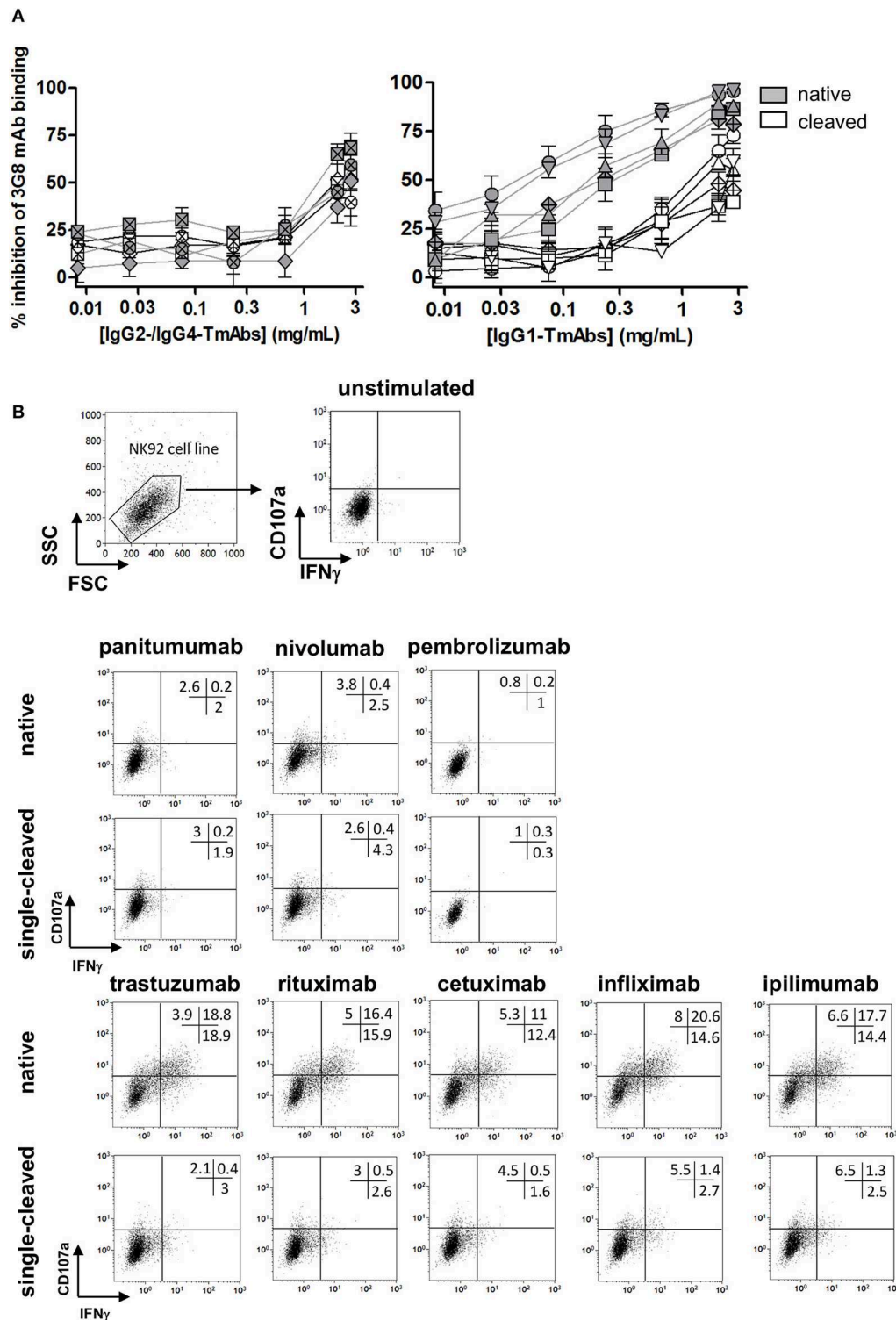


FIGURE 4 | Binding of sc-TmAbs to Fc γ RIIIA-transduced NK92 cells and Fc γ RIIIA-dependent functional responses. **(A)** Binding of cleaved or intact IgG2/IgG4 TmAbs (left) or IgG1 TmAbs (right) to Fc γ RIIIA-transduced NK92 cells. Percentage inhibition of 3G8 binding was analyzed as described previously (18). The eight TmAbs were used: trastuzumab (circle/TTZ), cetuximab (triangle/CTX), infliximab (crossed diamond/IFX), ipilimumab (square/IPI), rituximab (inverted triangle/RTX), panitumumab (diamond/PAN), nivolumab (crossed circle/NIV), and pembrolizumab (crossed square/PEM). **(B)** Gating strategy and flow cytometry analysis of Fc γ RIIIA-transduced NK92 cells incubated in the absence or presence of intact or cleaved plate-bound IgG2 or IgG4 TmAbs (row 2 and 3) or IgG1 TmAbs (row 4 and 5). The percentages of degranulation and IFN γ -producing cells are shown. Results are representative of three different experiments.

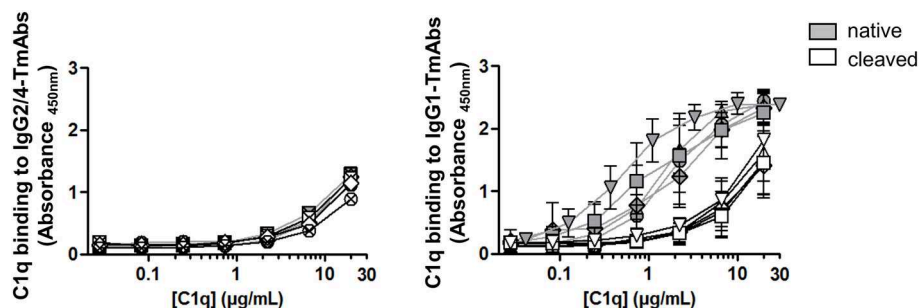


FIGURE 5 | C1q binding on sc-TmAbs. ELISA of C1q binding for the eight TmAbs: trastuzumab (circle), cetuximab (triangle), infliximab (crossed diamond), ipilimumab (square), rituximab (inverted triangle), panitumumab (diamond), nivolumab (crossed circle), and pembrolizumab (crossed square). C1q concentrations from 0.01 to 30 $\mu\text{g/mL}$ were incubated in plates sensitized with intact or single-cleaved TmAbs at saturating concentration. Horseradish peroxidase-conjugated anti-C1q was added to each well, then TMB as a substrate after 1 h, and absorbance was read at 450 nm. Data are mean (SD) for binding on IgG2/IgG4 TmAbs (left) or IgG1 TmAbs (right) ($n = 3$).

Several previous studies have shown that monoclonal IgG2 were almost completely resistant to cleavage by MMPs (11, 14). By contrast, their first HC was cleaved by IdeS, whereas the cleavage of their second HC was incomplete, as revealed by the simultaneous presence of sc-IgG2 and F(ab')_2 after 24 h of incubation (11). Our results confirmed that the IgG2 mAb panitumumab was MMP12-resistant and that the cleavage of its second HC by IdeS was reduced as compared with that of the other TmAbs. We could not compare different IgG2 TmAbs in our study and therefore cannot state that this is a general feature of these molecules. Replacing amino acids from an IgG1 hinge region with those of an IgG2 led to protease resistance (14), so the relative resistance of IgG2 is probably mainly, if not exclusively, dependent on the specific sequence of its lower hinge region.

All the other TmAbs we tested were cleaved, although at different levels by IdeS and MMP12. The cleavage kinetics of the two proteases differed. Indeed, as previously described, IdeS cleaved the first heavy HC extremely rapidly. F(ab')_2 was observed afterward, which indicates that the cleavage of the second HC occurred mainly on sc-TmAbs (21). Furthermore, this second cleavage was slow and incomplete even after 24 h. By contrast, MMP12 cleaved the first HC more slowly, and sc-TmAbs and F(ab')_2 were at a similar level at 4–6 h, which indicates that the cleavage of the two HCs occurred simultaneously. In addition, sc-TmAbs were no longer detected after 24 h (except for ipilimumab), so the cleavage of the second HC was faster and more complete than that observed with IdeS. In addition, we observed two additional bands at 24 h when IgG1 TmAbs were incubated with MMP12. These bands were detected after sc-TmAbs disappeared. They probably correspond to a third cleavage occurring on the F(ab')_2 in the upper hinge region (data not shown). Therefore, MMP12 can cleave the upper hinge region in the absence of the Fc region (Figure 1), whereas it was unable to cleave the lower hinge region in the absence of Fab (as shown in Figure 3 by the very low cleavage of the Fc portion of IgG1 TmAbs). Conversely, it has been proposed that IdeS interacts with the CH2 domain, before cleaving the hinge (8). This is in accordance with our finding that IdeS cleaved the Fc portion and the intact form of IgG1 TmAbs (excluding

ipilimumab) with very similar kinetic (Figures 1D, 3D). Hence, our results indicate that IdeS and MMP12 have a different site of interactions with IgG leading to different kinetics.

Using both proteases, we compared the cleavage of five IgG1 and two IgG4 TmAbs. Ryan et al. suggested that IgG1 and IgG4 mAbs were similarly susceptible to MMP3 and IdeS cleavage (6), and the latter has been shown to cleave IgG4 down to F(ab')_2 (22). Our results showed that the two IgG4 TmAbs tested were cleaved by MMP12 and IdeS. However, pembrolizumab and nivolumab were poorly and very strongly cleaved by IdeS, respectively, whereas both were highly cleaved by MMP12 (and more rapidly than all the IgG1 TmAbs tested). Thus, the sensitivity/resistance of TmAbs with the IgG4 format may differ substantially depending on the TmAb and the protease. Both TmAbs have the S228P mutation (6), which rules out that this structural characteristic may explain their differences in cleavage. The crystallographic resolution of pembrolizumab showed that one CH2 domain was rotated $\sim 120^\circ$ as compared with other known mAbs and the authors suggested that this new conformation may not be a crystallization artifact (23). Thus, assuming that the CH2 domain rotation is actually indicative of the structure of pembrolizumab in free solution and considering that IdeS must bind to the CH2–CH3 interface to cleave the hinge region (8), it may be hypothesized that the rotated CH2 of pembrolizumab could account for its reduced IdeS-mediated cleavage. The variability in cleavage kinetics observed with IgG4 TmAbs was confirmed when comparing TmAbs with the IgG1 format. Indeed, ipilimumab was strongly MMP12-resistant and IdeS-sensitive, whereas the other four IgG1 TmAbs were cleaved with similar and intermediate kinetics by each protease. Several previous studies have reported that monoclonal IgG1 molecules are cleaved efficiently by MMP3, MMP7, MMP12, and IdeS (6, 9, 10). Our results demonstrate that this is not a general feature. Even though the amino acid composition of the lower hinge region is clearly involved in the resistance of IgG2, the sequence is the same in a given subclass (i.e., the five IgG1 TmAbs and two IgG4 TmAbs tested). Therefore, the differences in the cleavage kinetics with the IgG1 and IgG4 TmAbs are due to other characteristics.

We hypothesized that the variability observed for ipilimumab among IgG1 TmAbs was due to its G1m3;1 allotype. Indeed, we have recently shown that the IgG1 allotype affected the affinity of an mAb for the FcRn, showing that a structural variation located outside an interaction site may nevertheless affect this interaction (17). However, we observed that the four allotypes of an mAb constructed on the basis of rituximab were cleaved similarly, which suggests that this polymorphism does not account for the feature of ipilimumab. It may be assumed that the glycans present in position N297 are involved in the cleavage modulation because glycosylation can affect the cleavage of the upper hinge region of IgG by papain (24). However, the binding of TmAbs to FcγRIIIA is influenced by the glycan structure (25), whereas we found similar binding of all tested IgG1 TmAbs including ipilimumab. Moreover, our results showed that the cleavage of ipilimumab Fc fragment by IdeS was superimposable to that of the 3 other IgG1 TmAbs Fc fragment. We conclude that the variability observed for intact ipilimumab is not related to natural structural differences located within its Fc portion (including glycosylation). We therefore propose that the Fab region could affect the cleavage kinetics of a given TmAb.

Among variations of the Fab related to bioengineering, the type of humanization could be important. In line with this assumption, ipilimumab was the sole fully human IgG1 tested in our study, whereas the other IgG1 TmAbs were chimeric or humanized. The fact that nivolumab and ipilimumab, which are both fully human TmAbs, were cleaved with opposite kinetics by MMP12 indicates that this type of engineering is not associated with a given cleavage sensitivity/resistance profile. Overall, our results confirm that the cleavage sensitivity/resistance by proteases might mainly depend on the subclass when comparing IgG2 vs. IgG1 or IgG4 TmAbs. They demonstrate for the first time a variability in this sensitivity/resistance balance among TmAbs of IgG1 and IgG4 subclasses, which likely results from TmAb characteristics probably related to and/or located in the Fab region and may be at least partially specific to a given TmAb.

The functional consequences of the proteolytic cleavage have been broadly studied with mAbs including TmAbs such as trastuzumab or pertuzumab, in *in vitro* and *in vivo* models (12, 13). We explored the ability of the eight TmAbs to bind to the membrane form of FcγRIIIA. A single cleavage decreased the binding, whatever the tested IgG1 TmAbs, in accordance with the results reported with trastuzumab by using ELISA with recombinant FcγR (12). Consequently, IgG1 sc-TmAbs were not able to induce FcγRIIIA-dependent IFNγ production and degranulation by NK92 cells on stimulation with plate-bound TmAbs, as compared with their intact forms. Due to the lack of a cell expressing all antigens recognized by the TmAbs tested, we could not compare the functional responses in a target cell-based assay. We however observed that IgG2 and IgG4 TmAbs, which are inefficient to mediate ADCC or CDC due to their reduced affinity for FcγRIIIA and C1q (confirmed in our study), were also inefficient to induce degranulation or cytokine production in our target cell-independent assay, conversely to intact IgG1 TmAbs. NK-cell degranulation assessed by CD107a labeling has been widely used as a surrogate marker for cytotoxic activity (26–28) including rituximab- trastuzumab- or cetuximab-mediated

ADCC directed against target cell lines expressing CD20, Her-2 or EGFR, respectively. The fact that IgG1 sc-TmAbs were inefficient as compared to intact forms in our assay, strongly suggest that the lack of activation would extend to functional responses (such as depletion) observed in target cell dependent assays. FcγRIIIA expression is not restricted to human NK cells. Several FcγRIIIA-expressing myeloid cells, including a subset of monocytes, macrophages, and neutrophils (at low levels) (29, 30) co-express FcγRIIIA. Both receptors are involved in myeloid cell-mediated functions such as ADCC, antibody-dependent cellular phagocytosis (ADCP) and trogocytosis (31–33). Several lines of evidence indicate that myeloid cells contribute substantially to the mechanism of action of cytolytic tmAbs [reviewed in (34)]. Indeed, targeting the myeloid-specific immune checkpoint CD47/SIRP-α pathway, triggers ADCP mediated by anti-CD20 and anti-Her2 mAbs *in vitro* and results in increased antitumor activity of TmAbs in diverse mouse models. The H131R polymorphism of *FCGR2A* gene encoding FcγRIIA, (whose expression is restricted to myeloid cells), is associated with patient responses to rituximab (lymphoma), cetuximab (colon cancer), and trastuzumab (breast cancer). Finally, a high tumor-associated macrophage infiltration is associated with favorable outcome in follicular lymphoma and breast cancer patients treated with rituximab and trastuzumab, respectively. Our results confirmed that the cleavage of a single H dramatically reduced the binding of IgG1 TmAbs to FcγRIIIA. It has been reported that it decreased similarly the binding to FcγRIIA and partially abrogated FcγRIIA-dependent functions induced by TTZ (12). Therefore, it may be assumed that the reduced FcγRIIIA-dependent functions mediated by NK cells reported herein with IgG1 sc-TmAbs, probably extend to FcγRIIIA- and FcγRIIA-dependent functions mediated by myeloid cells. This assumption is sustained by the fact that peripheral blood mononuclear cells (instead of NK cells) were used as effector cells, in the previous studies showing the reduced lysis mediated by sc-TmAbs compared with intact TmAbs (12, 13). Further studies are warranted to evaluate specifically the impact of the cleavage on FcγRIIA-mediated function such as ADCP. In addition, we observed impaired binding of C1q to IgG1 sc-TmAbs, which further suggests that the lower hinge cleavage may be an escape mechanism in cytolytic mAbs therapy.

The impact of the cleavage in TmAbs-based therapies is presently unknown. The cleavage of trastuzumab or pertuzumab has been associated with a weakened therapeutic effect in mouse xenograft tumor model (12, 13). In humans, increased tumor sc-IgGs were found to be associated with poor breast cancer patient outcomes (35) and high levels of MMP3-/MMP12-cleaved IgG were detected in sera from inflammatory bowel diseases patients, who did not respond to anti-TNFα therapy (10). These studies suggest that proteolytic degradation may contribute to compromised humoral immunity and/or non-responsiveness of patients to TmAbs. It is however of note that sc-IgG were detected in these studies, whereas, to the best of our knowledge, the presence of cleaved TmAbs in patients has not been reported so far. Our results underline the need to develop new assays to measure the levels of cleaved TmAbs *in vivo*, in order to evaluate/monitor the importance of the proteolytic

cleavage in their efficiency. The loss of interaction with immune effectors by IgG1 TmAbs after a single cleavage showed that this subclass loses its advantage over IgG2 or IgG4 TmAbs in terms of cytolytic activity. Ipilimumab, whose antitumor effect depends on the Fc region (although it is an antagonist) (36) was almost uncleaved by a relevant protease such as MMP12. The IgG2 or IgG4 format is favored in the case of neutralizing/antagonist TmAbs, which do not require Fc-mediated functions. However, a second cleavage producing F(ab')₂ would negatively affect the pharmacokinetics of these antibodies, which would be eliminated more quickly because of an absence of binding to FcRn. With these potential consequences, our results show the need to study each TmAb in the relevant protease microenvironment to assess its susceptibility/resistance balance. Even though non-cleavable structures are being developed by mutating the hinge region (14), we show that a natural format can resist the cleavage without structure modification. A better understanding of this phenomenon is required to limit the escape mechanism in TmAbs-treated patients.

DATA AVAILABILITY STATEMENT

All datasets generated for this study are included in the article/supplementary material.

REFERENCES

- Sondermann P, Huber R, Oosthuizen V, Jacob U. The 3.2-Å crystal structure of the human IgG1 Fc fragment–FcγRIII complex. *Nature*. (2000) 406:267–73. doi: 10.1038/35018508
- Ugurlar D, Howes SC, de Kreuk B-J, Koning RI, de Jong RN, Beurskens FJ, et al. Structures of C1-IgG1 provide insights into how danger pattern recognition activates complement. *Science*. (2018) 359:794–7. doi: 10.1126/science.aao4988
- Vidarsson G, Dekkers G, Rispens T. IgG subclasses and allotypes: from structure to effector functions. *Front. Immunol.* (2014) 5:520. doi: 10.3389/fimmu.2014.00520
- Porter RR. The hydrolysis of rabbit γ-globulin and antibodies with crystalline papain. *Biochem J.* (1959) 73:119–26. doi: 10.1042/bj0730119
- Nisonoff A, Wissler FC, Lipman LN. Properties of the major component of a peptic digest of rabbit antibody. *Science*. (1960) 132:1770–1. doi: 10.1126/science.132.3441.1770
- Ryan MH, Petrone D, Nemeth JF, Barnathan E, Björck L, Jordan RE. Proteolysis of purified IgGs by human and bacterial enzymes *in vitro* and the detection of specific proteolytic fragments of endogenous IgG in rheumatoid synovial fluid. *Mol Immunol.* (2008) 45:1837–46. doi: 10.1016/j.molimm.2007.10.043
- Gearing AJH, Thorpe SJ, Miller K, Mangan M, Varley PG, Dudgeon T, et al. Selective cleavage of human IgG by the matrix metalloproteinases, matrilysin and stromelysin. *Immunol Lett.* (2002) 81:41–8. doi: 10.1016/S0165-2478(01)00333-9
- Vincent B, von Pawel-Rammingen U, Björck L, Abrahamson M. Enzymatic characterization of the streptococcal endopeptidase, ides, reveals that it is a cysteine protease with strict specificity for igg cleavage due to exosite binding†. *Biochemistry*. (2004) 43:15540–9. doi: 10.1021/bi048284d
- Brezski RJ, Vafa O, Petrone D, Tam SH, Powers G, Ryan MH, et al. Tumor-associated and microbial proteases compromise host IgG effector functions by a single cleavage proximal to the hinge. *Proc Natl Acad Sci USA*. (2009) 106:17864–9. doi: 10.1073/pnas.0904174106
- Biancheri P, Brezski RJ, Di Sabatino A, Greenplate AR, Soring KL, Corazza GR, et al. Proteolytic cleavage and loss of function of biologic

AUTHOR CONTRIBUTIONS

QD, LL, and BB designed and performed the experiments. QD, LL, BB, and GT analyzed the results. QD, LL, and GT wrote the manuscript. LL and GT supervised the study design and GT supervised the study conception. All authors critically revised the work, provided substantial input, and gave final approval to the version to be published.

FUNDING

This study was supported by the program Investissements d'Avenir (Grant Agreement No. LabEx MABImprove ANR-10-LABX-53-01). This work was supported by the program ARD2020 Biomédicaments (Project BIO-S) and the French Ministry of Higher Education and Research as part of the Investissements d'Avenir program: LabEx MABImprove ANR-10-LABX-53-01.

ACKNOWLEDGMENTS

The authors thank Christine Dhomme and Laura Gisell Diaz Margarin for the technical assistance. The authors also thank Dr. Valérie Gouilleux-Gruart for the valuable discussions.

- agents that neutralize tumor necrosis factor in the mucosa of patients with inflammatory bowel disease. *Gastroenterology*. (2015) 149:1564–74.e3. doi: 10.1053/j.gastro.2015.07.002
- Brezski RJ, Oberholtzer A, Strake B, Jordan RE. The *in vitro* resistance of IgG2 to proteolytic attack concurs with a comparative paucity of autoantibodies against peptide analogs of the IgG2 hinge. *MAbs*. (2011) 3:558–67. doi: 10.4161/mabs.3.6.18119
- Fan X, Brezski RJ, Fa M, Deng H, Oberholtzer A, Gonzalez A, et al. A single proteolytic cleavage within the lower hinge of trastuzumab reduces immune effector function and *in vivo* efficacy. *Br Cancer Res.* (2012) 14:R116. doi: 10.1186/bcr3240
- Hsiao H-C, Fan X, Jordan RE, Zhang N, An Z. Proteolytic single hinge cleavage of pertuzumab impairs its Fc effector function and antitumor activity *in vitro* and *in vivo*. *Br Cancer Res.* (2018) 20:43. doi: 10.1186/s13058-018-0972-4
- Kinder M, Greenplate AR, Grugan KD, Soring KL, Heeringa KA, McCarthy SG, et al. Engineered protease-resistant antibodies with selectable cell-killing functions. *J Biol Chem.* (2013) 288:30843–54. doi: 10.1074/jbc.M113.486142
- Labrijn AF, Buijsse AO, van den Bremer ETJ, Verwilligen AYW, Bleeker WK, Thorpe SJ, et al. Therapeutic IgG4 antibodies engage in Fab-arm exchange with endogenous human IgG4 *in vivo*. *Nat Biotechnol.* (2009) 27:767–71. doi: 10.1038/nbt.1553
- Brezski RJ, Kinder M, Grugan KD, Soring KL, Carton J, Greenplate AR, et al. A monoclonal antibody against hinge-cleaved IgG restores effector function to proteolytically-inactivated IgGs *in vitro* and *in vivo*. *MAbs*. (2014) 6:1265–73. doi: 10.4161/mabs.29825
- Ternant D, Arnoult C, Pugnière M, Dhomme C, Drocourt D, Perouzel E, et al. IgG1 allotypes influence the pharmacokinetics of therapeutic monoclonal antibodies through FcRn binding. *J Immunol.* (2016) 196:607–13. doi: 10.4049/jimmunol.1501780
- Vincent M, Bessard A, Cochonneau D, Teppaz G, Solé V, Maillason M, et al. Tumor targeting of the IL-15 superagonist RLI by an anti-GD2 antibody strongly enhances its antitumor potency: RLI-based immunocytokine targeting GD2. *Int J Cancer.* (2013) 133:757–65. doi: 10.1002/ijc.28059
- Spoerry C, Hesse P, Lewis MJ, Paton L, Woof JM, von Pawel-Rammingen U. Novel IgG-degrading enzymes of the Igde protease family link substrate

- specificity to host tropism of streptococcus species. *PLoS ONE*. (2016) 11:e0164809. doi: 10.1371/journal.pone.0164809
20. Wang B, Gucinski AC, Keire DA, Buhse LF, Boyne II MT. Structural comparison of two anti-CD20 monoclonal antibody drug products using middle-down mass spectrometry. *Analyst*. (2013) 138:3058. doi: 10.1039/c3an36524g
 21. Vindebro R, Spoerry C, von Pawel-Rammingen U. Rapid IgG heavy chain cleavage by the streptococcal IgG endopeptidase IdeS is mediated by IdeS monomers and is not due to enzyme dimerization. *FEBS Lett*. (2013) 587:1818–22. doi: 10.1016/j.febslet.2013.04.039
 22. Falkenburg WJJ, van Schaardenburg D, Ooijevaar-de Heer P, Tsang-A-Sjoe MWP, Bultink IEM, Voskuyl AE, et al. Anti-hinge antibodies recognize IgG subclass- and protease-restricted neopeptides. *J Immunol*. (2017) 198:82–93. doi: 10.4049/jimmunol.1601096
 23. Scapin G, Yang X, Prosser WW, McCoy M, Reichert P, Johnston JM, et al. Structure of full-length human anti-PD1 therapeutic IgG4 antibody pembrolizumab. *Nat Struct Mol Biol*. (2015) 22:953–8. doi: 10.1038/nsmb.3129
 24. Raju TS, Scallan BJ. Glycosylation in the Fc domain of IgG increases resistance to proteolytic cleavage by papain. *Biochem Biophys Res Commun*. (2006) 341:797–803. doi: 10.1016/j.bbrc.2006.01.030
 25. Li T, DiLillo DJ, Bournazos S, Giddens JP, Ravetch JV, Wang L-X. Modulating IgG effector function by Fc glycan engineering. *Proc Natl Acad Sci USA*. (2017) 114:3485–90. doi: 10.1073/pnas.1702173114
 26. Alter G, Malenfant JM, Altfeld M. CD107a as a functional marker for the identification of natural killer cell activity. *J Immunol Methods*. (2004) 294:15–22. doi: 10.1016/j.jim.2004.08.008
 27. Bryceson YT, March ME, Barber DF, Ljunggren H-G, Long EO. Cytolytic granule polarization and degranulation controlled by different receptors in resting NK cells. *J Exp Med*. (2005) 202:1001–12. doi: 10.1084/jem.20051143
 28. Zhou Q, Gil-Krzeska A, Peruzzi G, Borrego F. Matrix metalloproteinases inhibition promotes the polyfunctionality of human natural killer cells in therapeutic antibody-based anti-tumour immunotherapy: MMP inhibition increases NK cell polyfunctionality. *Clin Exp Immunol*. (2013) 173:131–9. doi: 10.1111/cei.12095
 29. Bruhns P. Properties of mouse and human IgG receptors and their contribution to disease models. *Blood*. (2012) 119:5640–9. doi: 10.1182/blood-2012-01-380121
 30. Golay J, Valgardsdottir R, Musaraj G, Giupponi D, Spinelli O, Introna M. Human neutrophils express low levels of FcγRIIIA, which plays a role in PMN activation. *Blood*. (2019) 133:1395–405. doi: 10.1182/blood-2018-07-864538
 31. Graziano RF, Fanger MW. Fc gamma RI and Fc gamma RII on monocytes and granulocytes are cytotoxic trigger molecules for tumor cells. *J Immunol*. (1987) 139:3536–41.
 32. Huang Z-Y, Chien P, Indik ZK, Schreiber AD. Human platelet FcγRIIIA and phagocytes in immune-complex clearance. *Mol Immunol*. (2011) 48:691–6. doi: 10.1016/j.molimm.2010.11.017
 33. Taylor RP, Lindorfer MA. Fcγ-receptor-mediated trogocytosis impacts mAb-based therapies: historical precedence and recent developments. *Blood*. (2015) 125:762–6. doi: 10.1182/blood-2014-10-569244
 34. Mantovani A, Marchesi F, Malesci A, Laghi L, Allavena P. Tumour-associated macrophages as treatment targets in oncology. *Nat Rev Clin Oncol*. (2017) 14:399–416. doi: 10.1038/nrclinonc.2016.217
 35. Zhang N, Deng H, Fan X, Gonzalez A, Zhang S, Brezski RJ, et al. Dysfunctional antibodies in the tumor microenvironment associate with impaired anticancer immunity. *Clin Cancer Res*. (2015) 21:5380–90. doi: 10.1158/1078-0432.CCR-15-1057
 36. Ingram JR, Blomberg OS, Rashidian M, Ali L, Garforth S, Fedorov E, et al. Anti-CTLA-4 therapy requires an Fc domain for efficacy. *Proc Natl Acad Sci USA*. (2018) 115:3912–7. doi: 10.1073/pnas.1801524115

Conflict of Interest: The authors declare that the research was conducted in the absence of any commercial or financial relationships that could be construed as a potential conflict of interest.

Copyright © 2020 Deveuve, Lajoie, Barrault and Thibault. This is an open-access article distributed under the terms of the Creative Commons Attribution License (CC BY). The use, distribution or reproduction in other forums is permitted, provided the original author(s) and the copyright owner(s) are credited and that the original publication in this journal is cited, in accordance with accepted academic practice. No use, distribution or reproduction is permitted which does not comply with these terms.



A Comparison of Immunoglobulin Variable Region N-Linked Glycosylation in Healthy Donors, Autoimmune Disease and Lymphoma

Esther M. Vletter^{1,2}, Marvyn T. Koning², Hans Ulrich Scherer¹, Hendrik Veelken² and Rene E. M. Toes^{1*}

¹ Department of Rheumatology, Leiden University Medical Center, Leiden, Netherlands, ² Department of Hematology, Leiden University Medical Center, Leiden, Netherlands

OPEN ACCESS

Edited by:

Jean Harb,
INSERM U1064 Centre de Recherche
en Transplantation et
Immunologie, France

Reviewed by:

Martin Bachmann,
University of Bern, Switzerland
Véronique Blanchard,
Charité Medical University of
Berlin, Germany

*Correspondence:

Rene E. M. Toes
r.e.m.toes@lumc.nl

Specialty section:

This article was submitted to
B Cell Biology,
a section of the journal
Frontiers in Immunology

Received: 04 September 2019

Accepted: 29 January 2020

Published: 18 February 2020

Citation:

Vletter EM, Koning MT, Scherer HU,
Veelken H and Toes REM (2020) A
Comparison of Immunoglobulin
Variable Region N-Linked
Glycosylation in Healthy Donors,
Autoimmune Disease and Lymphoma.
Front. Immunol. 11:241.
doi: 10.3389/fimmu.2020.00241

N-linked glycans play an important role in immunity. Although the role of N-linked glycans in the Fragment crystallizable (Fc) region of immunoglobulins has been thoroughly described, the function of N-linked glycans present in Ig-variable domains is only just being appreciated. Most of the N-linked glycans harbored by immunoglobulin variable domain are of the complex biantennary type and are found as a result of the presence of N-linked glycosylation that most often have been introduced by somatic hypermutation. Furthermore, these glycans are ubiquitously present on autoantibodies observed in some autoimmune diseases as well as certain B-cell lymphomas. For example, variable domain glycans are abundantly found by anti-citrullinated protein antibodies (ACPA) in rheumatoid arthritis (RA) as well as by the B-cell receptors of follicular lymphoma (FL). In FL, variable domain glycans are postulated to convey a selective advantage through interaction with lectins and/or microbiota, whereas the contribution of variable domain glycans on autoantibodies is not known. To aid the understanding how these seemingly comparable phenomena contribute to a variety of deranged B-responses in such different diseases this study summarizes the characteristics of ACPA and other auto-antibodies with FL and healthy donor immunoglobulins, to identify the commonalities and differences between variable domain glycans in autoimmune and malignant settings. Our finding indicate intriguing differences in variable domain glycan distribution, frequency and glycan composition in different conditions. These findings underline that variable domain glycosylation is a heterogeneous process that may lead to a number of pathogenic outcomes. Based on the current body of knowledge, we postulate three disease groups with distinct variable domain glycosylation patterns, which might correspond with distinct underlying pathogenic processes.

Keywords: glycosylation, autoimmunity, lymphoma, antibodies, B-cells

INTRODUCTION

Immunoglobulins Provide Humoral Immunity

B cell antigen receptors (BCR) are rearranged at the pre-B cell stage during B-cell development, and may be present as membrane-bound B-cell receptors or as soluble immunoglobulins. Through distinction between foreign and self-antigens, immunoglobulins play a key role in the defense against infections. Immunoglobulins can initiate a variety of inflammatory effects throughout the organism, depending on e.g., the recognized target, the isotype used or the properties of the Fragment crystallizable (Fc) tail. Once a B cell has encountered antigen, the B cell becomes activated and is able to secrete the B-cell receptor, particularly after maturation to antibody-secreting plasma blasts and plasma cells, in soluble form as IgM. Upon further activation and acquisition of T cell-help, class switching from IgM to IgG, IgA, or IgE can occur, leading to the presence of antigen-specific, isotype-switched antibodies in serum and other bodily fluids (1). Of all immunoglobulins, IgG is the most prominent in serum, with a concentration of ~10 mg/mL (2, 3). IgG directly links the innate to the adaptive immune system by activating the complement system and binding to Fc receptors. Likewise, it can also mediate uptake of microbes by dendritic cells and macrophages, which transport the pathogen to secondary lymphoid organs for further initiation and activation of the adaptive immune response. Likewise, immunoglobulins can facilitate antibody-dependent cell mediated cytotoxicity (ADCC), a process in which FcγR-receptor activation leads to pathogen lysis by natural killer cells (4, 5). Furthermore, complement-dependent cytotoxicity (CDC) enhances cellular pathogen uptake for subsequent antigen presentation (5).

Addition of Glycans Shapes Immunoglobulin Function

Harboring of N-linked glycans is a result of the co-translational covalent addition of carbohydrate groups to asparagine residues in the lumen of the endoplasmic reticulum (ER). This process is primed by the presence of N-linked glycosylation motifs, which consist of an asparagine (N), followed by any amino acid but proline, followed by serine (S) or threonine (T) (N-X-S/T; X≠P). Initially, a pre-formed lipid-linked glycan consisting of two N-acetylglucosamines (GlcNAc) linked to nine mannose (Man) and three glucose (Glc) residues is attached *en bloc* (dolichol-P-P-GlcNAc₂Man₉Glc₃). When the protein is subsequently transferred to the Golgi complex, glycosylhydrolases and transferases further diversify the attached glycan (Figure 1) (11). Finally, three main types of glycans can be identified (Figure 1) (12). First, a high mannose-type glycan when the terminating mannoses remain uncleaved. Second, a “complex-type glycan” which can be heterogenous and is found in over 30 different species on antibodies (Table 1) (12). Complex glycans consist of at least two “antennae” formed by presence of N-acetylglucosamine residues to the mannose core, but can also express three-or four antennae

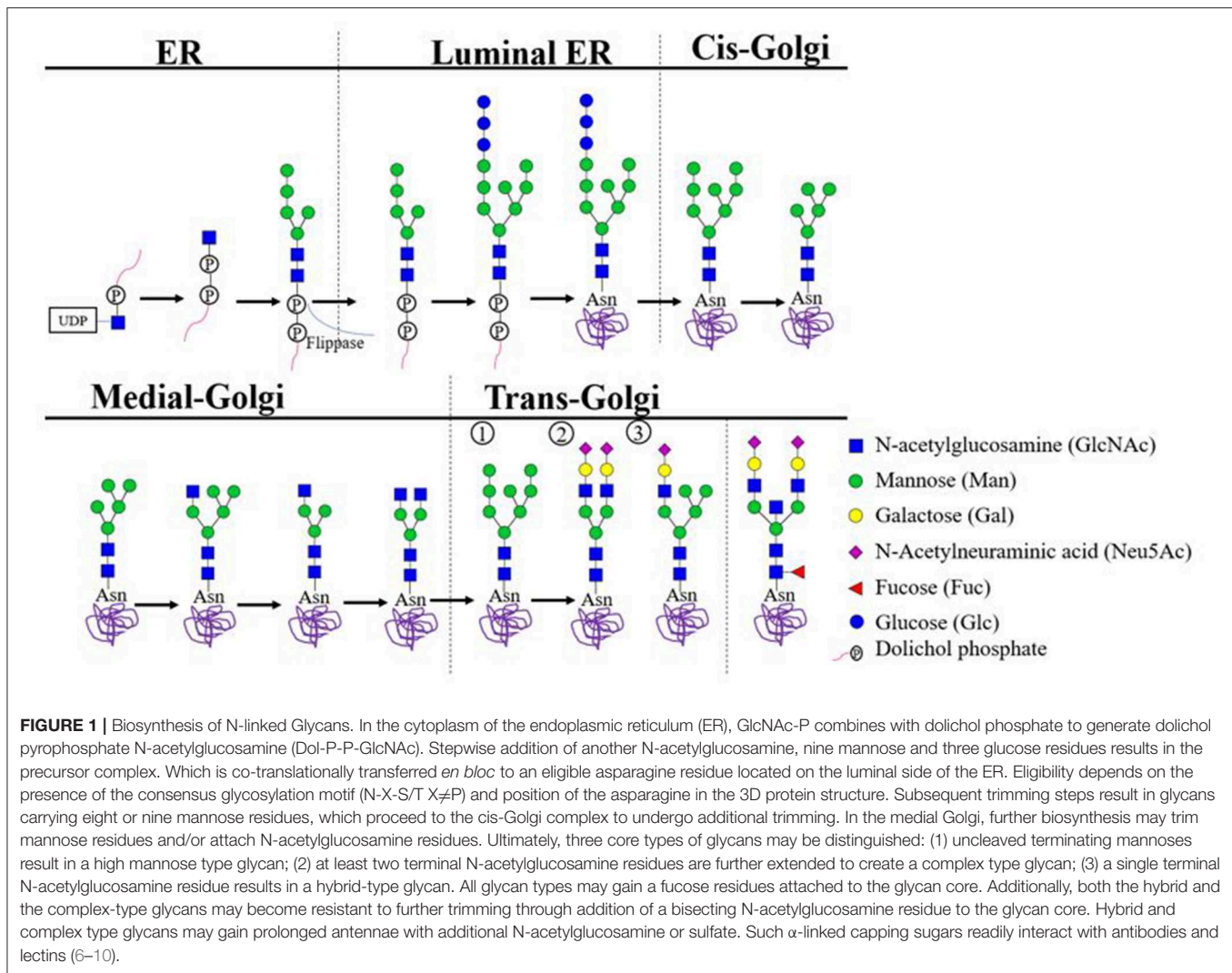
(12). These antennae can be extended through the addition of galactoses and terminal sialic acid. Furthermore, complex glycans can also contain a bisecting N-acetylglucosamine and a core fucose. The latter sugar moiety, when expressed by Fc-glycans of IgG, can mediate a strong impact on FcγR-binding (26). Third, a hybrid-type glycan which has one single terminal N-acetylglucosamine residue to which galactose and then sialic acid can be attached and one arm with mannoses (12).

Fc Glycosylation

Immunoglobulins are glycoproteins with conserved N-linked glycans in their Fc tail. For example, all IgG subclasses harbor N-linked glycans at heavy chain position N297 (27). It is becoming increasingly evident that these Fc-glycans can have major immunoregulatory functions (28, 29). For example, IgE Fc-glycosylation has been shown to play a role in allergic reactions by modulating the interaction of IgE to its Fc Receptor (30). Fc-glycan variability is relatively limited by the three-dimensional structure of the protein and peptide-glycan interactions. In addition, the limited accessibility of glycosyltransferases to the glycan mostly prevents extension of the glycan by sialylation and galactosylation (31, 32). Nevertheless, the Fc-glycans still vary greatly in composition and around 30 different glycan structures were observed for IgG, the majority of which are complex-type biantennary structures (33).

Variable Domain Glycosylation

In contrast to the ubiquitous N-linked glycosylation of the Fc-tail, only a proportion of immunoglobulins contains additional N-linked glycans in the variable domain. In the naïve human B-cell repertoire, N-linked glycosylation motifs are only present in the variable domain when rearrangements contain the V-segments IGHV1-8, IGHV4-34, or the more rarely used IGHV5-10, IGKV5-2, IGLV3-12, and IGLV3-22 (34). Additional N-linked glycosylation motifs may be found in naïve B cells when junctional diversity creates novel motifs in the complementary-determining region 3 (CDR3). Whereas, the influence of conserved N-linked glycans on the Fc tail effector functions is becoming increasingly well-understood (13, 21, 35–37), N-linked glycosylation of the antigen-binding fragment (Fab) arms, responsible for antigen binding, has been less studied (13, 29). As a consequence, the mechanisms and functions of variable domain glycosylation are less well-understood as compared to Fc glycosylation for which the immune-related impact and immune modulatory effects are well defined (38–41). For example, different IgG Fc-glycoforms can influence Fcγ-Receptor binding, and thereby control the activation of e.g., FcγRIII-expressing immune cells by immune complexes (42). Some Fc-glycoforms, expressing high levels of sialic acid-residues, have even been described to display anti-inflammatory effects, thereby contributing to the control of inflammation and inflammatory processes (26, 43). Nevertheless, it is highly conceivable that also variable domain glycosylation can have an impact on immune function since it is abundantly present in both autoimmune diseases and certain B-cell lymphomas (18–20, 22, 24, 44–47).



General Glycan Composition

The type of glycans present in the Fc-part and the Fab-part can differ considerably. Fc glycans show increased degrees of fucosylation as compared to variable domain glycans. Conversely, variable domain glycans are more often galactosylated, bisected, and sialylated, putatively due to the Fc glycan being shielded in between two heavy chains in the quaternary immunoglobulin protein structure, decreasing its accessibility for the glycosyltransferases responsible for the complex glycan structures (14). In contrast, the variable domain of antibodies is more likely to be exposed when traversing the Golgi complex, leading to more fully matured glycans. However, due to the inherently diverse nature of the variable domain, local changes due to differential VDJ usage and somatic hypermutation may result in varying local differences to enzyme accessibility (38). Furthermore, the influence of disease and physiological factors such as hormones, age, cytokine release, and pregnancy, may induce an altered expression of glycosyltransferases in B cells, skewing the newly attached

structures toward certain glycoforms in both the variable domain and the Fc-region alike (38, 48–50).

Variable Domain Glycosylation in Healthy Donors

Prevalence

Variable domain glycans have been estimated to be present in 15–20% of IgG immunoglobulins (combining heavy and light chain prevalence) in healthy individuals. In general, estimates from genetic analyses have been slightly lower than from protein-based strategies, such as the measurement of sialic acids to determine the presence of variable domain glycans (13, 29, 51–54). One explanation for this discrepancy, is offered by the observation that the stability of secreted immunoglobulin may be positively affected by the presence of variable domain glycans acquired during antigen-specific immune responses (thereby also potentially offering an *in vivo* selection mechanism for these antibodies) (55). As this enhanced stability would lead to an increased half-life, variable domain glycosylated serum

TABLE 1 | Overview of all the diseases mentioned and their N-linked glycan specifications.

	Frequency	Distribution	Glycan type	Proposed function
HD	15–20% (13)	CDR3	Complex (bisecting GlcNAc, sialylated) (14, 15)	
RA ACPA	>90% (13)	FR3 (16)	Complex (highly sialylated, bisecting GlcNAc, core fucose) (13)	Creates possible optimal balance
ANCA MPO	Unknown	FR3 (17)	Complex (galactosylated and mono-or di-sialylated) (18)	Impact functional and structural characteristics of the immunoglobulin
SLE	Unknown	Unknown	Unknown	
pSS anti-SS-A and/or anti-SS-B	~23% (19, 20)	FR3 (20)	Complex (20) (Sialylated)	Selection advantage
MG anti-MuSK	Unknown	Unknown	Unknown	
IgG4-RD	Unknown	Unknown	Complex (Sialylated) (21)	Unique effector function, interaction with Siglecs
FL	79–100% (22)	CDR2 (22, 23)	Mannose	Selection advantage
PCFCL	Unknown	CDR2 (24)	Unknown	
DCBCL	41% (22)	CDR3 (25)	Unknown	
BL	82% (22)	Unknown	Unknown	

HD, Healthy Donor; CDR3, Complementarity-Determining Region 3; RA, Rheumatoid Arthritis; FR3, Frame Work 3; ANCA MPO, Anti-Neutrophil Cytoplasmic Autoantibody (ANCA) Associated Vasculitis (AAV), myeloperoxidase; SLE, Systemic Lupus Erythematosus; pSS, primary Sjogren's Syndrome; SS-A, Anti-Sjögren's-syndrome-related antigen A; SS-B, Anti-Sjögren's-syndrome-related antigen B; MG, Myasthenia Gravis; MuSK, muscle-specific kinases; IgG4-RD, Immunoglobulin 4 Related Disease; FL, Follicular Lymphoma; CDR2, Complementarity-Determining Region 2; PCFCL, Primary Cutaneous Follicle Center cell Lymphoma; DCBCL, Diffuse large B-cell lymphoma; BL, Burkitt's Lymphoma.

immunoglobulins may be relatively abundant compared to their prevalence in the cellular compartment.

V Allele Distribution

Variable domain glycans were found to cluster around antigen-binding sites, suggesting that they are not randomly acquired, but rather lead to selective outgrowth of B cells (24, 53). A possible explanation is that the addition of these glycans induce a significant change in antigen affinity and binding, thereby modulating the interaction between antigen and antibody (53).

Glycan Composition

Over 90% of healthy donor IgG N-linked glycans contain a core fucose, of which the fucosylated digalactosylated form is the most abundant (14, 56). The majority of the N-linked glycans found on IgG plasma are of the complex biantennary type which are characterized by a high degree of conformational flexibility. In comparison with Fc glycans, the IgG variable domain glycans contain low percentages fucose and high percentages of sialic acids, bisecting GlcNAc and galactoses (15, 18, 57), with some differences between individuals depending on circumstances such as age and pregnancy (57). The high mannose type glycan is rare in healthy donor variable domains, estimated to represent only 4% of IgG variable domain glycans (38).

Subclass-Specific Differences

Within immunoglobulins, there are key differences found between subclasses. Recently, both IgE and IgG4 were shown to contain significantly more variable domain glycans than other isotypes (46, 54, 58). In particular, bone marrow-derived IgE was found to contain twice as many variable domain glycans

as other immunoglobulin subclasses in healthy donors (46), despite the fact that they often carried fewer mutations. IgE VDJ often retained germline-encoded N-linked glycosylation motifs and acquired additional ones at a faster pace than IgG and IgA. It has been suggested that in this way, variable domain glycosylation blocks antigen recognition sites and thereby creates a low-affinity resident IgE repertoire, which could protect against allergic reaction by occupation of Fcε receptors (54). Similarly, IgG4 contained more N-linked glycosylation motifs than IgG1-3. Indeed, the number of N-linked glycosylation motifs was similar to that found in IgE (46), which could suggest a commonality as both subclasses are known to be involved in T-helper 2 type responses.

Variable Domain Glycosylation in Autoimmune Diseases

Autoimmune diseases are characterized by an adaptive immune response against host tissues. A growing body of evidence shows an increased prevalence of autoantibody variable domain glycosylation in the context of many autoimmune diseases (59).

Immunoglobulin G4-Related Disease

In light of the differential variable domain glycosylation of immunoglobulin subclasses in healthy donors, immunoglobulin G4-related disease (IgG4-RD) represents a particularly interesting disease, as it is characterized by increased IgG4 titers. IgG4-RD is a multisystem fibroinflammatory condition, in which tumor-like masses related to organ dysfunction and tissue infiltration by IgG4⁺ plasma cells may be found in a number of anatomical locations, particularly the bile ducts (60, 61). Recently, variable domain glycosylation was found

to be increased in IgG4-RD patients in comparison to healthy controls and patients with non-IgG4-related primary sclerosing cholangitis (21). In particular, as detected by Sambucus nigra agglutinin (SNA) affinity chromatography, the presence of variable domain sialylation was increased in both IgG1 and IgG4 subclasses, even when corrected for the inherently higher N-linked glycosylation rates in IgG4 variable regions (46). This observation was corroborated by another study investigating combined variable domain and Fc-glycosylation in IgG4-RD patients (44). Although the role of increased variable domain glycosylation is unclear, it is suggested that increased variable domain sialylation could impart IgG4 immunoglobulins in the context of IgG4-RD with disease-specific immunomodulatory properties through binding of SIGLECs such as CD22 (62).

Rheumatoid Arthritis

Rheumatoid Arthritis (RA) is a destructive, autoantibody-mediated inflammatory disease of the joints which affects ~0.5–1% of the population (63, 64). The anti-citrullinated protein antibodies (ACPA), that are typically found in RA patients, target proteins that have undergone a post-translational conversion from arginine to citrulline (65). ACPA have been shown to bind their antigens with low affinity (66), and can occur in different isotype compartments including IgG, IgM, or IgA (67).

We were the first to observe the abundant presence of N-linked glycans in the variable domain of ACPA-IgG (45) and provided first evidence indicating that these glycans are introduced during somatic hypermutation and thereby could, potentially, influence the binding to citrullinated antigens. As previously mentioned, healthy control IgG contains 15–20% variable domain glycans, whereas this percentage is considerably increased in ACPA-IgG to over 90% (13). It has been postulated that these glycans modulate the antibody's interaction with citrulline. ACPA acquire this feature during affinity maturation as a consequence of somatic hypermutation. Indeed, for ACPA-IgM, no increase in variable domain glycosylation was observed (13). The latter observation is in line with the notion that T-helper cell activity is required for the generation of N-linked glycosylation-sites and hence the addition of variable domain glycans.

The ACPA-IgG variable domain glycans show high degrees of sialylation, could impart an immune-modulatory function (13, 68, 69). If this is the case, ACPA could locally shape immunological microenvironments at inflamed diseases sites, as synovial fluid-derived ACPA exhibited higher variable domain glycosylation prevalence than ACPA obtained from peripheral blood (13).

Anti-neutrophil Cytoplasmic Autoantibody

Anti-neutrophil cytoplasmic autoantibody (ANCA) associated vasculitis (AAV), is characterized by inflammatory lesions of the blood vessels (70, 71). Of the two predominantly recognized antigens, proteinase 3 (PR3) and myeloperoxidase (MPO) (72, 73), only the latter has been associated with increased levels of sialylated variable domain glycans (17). The recent description of SHM introduced glycosylation motifs, confirmed observations of increased variable domain glycan prevalence in AAV (17, 18). As

with other autoimmune diseases, the function and implication of these autoantibodies are as yet incompletely clarified (18).

Systemic Lupus Erythematosus

Systemic Lupus Erythematosus (SLE) is an autoantibody-mediated chronic disease characterized by multi-organ involvement that typically affects women (74, 75). In most cases of SLE, high titers of antinuclear antibodies (ANA) directed at nuclear and cytoplasmic cell components may be detected, and thus prove useful as a diagnostic marker (76, 77). Recently, it was observed that patients with SLE showed a 6% increase in the amount of acquired N-linked glycosylation motifs in the variable domain compared to a control data set (19). However, if variable domain glycosylation is truly enhanced on mature proteins, and whether it plays a role in SLE pathogenesis and/or disease activity or is rather a bystander-effect, needs yet to be confirmed.

Primary Sjogren's Syndrome

Primary Sjogren's Syndrome (pSS), is characterized by lymphocytic infiltrates in the exocrine glands (78). A hallmark of this disease is the presence of anti-RO (SS-A) and anti-La (SS-B) antibodies (79). Increased IgG variable domain glycosylation has been observed in pSS patients as compared to healthy controls (20). The authors noted an absence of evidence for antigen selection pressure in the variable region sequences, and proposed that antigen-independent interaction of the variable domain glycans with parotid gland microenvironmental lectins might represent an alternative stimulus for B-cell proliferation (20).

Myasthenia Gravis

In Myasthenia Gravis (MG), autoantibodies against neuromuscular junction protein impair neuromuscular transmission, resulting in skeletal muscle weakness (80). Although MG is typically characterized by antibodies against the acetylcholine receptor (81, 82), in rare cases the pathologic mechanisms derives from antibodies directed against muscle-specific kinases (MuSK) (83). These MuSK autoantibodies are present in 5–10% of the patients (80, 84) and are typically of the IgG4 subclass which are associated with anti-inflammatory responses. To a lesser extent, IgG1 anti-MuSK antibodies may be found alongside the IgG4 variants (85). To our knowledge, Koers et al. were the first to investigate the frequency and distribution of variable domain glycans in MG patients (46). In these studies, no differences were found in the distribution of the glycosylation motifs compared to healthy controls (46). However, recently variable domain glycans have been observed in monoclonal anti-MuSK-antibodies, although the phenomenon was not ubiquitous in this disease, leading the authors to suggest that variable domain glycosylation is not essential for the generation of anti-MuSK antibodies (85). Since it was also observed that the characteristics of bulk memory B cells in MuSK MG patient do not differ from healthy controls (46), the conclusion that variable domain glycosylation plays no major role in MuSK MG seems warranted. However, such conclusions should be corroborated by *in vivo* observations rather than genetic analyses, as IgG4 may undergo Fab-arm exchange with the potential of radically changing the antibody's properties (86).

In summary, variable domain glycans are present in high prevalence in a number of autoimmune diseases with disease-specific autoantibodies. For some (such as RA and AAV), the ubiquitous presence of variable domain glycans, suggest a mechanistic role, for example in the breach of immunological tolerance of variable domain glycans in these diseases. In other autoimmune diseases, variable domain glycosylation is less abundant (e.g., SLE, MG, and pSS). The reason for these differences is not known, but might relate to the type of antigens recognized or the chronicity/abundance of antigen-exposure. In comparison with healthy donor IgG, auto-antigen IgG from patients with autoimmune diseases can show an enhanced variable domain glycosylation (13). Nonetheless, the glycan composition of the overall IgG response is similar as in both situations complex-type glycans are observed, although an elevated level of highly sialylated glycan-species have been on auto-antigen-specific IgG in RA (13, 15, 18).

Variable Domain Glycosylation in B-Cell Malignancies

Intriguingly, the abundant presence of variable domain glycans has not only been observed in autoimmune disease, but also in the case of certain lymphomas. These findings are interesting as both disease groups may result from poor immune regulation and could therefore point to an unappreciated shared pathogenic mechanism.

Follicular Lymphoma

Follicular lymphoma (FL) is the most common indolent B-cell lymphoma, representing roughly 40% of all non-Hodgkin lymphomas (22). Immortalized by BCL-2 overexpression, FL cells remain situated in the germinal center stage leading to ongoing somatic hypermutation after malignant transformation (87). Already two decades ago, it was observed that FL BCR commonly feature SHM-induced N-linked glycosylation motifs (22). Indeed, such motifs are present in 79–100% of FL, and seemingly cluster around “hotspot” sites at positions 38 (CDR1), 55 (FR2), 107 (CDR3), and 125 (FR4) on the FL BCR (24). Such a ubiquitous presence of acquired glycans suggests a key role in lymphomagenesis. A popular theory involves glycan interaction with microenvironmental lectins, or alternatively with lectins from opportunistic bacteria. This interaction would stimulate the BCR via exposed variable domain glycans and in doing so provide additional growth and survival signals to the lymphoma cell (40, 88–90). An interesting and unusual finding on N-linked glycans found on FL B cells is that they appear to be rich in the otherwise rare oligomannoses in the variable regions, even though they feature complex-type glycans in the Fc domain (91, 92).

Primary Cutaneous Follicle Center Cell Lymphoma

Primary Cutaneous Follicle Center Cell Lymphoma (PCFCL) is an uncommon indolent B-cell lymphoma of unknown etiology that is found preferentially on the skin of the scalp and trunk (93). As to immunophenotyping and morphology, PCFCL mirrors FL (94, 95). Indeed, similar to FL it was recently observed that the vast majority of PCFCL BCR feature up to four acquired

variable domain glycans (24). Unlike FL however, there was no evidence of ongoing SHM, suggesting that the variable domain glycans must have been present already at malignant transformation. Although the majority of the acquired N-linked glycosylation motifs in PCFCL were found in the CDRs, the exact positions differ between the two diseases, with PCFCL showing no proclivity to cluster around hotspots. Whether these N-glycosylation motifs indeed lead to *in vivo* glycosylation, remains to be confirmed (24).

Burkitt's Lymphoma

Burkitt's lymphoma (BL) is an aggressive B-cell lymphoma associated with Epstein Barr virus and Human immunodeficiency virus which accounts for ~1–5% of the non-Hodgkin lymphomas (96). Like FL, BL may incidentally show intraclonal sequence variation (47, 97), although the true extent of this phenomenon has, at least to our knowledge, yet to be verified. Many BL, especially the endemic variant, acquire novel glycosylation sites (47). Additionally, many BL BCR which have not acquired novel variable domain glycans, have been found to express a rearranged IGHV4-34 gene which contains a germline-encoded variable domain glycan. Some cases lost their germline sites, but 75% of these had acquired a newly formed site. This implies that there is a selective pressure to maintain at least one variable domain glycan, although how this influences BL disease biology is currently unclear, as no functional experiments as with FL have been performed.

Diffuse Large B-Cell Lymphoma

Diffuse large B-cell lymphoma (DLBCL) is a common lymphoid malignancy and accounts for 40% of non-Hodgkin lymphoma. DLBCL is clinically heterogenous, but generally aggressive and characterized by the presence of mature B cells (98). One study showed variable domain glycosylation in up to 41% of DLBCL (22). However, since all DLBCL were included, this may represent an overestimation of primary DLBCL, as a subset might represent cases of the ubiquitously glycosylated FL which have undergone histological transformation. Therefore, it remains unclear whether variable domain glycans are found in an increased prevalence in primary DLBCL, as the relatively small datasets used do not provide sufficient evidence to support these observations (24).

Variable Domain Glycans May Serve to Distinguish Lymphoma Types

Summarizing, B-cell lymphomas with a follicular growth pattern have a strong proclivity to acquire variable domain glycans. Indeed, the variable domain glycans may in fact determine their follicular architecture as it links the cell to the germinal center microenvironment (22). Since normal plasma cells, memory B cells, multiple myeloma cells and chronic lymphocytic leukemia cells do not show a marked increase in N-linked glycosylation motifs, it appears that variable domain glycans are of less importance to cells that have exited the germinal center. Moreover, it appears that the mere presence of any variable domain glycan is not sufficient, but N-linked glycosylation motifs need to occur in specific locations, as

witnessed by the FL hotspots and the fact that naturally occurring IGHV4-34 variable domain glycans are often lost and replaced with novel motifs. Given these findings, antigen-independent BCR activation through interactions between glycans and microenvironmental lectins could represent a main driving mechanism for lymphomagenesis (89, 90).

A Comparison of Physiology, Autoimmune Diseases and Lymphoma

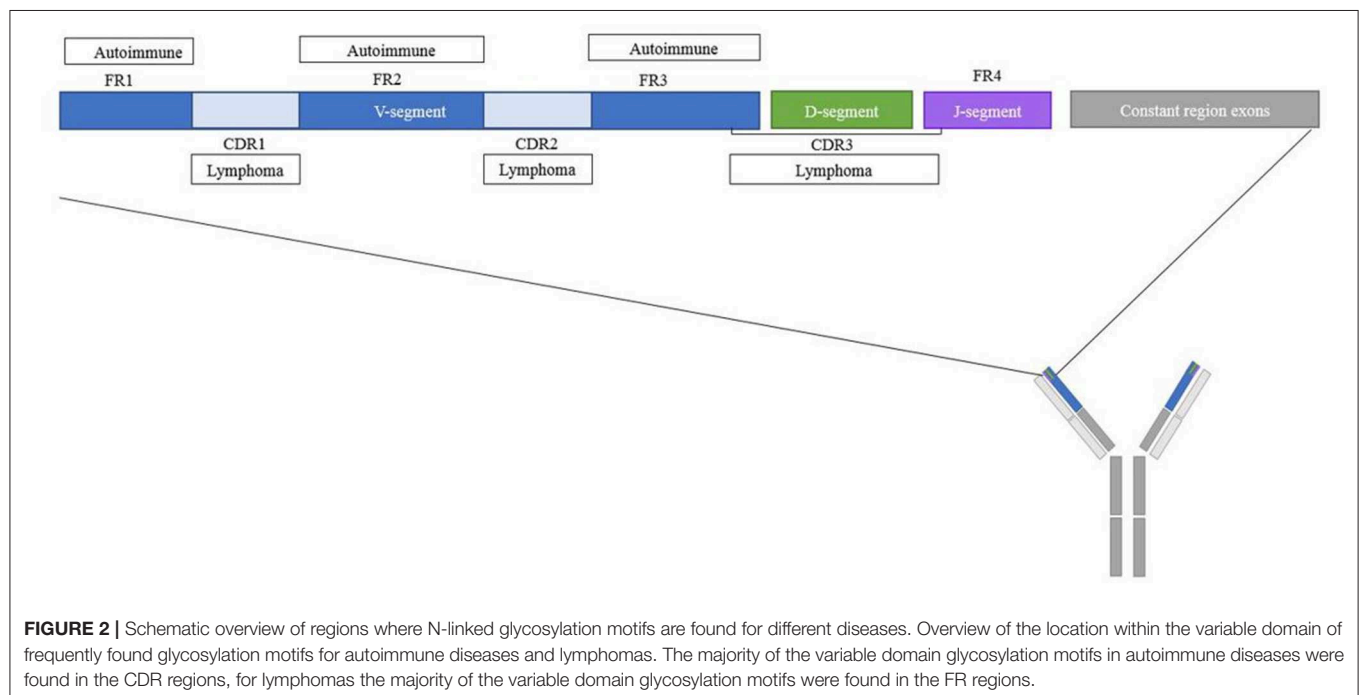
Distribution of the N-Linked Glycosylation Motifs

The position of an N-linked glycosylation motif in the variable region may prove informative for its functional consequences. Indeed, depending on the variable region position, glycans may block antigen-binding, contribute to antigen-specificity or interact with other molecules without interfering with the antigen-binding site. An analysis of structural regions containing the newly acquired glycans may help to make a rough distinction between these possibilities. The majority of the N-linked glycosylation motifs in patients with pSS, RA and AAV were observed in framework region 3 (FR3) (**Figure 2**, **Table 1**) (16, 17, 20). In addition, RA patients' ACPA showed a slight increase in the amount of glycosylation motifs in CDR1 and a slight decrease in CDR3 compared to healthy donors (16). This finding could be interesting since FR3 is known for its interaction with super-antigens which are known to stimulate B-cell differentiation and antibody secretion (42). The tendency of the N-linked glycosylation motifs to appear in the FR could even represent an alternative pathway for autoreactive B cells generation independent of classic antigenic selection (19). Indeed, less of such enrichment is thus far observed in healthy donors, for whom the majority of the glycosylation motifs were located in the CDR regions (16, 46, 53). Future determination of

variable domain glycan clustering in IgG4-RD, SLE, and MG may provide additional evidence toward this hypothesis.

In contrast to acquired variable domain glycans in autoimmune diseases, 87% of heavy chain variable domain glycosylation motifs of FL patients were observed in the CDR. Moreover, rather than clustering on particular regions, FL BCR acquired N-linked glycosylation motifs in a number of very specific hotspots (24), with the strongest hotspot located in CDR2 (**Figure 2**, **Table 1**) (22, 23). These latter sites were introduced during somatic hypermutation by introduction of an asparagine residue, which is an uncommon event for healthy B cells or CLL cells at this position (22). Likewise, acquired PCFCL variable domain glycans can often be found in the CDR2 region, although they do not cluster around the canonical FL hotspots (24). DLBCL variable domain glycans appear to cluster around the CDR3 region (25), and SHM-acquired BL variable domain-glycans also favor the CDRs, especially CDR2 (47, 99). Some authors have suggested super-antigens as a driver of clonal selection and expansion of variable domain glycosylated B cells in BL (99).

These differences in distribution indicate an interesting difference in variable domain glycosylation between lymphoma and autoimmune disease. The variable domain glycans typically found in lymphoma CDR, could prove to be detrimental to autoantibodies. Indeed since the CDR is intimately involved in antigen binding, blocking the antigen-binding site with a large glycan molecule may be expected to interfere with autoantibody recognition, a requirement for B-cell growth and selection. Conversely, the strong hotspot clustering of variable domain glycans in lymphoma BCR could also be explained as a result of glycans contributing to or “mimicking” antigen-binding, especially when those antigens are environmental or



bacterial lectins. Whether those antigens are indeed lectins, other microenvironmental antigens or the substrate of physiological B-cell activity before malignant transformation, is one of the key open questions to understand the importance of this phenomenon. Alternatively, the hotspot clustering may not signify antigen-recognition at all, but could contribute to auto-stimulatory properties due to tertiary formations of the BCR [as described by a different process in for example CLL (100)].

Composition of the Glycan

Although there is generally a decreased amount of Fc sialylation and galactosylation in autoimmune diseases (101, 102), N-linked sugars present on ACPA IgG variable domains form a notable exception with their high sialic acid content of up to 44% (13). Similarly, increased sialylation of variable domain glycans was, as compared to healthy controls also recently observed in the IgG variable domain glycans from patients with AAV and IgG4-RD, the latter regardless of Fab-arm exchange (18, 21). To underline the disease-specificity of this phenomenon, it is worth noting that even subgroups of patients with the same diseases, such as high-activity ANCA-PR3, have been reported to express strikingly low levels of variable domain sialylation. Nonetheless, variable domain sialylation may prove to be a common hallmark of autoantibodies in a plethora of autoimmune diseases (Table 1). Since sialic acids are so prominently present on variable domain glycans in ACPA B cells, it might be possible that they give these B cells a survival advantage compared to B cells without the sialic acids.

In contrast to the highly sialylated variable domain glycans in RA, AAV, and IgG4-RD patients, FL variable domain glycans were reported to be rich in high-mannose structures (Table 1) (91, 92, 103). Such glycans were solely observed at sites which were newly acquired through somatic hypermutation. In 85% of FL cases, non-germline variable domain glycans were found in the CDR, of which the majority were high-mannose structures (91). Their near-universal presence in this disease, may signify that they are beneficial or even essential to improve proliferation and survival (40). In healthy donors, these high mannose structures are normally not found on the cell surface, sparking the hypothesis that in FL the glycans do not fully mature inside the Golgi complex due to enzyme inaccessibility (91, 92).

Glycan-Lectin Interaction

The variable domain glycans of autoantibodies are, by and large, located at different positions as in FL and the mechanism by which the variable domain glycans of autoantibodies convey a survival advantage does not immediately become clear. However, it may be well-explained by interaction of highly sialylated variable domain glycans with sialic acid-binding immunoglobulin-type lectins (SIGLECs). Through interaction of sialic acids with for example SIGLEC CD22, an inhibitory co-receptor of the B-cell receptor (104), an optimal balance between stimulatory and inhibitory signals is achieved. By interfering with e.g., CD22 or other cellular lectins, the threshold for activation of ACPA-expressing B cells may be modified, leading to a selective advantage to those ACPA-expressing B cells that have introduced an N-linked glycosylation site. In case such interactions are

underlying the apparent selective advantage mediated by variable domain glycans to autoreactive B cells, it might explain the differential localization of these glycans in autoimmunity vs. FL.

As mentioned above, in case of FL, it has been proposed that interaction with environmental lectins act as a driving force behind the formation of variable domain glycans. In this case, glycan-lectin-interaction does not modulate or disrupt an inhibitory receptor, but rather serves as surrogate to mediate BCR-crosslinking. Indeed, it was shown that lectins can bind variable domain glycans introduced during somatic hypermutation, and in this way provide a survival signal for autoreactive B cells from the germinal center and onwards during development (88). Furthermore, experimental models confirmed interaction between lectins and FL high-mannose variable domain glycans, thereby stimulating the cells (40, 88). FL variable domain glycans have been reported to interact with C-type lectins, for example dendritic cell-specific intercellular adhesion molecule-3-grabbing non-integrin (DC-SIGN) (40). DC-SIGN is expressed by dendritic cells and macrophages, both of which may be abundantly found in FL biopsies. DC-SIGN binding was shown to trigger BCR signaling (88–90), but so did other lectins, such as those on opportunistic bacteria (40). In ultimo, it was hypothesized that lymphomagenesis through the latter pathway could be interrupted by targeted antibiotic treatment (24). However, more characterization of both the auto-lectins and lectins from opportunistic bacteria would be necessary to fully understand the pathogenesis of FL and create possible treatment options. Since PCFCL shares a few characteristics with FL, it is thought that the variable domain glycans of PCFCL patients are also mannosylated, potentially leading to stimulation from lectins from the cutaneous microbiome (24). Only little is known about the functionality of BL and DLBCL variable domain glycans, but it is possible that lectin interactions also plays a role in BCR activation in these diseases. Although a similar mechanism may mediate disease activity in variable domain glycosylated autoantibodies, we are unaware of any published experimental evidence to support or deny this possibility.

CONCLUSION

Concluding, variable domain glycans appear to play an important role in several B-cell diseases, both hemato-oncological and autoimmune in nature. However, in both fields the precise role and consequences of the variable domain glycosylation remain at best incompletely understood. There are, nonetheless, some observed commonalities between N-linked glycans in autoimmunity and in hematology. Lectin interaction is a recurring hypothesis in both autoimmune and malignant settings, although additional evidence is warranted to further support these paradigms.

Careful scrutiny of the distribution of variable domain glycans could hold the key to an increased understanding of any of these diseases. Currently, only RA ACPA and FL BCR have been investigated in extensive detail, which has led to corresponding pathogenic postulations of the variable domain

glycans. Researchers should aim to compile publicly accessible compendia for all other implied or potentially affected diseases, so side-by-side comparison may clarify important commonalities and differences for each disease.

A possible lead to further understanding of the contribution of variable domain glycans in different disease, is the different distribution and composition of variable domain glycans in autoimmunity and malignant hematological disease. Such differences suggest that in these disease groups, whilst both apparently resulting from deficient immune monitoring, variable domain glycosylation may play distinctly different roles.

On the other hand, defining common variable domain glycosylation patterns should help cluster diseases by shared underlying pathological mechanisms. Based in the current body of knowledge, we propose three such clusters: (1) near ubiquitous CDR-glycosylation with high-mannose structures, which is typical for certain lymphoma types and may depend on auto-lectin interactions potentially mimicking BCR-triggering; (2) near-ubiquitous FR(3)-glycosylation with extensive sialylation that may facilitate SIGLEC interaction, comprising some well-studied autoimmune diseases; and (3) Increased, but non-ubiquitous (FR) glycosylation in autoimmune diseases, which may well be a result of concurrent immune processes rather than an independent driving mechanism.

All in all, variable glycosylation in B-cell diseases is an emerging field of investigation. Through comparison of both

commonalities and differences in variable glycosylation of B-cell diseases across a number of fields, diseases may be clustered by shared pathogenesis and currently missing causative mechanisms may be clarified.

AUTHOR CONTRIBUTIONS

EV and MK screened, summarized and analyzed available literature, and wrote the manuscript. MK, HS, HV, and RT provided project supervision. All authors have critically read and approved the manuscript.

FUNDING

This study has received funding from the Innovative Medicines Initiative 2 Joint Undertaking under grant agreement No. 777357. This Joint Undertaking receives support from the European Union's Horizon 2020 research and innovation programme and EFPIA, was supported by a grant from the Dutch Arthritis Foundation (project no. 15-2-402 and no. 12-2-403, and funded as part of the Target to B! consortium by Samenwerkende Gezondheidsfondsen (SGF) consisting of 20 health funds including KWF kankerbestrijding and ReumaNederland, Topsectore life Sciences & Health (HealstH~Holland) and the business life, no. LSHM18055-SGF. EV was supported by Target-to-B! consortium grant.

REFERENCES

- Vidarsson G, Dekkers G, Rispens T. IgG subclasses and allotypes: from structure to effector functions. *Front Immunol.* (2014) 5:520. doi: 10.3389/fimmu.2014.00520
- Quast I, Lunemann JD. Fc glycan-modulated immunoglobulin G effector functions. *J Clin Immunol.* (2014) 34:51–5. doi: 10.1007/s10875-014-0018-3
- Cassidy JT, Nordby GL. Human serum immunoglobulin concentrations: prevalence of immunoglobulin deficiencies. *J Allergy Clin Immunol.* (1975) 55:35–48. doi: 10.1016/S0091-6749(75)80006-6
- Sun PD. Structure and function of natural-killer-cell receptors. *Immunol Res.* (2003) 27:539–48. doi: 10.1385/IR:27:2-3:539
- Russell A, Adua E, Ufrina I, Laws S, Wang W. Unravelling immunoglobulin G Fc N-glycosylation: a dynamic marker potentiating predictive, preventive and personalised medicine. *Mol Sci.* (2018) 19:E390. doi: 10.3390/ijms19020390
- Varki A. *Essentials of Glycobiology*. Cold Spring Harbor, NY: Cold Spring Harbor Laboratory Press (2015–2017).
- Waechter CJ, Lennarz WJ. The role of polyprenol-linked sugars in glycoprotein synthesis. *Annu Rev Biochem.* (1976) 45:95–112. doi: 10.1146/annurev.bi.45.070176.000523
- Kornfeld R, Kornfeld S. Assembly of asparagine-linked oligosaccharides. *Annu Rev Biochem.* (1985) 54:631–64. doi: 10.1146/annurev.bi.54.070185.003215
- Schenk B, Fernandez F, Waechter CJ. The ins(ide) and outs(ide) of dolichyl phosphate biosynthesis and recycling in the endoplasmic reticulum. *Glycobiology.* (2001) 11:61r–70r. doi: 10.1093/glycob/11.5.61R
- Berninsone PM, Hirschberg CB. Nucleotide sugar transporters of the Golgi apparatus. *Curr Opin Struct Biol.* (2000) 10:542–7. doi: 10.1016/S0959-440X(00)00128-7
- Schwarz F, Aebi M. Mechanisms and principles of N-linked protein glycosylation. *Curr Opin Struct Biol.* (2011) 21:576–82. doi: 10.1016/j.sbi.2011.08.005
- Stanley P, Schachter H, Taniguchi N. *Essentials of Glycobiology*. Varki A, Cummings RD, Esko JD, editors. Cold Spring Harbor, NY: Cold Spring Harbor Laboratory Press (2009).
- Hafkenschied L, Bondt A, Scherer HU, Huizinga TW, Wuhrer M, Toes RE, et al. Structural analysis of variable domain glycosylation of anti-citrullinated protein antibodies in rheumatoid arthritis reveals the presence of highly sialylated glycans. *Mol Cell Proteomics.* (2017) 16:278–87. doi: 10.1074/mcp.M116.062919
- Bondt A, Rombouts Y, Selman MHJ, Hensbergen PJ, Reiding KR, Hazes JMW, et al. Immunoglobulin G (IgG) fab glycosylation analysis using a new mass spectrometric high-throughput profiling method reveals pregnancy-associated changes. *Mol Cell Proteomics.* (2014) 13:3029–39. doi: 10.1074/mcp.M114.039537
- Anumula KR. Quantitative glycan profiling of normal human plasma derived immunoglobulin and its fragments Fab and Fc. *J Immunol Methods.* (2012) 382:167–76. doi: 10.1016/j.jim.2012.05.022
- Vergoesen RD, Slot LM, Hafkenschied L, Koning MT, van der Voort EIH, Grooff CA, et al. B-cell receptor sequencing of anti-citrullinated protein antibody (ACPA) IgG-expressing B cells indicates a selective advantage for the introduction of N-glycosylation sites during somatic hypermutation. *Ann Rheum Dis.* (2018) 77:956–8. doi: 10.1136/annrheumdis-2017-212052
- Lardinois OM, Deterding LJ, Hess JJ, Poulton CJ, Henderson CD, Jennette JC, et al. Immunoglobulins G from patients with ANCA-associated vasculitis are atypically glycosylated in both the Fc and Fab regions and the relation to disease activity. *PLoS ONE.* (2019) 2:e0213215. doi: 10.1371/journal.pone.0213215
- Holland M, Yagi H, Takahashi N, Kato K, Savage COS, Goodall DM, et al. Differential glycosylation of polyclonal IgG, IgG-Fc and IgG-Fab isolated from sera of patients with ANCA-associated systemic vasculitis. *Biochim Biophys Acta.* (2006) 1760:669–77. doi: 10.1016/j.bbagen.2005.11.021
- Visser A, Hamza N, Kroese FGM, Bos NA. Acquiring new N-glycosylation sites in variable regions of immunoglobulin genes by somatic hypermutation is a common feature of autoimmune diseases. *Ann Rheum Dis.* (2018) 77:e69. doi: 10.1136/annrheumdis-2017-212568

20. Hamza N, Hershberg U, Kallenberg CG, Vissink A, Spijkervet FK, Bootsma H, et al. Ig gene analysis reveals altered selective pressures on Ig-producing cells in parotid glands of primary Sjögren's syndrome patients. *J Immunol.* (2015) 194:514–21. doi: 10.4049/jimmunol.1302644
21. Culver EL, van de Bovenkamp FS, Derksen NIL, Koers J, Cargill T, Barnes E, et al. Unique patterns of glycosylation in immunoglobulin subclass G4-related disease and primary sclerosing cholangitis. *J Gastroenterol Hepatol.* (2019) 34:1878–86. doi: 10.1111/jgh.14512
22. Zhu D, McCarthy H, Ottensmeier CH, Johnson P, Hamblin TJ, Stevenson FK. Acquisition of potential N-glycosylation sites in the immunoglobulin variable region by somatic mutation is a distinctive feature of follicular lymphoma. *Blood.* (2002) 99:2562–8. doi: 10.1182/blood.V99.7.2562
23. McCann KJ, Johnson PWM, Stevenson FK, Ottensmeier CH. Universal N-glycosylation sites introduced into the B-cell receptor of follicular lymphoma by somatic mutation: a second tumorigenic event? *Leukemia.* (2006) 20:530–4. doi: 10.1038/sj.leu.2404095
24. Koning MT, Quinten E, Zoutman WH, Kielbasa SM, Mei H, Van Bergen CAM, et al. Acquired N-linked glycosylation motifs in B-cell receptors of primary cutaneous B-cell lymphoma and the normal B-cell repertoire. *J Invest Dermatol.* (2019) 139:2195–203. doi: 10.1016/j.jid.2019.04.005
25. Jardin F, Sahota SS, Ruminy P, Parmentier F, Picquenot JM, Rainville V, et al. Novel Ig V gene features of t(14;18) and t(3;14) de novo diffuse large B-cell lymphoma displaying germinal center-B cell like and non-germinal center-B cell like markers. *Leukemia.* (2006) 20:2070–4. doi: 10.1038/sj.leu.2404370
26. Pagan JD, Kitaoka M, Anthony RM. Engineered sialylation of pathogenic antibodies *in vivo* attenuates autoimmune disease. *Cell.* (2018) 172:564–77 e13. doi: 10.1016/j.cell.2017.11.041
27. Huber R, Deisenhofer J, Colman PM, Matsushima M, Palm W. Crystallographic structure studies of an IgG molecule and Fc fragment. *Nature.* (1976) 264:415–20. doi: 10.1038/264415a0
28. Dekkers G, Rispen T, Vidarsson G. Novel concepts of altered immunoglobulin G galactosylation in autoimmune diseases. *Front Immunol.* (2018) 9:553. doi: 10.3389/fimmu.2018.00553
29. van de Bovenkamp FS, Hafkenscheid L, Rispen T, Rombouts Y. The emerging importance of IgG Fab glycosylation in immunity. *J Immunol.* (2016) 196:1435–41. doi: 10.4049/jimmunol.1502136
30. Shade KT, Platzer B, Washburn N, Mani V, Bartsch YC, Conroy M, et al. A single glycan on IgE is indispensable for initiation of anaphylaxis. *J Exp Med.* (2015) 212:457–67. doi: 10.1084/jem.20142182
31. Lund J, Takahashi N, Pound JD, Goodall M, Jefferis R. Multiple interactions of IgG with its core oligosaccharide can modulate recognition by complement and human Fc gamma receptor I and influence the synthesis of its oligosaccharide chains. *J Immunol.* (1996) 157:4963–9.
32. Wormald MR, Rudd PM, Harvey DJ, Chang SC, Scragg IG, Dwek RA. Variations in oligosaccharide-protein interactions in immunoglobulin G determine the site-specific glycosylation profiles and modulate the dynamic motion of the Fc oligosaccharides. *Biochemistry.* (1997) 36:1370–80. doi: 10.1021/bi9621472
33. Adua E, Russell A, Roberts P, Wang YX, Song MS, Wang W. Innovation analysis on postgenomic biomarkers: glycomics for chronic diseases. *Omic.* (2017) 21:183–96. doi: 10.1089/omi.2017.0035
34. Lefranc MP, Giudicelli V, Ginestoux C, Bodmer J, Muller W, Bontrop R, et al. IMGT, the international ImMunoGeneTics database. *Nucleic Acids Res.* (1999) 27:209–12. doi: 10.1093/nar/27.1.209
35. Arnold JN, Wormald MR, Sim RB, Rudd PM, Dwek RA. The impact of glycosylation on the biological function and structure of human immunoglobulins. *Annu Rev Immunol.* (2007) 25:21–50. doi: 10.1146/annurev.immunol.25.022106.141702
36. Sondermann P, Huber R, Oosthuizen V, Jacob U. The 3.2-Å crystal structure of the human IgG1 Fc fragment-FcγRIII complex. *Nature.* (2000) 406:267–73. doi: 10.1038/35018508
37. Bruggeman CW, Dekkers G, Visser R, Goes NWM, van den Berg TK, Rispen T, et al. IgG glyco-engineering to improve IVIg potency. *Front Immunol.* (2018) 9:2442. doi: 10.3389/fimmu.2018.02442
38. Wright A, Tao MH, Kabat EA, Morrison SL. Antibody variable region glycosylation: position effects on antigen binding and carbohydrate structure. *EMBO J.* (1991) 10:2717–23. doi: 10.1002/j.1460-2075.1991.tb07819.x
39. Coloma MJ, Trinh RK, Martinez AR, Morrison SL. Position effects of variable region carbohydrate on the affinity and *in vivo* behavior of an antigen-(1–>6) dextran antibody. *J Immunol.* (1999) 162:2162–70.
40. Schneider D, Dühren-von Minden M, Alkhatib A, Setz C, van Bergen CA, Benkisser-Petersen M, et al. Lectins from opportunistic bacteria interact with acquired variable-region glycans of surface immunoglobulin in follicular lymphoma. *Blood.* (2015) 125:3287–96. doi: 10.1182/blood-2014-11-609404
41. Leibiger H, Wüstner D, Stigler R-D, Marx U. Variable domain-linked oligosaccharides of a human monoclonal IgG: structure and influence on antigen binding. *Biochem J.* (1999) 338:529–38. doi: 10.1042/bj3380529
42. Silverman GJ, Goodyear CS. Confounding B-cell defences: lessons from a staphylococcal superantigen. *Nat Rev Immunol.* (2006) 6:465–75. doi: 10.1038/nri1853
43. Ohmi Y, Ise W, Harazono A, Takakura D, Fukuyama H, Baba Y, et al. Sialylation converts arthritogenic IgG into inhibitors of collagen-induced arthritis. *Nat Commun.* (2016) 7:11205. doi: 10.1038/ncomms11205
44. Konno N, Sugimoto M, Takagi T, Furuya M, Asano T, Sato S, et al. Changes in N-glycans of IgG4 and its relationship with the existence of hypocomplementemia and individual organ involvement in patients with IgG4-related disease. *PLoS ONE.* (2018) 13:e0196163. doi: 10.1371/journal.pone.0196163
45. Rombouts Y, Willemze A, van Beers JJBC, Shi J, Kerkman PF, van Toorn L, et al. Extensive glycosylation of ACPA-IgG variable domains modulates binding to citrullinated antigens in rheumatoid arthritis. *Ann Rheum Dis.* (2015) 75:578–85. doi: 10.1136/annrheumdis-2014-206598
46. Koers J, Derksen NIL, Ooijevaar-de Heer P, Nota B, van de Bovenkamp FS, Vidarsson G, et al. Biased N-glycosylation site distribution and acquisition across the antibody V region during B cell maturation. *J Immunol.* (2019) 202:2220–8. doi: 10.4049/jimmunol.1801622
47. Zhu D, Ottensmeier CH, Du M-Q, McCarthy H, Stevenson FK. Incidence of potential glycosylation sites in immunoglobulin variable regions distinguishes between subsets of Burkitt's lymphoma and mucosa-associated lymphoid tissue lymphoma. *Br J Haematol.* (2003) 120:217–22. doi: 10.1046/j.1365-2141.2003.04064.x
48. Kapur R, Kustiawan I, Vestreim A, Koeleman CA, Visser R, Einarsdottir HK, et al. A prominent lack of IgG1-Fc fucosylation of platelet alloantibodies in pregnancy. *Blood.* (2014) 4:471–80. doi: 10.1182/blood-2013-09-527978
49. Menni C, Keser T, Mangino M, Bell JT, Erte I, Akmacic I, et al. Glycosylation of immunoglobulin g: role of genetic and epigenetic influences. *PLoS ONE.* (2013) 8:e82558. doi: 10.1371/journal.pone.0082558
50. Chen G, Wang Y, Qiu L, Qin X, Liu H, Wang X, et al. Human IgG Fc-glycosylation profiling reveals association with age, sex, female sex hormones and thyroid cancer. *J Proteomics.* (2012) 75:2824–34. doi: 10.1016/j.jpro.2012.02.001
51. Jefferis R. Antibody therapeutics: isotype and glycoform selection. *Expert Opin Biol Ther.* (2007) 7:1401–13. doi: 10.1517/14712598.7.9.1401
52. Kasermann F, Boerema DJ, Rueggsegger M, Hofmann A, Wymann S, Zuercher AW, et al. Analysis and functional consequences of increased Fab-sialylation of intravenous immunoglobulin (IVIg) after lectin fractionation. *PLoS ONE.* (2012) 7:e37243. doi: 10.1371/journal.pone.0037243
53. van de Bovenkamp FS, Derksen NIL, Ooijevaar-de Heer P, van Schie KA, Kruthof S, Berkowska MA, et al. Adaptive antibody diversification through N-linked glycosylation of the immunoglobulin variable region. *Proc Natl Acad Sci USA.* (2018) 115:1901–6. doi: 10.1073/pnas.1711720115
54. Koning MT, Trollmann IJM, van Bergen CAM, Alvarez Saravia D, Navarrete MA, Kielbasa SM, et al. Peripheral IgE repertoires of healthy donors carry moderate mutation loads and do not overlap with other isotypes. *Front Immunol.* (2019) 10:1543. doi: 10.3389/fimmu.2019.01543
55. van de Bovenkamp FS, Derksen NIL, van Breemen MJ, de Taeve SW, Ooijevaar-de Heer P, Sanders RW, et al. Variable domain N-linked glycans acquired during antigen-specific immune responses can contribute to immunoglobulin G antibody stability. *Front Immunol.* (2018) 9:740. doi: 10.3389/fimmu.2018.00740
56. Suhre K, Trbojevic-Akmacic I, Ugrina I, Mook-Kanamori DO, Spector T, Graumann J, et al. Fine-mapping of the human blood plasma N-glycome onto its proteome. *Metabolites.* (2019) 9:122. doi: 10.3390/metabo9070122
57. Bondt AWM, Kuijper TM, Hazes JM, Dolhain RJ. Fab glycosylation of immunoglobulin G does not associate with improvement of

- rheumatoid arthritis during pregnancy. *Arthritis Res Ther.* (2016) 18:274. doi: 10.1186/s13075-016-1172-1
58. Levin M, Levander F, Palmason R, Greiff L, Ohlin M. Antibody-encoding repertoires of bone marrow and peripheral blood—a focus on IgE. *J Allergy Clin Immunol.* (2017) 139:1026–30. doi: 10.1016/j.jaci.2016.06.040
 59. Biermann MH, Griffante G, Podolska MJ, Boeltz S, Sturmer J, Munoz LE, et al. Sweet but dangerous - the role of immunoglobulin G glycosylation in autoimmunity and inflammation. *Lupus.* (2016) 25:934–42. doi: 10.1177/0961203316640368
 60. Culver EL, Chapman RW. IgG4-related hepatobiliary disease: an overview. *Nat Rev Gastroenterol Hepatol.* (2016) 13:601–12. doi: 10.1038/nrgastro.2016.132
 61. Stone JH. IgG4-related disease: nomenclature, clinical features and treatment. *Semin Diagn Pathol.* (2012) 29:177–90. doi: 10.1053/j.semdp.2012.08.002
 62. Seite JF, Cornec D, Renaudineau Y, Youinou P, Mageed RA, Hillion S. IVIg modulates BCR signaling through CD22 and promotes apoptosis in mature human B lymphocytes. *Blood.* (2010) 116:1698–704. doi: 10.1182/blood-2009-12-261461
 63. Gibofsky A. Overview of epidemiology, pathophysiology, and diagnosis of rheumatoid arthritis. *Am J Manag Care.* (2012) 18:S295–302.
 64. Scott DL, Wolfe F, Huizinga TW. Rheumatoid arthritis. *Lancet.* (2010) 376:1094–108. doi: 10.1016/S0140-6736(10)60826-4
 65. Ge C, Tong D, Liang B, Lonnblom E, Schneider N, Hagert C, et al. Anticitrullinated protein antibodies cause arthritis by cross-reactivity to joint cartilage. *JCI Insight.* (2017) 2:93688. doi: 10.1172/jci.insight.93688
 66. Pratesi F, Tommasi C, Anzilotti C, Chimenti D, Migliorini P. Deiminated Epstein-Barr virus nuclear antigen 1 is a target of anti-citrullinated protein antibodies in rheumatoid arthritis. *Arthritis Rheum.* (2006) 54:733–41. doi: 10.1002/art.21629
 67. Burska AN, Hunt L, Boissinot M, Strollo R, Ryan BJ, Vital E, et al. Autoantibodies to posttranslational modifications in rheumatoid arthritis. *Mediators Inflamm.* (2014) 2014:492873. doi: 10.1155/2014/492873
 68. Kempers A.C., Hafkenscheid L, Dorjee A.L., Moutousidou E, van de Bovenkamp FS, Rispens T, et al. The extensive glycosylation of the ACPA variable domain observed for ACPA-IgG is absent from ACPA-IgM. *Ann Rheum Dis.* (2017) 77:1087–88. doi: 10.1136/annrheumdis-2017-211533
 69. Suwannalai P, Britsemmer K, Knevel R, Scherer HU, Levarht EW, van der Helm-van Mil AH, et al. Low-avidity anticitrullinated protein antibodies (ACPA) are associated with a higher rate of joint destruction in rheumatoid arthritis. *Ann Rheum Dis.* (2014) 73:270–6. doi: 10.1136/annrheumdis-2012-202615
 70. Savige J, Davies D, Falk RJ, Jennette JC, Wiik A. Antineutrophil cytoplasmic antibodies and associated diseases: a review of the clinical and laboratory features. *Kidney Int.* (2000) 57:846–62. doi: 10.1046/j.1523-1755.2000.057003846.x
 71. Hamour S, Salama AD, Pusey CD. Management of ANCA-associated vasculitis: current trends and future prospects. *Ther Clin Risk Manag.* (2010) 6:253–64. doi: 10.2147/TCRM.S6112
 72. Falk RJ, Jennette JC. anti-neutrophil cytoplasmic autoantibodies with specificity for myeloperoxidase in patients with systemic vasculitis and idiopathic necrotizing and crescentic glomerulonephritis. *N Engl J Med.* (1988) 318:1651–7. doi: 10.1056/NEJM198806233182504
 73. Niles JL, McCluskey RT, Ahmad ME, Arnaout MA. Wegener's granulomatosis autoantigen is a novel neutrophil serine proteinase. *Blood.* (1989) 6:1888–93. doi: 10.1182/blood.V74.6.1888.bloodjournal7461888
 74. Vuckovic F, Kristic J, Gudelj I, Teruel M, Keser T, Pezer M, et al. Association of systemic lupus erythematosus with decreased immunosuppressive potential of the IgG glycome. *Arthritis Rheumatol.* (2015) 67:2978–89. doi: 10.1002/art.39273
 75. Sjowall C, Zapf J, von Lohneysen S, Biermann MH, Winkler JS, Bily R, et al. Altered glycosylation of complexed native IgG molecules is associated with disease activity of systemic lupus erythematosus. *Lupus.* (2014) 24:569–81. doi: 10.1177/0961203314558861
 76. Tan EM. Antinuclear antibodies defining autoimmunity pathways. *Arthr Res Ther.* (2014) 16:104. doi: 10.1186/ar4482
 77. Han S, Zhuang H, Shumyak S, Yang L, Reeves WH. Mechanisms of autoantibody production in systemic lupus erythematosus. *Front Immunol.* (2015) 6:228. doi: 10.3389/fimmu.2015.00228
 78. Fox RI. Sjogren's syndrome. *Lancet.* (2005) 366:321–31. doi: 10.1016/S0140-6736(05)66990-5
 79. Hernandez-Molina G, Leal-Alegre G, Michel-Peregrina M. The meaning of anti-Ro and anti-La antibodies in primary Sjogren's syndrome. *Autoimmun Rev.* (2011) 10:123–5. doi: 10.1016/j.autrev.2010.09.001
 80. Hoch W, McConville J, Helms S, Newsom-Davis J, Melms A, Vincent A. Auto-antibodies to the receptor tyrosine kinase MuSK in patients with myasthenia gravis without acetylcholine receptor antibodies. *Nat Med.* (2001) 7:365–8. doi: 10.1038/85520
 81. Vrolix K, Fraussen J, Molenaar PC, Losen M, Somers V, Stinissen P, et al. The auto-antigen repertoire in myasthenia gravis. *Autoimmunity.* (2010) 43:380–400. doi: 10.3109/08916930903518073
 82. Chan KH, Lachance DH, Harper CM, Lennon VA. Frequency of seronegativity in adult-acquired generalized myasthenia gravis. *Muscle Nerve.* (2007) 36:651–8. doi: 10.1002/mus.20854
 83. McConville J, Farrugia ME, Beeson D, Kishore U, Metcalfe R, Newsom-Davis J, et al. Detection and characterization of MuSK antibodies in seronegative myasthenia gravis. *Ann Neurol.* (2004) 55:580–4. doi: 10.1002/ana.20061
 84. Klooster R, Plomp JJ, Huijbers MG, Niks EH, Straasheijm KR, Detmers FJ, et al. Muscle-specific kinase myasthenia gravis IgG4 autoantibodies cause severe neuromuscular junction dysfunction in mice. *Brain.* (2012) 135(Pt 4):1081–101. doi: 10.1093/brain/awt025
 85. Huijbers MG, Vergoossen DL, Fillie-Grijpma YE, van Es IE, Koning MT, Slot LM, et al. MuSK myasthenia gravis monoclonal antibodies: valency dictates pathogenicity. *Neurol Neuroimmunol Neuroinflamm.* (2019) 6:e547. doi: 10.1212/NXI.0000000000000547
 86. van der Neut Kolfschoten M, Schuurman J, Losen M, Bleeker WK, Martinez-Martinez P, Vermeulen E, et al. Anti-inflammatory activity of human IgG4 antibodies by dynamic Fab arm exchange. *Science.* (2007) 317:1554–7. doi: 10.1126/science.1144603
 87. Zhu D, Hawkins RE, Hamblin TJ, Stevenson FK. Clonal history of a human follicular lymphoma as revealed in the immunoglobulin variable region genes. *Br J Haematol.* (1994) 86:505–12. doi: 10.1111/j.1365-2141.1994.tb04780.x
 88. Coelho V, Krysov S, Ghaemmaghami AM, Emara M, Potter KN, Johnson P, et al. Glycosylation of surface Ig creates a functional bridge between human follicular lymphoma and microenvironmental lectins. *Proc Natl Acad Sci USA.* (2010) 107:18587–92. doi: 10.1073/pnas.1009388107
 89. Amin R, Mourcin F, Uhel F, Pangaout C, Ruminy P, Dupre L, et al. DC-SIGN-expressing macrophages trigger activation of mannoseylated IgM B-cell receptor in follicular lymphoma. *Blood.* (2015) 126:1911–20. doi: 10.1182/blood-2015-04-640912
 90. Linley A, Krysov S, Ponzone M, Johnson PW, Packham G, Stevenson FK. Lectin binding to surface Ig variable regions provides a universal persistent activating signal for follicular lymphoma cells. *Blood.* (2015) 126:1902–10. doi: 10.1182/blood-2015-04-640805
 91. Radcliffe CM, Arnold JN, Suter DM, Wormald MR, Harvey DJ, Royle L, et al. Human follicular lymphoma cells contain oligomannose glycans in the antigen-binding site of the B-cell receptor. *J Biol Chem.* (2007) 282:7405–15. doi: 10.1074/jbc.M602690200
 92. McCann KJ, Ottensmeier CH, Callard A, Radcliffe CM, Harvey DJ, Dwek RA, et al. Remarkable selective glycosylation of the immunoglobulin variable region in follicular lymphoma. *Mol Immunol.* (2008) 45:1567–72. doi: 10.1016/j.molimm.2007.10.009
 93. Willemze R, Kerl H, Sterry W, Berti E, Cerroni L, Chimenti S, et al. EORTC classification for primary cutaneous lymphomas: a proposal from the Cutaneous Lymphoma Study Group of the European Organization for Research and Treatment of Cancer. *Blood.* (1997) 90:354–71.
 94. Kim BK, Surti U, Pandya A, Cohen J, Rabkin MS, Swerdlow SH. Clinicopathologic, immunophenotypic, and molecular cytogenetic fluorescence *in situ* hybridization analysis of primary and secondary cutaneous follicular lymphomas. *Am J Surg Pathol.* (2005) 29:69–82. doi: 10.1097/01.pas.0000146015.22624.c7

95. Swerdlow SH, Campo E, Pileri SA, Harris NL, Stein H, Siebert R, et al. The 2016 revision of the World Health Organization classification of lymphoid neoplasms. *Blood*. (2016) 127:2375–90. doi: 10.1182/blood-2016-01-643569
96. Linch DC. Burkitt lymphoma in adults. *Br J Haematol*. (2012) 156:693–703. doi: 10.1111/j.1365-2141.2011.08877.x
97. Chapman CJ, Wright D, Stevenson FK. Insight into Burkitt's lymphoma from immunoglobulin variable region gene analysis. *Leukemia Lymphoma*. (1998) 30:257–67. doi: 10.3109/10428199809057539
98. Alizadeh AA, Eisen MB, Davis RE, Ma C, Lossos IS, Rosenwald A, et al. Distinct types of diffuse large B-cell lymphoma identified by gene expression profiling. *Nature*. (2000) 403:503–11. doi: 10.1038/35000501
99. Baptista MJ, Calpe E, Fernandez E, Colomo L, Cardesa-Salzmann TM, Abrisqueta P, et al. Analysis of the IGHV region in Burkitt's lymphomas supports a germinal center origin and a role for superantigens in lymphomagenesis. *Leukemia Res*. (2014) 38:509–15. doi: 10.1016/j.leukres.2014.01.001
100. Dühren-von Minden M, Übelhart R, Schneider D, Wossning T, Bach MP, Buchner M, et al. Chronic lymphocytic leukaemia is driven by antigen-independent cell-autonomous signalling. *Nature*. (2012) 489:309–12. doi: 10.1038/nature11309
101. Kemna MJ, Plomp R, van Paassen P, Koeleman CAM, Jansen BC, Damoiseaux JGMC, et al. Galactosylation and sialylation levels of IgG predict relapse in patients with PR3-ANCA associated vasculitis. *Ebiomedicine*. (2017) 17:108–18. doi: 10.1016/j.ebiom.2017.01.033
102. Plomp R, Ruhaak LR, Uh HW, Reiding KR, Selman M, Houwing-Duistermaat JJ, et al. Subclass-specific IgG glycosylation is associated with markers of inflammation and metabolic health. *Sci Rep UK*. (2017) 7:12325. doi: 10.1038/s41598-017-12495-0
103. Hollander N, Haimovich J. Altered N-linked glycosylation in follicular lymphoma and chronic lymphocytic leukemia: involvement in pathogenesis and potential therapeutic targeting. *Front Immunol*. (2017) 8:912. doi: 10.3389/fimmu.2017.00912
104. Muller J, Nitschke L. The role of CD22 and Siglec-G in B-cell tolerance and autoimmune disease. *Nat Rev Rheumatol*. (2014) 10:422–8. doi: 10.1038/nrrheum.2014.54

Conflict of Interest: The authors declare that the research was conducted in the absence of any commercial or financial relationships that could be construed as a potential conflict of interest.

Copyright © 2020 Vletter, Koning, Scherer, Veelken and Toes. This is an open-access article distributed under the terms of the Creative Commons Attribution License (CC BY). The use, distribution or reproduction in other forums is permitted, provided the original author(s) and the copyright owner(s) are credited and that the original publication in this journal is cited, in accordance with accepted academic practice. No use, distribution or reproduction is permitted which does not comply with these terms.



Analysis of the Targets and Glycosylation of Monoclonal IgAs From MGUS and Myeloma Patients

Adrien Bosseboeuf¹, Célia Seillier¹, Nicolas Mennesson¹, Sophie Allain-Maillet¹, Maeva Fourny¹, Anne Tallet², Eric Piver^{2,3}, Philippe Lehours^{4,5}, Francis Mégraud^{4,5}, Laureline Berthelot⁶, Jean Harb^{1,6,7}, Edith Bigot-Corbel^{1,7} and Sylvie Hermouet^{1,8*}

¹ CRCINA, Inserm, Université de Nantes, Université d'Angers, Nantes, France, ² Laboratoire de Biochimie, CHU de Tours, Tours, France, ³ Inserm UMR966, Tours, France, ⁴ Inserm U1053, Université de Bordeaux, Bordeaux, France, ⁵ Laboratoire de Bactériologie, Centre National de Référence des Campylobacters et des Hélicobacters, CHU de Bordeaux, Bordeaux, France, ⁶ Centre de Recherche en Transplantation et Immunologie UMR1064, Inserm, Université de Nantes, Nantes, France, ⁷ Laboratoire de Biochimie, CHU de Nantes, Nantes, France, ⁸ Laboratoire d'Hématologie, CHU de Nantes, Nantes, France

OPEN ACCESS

Edited by:

Harry W. Schroeder,
University of Alabama at Birmingham,
United States

Reviewed by:

Masaki Hikida,
Akita University, Japan
Dagmar Scheel-Toellner,
University of Birmingham,
United Kingdom

*Correspondence:

Sylvie Hermouet
sylvie.hermouet@univ-nantes.fr

Specialty section:

This article was submitted to
B Cell Biology,
a section of the journal
Frontiers in Immunology

Received: 20 September 2019

Accepted: 14 April 2020

Published: 27 May 2020

Citation:

Bosseboeuf A, Seillier C,
Mennesson N, Allain-Maillet S,
Fourny M, Tallet A, Piver E, Lehours P,
Mégraud F, Berthelot L, Harb J,
Bigot-Corbel E and Hermouet S
(2020) Analysis of the Targets and
Glycosylation of Monoclonal IgAs
From MGUS and Myeloma Patients.
Front. Immunol. 11:854.
doi: 10.3389/fimmu.2020.00854

Previous studies showed that monoclonal immunoglobulins G (IgGs) of “monoclonal gammopathy of undetermined significance” (MGUS) and myeloma were hyposialylated, thus presumably pro-inflammatory, and for about half of patients, the target of the monoclonal IgG was either a virus—Epstein–Barr virus (EBV), other herpes viruses, hepatitis C virus (HCV)—or a glucolipid, lysoglucosylceramide (LGL1), suggesting antigen-driven disease in these patients. In the present study, we show that monoclonal IgAs share these characteristics. We collected 35 sera of patients with a monoclonal IgA (6 MGUS, 29 myeloma), and we were able to purify 25 of the 35 monoclonal IgAs (6 MGUS, 19 myeloma). Monoclonal IgAs from MGUS and myeloma patients were significantly less sialylated than IgAs from healthy volunteers. When purified monoclonal IgAs were tested against infectious pathogens and LGL1, five myeloma patients had a monoclonal IgA that specifically recognized viral proteins: the core protein of HCV in one case, EBV nuclear antigen 1 (EBNA-1) in four cases (21.1% of IgA myeloma). Monoclonal IgAs from three myeloma patients reacted against LGL1. In summary, monoclonal IgAs are hyposialylated and as described for IgG myeloma, significant subsets (8/19, or 42%) of patients with IgA myeloma may have viral or self (LGL1) antigen-driven disease.

Keywords: monoclonal immunoglobulin A (IgA), multiple myeloma, monoclonal gammopathy of undetermined significance (MGUS), infectious antigens, Epstein–Barr virus, hepatitis C virus, lysoglucosylceramide (LGL-1), sialylation

INTRODUCTION

Myeloma is preceded by an asymptomatic stage termed monoclonal gammopathy of undetermined significance (MGUS) (1–4). In MGUS and myeloma, clonal plasma cells produce large quantities of a so-called “monoclonal” immunoglobulin (Ig). In MGUS, clonal plasma cells represent <10% of bone marrow cells, and the amount of monoclonal Ig in blood is <30 g/L. Following the acquisition of genetic alterations in clonal plasma cells, a fraction of MGUS progress over time toward smoldering, then overt myeloma (5, 6). The rate of transformation of MGUS toward myeloma is 1% per year per individual. In myeloma, patients suffer from diverse renal, bone, and hematological complications; clonal plasma cells represent >10% of bone marrow cells, and the

amount of monoclonal Ig in blood is >30 g/L (6). For 55–60% of MGUS and myeloma patients, the monoclonal Ig is type G, for 20–25%, it is type A, and for $<5\%$, it is type D, M, or E; light chain myeloma represent $\sim 15\%$ cases (7).

The causes of MGUS have long remained unknown, although it is established that chronic infection may lead to the emergence of oligoclonal and eventually, monoclonal plasma cells and the subsequent production of a so-called “monoclonal Ig.” In addition, it is thought that certain genetic backgrounds, ethnicity, lipid disorders, and obesity may increase the risk of developing myeloma. Consistent with these observations, the study of Ig genes in malignant plasma cells had revealed restricted heavy-chain variable-region use and highly hypermutated Ig heavy- and light-chain genes, which supports antigen-mediated selection of the malignant clone (8, 9). Recent studies identified several types of antigens that are specifically recognized by monoclonal IgGs, notably lysoglycosylceramide (LGL1) (10, 11), and infectious antigens (12–14). Thus, it has been proposed that chronic stimulation by glucolipidic auto-antigens or by infectious antigens may underlie the pathogenesis of subsets of IgG MGUS and myeloma.

Identification of LGL1 as a frequent target of the plasma cell clone in MGUS and in myeloma resulted from the study of patients with Gaucher disease (10, 11). Gaucher disease is a genetic disorder in which a glucocerebroside (or glucosylceramide) accumulates, and MGUS and myeloma are more frequent in Gaucher patients than in the general population. Nair et al. demonstrated that the monoclonal Ig of patients with Gaucher disease frequently target LGL1, a glucosylceramide present in excess in these individuals (10, 11). Moreover, up to a third of monoclonal IgG from patients without Gaucher disease—with sporadic MGUS or myeloma—may also target LGL1, which suggested a link between chronic stimulation by a self-antigen and the development of MGUS and myeloma (10, 11). In parallel, our group investigated whether an abnormal immune response to latent infection may lead to MGUS and eventually, myeloma. We designed a new assay, called the multiplexed infectious antigen microarray (MIAA), which carries proteins and lysates from nine infectious pathogens, to analyze the specificity of infectious antigen recognition of purified monoclonal IgGs from MGUS or myeloma patients (15). Using the MIAA assay, we found that purified monoclonal IgGs reacted with several infectious pathogens known to cause latent infection. These pathogens include herpesviruses, especially Epstein–Barr virus (EBV), and hepatitis C virus (HCV) (12–15). EBV and HCV are oncogenic viruses associated with solid cancers and B-cell malignancies such as Hodgkin and non-Hodgkin lymphoma, mostly directly via cell infection and transformation (16–19). In contrast, EBV DNA is rarely detected in malignant plasma cells (20). Thus, in MGUS and myeloma with EBV-specific IgG, malignant transformation presumably occurs indirectly, without infection of tumor cells, *via* chronic antigen-driven stimulation of the B-cell receptor (BCR) that has identical heavy and light chain specificity to the secreted IgG. Interestingly, monoclonal IgGs may contribute to the inflammation associated with MGUS and myeloma, since they have a very low level of sialylation of the Fc fragment,

a characteristic typically associated with a pro-inflammatory action (21).

In contrast to the monoclonal IgGs of MGUS and myeloma patients, the characteristics and antigenic targets of monoclonal IgAs have not been studied. IgA myeloma is relatively rare and differs from IgG myeloma by a worse prognosis and shorter survival: patients with IgA myeloma are considered more at risk of bone destruction, extra-medullary disease, infection, and hyper-viscosity facilitated by greater polymerization of IgAs compared to IgGs (22–28). In the present study, we were able to collect serum from 35 patients with a monoclonal IgA; 25/35 monoclonal IgAs were successfully separated from other IgG. The specificity of antigenic recognition of the purified monoclonal IgAs was analyzed using the MIAA and an adapted LGL1 assay; the isotype of monoclonal IgAs was also determined, and their degree of sialylation was quantified.

MATERIALS AND METHODS

Patients

We examined 35 patients with a monoclonal IgA (6 MGUS, 29 myeloma). Among those, 6 MGUS and 22 myeloma were diagnosed at the University Hospitals (CHUs) in Tours and Bordeaux (France) over the 2010–2016 period. Samples of blood serum from seven additional patients with IgA myeloma from international cohorts of relapsed myeloma were provided by Novartis (Basel, Switzerland).

Purification of Monoclonal IgAs and Determination of Isotype

After clotting, blood samples were centrifuged at $2,200 \times g$ (4°C), and serum aliquots were frozen. Measurement of Ig concentration, separation of monoclonal IgAs from other IgG, and verification of purity were performed as described previously (12–15, 21). Briefly, the presence of a monoclonal IgA in serum is first established in clinical laboratories, then purification of the monoclonal IgA is performed. The protocol of purification starts with a high resolution agarose gel electrophoresis (SAS-MX high resolution; Helena Biosciences, Gateshead, UK), which allows us to elute the monoclonal Ig from the gel, for elution in PBS. The purity of the monoclonal IgA preparation is then verified by isoelectrofocusing on an agarose gel (pH 3–10) followed by blotting and immunorevelation by an anti-human IgA alpha chain antibody labeled with peroxidase. In some cases, the monoclonal IgA preparation still contains very small amounts of other IgAs (oligo- or poly-clonal), always in very low concentration and not detectable by our techniques. Moreover, eventual contamination by IgG is not relevant here because all further assays are revealed using anti-human IgA alpha chain antibodies.

To determine the A1/A2 isotype, 96-well plates (Nunc MaxiSorp™) were coated overnight at 4°C with $50 \mu\text{l}$ of goat anti-human IgA antibody (Southern Biotech, Birmingham, AL, USA) diluted 1:500 in 25 mM borate buffer pH 9. After washing with PBS-Tween 0.05%, wells were saturated for 2 h at 37°C with 0.25% B-grade bovine gelatin (Sigma, St. Louis, MO, USA) diluted in 0.1% PBS-Tween; $50 \mu\text{l}$ of monoclonal IgA (400 ng/ml)

was then added (2-h incubation, 37°C). After washing, 50 µl of biotinylated mouse anti-human IgA1 or IgA2 antibody (0.5 µg/ml; Southern Biotech, Birmingham, AL, USA) was added (2-h incubation, 37°C). After washing, 50 µl of streptavidin-HRP (1 µg/ml; Vector Laboratories, Burlingame, CA, USA) was added (1-h incubation, 37°C). After washing, 50 µl of 3,3',5,5'-tetramethylbenzidine (TMB) was added. The reaction was stopped with 50 µl of sulfuric acid (0.5 M). Optical density was read at 450 nm using a Spark 10 M multimode microplate reader (Tecan, Männedorf, Switzerland).

The MIAA Assay

The MIAA assay allows testing for panels of commercially available proteins, antigens, or/and lysates from EBV, herpes simplex virus 1 (HSV-1), HSV-2, cytomegalovirus (CMV), varicella zoster virus (VZV), HCV, *Helicobacter pylori* (*H. pylori*), *Toxoplasma gondii* (*T. gondii*), and *Borrelia burgdorferi* (*B. burgdorferi*) (12–15, 21). For incubation on MIAA arrays, Ig concentrations were adjusted to 400 µg/ml (serum) or 50–200 µg/ml (purified monoclonal IgAs) in 80 µl. After washing, MIAA slides were incubated with Dylight™ 680-labeled goat anti-human IgA Fc antibody (1:2,500; 0.4 µg/ml; Immuno Reagents, Raleigh, NC, USA). Fluorescence signals were detected with the Odyssey infrared imaging system scanner at 21-µm resolution (LI-COR Biosciences, Lincoln, NE, USA) and quantified using the GenePix® Pro 4 Microarray Acquisition and Analysis Software (Molecular Devices, Sunnyvale, CA, USA) (12–15, 21). Five fluorescence thresholds of specific positivity were determined using positive and negative controls: 500, for HCV, *H. pylori*, *T. gondii*; 1,000, for HSV-1 and HSV-2; 1,200, for CMV; 1,400, for EBV and VZV; and 1,800 for *B. burgdorferi*. Fluorescent signals below the thresholds were considered negative (12, 21).

Dot Blotting Assays

Nitrocellulose membranes (Amersham, Buckinghamshire, UK) were spotted with recombinant EBNA-1 protein, relevant and irrelevant EBV peptides, or HCV core protein, then dried (12). Saturation of membranes, and incubation with serum or purified monoclonal IgA were performed as published (12). Antigen–IgA complexes were revealed using an HRP-labeled goat anti-human IgA (α chain) from Bethyl Laboratories (Montgomery, TX, USA).

LGL1 Immunoblotting Assay

For LGL1-specific immunoblotting, polyvinylidene fluoride (PVDF) membranes were incubated for 90 min in 100 µg/ml of LGL1 in 0.1 M sodium bicarbonate, rinsed 3 times in PBS and 0.1% Tween 20 detergent, then blocked for 2 h with 5% bovine serum albumin (BSA) (10, 29). Samples of serum or purified monoclonal IgAs were submitted to agarose gel electrophoresis; then, the gels were blotted onto the LGL1-saturated membranes by diffusion blotting during 12 min (10, 30). After blocking for 1 h with 2.5% BSA in PBS and 0.1% Tween 20, membranes were incubated with anti-human IgA horseradish peroxidase (HRP)-conjugated secondary antibody for 1 h, then washed and revealed with Super Signal West Pico chemiluminescent substrate (Thermo Scientific).

Analysis of the Sialylation of Serum IgAs

An enzyme linked lectin assay (ELLA) was developed to analyze IgA sialylation, and an enzyme linked immuno-sorbent assay (ELISA) was used for the detection of total IgAs, as previously described (21). Ninety-six well plates (Nunc MaxiSorp™) were coated overnight at 4°C with 50 µl of goat anti-human IgA (Bethyl Laboratories, Montgomery, TX, USA) diluted 1:250 (4.0 µg/ml; ELLA) and 1:1,000 (1.0 µg/ml; ELISA) in 25 mM borate buffer pH 9. After three washes with 200 µl of PBS-Tween 0.05% (Sigma, Saint Louis, USA), 100 µl of periodic acid (5 mM) per well was added for 10 min at room temperature, protected from light. The plates were then saturated with 100 µl of 0.25% B-grade bovine gelatin (Sigma, St. Louis, MO, USA) in PBS-Tween 0.01%, at 37°C, for 2 h. After three washes, samples were diluted in PBS-Tween 0.1% and deposited in triplicate wells containing 1.25 ng of Ig for the detection of total IgA, or 2.5 ng of IgA for sialylation studies. The total IgA quantity was assessed by incubating the plates with 50 µl of HRP-coupled goat anti-human IgA diluted 1:1,000 for 1 h (Bethyl Laboratories, Montgomery, TX, USA). Sialic acid was revealed using 50 µl of biotinylated *Sambucus nigra* agglutinin (SNA) diluted 1:750 (2 µg/ml; Glycidiag, Orléans, France) for 90 min and then 50 µl of streptavidin HRP diluted 1:1,000 (1 µg/ml; Vector laboratories, Burlingame, CA, USA) for 1 h, at 37°C. Then, 50 µl of TMB, the chromogenic substrate for HRP (Sigma-Aldrich, St. Louis, MO, USA) was added, and the reaction was stopped by 50 µl of 0.5 M sulfuric acid, after 3 min for IgA detection, and after 5 min for sialic acid detection. Optical densities (OD) were measured using a Spark 10 M multimode microplate reader (Tecan, Männedorf, Switzerland) at 450 nm. The percentage of sialylation was calculated as follows: $[\text{SNA OD signal/IgA OD signal}]/[\text{ng IgA in SNA well/ng IgA in IgA well}] \times 100$. In all experiments, internal controls were used to assess reproducibility.

Statistics

Data analysis was performed by GraphPad Prism 6.01 software. Patient parameters were expressed as medians and ranges, or/and means ± standard error of the mean (SEM). The Chi-2 test was used. For continuous variables, a Mann–Whitney *U*-test or a Kruskal–Wallis test followed by Dunn's *post-hoc* test was performed. The tests used are indicated in the legends of figures and tables. A value of $p < 0.05$ was considered statistically significant.

Study Approval

The study was promoted by the CHU of Nantes, France (# RC12 0085) with the approval of the local and national ethical committee [Comité Consultatif de Protection des Personnes dans la Recherche Biomédicale, Commission Nationale de l'Informatique et des Libertés (CNIL #912335)]. Written informed consents were obtained from patients and healthy donors, by the blood bank (Etablissement Français du Sang (EFS), Nantes, France). A convention was signed between CRCINA and EFS Pays de La Loire.

RESULTS

Characteristics of Patients With a Monoclonal IgA

In this retrospective study, 35 patients with a monoclonal IgA were recruited (6 MGUS, 29 myeloma). Annotated clinical data were available for 26 patients (6 MGUS, 20 myeloma); the biological and clinical characteristics of patients are shown in **Table 1**. The male/female ratios were 33.3% for MGUS and 45.0% for myeloma, and the median age of MGUS and myeloma patients with monoclonal IgA at the time of diagnosis was 76.6 and 75.1, respectively. Thus, in this cohort, patients with IgA myeloma were older than in the series of 135 IgG myeloma patients we studied previously (median age at the time of diagnosis: 75.1 years for IgA myeloma vs. 63.8 years for IgG myeloma) (12, 21). Compared to IgG myeloma, the quantity of monoclonal Ig produced at the time of diagnosis of IgA myeloma was low (median quantity of monoclonal Ig: 17.0 g/L for IgA vs. 26.7 g/L for IgG), and the median percentage of plasma cells in the bone marrow was high: 52 vs. 33% for IgG myeloma (12). All but one patients with IgA myeloma presented with bone lesions, and the International Staging System (ISS) and Durie–Salmon Staging (DSS) scores indicated that 50.0% of patients presented with ISS stage III at the time of diagnosis (median DSS stage III: 59.1%).

Serological Status of MGUS and Myeloma Patients With a Monoclonal IgA

The unseparated IgG and IgA serological status was determined for 32 patients (6 MGUS, 26 myeloma) using the MIAA, which tests for reactivity to lysates and/or antigens representing nine infectious pathogens (12, 15, 21). The MIAA assay can be revealed either with a fluorescent goat anti-human IgG Fc antibody (for IgG serology) or with a fluorescent goat anti-human IgA Fc antibody (for IgA serology), which allowed us to analyze in parallel IgG and IgA reactivity in the serum of patients (**Table 2**). Overall, the rates of positive IgG serology for EBV, CMV, HSV-1, *T. gondii* of MGUS, and myeloma patients were comparable to those of our previous studies and to those observed in the general population. The rates of positive IgG serology differed for HSV-2 (high frequency of positivity in the IgA cohort) and VZV (likely underestimated by the MIAA) (12, 15, 21). Patients also had a positive IgA serology for EBV, CMV, HSV-1, as reported for the general population (31–35). The rates of positive IgA serology were significantly lower than the rates observed for IgG serology for EBV, CMV, HSV-1 ($p < 0.00001$, Fisher exact test), and HSV-2 ($p = 0.0272$, Fisher exact test) (**Table 2**). They were similar to those of IgG for *H. pylori* and *T. gondii*, and increased for VZV.

Identification of the Infectious Targets of Purified Monoclonal IgAs

Monoclonal IgAs were separated individually from other Igs from blood serum, then incubated on the MIAA. In general, monoclonal IgAs were more difficult to purify than monoclonal IgGs because of their migration in agarose in the beta–gamma zone (**Figure 1**). Altogether, purity was achieved for 25 (71.4%)

TABLE 1 | Characteristics of patients with IgA monoclonal gammopathy of undetermined significance (MGUS) or IgA myeloma.

	MGUS	Myeloma
Patients, <i>n</i>	6	29
Patients with available biological data, <i>n</i>	6	20
Male sex, <i>n</i> (%)	2 (33.3%)	9 (45.0%)
Age (year)		
Median	76.6	75.1
Range	66–97	57–95
Monoclonal IgA (g/L)		
Median	8.0	17.0
Range	3.0–19.0	4.0–57.0
Bone marrow plasma cells (%)	<i>n</i> = 2	<i>n</i> = 19
Median	8	52
Range	1–16	1–89
β_2-microglobulin (mg/L)		
Median	NA	4.2
Range	NA	1.1–14.0
Leukocytes ($\times 10^9/L$)		
Median	7.1	4.6
Range	4.1–11.8	1.3–9.0
Hemoglobin (g/dl)		
Median	11.2	9.7
Range	7.6–126	5.4–15.3
Platelets ($\times 10^9/L$)		
Median	218.5	164.0
Range	132–356	24–269
ISS (<i>n</i> = 8)*		
Stage I, <i>n</i> (%)	-	2 (25.0%)
Stage II, <i>n</i> (%)	-	2 (25.0%)
Stage III, <i>n</i> (%)	-	4 (50.0%)
DSS (<i>n</i> = 22)		
Stage I, <i>n</i> (%)	-	0 (0%)
Stage II, <i>n</i> (%)	-	9 (40.9%)
Stage III, <i>n</i> (%)	-	13 (59.1%)

n, number; NA, not available; ISS, International System Staging; DSS, Durie–Salmon Staging. *The β_2 -microglobulin level was available for only eight myeloma patients.

monoclonal IgAs (6 MGUS, 19 myeloma). The A1 or A2 isotype was determined for 21 monoclonal IgAs: 20 were IgA1s (5 MGUS, 15 myeloma) and 1 was an IgA2 (1 MGUS, X01). None of the monoclonal IgAs from MGUS patients recognized any infectious pathogen in the MIAA (**Figure S1**), whereas the purified monoclonal IgAs from five (26.3%) myeloma patients in this series specifically recognized a single recombinant protein from a single pathogen. Four recognized EBV nuclear antigen-1 (EBNA-1) (**Figures 2A–E**), and one recognized HCV core protein (**Figure 2F**). MIAA results of other myeloma patients are shown in **Figure S1**. Dot blots with recombinant EBNA-1 or HCV core proteins confirmed a positive reaction for the monoclonal IgAs specific for EBNA-1 (**Figure 3A**) or HCV core (**Figure 3B**). EBNA-1-specific monoclonal IgAs were then tested against an immuno-dominant B-cell public epitope sequence, PGRRPFF (EBNA-1 residues 400–406), reported to be a target

TABLE 2 | IgG and IgA serological status of MGUS and myeloma patients with monoclonal IgA, as determined with the multiplexed infectious antigen micro-array (MIAA) assay.

Pathogens	MGUS (n = 6)		Myeloma (n = 26)		MGUS and Myeloma (n = 32)	
	Negative	Positive	Negative	Positive	Negative	Positive
IgG serology						
EBV, n (%)	0	6 (100%)	0	26 (100%)	0	32 (100%)
HCV, n (%)	6	0 (0.0%)	25	1 (3.1%)	31	1 (3.1%)
CMV, n (%)	4	2 (33.3%)	12	14 (53.8%)	16	16 (50.0%)
HSV-1, n (%)	1	5 (83.3%)	7	19 (73.1%)	8	24 (75.0%)
HSV-2, n (%)	3	3 (50.0%)	15	11 (42.3%)	18	14 (43.8%)
VZV, n (%)	5	1 (16.7%)*	22	4 (15.4%)*	27	5 (15.6%)*
<i>H. pylori</i> , n (%)	4	2 (33.3%)	19	7 (26.9%)	23	9 (28.1%)
<i>T. gondii</i> , n (%)	5	1 (16.7%)	17	9 (34.6%)	22	10 (31.2%)
<i>B. burgdorferi</i> , n (%)	5	1 (16.7%)	26	0 (0.0%)	31	1 (3.1%)
IgA serology						
EBV, n (%)	2	4 (66.7%)	13	13 (50.0%)	15	17 (53.1%) ^a
HCV, n (%)	6	0 (0.0%)	25	1 (3.8%)	31	1 (3.1%)
CMV, n (%)	5	1 (16.7%)	26	0 (0.0%)	31	1 (3.1%) ^b
HSV-1, n (%)	4	2 (33.3%)	24	2 (7.7%)	28	4 (12.5%) ^c
HSV-2, n (%)	5	1 (16.7%)	22	4 (15.4%)	27	5 (15.6%) ^d
VZV, n (%)	4	2 (33.3%)	14	12 (46.2%)	18	14 (43.8%) ^e
<i>H. pylori</i> , n (%)	5	1 (16.7%)	18	8 (30.8%)	23	9 (28.1%)
<i>T. gondii</i> , n (%)	5	1 (16.7%)	23	3 (11.5%)	28	4 (12.5%) ^f
<i>B. burgdorferi</i> , n (%)	5	1 (16.7%)	21	5 (19.2%)	26	6 (18.8%)

Prior to the analysis of the specificity of purified monoclonal IgAs, the IgG serology status and the IgA serology status were assessed in parallel for 32 patients (6 MGUS, 26 myeloma) by analyzing serum samples (containing unseparated IgGs, unseparated IgAs, and monoclonal IgA) with the MIAA assay, revealed with either a Dylight™ 680-labeled goat anti-human IgG Fc antibody or a Dylight™ 680-labeled goat anti-human IgA Fc antibody.

*Underestimated by the MIAA assay, the percentage of positive IgG serology for VZV in the general population being >90%.

^a $p < 0.00001$.

^b $p < 0.00001$.

^c $p < 0.00001$.

^d $p = 0.0272$.

^e $p = 0.0272$.

^f $p = 0.1289$ compared to the IgG serology, Fisher exact test.

EBV, Epstein-Barr virus; HCV, hepatitis C virus; CMV, cytomegalovirus; HSV, herpes simplex virus 1; VZV, varicella zoster virus; *H. pylori*, *Helicobacter pylori*; *T. gondii*, *Toxoplasma gondii*; *B. burgdorferi*, *Borrelia burgdorferi*.

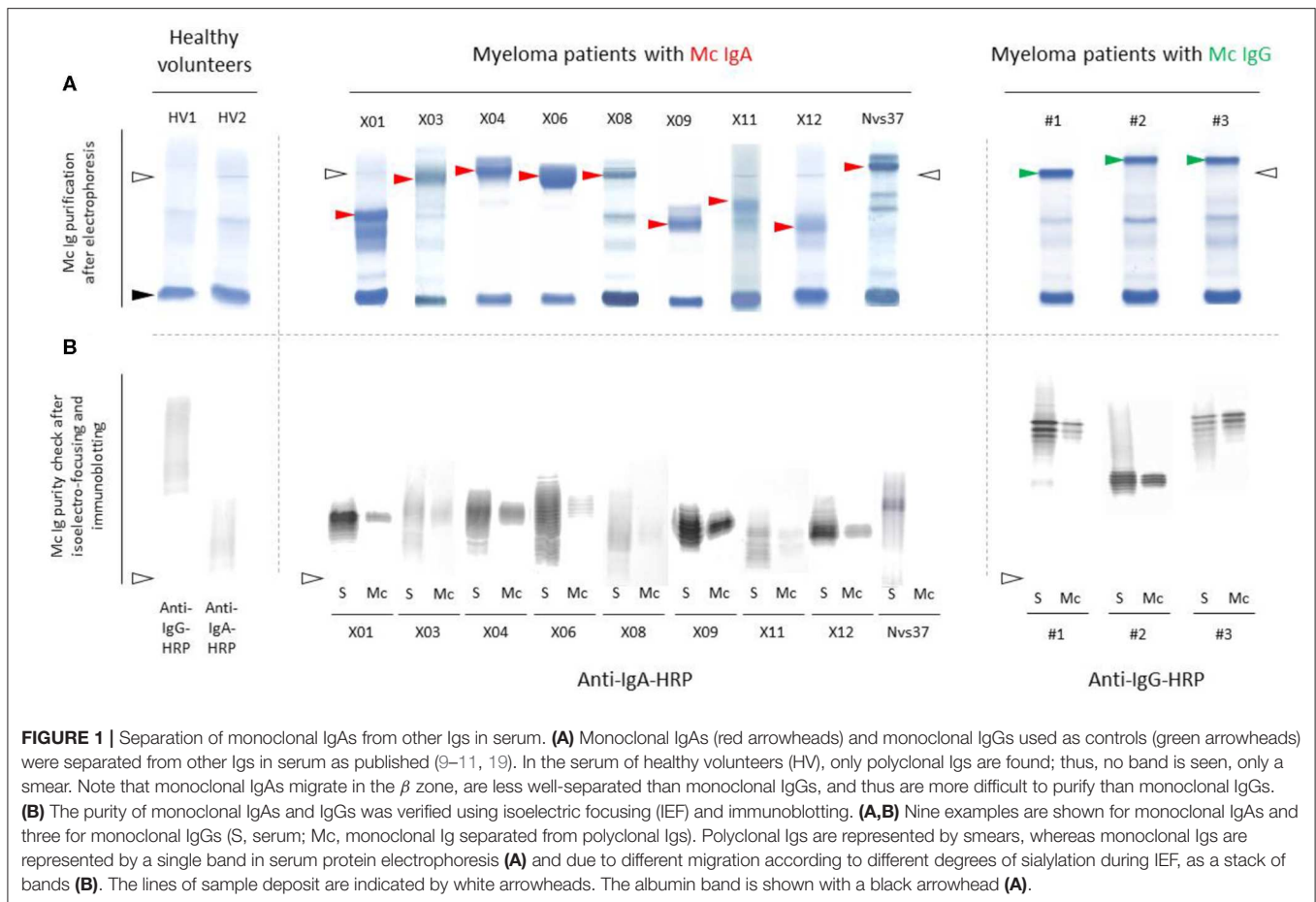
for polyclonal IgG from 86.3% of the general population (36). However, we previously found that the PGRPF sequence was recognized by only 2/32 (6.25%) of EBNA-1-specific monoclonal IgGs (12). In this cohort of IgA myelomas, none of the four EBNA-1-specific monoclonal IgAs recognized PGRPF (data not shown).

Identification of Monoclonal IgAs That Target LGL1

Purified monoclonal IgAs from MGUS and myeloma patients were analyzed with the LGL1 assay adapted from Nair et al. (10). As shown in **Figure 4**, only three monoclonal IgAs reacted with LGL1, and all were from myeloma patients (X03, X08, Nvs37). The monoclonal IgA of each of the three patients did not recognize any pathogen of the MIAA assay (their MIAA assay was negative, an indirect proof of purity of the monoclonal IgA preparation). Thus, 3/19 (15.8%) of myeloma monoclonal IgA targeted LGL1 in this series.

Characteristics of Myeloma Patients With a Monoclonal IgA Specific for EBNA1 or LGL1

We compared the clinical characteristics of the four myeloma patients with EBNA-1-specific monoclonal IgA ["EBNA-1(+)" patients] with those of the 17 myeloma patients with a monoclonal IgA that was non-reactive for pathogens of the MIAA assay ["MIAA(-)" patients] (**Table 3**). Compared to other IgA myeloma patients, myeloma patients with EBNA-1-specific IgA were relatively young at the time of diagnosis (≤ 63 years old), as reported for myeloma patients with EBNA-1-specific monoclonal IgG (12). Regarding patients with an LGL1-specific monoclonal IgA, Nair et al. reported a tendency toward a mild form of disease for LGL1-associated myeloma (10). Here, clinical and biological characteristics were available for only two patients. The data did not suggest a mild disease since both had bone lesions: one had >50% plasma cells in the bone marrow, and one had a DSS stage III (**Table 4**).



Glycosylation of IgAs

As published for monoclonal IgGs, the sialylation level of unseparated, total IgAs, assessed in serum, expressed in % sialylation, was lower for MGUS and myeloma patients with a monoclonal IgA than for healthy volunteers (41.2 vs. 63.4%, respectively; $***p < 0.0001$, Mann-Whitney U -test) (Figure 5A) (12, 21). No difference was observed according to age (healthy donors under or over 60 years), nor between MGUS and myeloma (Figure 5B). In addition, there was no difference in IgA sialylation depending on the antigenic specificity (MIAA+ vs. MIAA-) of the monoclonal IgA (Figure 5C, Table 4). However, due to the small size of the cohorts, these results will need to be confirmed in larger studies.

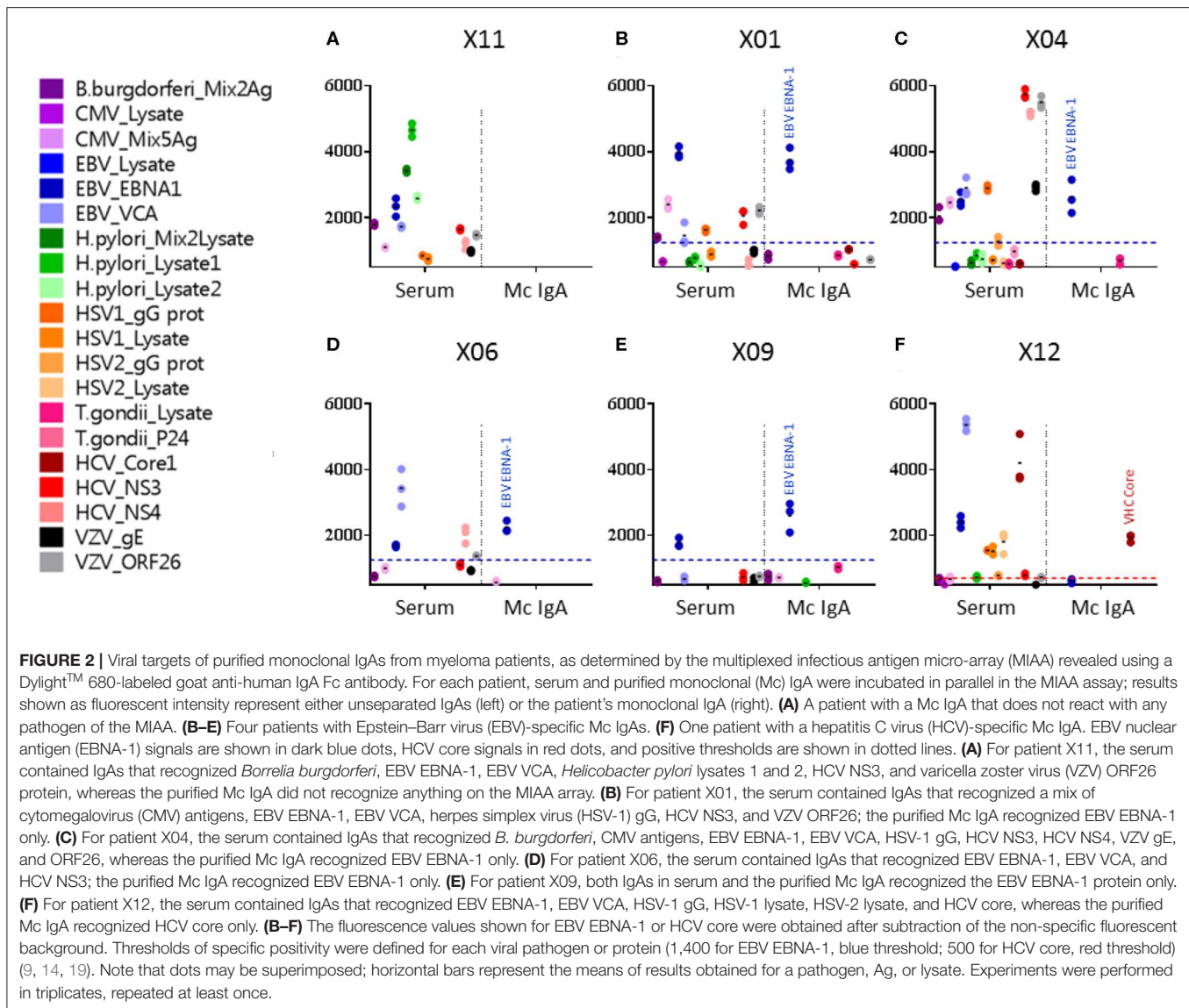
DISCUSSION

This is the first analysis of the antigenic origins of IgA myeloma. In this small cohort, no antigenic target was identified for the monoclonal IgAs from MGUS patients, but for patients with IgA myeloma, two viruses (EBV, HCV) were candidate targets for the monoclonal IgA of 5/19 patients (26.3%). In addition, the monoclonal IgA of 3/19 myeloma patients (15.8%) reacted with LGL1, a glucolipidic auto-antigen. These results imply that

chronic stimulation by viral antigens or auto-antigen LGL1 may underlie the initiation of ~40% of IgA myeloma, as reported for MGUS and myeloma with a monoclonal IgG (10, 12).

In this study, myeloma patients with a monoclonal IgA were typically older and had stage III disease, consistent with IgA myeloma being more severe than IgG myeloma (22–28). Analysis of the IgG and IgA serology status of MGUS and myeloma patients revealed that despite stage III disease, patients maintained detectable levels of polyclonal IgGs and IgAs directed against common pathogens. The rates of positive IgG serology against EBV, CMV, HSV-1, and HSV-2 observed for IgA myeloma patients were similar to those of the general population. The rates of positive IgA serology of these patients were lower than those of IgG for EBV, CMV, HSV-1, and HSV-2, as expected (31–35). They were similar to the rates of positive IgG serology for *H. pylori*, *T. gondii*, *B. burgdorferi*, and higher for VZV. Thus, this cohort of patients with IgA myeloma maintained IgG- and/or IgA-mediated protection against EBV, CMV, HSV-1, HSV-2, and VZV.

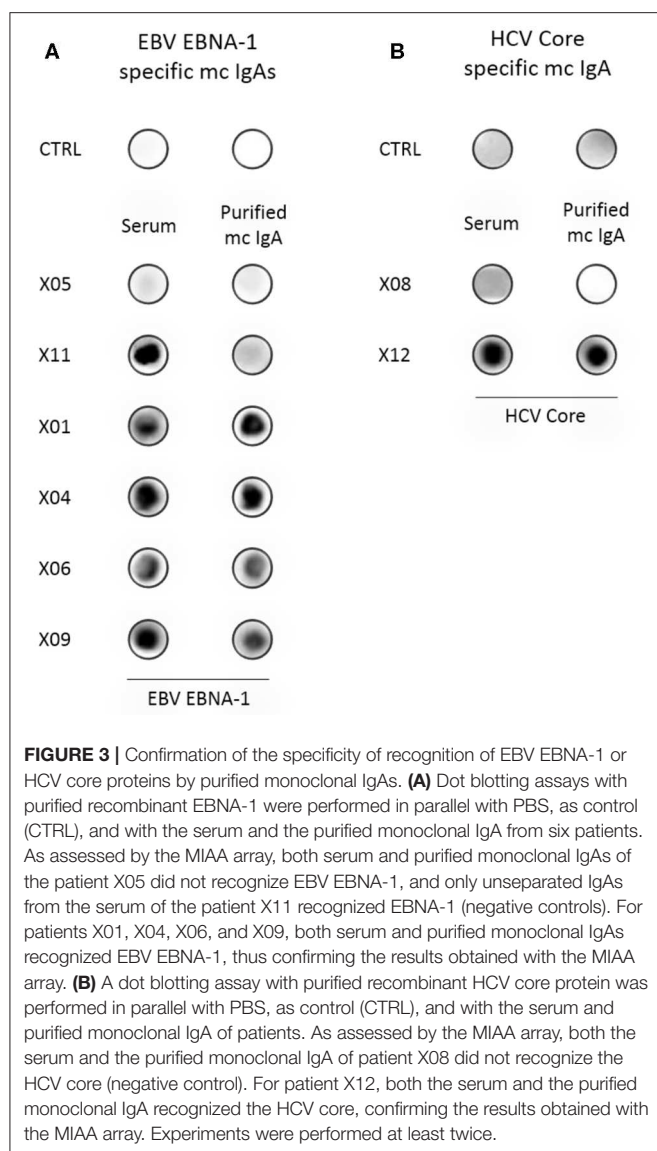
Two viral proteins, EBV EBNA-1 and HCV core, were specifically recognized by monoclonal IgAs from certain myeloma patients; these proteins are also the targets of monoclonal IgGs in both MGUS and myeloma (12–15). Because IgAs are linked with the digestive tract and other mucosal tissues,



it is not surprising that monoclonal IgAs reacted with pathogens found in mucosal or digestive and hepatic tissues (HCV) or in saliva (EBV) (31, 35, 37). The PGRPPFF sequence, identified as a frequent EBNA-1 epitope for the general population, was not recognized by EBNA-1-reactive monoclonal IgAs, an observation also made for EBNA-1-reactive monoclonal IgGs (12, 36). It will be important to determine whether the amino acid sequences targeted by monoclonal IgAs from myeloma patients differ from those of IgAs from healthy individuals. Future characterization of the EBNA-1 sequences recognized by monoclonal IgGs and IgAs should help determine whether certain epitope “hotspots” are overrepresented in the BCR specificity of malignant B cells in myeloma. For instance, knowing the viral sequences linked to MGUS and myeloma would permit their elimination from the future EBV vaccines in development (38, 39). In addition, for 15.8% of patients with IgA myeloma in this cohort, the purified monoclonal IgA reacted with LGL1, a self-antigen

initially described as a target of monoclonal IgAs in the context of Gaucher disease (10, 11). In future studies, it would be of interest to determine whether MGUS and myeloma patients with an anti-LGL1 monoclonal Ig present a mild, unsuspected metabolic deficiency resulting in sphingolipid accumulation.

Altogether, our findings suggest that for a significant fraction (>30%) of patients with IgA or IgG myeloma, the initial cause of disease may be chronic antigen stimulation due to a viral infection (particularly by EBV or HCV) or autoimmunity against LGL1 (10–14). These observations may be compared to the ~50% chronic lymphocytic leukemia (CLL) where the malignant clone displays somatically mutated Ig heavy (H) chain variable (IGHV) genes, indicative of antigen-driven disease (40, 41). Importantly, antigen-driven disease may be associated with a distinct prognosis: patients with antigen-driven CLL seem to have a more favorable clinical course than other CLL patients, whereas myeloma patients with EBNA-1-associated myeloma tend to



present with more severe disease (12, 42, 43). In this small cohort, myeloma patients with EBNA-1-specific monoclonal IgA were relatively young at diagnosis (≤ 63 years), with severe (59–93%) plasma cell infiltration of the bone marrow, characteristics similar to those reported for myeloma patients with EBNA-1-specific monoclonal IgG (12). Regarding LGL1-associated myeloma, Nair et al. suggested that it may represent a mild form of myeloma (10). In the present study, the two myeloma patients with LGL1-specific IgA did not have mild disease. Studies performed on large cohorts of well-annotated patients (with cytometry, cytogenetics, genetic data) are necessary for the full characterization of myeloma linked to LGL-1 or EBV EBNA-1.

The antigenic targets of malignant clones of B-cell lineage have been studied in the context of CLL, using different technical approaches (phage-display technology, mass spectrometry). Several auto-antigens have been associated with CLL, notably cytoskeleton components (non-muscle myosin heavy chain IIA,

TABLE 3 | Characteristics of myeloma patients with a monoclonal IgA specific for EBV nuclear antigen 1 (EBNA-1).

	Myeloma with or without a monoclonal IgA specific for EBV or HCV			
	HCV(+)	EBNA-1(+)	MIAA(-)	p-value
Patients, <i>n</i>	1	4	17	
Male sex, <i>n</i> (%)	1	0 (0%)	7 (41.2%)	
Age at Diagnosis (year)				
Patients, <i>n</i>	1	3	17	
Median	NA	60.6	75.1	
Mean \pm SD	NA	60.2 \pm 2.9	73.5 \pm 8.8	$p = 0.0254^*$
Range, min-max	94	57–63	57.1–86.5	
Leukocytes ($10^9/L$)				
Patients, <i>n</i>	1	3	16	
Median	NA	3.6	5.1	NS
Range, min-max	NA	3.4–4.6	1.3–9.0	
Hemoglobin (g/dl)				
Patients, <i>n</i>	1	3	16	
Median	NA	9.8	9.7	NS
Range, min-max	NA	8.5–12.5	5.4–15.3	
Platelets ($10^9/L$)				
Patients, <i>n</i>	1	3	16	
Median	NA	140	169	NS
Range, min-max	NA	113–237	24–269	
Bone Marrow Plasma Cells (%)				
Patients, <i>n</i>	1	3	16	
Median	NA	74	46.5	$p = 0.0572^*$
Range, min-max	NA	59–93	1 [#] –89	
Calcemia (mmol/L)				
Patients, <i>n</i>	1	3	17	
Median	NA	2.4	2.2	NS
Range, min-max	NA	2.3–2.6	1.8–2.7	
Creatinin ($\mu\text{mol/L}$)				
Patients, <i>n</i>	1	3	17	
Median	NA	59.0	69.0	NS
Range, min-max	NA	57–117	36–763	
β_2-Microglobulin (mg/L)				
Patients, <i>n</i>	1	2	5	
Median	NA	5.6	4.5	NS
>3.5 mg/L, <i>n</i> (%)	NA	1 (50.0%)	2 (40.0%)	
Range, min-max		3.05–8.2	1.1–14.2	
Monoclonal IgA (g/L)				
Patients, <i>n</i>	1	4	17	
Median	NA	33.0	16.0	NS
Range, min-max	NA	17.0–57.0	4.0–57.0	
Bone Lesions				
Patients, <i>n</i>	1	3	17	
With bone lesions, <i>n</i> (%)	NA	3 (100%)	15 (88.2%)	NS
DSS Stage				
Patients, <i>n</i>	1	4	17	
Stage I	NA	0	0	
Stage II	NA	1	7	
Stage III, <i>n</i> (%)	NA	3 (75.0%)	10 (58.8%)	NS

(Continued)

TABLE 3 | Continued

	Myeloma with or without a monoclonal IgA specific for EBV or HCV			
	HCV(+)	EBNA-1(+)	MIAA(-)	<i>p</i> -value
ISS Stage				
Patients, <i>n</i>	1	4	5	
Stage I, <i>n</i>	NA	2	1	
Stage II, <i>n</i>	NA	0	2	
Stage III, <i>n</i> (%)	NA	2 (50.0%)	2 (40.0%)	NS
Serum IgA Sialylation (%)				
Patients, <i>n</i>	1	3	17	
Median (mean)	49.7 (49.7)	53.4 (41.7)	40.8 (43.1)	
Range, min–max	NA	11.9–59.7	35.9–57.9	NS

n, number; NA, not applicable; NS, not significant; HCV+, patient with HCV-specific purified monoclonal IgA; EBNA-1+, patients with EBNA-1-specific purified monoclonal IgA; MIAA-, Patients with a purified monoclonal IgA not specific for any infectious pathogen of the MIAA. Because biological information was not available for all patients, and was partial for some patients, the number of patients with data may vary. Statistical analysis was performed using the Chi-2 test for categorical variables and the *Mann-Whitney test for continuous variables. Significant differences are indicated. *MM patient with 29g/L monoclonal IgG.

TABLE 4 | Characteristics of myeloma patients with a lysoglycosylceramide (LGL1)-specific monoclonal IgA.

	Patient X03	Patient X08	Patient Nvs37
Sex (M/F)	F	F	M
Age (year)	76	66	51
Leukocytes ($\times 10^9/L$)	2.4	7.2	NA
Hemoglobin (g/dl)	6.9	12.8	NA
Platelets ($\times 10^9/L$)	191	269	NA
Bone marrow plasma cells (%)	51	16	NA
Calcemia (mmol/L)	2.16	2.36	NA
Creatinin ($\mu\text{mol/L}$)	66	38	NA
β_2 -microglobulin (mg/L)	NA	NA	NA
Monoclonal IgA (g/L)	28.0	8.0	23.2
Bone lesions	Yes	Yes	NA
ISS stage	NA	NA	NA
DSS stage	NA	III	NA
Serum IgA sialylation (%)	36.1%	46.3%	NA

NA, not available; ISS, International System Staging; DSS, Durie-Salmon Staging.

vimentin, cofilin-1, filamin B), cardiolipin, proline-rich acidic protein-1 (PRAP-1), dUTPase, and auto-antigens at the surface of apoptotic cells and bacteria (*Streptococcus pneumoniae* for instance) (44–51). Evidence of virus (HCV, HIV)-driven CLL has been less reported (52–54). Regarding EBV, EBV DNA is typically not detected in malignant CLL or myeloma cells (20). The variability of EBV DNA loads in blood and the patterns of anti-EBV Ig responses of patients have been well-analyzed in CLL, but the findings of these studies appear to mostly reflect the deficient immune system of aged CLL patients (55–58). Thus, formal evidence of EBV antigen-driven CLL disease is still lacking,

and identified CLL-associated antigens are predominantly auto-antigens linked to bacterial infection and/or apoptotic cell removal, and to a lesser degree, viral antigens (44, 45, 52–54). In contrast, the most frequent antigenic targets associated so far with MGUS and myeloma are viral proteins (especially from EBV, HSV, HCV) and a ganglioside, LGL1 (10–14). Of note, several groups reported that gangliosides facilitate cell entry of viruses (59). Knowing whether anti-LGL1 monoclonal IgAs can counter virus cell entry would be of interest.

IgA glycosylation was also analyzed. Monoclonal IgAs differed from IgAs from healthy donors by their low level of sialylation, a characteristic observed for monoclonal IgGs and associated with a pro-inflammatory action of the Ig Fc fragment upon binding to FcγR, notably in monocytes and macrophages (21). However, sialylation did not differ depending on the antigenic specificity of the monoclonal IgA. Further studies are needed to determine whether monoclonal IgAs from MGUS and myeloma patients contribute to the production of pro-inflammatory cytokines, as reported for patients with hyposialylated IgGs (polyclonal or/and monoclonal) (21).

In aging populations, the incidence of MGUS and the subsequent risk of myeloma and other MGUS-associated diseases increase (60, 61). The detection of antigen-initiated MGUS and myeloma cases, and the determination of the antigenic target of the monoclonal Ig, should be useful additions to the diagnostic work-up of MGUS and myeloma because they allow new possibilities of prevention and treatment. First, disease-initiating antigenic targets could serve as new risk markers. Second, MGUS patients, who are not treated presently, and myeloma patients could benefit from antigen-reduction treatments. Supporting this approach, several groups reported that the addition of anti-viral treatment to myeloma protocols resulted in disease regression and/or improved response to chemotherapy, notably for HCV-associated myeloma (62, 63). Drugs that target BCR signaling may also be considered (64, 65). Moreover, new drugs are currently being developed that specifically target EBV (66, 67). Clearly, if one could clear the MGUS-associated underlying chronic infection early on, it may be possible to prevent the development of myeloma (68). Regarding myeloma patients with an LGL1-specific monoclonal Ig, reduction of LGL1 levels may be envisioned as a complementary treatment. Indeed, LGL1 reduction has been successfully achieved in Gaucher patients for many years (69–73). Importantly, glucolipid reduction prevents associated B-cell malignancies in murine models (74, 75). Recently, Nair et al. reported that glucolipid reduction treatment resulted in decreased amount of monoclonal Ig in Gaucher patients with monoclonal gammopathy (76).

In conclusion, EBV EBNA-1, the HCV core protein, and LGL1, a glucolipid, were identified as candidate antigenic targets of the purified monoclonal IgAs of patients with IgA myeloma. An abnormal immune response to these viruses or to LGL1 may therefore be part of the pathogenesis of IgA myeloma, as reported for IgG myeloma. Detecting patients who present with LGL1- or virus-associated MGUS or myeloma is important since it is possible to add antigen target reduction to classic treatments.

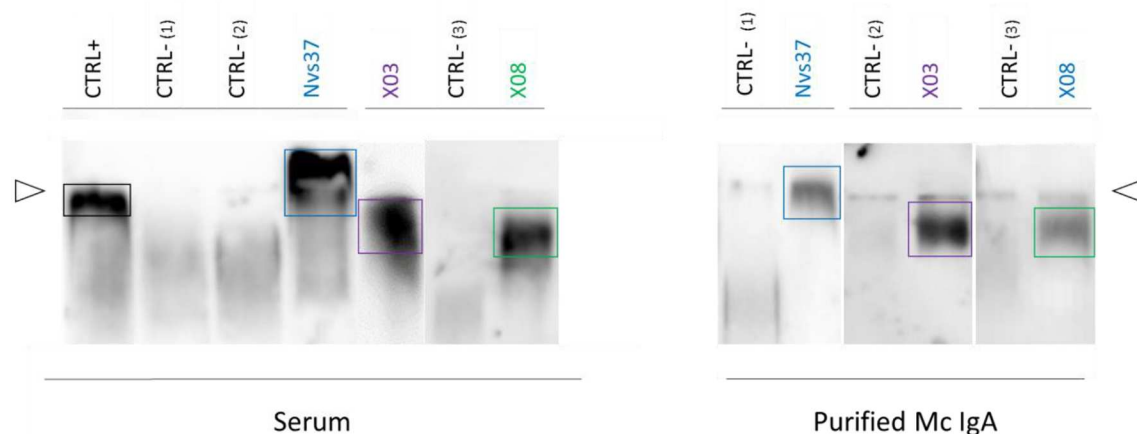


FIGURE 4 | Lysoglucosylceramide (LGL1) is specifically recognized by subsets of purified monoclonal IgAs. LGL1-specific immunoblotting assays were performed as described in the Materials and Methods section (7, 27, 28). Samples of serum (left) or purified monoclonal IgAs (right) were first submitted to agarose gel electrophoresis; then, the gels were blotted onto LGL1-saturated membranes. After blocking for 1 h, membranes were incubated with anti-human IgA horseradish peroxidase (HRP)-conjugated secondary antibody, then washed and revealed by chemiluminescence. The positive control (CTRL+, left) was a sample of serum from a patient known to have LGL1-specific IgAs. Negative controls (CTRL-) were samples of serum without LGL1-reactive IgAs (one from a healthy volunteer, two from patients). The lines of sample deposit are indicated by white arrowheads. The positive signals characteristic of LGL1-reactive Igs are encircled. Patterns of migration may differ for serum and purified monoclonal IgAs because serum may contain both monoclonal and polyclonal LGL1-reactive IgAs.

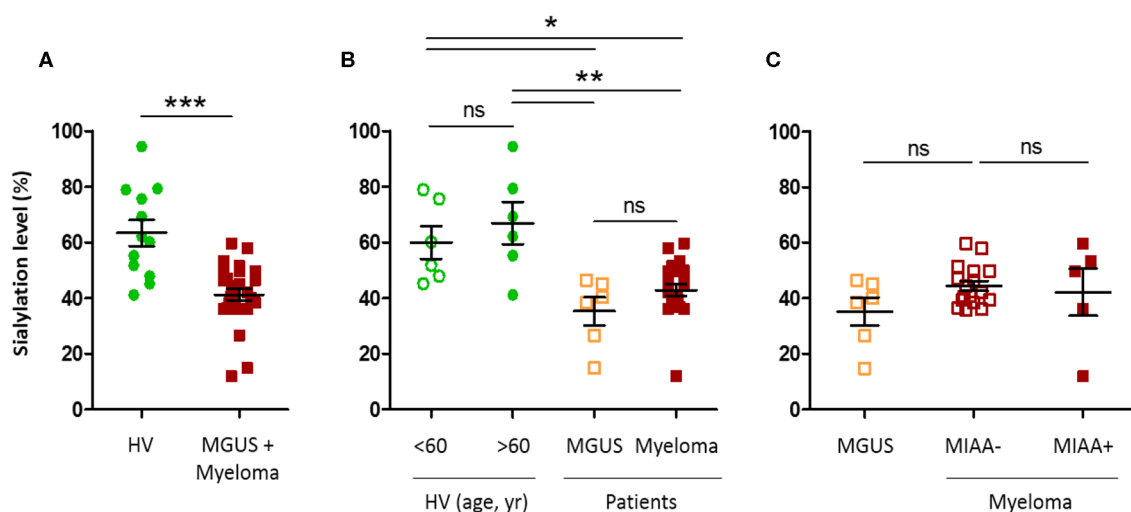


FIGURE 5 | Hyposialylation of IgAs from monoclonal gammopathy of undetermined significance (MGUS) and myeloma patients. The sialylation level of IgAs in the serum of healthy volunteers (HV, $n = 12$), MGUS ($n = 6$), and myeloma ($n = 22$) patients was assessed using an enzyme-linked lectin assay (ELLA) technique, as described in the Materials and Methods section. Unfortunately, we were not able to constitute a control cohort of patients with excessive amounts of non-clonal IgAs. Results are expressed as percentages of sialylated forms of IgAs in serum. **(A)** Sialylation level of IgAs from HV (green dots) and MGUS and myeloma (MM) patients (red dots); $***p < 0.001$, Mann-Whitney U -test. **(B)** Sialylation level according to age, in HV under or over 60 (green dots), and according to the diagnosis of MGUS (orange squares) or MM (red squares). **(C)** Sialylation level of IgAs from MM patients with a pathogen-specific monoclonal IgA, as determined by the MIAA (filled red squares, MIAA+) and MM patients with a monoclonal IgA of undetermined specificity (open red squares, MIAA-), compared to MGUS patients (orange squares). Bars indicate means \pm SEM. **(B,C)** Significant differences are indicated by stars; $*p < 0.05$ and $**p < 0.01$, Kruskal-Wallis test followed by Dunn's *post-hoc* test (ns, not significant).

DATA AVAILABILITY STATEMENT

The datasets generated for this study are available on request to the corresponding author.

ETHICS STATEMENT

The studies involving human participants were reviewed and approved by Local ethics committee, CHU Nantes. The

patients/participants provided their written informed consent to participate in this study.

AUTHOR CONTRIBUTIONS

SH, AB, EB-C, and JH designed the research, analyzed the data, and wrote the manuscript. AB, CS, NM, SA-M, MF, EB-C, and JH performed the experiments and edited the manuscript. AT, EP, PL, and FM contributed patient samples and data. All approved the version to be submitted for publication and agreed to be accountable for all aspects of the work in ensuring that questions related to the accuracy or integrity of any part of the article are appropriately investigated and resolved.

FUNDING

The study has been supported by grants to SH from the Ligue Nationale contre le Cancer, the Cancéropôle Grand Ouest and Région Pays de la Loire (2015–2016), and Janssen USA. EP benefited from a grant from the Cancéropôle Grand Ouest and Région Centre (2015–2016). The salary of AB was supported

by the Cancéropôle Grand Ouest/Région Pays de la Loire (HII-GO project, June 2015 to December 2016), then Janssen USA (January 2017 to December 2017). The salary of NM was supported by Janssen USA (September 2016 to April 2019).

ACKNOWLEDGMENTS

We thank all the colleagues from the Departments of Hematology or Internal Medicine of the University Hospitals in Tours and Bordeaux, who contributed to the diagnosis and care of patients in this study, and Novartis (Basel, Switzerland) for providing seven IgA myeloma serum samples. We also thank Dr. Pierre Weigel and Dr. Cathy Charlier (CNRS UMR6286) and the IMPacT platform (impact-plateforme.com) at the University of Nantes, in Nantes, France.

SUPPLEMENTARY MATERIAL

The Supplementary Material for this article can be found online at: <https://www.frontiersin.org/articles/10.3389/fimmu.2020.00854/full#supplementary-material>

REFERENCES

- Kyle RA. Monoclonal gammopathy of undetermined significance. Natural history in 241 cases. *Am J Med.* (1978) 64:814–26. doi: 10.1016/0002-9343(78)90522-3
- Kyle RA, Therneau TM, Rajkumar SV, Offord JR, Larson DR, Plevak MF, et al. A long-term study of prognosis of monoclonal gammopathy of undetermined significance. *N Engl J Med.* (2002) 346:564–9. doi: 10.1056/NEJMoa01133202
- Dhodapkar MV. MGUS to myeloma: a mysterious gammopathy of underexplored significance. *Blood.* (2016) 128:2599–606. doi: 10.1182/blood-2016-09-692954
- Kyle RA, Larson DR, Therneau TM, Dispenzieri A, Kumar S, Cerhan JR, et al. Long-term follow-up of monoclonal gammopathy of undetermined significance. *New Engl J Med.* (2018) 378:241–9. doi: 10.1056/NEJMoa1709974
- Kyle RA, Greipp PR. Smoldering multiple myeloma. *N Engl J Med.* (1980) 302:1347–9. doi: 10.1056/NEJM198006123022405
- Rajkumar SV, Dimopoulos MA, Palumbo A, Blade J, Merlini G, Mateos MV, et al. International myeloma working group updated criteria for the diagnosis of multiple myeloma. *Lancet Oncol.* (2014) 15:e538–48. doi: 10.1016/S1470-2045(14)70442-5
- Bergón E, Miravalles E. Retrospective study of monoclonal gammopathies detected in the clinical laboratory of a Spanish healthcare district: 14-year series. *Clin Chem Lab Med.* (2007) 45:190–6. doi: 10.1515/CCLM.2007.029
- Vescio RA, Cao J, Hong CH, Lee JC, Wu CH, Der Danielian M, et al. Myeloma Ig heavy chain V region sequences reveal prior antigenic selection and marked somatic mutation but no intraclonal diversity. *J Immunol.* (1995) 155:2487–97.
- Sahota SS, Leo R, Hamblin TJ, Stevenson FK. Myeloma VL and VH gene sequences reveal a complementary imprint of antigen selection in tumor cells. *Blood.* (1997) 89:219–26. doi: 10.1182/blood.V89.1.219.219_226
- Nair S, Branagan AR, Liu J, Boddupalli CS, Mistry PK, Dhodapkar M V. Clonal immunoglobulin against lysolipids in the origin of myeloma. *N Engl J Med.* (2016) 374:555–61. doi: 10.1056/NEJMoa1508808
- Nair S, Sng J, Sekhar Boddupalli C, Seckinger A, Chesi M, Fulciniti M, et al. Antigen-mediated regulation in monoclonal gammopathies and myeloma. *J Clin Invest Insight.* (2018) 3:e98259. doi: 10.1172/jci.insight.98259
- Bosseboeuf A, Feron D, Tallet A, Rossi C, Charlier C, Garderet L, et al. Monoclonal IgG in MGUS and multiple myeloma target infectious pathogens. *J Clin Invest Insight.* (2017) 2:e95367. doi: 10.1172/jci.insight.95367
- Hermouet S, Corre I, Gassin M, Bigot-Corbel E, Sutton CA, Casey JW. Hepatitis C virus, human herpesvirus 8, and the development of plasma-cell leukemia. *N Engl J Med.* (2003) 348:178–9. doi: 10.1056/NEJM200301093480219
- Bigot-Corbel E, Gassin M, Corre I, Le Carrer D, Delaroché O, Hermouet S. Hepatitis C virus (HCV) infection, monoclonal immunoglobulin specific for HCV core protein, and plasma-cell malignancy. *Blood.* (2008) 112:4357–8. doi: 10.1182/blood-2008-07-167569
- Feron D, Charlier C, Gourain V, Garderet L, Coste-Burel M, Le Pape P, et al. Multiplexed infectious protein microarray immunoassay suitable for the study of the specificity of monoclonal immunoglobulins. *Anal Biochem.* (2013) 433:202–9. doi: 10.1016/j.ab.2012.10.012
- Plummer M, de Martel C, Vignat J, Ferlay J, Bray F, Franceschi S. Global burden of cancers attributable to infections in 2012: a synthetic analysis. *Lancet Glob Health.* (2016) 4:e609–16. doi: 10.1016/S2214-109X(16)30143-7
- Seifert M, Scholtysik R, Küppers R. Origin and pathogenesis of B cell lymphomas. *Methods Mol Biol.* (2013) 971:1–25. doi: 10.1007/978-1-62703-269-8_1
- Saha A, Robertson ES. Epstein-Barr virus-associated B-cell lymphomas: pathogenesis and clinical outcomes. *Clin Cancer Res.* (2011) 17:3056–63. doi: 10.1158/1078-0432.CCR-10-2578
- Franceschi S, Lise M, Trépo C, Berthillon P, Chuang SC, Nieters A, et al. Infection with hepatitis B and C viruses and risk of lymphoid malignancies in the European prospective investigation into cancer and nutrition (EPIC). *Cancer Epidemiol Biomarkers Prev.* (2011) 20:208–14. doi: 10.1158/1055-9965.EPI-10-0889
- Hermouet S, Sutton CA, Rose TM, Greenblatt RS, Corre I, Garand R, et al. Qualitative and quantitative analysis of human herpesvirus expression in chronic and acute B-cell lymphocytic leukemia and in multiple myeloma. *Leukemia.* (2003) 17:185–95. doi: 10.1038/sj.leu.2402748
- Bosseboeuf A, Allain S, Mennesson N, Tallet A, Rossi C, Garderet L, et al. Pro-inflammatory state in MGUS and myeloma is characterized by low sialylation of pathogen-specific and other monoclonal and polyclonal immunoglobulin G. *Front Immunol.* (2017) 8:1347. doi: 10.3389/fimmu.2017.01347
- Nair B, Waheed S, Szymonifka J, Shaughnessy JD, Crowley J Jr, Barlogie B. Immunoglobulin isotypes in multiple myeloma: laboratory correlates and prognostic implications in total therapy protocols. *Br J Haematol.* (2009) 145:134–7. doi: 10.1111/j.1365-2141.2008.07547.x

23. Krejci M, Hajek R, Buchler T, Krivanova A, Svobodnik A, Pour L, et al. Simple variables predict survival after autologous transplantation: a single centre experience in 181 multiple myeloma patients. *Neoplasma*. (2007) 54:143–8.
24. Pasqualetti P, Colantonio D, Collacciani A, Casale R, Natali G. Classification and prognostic evaluation in multiple myeloma. A retrospective study of relationship of survivals and responses to chemotherapy to immunological types, 20 single prognostic factors, 15 clinical staging systems, and 6 morphological classifications. *Panminerva Med*. (1991) 33:93–110.
25. Wang L, Jin F-Y, Li Y, Sun J-N, Zhang J-J, Tang R, et al. IgA type multiple myeloma, clinical features, and prognosis. *Chinese Med J*. (2018) 131:1249–50. doi: 10.4103/0366-6999.231513
26. Gemenetzi K, Agathangelidis A, Papalexandri A, Medina A, Genuardi E, Moysiadis T, et al. Distinct immunogenetic signatures in IgA versus IgG multiple myeloma. *58th American Society of Hematology (ASH) Annual Meeting & Exposition*. San Diego, CA: Poster (2016) doi: 10.1182/blood.V128.22.2062.2062
27. Roberts-Thomson PJ, Mason DY, MacLennan ICM. Relationship between paraprotein clinical features in IgA polymerization and myeloma. *Br J Haematol*. (1976) 33:117–30. doi: 10.1111/j.1365-2141.1976.tb00978.x
28. Kyle RA, Remstein ED, Therneau TM, Dispenzieri A, Kurtin PJ, Hodnefield JM, et al. Clinical course and prognosis of smoldering (asymptomatic) multiple myeloma. *New Engl J Med*. (2007) 356:2582–90. doi: 10.1056/NEJMoa070389
29. Nooij FJ, Van der Sluijs-Gelling AJ, Jol-Van der Zijde CM, Van Tol MJ, Haas H, Radl J. Immunoblotting techniques for the detection of low level homogeneous immunoglobulin components in serum. *J Immunol Methods*. (1990) 134:273–81. doi: 10.1016/0022-1759(90)90389-D
30. Braun W, Abraham R. Modified diffusion blotting for rapid and efficient protein transfer with PhastSystem. *Electrophoresis*. (1989) 10:249–53. doi: 10.1002/elps.1150100406
31. Hadar T, Rahima M, Kahan E, Sidi J, Rakowsky E, Sarov B, et al. Significance of specific Epstein-Barr virus IgA and elevated IgG antibodies to viral capsid antigens in nasopharyngeal carcinoma patients. *J Med Virol*. (1986) 20:329–39. doi: 10.1002/jmv.1890200405
32. Levy E, Margalith M, Sarov B, Sarov I, Rinaldo CR, Detels R, et al. Cytomegalovirus IgG and IgA serum antibodies in a study of HIV infection and HIV-related diseases in homosexual men. *J Med Virol*. (1991) 35:174–9. doi: 10.1002/jmv.1890350306
33. Friedman MG, Kimmel N. Herpes Simplex virus-specific serum immunoglobulin A: detection in patients with primary or recurrent herpes infections and in healthy adults. *Infect Immun*. (1982) 1:374–7. doi: 10.1128/IAI.37.1.374-377.1982
34. Wittek AE, Arvin AM, Koropchak CM. Serum immunoglobulin A antibody to varicella-zoster virus in subjects with primary varicella and herpes zoster infections and in immune subjects. *J Clin Microbiology*. (1983) 18:1146–9. doi: 10.1128/JCM.18.5.1146-1149.1983
35. Urita Y, Hike K, Torii N, Kikuchi Y, Kurakata H, Kanda E, et al. Comparison of serum IgA and IgG antibodies for detecting helicobacter pylori infection. *Int Med*. (2004) 43:548–52. doi: 10.2169/internalmedicine.43.548
36. Xu GJ, Kula T, Xu Q, Li MZ, Vernon SD, Ndung'u T, et al. Viral immunology. Comprehensive serological profiling of human populations using a synthetic human virome. *Science*. (2015) 348:aaa0698. doi: 10.1126/science.aaa0698
37. González-Quintela A, Alende MR, Gamallo R, González-Gil P, López-Ben S, Tomé S, et al. Serum immunoglobulins (IgG, IgA, IgM) in chronic hepatitis C. A comparison with non-cirrhotic alcoholic liver disease. *Hepatogastroenterol*. (2003) 54:2121–6.
38. Cohen JI. Epstein-Barr virus vaccines. *Clin Translat Immunol*. (2015) 4:e32. doi: 10.1038/cti.2014.27
39. Cohen JI. Vaccine development for Epstein-Barr virus. *Adv Exp Med Biol*. (2018) 1045:477–93. doi: 10.1007/978-981-10-7230-7_22
40. Fais F, Ghiotto F, Hashimoto S, Sellars B, Valetto A, Allen SL, et al. Chronic lymphocytic leukemia B cells express restricted sets of mutated and unmutated antigen receptors. *J Clin Invest*. (1998) 102:1515–25. doi: 10.1172/JCI3009
41. Henriques A, Rodríguez-Caballero A, Criado I, Langerak AW, Nieto WG, Lécresse Q, et al. Molecular and cytogenetic characterization of expanded B-cell clones from multiclonal versus monoclonal B-cell chronic lymphoproliferative disorders. *Haematologica*. (2014) 99:897–907. doi: 10.3324/haematol.2013.098913
42. Damle RN, Wailly T, Fais F, Ghiotto F, Valetto A, Allen SL, et al. Ig V gene mutation status and CD38 expression as novel prognostic indicators in chronic lymphocytic leukemia. *Blood*. (1999) 94:1840–7. doi: 10.1182/blood.V94.6.1840.418k06_1840_1847
43. Hamblin TJ, Davis Z, Gardiner A, Oscier DG, Stevenson FK. Unmutated Ig VH genes are associated with a more aggressive form of chronic lymphocytic leukemia. *Blood*. (1999) 94:1848–54. doi: 10.1182/blood.V94.6.1848.418k05_1848_1854
44. Chiorazzi N, Hatzi K, Albesiano E. B-cell chronic lymphocytic leukemia, a clonal disease of B lymphocytes with receptors that vary in specificity for (auto)antigens. *Ann N Y Acad Sci*. (2005) 1062:1–12. doi: 10.1196/annals.1358.002
45. Karp M, Giannopoulos K. Antigen stimulation in the development of chronic lymphocytic leukemia. *Postepy Hig Med Dosw*. (2013) 67:1204–13. doi: 10.5604/17322693.1078852
46. CATERA R, Silverman GJ, Hatzi K, Seiler T, Didier S, Zhang L, et al. Chronic lymphocytic leukemia cells recognize conserved epitopes associated with apoptosis and oxidation. *Mol Med*. (2008) 14:665–74. doi: 10.2119/2008-00102.CATERA
47. Chu CC, CATERA R, Hatzi K, Yan XJ, Zhang L, Wang XB, et al. Chronic lymphocytic leukemia antibodies with a common stereotypic rearrangement recognize nonmuscle myosin heavy chain IIA. *Blood*. (2008) 112:5122–9. doi: 10.1182/blood-2008-06-162024
48. Lanemo Myhrinder A, Hellqvist E, Sidorova E, Söderberg A, Baxendale H, Dahle C, et al. A new perspective: molecular motifs on oxidized LDL, apoptotic cells, and bacteria are targets for chronic lymphocytic leukemia antibodies. *Blood*. (2008) 111:3838–48. doi: 10.1182/blood-2007-11-125450
49. Seiler T, Woelfle M, Yancopoulos S, CATERA R, Li W, Hatzi K, et al. Characterization of structurally defined epitopes recognized by monoclonal antibodies produced by chronic lymphocytic leukemia B cells. *Blood*. (2009) 114:3615–24. doi: 10.1182/blood-2009-01-197822
50. Rosén A, Murray F, Evaldsson C, Rosenquist R. Antigens in chronic lymphocytic leukemia—implications for cell origin and leukemogenesis. *Semin Cancer Biol*. (2010) 20:400–9. doi: 10.1016/j.semcancer.2010.09.004
51. Williams M, Ariza ME. EBV positive diffuse large B cell lymphoma and chronic lymphocytic leukemia patients exhibit increased Anti-dUTPase antibodies. *Cancers (Basel)*. (2018) 10:129. doi: 10.3390/cancers10050129
52. Casabonne D, Almeida J, Nieto WG, Romero A, Fernández-Navarro P, Rodríguez-Caballero A, et al. Common infectious agents and monoclonal B-cell lymphocytosis: a cross-sectional epidemiological study among healthy adults. *PLoS ONE*. (2012) 7:e2808. doi: 10.1371/journal.pone.0052808
53. Arcaini L, Merli M, Volpetti S, Rattotti S, Gotti M, Zaja F. Indolent B-cell lymphomas associated with HCV infection: clinical and virological features and role of antiviral therapy. *Clin Dev Immunol*. (2012) 2012:638185. doi: 10.1155/2012/638185
54. Hwang K-K, Trama AM, Kozink DM, Chen X, Wiehe K, Cooper AJ, et al.IGHV1-69 B cell chronic lymphocytic leukemia antibodies cross-react with HIV-1 and hepatitis C virus antigens as well as intestinal commensal bacteria. *PLoS ONE*. (2014) 9:e90725. doi: 10.1371/journal.pone.0090725
55. Visco C, Falisi E, Young KH, Pascarella M, Perbellini O, Carli G, et al. Epstein-Barr virus DNA load in chronic lymphocytic leukemia is an independent predictor of clinical course and survival. *Oncotarget*. (2015) 6:18653–63. doi: 10.18632/oncotarget.4418
56. Teras LR, Rollison DE, Pawlita M, Michel A, Brozy J, de Sanjose S, et al. Epstein-Barr virus and risk of non-Hodgkin lymphoma in the cancer prevention study-II and a meta-analysis of serologic studies. *Int J Cancer*. (2015) 136:108–16. doi: 10.1002/ijc.28971
57. Casabonne D, Benavente Y, Robles C, Costas L, Alonso E, Gonzalez-Barca E, et al. Aberrant Epstein-Barr virus antibody patterns and chronic lymphocytic leukemia in a Spanish multicentric case-control study. *Infect Agent Cancer*. (2015) 10:5. doi: 10.1186/1750-9378-10-5
58. Ferrajoli A, Ivan C, Ciccone M, Shimizu M, Kita Y, Ohtsuka M, et al. Epstein-Barr virus microRNAs are expressed in patients with chronic lymphocytic leukemia and correlate with overall survival. *EBioMedicine*. (2015) 2:572–82. doi: 10.1016/j.ebiom.2015.04.018
59. Martínez MA, López S, Arias CF, Isa P. Gangliosides have a functional role during rotavirus cell entry. *J Virol*. (2013) 87:1115–22. doi: 10.1128/JVI.01964-12

60. Therneau TM, Kyle RA, Melton LJ 3rd, Larson DR, Benson JT, Colby CL, et al. Incidence of monoclonal gammopathy of undetermined significance and estimation of duration before first clinical recognition. *Mayo Clin Proc.* (2012) 87:1071–9. doi: 10.1016/j.mayocp.2012.06.014
61. Bida JP, Kyle RA, Therneau TM, Melton LJ 3rd, Plevak MF, Larson DR, et al. Disease associations with monoclonal gammopathy of undetermined significance: a population-based study of 17,398 patients. *Mayo Clin Proc.* (2009) 84:685–93. doi: 10.4065/84.8.685
62. Panfilio S, D'Urso P, Annechini G, D'Elia GM, De Angelis F, Stefanizzi C, et al. Regression of a case of multiple myeloma with antiviral treatment in a patient with chronic HCV infection. *Leuk Res Rep.* (2013) 2:39–40. doi: 10.1016/j.lrr.2013.01.002
63. Rodríguez García A, Linares M, Mennesson N, Sanchez-Vega B, Sanchez R, Alonso Fernandez R, et al. The role of Hepatitis C virus in the development of multiple myeloma: A case study. 60th Annual Meeting of the American Society of Hematology (ASH), San Diego, CA, USA, December 1–4, (2018). Abstract Nbr: 5592, Submission ID: 112842. *Blood.* (2018) 132:5592. doi: 10.1182/blood-2018-99-112842
64. Pal Singh S, Dammeijer F, Hendriks RW. Role of Bruton's tyrosine kinase in B cells and malignancies. *Mol Cancer.* (2018) 17:57. doi: 10.1186/s12943-018-0779-z
65. Burger JA, Chiorazzi N. B cell receptor signaling in chronic lymphocytic leukemia. *Trends Immunol.* (2013) 34:592–601. doi: 10.1016/j.it.2013.07.002
66. Pagano JS, Whitehurst CB, Andrei G. Antiviral drugs for EBV. *Cancers (Basel).* (2018) 10:E197. doi: 10.3390/cancers10060197
67. Verma D, Thompson J, Swaminathan S. Spironolactone blocks epstein-barr virus production by inhibiting EBV SM protein function. *Proc Natl Acad Sci USA.* (2016) 113:3609–14. doi: 10.1073/pnas.1523686113
68. Tomasson MH, Ali M, De Oliveira V, Xiao Q, Jethava Y, Zhan F, et al. Prevention is the best treatment: the case for understanding the transition from monoclonal gammopathy of undetermined significance to myeloma. *Int J Mol Sci.* (2018) 19:E3621. doi: 10.3390/ijms19113621
69. Weinreb NJ, Charrow J, Andersson HC, Kaplan P, Kolodny EH, Mistry P, et al. Effectiveness of enzyme replacement therapy in 1028 patients with type 1 gaucher disease after 2 to 5 years of treatment: a report from the gaucher registry. *Am J Med.* (2002) 113:112–9. doi: 10.1016/S0002-9343(02)01150-6
70. Weinreb NJ, Goldblatt J, Villalobos J, Charrow J, Cole JA, Kerstenetzky M, et al. Long-term clinical outcomes in type 1 Gaucher disease following 10 years of imiglucerase treatment. *J Inherit Metab Dis.* (2013) 36:543–53. doi: 10.1007/s10545-012-9528-4
71. Mistry PK, Lukina E, Ben Turkia H, Amato D, Baris H, Dasouki M, et al. Effect of oral eliglustat on splenomegaly in patients with Gaucher disease type 1 : the ENGAGE randomized clinical trial. *JAMA.* (2015) 313:695–706. doi: 10.1001/jama.2015.459
72. Wasserstein MP, Diaz GA, Lachmann RH, Jouvin MH, Nandy I, Ji AJ, et al. Olipudase alfa for treatment of acid sphingomyelinase deficiency (ASMD): safety and efficacy in adults treated for 30 months. *J Inherit Metab Dis.* (2018) 41:829–38. doi: 10.1007/s10545-017-0123-6
73. Lachmann RH. Treating lysosomal storage disorders: what have we learnt? *J Inherit Metab Dis.* (2019) 43:125–32. doi: 10.1002/jimd.12131
74. Lwin ST, Olechnowicz SW, Fowler JA, Edwards CM. Diet-induced obesity promotes a myeloma-like condition *in vivo*. *Leukemia.* (2015) 29:507–10. doi: 10.1038/leu.2014.295
75. Pavlova EV, Archer J, Wang S, Dekker N, Aerts JM, Karlsson S, et al. Inhibition of UDP-glucosylceramide synthase in mice prevents Gaucher disease-associated B-cell malignancy. *J Pathol.* (2015) 235:113–24. doi: 10.1002/path.4452
76. Nair S, Bar N, Xu ML, Dhodapkar M, Mistry PK. Glucosylsphingosine but not saposin C, is the target antigen in Gaucher disease-associated gammopathy. *Mol Genet Metab.* (2020) 129:286–91. doi: 10.1016/j.ymgme.2020.01.009

Conflict of Interest: The authors declare that this study received funding from Janssen (USA). Janssen had no role in study design, data collection and analysis, or preparation of the manuscript.

Copyright © 2020 Bosseboeuf, Seillier, Mennesson, Allain-Maillet, Fourny, Tallet, Piver, Lehours, Mégraud, Berthelot, Harb, Bigot-Corbel and Hermouet. This is an open-access article distributed under the terms of the Creative Commons Attribution License (CC BY). The use, distribution or reproduction in other forums is permitted, provided the original author(s) and the copyright owner(s) are credited and that the original publication in this journal is cited, in accordance with accepted academic practice. No use, distribution or reproduction is permitted which does not comply with these terms.

Advantages of publishing in Frontiers



OPEN ACCESS

Articles are free to read
for greatest visibility
and readership



FAST PUBLICATION

Around 90 days
from submission
to decision



HIGH QUALITY PEER-REVIEW

Rigorous, collaborative,
and constructive
peer-review



TRANSPARENT PEER-REVIEW

Editors and reviewers
acknowledged by name
on published articles

Frontiers

Avenue du Tribunal-Fédéral 34
1005 Lausanne | Switzerland

Visit us: www.frontiersin.org

Contact us: info@frontiersin.org | +41 21 510 17 00



REPRODUCIBILITY OF RESEARCH

Support open data
and methods to enhance
research reproducibility



DIGITAL PUBLISHING

Articles designed
for optimal readership
across devices



FOLLOW US

[@frontiersin](https://twitter.com/frontiersin)



IMPACT METRICS

Advanced article metrics
track visibility across
digital media



EXTENSIVE PROMOTION

Marketing
and promotion
of impactful research



LOOP RESEARCH NETWORK

Our network
increases your
article's readership